A BLOOD-BASED SIGNATURE OF NEOCORTICAL AMYLOID BURDEN AN EARLY DIAGNOSTIC POPULATION SCREENING TOOL FOR ALZHEIMER'S DISEASE

Ashton, Nicholas James

Awarding institution:
King's College London

A BLOOD-BASED SIGNATURE OF NEOCORTICAL AMYLOID BURDEN: AN EARLY DIAGNOSTIC POPULATION SCREENING TOOL FOR ALZHEIMER'S DISEASE

Nicholas James Ashton

Submitted to King's College London University in fulfilment of the requirements for the degree of Doctor of Philosophy

2017

ABSTRACT

Alzheimer´s disease (AD) biomarkers that can detect and track disease progression at its earliest stages to aid the critical search for a disease modifying therapy is much needed. Markers of *in vivo* amyloid-beta (Aβ) deposition (e.g. ^{11}C-PiB) combined with positron emission tomography (PET) or cerebrospinal fluid (CSF) examination are becoming widely utilised as essential criterion for AD prevention trials. Although necessary, this is likely to come at a great cost and will restrict the progression of some trials. The inexpensive and accessible nature of a blood-based prediction for AD risk would be of considerable value in a population screening process. The traditional "case versus control" design frequently disregards the clinical heterogeneity in AD, with active preclinical neuropathology overlooked. Therefore, deriving biologically relevant markers associated with *in vivo* surrogates of AD pathology is considered a superior approach. Here, we aimed to identify single and multi-analyte plasma biomarkers associated with neocortical Aβ burden (NAB) using two proteomic approaches.

One dimensional gel electrophoresis (1DGE) coupled with Mass Spectrometry was performed on 78 individuals with extreme ranges of NAB. Immunoassay-based techniques were utilised to validate protein candidates in independent cohorts. Further to this, an improved proteomic strategy incorporating high-resolution peptide separation was able to increase the number of quantifiable targets and widen plasma proteome coverage. This enhanced methodology was applied to 297 individuals from two cohorts stratified by Aβ PET. In both discoveries, the relationship between plasma protein levels and NAB modalities was examined, with an attempt to build multi-modal predictions of NAB.

In the first discovery study, several candidates associated with NAB were selected for technical replication. Plasma FGγ models predicted NAB with a sensitivity of 59% and specificity of 78%. FGγ was further shown to associate with Aβ using core CSF biomarkers as surrogate measures. The secondary discovery study demonstrated a larger number of single markers associated with NAB, along with the verification

of brain-derived proteins found to be present in plasma. A machine learning analysis built a multi-analyte panel for NAB prediction which was shown to replicate, in an independent cognitively normal cohort, with an accuracy of 86.6%. This predictive panel indicated the convergence of pathways related to coagulation, APP processing, neuronal transcription factors and axonal injury to be of central importance in predicting NAB.

ACKNOWLEDGEMENTS

Firstly, I would like to express my immense appreciation and thanks to Dr. Abdul Hye for his guidance, friendship and fantastic opportunities that he has offered to me throughout the duration of my PhD. I would also like to thank my other supervisors Professor John Powell and Professor Simon Lovestone for their constant support and advice.

Further thanks must go to Professor Ralph Martins, Dr. Chantal Bazenet, Dr. Steven Kiddle, Dr. Malcolm Ward and Dr. Alejo Nevado-Holgado as key collaborators, in which, this work would not have been possible. Thanks to all of my colleagues, past and present, at the Institute of Psychiatry, Psychology and Neuroscience for a supportive and friendly environment.

I am also grateful to the Rosetree Trust UK and GE Health Care for their financial support of my PhD. I would also like to express my appreciation to all the participants who volunteered to be a part of the various research studies included in this thesis. Their contribution and continued commitment to dementia research is imperative in advancing our knowledge and developing treatments for Alzheimer's disease.

Lastly, I would like to give special recognition to my family: Mum, Dad, Claire, Andy, Helen, Olly and Noah for their welcome distraction, patience and encouragement throughout my PhD.

PUBLICATIONS AND PRESENTATIONS

PEER REVIEWED RESEARCH PAPERS

Ashton NJ, Baird AL, Lim K, Lynham S, Ward M, Fischer R, Lovestone S and Hye A. In-depth proteomic profiling of blood plasma; an application for the discovery of peripheral biomarkers of neurological disease. *PROTEOMICS*, 2017 (in review).

Westwood S, Leoni E, Hye A, **Ashton NJ**, Kiddle SJ, Baird AL, Sainz-Fuertes R, Leung R, Graf J, Hehir CT, Baker D, Cereda C, Bazenet C, Ward M, Thambisetty M and Lovestone S. Blood-based biomarker candidates of cerebral amyloid using PiB PET in non-demented elderly. *Journal of Alzheimer's Disease*, 2016: 29, 561-72.

Voyle N, Kim M, **Ashton NJ**, Baird AL, Bazenet C, Hye A, Westwood S, Chung R, Ward M, Rabinovici GD, Lovestone S, Breen G, Legido-Quigley C, Dobson RJB, Kiddle SJ for the Alzheimer's Disease Neuroimaging Initiative. (2016) Blood metabolite markers of neocortical amyloid-β burden: discovery and enrichment using candidate proteins. *Translational Psychiatry*, 2016: 6, 1-8.

Ashton NJ, Kiddle SJ, Graf J, Ward M, Baird AL, Hye A, Westwood S, Wong KV, Dobson RJB, Rabinovici GD, Miller BL, Rosen HJ, Torres A, Zhang Z, Thurfjell L, Covin A, Tan Hehir C, Baker D, Bazenet C, Lovestone S and the AIBL Research Group. Blood protein predictors of brain amyloid for enrichment in clinical trials? *Alzheimers Dement (Amst)*, 2015; 1, 48-60.

Kiddle SJ, Steves CJ, Mehta M, Simmons A, Newhouse S, **Ashton NJ**, Bazenet C, Killick R, Adnan J, Westman E, Nelson S, Soininen H, Kloszewska I, Mecocci P, Tsolaki M, Vellas B, Curtis C, Breen G, Williams SCR, Lovestone S, Spector TD and R J B Dobson RJB. Plasma protein biomarkers of Alzheimer's disease endophenotypes in asymptomatic older twins: early cognitive decline and regional brain volumes. *Translational Psychiatry*, 2015: 5, 1-6.

CONFERENCE PRESENTATIONS (ORAL)

Ashton NJ. Plasma biomarkers of neocortical amyloid burden; an in-depth plasma profile using LC-MS/MS. *Biofluid Based Biomarker PIA (BBB-PIA), Association International Conference*; 23rd July 2016, Toronto, Canada.

Ashton NJ. Plasma biomarkers for Alzheimer's disease. *Alzheimer's Research UK (ARUK) network dementia symposium*; 4th September 2015, London, UK.

Ashton NJ. FGγ a candidate blood protein markers of neocortical amyloid burden (NAB) for enrichment in clinical trials. *Alzheimer's Association International Conference*; 17th July 2014, Copenhagen, Denmark.

CONFERENCE PRESENTATIONS (POSTER)

Ashton NJ, Narvardo A, Lynham S, Ward M, Baird AL, Gupta V, Chatterjee P, Goozee K, Hone E, Pedrini S, Laws S, Rainey-Smith SR, Bush AI, Rowe CC, Villemagne VL, Amnes D, Masters C, Lovestone S, Martins R and Hye A. Plasma biomarkers of neocortical amyloid burden; an in-depth plasma profile using LC-MS. *Alzheimer's Association International Conference*; July 2016, Toronto, Canada.

Ashton NJ, Baird AL, Lin K, Fischer R, Lynham S, Ward M, Lovestone S and Hye A. In-depth mining of blood plasma for biomarkers of Neurodegeneration. *Alzheimer's research UK Conference*; March 2016, Manchester, England.

Ashton NJ, Kiddle SJ, Graf J, Ward M, Baird AL, Hye A, Westwood S, Wong KV, Dobson RJB, Rabinovici GD, Miller BL, Rosen HJ, Torres A, Zhang Z, Thurfjell L, Covin A, Tan Hehir C, Baker D, Bazenet C and Lovestone S. Candidate blood protein markers of neocortical amyloid burden (NAB) for enrichment in clinical trials. *Alzheimer's Association International Conference*; July 2014, Copenhagen, Denmark.

Ashton NJ, Hye A, Baird AL, Ward M, Bazenet C and Lovestone S. Peripheral biomarkers of Alzheimer's disease; widening the limits of detection in large scale biomarker discovery projects using LC-MS/MS. *Alzheimer's & Parkinson's Diseases Congress*; March 2013, Florence, Italy.

TABLE OF CONTENTS

CHAPTER CONTENTS

LIST OF TABLES

CHAPTER 1

CHAPTER 2

CHAPTER 3

CHAPTER 4

CHAPTER 5

LIST OF FIGURES

CHAPTER 1

CHAPTER 2

CHAPTER 3

CHAPTER 4

CHAPTER 5

CHAPTER 6

LIST OF SUPPLEMENTARY MATERIAL

Supplementary Material 1

An R script for "Pre-processing for Relative Quantification 1" (PRQ-1).

Supplementary Material 2

An R script for "Pre-processing for Relative Quantification 2" (PRQ-2).

Supplementary Material 3

Full LC-MS/MS results extracted from PRQ-1 examining the relationship of 1,139 protein group MW isoforms with ^{11}C-PiB as binary and continuous measures in the AIBL-1 cohort.

Supplementary Material 4

The numbers of peptide spectral matches for the identification of 7,439 unique proteins groups have been database matched (at 5% FDR) in 15 proteomic methodologies investigated Chapter 4.

Supplementary Material 5

The identification of 468 highly expressed cerebral cortex protein groups that have peptide spectral evidence (at 5% FDR) of plasma expression in the OGE-9 methodology highlighted in Chapter 4. A total of 311/468 protein groups have been described as "Grouped Enriched" (n = 88) or "Tissue Enhanced" (n = 223) by Human Protein Atlas. These are protein groups that have five-fold higher expression in cerebral cortex but also exhibit substantial expression in other tissues.

ABBREVIATIONS

^{11}C-PiB	Pittsburgh compound B
^{18}FBB	Florbetaben
1DGE	One dimensional gel electrophoresis
2DGE	Two dimensional gel electrophoresis
A1AT	α1-Antitrypsin
ACh	Acetylcholine
ACN	Acetonitrile
AD	Alzheimer's disease
AGC	Automatic Gain Control
AGP	α1-Acid glycoprotein
AIBL	Australian Imaging, Biomarkers and Lifestyle Flagship Study of Ageing
ALS	Amyotrophic lateral sclerosis
Ambic	Ammonium Bicarbonate
ANM	AddNeuroMed study
ANOVA	Analysis of variance
apo(a)	apolipoprotein(a)
apoA1	apolipoprotein A-I
apoA2	apolipoprotein A-II
apoA4	apolipoprotein A-IV
ApoE	apolipoprotein E (protein)
APOE	apolipoprotein E (gene)
apoL1	apolipoprotein L1
APP	amyloid precursor protein
APP	Amyloid precursor protein (gene)
AUC	Area Under the Curve
Aβ	Amyloid-beta
BACE1	β-secretase
BBB	Blood-brain barrier
BDP	Brain-derived protein
C18	C18-bonded silica
C4α	complement C4-A

CAA	Cerebral amyloid angiopathy
CART	Classification and Regression Trees
CC3	complement C3
CDR	Clinical Dementia Rating
CFB	complement factor B
CFH	complement factor H
CJD	Creutzfeldt-Jakob disease
CNS	Central nervous system
CSF	Cerebrospinal fluid
CSF $A\beta_{1-42}$-	Cerebrospinal fluid beta-amyloid negative
CSF $A\beta_{1-42}$+	Cerebrospinal fluid beta-amyloid positive
CV	Coefficient of Variation
Da	Daltons
DAVID	Database for Annotation, Visualization and Integrated Discovery
ddH_20	Double distilled water
DIAN	Dominantly Inherited Alzheimer Network
DLB	Dementia with Lewy Bodies
DS	Down Syndrome
DTT	Dithiothreitol
ELISA	Enzyme-linked immunosorbent assay
EMIF	European Medical Informatics Framework
EMIF-AD	European Medical Informatics Framework for Alzheimer's disease
ENO2	neuron specific enolase
EOAD	Early onset Alzheimer's disease
FA	Formic acid
FDA	Food and Drug Administration
FDG	Fludeoxyglucose
FDR	False discovery rate
FGα	fibrinogen α chain
FGβ	fibrinogen β chain
FGγ	fibrinogen γ chain
FHR-1	complement factor H related protein 1
FTD	Frontotemporal Dementia
FTLD	Frontotemporal lobar degeneration
x g	Acceleration due to gravity

GFAP	glial fibrillary acidic protein
GLM	Generalised linear model
GWAS	Genome-wide association study
h	Hours
HA	Heterophilic antibodies
HCD	Higher Collision induced Dissociation
HD	Huntington's disease
HEC	Healthy elderly control
HPA	Human Protein Atlas
HRG	histidine-rich glycoprotein
HRP	Horseradish peroxidase
IAA	Iodoacetamide
IDE	Insulin degrading enzyme
IEF	Isoelectric focusing
IgA	Immunoglobulin A
IgG	Immunoglobulin G
IGHA1	Ig alpha-1 chain C region
IgM	Immunoglobulin M
IPG	Immobilised pH gradient
IV	Intravenous
kDa	Kilodaltons
KEGG	Kyoto Encyclopedia of Genes and Genomes
kVh	Kilo voltage hours
LASSO	Least absolute shrinkage and selection operator
LC	Liquid chromatography
LC-MS/MS	Liquid chromatography – tandem mass spectrometry
LOAD	Late onset Alzheimer’s disease
LOD	Limit of detection
LP	Lumbar puncture
LTQ	Linear Trap Quadrupole
M	Molar
m/z	Mass-to-charge ratio
MBL	Mannose-binding lectin
MCI	Mild cognitive impairment
mg	Milligram

mL	Millilitre
mM	Millimolar
MMSE	Mini Mental State Examination
MOG	myelin-oligodendrocyte glycoprotein
MRI	Magnetic resonance imaging
MS	Mass spectrometry
MS/MS	Tandem mass spectrometry
MSA	Multiple system atrophy
MSD	Mesoscale discovery
MTL	Medial temporal lobe
MW	Molecular weight
n	Number
NAB	Neocortical amyloid burden
NaCl	Sodium chloride
NDEs	Neuronal-derived exosomes
NEFL	neurofilament light
NFT	Neurofibrillary tangles
NGS	Next generation sequencing
nL	Nanolitres
nm	Nanometers
NMDA	N-Methyl-D-Aspartate
NPV	Negative predcitive value
NRGN	neurogranin
Qalb	CSF/plasma albumin ratio
OGE	OFFGEL fractionation
OPALIN	oligodendrocytic myelin paranodal and inner loop protein
OR	Odds ratio
pAGC	predictive automatic gain control
PARK7	protein deglycase DJ-1
PBS	Phosphate buffered saline
PCA	Principle component analysis
PD	Parkinsons disease
PDD	Parkinsons disease dementia
PET	Positron emmision tomography
pH	Potential of Hydrogen

PHF	Paired helical filaments
pI	Isoelectric point
PiB-	Pittsburgh compound B negative
PiB+	Pittsburgh compound B positive
PLP1	proteolipid Protein 1
PPD	Plasma Proteome Database
ppm	Parts per million
PPV	Postivie predictive value
PPY	pancreatic polypeptide
PRQ-1	Pre-processing for Relative Quantification 1
PRQ-2	Pre-processing for Relative Quantification 2
PSEN1	Presenilin 1 (gene)
PSEN2	Presenilin 2 (gene)
PSM	Peptide spectral matches
PSP	Progressive supranuclear palsy
PTM	Post translational modification
QC	Quality control
RBM	Rules-Based Medicine
RF	Random Forest
ROC	Receiver Operator Characteristic
ROI	Region of interest
rpm	Revolutions per minute
RT	Room temperature
S.D	Standard deviation
S100B	S100 calcium-binding protein B
SCX	Strong cation exchange
SDS	Sodium dodecyl sulfate
SIMOA	Single-molecule enzyme-linked immunosorbent assay
SMC	Subjective memory complaints
SNAP	Suspected Non Amyloid Pathology
SNAP-25	synaptosome associated protein 25kDa
SNCA	α-synuclein
SNCB	β-synuclein
SNP	Single nucleotide polymorphism
SRM	Selection reaction monitoring

SOD1	Superoxide dismutase [Cu-Zn]
SUV	Standardized uptake values
SUVR	Standardized uptake values ratio
$t_{1/2}$	Half-life
TBI	Traumatic brain injury
TCEP	Tris (2-carboxyethyl) phosphine
TEAB	Tetraethylammonium bromide
TF	serotransferrin
TFA	Trifluoroacetic acid
TMB	3,3',5,5'-Tetramethylbenzidine
TMT	Tandem Mass Tags
UCSF	University of California, San Francisco
UCH-L1	Ubiquitin carboxy-terminal hydrolase L1
V	Voltage
VaD	Vascular dementia
w/v	Water / volume percentage
α2m	alpha-2-Macroglobulin
µg	Micrograms
µL	Microlitres

GENERAL INTRODUCTION

1.1 A brief history of dementia: Auguste Deter to present day

In 1906, Alois Alzheimer presented for the first time a form of dementia that was later acknowledged as Alzheimer's disease (AD). Alzheimer described the rapid clinical decline of his patient, Auguste Deter, who had shown progressive cognitive impairment, memory loss, delusional behaviour and psychosocial difficulties. Upon *post mortem* examination, Alzheimer demonstrated the extensive atrophy of the cerebral cortex as well as extracellular and intracellular protein aggregates. Although these observations had been previously reported by other scientists, it was the young age and rapid decline of Auguste Deter that made this case so unique.

Since Alzheimer's first account of Auguste Deter, significant discoveries and breakthroughs for AD have been hard to come by. It wasn't until 1984 when the extracellular protein deposits that Alzheimer described in Auguste Deter were found to be amyloid-beta (Aβ) and in 1985, researchers discovered that the key component of the intracellular tangles was hyperphosphorylated tau. Genetic studies identified the first gene for inherited familial AD (amyloid precursor protein; *APP*) in 1987, with the first major risk factor gene (apolipoprotein ε4; *APOE* ε4) being identified in 1993. The first drug approved by the Food and Drug Administration (FDA) for the symptomatic treatment of AD was made in 1996, with three further symptomatic only treatments approved since. The discovery of the imaging agent Pittsburgh Compound B (PiB) in 2004 was a major breakthrough in disease monitoring and early detection by the *in vivo* assessment of neocortical Aβ deposition. This contributed to the development of a hypothetical model being published in 2010, based upon growing evidence, that changes in AD related pathology occurs decades before clinical onset (Aβ being the earliest). New criteria and guidelines for AD diagnosis quickly followed. The first major Phase III preventive trials that targeted Aβ production and clearance commenced in 2008, with several others underway and concluded since.

While in recent year's major landmark breakthroughs for the cause and understanding of AD have been deduced, there is still no disease modifying treatment. Since the description of Auguste Deter in 1906, the prevalence and concern for AD has grown immeasurably. In 1976, AD was for the first time declared the most common cause of dementia and a major public health concern for the future. At that time, the estimated prevalence of AD was thought to be between 880,000 – 1.2 million [1].

Today, there are more than 40 million worldwide dementia sufferers, mostly older than 60 years of age, which is expected to rise to 115 million by 2050 [2]. Of major concern, these projected increases in dementia prevalence are proportionally much higher for developing countries than for Western Europe and the USA, which already have a much older populations [3]. The global economic burden of dementia care is currently estimated at $604 billion and like prevalence rates this figure is set to exponentially increase with a projected 85% rise in costs within the next 20 years.

These figures can be revised if interventions are found to delay or prevent the clinical onset of dementia. AD is the main cause of dementia and accounts for around 60-80% of all cases. AD has therefore been highlighted as a major global priority to search for early diagnostics, preventative and or disease-modifying therapies.

1.2 Alzheimer's disease pathology

AD is primarily characterised by two neuropathological hallmarks; extracellular deposits of senile plaques and intracellular neurofibrillary tangles (NFTs). Senile plaques exist in various morphological forms including diffuse ('pre-amyloid'), primitive neuritic, classic ('dense-cored') plaques [4]. The major component of senile plaques is amyloid-beta (Aβ), a 38-43 amino acid peptide, which is derived by the secretase cleavage of the amyloid precursor protein (APP) [5]. A variety of Aβ peptides are present within these plaques with the most common peptide being $Aβ_{42/43}$, whereas the more soluble $Aβ_{40}$ is also found in association with blood vessels [6]. Diffuse plaques contain $Aβ_{42/43}$ as well as APP fragments lacking the C-terminus while more mature classic plaques contain $Aβ_{40}$ in addition to $Aβ_{42/43}$ [7]. While senile plaques are primarily composed of the Aβ peptides, a host of 'secondary' constituents have been colocalised with Aβ in the AD brain, this includes; proteoglycans, inflammatory molecules (e.g. acute phase proteins, cytokines, chemokines, complement proteins and immunoglobins), serum related molecules (e.g. amyloid-P), metal ions, protease and clearance related elements (e.g. alpha-1-antichymotrypsin), antioxidant defense proteins (e.g. ferritin and ceruloplasmin) as well as apolipoprotein E and the multifactoral protein clusterin (reviewed in [8-7]).

The cleavage of APP predominately occurs by the action of α-secretase followed by γ-secretase to produce non-amyloidogenic products. The cleavage of α-secretase releases a large soluble ectodomain of APP (sAPPα) and a carboxyl terminal fragment (αCTF) [9]. The γ-secretase cleavage of αCTF produces APP interacellular cytoplasmic domain (AICD) and soluble peptide P3 [10]. However, a proportion of APP is cleaved by β-secretase (BACE1) rather than α-secretase to produce sAPPβ and βCTF. The following cleavage by γ-secretase produces an Aβ fragment and AICD which are transported, via exocytosis, in the extracellular space [9, 11-12] (Figure 1-1). The predominate forms of Aβ produced by the amyloidogenic pathway are $Aβ_{1-40}$ and $Aβ_{1-42,}$ of which the latter is considered to be the more neurotoxic and tends to aggregate into oligomers, protofibers and fibrils [13-14]. Subsequent diffuse Aβ plaque formation leads to localised microglial activation, cytokine release, astrocytosis and a multi-protein inflammatory response [15-16].

Three forms of APP have been described and are referred to as APP695, APP751 and APP770, reflecting the number of amino acids encoded for by their respective complementary DNAs [17]. The two larger APPs contain a 57-amino-acid addition with striking homology to the Kunitz family of protease inhibitors [18-19]. It has been shown that the deduced amino-terminal sequence of APP is identical to the sequence of a cell-secreted protease inhibitor, protease nexin-II (PN-II). Nexin-II potently inhibits serine proteases, including trypsin and coagulation factors [20]. This identification of APP as a secreted protease nexin has offered new insights into the pathogensis of AD; not only is the protease activities of APP are of importance but also the reuptake and degradation APP-protease complexes.

The "amyloid cascade hypothesis", supported by genetics, has been the prevailing theory to explain AD pathogenesis. This model suggests that APP mismetabolism and subsequently the increased production then deposition of toxic Aβ acts as a pathological trigger that leads to neurotic injury, NFT formation and cell death which underpin neurodegeneration in AD [21]. This has been further supported by substantial genetic, biochemical and pathological evidence [22]. Recent evidence suggests that the failure or imbalance of Aβ clearance, rather than excess formation, is the major contributor to toxic deposition [23-24]. This would attribute mechanisms implicated in the degradation of toxic Aβ (i.e. neprilysin, insulin degrading enzyme (IDE), intracellular lysosomal degradation and microglia activation) a central importance in the development of Aβ pathology [11, 25].

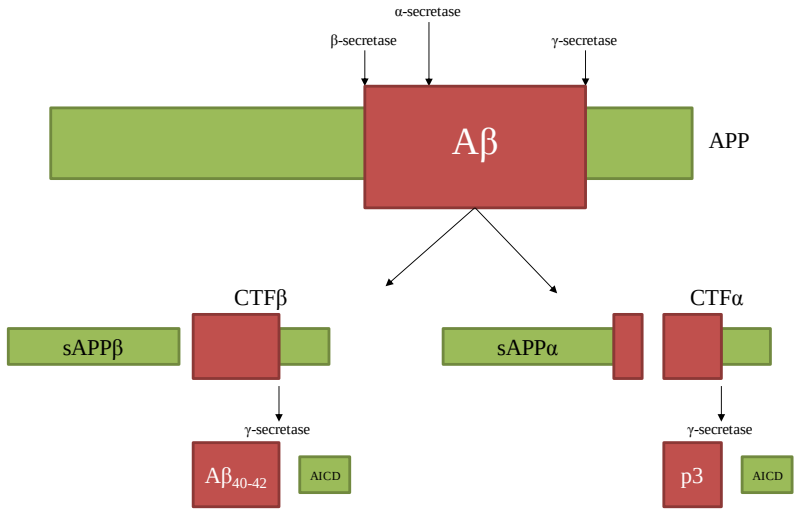

Figure 0-1: Sequential cleavage of the amyloid precursor protein (APP) occurs by two main pathways. The non-amyloidogenic processing of APP involves α-secretase followed by γ-secretase. The amyloidogenic processing of APP involves BACE1 followed by γ-secretase. Both processes generate soluble ectodomains (sAPPα and sAPPβ) and identical intracellular C-terminal fragments (AICD).

Although Aβ peptides are produced in high amounts in pathological conditions, they are also present at low levels in normal brains, particularly during synaptic activity. It was thought for many years that Aβ was a bi-product of APP catabolism and had no non-pathological role. APP is an essential membrane protein with high affinity to copper which is ubiquitously expressed [26]. It has been reported that APP is involved in neurodevelopment and is required for neuronal growth [26], synaptogenesis and cell adhesion [27]. At nanomolar and micromolar concentrations Aβ causes neurotoxicity and cell death, however at picomolar levels Aβ has been shown to act as a key growth factor and modulator synaptic activity and plasticity, with relation to memory and learning highly important for normal individuals [28-29]. This is supported by anti-APP antibodies being shown to block memory formation [30]. Furthermore, low concentrations of Aβ could work as antioxidants, due to its ability to capture redox metals, such as Copper, Iron and Zinc, and therefore, preventing their participation in redox cycling with other ligands [31]. Considering the positive or negative effects of Aβ at differing concentrations, it is proposed that the peptide exhibits dual effects: neurotrophic or neurotoxic

The hyperphosphorylation of the microtubule-associated protein tau causes the production of NFTs in the intracellular space [32-33]. Neurodegeneration, synaptic loss and cognitive symptoms observed in AD patients are more associated with the density and distribution of NFT pathology than Aβ deposition [34]. In the adult brain, six tau isoforms are coded for by a single gene located on chromosome 17 [35]. A prominent feature of the primary structure of tau is the three or four repeat of an 18 amino acid sequence located at the C-terminal half (3R and 4R tau). This microtubule binding domain is involved in the microtubule polymerisation and stabilisation [36]. In neurons, the cytoskeleton undergoes continuous change and tau protein regulates this process. The abnormal hyperphosphorylation of tau prevents the primary function of tau binding to microtubules and ultimately causes cell death by leading to the destabilisation of axons, impairment of axonal transport, axonal degeneration and neuronal dysfunction [37]. Hyperphosphorylated tau also forms insoluble aggregates, paired helical filaments (PHF), the foremost constituent of NFTs found in AD and other tauopathies [38]. Tau isolated from AD brains has a 4-fold increase in phosphorylation [39] and all tau isoforms are found to be aggregated in PHFs [40]. Contrary to this causative role, recent evidence from mouse models also points towards a protective element of tau in early AD. This is by the specific phosphorylation of threonine-205 at post-synaptic terminals [41].

There is growing evidence of the direct or indirect interaction of Aβ pathology and tau to accelerate NFT formation. The dominant view is that Aβ precedes and initiates a cascade that results in NFT and other pathologies [42]. Evidence from genetic studies that increase Aβ production demonstrates the enhanced development of tau pathology [43] and whilst hyperphosphorylation of tau promotes aggregation and NFT formation, tau kinase activation can be induced by Aβ [43-44]. Furthermore, inflammatory cytokine activation and impairment of degrading enzymes that increase tau phosphorylation can be modulated by Aβ [43].

Although the relationship of Aβ accumulation and tau pathology remain unclear they both finally converge to cause widespread and progressive cell death and neuronal loss. *Post mortem* analysis indicates the medial temporal lobe (MTL), including the hippocampus, parahippocampus and entorhinal cortex, to be the first affected by AD pathology [45]. In addition, extensive degeneration of cholinergic processes from the

basal nucleus of Meynert to the neocortex is an early observation in the disease process [45]. As the disease progresses, significant neuronal loss in the cerebral cortex, specifically the lateral temporal and medial parietal lobes are observed, followed by atrophy of the lateral parietal and frontal lobes [46]. Upon clinical presentation, an AD sufferer will have extensive atrophy of the temporal, parietal and frontal cortices with relative preservation of the primary occipital and primary sensor-motor cortex [45, 47]. The extent of clinic symptoms due to AD is more strongly correlated with the anatomical extent and number of NFTs in the cortex [48]. This observation has led to the "tau propagation" hypothesis where tau may systemically develop and progress independently throughout the brain [49]. Investigations using animal models strongly point towards NFTs propagation from the MTL to the cortex being driven by Aβ [50-51].

1.3 Genetic, epigenetic and lifestyle risks

1.3.1 Genetics of Alzheimer's disease

Early onset Alzheimer's disease (EOAD) and genetic risk

EOAD compromises the minority of all AD cases (5-10%) with an onset normally between 30-65 years of age. EOAD can be categorised by a classic Mendelian inheritance pattern, usually autosomal-dominant, however it can present without any family history ("sporadic" EOAD). Although autosomal-dominant AD is very rare (<1%), discovery of the causative mutations is the basis of unravelling the pathogenesis of AD and are now at the centre of current diagnosis and drug development.

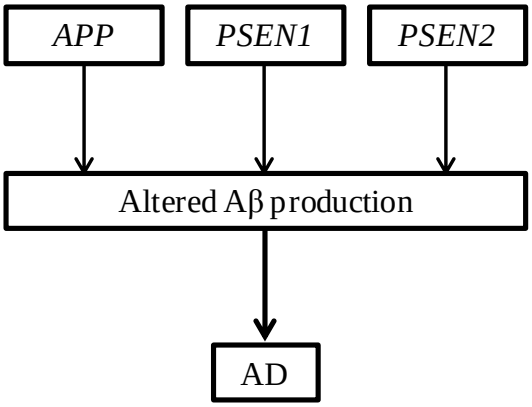

Figure 0-2: Three genes implicated in early onset AD; amyloid precursor protein (*APP*), presenilin 1 (*PSEN1*) and presenilin 2 (*PSEN2*).

Highly-penetrant mutations in three genes are considered the main risk factors for EOAD (Figure 1-2): *APP* [52-54], *PSEN1* [55-56] and *PSEN2* [57]. These mutations have been shown to alter Aβ production to increase the $A\beta_{1-42}$ to $A\beta_{1-40}$ ratio leading to dementia [58-60]. *PSEN1* mutations are the most common and most severe cause of autosomal-dominant AD with full penetrance and the age of onset occuring as early as 25 years of age [61] (Figure 1-3).

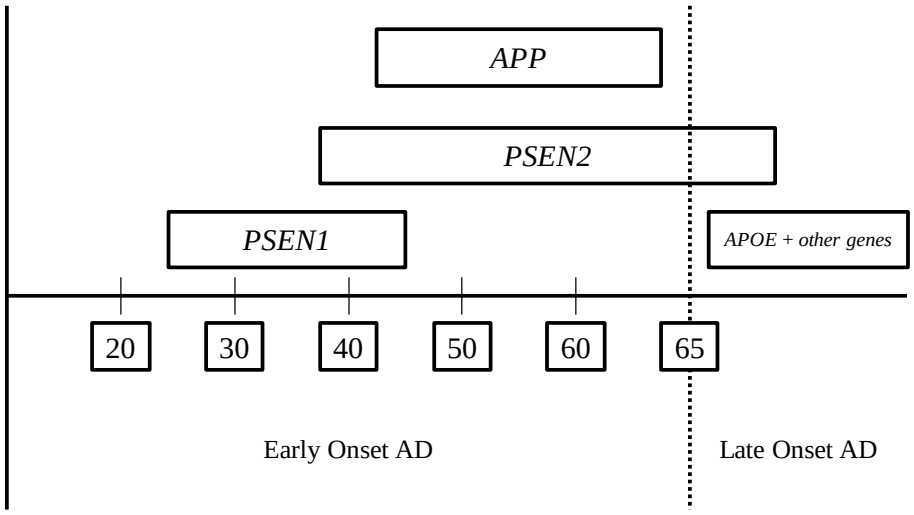

Figure 0-3: The age onset of Alzheimer's disease depending on the different involvement of genes.

Late onset Alzheimer's disease (LOAD) and genetic risk

Late onset AD is considered to be a multifactorial disease; nonetheless, there is a considerable genetic contribution. The *APOE* gene, located on chromosome 19, is an important genetic risk factor for LOAD. Apolipoprotein E (ApoE) protein is the major cholesterol carrier in the brain and has key roles in neuronal growth, tissue injury repair and immunoregulation. ApoE binds to numerous cell surface receptors which are implicated in lipid delivery and transport as well as mitochondrial function and glucose metabolism. Three predominate allelic variations are found in the *APOE* gene (ε2, ε3 and ε4) encoding for different protein isoforms that differ in two sites of the amino acid sequence [62]. *APOE* ε3 is the most common variant (77%), while ε2 (8%) and ε4 (15%) alleles are less common [63]. Conversely, the frequency of ε4 carriers in the AD population is much larger, approximately 60% [64] and substantially increases the risk in both familial AD and sporadic AD [65-66]. Typically, ApoE binds to Aβ peptides and effectuates the clearance of soluble Aβ and its aggregates [67-68] however the *APOE* ε4 variant is less efficient in the clearance of Aβ [68]. Furthermore, transgenic mouse models that express *APOE* ε4 show a disinhibition of cyclophlin A signalling in the pericytes of the brain-blood vessels and this results in degeneration of these vessel and leakage of the blood-brain barrier (BBB) and neurodegeneration independent of Aβ [69]. Nonetheless, the presence of the *APOE* ε4 allele alone is not sufficient for the development of AD pathology [66]. Not only has the ε4 allele found to increase risk but it is also implicated in the reduction in the age of onset [62, 70] and

increases the rate of cognitive decline [71-72]. The *APOE* ε4 allele has also been found to have a stronger association with risk in women than in men [73-74]. The disease risk effect in heterozygous ε4 carriers is estimated at 3-fold whereas a 15-fold risk is reported in homozygous ε4 carriers [62, 65, 67]. The *APOE* ε2 allele is considered to be protective and to delay disease onset [66, 75-76], although in certain populations *APOE* ε2 has been shown not to have protective effect in relation to AD [77]. More recent evidence suggests a protective mechanism whereby *APOE* ε2 allele reduces the accumulation of Aβ pathology in the ageing brain [78].

Genome wide association studies (GWAS) have identified a number of novel loci for late onset AD, including polymorphisms in: *SORL1*, *BIN1*, *CR1*, *CLU* and *PICALM* (Table 1-1) [79-85]. This analysis approach has so far highlighted pathways related to cholesterol and lipid metabolism, energy metabolism, immune system, inflammatory responses, endosomal vesicle cycling and risk genes connected with Aβ and Tau pathology (Table 1-1). On-going large meta-analyses continue to be published and identify new susceptibility genes adding further weight to the implicated pathways in AD [86]. Moreover, GWAS studies have revealed several additional susceptibility loci located in gene dense regions; *MS4A6A* locus, *HLA-DRB5* locus, *ZCWPW1* locus, *SLC24A4/RIN3* locus, *NME8* locus and *CELF1* locus [64]. It is yet to be determined which gene in these regions is responsible for the association. More recently, GWAS studies have indentified novel genetic loci associated with hippocampal volume [87] and novel AD loci encoding in proximity to the gene that encoded for tau (*MAPT*) [88]. None of these indentified risk loci attain the magnitude of *APOE* ε4, yet they provide information on the pathological pathways implicated in the disease process (Table 1-1).

Table 0-1: Overview of the single locus susceptibility genes identified for AD by GWAS with functional and pathway characteristics (adapted from Van Cauwenberge C et al., 2016).

Gene	Location	OR (95% CI)	Pathway/Function	Effect on APP/Tau pathway
APOE	19q13.32	3.78 (2.60-5.48)	Cholesterol and lipid metabolism and immune response	Aβ aggregation and clearance
SORL1	11q24.1	1.30 (1.22-1.39)	Endosomal vesicle cycling	Aβ generation and clearance
BIN1	2q14.3	1.33 (1.18-1.25)	Endosomal vesicle cycling	Tau toxicity
CR1	1q32.2	1.18 (1.14-1.22)	Immune response	Aβ clearance
CLU	8p21.1	1.16 (1.12-1.19)	Cholesterol and lipid metabolism	Aβ aggregation and clearance
PICALM	11q14.2	1.15 (1.12-1.18)	Endosomal vesicle cycling	APP trafficking and Aβ clearance
ABCA7	19p13.3	1.15 (1.11-1.19)	Lipid metabolism and immune response	Aβ clearance
FERMT2	14q22.1	1.14 (1.09-1.19)	Cytoskeletal function and axonal transport	Tau toxicity
CASS4	20q13.31	1.14 (1.09-1.19)	Cytoskeletal function and axonal transport	-
EPHA1	7q35	1.11 (1.08-1.14)	Endosomal vesicle cycling and immune system	-
PTK2B	8p21.2	1.10 (1.08-1.13)	Cell migration and synaptic function	-
CD2AP	6p12.3	1.10 (1.07-1.13)	Endosomal vesicle cycling	Aβ clearance and Tau toxicity protection
INPP5D	2q37.1	1.08 (1.05-1.11)	Immune response	-
MEF2C	5q14.3	1.08 (1.05-1.11)	Immune response and synaptic function	-
CD33	19q13.41	1.06 (1.04-1.10)	Immune system and inflammatory response	Aβ clearance

Abbreviations: CI, Confidence interval; OR, Odds ratio.

Recent next-generation sequencing (NGS) studies and GWAS on very large cohorts have revealed rare variants associated with AD. Multiple rare, missense variants in *TREM2* (1-2% frequency) have been reported to increase the risk for late onset AD [89-91] and FTD [92]. People homozygous for *TREM2* variants develop Nasu-Hakola

disease characterised by early onset cognitive problems and with bone fractures and cysts. The most common disease-associated variant in *TREM2* (R47H) is found within European populations and is reported to have an effect size comparable to *APOE* ε4. TREM2 is a highly expressed receptor in microglia where it is thought to have an important role in phagocytosis (including Aβ) and inflammatory pathways [89, 93].

1.3.2 Epigenetics

Epigenetics refers to the change in gene regulation caused by modifications to the DNA's packaging protein or the DNA molecules themselves without changing the underlying nucleotide sequence [94-95]. Epigenetic modifications have found to be a cause of phenotypic plasticity loss associated with the ageing process [96]. Since ageing is the biggest risk factor for AD and other neurodegenerative diseases, it is hypothesised that epigenetic modifications play a prominent role in disease pathogenesis [97-98]. At the molecular level two dominant epigenetic modifications are known: direct methylation of DNA or modification of the histones that package DNA [99-100]. There have been several reports of a genome-wide change in DNA methylation in AD patients [101-103]; whereas epigenome-wide association studies (EWAS) have identified hypermethylated genes (SORBS3 and ANK1) in AD vulnerable brain regions [104-106]. The less studied histone modifications have been shown to be decreased [107] and increased [108] in AD *post mortem* studies. Pharmacologically targeting DNA methylation or histone acetylation maybe of potential benefit to AD sufferers. Folic acid and Vitamin B_{12} influence DNA methylation through their role in 1-Carbon metabolism [109] whereas histone deacetylase (HDAC) modifiers (2-valproate) have been used to target histone acetylation [110].

1.3.3 Lifestyle and vascular risk factors

There is a large collection of data describing the major risk factors for AD including age [111], genetics [112] and head injury [113]. However, given that AD develops over a long preclinical period of several decades; modifiable lifestyle choices may have a large impact in the development and onset of AD. Sufficient evidence points towards physical activity and exercise [114-116], midlife obesity [117], alcohol

consumption [118], nutrition [119], education [120] and smoking [121-122] being the most crucial modifiable risk factors for AD.

Regular physical exercise has been shown to delay the onset of AD with even low intensity activity shown to be beneficial [115-116]. Exercise was shown to enhance hippocampal neurogenesis [123] and learning in rodents [124]. Moreover, a significant protective effect of regular exercise was found in persons with *APOE* ε4 risk [125]. Higher BMI in middle aged is a risk factor for many dementias [117, 126] and many studies link midlife obesity to cognitive decline and directly to AD [127-128]. Conversely, in the elderly, a significant decrease in BMI was associated with the onset of AD within 5-6 years [129-130]. Alcohol consumption is a widely recognised risk for dementia. Middle-aged heavy drinkers are at a 3-fold greater risk to develop AD later in life [131]. There is a significant reduction in risk for light and moderate consumers [132-133] however, alcohol consumption at all levels has been found to be related to brain atrophy and volume loss [134]. Meta-analysis and systemic review of large datasets have shown that enhanced cognitive reserve (a model combing education, mental activity and occupation) may have a protective mechanism in delaying the onset of dementia [135] with education being the most influencing factor [135]. A number of studies assessing smoking on cognitive health concluded that a current smoker was 1.5-fold more likely to develop AD [122], with the risk greater in *APOE* ε4 non-carriers [122].

The lifestyle factors mentioned above may contribute to the development of treatable medical conditions that are also associated in the development in AD. Stroke [136-137], atherosclerosis [138], type 2 diabetes [139-141], midlife hypertentsion [142-143] and midlife hypercholesterolaemia [144-146] have been associated with an increased risk of AD. Evidence from the Rotterdam study suggests that a 30% reduction in the incidence of dementia would occur if the major modifiable cardiovascular risks could be managed or prevented [143].

A number of intervention studies addressing modifiable risk factors to address the development of AD have been conducted, with variable results. Many studies link hypertension to increased brain atrophy and NFT generation [147] however randomised controlled trials addressing hypertension have shown little benefit in reducing the

incidence of dementia [148]. There is also insufficient evidence to support dietary supplements in reducing the incidence of AD [149-150] and similarly vitamin supplements do not seem to be effective [151]. However, there is continued support for the components of a Mediterranean diet in a having an encouraging effect on cognition [152-153]. Furthermore, a moderate benefit of applying cognitive stimulation in older adults has been observed [135, 154]. Many modifiable risk factors of AD do overlap, explaining why altering one lifestyle strategy alone has made little impact in reducing the incidence of AD. It has been postulated that a more general approach to promote healthy living, with a focus on exercise, is the most promising approach [14] until more robust longitudinal evidence about modifiable risk factors for AD are available.

1.4 Clinical timeline of symptom development

1.4.1 Clinical Alzheimer's disease

A definitive AD diagnosis can only be made at *post mortem* and only a "probable" diagnosis of AD can be made clinically. AD is characterised by multiple cognitive deficits and memory decline which is assessed by a detailed history (by patient and carer) to determine the impact on social or occupational functioning [14]. The National Institute on Neurological and Communicative Disorders and Stroke and Alzheimer Related Disorders Association (NINCDS/ADRDA) proposed the criteria for the diagnosis of AD [155] with later revisions made to incorporate advancements in clinical, imaging and fluids assessments [24, 156-158]. The revised NINCDS/ADRDA criteria in 2011 recognised that the clinical diagnosis of AD could only be designated as "probable" while the patient was alive and could not be made "definite" until AD pathology had been confirmed *post mortem*. The recent NINCDS/ADRDA criteria also addressed the development of *in vivo* assessment of AD pathology. The clinical guidelines alone demonstrated a good sensitivity and specificity (>80%) of distinguishing AD patients from non-demented individuals [159] but were inconsistent in separating the subtypes of dementia [159].

More recent criteria set out by the International Working Group (IWG) for New Research Criteria for the Diagnosis of Alzheimer's Disease (AD) proposed criteria that is reliant on the *in vivo* biomarker evidence of pathophysiology indicative of AD (discussed further in section 1.7) [158]. Nonetheless the clinical criteria set out for AD remains important for clinics without advanced neuroimaging or cerebrospinal fluid testing.

The initial presentation of cognitive impairment follows a long preclinical phase of AD pathology [160]. Individuals with early AD may present clinically normal with only slight impediment of daily living. The decline of cognitive impairment is variable but often slow in the early symptomatic phase. Significant decline in short term memory are the main complaints by the individual or informant but symptoms of aphasia or spatial disorientation are commonly described [161]. Individuals with early AD experience difficulty with executive function and reduced verbal fluency. Subtle mood changes occur in 20-30% of early AD patients, with behavioural and

personality changes observed in 25-50% of cases [162]. Conversely, agitation, psychosis and anxiety are rare in early AD but the frequency tends to increase as the disease develops [163]. Moderate to severe AD has significant impact on daily living with functional impairment and dependency on others. Individuals with moderate to severe AD have extreme difficulty in retaining new information, develop prosopagnosia (deficit in recognising familiar people) and executive function is significantly deteriorated. Behavioural symptoms (hallunications, delusions, aggression and anxiety) are not always apparent but are increased in the advanced stages of AD. Basic motor functions (dysphagia) can become impaired and almost all cognitive functions are lost in severe AD with individuals completely dependent on comprehensive care.

1.4.2 Differential clinical diagnosis

AD accounts for between 60-80% of dementia cases seen in clinical practice, which has been confirmed by *post mortem* studies [164-166]. In pathological studies, approximately half of *post mortem* confirmed AD cases have a "pure AD" pathological phenotype; the remainder have substantial pathology relating to other dementias (i.e DLB or VaD) [165]. Conversely, a considerable proportion of cases diagnosed with non-AD dementia still demonstrate classical AD pathology; DLB (66%-70%) and VaD (74%) [164, 166]. Given this large overlap between the pathological presentation of AD and other dementias, neurological evidence that can be derived within clinics to suggest differential causes should be pursued.

Dementia with Lewy Bodies (DLB) is widely considered to be the second most common form of dementia, with 30-40% of *post mortem* dementia cases having sufficient pathology to be diagnosed with DLB [167-168]. In addition to the symptoms of dementia, core DLB indicators are visual hallucinations (42%), spontaneous Parkinsonism (55%) and cognitive fluctuations [169]. Sleep disorders, neuroleptic sensitivity, repeated falls, syncope (temporary loss of consciousness), autonomic dysfunction and depression are also suggestive features of DLB [169]. A "definite" DLB clinical diagnosis is made with the presence of at least 2/3 core features, whereas a "probable DLB" diagnosis is made with one core feature with the addition of a suggestive feature. Compared with AD, a DLB patient is more likely to be

impaired in executive, visuoperceptual and psychomotor functions [170] and less likely to have verbal recall disruption [171]. Furthermore, early psychiatric symptoms (hallucinations and delusions) and passive personality traits are more apparent in DLB [172-173]. Vascular dementia (VaD) is a heterogeneous phenotype resulting from a wide variety of vascular pathologies and there is no single clinical profile indicative of VaD [174]. Nevertheless, abstract thinking, information processing and working memory seem to be more affected in VaD [175]. The decline of cognition is generally slower [174], with a preserved verbal memory [176] while increased mortality rates are observed compared with AD [174]. However, vascular abnormalities do contribute to the pathological development of AD, particularly cerebrovascular lesions in the early stages. As a consequence VaD is considered to be over diagnosed as a direct cause of dementia [164]. Frontotemporal lobar degeneration (FTLD) typically presents between the ages of 45-65 and in this demographic proportion has equal prevalence as AD [177]. FTLD is characterised as a progressive neurodegeneration in the frontal and anterior temporal cortices and has three subtypes: Frontotemporal lobar degeneration (FTD), semantic dementia and non-fluent aphasia. FTD typically presents with behavioural and personality changes including disinhibition, apathy, executive dysfunction as a result of right frontal lobe involvement. Semantic dementia characteristically presents anomia and deficits in empathy whereas non-fluent aphasia displays with phonological errors and speech apraxia. The distinction between AD and advanced FTLD is not challenging clinically, however is harder to differentiate in the mild stages of development. Imaging biomarkers measuring hypometabolism and Aβ have helped with this distinction (Discussed in 1.7). The clinical presentation of depression can mirror early features observed in AD. AD and depression can overlap, with 20% of early stage AD patients displaying clinical depression [178]. Pronounced memory complaints with minor cognitive deficits along with apathy are commonly observed with depression in the elderly [178]. However, focal deficits such as apraxia and aphasia should point towards a diagnosis of dementia and not depression.

1.4.3 Mild Cognitive Impairment

Individuals classified with Mild Cognitive impairment (MCI) are regularly included in AD research studies as an opportunity to investigate prodromal AD, with MCI

seen as the intermediate state between normal ageing and AD. Indeed MCI patients are known to have an increased risk for developing AD with an annual conversion rate of 10-15% compared to 1-2% in nondemented individuals [165]. However a meta-analysis of 41 research studies, documenting the clinical conversion to AD from an MCI state, revealed that only 30-34% of MCI individuals progressed to AD within 10 years [179]. Therefore, the original criteria for MCI diagnosis [180] were changed to recognise impairment other than memory deficits, leading to the creation of amnestic MCI (including memory impairment) and nonamnestic [181-182]. Amnestic MCI has many common behavioural and neurobiological features with AD [183] as well as *in vivo* biomarkers similarities [184].

1.4.4 Healthy cognitive ageing

Several cognitive changes are associated with increasing age however without significant underlying pathology these changes are sporadic, inconsistent and not progressive. The speed of mental processing, reaction and perception time decline the most compared with young individuals however in the absence of a dementia they do not have a significant functional impact [165]. Short-term memory loss without immediate and long memory loss is reported in the healthy elderly. Decline in verbal fluency is expected with all other language characteristics unimpaired [185]. Unlike AD, insight, social engagement and visuospatial functions are retained [186] and the ability of learning new tasks is reserved. Longitudinal studies investigating the healthy elderly have been difficult to conduct due to the number of subjects with asymptomatic dementias researched as healthy elderly. However successful studies have demonstrated that the healthy elderly generally have a flat cognitive trajectory until 90 years of age [187].

1.5 Therapeutic interventions for Alzheimer's disease

1.5.1 Symptomatic treatment

There is currently no cure or preventative treatment for AD, however treatments that help ameliorate the cognitive and behavioural symptoms are available. Their clinical effects are largely palliative however the use of symptomatic relief in combination with disease-modifying treatments has yet to be explored. There are two main groups of classes of drugs approved for AD treatment: Acetylcholinesterase inhibitors and NMDA receptor antagonists.

Acetylcholinesterase inhibitors

Acetylcholine (ACh) modulation plays a central role in facilitating learning and memory. The cholinergic hypothesis describes the degeneration of cholinergic neurons and loss of cholinergic neurotransmission to the neocortex and hippocampus that contribute significantly to the decline in cognitive function in AD. Several *post mortem* studies have demonstrated decreases in acetyltransferase (ChAT) and ACh release in the cerebral cortex and hippocampus of AD patients [188]. Acetylcholinesterase inhibitors act by promoting the availability of ACh at the synapse by deterring the enzyme that degrades ACh [189]. Currently three approved acetylcholinesterase inhibitors are routinely used in clinic for the symptomatic relief for AD: Rivastigmine, galantamine and donepezil [190]. Furthermore, tacrine, xanthostigmine, para-aminobenzoic acid, coumarin, flavonoid and pyrroloisoxazole are also being studied in relation to AD and cognition. Ladostigil is an acetylcholinesterase inhibitor currently in Phase II clinical trials as a reversible inhibitor of ACh that also promote antidepressant effects by the inhibition of monoamine oxidases A and B [191-192]. Recent reports show that ladostigil failed to reach its primary endpoint but trended in the direction of a treatment benefit. In general, acetylcholinesterase inhibitors are well tolerated by patients and the adverse effects are dose-dependent [193].

N-Methyl-D-Aspartate (NMDA) receptor antagonists

NMDA receptor antagonists act to block glutamate-mediated excitotoxicity. This overstimulation is known to trigger calcium overload and mitochondrial dysfunction causing neuronal apoptosis by the elevated generation of nitric oxide. Memantine

acts to decreases glycogen synthase kinase (GSK-3β), therefore reducing tau phosphorylation and protecting neurons. Memantine was approved by the FDA for the treatment of moderate-severe AD but is also shown to have small or no impact on cognition in mild AD [194-195]. NMDA receptor antagonists can be prescription alone or in combination with acetylcholinesterase inhibitors [196], although combination therapy has yet to show a positive clinical benefit [190].

Other neurotransmitter systems

Serotonin and histamine receptors are also expressed ubiquitously in brain regions involved in memory and learning. The inhibition of the 5-HT_6 serotonin receptors has shown to stimulate ACh release [197], which have cognitive benefit in animals studies [198]. It has been postulated that 5-HT_6 antagonists would be of benefit to mild AD patients [191]. Similarly, H_3 receptor antagonists may improve cholinergic neurotransmission. Phase I and II studies for 5-HT_6 and H_3 antagonists are currently underway [191, 199].

1.5.2 Disease modifying therapies

The search for disease-modifying interventions is largely focused on targeting Aβ, based on the amyloid cascade hypothesis. Intervention strategies are focused upon (1) the inhibition of Aβ production and plaque formation and (2) to promote the removal of Aβ deposits and plaques to successfully halt or slow the progression of the disease. Finally, an alternative to an Aβ focused strategy would be to target the formation of insoluble PHF which form NFTs which have a greater correlation with cognitive decline.

Modulators and inhibitors of secretases

The generation of Aβ from APP occurs by the initial cleavage of either α-secretase or β-secretase. The resulting fragments are finally processed by γ-secretase. The over activation of β-secretase or γ-secretase and the age-dependent decline in α-secretase processing has led to the investigation of secretase inhibitors for the reduction of Aβ production.

The development of β-secretase (BACE1) inhibitors can lead to significant side effects. BACE1 targets many other substrates in the CNS, including proteins of myelin metabolism. However, during the past few years much progress had been made on the development of BACE1 inhibitors, which have been shown to have positive effects in experimental animal models. GRL-8234 was shown to rescue age-related cognitive decline in transgenic APP mice (Tg2576) [200]. Human trials of BACE1 inhibitors (E2609, MK8931, LY3314814 and LY2886721) have all shown to reduce Aβ production of up to 90% [201-202]. Yet, no BACE1 inhibitor has successfully been approved for the use in AD. In a similar fashion γ-secretase inhibitors secondary off-target effects are a major concern. A key target of γ-secretase is Notch signalling which has central roles in regulating cell proliferation, development and cellular communication [203-204]. Clinical studies of γ-secretases (Semagacestat and Avagacestat) were discounted as a result of serious adverse effects and lack of efficacy [205-206]. Selective γ-secretase modulators (SGSM) are currently being investigated which aim to block the process of APP processing while preserving other signalling pathways [207]. Lastly, the up regulation of metalloproteinases (ADAM10 and ADAM17), key enzymes in the proteolytic processing of α-secretase, have been studied to prevent Aβ generation [208]. In AD transgenic mice the overexpression of metalloproteinases has been shown to prevent cognitive decline [209]. Furthermore, melatonin also encourages α-secretase activity by the positive regulation of ADAM10 and AMAM17 [210].

Inhibition of Aβ peptide aggregation

Given the overproduction of toxic Aβ due to faulty activity of α, β, γ-secretases, compounds that prevent the formation Aβ aggregates have been widely investigated. The only inhibitor of Aβ aggregation that has reached Phase III trials is Tramiprosate [211-212], with three other small molecules investigated in phase II clinical trials (Clioquinol, Scylloinositol and Epigallocatechin-3-gallate) [213-214 215]. Although these agents effectively prevented Aβ fibril formation they failed to pass phase II and III trials due to lack of efficacy.

Anti-Aβ immunotherapy

Active and passive immunotherapy attempts to promote Aβ clearance in AD patients, with the aim of reducing Aβ load and thereby slowing cognitive decline. Active immunotherapy uses $A\beta_{1-42}$ or synthetic fragments to stimulate an immune response that produce anti-Aβ antibodies. Initial results from active immunotherapy phase II clinical trials (AN1792) demonstrated Aβ plaque clearance, a reduction in CSF tau and minor cognitive benefits. However, serious adverse effects of AN1792 lead to the halting of the clinical trial due to 6% of the participants developing aseptic meningoencephalitis as a result of T cell-mediated autoimmune response [216]. Second generation vaccines have been designed using shorter Aβ peptides ($A\beta_{1-6}$ and $A\beta_{1-15}$) and have shown to be free from adverse inflammatory reactions. Phase II clinical trials investigating these immunotherapies are currently ongoing [191, 217].

Passive immunotherapy is the direct administration of monoclonal or polyclonal antibodies directed against Aβ. A potential advantage of passive immunotherapy over active immunotherapy is to prevent a potential proinflammatory immune response [191]. The passive Aβ immunotherapies investigated for AD are summarised in Table 1.2. Solanezumab and Bapineuzumab are monoclonal antibodies that have both reached Phase III clinical trials for AD, however they both lacked clinical efficacy in patients with mild-moderate AD [218-219]. Solanezumab is directed to the mid-domain of the Aβ peptide ($A\beta_{12-28}$) binding only soluble Aβ species that are directly toxic to synaptic function. The Solanezumab trial indicated a promising effect on mild AD patients, albeit statistical significance was not achieved [219]. Solanezumab continues to be trialled in cognitively normal older individuals who are at risk for AD. Bapineuzumab binds to fibrillar and soluble Aβ promoting its clearance as well as microglial phagocytosis and cytokine activation. Bapineuzumab failed to produce a positive change in cognitive function despite demonstrating significant reduction in Aβ plaques and positive changes in core CSF biomarkers [220].

Gantenerumab, Crenezumab, Aducanumab and BAN2401 are also monoclonal antibodies that act by prompting microglia recruitment that will act to dissemble and degradation Aβ [221] and are currently in on-going Phase III clinical trials. Gantenerumab, alongside Solanezumab, trials are being investigated patients with

risk of Aβ accumulation due to genetic mutation, Aβ accumulators who are cognitively normal and mild AD [222-225].

Table 0-2: A summary of passive Aβ immunotherapy investigated in AD.

Passive Immunotherapy	Aβ epitope	Effect on biomarkers	Adverse effects	Clinical trials
Bapineuzumab (Janssen/Pfizer)	$A\beta_{1-5}$	Reduction cerebral Aβ, CSF p-tau and t-tau	Vasogenic cerebral edema	Phase III (Discontinued 2012)
Solanezumab (Eli Lilly & Co.)	$A\beta_{13-28}$	Increased CSF $A\beta_{1-42}$	None	Phase III
Gantenerumab (Roche)	$A\beta_{1-11}$	Reduction of Aβ plaques	Vasogenic edema	Phase III
Crenezumab (Roche)	$A\beta_{12-23}$	Increased CSF $A\beta_{1-42}$	None	Phase III
Aducanumab (Biogen)	Insoluble fibrillar human Aβ	Reduction of Aβ plaques	None	Phase III
Ponezumab (Pfizer)	$A\beta_{33-40}$	Increased plasma $A\beta_{1-42}$	None	Phase II (Discontinued 2011)
BAN2401 (Biogen/Eisai)	Large Aβ species (>100kDa)	Reduction of Aβ protofibrils	None	Phase II

Promoting Aβ degrading enzymes

Another mechanism that would promote the removal of Aβ is addressing the reduced activity of enzymes that degrade Aβ aggregates and plaques which has been extensively observed in AD [226-227]. There are number of proteases that act to degrade Aβ plaques (neprilysin, plasmin, angiotensin and endothelin converting enzyme) however strategy with this mode of action has not reached advanced clinical trials.

Therapeutic strategies focused on Tau

Another potential therapeutic strategy distinct from Aβ-based interventions is the prevention of tau hyperphosphorylation and aggregation. Tau active immunotherapy has been developed (AADvacl and ACI-35) with phase II clinical trials currently underway [189]. Both immunotherapies have produced positive results in relation to cognition within rodent models with no adverse affects [189, 228]. Inhibitors of tau phosphorylation (i.e. tideglusib) have been investigated with no significant benefits observed [189]. There have been successes in identifying molecules that act as good

inhibitors of tau aggregation. Leucomethylthioninium (LMTX) and methylthioninium chloride (MTC) have been shown to reduce tau aggregation and restore cognition in transgenic mice [229]. However, recent reports have shown that LMTX has failed to slow cognitive decline in two recent AD trials.

Participant recruitment for therapeutic trials

Multiple failures in drugs trials, mainly targeting the Aβ pathway, have been disappointing and there are several suggested reasons for such failures: (1) Approximately 20% of trial participants recruited into Solanezumab and Bapineuzumab Phase III trials had little or no Aβ when studied later using retrospective neuroimaging [218, 230]. This is a concern for such trials when a large minority of trial subjects fail to have the primary target pathology (Aβ or tau), which may mask positive outcomes in pathology positive subjects. (2) Participants recruited for Phase III clinical trials are in the advanced stages of the disease and intervention is unlikely to have an effect. This has prompted clinical trials to target individuals in the early stages of AD, with little or no cognitive deficits.

Successful recruitment of individuals of preclinical AD with the target pathology will be a key factor for these preventative clinical trials and the use of biomarkers for subject selection is imperative. Current imaging methods to detect AD pathology in cognitively healthy individuals will substantially increase the cost of these trials, whereas CSF biomarkers may not be suitable for widespread implementation and repeated sampling. A more practical approach would be to use a blood-based indicator of AD pathology. A relatively accurate blood test implemented as a trial entry criterion would be minimally invasive, easy to implement and could also be used to help triage subjects to further testing using imaging methods. However, to date, an accurate blood-based marker of centralised AD pathology does not exist.

1.6 Pathological timeline of Alzheimer's disease

The clinical presentation of AD is thought to be the end result of 10-20 years of gradual unseen changes in various pathological processes. The timeline of AD development can be generally divided into three stages: preclinical, prodromal and dementia. The study of clinical development, although progressive and informative, is now thought to be at an advanced stage of disease. Preclinical and prodromal development can now be investigated with established biomarkers to measure *in vivo* AD pathology; for example Aβ (^{11}C-PiB PET) and glucose metabolism imaging tracers imaging (FDG PET), structural imaging (MRI), and CSF protein measures.

These studies have shown that AD biomarker abnormalities do precede clinical onset with Aβ accumulation (measured by Aβ PET and CSF $A\beta_{1-42}$) being the earliest abnormal change [231-237]. These changes are followed by subsequent markers of NFT formation (CSF tau measures and FDG PET) [234-238] and subtle changes using MRI becoming apparent before clinical onset occurs [239-240]. These biomarkers enhance with disease severity, with each biomarker developing at different rates and reaching differing plateau points. A theoretical time-dependant *in vivo* staging established AD biomarkers was first proposed in 2010 [241] and later revised in 2013 [242] which describes that AD biomarkers become abnormal in a temporally ordered manner (Figure 1-4). This model is now an accepted but simplified version of typical AD development, hypothesising asymptomatic individuals with underlying pathology would eventually develop clinical AD. Evidence generated from several studies has concluded that a sigmoidal trajectory of Aβ, tau and glucose metabolism biomarkers occurs and approaches a plateau at different disease phases [242]. The model also recognises that AD risks factors (genetics, life style and diminished cognitive reserve) can shift the onset of cognitive impairment to an earlier stage.

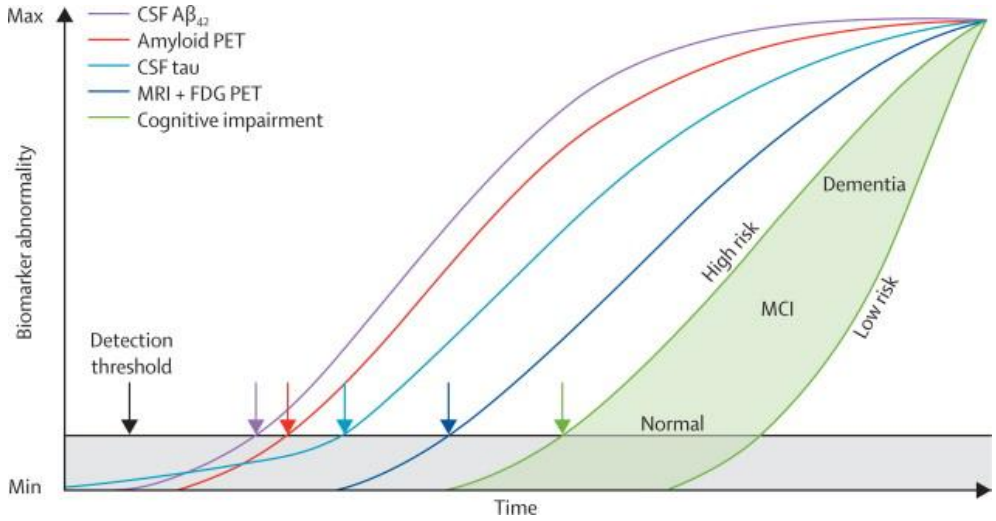

Figure 0-4: An *in vivo* model of the AD pathological cascade, taken from Jack CR et al., 2013. The theoretical model is based on imaging, biofluid and autopsy studies and describes an initial change in CSF $A\beta_{1-42}$ followed by Aβ PET in preclinical AD. CSF tau, FDG PET and MRI changes are observed before the clinical onset of dementia.

Cross-sectional comparisons in healthy ageing, MCI and AD patients by *in vivo* Aβ imaging revealed that ~20% of healthy ageing individuals had an equivalent Aβ level as AD patients. Conversely, there was minimal overlap of the clinical groups when comparing hippocampal volume with structural imaging by magnetic resonance imaging (MRI) [243]. This is evidence to suggest that substantial plaque deposition occurs prior to neurodegeneration with significant Aβ load accumulated in pre-symptomatic subjects. Reduced CSF $A\beta_{1-42}$ measures in pre-symptomatic individuals have also been shown to reflect this increased Aβ load [244]. Longitudinal studies have shown that rate of change in Aβ biomarkers do not change between clinical group whereas biomarkers observed with MRI (ventricular volume and hippocampal atrophy) are more associated with MCI and AD [245]. This implies that changes in cognition are more associated with neurodegenerative processes than with Aβ accumulation. This supports the theory that Aβ initiates a series of events that lead to neurodegeneration. Reports from the dominantly inherited Alzheimer's network (DIAN) [246] support the concept of Aβ being the initiating event in the pre-symptomatic stage but with CSF $A\beta_{1-42}$ preceding Aβ imaging biomarkers.

CSF tau measures have been shown to be elevated in cognitively healthy and MCI, assumed to reflect NFT formation, although these have been shown to be less evident and later in the disease course than CSF $A\beta_{1-42}$ [247-249]. Patients with early AD and

individuals who are cognitively normal that later convert to dementia, have marked brain metabolic reduction, as measured by FDG PET [250] demonstrating that FDG PET changes occur in the early stages of the disease. However on several occasions this has been shown to occur after Aβ biomarkers [249, 251] with hypometabolism being more pronounced in the later stages of the disease [252]. Furthermore, FDG PET measures correlate highly with CSF tau biomarkers [253] but abnormal CSF tau measures precede FDG PET biomarkers [246]. Subtle brain atrophy at the preclinical stage has also been observed [247] [239] however, these changes observed by MRI are more associated with the clinical severity of AD and therefore a biomarker of established disease rather than prodromal or preclinical AD [240]. MRI is also superior in predicting future conversion to AD than CSF measures [254].

1.7 Biomarkers – Neuroimaging

The current role for neuroimaging in AD is the exclusion of another disease that may be the primary cause of cognitive decline. The two types of neuroimaging most commonly used as AD biomarkers include Magnetic Resonance Imaging (MRI) and Positron Emission Tomography (PET). MRI is predominantly utilised to investigate *in vivo* structural changes in an AD setting and is preferred to computed tomography (CT) due to its superior resolution of tissues. PET is generally coupled to radio-labelled ligands which measure *in vivo* metabolic and neurochemical processes. In AD research, two types of PET ligands are primarily exploited: (1) ^{18}F-fluorodeoxyglucose (FDG), which measures brain metabolism and (2) Aβ tracers which bind to fibrillar Aβ plaques.

1.7.1 Aβ imaging in Alzheimer's disease

The development of PET tracers for Aβ aggregates has allowed the *in vivo* evaluation of Aβ pathology. Several hundred Aβ PET studies have been published since the first human study was reported in 2004 [231], improving our knowledge on the accumulation pattern, variability and timing of Aβ deposition in the human brain. Quantitative PET studies using diverse range of Aβ tracers have consistently demonstrated a significant increase in retention between AD and elderly controls, with the binding particularly elevated in the frontal, cingulate, precuneus, striatum, parietal and lateral temporal cortices [255]. PET imaging also presents an accumulation pattern that is representative of the Aβ deposition at *post mortem* [231, 256]. Longitudinal studies examining Aβ accumulation have shown that it is slow and relatively stable measure across early clinical stages, but tends to accelerate with increasing Aβ load and plateau at the late stages of amyloidosis [242, 257].

^{11}C-PiB – Pittsburgh Compound B

Initial investigation in mouse models demonstrated the rapid neocortical uptake of ^{11}C-PiB upon intravenous injection. ^{11}C-PiB also demonstrated rapid clearance from healthy neuronal tissue while retention remained in the AD cases [258]. ^{11}C-PiB was the first radiotracer to be developed for binding with fibrillar Aβ plaques in humans [231] and later studies confirmed its high affinity and specificity to fibrillar plaques [259-260]. Furthermore, ^{11}C-PiB *in vivo* signal demonstrates excellent neuropathological

concordance with *in vitro* measures of Aβ in *post mortem* brain [261-262]. Compared with elderly controls, ^{11}C-PiB PET scans of AD patients show higher overall retention, with 90% of clinically confirmed cases having elevated ^{11}C-PiB [259-260]. In comparison, 60% of clinically defined MCI cases and 25-30% of cognitively normal cases also exhibit high ^{11}C-PiB retention [263-264]. The regional distribution of ^{11}C-PiB is known to contain large amounts of Aβ plaques [231, 260, 262]. This distinct pattern can aid the differential diagnosis from other neurodegenerative diseases [260] but not all [233, 259]. Longitudinal studies with ^{11}C-PiB have shown that significant changes in Aβ deposition can be measured at all stages of cognition [245, 257, 265].

^{11}C has a half-life ($t_{1/2}$) of 20 minutes, limiting its use to facilities capable of onsite isotope production. ^{18}F labelled radiotracers for Aβ, with a longer $t_{1/2}$ (110 minutes), may foster greater utility and a number are being used within clinical trials.

^{18}F-GE067 – Flutemetamol

Flutemetamol is the structural analogue of ^{11}C-PiB and therefore it is unsurprising that the neuronal uptake and Aβ affinity of this radiotracer closely resembles ^{11}C-PiB [266-267]. However, it has been demonstrated that higher non-specific white matter background can be visualised with Flutemetamol even in healthy controls [232]. This may lead to the false assignment of an Aβ positive (Aβ+) diagnosis.

^{18}F-AV-45 – Florbetapir

Florbetapir is the first ^{18}F radiotracer to be approved by the FDA for the clinical investigation of patients with suspecting AD. Florbetapir has been able to accurately replicate the findings of ^{11}C-PiB [268] with a high affinity for Aβ plaques and encouraging pharmacokinetics [269]. Florbetapir rapidly enters the brain, and clears circulation illustrating clear Aβ positivity or negativity within 20 minutes of injection [270]. Phase III clinical trials utilising Florbetapir are currently in use demonstrating a significant correlation with Aβ distribution upon *post mortem* examination on trial participants [270].

^{18}F-BAY94-9172 – Florbetapen

Florbetapen (^{18}FBB) is used for the examination of Aβ aggregates in AD and other dementias. The cortical distribution of ^{18}FBB is similar to that of ^{11}C-PiB [271]. The

sensitivity of ^{18}FBB has been able to distinguish DLB patients from AD despite the similar pattern of Aβ pathology [233] thus it may prove useful in the differential diagnosis of other dementias and amyloidopathies.

^{18}F-FDDNP

FDDNP was initially developed for the visualisation of senile plaques in AD however, it also binds to NFTs [272]. Early studies using FDDNP demonstrated significant binding of regions consistent with Aβ plaques but also NFTs, later confirmed by *post mortem* examination [273]. Therefore, uptake in the MTC, which is among the first areas to develop NFTs, is relatively high when compared with ^{11}C-PiB. In contrast to other Aβ radiotracers, the clearance time of FDDNP maybe inversely correlated with the degree of cognitive impairment [272].

Table 0-3: List of radiotracers designed for PET analysis of AD pathology

Radiotracer	$t_{1/2}$	Specificity	Disease Condition
^{11}C-PiB (Pittsburgh Compound B)	20 minutes	Aβ	AD
^{11}C-AZD2184	20 minutes	Aβ	AD
^{18}F-AV-45 (Florbetapir)	110 minutes	Aβ	AD
^{18}F-FDDNP	110 minutes	Aβ/Tau	AD
^{18}F-BAY94-9172 (^{18}FBB)	110 minutes	Aβ	AD
^{18}F-GE067 (Flutemetamol)	110 minutes	Aβ	AD
^{18}F-AZD4694	110 minutes	Aβ	AD
^{11}C-BF-227	20 minutes	Aβ	AD
^{11}C-SB-13	20 minutes	Aβ	AD
^{18}F-THK523	110 minutes	Tau	tauopathies
^{18}F-THK5105	110 minutes	Tau	tauopathies
^{18}F-THK5107	110 minutes	Tau	tauopathies
^{18}F-T807	110 minutes	Tau	tauopathies
^{18}F-T808	110 minutes	Tau	tauopathies
^{11}C-PBB3	20 minutes	Tau	tauopathies
^{11}C-PK11195	20 minutes	PBR-TSPO	Neuroinflammation
^{11}C-DPA713	20 minutes	PBR-TSPO	Neuroinflammation
^{11}C-CLINME	20 minutes	PBR-TSPO	Neuroinflammation
^{18}F-DPA714	110 minutes	PBR-TSPO	Neuroinflammation
^{18}F-PBR111	110 minutes	PBR-TSPO	Neuroinflammation
^{11}C-DED	20 minutes	I_2BS	Neuroinflammation
^{11}C-FTIMD	20 minutes	I_2BS	Neuroinflammation

1.7.2 Aβ imaging in other disorders

The investigation of Aβ imaging across a wide spectrum of neurodegenerative disorders has allowed the assessment of the pattern of Aβ presence or absence as a biomarker in differing conditions.

Co-pathology of Aβ, tau and α-synuclein is present in several neurodegenerative diseases, including AD, Parkinson's (PD), Parkinson's dementia (PDD), DLB and Multiple system atrophy (MSA). Cortical ^{11}C-PiB retention in DLB is more subtle and variable than AD [274]. *Post mortem* studies have confirmed that 50-80% of DLB cases have cortical Aβ deposits with a distribution pattern similar to AD [275] and that a pure α-synuclein DLB is relatively uncommon. DLB patients with negative Aβ scans have been neuropathologically confirmed to have little diffuse Aβ plaques [276]. An overlap in early cognitive signs with AD makes a differential diagnosis of DLB difficult and with a mixed DLB/AD pathology commonly found, Aβ imaging maybe only useful in identifying pure DLB cases. Despite this, ^{18}F Aβ tracers are beginning to show the sensitivity to distinguish between AD and DLB [233]. Furthermore, DLB, PD and PDD patients have been described to have higher ^{11}C-PiB retention in the occipital lobe when compared with AD [274]. No differences between DLB and PDD global ^{11}C-PiB retention has been reported but a lower PDD retention is more commonly observed [277]. ^{11}C-PiB has also been used successfully as a tool to separate DLB and MSA patients given the similar clinical presentations [278].

FTD can also be extremely difficult to be clinically distinguished from AD. Aβ deposition is not a common pathological trait of FTD and three intraneuronal inclusions are often found: tau, TDP-43 and FUS [279]. It has been widely shown that Aβ imaging is helpful in the differential diagnosis between FTD and AD [280]. Cerebral amyloid angiopathy (CAA) is characterised by Aβ build-up around small arteries and arterioles of the cerebral cortex [281]. ^{11}C-PiB in patients with CAA has demonstrated a distinct pattern of Aβ, specifically in the occipital regions, that can be distinguishable from AD [282]. No cortical ^{11}C-PiB retention is found in sporadic prion diseases like Creutzfeldt-Jakob disease (CJD) [283]. Given the rapid phase of the symptomatic illness, plaque formation is unlikely to occur although sub-types of CJD

have been shown to have small synaptic and perivascular Aβ deposits [284]. Aβ PET imaging can distinguish other spongiform encephalopathies and CJD [285].

Patients with Down Syndrome (DS) have an extremely high incidence of early-onset dementia and this is likely due to the overexpression of the *APP* gene by chromosome 21 triplication. Studies using ^{11}C and ^{18}F Aβ tracers have all concluded an age-dependant accumulation of Aβ in age brain of DS patients [286]. Aβ imaging in DS patients has been used as a model of the natural history of Aβ deposition. The early detection of Aβ accumulation is critical in the development of anti-Aβ therapies, in which DS patients may benefit. With little influence from contaminant diseases such as VaD, dementia formed in DS patients is likely to be Aβ driven. Thus, Aβ PET imaging studies in DS patients would help study the role of *APP* and Aβ accumulation in the pathogenesis of AD [287].

1.7.3 FDG imaging in Alzheimer's disease

FDG PET measures brain glucose metabolism and investigations have shown that in AD a decline in glucose consumption is progressive and correlates with disease severity. The typical "AD pattern" in FDG PET studies demonstrate posterior cingulate, parietal, temporal, and prefrontal cortex hypometabolism with relative sparing of the basal ganglia, thalamus, cerebellum and primary sensorimotor cortex [288]. A similar pattern of hypometabolism has been reported in MCI [289] and asymptomatic subjects with mutations in *APP*, *PSEN1* and *PSEN2* genes [290]. Glucose metabolism abnormalities identified using FDG PET also have been found to successfully predict conversion from MCI to AD with very early metabolic deficits reported in the medial parietal cortex [291]. Reviews on FDG PET have reported an average diagnostic accuracy of 93% in differentiating AD from healthy controls and can discriminate AD from other dementias with an accuracy of 94% [291-292].

The relationship between Aβ imaging and FDG PET

On the whole, no relationship can be found between FDG PET and Aβ imaging in AD subjects [293]. There are conflicting reports in the non-demented group with correlations in the parietal and temporal cortices with ^{11}C-PiB and FDG PET [231, 294] whereas others have reported no correlations in any brain regions [291, 295]. A study

conducted in a large group of participants concluded that there was no association between regional fibrillar Aβ and hypometabolism in clinically defined AD and controls patients. However, a strong positive correlation was observed in the MCI group [296].

1.7.4 MRI in Alzheimer's disease

Brain atrophy measured by structural MRI is repeatedly reported as an AD biomarker. While brain atrophy is not specific to AD, many studies have associated the atrophy of structures in the MTL and ventricular enlargement with changes in cognition and disease progression [240, 297]. Notably, atrophy of the entorhinal cortex and hippocampus are of considerable value in predicting conversion from cognitively normal to MCI and MCI to AD [297]. Hippocampal volume is reduced in AD patients by up to 40%, with a 15% reduction in MCI patients [298]. Serial MRI measures from a preclinical stage through to moderate dementia show a non-linear relationship between cognition and brain atrophy, with the rate of atrophy increasing with disease severity [254]. AD patients have an atrophy rate of 4-6% each year, whereas aged-matched controls typically have a decline of 1-2% per year [299]. This demonstrates that although MRI has the ability as a diagnostic pre-clinical biomarker, its main strength lies after the onset of clinical symptoms to follow cognitive decline.

Other structural MRI techniques include Diffusion Weighted Imaging (DWI) and Magnetisation Transfer Imaging (MTI). DWI is used to investigate white matter changes in the temporal lobe and hippocampus in relation to AD [300]. MTI is able to detect structural changes reflecting tissues homogeneity from pathological changes associated with AD [301]. Functional MRI (fMRI) can assess the decline of neuronal activity and connectivity as a consequence of neuropathology. These images are determined by changes in cerebral blood flow or changes revealed by blood oxygen level (BOLD) effect [300]. Compared to controls, AD patients exhibit a decreased hippocampal and parahippocampal activity as well as a disruption in the default mode network (DMN) [302].

The relationship between Aβ imaging and MRI

The relationship between Aβ deposition and atrophy is inconclusive. In AD, no direct association between hippocampal Aβ load and hippocampal atrophy has been found [303], although other regional relationships between Aβ load and atrophy have been reported at certain stages of the disease [304]. In the cognitively normal, some reports find the association of hippocampal atrophy and elevated global ^{11}C-PiB [243] while others did not [305]. Furthermore, an inverse relationship between temporal lobe volume and Aβ load (larger temporal volume and high Aβ deposition) has been implicated as a sign of resistance, as these individuals seem to have the ability to have a greater tolerance to the presence of Aβ plaques [304].

1.7.5 Tau imaging in Alzheimer's disease

The limitation of Aβ imaging is that presence of Aβ plaques alone is not sufficient for complete diagnosis of AD, whereas a PET Tau tracer would aid and affirm this diagnosis. The development of Tau radiotracers is somewhat more difficult given the intracellular location of tau aggregation. A successful PET tau tracer would have selective binding to PHF over Aβ, high permeability to the BBB, low metabolism and non-specific binding to white matter.

Initial studies of the radiotracer ^{18}F-THK523 demonstrated high affinity to PHFs compared to Aβ [306] and does not have an association with any Aβ radiotracers [307]. Regional retention of THK523 has been found in the hippocampus, orbitofrontal, lateral and temporal regions however this was not found to differ between AD and elderly controls [308]. ^{18}F-THK5105 has been shown to have retention in the lateral mesial temporal lobes, areas known to have a high accumulation of NFTs [309]. Further to this, the intensity of the radiotracer in these regions is seen to be correlated with the degree of dementia and neuronal atrophy [309]. ^{18}F-T807 has very weak selectivity to Aβ and human studies demonstrate excellent concordance of radiotracer retention and typical NFT distribution in the brain [310]. ^{18}F-T807 also has favourable kinetics, rapid delivery into the brain and clearance from the white matter [311]. The initial success of ^{18}F-T807 has moved this radiotracer into Phase II clinical trials of AD and other tauopathies and will likely be used to monitor the ability of tau-targeted therapeutics that are in development.

1.7.6 Neuroinflammation imaging in Alzheimer's disease

Neuroinflammation is a significant process in the progression in all neurodegenerative diseases. Inflammation is associated with microglial activation that is triggered by neuronal degradation in the early stages of AD. Therefore, molecular imaging that could detect and monitor neuroinflammation would be of considerable use in further characterising AD. ^{11}C-PK11195 is the leading PET based radiotracer for neuroinflammation and specifically binds TSPO, an 18kDa translocator protein. TSPO is upregulated in response to inflammatory microglia activation; therefore ^{11}C-PK11195 could act as a putative biomarker for neuroinflammation [312]. Indeed, initial studies have demonstrated notably high retention of ^{11}C-PK11195 in AD patients compared with aged matched controls [313]. However, due to increased reports of nonspecific binding ^{11}C-PK11195 may have limited use in neuroinflammation. Radiotracers ^{11}C-DPA713 and ^{11}C-CLINME, and more recently their equivalent F^{18} ligands, have shown a decreased likelihood of nonspecific neuronal interaction and are sensitive to subtle TSPO expression due to their high affinity for the receptor [313]. Radiotracers ^{11}C-DED and ^{11}C-FTIMED have been developed for the imaging of imidazoline 2 binding sites (I_2BS) [314]. The increased expression of I_2BS is a prominent hallmark of astrocytosis, another key feature of neuroinflammation and neurodegeneration.

The relation of neuroinflammation imaging and Aβ imaging

Most reports have reported no association between Aβ retention and microglia activation measured by ^{11}C-PK11195 [277, 315] but a correlation between ^{11}C-PK11195 and hypometabolism [277, 316]. Similarly, no regional association between PET astrocytosis and ^{11}C-PiB have been found [317].

1.8 Fluid Biomarkers – Cerebrospinal Fluid

CSF is in direct contact with the extracellular space of the brain and serves as a substrate for biochemical changes related to brain pathology. The single cell epithelium layer that separates the two compartments allows an almost unimpeded flow of molecules from the brain towards the CSF.

A lumbar puncture (LP) must be performed to obtain CSF. The perceived invasive nature of an LP has made the routine implementation of CSF analysis in AD diagnostics and research troublesome. However, several large prospective studies have demonstrated that the incidence of post-LP complications is very low in the elderly [318-319]. International collaborative efforts have standardised the use of small gauge needles and atraumatic techniques in CSF sampling to further reduce the concerns of post-LP headache. Particular attention has been paid to the standardisation of pre-analytical treatment of CSF [320] and measurements of core CSF AD biomarkers given the reported large inter-laboratory variation in concentrations [321-324]. The results have produced fully validated mass-spectrometry references for CSF $A\beta_{1-42}$ [325] and automated assays that are reproducible between laboratories [3].

This global effort in standardisation and safety has made CSF analysis a rapidly expanding research field. The direct interaction with the disease organ and cost effective alternative to neuroimaging biomarkers has ensured the introduction of CSF analysis routinely implemented into AD diagnostics.

1.8.1 Core CSF biomarkers

The core CSF biomarkers for AD are $A\beta_{1-42}$, total tau (t-tau) and phosphorylated tau (p-tau) and these markers are thought to reflect cortical Aβ deposition, neuronal loss and neurofibrillary tangles respectively [326]. These biomarkers are now included in AD diagnostic guidelines to help increase the accuracy of an early preclinical or prodromal AD diagnosis for a research setting [327-328].

CSF $A\beta_{1-42}$ concentrations are widely reported to be reduced in AD patients, where an approximate decrease of 50% is expected when compared to healthy controls [329]. The inverse relationship of CSF $A\beta_{1-42}$ and cortical ^{11}C-PiB binding suggest that this

CSF measure is a strong surrogate marker for *in vivo* neocortical Aβ burden (NAB) [247]. Autopsy investigations also demonstrated reduced CSF $A\beta_{1-42}$ is correlated with neuropathological Aβ [330]. In the preclinical phase of the disease, a reduction in CSF $A\beta_{1-42}$ has been shown to predict subsequent conversion to dementia [331]. Furthermore, a significant change in CSF $A\beta_{1-42}$ [332-333] but not t-tau or p-tau [334] in cognitively normal participants were more likely to later develop AD.

Increases in CSF t-tau and p-tau have been associated with neocortical neurofibrillary pathology, cognition and temporal lobe hypometabolism. CSF t-tau assays, that detect all tau isoforms independent of phosphorylation site, have shown increases of 50-300% in AD subjects [335]. Although increases in CSF p-tau concentrations are somewhat less dramatic between clinical classifications than CSF t-tau, p-tau is thought to be a more accurate reflection of neuronal degeneration, with sensitivity for AD reported at 85% [235, 336]. Both t-tau and p-tau have demonstrated correlation with ^{11}C-PiB binding in the healthy subjects but the relationship is considerably weaker than CSF $A\beta_{1-42}$ and ^{11}C-PiB [247]. Abnormal CSF concentrations of tau have been reported before the clinical presentation of AD, indicating an ability of future conversion to dementia [336].

Ratios of the core AD CSF markers have also been identified as useful AD biomarkers. The diagnostic performance of the core CSF biomarkers to discriminate AD from non-demented older adults is extremely accurate (~85-90%). During life CSF measures combined with neuropathological conformation demonstrated that CSF core measures had a specificity of 96% for AD [235, 337]. Normal CSF levels with cognitive symptoms could be indicative of depression or PD, whereas p-tau aids to differentiate AD from FTD and DLB [338]. CSF $A\beta_{1-42}$/t-tau has been identified as a good predictive marker of future conversion from MCI to AD [240, 326]. Later studies with comprehensive clinical follow-up demonstrated than combinations of the core CSF biomarkers (t-tau, p-tau and $A\beta_{1-42}$) have a predictive ability of 95% to differentiate MCI cases into stable, converting and other underlying pathology [339]. The uses of these markers to identify prodromal AD have been confirmed in other large studies [236-237]. Studies investigating CSF $A\beta_{1-42}$/t-tau and $A\beta_{1-42}$/p-tau also show that core CSF biomarkers predict cognitive in cognitively normal with high accuracy [234].

1.8.2 Novel CSF biomarkers

The pathobiological variance observed in AD precludes any biomarker from having a diagnostic accuracy of 100%. However, additional biomarkers of the pathogenic processes that can further differentiate AD from healthy controls and other dementias would be of considerable value. Synaptic dysfunction and degeneration is an early pathological event [340] and is likely the direct cause of cognitive deterioration in AD [341]. High CSF concentrations of the post-synaptic protein neurogranin (NRGN) predict progression from MCI to AD and correlate with rapid cognitive decline [342-344]. Additionally, the pre-synaptic protein synaptosome associated protein 25kDa (SNAP25) increases substantially during the prodromal stage of the disease [345]. Neurofilament light (NEFL) is a global marker of axonal damage and is shown to be increased in AD compared with controls [346]. However, high levels of CSF NEFL have also shown to be associated with FTD [347-348] with the highest levels associated Amyotrophic lateral sclerosis (ALS) [349]. A recent CSF biomarker meta-analysis by Olsson and colleagues [350] demonstrated that CSF NEFL had the second highest effect size (2.35) at discriminating AD subjects from control after t-tau. The same analysis highlighted that CSF measures neuron specific enolase (ENO2), visinin-like protein 1 (VLP-1), heart fatty acid binding protein (HFABP) and chitinase-3-like protein 1 (YKL-40) to moderately distinguish AD from healthy controls [350]. Further to this, early changes in CSF TREM2 levels have recently been reported [351]. This study points towards the activation of microglial before the clinical onset, but after CSF Aβ and neuronal injury biomarkers.

1.9 Fluid Biomarkers – Blood

1.9.1 Proteomic approaches for blood-based biomarker discovery

The difficultly and complexity of discovering blood-based measures indicative of AD and its pathology is reflected in the number of analytical approaches that are routinely employed. To date, single and multi-analyte immunocapture and to a lesser extent Mass Spectrometry (MS) have been utilised. These approaches have advantages and disadvantages which will be discussed further. More recently, advanced multi-analyte and ultra-sensitive assays have been developed for targeted proteomics.

Immunocapture assays

The most commonly used method for soluble protein quantification is a "sandwich" or "in-direct" ELISA but this method only allows the measurement of one analyte per assay. There is a need to maximise the use of valuable clinical samples and therefore multiplexing immunocapture assays are a rapidly developing field.

Mesoscale discovery (MSD) and Luminex xMAP technology are in principle sandwich ELISAs but with modifications that allow the measurement of multiple analytes. For the MSD assay, capture antibodies for multi-targets are coated onto the base of the microtitre plates. Electrochemiluminescence (SULFO-TAG) labels are then bound to the detection antibody and upon electrical stimulation the SULFO-TAG emits light signals that are unique to the protein of interest. Alternatively, Luminex xMAP employ a microsphere technology. The capture antibody and fluorescently labelled detection antibody are coated onto microsphere beads (polystyrene or magnetic) in suspension. This will allow for microspheres to be labelled with differing capture antibodies. Luminex xMAP technology has a greater capacity for multiplexing than MSD. Blood-based investigations in AD using MSD and Luminex xMAP have been conducted [352-357]. More recently, the ultra-sensitive single molecule arrays (SIMOA) divides samples into femtoliter-size chambers and allows higher detection of signal to background [358]. This assay has been shown to detect tau in plasma with a sensitivity of 0.02pg/mL far superior than other immunocapture assays [359-361]. SIMOA has also been used to successfully detect other

neurodegenerative markers in blood; Aβ [362] and NEFL [363-364]. However, at this time, the numbers of multiplex assays available for SIMOA are limited.

Whichever approach is selected these methods are solely reliant on the availability, quality and binding characteristics of the antibodies being used. Immunocapture assays are useful tools for targeted or semi-targeted investigations where a protein or pathway is of particular interest and are not feasible for unbiased hypothesis generating experiments. Additionally, protein quantification will largely depend on the epitope determined by the capture antibody. This is important to note when comparing results generated by other immunocapture assays and antibody-free technologies such as MS.

Aptamer-based multiplexing

Aptamers are single-stranded oligomucleotides, which recognise and bind target proteins with high affinity [365]. Somalogic™ have developed a panel of >1300 analytes that can be targeted in a single sample, making this approach ideal for clinical samples with limited volume. However, just as with antibody-based approaches, aptamer arrays are limited to those which have been designed. Aptamer studies in blood related to AD phenotypes have been conducted [366-367].

Mass Spectrometry

At the discovery level, MS has a key advantage of measuring features present within a sample having without prior knowledge of its contents. This enables MS to be a hypothesis-generating tool which can be confirmed using targeted approaches. Multiple variants in MS-based proteomics can be employed but typically plasma proteins undergo enzymatic digestion. The resulting peptides are resolved using reserve-phase liquid chromatography (LC) and analysed by MS. The peptides sequences identified are probability matched to unique protein groups by databases. The development of isobaric chemical labelling (TMT and iTRAQ) for peptides or proteins has enabled multiplexing of clinical samples within one MS analysis, increasing throughput, with relative quantitation [368]. An obvious disadvantage of MS-based studies is the inability to detect low abundant proteins within plasma. Plasma is a highly complex biofluid but is constituted by 20 highly abundant proteins including albumin, immunoglobulins, transferrin and haptoglobin, which make up

99% of the total protein content [369]. Therefore, upfront fractionation, in addition to reserve-phase chromatography, is required to divide plasma into manageable portions. Furthermore, immunodepletion of the most highly abundant proteins has been widely explored.

There have been several blood-based biomarker studies for AD utilising MS with fractionation and isobaric labelling, typically but not exclusively employing a case-control design [370-375]. Blood-based biomarker discovery employing protein and peptide isobaric labelling, upfront fractionation and immunodepletion in an endophenotype fashion are discussed in Chapters 3, 4 and 5 of this thesis.

1.9.2 Blood-based measures of Aβ and Tau

Due to the central importance of Aβ and tau in the neuropathology of AD and with the successful translation of CSF $A\beta_{1-42}$, p-tau and t-tau in classifying AD from healthy controls, it is unsurprising that there has been a substantial focus on measuring these targets within blood.

$A\beta_{1-40}$ and $A\beta_{1-42}$ as blood-based biomarkers

To date, $A\beta_{1-40}$ and $A\beta_{1-42}$ have been the predominant Aβ species investigated in blood. However, contradictory and largely unsuccessful results have been reported in several studies. Large systematic reviews and meta-analyses of blood $A\beta_{1-40}$ and $A\beta_{1-42}$ have reported significant findings [376-377]. Koyama and colleagues [377] conducted a meta-analysis of 10,303 subjects, which demonstrated significant association of $A\beta_{1-40}/A\beta_{1-42}$ ratios in the development of AD. However, this study also showed that stand-alone measures of $A\beta_{1-40}$ and $A\beta_{1-42}$ blood measures were not associated with AD. Similar conclusions were made by Song and colleagues with the addition of a non-significant decrease in $A\beta_{1-42}$ in AD subjects. Furthermore, a recent meta-analysis investigating all potential fluid biomarkers for AD found no significant differences between plasma or serum concentration of Aβ markers in AD and controls [378]. Due to the wide confidence intervals created by large inter study variability these studies concluded that blood $A\beta_{1-40}$, $A\beta_{1-42}$ and ratios are unlikely to be useful in the classification of AD from healthy controls.

In relation to disease progression, decreased plasma $A\beta_{1-42}$ has been correlated with rapid cognitive decline [379], conversion from healthy to MCI [380] and MCI to AD [381]. In contrast to this, other studies have reported opposite results to these findings, demonstrating that an increase in plasma $A\beta_{1-42}$ is a significant factor in disease conversion [382-383]. However, a large longitudinal community-based study of plasma $A\beta_{1-40}$ and $A\beta_{1-42}$ conducted in 2,000 cognitively healthy individuals reported that decreased plasma $A\beta_{1-42}$ was associated with the development of AD [384]. Given the size and duration of the study, this may be the most promising blood Aβ result to date. The results of blood $A\beta_{1-40}$ are less promising than $A\beta_{1-42}$, given the contradictory reports. Both increased serum $A\beta_{1-40}$ and decreased plasma $A\beta_{1-40}$ have been reported in AD individuals [385-386]. A decrease in plasma $A\beta_{1-40}$ has been attributed to rapid cognitive decline [379] however the majority of studies report no change in plasma $A\beta_{1-40}$ in relation to a range of AD modalities [381, 384]. The conflicting reports in Aβ studies may suggest that Aβ measures are unsuitable or time dependant [382]. Blasko and colleagues [382] demonstrated that $A\beta_{1-42}$ levels were a good measure in predicting the conversion from healthy elderly to MCI but not conversion to AD. This is supported by $A\beta_{1-42}$ appearing to be a predictive marker of AD development in an 8-year longitudinal study in cognitively healthy individuals.

The clearance of CSF Aβ into the blood [387] gives the reasonable assumption that plasma $A\beta_{1-42}$ would follow the same disease related trend as CSF $A\beta_{1-42}$. However, most investigations into the relationship between plasma and CSF Aβ measures report poor correlations [246]. The relationship between plasma Aβ and neuropathology is also inconclusive. Levels of plasma $A\beta_{1-40}$ and $A\beta_{1-42}$ taken 1 year prior to *post mortem* did not correlate with $A\beta_{1-40}$ and $A\beta_{1-42}$ burden at *post mortem* examination [388]. However, a link between plasma $A\beta_{1-40}/A\beta_{1-42}$ ratios and *in vivo* Aβ imaging have been reported [380, 389-390].

The results discussed above point toward a potential use of blood Aβ in disease classification or in relation to disease pathology but the huge discrepancy in findings highlighted by individual studies and large meta-analysis suggest further work is needed. The most promising studies have been described in preclinical stages of AD, suggesting that disease-stage testing of plasma Aβ is critical. In addition, technical

challenges in plasma Aβ measurements will invariably account for a substantial proportion of the variation. Large intra-subject variability in Aβ plasma measures were reported in plasma samples from the same individuals obtained four weeks apart [385]. Aβ show signs of a circadian rhythm in its levels [391] and therefore standardisation of sampling times for Aβ need to be considered [365]. Further to this, the standardisation of assays used to measure plasma Aβ in clinical studies needs to be addressed. For example, the influence of heterophilic antibodies (HAs) in Aβ assays for CSF but particualrly blood needs to be made uniform [392]. Plasma Aβ studies routinely use commercial and in-house ELISA [246, 379, 381-383, 385, 388-389], Luminex xMAP assay [380, 384, 393] and immunomagnetic reduction (IMR) assays [390] which all use a range of antibodies that recognise differing epitopes of Aβ.

Tau as a blood-based biomarker

Plasma tau is a brain-specific axonal protein that is expected to be transferred to the peripheral system from brain interstitial fluid [360]. It is therefore a prime candidate for a reflection of centralised AD pathology however low abundances in plasma have made it a great challenge to report consistent results [365]. Studies on hypoxic brain injury describe a rapid clearance of plasma tau from blood stream, again highlighting a difficulty in applying plasma tau as reliable biomarker [394]. The vast majority of plasma tau studies have been underpowered and reported contradictory results. Substantially elevated and mild elevations of plasma tau in AD individuals have been reported [390, 395-396]. Conversely, reduced plasma tau in AD [397-398] and no change compared with healthy controls have also been reported [399]. Efforts have been made to develop more sensitive assays for the detection and quantification of plasma tau. Firstly, a measurement of specific tau fragments (Tau-A and Tau-C) using an ELISA method was correlated with cognitive decline in AD. However, this was not associated with CSF tau measures [400]. Likewise, a digital array technology (SiMoA) demonstrated elevated plasma tau in AD subjects with no correlation with CSF tau [359]. A large replication study in two cohorts confirmed the increase in plasma tau with SiMoA in the AD population with mild association with CSF biomarkers but with significant cohort differences [360]. Lastly, SQUID-IMR technology also verified the increased levels of plasma tau in AD subjects with significant correlations with regional brain volume [396].

1.9.3 Blood-based biomarkers of AD: case versus control design

The blood-brain barrier (BBB) dysfunction described in AD, the movement of content from the CSF into the blood and the failure to consistently demonstrate blood Aβ and tau as biomarkers are all reasons why the field is now focused on the detection of novel blood markers of AD. An enormous amount of effort, using a wide range of proteomic techniques, has been dedicated to discover single blood markers that can differentiate AD individuals from healthy controls or MCI [370, 401-411]. One of the first large-scale AD plasma studies discovered several differences in the blood of AD individuals [372]. Most notably complement factor H (CFH), an innate immunity marker, which has been replicated by several research groups [412-414].

It was soon apparent that a single protein marker in blood is unlikely to achieve the sensitivity or specificity required for clinical implementation. A multi-variate signature approach has been taken by many research groups [355, 406, 412-413, 415-420]. Ray and colleagues [421] identified a panel of 18 cytokines which illustrated a diagnostic accuracy of 90%. This multi-analyte signature pointed towards the dysregulation of immune response, neuronal support and apoptosis [422]. However, subsequent validation attempts in independent cohorts have been unsuccessful [423-425]. These studies comparing established disease to healthy individuals have clearly demonstrated that a signature of AD and/or dementia in blood does exist. However, a more constructive signature would be one of prodromal disease and therefore a signature of MCI patients that later convert to AD compared with stable MCI and healthy ageing has been investigated [426-427]. Hye and colleagues [357] demonstrated a 10 protein panel with an accuracy of 87% to predict future conversion from MCI to AD. Replication studies in multiple cohorts are examining this panel further.

A major concern for the field has been the lack of reproducibility in plasma markers of AD diagnosis or disease progression. Technical, assay, sampling and cohort variation might explain these discrepancies however it is likely that the heterogeneity of AD is partially accountable for the failure of replication using a "case versus control" design. Such approaches are inherently flawed in AD, as a considerable proportion of cognitively unimpaired individuals will be in the prodromal phase of the disease where substantial pathology has accumulated without clinical

presentation. Therefore, in a "case versus control" design individuals in the prodromal phase of the disease would be incorrectly classified as "control". Furthermore, the recent failure in Phase III anti-Aβ clinical trials has shown that a considerable proportion of AD subjects do not exhibit Aβ pathology [218, 220] and this highlights the importance of participant selection based upon neuropathology biomarkers. The inevitable triage based on CSF measures and/or neuroimaging is likely to be costly and unfeasible to widely implement given the expected failure rates. Therefore, a minimally invasive and accessible blood-based measure of AD pathology could be of considerable use in early diagnosis and reducing screen failure rates for therapeutic trials.

1.9.4 Blood-based biomarkers of AD: endophenotype design

Increasingly, blood-based biomarker studies are increasingly using other variables, besides clinical outcome, to discover markers reflecting AD. The endophenotype approach has utilised measures of brain atrophy (MRI), cognitive decline and NAB (Aβ PET) to investigate disease activity and pathology, including preclinical disease.

Blood-based biomarkers of cognitive decline and brain atrophy

Thambisetty and colleagues reported the first results from an endophenotype approach, which investigated plasma biomarkers of brain atrophy and rate of clinical progression [373]. A panel of 7 proteins (complement C3 (CC3), fibrinogen gamma (FGγ), albumin, complement factor-I (CFI), alpha-1-macroglobin (α1m), clusterin and serum amyloid-P (SAP)) were found to explain 34% of the variance in hippocampal atrophy [373]. This was later replicated in an independent cohort [428]. In the same discovery investigation, 5 proteins were able to classify "fast" and "slow" cognitive decliners (complement C4-A (C4α), complement C8, clusterin, apolipoprotein A1 (apoA1) and transthyretin) [373]. Transthyretin was more recently replicated in an independent cohort to be plasma biomarker of faster cognitive decline [429]. Plasma clusterin (also known as apolioprotein J) was found to be important in the panels of both hippocampal atrophy and cognitive decline [373]. Since these initial discoveries, additional studies have further implicated plasma Clusterin in cognitive decline [366, 430-431], brain atrophy [357, 432] and NAB [374, 433].

Other studies have investigated the role of inflammatory plasma proteins in AD [356, 434]. A five protein panel (IL-1ra, IL-6, IL-10, TNFα and IL-13) was able to distinguish "high" and "low" atrophy measures [356] whereas a panel of six proteins (Il-4, IL-10, G-CSF, IL-2, IFN-γ and PDGF) were associated with the rate of cognitive decline [356]. Further to this, inflammatory proteins CCL3 and chromogranin A were found to be related to brain atrophy [435].

Blood-based biomarkers of neocortical Aβ

The inconclusive findings of Aβ species as blood markers for AD or correlation with Aβ pathology has meant that novel peripheral markers of neocortical Aβ (determined by Aβ PET) have been investigated. The initial studies utilising this endophenotype approach used a range of technologies: two-dimensional gel electrophoresis (2DGE) [373] and Rules-Based Medicine (RBM) [436-437]. The first study to utilise an unbiased Mass Spectrometry discovery approach and the subsequent immunoassay-based verification for the detection of plasma biomarkers of neocortical Aβ is presented in detail in Chapter 3 [374]. This study is also the first to use CSF $A\beta_{1-42}$ measure in an endophenotype design.

Thambisetty and colleagues [373] demonstrated a panel of six plasma proteins (ApoE, CC3, albumin, plasminogen, haptoglobin and IgG C chain receptor) to distinguish individuals with elevated neocortical Aβ burden (NAB) from those without using ^{11}C-PiB. A further validation study only confirmed the association of ApoE with NAB [428]. Kiddle and colleagues [436] used a commercially available platform (RBM) to identify a panel of 13 proteins that predict elevated NAB at a sensitivity and specificity of 92% and 55% respectively. Burnham and colleagues [437] also utilised the RBM panel to produce a biomarkers signature that achieve a sensitivity of 79% and specificity of 78% [437]. Despite the same discovery platform employed, only pancreatic polypeptide (PPY) was a common feature observed in these studies.

Table 0-4: The findings from initial blood-based discovery studies of Aβ PET endophenotypes.

Protein classifier	Aβ PET	Sample size (*n*)	Analytical platform	Study
ApoE, CC3, albumin, plasminogen, haptoglobin, IgG C chain region	^{11}C-PiB	57 (replication study *n* = 42)	2DGE	[373]
C-peptide, fibrinogen, α1AT, PPY, CC3, vitronectin, cortisol, AXL receptor kinase, IL-3, IL-13, MMP9, apoE and IgE **(with age, *APOE* predicts NAB with sensitivity 92% and specificity 52%)**	^{11}C-PiB	71	Luminex xMAP (RBM)	[436]
$A\beta_{1-42}$, CXCL-13, IL-17, IgM-1, PPY and VCAM-1 **(with age, *APOE* predicts NAB with sensitivity 79% and specificity 76%)**	^{11}C-PiB	273 (replication study *n* = 82)	Luminex xMAP (RBM)	[437]
α2m, FHR-1 and FGγ **(with age, sensitivity 59% and specificity 78%)**	^{11}C-PiB	78 (replication study *n* = 79)	TMT-LC-MS/MS ELISA	[374]

Abbreviations: apoE, apolipoprotein E; CC3, complement C3; A1AT, α1-antitrypsin; PPY, pancreatic polypeptide; IL-3, interleukin-3; IL-13, interleukin-13; MMP9, matrix metalloproteinase-9; IgE, Immunoglobulin E; CXCL-13, chemokine ligand 13; IL-17, interleukin-17; IgM-1, Immunoglobulin M; VCAM-1, vascular cell adhesion protein; α2m; alpha-2-macroglobin; FHR-1, complement factor related protein-1; FGγ, fibrinogen gamma chain.

Since these original investigations, other studies have reported blood-based signatures of NAB. Plasma IL-6 receptor, clusterin and apoE together with clinical, MRI imaging and demographic data revealed a 79% and 83% sensitivity and specificity for NAB [427]. A reduced level plasma BDNF was also related to widespread brain amyloidosis [438]. Westwood and colleagues [375] presented a number of plasma proteins associated with longitudinal ^{11}C-PiB in cognitively normal individuals using a 2DGE methodology. Proteins that were associated with three separate time-points were α2m, albumin, apoA1, CC3, complement C4-B, haptoglobin and Ig kappa chain C region. Despite platform differences across all these studies, commonalities in candidate proteins related to NAB do exist (PPY,

CC3, apoE, fibrinogen, α2m and haptoglobin). An effort was made to replicate targets using a SOMAscan platform in an independent cohort. This work confirmed the association of two proteins with NAB: PPY and IgM [439]. This was a disappointing replication finding; however, the lack of translation between multiple platforms (Mass Spectrometry, immunocapture and SOMAscan) is unsurprising.

The endophenotype approach to biomarker discovery is still in its infancy but has already yielded promising results. However, it is likely that these markers will be more variable than CSF measures. Firstly, proximity and reduced interaction with the diseases organ is far greater and secondly, blood-biomarker standardisation of sample pre-analytics and assay choice are at the preliminary stage [440]. In addition, the majority of blood-based endophenotype studies have utilised ^{11}C-PiB as the surrogate measure Aβ pathology. ^{11}C-PiB detects insoluble fibrillary Aβ and not the neurotoxic insoluble oligomeric Aβ. It is then critical that the reproducibility and robustness of plasma proteins associated with NAB are assessed in (1) large independent cohorts, (2) multiple technical platforms and (3) alternative measures of NAB (^{18}F PET tracers or CSF $A\beta_{1-42}$).

Other endophenotype approaches

Other types of biomarkers within blood have been investigated in AD individuals. Metabolomic [407, 441-443] and transcriptomic markers [444] have shown promise but have predominantly used a case-control design. A recent metabolomic study demonstrated a 5 analyte panel that could predict elevated NAB with 72% accuracy with increased accuracy shown with the addition of proteomic results discovered in this thesis [445]. Further research is needed to examine how these markers relate to disease endophenotypes and if in combination with proteomic markers can improve the prediction of AD pathology.

1.10 Conclusion

Biomarkers for AD are dynamic with disease development. These changes start at an early preclinical stage and progress until clinical symptoms manifest in the later stages of the disease. Biochemical changes measured by neuroimaging and CSF sampling have been successful in tracking AD pathology but will prove difficult to implement as population screening tools for clinical application and clinical trial selection. The most suitable application for biomarker investigation at all stages of disease is venipuncture for blood analysis. The reduced cost, simplicity, accessibility and perceived non-invasive nature of blood testing compared with CSF sampling and neuroimaging will allow for large nondemented and demented populations to be extensively studied and followed longitudinally. The complexity of blood makes the search for these biomarkers a challenging task and in-depth unbiased profiling to discover protein markers at high and more importantly low abundances are required. Multiple pre-analytical procedures as well as varying technical platforms may need to be utilised in combination to provide a comprehensive coverage of the proteome for the discovery and validation of blood biomarkers.

This work will therefore investigate multiple proteomic platforms, focusing primarily on LC-MS/MS, for the unbiased identification, replication and validation of single and multi-analyte panels predictive of elevated Aβ pathology at the preclinical to advanced stages of AD. An endophenotype approach will be taken so that individuals will be classified as either “high pathology” or “low pathology” by Aβ PET neuroimaging (^{11}C-PiB and ^{18}FBB) as well as core CSF biomarkers ($A\beta_{1\text{-}42}$, p-tau and t-tau).

1.11 Aims and Objectives

Overall aim

To investigate blood-based markers of neocortical Aβ burden (NAB) to establish plasma derived protein signatures of for Alzheimer's disease (AD) pathology that could be used as a population screening tool for therapeutic trials.

Specific aims

1. To use established proteomic approaches to investigate abundant plasma proteins that are associated with elevated NAB using an extreme endophenotype research design.
    a. LC-MS/MS discovery will be used to relate proteins with elevated NAB as determined by Pittsburgh compound B (^{11}C-PiB) PET.
    b. To select and target proteins from LC-MS/MS discovery phase and replicate the findings by immunoassay in independent cohorts of differing NAB modalities:
        i. ^{11}C-PiB PET imaging
        ii. Core CSF biomarkers ($A\beta_{1-42}$, p-tau and t-tau)
2. To review, assess and improve upon current plasma proteomic LC-MS/MS approaches for the investigation of plasma biomarkers. Several modalities coupled to LC-MS/MS will be investigated including immunodepletion, fractionation and isobaric labelling methods. Outcomes of each methodology will be assessed by comparing;
    a. The total numbers of quantified protein groups and peptides.
    b. The number of protein groups of low abundance (<100ng/mL).
    c. The identification of brain specific protein groups and protein groups related to neurodegenerative pathogenesis.
3. To apply the developed LC-MS/MS methodology to two larger, predominately cognitively normal, cohorts to discover single and multi-analyte protein panels that can predict elevated NAB as measured by Aβ PET neuroimaging (^{11}C-PiB and ^{18}FBB) in the preclinical stage of AD.

CHAPTER 2

MATERIALS AND METHODOLOGY

2.1 Participants

2.1.1 The Australian Imaging, Biomarkers and Lifestyle Flagship Study of Ageing

The Australian Imaging, Biomarkers and Lifestyle Flagship Study of Ageing (AIBL) study was initiated in 2006 with the view to recruit participants, over the age of 60, for the primary purpose of prospective research into AD. AIBL is one of the largest longitudinal studies of ageing (>1000 participants) that incorporates neuroimaging, fluid biomarkers, lifestyle, clinical and neuropsychological assessment. The AIBL study was approved by the institutional ethics committees of Austin Health, St. Vincent's Health, Hollywood Private Hospital and Edith Cowan Univeristy. All volunteers gave written consent before participating in the study [446].

In this work, two distinct AIBL populations were selected as discovery cohorts. AIBL-1 (Chapter 3) consisted of plasma samples from 78 participants selected on the premise of an extreme endophenotype approach based on measures by ^{11}C-PiB PET imaging. AIBL-2 (Chapter 5) was a larger cohort which consisted of plasma samples from 190 individuals. Here, participants were selected based upon baseline ^{11}C-PiB PET neuroimaging but an extreme endophenotype was not used. AIBL-2 was enriched to principally include cognitively normal individuals with longitudinal Aβ PET and cognitive examinations.

Positron emission tomography (PET) acquisition and analysis

An initial T1-weighted MRI for screening and co-registration with the PET images was initially performed on all participants. Within 11 ±22 days of the neuropsychological assessment all participants (AIBL-1 and AIBL-2) received an ^{11}C-PiB PET scan, which has been previously described [447]. In brief, individuals received ~370 MBq ^{11}C-PiB PET IV over 1 minute. Imaging was performed on a Phillips Allegro PET camera. A rotation transmission sinogram acquisition was

performed before the injection of the radiotracer for attenuation correction. A 90-minute list-mode emission acquisition was performed in 3D mode after injection of PiB. List-mode raw data were classified off line into four 30-seconds, nine 1-minute, three 3-minute, ten 6-minute, and two 10-minute frames. Classified sinograms were reconstructed using a 3D RAMLA algorithm [448]. PET standardized uptake values (SUV) were acquired 40–70 minutes post-PiB injection and were summed and normalised to the cerebellar cortex SUV, resulting in a region to cerebellar ratio termed the SUV ratio (SUVR). The cerebellar cortex was used as a reference region as it is relatively devoid of senile plaques and shows no PiB binding in controls or AD [448]. Regions of interest (ROIs) were determined by the individual's MRI. Mean radioactivity values were obtained from ROIs for cortical, subcortical and cerebellar regions. Neocortical Aβ burden (NAB) was expressed as the average SUVR of the area-weighted mean for the following cortical ROIs. ROC's were performed to establish the most accurate cut-off value to distinguish AD from Healthy. This approach generated a cut-off value for ^{11}C-PIB SUVR of 1.3 for AIBL-1 and 1.5 for AIBL-2, which was used to categorise participants into those with 'AD-like' (PiB positive (PiB+) images or those with 'Control' (PiB-negative (PiB-) [447].

Cognitive assessment

Various cognitive assessments were implemented based on internationally recognised literature. The full battery comprised of Mini Mental State Examination (MMSE) [449], California Verbal Learning Test (CVLT-II), 30-item Boston Naming Test (BNT), Wechsler Test of Adult Reading (WTAR), Digit Span and Digit Symbol-Coding subtests of the Wechsler Adult Intelligence Scale (WAIS-III), the Stroop task and the Rey Complex Figure Test (RCFT) [446]. In addition, participants also completed the CogState battery examination (www.cogstate.com). The Hospital Anxiety and Depression Scale (HADS) were also completed to complement the GDS performed at screening [446].

For participants with a diagnosis of MCI or AD, an informant was asked to provide supplementary information about the functional performance of the research participant and to complete the Informant Questionnaire on Cognitive Decline (IQCODE). Dementia severity was assessed by the Clinical Dementia Rating scale (CDR) [450]. CDR assesses six categories of function (memory, orientation, problem

solving, home and hobbies, community affairs, self-care) and is scored to indicate whether dementia is absent (CDR = 0), questionable (CDR = 0.5), mild (CDR = 1), moderate (CDR = 2) or severe (CDR = 3). This decision is made from retrospective information obtained from the cognitive testing and from an informant and/or from the participants' clinician.

Blood sampling

All sampling took place in the morning with participants required to fast overnight. Whole blood was collected by venipuncture at two separate sampling sites within Australia (Melbourne and Perth). Samples were inverted several times and incubated on an orbital shaker for approximately 15 minutes at room temperature (RT) prior to being fractionated. For plasma preparation, whole blood was spun at 200 x *g*, at 20°C, for 10 minutes. The resulting supernatant was transferred to a new 15mL tube and spun at 800 x *g* at 20°C for 15 minutes, to obtain the platelet depleted plasma. Resulting plasma was then aliquoted into 1mL polypropylene tubes and immediately frozen on dry ice before long term storage in liquid nitrogen vapour tanks [446].

2.1.2 The University of California, San Francisco Memory and Ageing Cohort

The University of California, San Francisco (UCSF), Memory and Aging Centre (MAC) is a tertiary care dementia clinic and research program. Established in 1985, the primary focuses at UCSF-MAC were to conduct longitudinal research in the clinical, genetic, neuroimaging, emotional and diagnostic features of MCI, AD and non-AD dementias. Written informed consent was obtained from all patients (or guardians of patients) participating in the study. Biomarkers studies were approved by the University of California (San Francisco and Berkeley) and Lawrence Berkeley National Laboratory institutional review boards for human research.

In this study, the UCSF cohort was utilised as an independent replication in Chapter 3. UCSF participants predominantly were given an FTD diagnosis but this replication utilised brain Aβ measures that had been obtained and not a clinical represtnation. A total of 79 participants were selected based upon an extreme endophenotype approach using either ^{11}C-PiB PET SUVR or ^{11}C-PiB visual examination to categorise subjects into PiB- or PiB+ groups. UCSF participants must also have had *APOE* genotyping, neurological and cognitive investigations.

Positron emission tomography (PET) acquisition and analysis

Subjects underwent ^{11}C-PiB on a Siemens ECAT EXACT HR scanner at Lawrence Berkeley National Laboratory or Biograph Truepoint 6 PET/CT [451]. Approximately 15mCi ^{11}C-PiB was injected as a bolus into an antecubital vein and dynamic acquisition frames were obtained for 90 minutes. Thirty minutes of emission data was collected at 30-60 minutes after tracer injection. Ten minute transmission scans for attenuation correction were obtained immediately after each PiB scan. PET data were reconstructed using an ordered subset expectation maximisation algorithm with weighted attenuation [451]. Image processing and analysis was performed using Statistical Parametric Mapping software (www.fil.ion.ucl.ac.uk). As with AIBL, the cerebellum was utilised as a reference region to create SUVR's and a PiB+ cut-off was set 1.5.

Patient ^{11}C-PiB PET scans were also visually rated by two experienced investigators (Professor Howard Rosen and Professor William Jagust) blinded to clinical data. ^{11}C-PiB scans were rated as "PiB-positive (PiB+)" if tracer binding was thought to be greater in cortical gray matter than in white matter and as "PiB-negative (PiB-)" if only nonspecific white matter binding was observed [451].

Cognitive assessment

All UCSF participants underwent standardised cognitive and behavioural testing. Cognitive testing was obtained within three months of the participants' blood draw and neuroimaging scan [452]. As with AIBL, a CDR was completed for each patient based on an interview with their informant and/or from the participants' clinician. Face-to-face neuropsychological testing that overlapped with AIBL included the MMSE, GDS and D-KEFS verbal fluency [453].

Blood sampling

Whole blood was collected by venipuncture. The blood was centrifuged at 2000 *g* at room temperature for 15 minutes. Plasma was carefully collected, aliquoted and stored at -80°C until further use [452].

2.1.3 European Medical Informatics Framework

The European Medical Informatics Framework (EMIF; www.imi.europa.eu) project aims to develop a common information framework of data to facilitate access to medical and research cohorts. The EMIF-AD platform provides a catalogue on study characteristics of AD cohorts in Europe that can be accessed by other research groups. To date EMIF-AD consists on information on 23 cohort studies. These cohorts have accessible to data for 4,000 subjects with normal cognition, 1,500 with subjective memory complaints (SMC), 5,000 with MCI and 3,000 with AD.

In this work, the EMIF-AD cohort was used as an independent replication and in Chapter 3. EMIF-AD consisted of plasma samples from 489 participants from three European centres selected on the primary premise of CSF $A\beta_{1-42}$ stratified as CSF $A\beta_{1-42}$+ (high NAB) or CSF $A\beta_{1-42}$- (low NAB). Furthermore, participants were also stratified by CSF t-tau, p-tau and a CSF algorithm which incorporated all three measures [454]. EMIF-AD participants must also have had *APOE* genotyping, neurological and cognitive investigations.

Cerebrospinal fluid (CSF) sampling and analysis

CSF was obtained by LP using a 25-gauge needle and collected in 10mL polypropylene tubes. CSF samples were centrifuged at 1800 × *g* for 10 minutes at 4°C within 2 h of collection. CSF was aliquoted in polypropylene tubes of 0.5 or 1 ml and stored at −80 °C until further analysis. CSF $A\beta_{1-42}$, t-tau, and p-tau were measured with INNOTEST ELISA at each cohort site. The inter-assay coefficient of variation (CV) was under 12% for all analytes at all sites.

Cognitive assessment

All EMID-AD participants underwent a different battery of cognitive assessment at different cohort sites. Consistent with AIBL and UCSF, a CDR was completed for each patient and face-to-face neuropsychological testing included MMSE and GDS.

Blood sampling

All EMIF-AD cohorts all followed a similar blood processing pipeline. Blood samples were obtained in the morning after an overnight fast, centrifuged at 2000 x *g* for 30 min at 4°C. Plasma was collected and stored in 1.5ml aliquots at -80◦C.

2.1.4 The McCusker Kerr Ageing Research cohort

The McCusker Kerr Anglican Retirement Village Initiative in Ageing Health Research cohort (KARVIAH) study is a two year health and lifestyle evaluation incorporating a one year curcumin intervention focused on AD prevention (Martins R et al., unpublished). The study includes a two stage design to evaluate the health and risk factors of older people (65-90 yrs) living in independent living retirement complexes. Stage 1 will involve a physical assessment including blood collection, neuropsychological assessment and the completion of lifestyle questionnaires. Eligible participants, based on the defined inclusion / exclusion criteria, will progress to Stage 2 of the study where the participants will in addition to the preceding investigations, undergo retinal and brain imaging. At the completion of the Stage 2 baseline assessment, the participant will then be provided with either the intervention Biocurcumax™ or placebo, through a double blind, randomly allocated process. The participants will be assessed at three monthly intervals for two years.

In this study, the 94 KARVIAH participants were utilised as an independent replication cohort in Chapter 5. It was not the intention to investigative the affects of curcumin and therefore only baseline plasma samples, before intervention, were utilised. Selection was dependant on the availability of ^{18}FBB images for each subject. All KARVIAH participants were categorised as Aβ+ and Aβ- however all were clinically defined as healthy controls. Cognitive assessments as well as *APOE* genotyping needed to be available for inclusion into this study.

Positron emission tomography (PET) acquisition and analysis

All participants receiving PET scans also underwent an anatomical MRI procedure for anatomical localisation of ROIs. All KARVIAH participants underwent PET imaging using the ligand ^{18}FBB within three months of blood collection, at the Macquarie Medical Imaging centre in Macquarie University Hospital, Sydney, Australia. Participants were administered an IV bolus of ^{18}FBB over 30 seconds at resting state. Images were acquired over a 20 minute scan beginning 50 minutes post ^{18}FBB injection. NAB was calculated as the mean SUVR of the frontal, superior parietal, lateral temporal, lateral occipital, and anterior and posterior cingulate. An SUVR cut-off value of 1.35 was utilised to categorise participants into Aβ+ and Aβ-.

Cognitive assessment

The battery of neuropsychological tasks followed the same protocol as the AIBL study [446]. As with AIBL, only MMSE and CDR assessments were utilised in this study.

Blood sampling

Whole blood was collected by venipuncture and followed the same plasma collectionpre-analytical procedure as the AIBL cohort [446].

2.2 Materials

The following is a list of reagents and the suppliers they were acquired.

Reagent	Supplier	Catalogue #
Acetonitrile (ACN), hypergrade for LC-MS	Merk Millipore	100029
alpha-2-Macroglobulin (α2m) Human ELISA kit	USCN Life Science	SEB017Hu
Ammonium Bicarbonate (Ambic)	Sigma	A6141
apolipoprotein A-I (apoA1) Human ELISA kit	USCN Life Science	SEA519Hu
apolipoprotein A-IV (apoA4) Human ELISA kit	USCN Life Science	SEC543Hu
apolipoprotein L1 (apoL1) Human ELISA kit	USCN Life Science	SEC560Hu
apolipoprotein(a) (apo(a)) Human ELISA kit	Cusabio	CSB-E15088h
clusterin Human ELISA kit	USCN Life Science	SEB180Hu
complement C3 (CC3) Human ELISA kit	USCN Life Science	SEA861Hu
complement C4 (C4α) Human ELISA kit	USCN Life Science	SEA888Hu
complement factor B (CFB) Human ELISA kit	Abcam	ab137973
complement factor H (CFH) Human ELISA kit	Abcam	ab137975
complement factor H related protein 1 (FHR-1) Human ELISA kit	Cusabio	CSB-EL005274Hu
Dithiothreitol (DTT)	Sigma	D5545
EASY-Column™ capillary analytical column	Fisher Scientific Ltd	SC003
EASY-Column™ capillary guard column	Fisher Scientific Ltd	SC001
fibrinogen Alpha Chain (FGα) Human ELISA kit	USCN Life Science	SEB154Hu
fibrinogen γ chain (FGγ) Human ELISA kit	USCN Life Science	SEC477Hu
Formic acid (FA)	Merk Millipore	100264
gelsolin Human ELISA kit	USCN Life Science	SEA372Hu
Glycercol	Sigma	G5516

haptoglobin Human ELISA kit	Genway	17Q1
High resolution IPG strips, pH 3-10	Agilent Technologies	5188-6424
histidine Rich Glycoprotein (HRG) Human ELISA kit	USCN Life Science	SEC534Hu
Hydroxylamine solution	Sigma	438227
Imperial Protein Stain	Fisher Scientific Ltd	24615
Iodoacetamide (IAA)	Sigma	I1149
Low resolution IPG strips, pH 3-11	Agilent Technologies	5188-6425
Methanol, hypergrade for LC-MS	Sigma	34966
Minerial Oil	Sigma	M3516
NuPAGE® MOPS SDS Running Buffer (20X)	Fisher Scientific Ltd	NP0001
NuPAGE® Novex 10% Bis-Tris 1.5 mm	Invitrogen	NP0316BOX
Phosphate buffered saline (PBS)	Sigma	P4417
Pierce™ Top 2 Abundant Protein Depletion Spin Columns	Fisher Scientific Ltd	85162
ProteoPrep Immunoaffinity Albumin & IgG Depletion Kit	Sigma	PROTIA-1KT
Sample Buffer, Laemmli 2× Concentrate	Sigma	S3401
serotransferrin (TF) Human ELISA kit	USCN Life Science	SEC036Hu
Sodium dodecyl sulfate (SDS)	Sigma	5030
SOLA HRP SPE Cartridge	Fisher Scientific Ltd	60109-001
Tetraethylammonium bromide (TEAB)	Sigma	T7408
TMT10plex™ Isobaric Label Reagent Set, 1 x 5 mg	Fisher Scientific Ltd	90406
TMTsixplex™ Isobaric Label Reagent Set, 5 x 0.8 mg	Fisher Scientific Ltd	90066
Trifluoroacetic acid (TFA), hypergrade for LC-MS	Merk Millipore	1.08262.0100
Tris (2-carboxyethyl) phosphine (TCEP)	Sigma	C4706
Trypsin, Modified Sequencing Grade	Roche	11418025001

2.3 Solutions

All solutions were made up with 18MΩcm ultra-pure water (ddH_20) unless stated otherwise.

Stock	Procedure
Ambic 100mM	0.79g Ambic 100mL ddH_20
DTT 100mM	15mg DTT 1mL 100mM Ambic
Hydroxylamine 5	20µL Hydroxylamine 50% 180µL ddH_20
IAA 150mM	27.74mg IAA 1mL200mM TEAB
LC-MS/MS sample solution (2% ACN, 0.1% FA)	200µL ACN 10µL FA 9.79mL ddH_20
OGE rehydration solution (24 well frame)	960µL OGE peptide stock solution 240µL ddH_20
OGE rehydration solution (12 well frame)	560µL OGE peptide stock solution 140µL ddH_20
OGE peptide stock solution	600µL OGE buffer Glyercol 6mL 43.4mL ddH_20
OGE peptide sample (24 well frame)	1mg TMT10plex dried sample 360µL ddH_20 1.44mL OGE peptide stock solution
OGE peptide sample (12 well frame)	1mg TMT10plex dried sample 720µL ddH_20 2.88mL OGE peptide stock solution
SDS 2%	20mg SDS 1mL ddH_20
TCEP 0.5M	125mg TCEP 1mL ddH_20

TCEP 200mM	70µL 0.5M TCEP 70µL ddH_20 35µL 1M TEAB
TEAB 200mM	600µL 1M TEAB 2.4mL ddH_20
Trypsin 0.1% TFA	250µl 0.1% TFA 25µg Trypsin

2.4 Methodology for Chapter 3

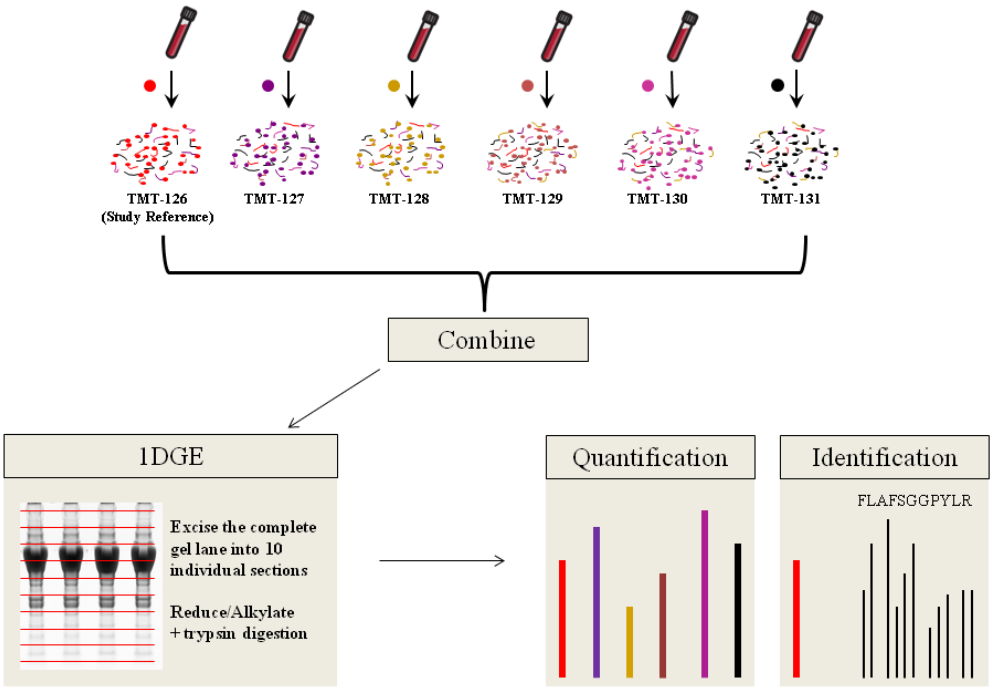

Figure 2-1: Schematic diagram of the LC-MS/MS workflow applied to AIBL-1 cohort in Chapter 3.

2.4.1 Tandem Mass Tag 6plex (TMT6plex) protein labelling

TMT tags were utilised for multiplexing clinical samples and relative quantification against a study reference. TMT chemical tags contain four regions; a mass reporter region, a cleavable linker region, a mass normalisation region and a protein reactive group (Figure 2-2). Although chemically identical, each TMT tag has isotope replacements at differing locations. This ensures that the mass normaliser and mass reporter have differing molecular masses in each tag. As the full structure and molecular weight of each TMT tag is identical, the differing TMT labels cannot be distinguished during protein fractionation, liquid chromatography (LC) or MS1 fragmentation. Fragmentation is achieved upon MS2 (MS/MS) by high energy collision dissociation (HCD), cleavage of the peptide back bone and linker give rise to sequence and quantitation simultaneously.

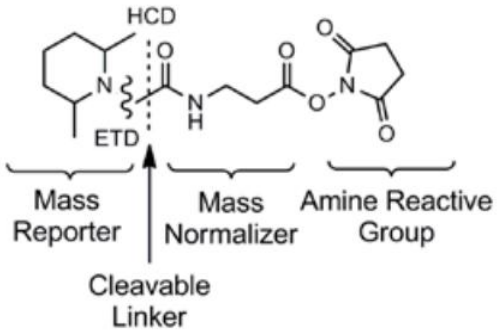

Figure 2-2: Functional regions of TMT tag structure including MS/MS fragmentation sites by higher energy collision dissociation (HCD). During MS2 fractionation by HCD the cleavable linker is broken to give produce a unique Mass Reporter.

Total protein quantification was determined by a NanoDrop™ 1000 Spectrophotometer (Thermo Scientific) and 100µg of protein from each sample was extracted for TMT6plex protein labelling. Each sample was randomly assigned and labelled with an amine reactive TMT reagent (TMT-127, TMT-128, TMT-129, TMT-130 and TMT-131) with TMT-126 being used to label the study reference, an equal pool of the plasma obtained from all samples included in the study (Figure 2-1).

One hundred micrograms of lyophilised plasma sample was solubilised in 200mM Tetraethylammonium bromide (TEAB) and 2% SDS, reduced in 200mM tris (2-carboxyethyl) phosphine (TCEP) for 1 h at 55˚C and then alkylated in 150mM iodoacetamide (IAA). The TMT6plex protein reagents were reconstituted in 24µL acetonitrile (ACN) and 18.5µL was added to the appropriate pre-designated sample and incubated at RT for 1 hour. Plasma samples were then quenched with 4µL of 5% hydroxylamine and incubated at RT for a further 15 minutes. The TMT6plex's were completed by combining one of each sample with a TMT-127, TMT-128, TMT-129, TMT-130 and TMT-131 reagent, plus a study reference (TMT-126). The resulted in the formation of 16 TMT6plex's, each with a total of 600µg of protein, were further treated with 8µL of 5% hydroxylamine before being divided into 100µg aliquots, frozen at -80˚C and lyophilised until completion.

2.4.2 One dimensional gel electrophoresis (1DGE)

One hundred micrograms of each TMT6plex were reconstituted in 15µL 50mM TEAB. An equal volume of 2x sample buffer (4% SDS, 20% glycerol, 10% 2-mercaptoethanol, 0.004% bromphenol blue and 0.125 M Tris HCl, pH ~6.8) was added to the TEAB sample and incubated at 90˚C for 10 minutes. TMT6plex protein samples were loaded onto a single NuPAGE® Novex 10% Bis-Tris 1.5 mm precast gel. To avoid overloading only 4 TMT6plex's were run on one 1DGE gel. Gels were run at constant 150V for 90 minutes, stained with Imperial™ Protein stain (Thermo Scientific) for 2 h and destained with ddH_20 overnight. A pre-stained reference (SeeBlue® Plus2 Pre-stained Protein Standard) was run on each gel. All gel lanes were cut manually into 10 equal sized fractions (Figure 2-3) and frozen at -80˚C.

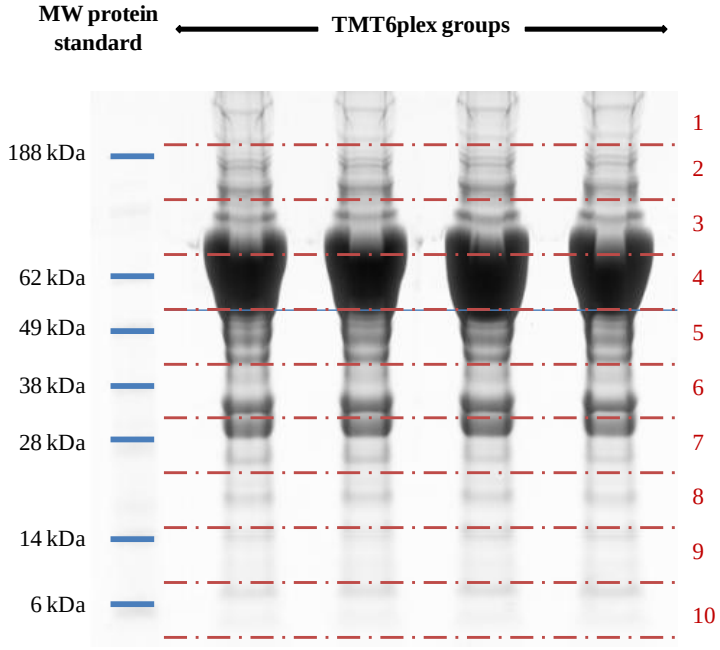

Figure 2-3: A schematic diagram demonstrating the equal fractions excised for enzymatic digestion for all 16 TMT6plex groups. Four representative TMT6plex's are shown.

2.4.3 Enzymatic digestion

Excised gel fractions were further cut into ~2mm^3 cubes and washed firstly with 100mM of ammonium bicarbonate (ambic) for 5 minutes and then decanted. ACN was added in excess, decanted, and then the same volume was added to fully and quickly dehydrate the gel cubes. After the removal of the second round of ACN, gel

cubes were vacuum dried for 15 minutes. The gel cubes were reduced in 10mM Dithiothreitol (DTT), incubated at 56˚C for 1 h before being dehydrated by two rounds of ACN washes before being vacuum dried for 10-15 minutes. Next 55mM IAA was added to alkylate the gel cubes and incubated at RT for 20 minutes, protected from light. Three further washes included 100mM ambic, 50% ACN and 100% ACN with a final vacuum stage. Trypsin solution was prepared by adding 200µL of ambic to each aliquot containing 0.1% Trifluoroacetic acid (TFA) to give a final concentration of 13ng/µL trypsin. Gel cubes were fully submersed in the trypsin solution and incubated at 4˚C for 20 minutes. Finally, 20µL of 50mM ambic was added to the gel pieces, to keep moist during enzyme cleavage and incubated at 37˚C for 4 hours then overnight at RT.

2.4.4 Peptide extraction

Supernatant from the overnight tryptic digestion was decanted and collected into a new Eppendorf tube (primary collection). A minimal volume of 50mM Ambic (enough to cover the gel cubes) was added to each gel fraction and incubated on a heat shaker (37˚C) for 5 minutes. The supernatant was collected and added to the primary collection. Gel cubes were next dehydrated with ACN for 10 minutes at 37˚C, after which the supernatant was again decanted and into the primary collection Eppendorf tube. The rehydrating and dehydrating step was repeated once more, with the supernatant being added to the primary collection Eppendorf tube each time. The pooled supernatant of tryptic peptides was then frozen and vacuum dried to completion prior to MS analysis.

2.4.5 Liquid Chromatography – Tandem Mass Spectrometry acquisition

Prior to LC-MS/MS analysis, peptide extracts from all 160 gel fractions were reconstituted in 0.1% formic acid (FA), 2% ACN and de-ionised water then shaken at 37˚C, vortexed and centrifuged thoroughly. Each peptide extract was reconstituted to a concentration of 0.5µg/µL with retrospective protein concentration of peptide extracts estimated by densitometry (Odyssey®; LI-COR Biosciences) of the 1DGE images.

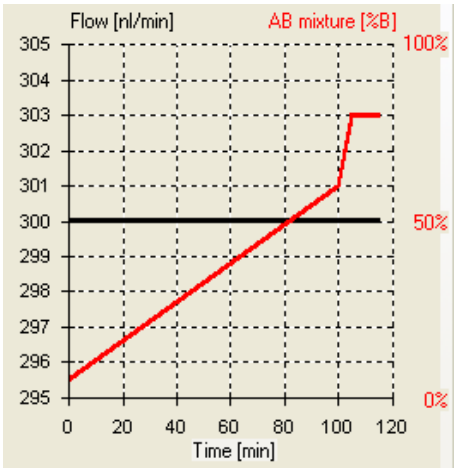

Time	Duration	Flow [nl/min]	%B
00:00	N/A	300	5
100:00	100:00	300	60
105:00	05:00	300	80
115:00	10:00	300	80

Figure 2-4: Method of chromatographic separation for TMT6plex labelled peptides in AIBL-1. A linear increase of 5% solvent B (0.1% FA in 100% ACN) was run for 100 minutes before a 5 minute wash at 80% solvent B.

Chromatographic separation was achieved by a two column configuration; 4µL of sample (~2µg) was injected first onto a 0.1 × 20 mm pre-column (Thermo Scientific) packed with octadecyl carbon chain C18-bonded silica (C18) using the Thermo Scientific Proxeon EASY-nLC II system. Peptides were then resolved using a linear gradient of 0.1% FA in ACN (10% to 65% over 115 minutes) through a 0.075 × 150 mm C18 analytical column (Thermo Scientific) at a flow rate of 300nL/min (Figure 2-4). Mass spectra were acquired on a Thermo Scientific LTQ Orbitrap Velos instrument throughout the chromatographic run which operated in data-dependent mode to automatically switch between full scan MS and MS/MS acquisition. Instrument control was through Tune 2.6.0 and Xcalibur 2.1 (Thermo Scientific). A Higher Collision induced Dissociation (HCD) Top10 method was used; survey full scan MS spectra (from *m/z* 400–2,000) were acquired in the Orbitrap system with resolution at 30,000 after accumulation to an Automatic Gain Control (AGC) ion injection target value of $1x10^6$ (500ms max injection time). The ten most intense peptide ions, with charge states $\geq$2, were sequentially isolated to an AGC target value of 50,000 (250ms max ion injection time). Selected ions were then put on a dynamic exclusion list for 30secs (10 ppm *m/z* window). Fragmentation in the HCD collision

cell was achieved with normalised collision energy of 40%. The resulting fragments were detected in the Orbitrap system with resolution of 7,500. Real-time calibration and therefore greater mass accuracy was achieved using the polysiloxane peak at 445.120024 *m/z* as a lock-mass. Other standard MS conditions for all experiments were as described in Olsen and colleagues [455]; spray voltage, 2.2 kV; no sheath and auxiliary gas flow; heated capillary temperature, 200°C; predictive automatic gain control (pAGC) enabled and an S-lens RF level of 50–60%.

2.4.6 Computational Mass Spectrometry

Pre-processing of LC-MS/MS data

Raw data files produced in Xcalibur software 2.1 were processed using Proteome Discoverer, (ver. 1.3; Thermo Scientific) to determine peptide identification (Figure 2-5); the subsequent Mascot (ver. 2.3; available at: http://www.matrixscience.com) output file was used for additional pre-processing and analysis.

Prior to database searching a spectrum selector threshold was applied; minimum 700 Da and maximum 10000 Da. Within Mascot, mass spectra were searched against the uniprot/Swiss-prot database (ver. 4.11), taxonomy was set to human with precursor and fragment mass tolerances were set to ±5ppm and 0.5 Da respectively. Dynamic modifications included TMT6plex modification of the lysine residue (TMT (K)), TMT6plex modification of the peptide N-Terminus (TMT (N-Term)), deamidation (NQ) and oxidation of the methionines. Additionally, carbamidomethylation of cysteine residues was set as a fixed modification and three miss cleavages were allowed. The results of this database search were further filtered to include peptides with an "ion score" $\geq$15 and those described by mascot as "Bold Red" (at least one top-scoring peptide appearing for the first time in a protein; [370]). The LC-MS/MS peak lists were further processed to pull out the six TMT reporter ion intensities for each peptide that passed the criteria mentioned above; this was generated by a bespoke in-house perl script [370].

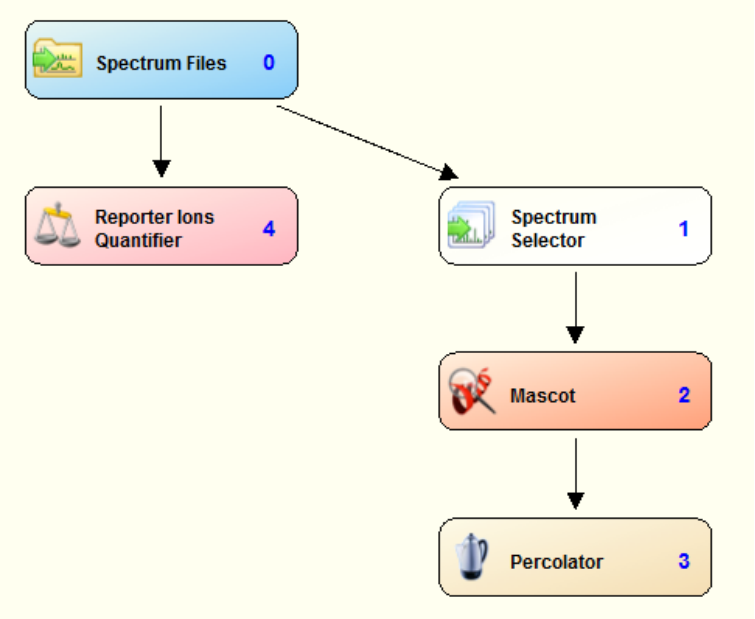

Figure 2-5: Proteome Discoverer workflow for database searching of MS/MS spectra in Chapter 3. Spectrum selector thresholds were set as 700Da-10000 Da. In Mascot, precursor and fragment tolerances were set to ±5ppm and 0.5 Da. Modifications included TMT (K), TMT (N-Term), deamidation (NQ), oxidation (M) and carbamidomethylation (C) of cysteine residues. Three miss cleavages were allowed.

Pre-processing for Relative Quantification (PRQ-1)

A script was written in R to complete the pre-processing of LC-MS/MS data acquired. The script, named Pre-processing for Relative Quantification (PRQ-1) can be viewed in Supplementary Material 1. PRQ-1 performs (1) median ratio normalisation [456], (2) calculates within TMT6plex ratios for each peptide, (3) derives within TMT6plex protein level data from all corresponding peptide scores, and (4) collects the protein group scores across all TMT6plex experiments. A protein group is defined as the number of protein identification in which this peptide is found.

Median normalisation to correct for TMT6plex labelling and MS-run variation (Step 1) is performed within each sample and gel fraction. This involves calculating the median of the ratios of all peptide intensities from one sample versus the corresponding intensities measured in the reference sample. All intensities relating to that sample and gel fraction are then divided by the median ratio. Ratio scores for each peptide are then calculated (Step 2) by taking the ratios of the normalised data for each peptide by dividing it to the reference intensity. Ratios corresponding to the

same source protein, peptide sequence and gel fraction are then summed. Protein level data is derived from these summed peptide scores (Step 3) by taking either the mean or median of all peptide scores from the same source protein and gel fraction. This protein level data is then collected across all sixplexs (Step 4).

Post PRQ-1 data clean up included the removal of all non-TMT peptides. The isobaric multiplex approach applied subsequently meant that only proteins with full quantifiable TMT information were carried forward for statistical evaluation. In addition, only protein data with information from $\geq$50% of subjects were considered a reliable measurement of plasma protein expression. In the instance of LC-MS/MS data separated with 1DGE a single protein can be observed in multiple fractions. These mass differences could be explained by Post-Translational Modifications (PTM), single nucleotide polymorphism (SNP), proteolytic cleavage, alternative splicing or terminal fragments of a protein sequence. Therefore, identical protein identifications observed in different fractions were considered as separate entities known as protein group molecular weight (MW) isoforms.

Manual assessment of MS spectra

Manual examination of assigned spectra in Proteome Discoverer was only performed for significantly associated proteins. The manual examination of MS/MS spectra is subjective; however it is an essential step when confirming the identity of a peptide sequence, especially at a relaxed assignment criterion (5% FDR) or for proteins of lower abundance. MS/MS spectra would typically be confirmed by the presence of overlapping *b* and *y* ions that give full coverage of the peptide sequence (good quality, Figure 2-6) or significant coverage series of *b* or *y* ions with strings of adjacent *b* or *y* ions being identified together (moderate quality, Figure 2-7). The criterion set out by Tabb and colleagues [457] was followed were possible.

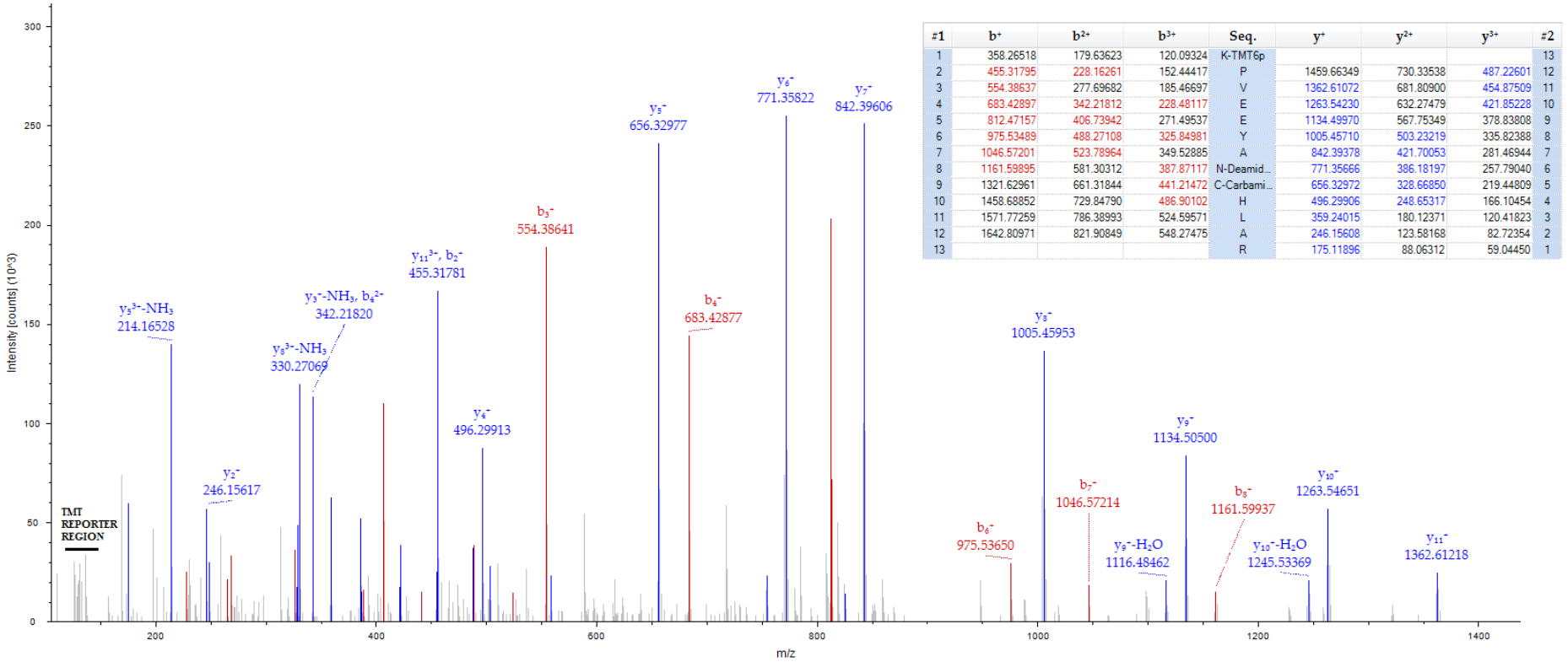

#1	b+	b2+	b3+	Seq.	y+	y2+	y3+	#2
1	358.26518	179.63623	120.09324	K-TMT6p				13
2	455.31795	228.16261	152.44417	P	1459.66349	730.33538	487.22601	12
3	554.38637	277.69682	185.46697	V	1362.61072	681.80900	454.87509	11
4	683.42897	342.21812	228.48117	E	1263.54230	632.27479	421.85228	10
5	812.47157	406.73942	271.49537	E	1134.49970	567.75349	378.83808	9
6	975.53489	488.27108	325.84981	Y	1005.45710	503.23219	335.82388	8
7	1046.57201	523.78964	349.52885	A	842.39378	421.70053	281.46944	7
8	1161.59895	581.30312	387.87117	N-Deamid...	771.35666	386.18197	257.79040	6
9	1321.62961	661.31844	441.21472	C-Carbami...	656.32972	328.66850	219.44809	5
10	1458.68852	729.84790	486.90102	H	496.29906	248.65317	166.10454	4
11	1571.77259	786.38993	524.59571	L	359.24015	180.12371	120.41823	3
12	1642.80971	821.90849	548.27475	A	246.15608	123.58168	82.72354	2
13				R	175.11896	88.06312	59.04450	1

Figure 2-6: Example of a good quality MS/MS spectrum identified at 5% FDR. There is a large intensity ion count and full series of overlapping *b* and *y* ions are indentified. TMT reporter region is not contributing to peptide score in Mascot. MS/MS spectrum of m/z 605.98 for the $[M+3H]^{3+}$ molecular ion for a peptide of 1815.94 Da with corresponding sequence KPVEEYANCHLAR unique to serotransferrin (TF).

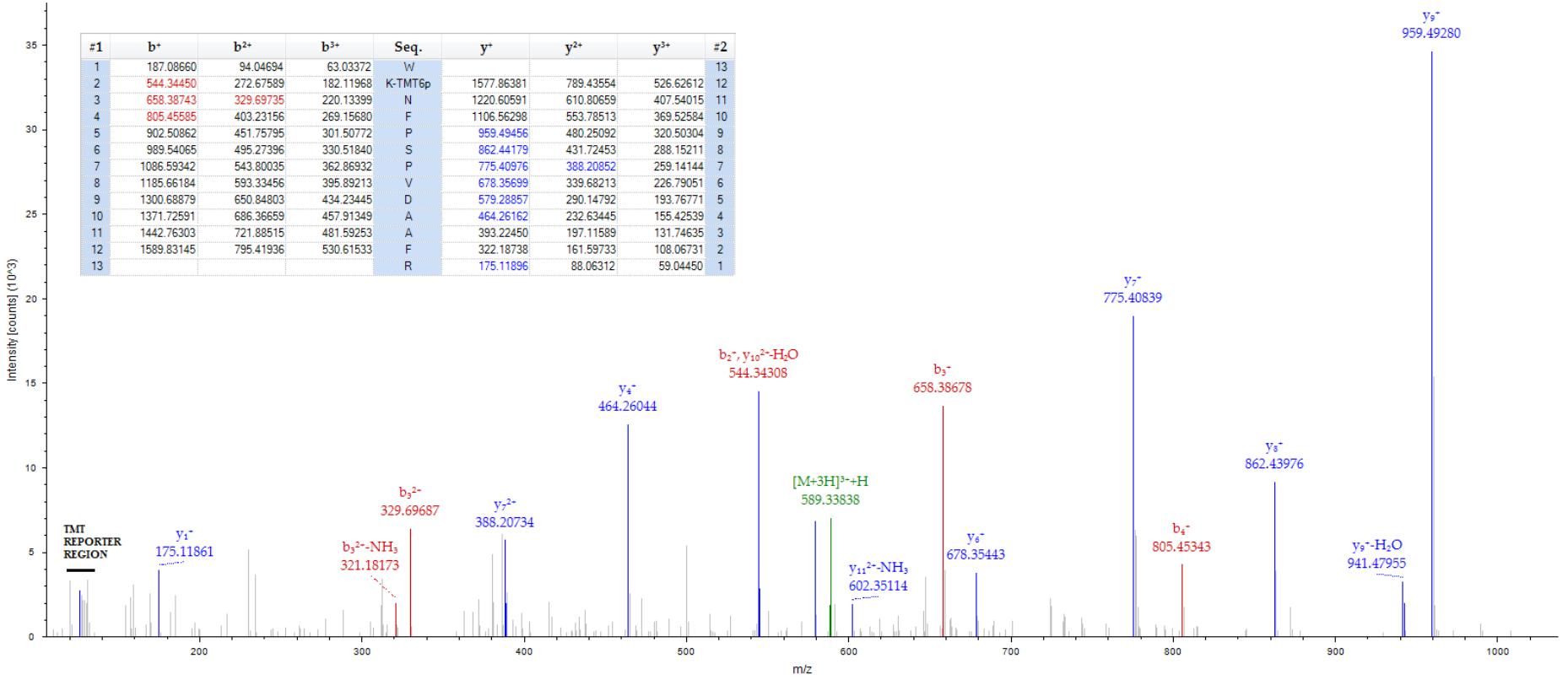

Figure 2-7: Example of a moderate quality MS/MS spectrum identified at 5% FDR. There is a large intensity ion count and the majority but not all *b* and *y* ions are accounted for. TMT reporter region is contributing small proportion to peptide score in Mascot and a small amount of the precursor ion remains. MS/MS spectrum of m/z 588.65 for the $[M+3H]^{3+}$ molecular ion for a peptide of 1763.95 Da with corresponding sequence WKNFPSPVDAAFR unique to hemopexin.

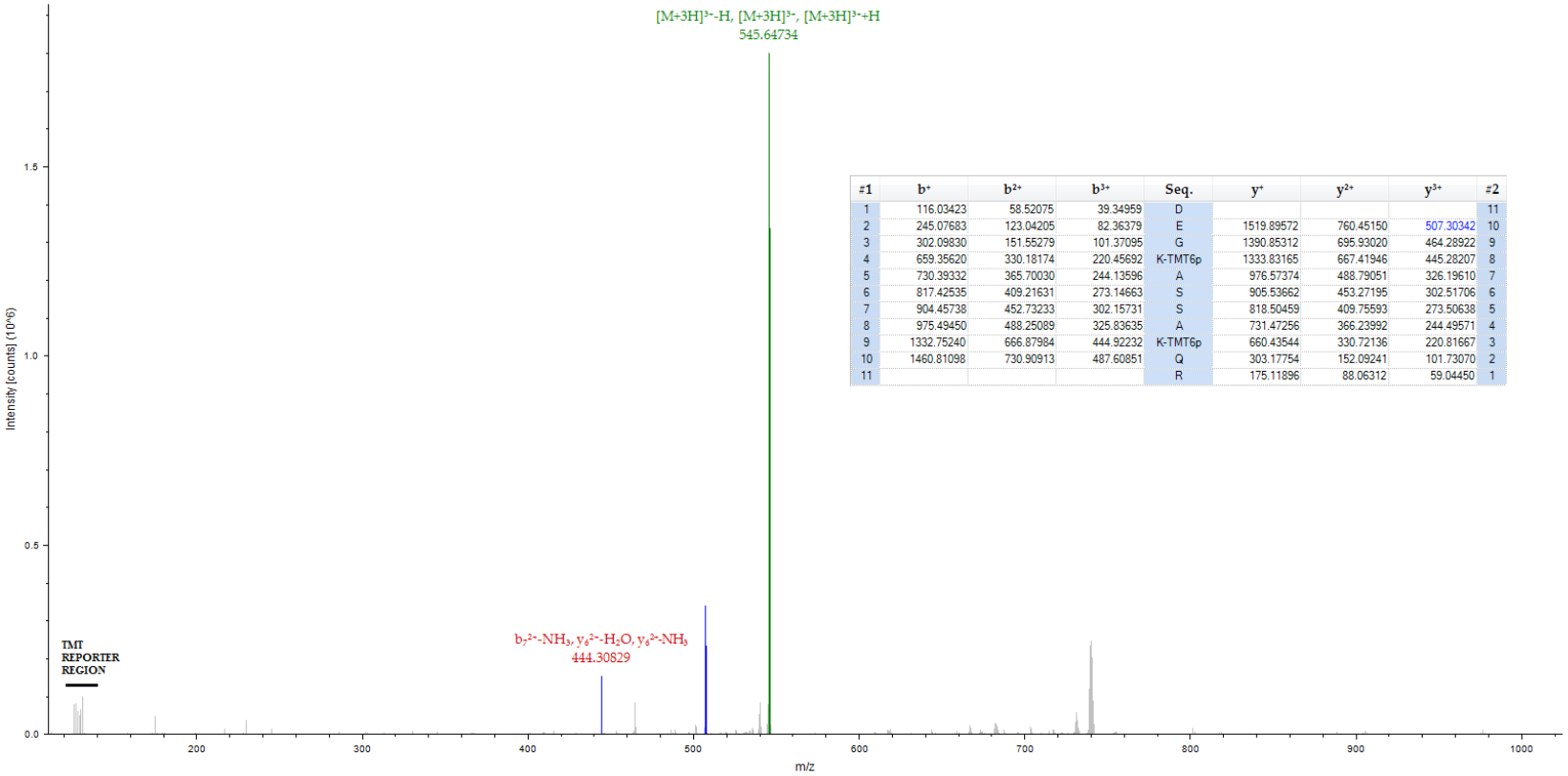

#1	b+	b2+	b3+	Seq.	y+	y2+	y3+	#2
1	116.03423	58.52075	39.34959	D				11
2	245.07683	123.04205	82.36379	E	1519.89572	760.45150	507.30342	10
3	302.09830	151.55279	101.37095	G	1390.85312	695.93020	464.28922	9
4	659.35620	330.18174	220.45692	K-TMT6p	1333.83165	667.41946	445.28207	8
5	730.39332	365.70030	244.13596	A	976.57374	488.79051	326.19610	7
6	817.42535	409.21631	273.14663	S	905.53662	453.27195	302.51706	6
7	904.45738	452.73233	302.15731	S	818.50459	409.75593	273.50638	5
8	975.49450	488.25089	325.83635	A	731.47256	366.23992	244.49571	4
9	1332.75240	666.87984	444.92232	K-TMT6p	660.43544	330.72136	220.81667	3
10	1460.81098	730.90913	487.60851	Q	303.17754	152.09241	101.73070	2
11				R	175.11896	88.06312	59.04450	1

Figure 2-8: Example of a poor quality MS/MS spectrum identified at 5% FDR. There is a large intensity ion count which is caused by the non-fragmented precursor ion. Only one y ion matched with no subsequent b ions matched. MS/MS spectrum of m/z 545.64 for the [M+3H]3+ molecular ion for a peptide of 1634.92 Da with corresponding sequence DEGKASSAKQR unique to hemopexin.

2.4.7 Technical verification and validation: Enzyme-linked Immunoabsorbent assays (ELISA)

Candidate markers discovered by LC-MS/MS underwent technical verification using commercially available ELISAs. Technical verification was performed in the same 78 subjects from the AIBL-1 imaging sub-cohort, as we sought to translate our discovery findings to a simple-to-use format. Further validation in independent cohorts (UCSF and EMIF-AD) was performed using the same commercial ELISA as the technical verification.

Sandwich ELISA

Plasma samples were tested for optimal dilution by testing each kit using a pool of elderly control and AD plasma all standards were diluted as recommended in the protocol for each ELISA kit (Table 2-1). All kit components and samples were brought to RT (18-25˚C) before use. The variations between assay protocols were minimal and differences in volumes, incubation times/temperatures are indicated in Table 2-1. In general, 100µL of the standard and diluted plasma samples were added to the appropriate wells and incubated for 2 h at 37˚C with agitation on an orbital shaker. The liquid from each well was aspirated and 100µL of detection antibody was added, and incubated for 1 h at 37˚C. The plate was then washed 3 times with 350µL of wash buffer by an automated plate washer (Bio-Rad) and incubated for 30 minutes with 100µL secondary antibody. The plate was further washed 5 times as before and 90µL 3,3’,5,5’-Tetramethylbenzidine (TMB) substrate solution was added to each well and incubate at 37˚C for 5-20 minutes (protected from the light). Finally, 50µL of stop solution was added to each well and the absorbance at 450nm was measured on a micro plate reader (PHERAStar FS). The plate was also read at 595nm to account for background interference.

Before statistical analysis, the performance of each assay was examined using quality checks (QC; Table 2-3). Sample replicates were averaged and standard values were exported into Sigma plot (Systat Software; version 12) for estimation of protein concentrations using a 5-parameter logistic curve fitting method. Any sample that recorded a coefficient of variation (CV) >15% for either duplicate was eliminated; if both duplicates were out of range then both data points were excluded. Ideally, a spike and recovery assessment should be performed on each commercial

assay to determine its performace. In spike and recovery, a known amount of analyte is added (spiked) into the natural test sample matrix. Then the assay (ELISA) is run to measure the response (recovery) of the spiked sample matrix compared to an identical spike in the standard diluent. This was not performed for commercial assays displayed in Table 2-1.

Table 2-1: Sandwich ELISA protocol variations for proteins selected for technical replication and validation.

Protein Name	Manufacturer	Dilution factor	Primary Incubation, hrs (Temp)	Detection Antibody Volume (Time, hrs)	Secondary Antibody Volume (Time, hrs)	TMB substrate Volume (Time, mins)
α-2-macroglobulin (α2m)	USCN Life Sciences Inc.	40,000	2 (37°C)	100µL (1)	100µL (0.5)	90µL (10)
apolipoprotein(a) (apo(a))	Cell BioLabs Inc.	2,000	16 (4°C)	100µL (1)*	100µL (1)*	100µL (12)
apolipoprotein A-I (apoA1)	USCN Life Sciences Inc.	5,000	2 (37°C)	100µL (1)	100µL (0.5)	90µL (8)
apolipoprotein A-IV (apoA4)	USCN Life Sciences Inc.	1000+	2 (37°C)	100µL (1)	100µL (0.5)	90µL (15)
apolipoprotein L-1 (apoL1)	USCN Life Sciences Inc.	500+	2 (37°C)	100µL (1)	100µL (0.5)	90µL (15)
clusterin	USCN Life Sciences Inc.	10,000	2 (37°C)	100µL (1)	100µL (0.5)	90µL (10)
complement C3 (CC3)	USCN Life Sciences Inc.	10,000	2 (37°C)	100µL (1)	100µL (0.5)	90µL (10)
complement C4a (C4α)	USCN Life Sciences Inc.	20,000	2 (37°C)	100µL (1)	100µL (0.5)	90µL (6)
complement factor B (CFB)	Abcam	5,000	2 (37°C)	50µL (1)	50µL (0.5)	50µL (12)
complement factor H (CFH)	Abcam	200,000	2 (37°C)	50µL (1)	50µL (0.5)	50µL (20)
fibrinogen-α-Chain (FGα)	USCN Life Sciences Inc.	25+	2 (37°C)	10 µL (1)	100µL (30)	90µL (10)
fibrinogen-γ-Chain (FGγ)	USCN Life Sciences Inc.	10,000	2 (37°C)	100µL (1)	100µL (30)	90µL (10)
geloslin	USCN Life Sciences Inc.	250+	2 (37°C)	100µL (1)	100µL (30)	90µL (15)
haptoglobin	GenWay	50,000	0.25 (25°C)	100µL (0.25)	N/A	100µL (5)
histidine-rich glycoprotein (HRG)	USCN Life Sciences Inc.	20,000	2 (37°C)	100µL (1)	100µL (30)	90µL (10)
serotransferrin (TF)	USCN Life Sciences Inc.	200,000	2 (37°C)	100µL (1)	100µL (30)	90µL (12)

Table 2-2: Immunoassay quality control (QC) criteria (adapted from Hye A et al., 2014). Analytes were assessed for quality by applying rank according to the assay performance and defined using a scoring system based on four criteria as follows. All plasma analytes passed these criteria.

1- Standard Curve Rank	1 = Good quality – samples within linear section on standard curve. 2 = Moderate quality – samples spread across the linear section on standard curve. 3 = Poor quality – not on linear section at all.
2- Intra-assay CV	Intra-assay CV (%) for assay standards 1-4, CV<15% accepted.
3- Inter-assay CV	Inter-assay CV (%) for in-house pooled sample (master mix), CV<20% accepted.
4- Missing data	Missing data defined as samples that could not be reliably extrapolated from the standard curve. (1) OD values outside the quantifiable range. (2) Technical failure resulting in no OD value being generated.

Competitive ELISA: complement Factor H related protein 1 (FHR-1)

For FHR-1, a competitive ELISA was utilised. Briefly, 50µL of standards and diluted plasma (1 in 400) were added to a pre-coated 96 well micro plate pre-coated. Immediately, 50µL of the HRP-conjugate (FHR-1) secondary antibody is added to each well and then incubated for 1 hr at 37˚C. The plate was then washed 5 times with 200µL of wash buffer by an automated plate washer, allowing standing for 2 minutes after each wash. Then, 90µL of TMB substrate was added to each well and incubated at 37˚C and after 20 mins 50µL stop solution was added. FHR-1 plates were measured in the same fashion as a sandwich ELISA.

With a competitive ELISA, analyte concentration is measured by noting the extent of the signal reduction. If there is a high concentration of antigen in the sample, then there will be a significant reduction in signal output of the assay. Conversely, if there is little analyte in the sample, there will be minimal reduction in signal and the HRP-

conjugate with bind to the capture antibody. A competitive ELISA is often used when only one antibody is available to the antigen of interest or when the analyte is small and cannot be bound by two different antibodies. On the other hand, a sandwich ELISA is considered to be highly specific as two antibodies are used to capture and detected the antigen and therefore more suitable for complex samples.

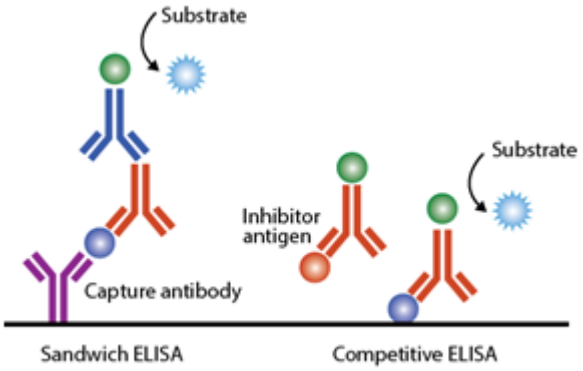

Figure 2-9: A schematic diagram illustrating the differences between a sandwich and competitive ELISA. The sandwich ELISA measures an analyte by two primary antibodies – the capture antibody and the detection antibody. For a competitive ELISA unlabelled antigen from the sample and the HRP labelled antigen compete for binding to the capture antibody. A decrease in signal from purified antigen indicates the presence of the antigen in samples.

2.4.8 Statistical analysis

All statistical analyses were performed in SPSS (version 21) and R statistical packages. For Logistic and Linear regressions, age, gender and presence of *APOE* ε4 allele were used as standard confounding factors upon the data (covariates).

For LC-MS/MS discovery data in AIBL-1, each protein group MW isoform underwent four statistical tests for either correlation with ^{11}C-PiB SUVR (Spearman's Rank Correlation and Linear Regression) or to assess association with ^{11}C-PiB SUVR as an extreme endophenotype (PiB-, PiB+; Mann Whitney-U and Logistic Regression). These statistical tests were performed on both median and mean protein roll up methods (PRQ-1; Step 3). Benjamini-Hochberg *Q* values were calculated as a multiple testing correction.

For the ELISA analysis of technical replication (AIBL-1) and validation (UCSF) studies, data outliers were excluded (±3 standard deviations). Protein values were $\log_{10}$ transformed to achieve normal distribution. Again, protein values were assessed for their association with ^{11}C-PiB SUVR as a continuous and binary measure. Only Linear Regression and Logistics Regressions were performed with a fourth covariate, assay plate, being added. PET scanner type was added as an additional covariate for only the UCSF data. Multiple testing corrections were calculated using Benjamini-Hochberg *Q* values. The package 'CARET' [458], with default parameters, was used to perform Random Forest and partitioning multivariate classifications. The package 'ROCR' [459] was used to calculate classifier performance.

For the ELISA analysis in the EMIF-AD cohort there was no confounding affect of age or gender. However, EMIF-AD is a multi-centre cohort and therefore, protein values were adjusted by a Generalised Linear Model (GLM) for cohort differences as well as assay plate difference. The residuals produced from the GLM, for each individual sample, were added to mean of raw protein value. Protein values were assessed with CSF $A\beta_{1\text{-}42}$, p-tau, t-tau and CSF algorithm as continuous and endophenotype binary measures. *APOE* ε4 was added as a covariate separately. The identical protein model developed in AIBL-1 and UCSF was tested in EMIF-AD. The package 'CARET' was used to create confusion matrices to calculate negative predictive value (NPV), positive predictive value (PPV), sensitivity and specificity. Pathway analysis was performed using the Database for Annotation, Visualization and Integrated Discovery (DAVID, http://david.abcc.ncifcrf.gov/) [460-461], based on Kyoto Encyclopedia of Genes and Genomes (KEGG) annotations [462].Methodology for Chapter 4

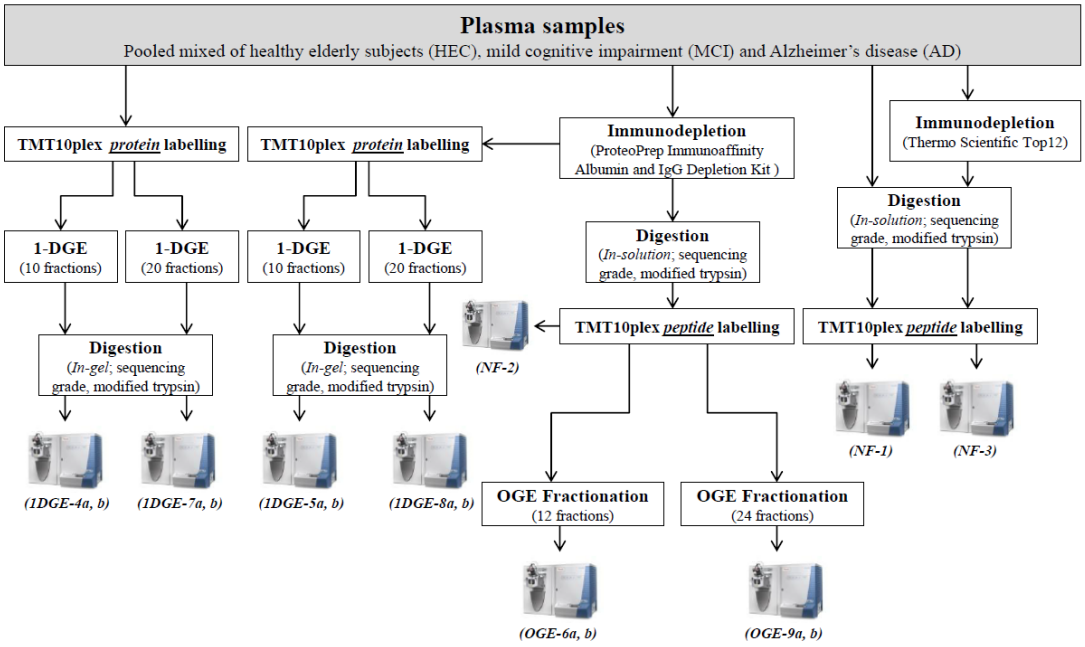

Figure 2-10: Schematic flow diagram represents the 15 proteomic workflows investigated to establish a workflow to detect a broad range, low abundant and brain derived plasma proteins circulating within plasma.

2.4.9 Immunodepletion

Two commercially available immuodepletion kits were investigated: The ProteoPrep® Immunoaffinity Albumin and IgG Depletion Kit (PROTIA, Sigma-Aldrich, Saint Louis, USA) and Pierce™ Top12 Abundant Protein Depletion Spin columns (Pierce Biotechnology, Rockford, USA).

ProteoPrep® Immunoaffinity Albumin and IgG Depletion

The depletion spin columns were brought to RT and 30µL (~1.8mg) of plasma was diluted in 70µl of equilibration buffer before performing the depletion process. After column preparation and equilibration (as per manufactures instructions), diluted plasma was loaded onto the column and incubated for 15 minutes at RT. Samples were then collected by centrifugation 8000 x *g* for 60 seconds. The eluate collected was then re-applied to the medium bed and incubated for a further 10 minutes. The twice depleted plasma was centrifuged again at 8000 x *g* for 1 minute. Finally, 125µl of equilibration buffer was added to the medium bed and centrifuged for 60 seconds to wash through any remaining unbound proteins from the spin column. Total protein quantification of the "twice depleted" sample was determined by a

NanoDrop™ 2000 Spectrophotometer for further downstream fractionation or analysis.

Pierce™ Top12 Abundant Protein Depletion

The Pierce™ Top12 Abundant Protein Depletion spin columns was utilised to remove 12 highly abundant proteins from plasma to assist the identification and quantitation of low abundant proteins

Table 2-3: The Top 12 proteins removed by the Pierce™ Top12 Abundant Protein Depletion spin columns

alpha-1-Acid glycoprotein (AGP)	fibrinogen
alpha-1-Antitrypsin (α1AT)	haptoglobin
alpha-2-Macroglobulin (α2m)	Immunoglobulin A (IgA)
albumin	Immunoglobulin G (IgG)
apolipoprotein A-I (apoA1)	Immunoglobulin M (IgM)
apolipoprotein A-II (apoA2)	transferrin

The depletion spin column was brought to RT and 10µL (~600µg) of plasma was added directly to the resin slurry. The column was inverted several times until the resin was completely suspended in the solution. The sample was then further incubated for 60 minutes on an end-over-end mixer at RT. The column was then centrifuged for 2 minutes at 1000 x *g* and the flow through collected in separated tube. The sample, depleted of the top 12 proteins, is in a solution of 10mM PBS, 0.15M NaCl, 0.02%. The sample was frozen and vacuum dried to completion for further downstream fractionation or analysis.

2.4.10 Tandem Mass Tag 10plex (TMT10plex) labelling

TMT10plex labelling utilise the same reporter regions as TMT6plex however an elemental isotope different of 0.0063 Da in tags 127, 128, 129 and 130 created four additional tags for multiplexing.

TMT10plex protein labelling

The process of TMT10plex protein labelling followed the same technical process as TMT6plex protein labelling (see Chapter 2.4.1). Each sample was randomly assigned amine-reactive TMT10plex tag (TMT-127N, TMT-127C, TMT-128N, TMT-128C, TMT-129N, TMT-129C, TMT-130N, TMT-130C and TMT-131) with TMT-126 assigned as a static study reference.

TMT10plex peptide labelling and in-solution digests

TMT10plex peptide labelling commences following in-solution tryptic digestion. Briefly, for in-solution digests, 100µg of each plasma sample was initially dried to completion and incubated with 100mM TEAB and 0.1% SDS [w/v]. Reduction and alkylation was achieved in 1mM tris (2-carboxyethyl) phosphine (TCEP) for 1 hour at 55˚C followed by incubation in 7.5mM iodoacetamide (IAA). Proteins were digested overnight in 4µg trypsin (sequencing grade) reconstituted in 100mM TEAB. TMT10plex reagents were reconstituted in ACN then added to the appropriate sample to reach a final concentration of 15mM and incubated for 1 h at RT. Plasma samples were treated with 5% hydroxylamine (0.25% [w/v]) and incubated at RT for 15 minutes. After combining all samples together, the samples were incubated at RT for a further 15 minutes. Again, each sample was randomly assigned amine-reactive TMT10plex tag with TMT-126 assigned as the study reference.

2.4.11 One dimensional gel electrophoresis (1DGE)

All information on the 1DGE procedure is outlined in Chapter 2.4.2. After destaining**,** gel lanes were cut manually and frozen at -80˚C. For methods that required 10 fractions (1DGE-4 and 1DGE-5) or 20 fractions (1DGE-7 and 1DGE-8) gel pieces were excised to maximise gel bands displayed by protein staining and was kept uniform across all replicates (Figure 2-11, Figure 2-12, Figure 2-13 and Figure 2-14). The process of enzymatic digestion (2.5.3) and peptide extraction (2.5.4) was identical between all methods and has been previously described.

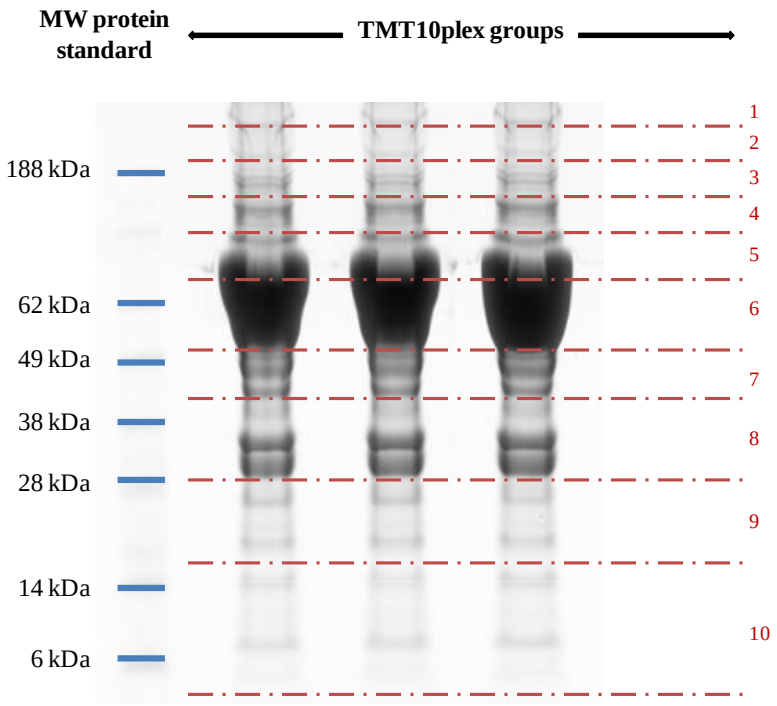

Figure 2-11: A schematic diagram demonstrating the fractions excised for enzymatic digestion for undepleted TMT10plex groups with 10 fractions (1DGE-4).

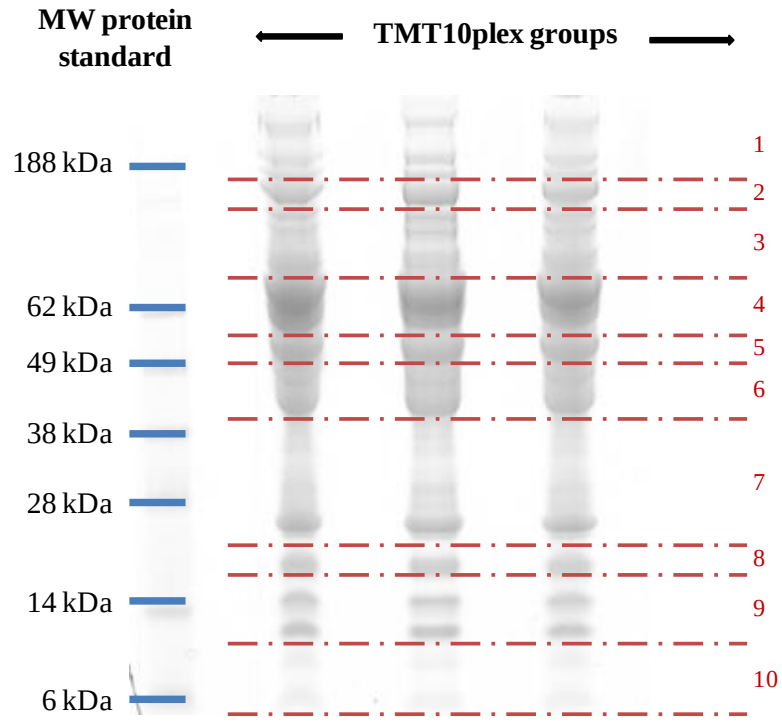

Figure 2-12: A schematic diagram demonstrating the fractions excised for enzymatic digestion for Top2 depleted TMT10plex groups with 10 fractions (1DGE-5).

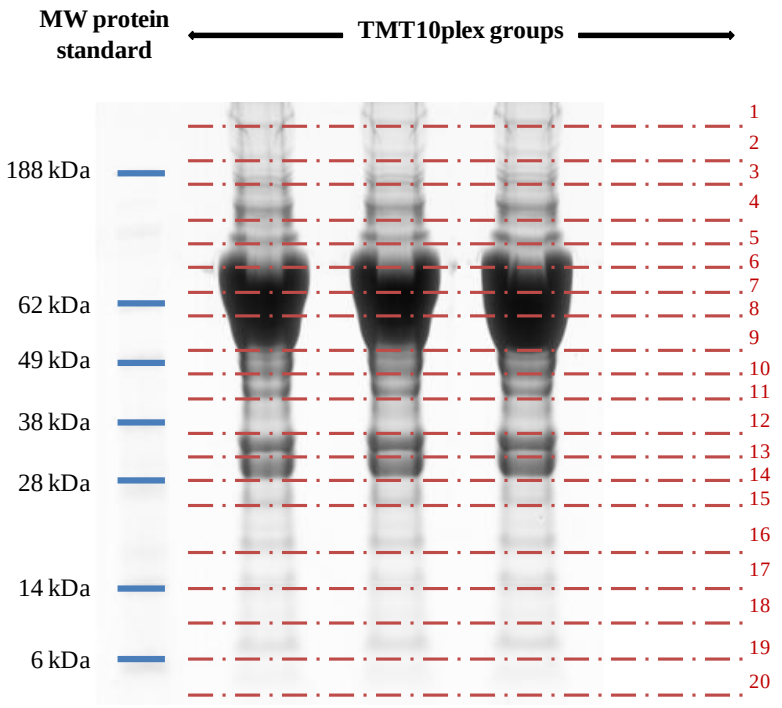

Figure 2-13: A schematic diagram demonstrating the fractions excised for enzymatic digestion for undepleted TMT10plex groups with 20 fractions (1DGE-7).

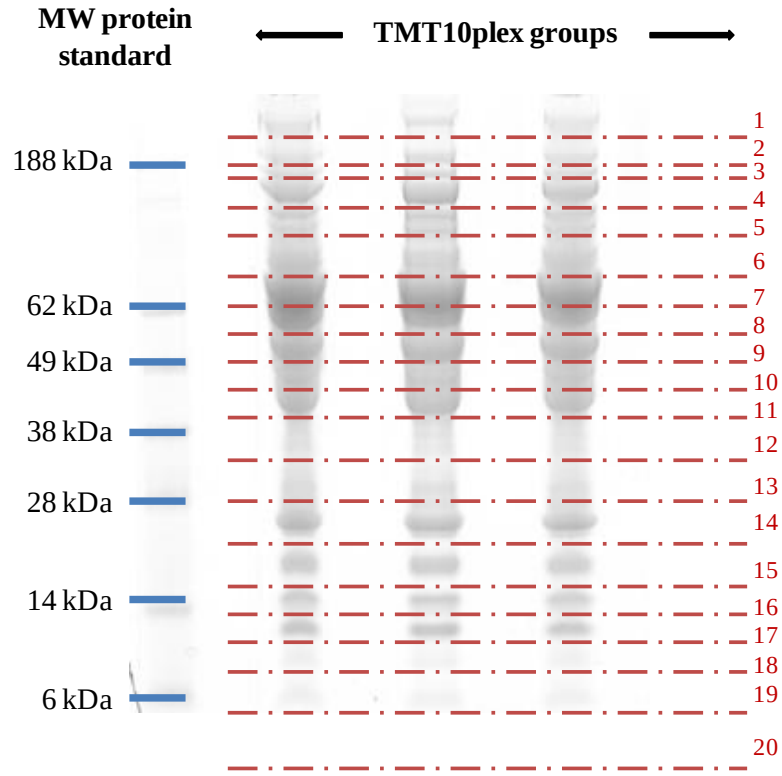

Figure 2-14: A schematic diagram demonstrating the fractions excised for enzymatic digestion for Top2 depleted TMT10plex groups with 20 fractions (1DGE-8).

2.4.12 OFFGEL (OGE) fractionation

OFFGEL fractionation (OGE) technology enables separation based on immobilised pH gradient (IPG) strips. Unlike the traditional workflow of gel electrophoresis, protein/peptides present in the liquid phase are forced to migrate through the gel from one compartment to another until reaching their isoelectric point (pI). These molecules are then retained in the solution as their net charge equals zero and therefore enabling the recovery of protein/peptides from the liquid phase (Figure 2-15).

Isoelectric point-based (pI) OGE for peptides was carried out as specified by manufacturer's instructions. In brief, 1mg of TMT10plex labelled peptides were dried to completion and re-suspended in OGE stock solution (1.25X). Prior to separation, each IPG strip was rehydrated with 40µL (per well) OGE rehydration solution for 15 minutes. Peptides were separated using both a 12-multiwell and 24-multiwell format encompassing IPG strips (pH 3-10, 13cm; pH 3-10, 24cm), focused for 50kVh with a maximum current of 50µA and maximum voltage of 4500 V. Upon completion peptide fractions were held at 500 V and current of 20µA prior to collection. Liquid fractions (12 and 24) were collected into separate Eppendorf tubes (passive recovery). To extract larger peptides retained in the IPG strips, 150µL of 50% ACN/0.1% FA was added in each compartment and incubated for 30 minutes. The solution (second recovery) was retrieved and added to extract from the passive recovery. Peripheral fractions (1-3 and 22-24) were combined to emulate the number of fractions as included in 1DGE methods and each fraction was cleaned by a SOLA HRP solid phase extraction cartridge (Thermo Scientific). Each fraction was vacuum-dried to completion and re-suspended in 2% ACN/0.1% FA at concentration of 0.5µg/µL for MS analysis.

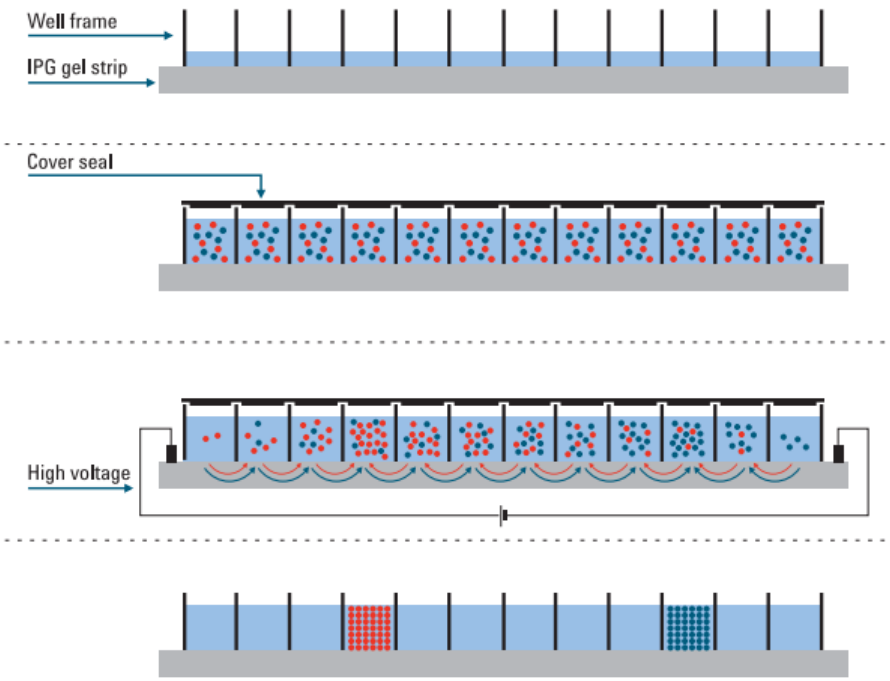

Figure 2-15: Schematic diagram to demonstrate the process of OFFGEL fractionation. Protein/peptide sample is evenly distributed across all compartment of the IPG strip. In response to high voltage, molecules move through the compartment until their isoelectric point is found. Protein/peptides are removed in a liquid fraction ready for LC-MS/MS analysis.

Diagram has been adapted with permission from Agilent Technologies.

2.4.13 Liquid Chromatography – Tandem Mass Spectrometry acquisition

All LC-MS/MS acquisition was performed in an identical manner, regardless of proteomic workflow employed. As previous (Chapter 2.4.5), chromatographic separation was achieved by a two column configuration and mass spectra were acquired on a Thermo Scientific LTQ Orbitrap Velos instrument controlled through Tune 2.6.0 and Xcalibur 2.1 (Thermo Scientific). There were two major modifications made to the LC-MS/MS acquisition that differed from the methodology used in Chapter 2.4.5.

1. Peptides were resolved using a **modified linear gradient** of 0.1% FA in ACN (10% to 65% over 115 minutes) through a 0.075 × 150 mm C18 analytical column (Thermo Scientific) at a flow rate of 300nL/min (Figure 2-16).

2. A HCD Top10 method was used; survey full scan MS spectra (from *m/z* 400–2,000) were acquired in the Orbitrap system with resolution **60,000** after accumulation to an AGC ion injection target value of $1x10^6$ (500ms max injection time). The higher resolution was needed for the incorporation of TMT10plex.

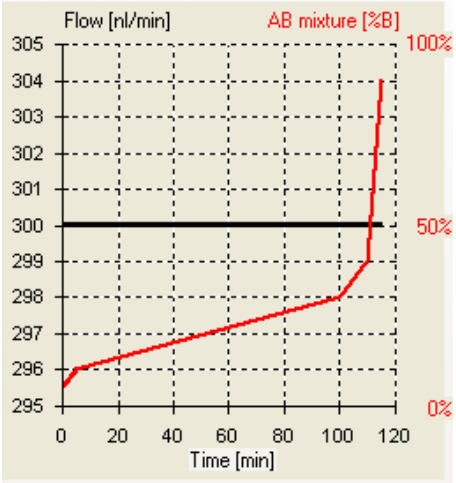

Time	Duration	Flow [nl/min]	%B
00:00	N/A	300	5
05:00	05:00	300	10
100:00	95:00	300	30
110:00	10:00	300	40
115:00	05:00	300	90

Figure 2-16: Method of chromatographic separation for TMT10plex labelled peptides. A modified linear gradient of 0.1% FA in ACN (10% to 65% over 115 minutes) was applied to peptide extracts from all methodologies.

2.4.14 Computational Mass Spectrometry and statistical analysis

Raw data files produced in Excalibur software (Thermo Scientific) were processed using Proteome Discoverer (ver. 1.4) to determine peptide identification and quantitation. All methods underwent a sequential database searching, where all individual fraction(s) were processed as separate entities and merged to create one file. In addition, methodologies with multiple fractions (4-9) also underwent MudPIT database searching where all fractions were merged prior to pre-processing indentified as 4b, 5b, 6b, 7b, 8b and 9b (Figure 2-10). Within Proteome Discoverer, mass spectra were searched against two sequence databases side-by-side (Figure 2-17). For Mascot based searching against the uniprot/Swiss-prot database (ver. 4.11) taxonomy was set to human and precursor and fragment mass tolerances were set to

±5ppm and 0.5Da respectively. Dynamic modifications included TMTPlex modification of the lysine residue (TMT (K)), TMTPlex modification of the peptide N-Terminus (TMT (N-Term)), deamidation (NQ) and oxidation of the methionines. Additionally, carbamidomethylation of cysteine residues was set as a fixed modification and three missed cleavages were allowed. Sequest HT searching parameters were identical to Mascot. Validation of merged Mascot and Sequest database results were conducted by Percolator at FDR of 0.05.

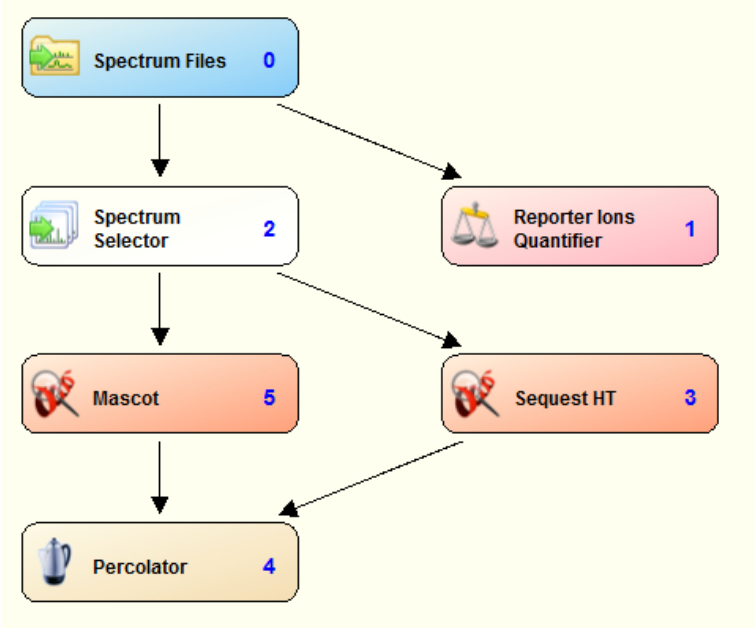

Figure 2-17: Proteome Discoverer workflow for database searching of MS/MS spectra for methods in Chapter 4 and 5. Two database search engines were utilised (Mascot and Sequest HT) with identical parameters.

LC-MS/MS peak lists with TMT reporter raw intensities were exported from Proteome Discoverer. Each methodology reported the number of proteins groups, unique peptides, PSMs (peptide spectral matches) and spectral yield (unique peptides/PSMs) at 1% and 5% FDR to assess the number of indentified features for each methodology.

To assess the depth of proteome coverage, each workflow was compared with the Plasma Proteome Database (PPD, www.plasmaproteomedatabase.org) that has reported the concentrations of >1,200 proteins [463]. Protein concentrations in PPD matched with our LC-MS/MS peak lists were extracted and $\log_2$ transformed to

achieve a normal distribution. In SPSS (ver. 22), an Analysis of variance (ANOVA) was used to compare the mean differences of protein concentration between each method and illustrated with a box plot (to demonstrate range) with vertical bins (to demonstrate frequency) was created in R. The Human Protein Atlas (HPA) (http://www.proteinatlas.org/; download date from HPA 20/10/2016) was utilised to assess brain-derived proteins (BDP) present within plasma. The "Tissue Enriched" category in HPA (>five-fold increased expression in the cerebral cortex compared with all other tissues) was used as an indication of a BDP and compared with our LC-MS/MS plasma protein list. Spectra of LC-MS/MS plasma proteins that matched in HPA were manually assessed to confirm the database identification (same criteria as 2.4.6).

For TMT quantification, a threshold of >50 counts was applied to all PSM (as applied by PRQ-1), therefore <50 was considered to be background noise and removed as a TMT assignment. Any PSM with >4/10 TMT reporter channels present was also removed from the TMT analysis. The assessment TMT quantification for each method was reported as a percentage of total identified PSMs that could be quantified by TMT.

2.5 Methodology for Chapter 5

The LC-MS/MS based proteomic workflow utilised in this study is outlined in Figure 2-18. This method has been shown to produce a superior coverage of the plasma proteome over other conventional proteomic methodologies (Chapter 4). The process of immunodepletion, enzymatic digestion, OGE fractionation and LC-MS/MS acquisition were perform as described in either Chapter 2.5.

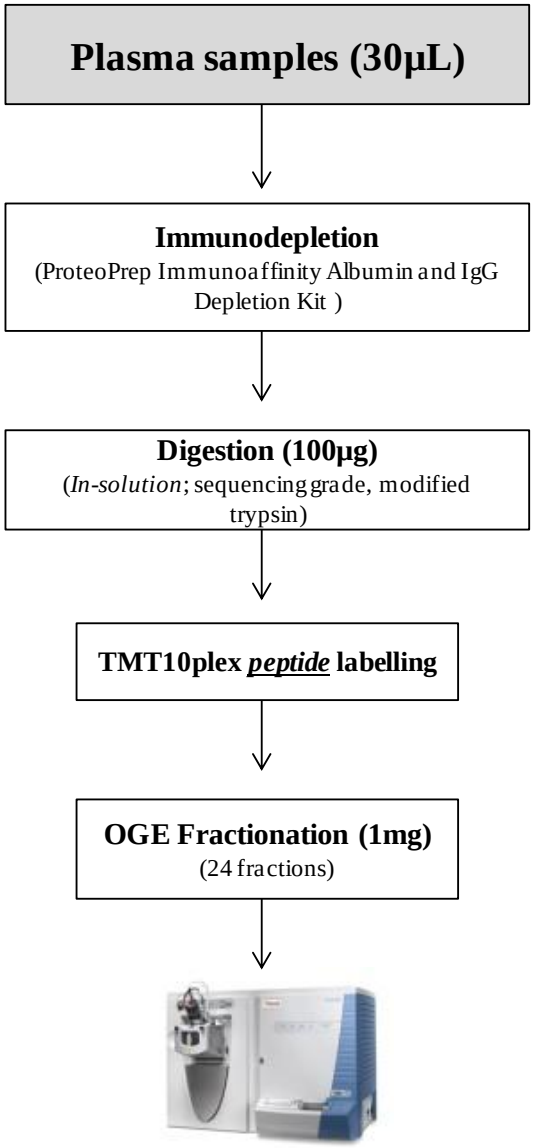

Figure 2-18: Methodology workflow employed in to examine plasma samples from AIBL-2 and KARVIAH in Chapter 5.

2.5.1 Tandem Mass Tag 10plex (TMT10plex) peptide labelling

TMT10plex peptide labelling was performed identically as described above. In a different manner to previous TMT methodologies, Chapter 5 employed a dynamic study reference. Previously, a TMT study reference had been made static, usually TMT-126 being assigned as the study reference channel. Here, the study reference channel was randomly assigned in each TMT10plex group and therefore reducing any bias toward a chemical label.

2.5.2 Computational Mass Spectrometry

Raw data files produced in Excalibur software (Thermo Scientific) were processed using Proteome Discoverer (ver. 1.4) to determine peptide identification and quantitation as previously described (Figure 2-17). The use of peptide isoelectric focusing based fractionation means that protein MW isoforms cannot be studied. Therefore, for each TMT10plex the database search results for all OGE fractions can be merged in one file for analysis. This requires a differing but more simplified script for LC-MS/MS pre-processing than PRQ-1.

As with PRQ-1, this modified script (PRQ-2; Supplementary Material 2) performs median ratio normalisation and calculates within TMT10plex ratios for each peptide. However, this is performed across all fractions simultaneously rather than within each fraction. PRQ-2 then continues to derive within TMT10plex protein level data from all corresponding peptide scores and then collects protein scores across all TMT10plex experiments. A protein matrix table was then produced with all identified protein groups and their corresponding TMT scores for each individual within the study. This was done so that "missingness" and technical variability could be assessed by principle component analysis (PCA).

2.5.3 Statistical analysis

All statistical analyses were performed in SPSS (version 22) and R statistical packages. TMT ratios were $\log_{10}$ transformed to achieve normal distribution. Only protein groups extracted by PRQ-2 with >50% participant data, BDPs from HPA and specific proteins of interest in disease pathogenesis were extracted from the protein

matrix table for further analysis. Covariates including age, gender, cohort and technical variables (TMT10plex group, TMT10plex label, OGE fractionation date, depletion date and MS analysis date) were investigated. We found that a large proportion of protein groups were affected by these covariates and therefore a GLM was used to adjust the data. The function "glm" in R package "STATS" was used to performed this. All subsequent analysis was performed on residuals from GLM adjusted data.

Univariate analysis was performed in SPSS (version 22). A Mann Whitney-U test was performed to examine the association of all protein group GLM adjusted data with *APOE* genotype. Spearman's Rank Correlation was used to examine associations of protein groups with PET SUVR as a continuous measure. Furthermore, a partial correlation (adjusting for *APOE* genotype) was performed on protein groups found to be significant from this analysis that were also associated with *APOE* genotype. Protein groups were also examined individually in an endophenotype group-wise analysis (Aβ- versus Aβ+) using a Mann Whitney-U test. A modified GLM, including *APOE* genotype, was performed on protein groups found to be significantly associated with both *APOE* genotype and group-wise analysis. Benjamini-Hochberg *Q* values were calculated as a multiple testing correction. Classification analysis was performed in R. Functions "svm" and "glmnet" from packages "MASS", "e1071" and "glmnet" were utilised. Missing values were imputed by using the average score of the protein group. Protein groups were assessed by LASSO (Least Absolute Shrinkage and Selection Operator) with 10,000 iterations. Supervised learning models (Support Vector Machine (SVM)) were built using protein groups in the AIBL-2 dataset and assessed by 100 repeats of a 5-fold cross validation. The performance of a classifier was assessed in KARVIAH to test prediction accuracy.

CHAPTER 3

BLOOD PROTEIN PREDICTORS OF NEOCORTICAL AMYLOID PATHOLOGY FOR ENRICHMENT IN THERAPEUTIC TRIALS

3.1 Introduction

The diagnosis of AD can only be confirmed, with certainty, by histological examination of brain tissue at autopsy. This inspection should demonstrate substantial evidence of the classical pathological hallmarks of AD. Although an age-related disease usually affecting people over the age of 65 it is believed the accumulation of Aβ plaques begins 15-20 years prior to clinical presentation [233] and plateaus when cognitive, functional and behavioural decline occurs [464]. As elevated brain Aβ is an important risk factor for AD, it has become critical to identify individuals at the early stages of Aβ deposition to recruit into clinical trials of potentially disease-modifying therapeutics.

At present neuroimaging and CSF biomarkers are the accepted standards used to provide evidence of on-going AD pathophysiology related to Aβ plaques. ^{11}C-PiB coupled with PET is widely used in research in measuring *in vivo* Aβ deposition as its uptake in AD correlates with Aβ plaques measured neuropathologically in the same brains [261]. The availability of longer lived ^{18}F-labelled Aβ PET tracers, such as Flutemetamol [266], Florbetapir [269] and ^{18}FBB [465] could foster wider utilisation in clinical use [466]. Several large studies have shown that ^{11}C-PiB PET could discriminate between AD and non-Aβ dementias [260, 448, 451]. Some, but not all [467-468], studies also show that Aβ deposition as measured using ^{11}C-PiB PET either predicts decline in cognitive measures or tracks with such [233, 257].

Disease modifying therapeutics that are being developed target primarily Aβ generation, deposition or clearance [469]. Recent Phase III trials targeting Aβ reported that approximately 20% of trial participants actually had little or no Aβ when

studied later using retrospective PET imaging (Suspected Non Amyloid Pathology; SNAP) [218]. This is a concern for such trials when a large minority of trial subjects fail to have the primary target pathology. A solution is to use Aβ PET imaging to ensure primary target pathology for patient stratification or recruitment. The first study to use this strategy is the anti-Aβ in Asymptomatic AD (A4) prevention trial [470]. In A4, the screen failure rate is anticipated to be even higher (~66%) due to the use of only asymptomatic subjects. The great expense of the anticipated Aβ PET screen failure rates for clinical and prevention anti-Aβ trials means that a blood test, with even relatively low predictive accuracy for neocortical Aβ burden (NAB), has the potential to greatly reduce costs. This would work by applying the blood tests to large numbers of potentially eligible subjects and only performing neuroimaging or CSF measures on those whose blood tests are positive. This would reduce the screen failure rates as well as reducing costs and recruitment time as the blood test would be inexpensive comparatively and more widely accessible. Therefore, a blood-based measure that correlates with NAB would be of considerable value as an enrichment filter for clinical trials.

The obvious blood candidate biomarker of NAB would be Aβ itself but numerous studies, examining the correlation between Aβ plasma levels and NAB, have produced conflicting results [377]. There has been considerable effort in the search for AD blood-based biomarkers. Most studies use a "case versus control" design, based on a clinical diagnosis of AD as determined by medical history, cognitive assessments and clinical examination. This classical approach has identified a large number of putative plasma biomarkers. However, such approaches are intrinsically flawed in the context of AD where a considerable proportion of cognitively unimpaired controls will be in the prodromal phase of AD, e.g. asymptomatic but with elevated NAB. An approach to overcome this is to use a non-apparent measure of disease activity (endophenotype paradigm). The endophenotype approach is increasingly being adopted for a range of modalities related to AD [357, 366, 370, 430, 432, 471]. More recently, blood-based biomarkers of NAB, as measured by ^{11}C-PiB PET, have been reported by utilising the Rules-Based Medicine (RBM) panel of 190 analytes [436-437]. In a different approach, 2DGE coupled with Mass Spectrometry (MS) was utilised to identify protein spots associating with NAB in an unbiased fashion [373]. This study identified 6 proteins from spots associated with NAB,

including ApoE and CC3 which were independently replicated in the Kiddle and colleagues study [436]. 2DGE is a well established technique for blood biomarker research and offers many advantages. 2DGE enables the separation of proteins in a complex sample according to charge (pH/pI) in the first dimension followed by molecular weight (MW) in the second dimension. However, it is restricted by a lengthy procedure with poor reproducibility that can only identify a small number of "candidate spots" in limited sample sets.

In this study we employed a methodology (Figure 3-1) that combines the unbiased approach of gel-based proteomics (1DGE) with high-throughput multiplex technology (TMT). Isobaric labelling is a critical step in LC-MS/MS discovery primarily because of its application in measuring multiple samples in a single acquisition. This is fundamental to drive down cost, reduce analytical time and increase sample size consequently improving statistical power. Coupled to high-resolution MS instrumentation this method has enabled the identification of several hundred proteins, comparable to most panel based arrays, without losing the key advantages of unbiased gel-based discovery. This is the first application of this approach to identify blood-based biomarkers of NAB, and was applied to a subset of patients from the AIBL-1 cohort with either high or low NAB. These results were then tested in independent cohorts differing measures of NAB (neuroimaging and CSF).

3.2 Aims

To use 1DGE, isobaric TMT protein labelling and LC-MS/MS to identify proteins predictive of neocortical Aβ burden (NAB). An extreme endophenotype approach has been employed to stratify participants as "high Aβ (PiB+)" or "low Aβ (PiB-)" as determined by ^{11}C-PiB PET. Replication of LC-MS/MS candidates by an orthogonal platform was performed in the same discovery cohort (technical replication) to confirm the proteins most predictive of NAB. The most associated candidates were further examined in two independent cohorts (UCSF and EMIF-AD) that reflect NAB by differing surrogate measures (1) ^{11}C-PiB PET and (2) CSF $A\beta_{1-42}$ and other core CSF biomarkers.

3.3 Methodological Overview

The LC-MS/MS proteomic workflow utilised in this study is outlined in Figure 3-1. The detailed methodological protocols for each procedure are outlined in Chapter 2.4.

This MS-based proteomic workflow utilises TMT6plex protein isobaric tagging for LC–MS/MS based quantification. 1DGE was utilised for the pre-fractionation of TMT6plex labelled proteins prior to LC-MS/MS acquisition. Each protein gel was divided into 10 equal fractions, digested and resulting peptides were extracted for LC-MS/MS analysis. This was performed on 16 TMT6plex groups, which included 78 individual from the Australian Imaging, Biomarkers and Lifestyle Flagship Study of Ageing (AIBL-1). All peptides extracts were resolved using on a liquid chromatography (LC) linear gradient for 115 minutes through a C18 analytical column and mass spectra were acquired on a LTQ Orbitrap Velos instrument.

Candidate markers discovered by LC-MS/MS underwent technical replication (AIBL-1 cohort) and further replication and validation (UCSF and EMIF-AD cohorts) using commercially available ELISAs (Table 2-1).

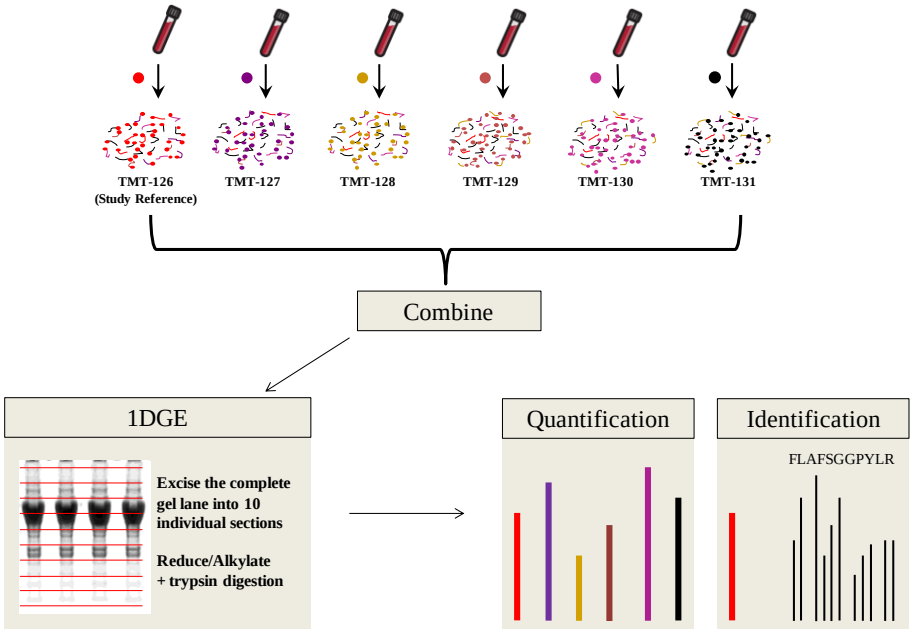

Figure 3-1: Methodological Overview: Schematic flow diagram represents the LC-MS/MS proteomic workflow applied to the discovery cohort (AIBL-1) in Chapter 3.

3.4 Results

3.4.1 Demographic characteristics

Discovery and technical replication cohort (AIBL-1)

Participants (n = 78) were selected from the Australian Imaging, Biomarkers and Lifestyle Flagship Study of Ageing (AIBL-1) imaging sub-cohort previously described (Chapter 2.1.1) and by Ellis and colleagues [446]. These individuals must have undergone baseline ^{11}C-PiB PET, cognitive assessment and *APOE* genotyping to be included in the study. A standardised uptake value ratio (SUVR) was calculated and a cut-off of 1.3 was used to classify subjects as belonging to Aβ positive (PiB+) or Aβ negative (PiB-) groups. Subjects were selected by an extreme endophenotype strategy and enriched for clear cases of PiB PET negativity and positivity (Figure 3-2). Table 3-1 summarises the full demographic characteristics of subjects selected for the AIBL-1 cohort.

Table 3-1: Subject demographics for participants selected for the AIBL-1 cohort.

	Low Neocortical SUVR (PiB-)	**High Neocortical SUVR (PiB+)**	***P* value**
Number of subjects (*n*)	38	40	
^{11}C-PiB PET SUVR (mean (S.D))	1.11 (0.06)	2.34 (0.33)	2.4×10^{-25}
Gender; females (*n* (%))	18 (47%)	20 (50%)	0.830
Age in years (mean (S.D))	75.8 (6.53)	80.9 (8.22)	0.004
Clinical diagnosis (*n* (%))	HEC: 13 (34%)	HEC: 6 (15%)	0.004
	SMC: 18 (47%)	SMC: 13 (40%)	
	MCI: 7 (19%)	MCI: 16 (30%)	
	AD: 0 (0%)	AD: 6 (15%)	
APOE ε4 carrier (*n* (%))	14 (37)	25 (63)	0.360
MMSE (mean (S.D))	28.3 (1.8)	26.8 (4.1)	0.038

Abbreviations: HEC, Healthy elderly control; SMC, Subjective memory complaints; MCI, Mild cognitive impairment; AD, Alzheimer's disease; SUVR, Standardized uptake values ratio; S.D; Standard deviation; MMSE, Mini mental state examination.

Subjects were matched for gender and *APOE* ε4 but a significant difference was observed between the two groups for age, diagnosis and consequently MMSE.

Figure 3-2 shows the distribution of ^{11}C-PiB PET SUVR values across selected subjects from the AIBL-1 imaging cohort. This histogram displays the two distinct populations of ^{11}C-PiB PET SUVR values included in the study. The PiB- group SUVR range from 0.95–1.21 whereas the more diverse PiB+ group range from 1.82–3.18.

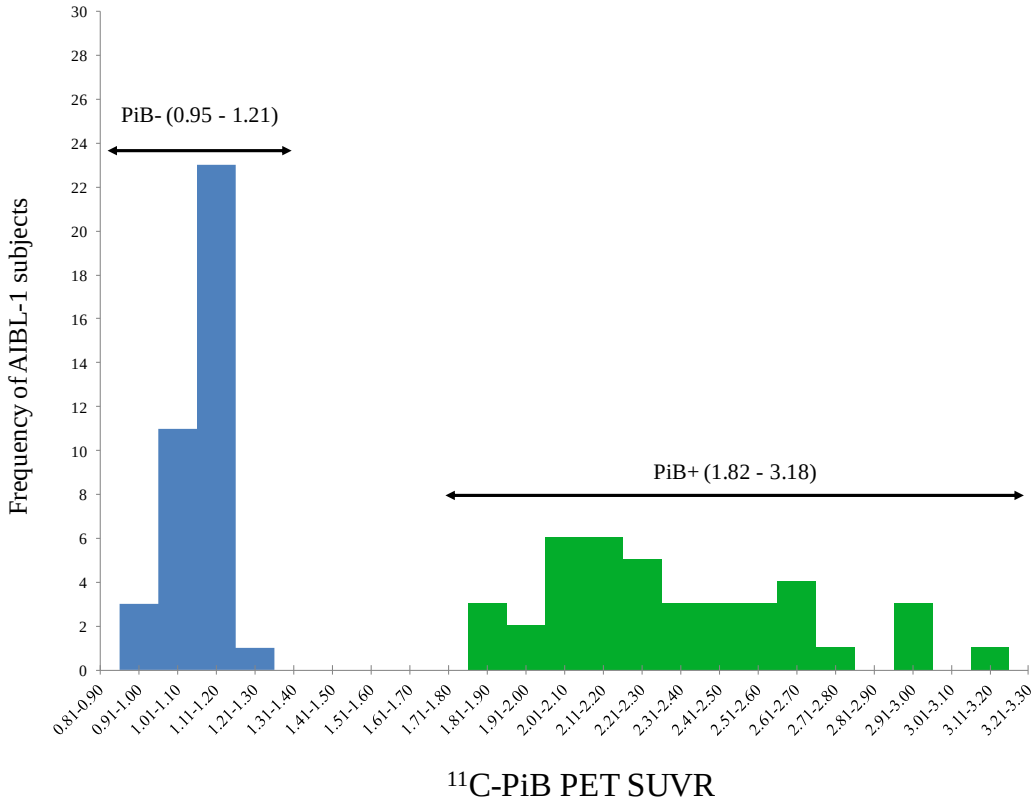

Figure 3-2: Histogram displaying the distribution of ^{11}C-PiB PET SUVR values for 78 participants selected from the AIBL-1 imaging cohort.

Aβ endophenotype replication cohort (UCSF)

The replication cohort consisted of plasma samples from participants (*n* = 79) enrolled in the University of California, San Francisco (UCSF) memory and ageing centre (Table 3-2) which has been previously described (Chapter 2.1.2). All subjects underwent *APOE* genotyping, neurological and cognitive assessments [451], as well as plasma collection and storage as previously described [452]. Clinical diagnoses of AD, FTD and MCI were made by consensus applying standard research criteria [155, 472-473].

Although a mixed diagnosis cohort that differs in dementias from AIBL-1, the UCSF cohort was utilised as a replication of Aβ positivity and not clinical diagnosis. All subjects underwent ^{11}C-PiB PET at Lawrence Berkeley National Laboratory on either a Siemens ECAT EXACT HR PET (*n* = 70) or Biograph Truepoint 6 PET/CT (*n* = 9) [262]. Scans were also visually rated as PiB+ or PiB- by two experienced physicians blinded to clinical data [262]. The UCSF endophenotype design differed to AIBL-1 by having an ^{11}C-PiB PET SUVR cut-off at 1.5. Figure 3-3 shows the distribution of ^{11}C-PiB PET SUVR values and visual classification of ^{11}C-PiB PET images in the UCSF cohort. There is a relatively good concordance between the two assessments, with only three subjects visually classified as PiB+ having an SUVR of <1.5 and only one subject visually classified as PiB- with an SUVR of >1.5. Three UCSF subjects did not have quantifiable SUVR values recorded and are not included in Table 3-2; however a visual examination was completed on these subjects (1 = PiB-, 2 = PiB+). As with AIBL-1, gender did not affect the two PiB groups however there was a significant difference between *APOE* genotype as well as diagnostic status and MMSE. There was no significant difference between ages (Table 3-2).

Table 3-2: Subject demographics for participants selected from the UCSF cohort.

	Low Neocortical SUVR (PiB-)	**High Neocortical SUVR (PiB+)**	***P* value**
Number of subjects (*n*)	47	32	
^{11}C-PiB PET SUVR (mean (S.D) [missing])	1.2 (0.12) [1]	2.2 (0.35) [2]	4.2×10^{-16}
Gender; females (*n* (%))	18 (38%)	14 (44%)	0.650
Age in years (mean (S.D))	65 (8.8)	64 (8.4)	0.610
Clinical diagnosis (*n* (%))	HEC: 2 (4.3%)	HEC: 1 (3.1%)	1.9×10^{-10}
	MCI: 1 (2.1%)	MCI: 1 (3.1%)	
	AD: 2 (4.3%)	AD: 23 (72%)	
	FTD: 42 (89.3%)	FTD: 7 (21.8%)	
APOE ε4 carrier (*n* (%))	8 (17%)	13 (41%)	0.036
MMSE (mean (S.D))	26 (4.3)	21 (6.9)	0.001

Abbreviations: HEC, Healthy elderly control; MCI, Mild cognitive impairment; AD, Alzheimer's disease; FTD, Frontotemporal dementia; SUVR, Standardized uptake values ratio; S.D; Standard deviation; MMSE, Mini mental state examination.

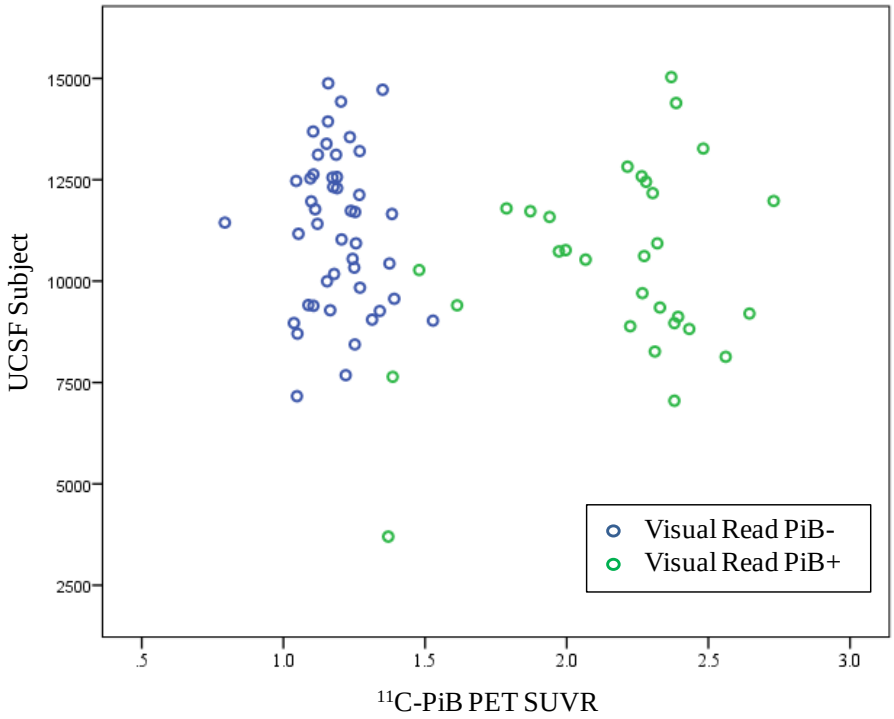

Figure 3-3: Scatter plot demonstrating the distribution of ^{11}C-PiB PET SUVR for the UCSF imaging cohort. The individual SUVR values are coded by the visual classification of the PET images; PiB- (blue) or PiB+ (green).

Validation cohort (EMIF-AD)

An original 510 participants were recruited from the European Medical Informatics Framework (EMIF-AD) previously described (Chapter 2.1.3); however 21 participants were removed from this study for not having the basic demographics available (*APOE* genotype, cognitive scores or CSF measures).

Participants were categorised into two groups (Table 3-3; Figure 3-4); CSF $A\beta_{1-42}$ negative (CSF $A\beta_{1-42}$- (550.5 – 2066 pg/mL)) and CSF $A\beta_{1-42}$ positive (CSF $A\beta_{1-42}$+ (151 – 550 pg/mL)). A low CSF $A\beta_{1-42}$ measure (CSF $A\beta_{1-42}$+) is indicative, but not exclusively, of PiB+ subjects. We also examined CSF $A\beta_{1-42}$ as a continuous measure. CSF t-tau and p-tau were also classified into endophenotype groups based upon their individual measures (Figure 3-5 and Figure 3-6). The CSF t-tau- group ranged from 15 – 372 pg/mL (n = 262), with the CSF t-tau+ groups ranging from 377 – 2114 pg/mL (n = 227; Figure 3-5). The CSF p-tau- group ranged from 9 – 52 pg/mL (n = 209), with the CSF t-tau+ groups ranging from 52.5 – 328 pg/mL (n = 280; Figure 3-6).

A CSF algorithm that incorporated $A\beta_{1\text{-}42,}$ t-tau and p-tau measures was also investigated in this study [454]. A low CSF algorithm score is considered to be more healthy (CSF algorithm–; 0.47 – 0.997) whereas a high CSF algorithm score is a more high risk group (CSF algorithm+; 1.00 – 9.166). An overlap of CSF algorithm values when stratifying by CSF Aβ group is observed and this is because of the inclusion of CSF t-tau and p-tau measures in the algorithm (Table 3-3; Figure 3-7). If subjects were stratified by CSF algorithm (CSF algorithm- and CSF algorithm+) we can see a number of CSF $A\beta_{1\text{-}42}$+ subjects would be classed as CSF algorithm- (Figure 3-7). However, there was still a highly significant correlation between the CSF algorithm and all modalities, with CSF $A\beta_{1\text{-}42}$ being the most significant association (Figure 3-8; Rho = -0.915, $P = 2.097 \times 10^{-195}$).

As with AIBL-1 and UCSF there was no significant difference of gender with the two groups. However, age, clinical diagnosis and *APOE* ε4 carrier status were vastly different (Table 3-3).

Table 3-3: Subject demographics for participants selected from the EMIF-AD cohort.

	CSF $A\beta_{1\text{-}42}$ Negativity (CSF $A\beta_{1\text{-}42}$-)	**CSF $A\beta_{1\text{-}42}$ Positivity (CSF $A\beta_{1\text{-}42}$+)**	***P* value**
Number of subjects (*n*)	268	221	
CSF $A\beta_{1\text{-}42}$ pg/mL (mean (S.D, range)	881.78 (276.97, 151-550)	397.65 (99.03, 550.5-2066)	5.54×10^{-88}
CSF algorithm (mean (S.D, range)	0.82 (0.42, 0.25-2.30)	2.38 (1.24, 0.84-9.17)	1.15×10^{-62}
Gender; females (*n* (%))	146 (55%)	131 (59%)	0.388
Age in years (mean (S.D))	66.8 (10.1)	70.3 (7.9)	2.90×10^{-5}
Clinical diagnosis (*n* (%))	HEC: 82 (30.6%)	HEC: 12 (5.4%)	4.16×10^{-36}
	MCI: 158 (59%)	MCI: 76 (34.4%)	
	AD: 28 (10.4%)	AD: 133 (49.1%)	
APOE ε4 carrier (*n* (%))	74 (27.6%)	115 (52.2%)	2.21×10^{-8}

Abbreviations: HEC, Healthy elderly control; MCI, Mild cognitive impairment; AD, Alzheimer's disease; SUVR, Standardized uptake values ratio; S.D; Standard deviation; MMSE, Mini mental state examination.

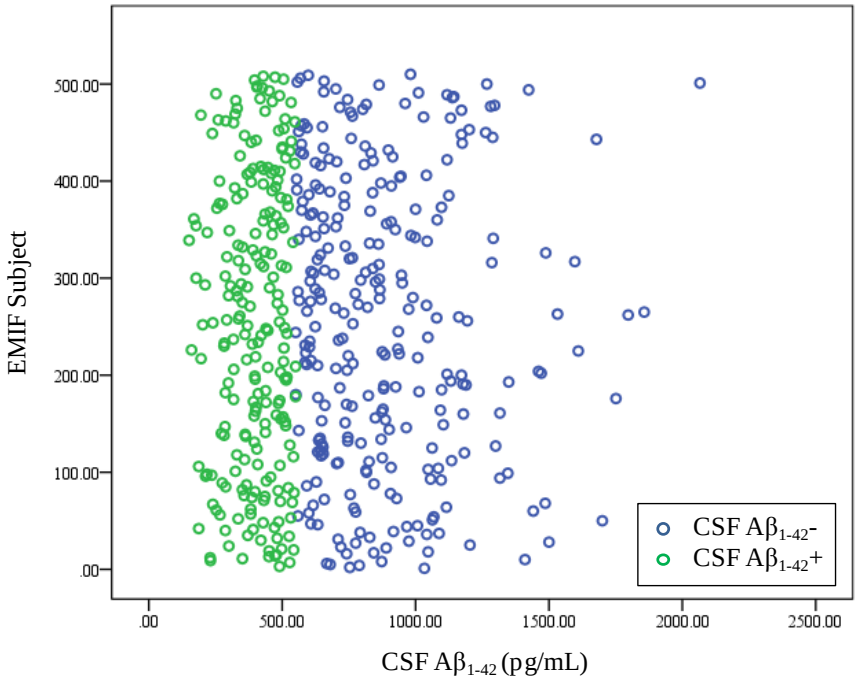

Figure 3-4: Scatter plot demonstrating the CSF $A\beta_{1-42}$ distribution of the selected subjects from the EMIF-AD cohort. The EMIF-AD individuals are colour coded by CSF $A\beta_{1-42}$ category alone; CSF $A\beta_{1-42}$- (blue) or CSF $A\beta_{1-42}$+ (green).

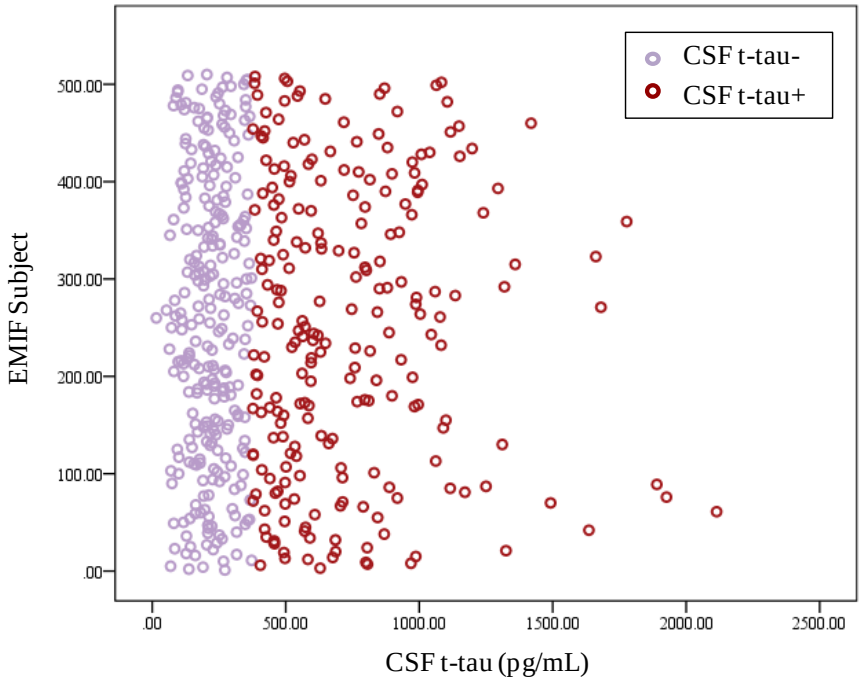

Figure 3-5: Scatter plot demonstrating the CSF t-tau distribution of the selected subjects from the EMIF-AD cohort. The EMIF-AD individuals are colour coded by CSF t-tau category alone; CSF t-tau- (purple) or CSF t-tau+ (red).

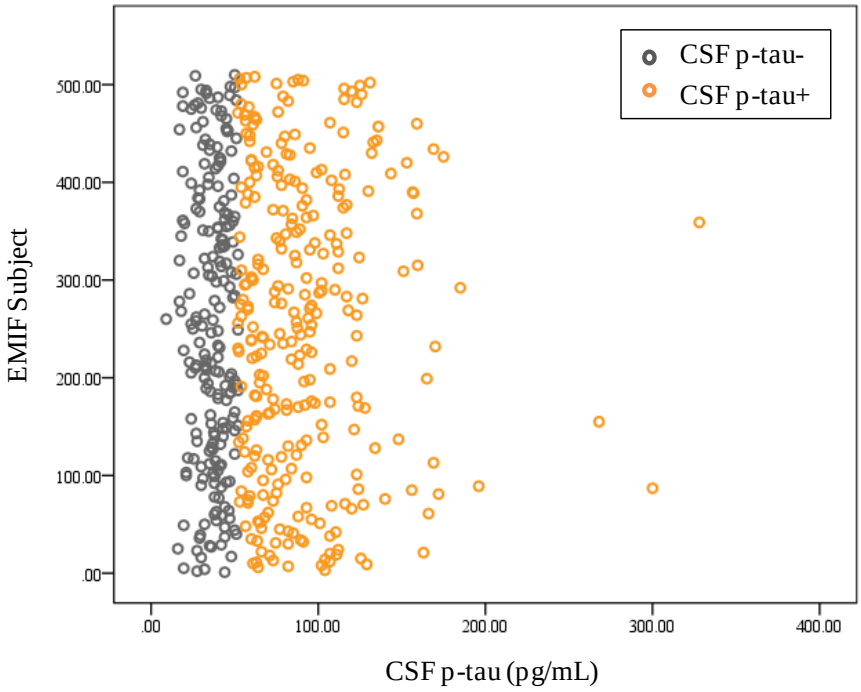

Figure 3-6: Scatter plot demonstrating the CSF p-tau distribution of the selected subjects from the EMIF-AD cohort. The EMIF-AD individuals are colour coded by CSF p-tau category alone; CSF p-tau- (grey) or CSF p-tau+ (orange).

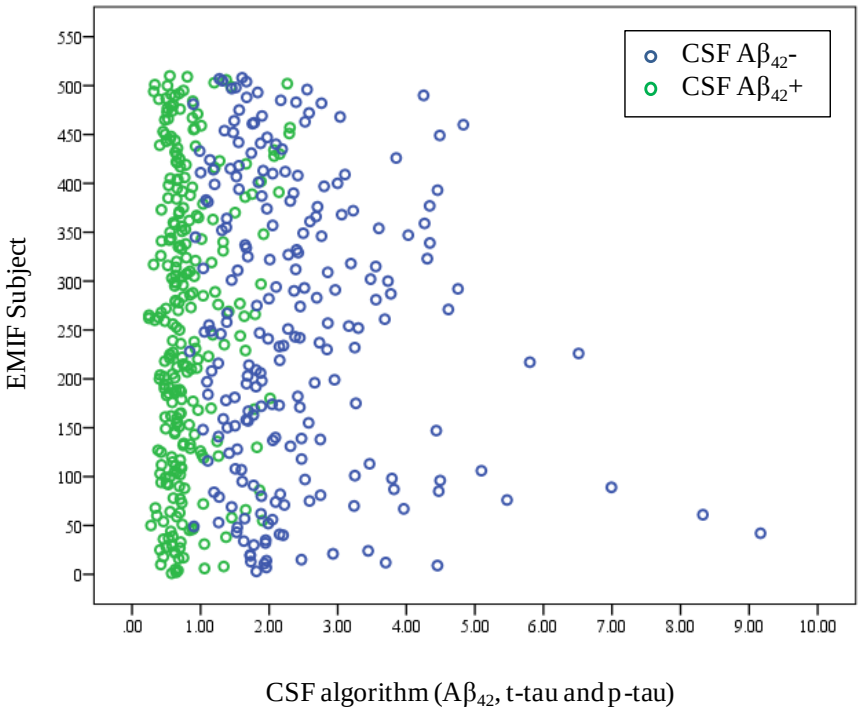

Figure 3-7: Scatter plot demonstrating the CSF algorithm (CSF $A\beta_{1\text{-}42}$, t-tau and p-tau) distribution of the selected subjects from the EMIF-AD cohort. The EMIF-AD individuals are colour coded by CSF $A\beta_{1\text{-}42}$ category alone; CSF $A\beta_{1\text{-}42}$- (blue) or CSF $A\beta_{1\text{-}42}$+ (green).

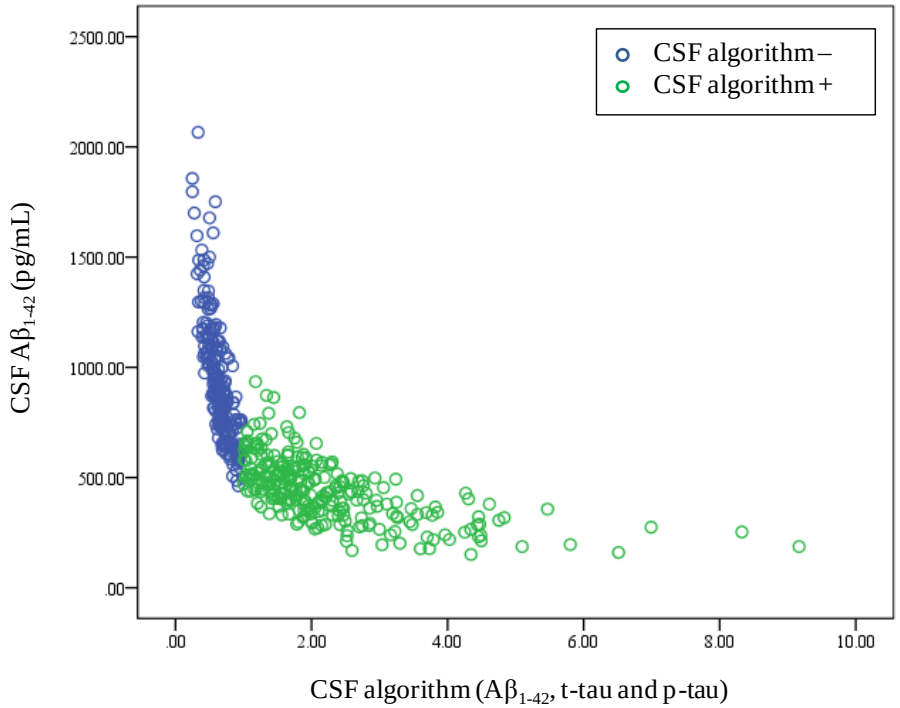

Figure 3-8: Scatter plot demonstrating the CSF algorithm correlation with $A\beta_{1-42}$ measures (P = 2.097 x10^{-195}) of the selected subjects from the EMIF-AD cohort. The EMIF-AD individuals are colour coded by CSF algorithm category alone; CSF algorithm – (blue) or CSF algorithm+ (green).

3.4.2 LC-MS/MS performed on AIBL-1 subjects

TMT protein labelling, gel-based proteomics and LC-MS/MS analysis (Chapter 2.4) was performed on plasma samples from 78 subjects from the AIBL-1 imaging cohort, whose demographics are shown in Table 3-1. Technical variance was assessed by the sum of MS/MS events for each TMT6plex experiment (Table 3-4). MS/MS events are an indication of how many MS1 precursor ions has been selected for subsequent fragmentation. A lower number of MS/MS events may indicate a decreased instrument performance or sample quality.

Table 3-4: The number of MS/MS events acquired for each TMT6plex included in the study. Each TMT6plex included 5 clinical samples from the AIBL-1 cohort plus a study reference.

TMT6plex #	MS/MS events		
1	55638	9	71399
2	74521	10	72816
3	72141	11	67710
4	62419	12	74161
5	77941	13	73276
6	83123	14	76425
7	85936	15	73884
8	70142	16	72489

Mean	Standard Dev.	Coefficient of Variation (CV %)
72751.31	7130.38	9.80%

A CV of <10% for MS/MS events across all 16 TMT6plex experiments signifies consistent sample preparation and instrument performance. The number of MS/MS events is directly proportional to the number peptide spectral matches (PSM) and therefore related to the number of unique peptides and protein groups that will be assigned by a database. Features inconsistently measured across several experiments would be rejected from downstream analysis and therefore it is imperative to keep the number of identifications reliable across each TMT6plex. TMT6plex 1 had a reduced number of MS/MS events in comparison to all other experiments and this is reflected in the number of PSM assignments (Figure 3-9). Despite this, the resulting number of unique peptides and protein groups, although the lowest in the study, was not out of the norm when compared to all other experiments (Table 3-5 and Table 3-6).

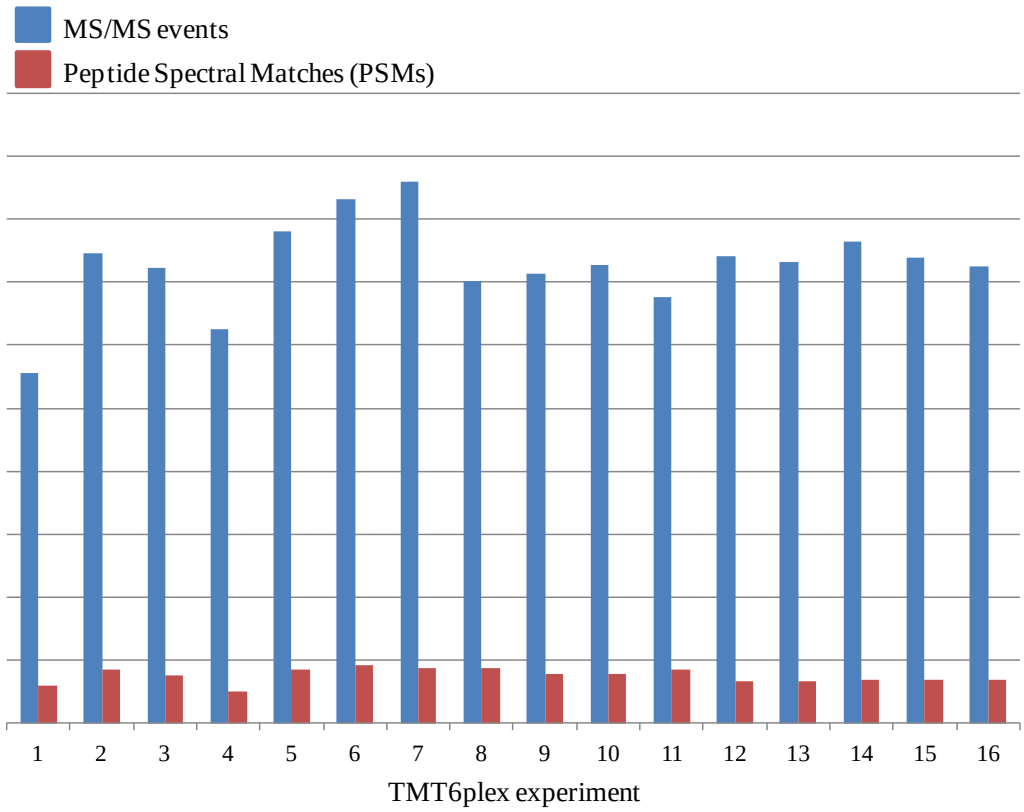

Figure 3-9: A visualisation of the number of MS/MS events (blue) compared to number of peptide spectral matches (PSMs; red) for each TMT6plex experiment.

The number of protein groups, peptides, PSMs and spectral yield rates of each TMT6plex at 5% FDR were examined (Table 3-5) and contrasted this to 1% FDR (Table 3-6). As expected, on average there was a reduction in protein groups (6.8%), peptides (8.6%), PSMs (6.7%) and spectral yield performance when applying a more stringent FDR to the dataset. For discovery proteomics and to maximise potential targets related to disease all further analysis was carried on data with 5% FDR applied.

Table 3-5: The performance of each TMT6plex by number of protein groups, peptides, PSM and spectral yield at false discovery rates of 5%.

	5% FDR			
	Protein Groups	Peptides	Peptide Spectral Matches (PSMs)	Spectral Yield
1	221	1082	5893	0.11
2	319	1405	8553	0.11
3	258	1198	7573	0.10
4	221	1012	5057	0.08
5	250	1280	8656	0.11
6	308	1424	9209	0.11
7	292	1459	8675	0.10
8	285	1415	8754	0.12
9	277	1364	7770	0.11
10	326	1480	7966	0.11
11	340	1489	8454	0.12
12	275	1261	6624	0.09
13	270	1282	6620	0.09
14	278	1330	6827	0.09
15	268	1281	6985	0.09
16	262	1326	6911	0.10
Mean	278.13	1318.00	7532.94	0.10
Standard Dev.	33.75	135.89	1173.73	0.01
Coefficient of Variation (CV %)	12.13%	10.31%	15.58%	12.35%

Table 3-6: The performance of each TMT6plex by number of protein groups, peptides, PSM and spectral yield at false discovery rates of 1%.

TMT6plex #	1% FDR			
	Protein Groups	Peptides	Peptide Spectral Matches (PSMs)	Spectral Yield
1	209	995	5554	0.10
2	298	1287	8043	0.11
3	240	1096	7037	0.10
4	208	901	4579	0.07
5	235	1157	8061	0.10
6	286	1297	8695	0.10
7	262	1330	8144	0.09
8	264	1279	8143	0.12
9	256	1244	7159	0.10
10	304	1334	7391	0.10
11	318	1365	7863	0.12
12	254	1135	6050	0.08
13	255	1199	6152	0.08
14	261	1227	6454	0.08
15	251	1219	6548	0.09
16	247	1221	6499	0.09
Mean	259.25	1205.38	7023.25	0.10
Standard Dev.	30.65	125.60	1123.82	0.01
Coefficient of Variation (CV %)	11.82%	10.42%	16.00%	12.66%

Combining data from all MS/MS acquisitions, 4,518 unique peptides sequences were identified that corresponded to 789 unique protein groups at 5% FDR. The statistical pipeline Pre-processing for Relative Quantification (PRQ-1; Chapter 2.4.6) extracted 2,319 unique TMT peptides, 1,139 protein group MW isoforms and 379 unique protein groups (Supplementary Material 3). In the instance of LC-MS/MS data separated by 1DGE a single protein group can be observed in multiple fractions. Therefore, identical protein identifications observed in different fractions were considered as separate entities and termed molecular weight (MW) protein group isoforms. This list of unique protein groups further reduced to 116 confidently annotated unique protein groups when applying post-PRQ-1 restrictions (Figure 3-10); this consisted of 381 protein MW group isoforms (Appendix 1) which underwent statistical analysis in relation to ^{11}C-PiB retention.

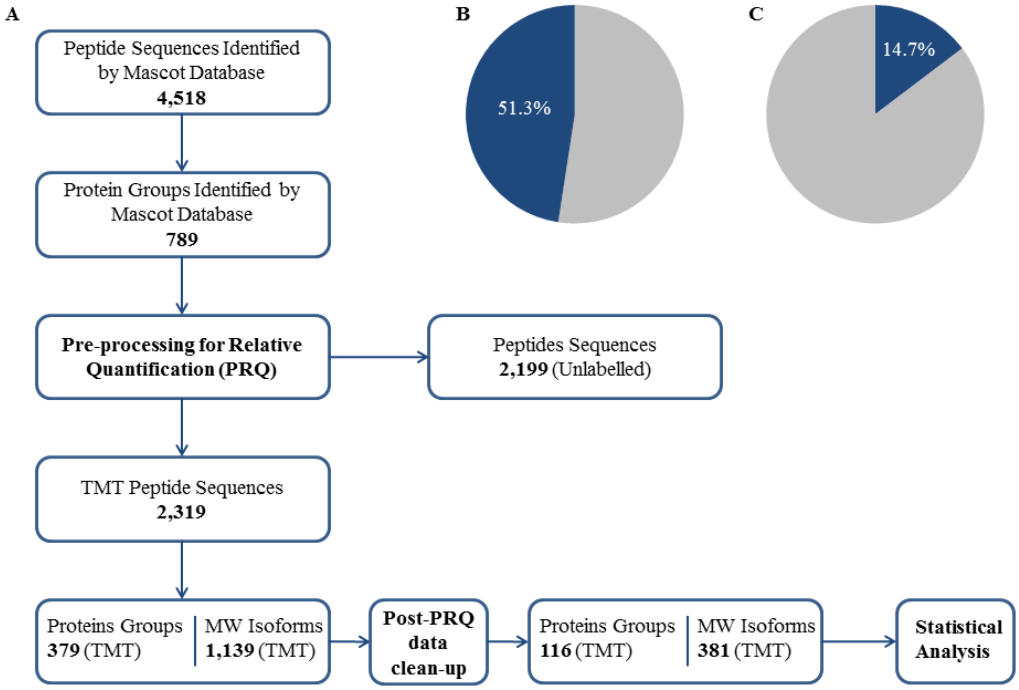

Figure 3-10: (A) Schematic diagram demonstrating the selection process of unique protein groups and protein group MW isoforms for statistical analysis. Pie charts illustrate (B) the percentage of all peptides identified by Mascot that could be quantified by TMT and (C) the percentage all protein groups identified by mascot could be quantified by TMT.

3.4.3 Plasma protein markers associated with ^{11}C-PiB PET in AIBL-1

Each of the identified 381 protein group MW isoforms (Appendix 1) was investigated by Mann-Whitney U tests and Logistic Regression to compare PiB+ and PiB- groups. In addition, Spearman Rank Correlation and Linear Regression were used to correlate protein group MW isoform levels against ^{11}C-PiB retention as a continuous measure. This was completed for both the mean and median protein roll-up methods separately (described in Chapter 2.4.6), giving a total of eight statistical tests per protein group MW isoform. The significant protein group MW isoforms using the mean protein roll-up method are displayed in Table 3-7 and Table 3-8. The significant protein group MW isoforms using the median protein roll-up method are presented in Table 3-9 and Table 3-10. A summary of these results ranked by the number of statistical tests that each protein group MW isoform passes is displayed in Table 3-11.

Table 3-7: Protein group MW isoforms measured by LC-MS/MS significantly associated with NAB groups (PiB- and PiB+) when applying a "mean of all peptides" method. For regressions age, gender and presence of *APOE* ε4 was used as covariates. Protein group MW isoforms that passed a significance of *P* = <0.05 are highlighted (green). All multiple testing corrections = *Q* > 0.75.

				Mean over all peptides mapping to protein			
				Logistic Regression		**Mann-Whitney U**	
UniProt ID	**Gene Name**	**1DGE Fraction**	**Samples Present (%)**	**Beta**	***P* value**	**Median difference**	***P* value**
P01876	*IGHA1*	4	93.75	-0.863	0.008	-0.410	0.058
P02647	*APOA1*	10	68.75	-0.877	0.014	-0.173	0.070
P00738	*HP*	8	81.25	-0.932	0.015	-0.331	0.011
P00738	*HP*	5	100	-0.728	0.023	-0.521	0.017
P01700	n/a	7	81.25	-0.747	0.024	-0.195	0.050
P00747	*PLG*	1	62.50	0.901	0.026	0.610	0.078
Q06033	*ITIH3*	2	56.25	1.525	0.027	0.297	0.099
P04196	*HRG*	5	62.50	-0.996	0.031	-0.093	0.150
P00450	*CP*	6	75.00	-2.088	0.032	-0.222	0.019
P01023	*A2M*	9	75.00	-0.749	0.035	-0.246	0.112
P01768	n/a	6	56.25	-1.586	0.036	-0.195	0.100
P0C0L4	*C4A*	7	100	-0.656	0.038	-0.235	0.027
P02647	*APOA1*	9	93.75	-0.599	0.039	-0.061	0.255
P04196	*HRG*	3	68.75	1.205	0.039	0.334	0.034

Q14624	*ITIH4*	1	56.25	1.244	0.041	0.187	0.118
P02747	*C1QC*	2	56.25	-0.746	0.043	-0.460	0.095
P01876	*IGHA1*	1	93.75	-0.537	0.046	-0.329	0.099
O14791	*APOL1*	5	81.25	0.829	0.048	0.731	0.004
P02790	*HPX*	6	87.50	0.587	0.049	0.216	0.053
P01024	*C3*	8	93.75	-0.569	0.058	-0.480	0.030
P08519	*LPA*	1	62.50	0.929	0.062	0.315	0.030
P04220	n/a	4	62.50	-0.954	0.063	-0.256	0.020
P19823	*ITIH2*	4	75.00	-0.762	0.067	-0.294	0.026
O43866	*CD5L*	5	75.00	-0.929	0.110	-0.398	0.013
Q03591	*CFHR1*	8	87.50	1.667	0.120	0.313	0.008
P06396	*GSN*	5	75.00	1.018	0.251	0.174	0.033
Q92620	*DHX38*	2	87.50	-0.383	0.351	0.046	0.044
P01700	n/a	8	68.75	-0.218	0.510	-0.366	0.002
P25311	*AZGP1*	7	62.50	0.140	0.681	0.327	0.043
P01762	n/a	4	68.75	0.018	0.952	-0.273	0.042

Table 3-8: Protein group MW isoforms measured by LC-MS/MS significantly associated with NAB as continuous measure, using a "mean of all peptides" method. For regressions age, gender and presence of *APOE* ε4 was used as covariates. Protein group MW isoforms that passed a significance of *P* = <0.05 are highlighted (green). All multiple testing corrections = *Q* > 0.75.

				Mean over all peptides mapping to protein			
				Linear Regression		**Spearman's Rank Correlation (SRC)**	
UniProt ID	**Gene Name**	**1DGE Fraction**	**Samples Present (%)**	**Beta**	***P* value**	**Rho**	***P* value**
P01876	*IGHA1*	4	93.75	-0.225	0.002	-0.186	0.116
P00738	*HP*	5	100	-0.198	0.005	-0.280	0.013
P01876	*IGHA1*	6	100	-0.194	0.005	-0.144	0.209
P0C0L4	*C4A*	1	56.25	0.241	0.009	0.160	0.293
P04196	*HRG*	5	62.50	-0.228	0.011	-0.238	0.096
Q14624	*ITIH4*	1	56.25	0.251	0.013	0.222	0.142
P02647	*APOA1*	10	68.75	-0.211	0.013	-0.204	0.136
P00739	*HPR*	5	62.50	0.209	0.016	0.232	0.104
P01768	n/a	6	56.25	-0.209	0.018	-0.124	0.416
P0C0L4	*C4A*	7	100	-0.162	0.019	-0.302	0.007
P02768	*ALB*	1	100	0.160	0.020	0.100	0.385
P02647	*APOA1*	6	100	-0.157	0.023	-0.189	0.098
P02747	*C1QC*	2	56.25	-0.201	0.024	-0.210	0.165
P00738	*HP*	8	81.25	-0.170	0.026	-0.248	0.047
P00734	*F2*	6	68.75	0.190	0.027	0.208	0.135
P04003	*C4BPA*	7	100	-0.153	0.028	-0.156	0.173

P00450	*CP*	2	87.50	0.167	0.029	0.000	0.998
P0CG04	*IGLC1*	6	68.75	-0.176	0.031	-0.098	0.486
P04220	n/a	4	62.50	-0.197	0.034	-0.312	0.027
O14791	*APOL1*	5	81.25	0.165	0.035	0.308	0.014
P01024	*C3*	6	100	-0.148	0.035	-0.107	0.351
P01023	*A2M*	9	75.00	-0.196	0.037	-0.092	0.482
P10909	*CLU*	6	87.50	-0.159	0.037	-0.102	0.408
Q92620	*DHX38*	5	62.50	0.197	0.038	0.144	0.318
P01700	n/a	3	68.75	0.177	0.044	0.377	0.005
P01700	n/a	7	81.25	-0.156	0.044	-0.191	0.134
O75636	*FCN3*	6	75.00	-0.152	0.044	0.034	0.798
P04196	*HRG*	6	56.25	-0.185	0.049	-0.194	0.214
P02671	*FGA*	4	100	-0.142	0.052	-0.284	0.012
P19823	*ITIH2*	4	75.00	-0.159	0.061	-0.267	0.039
P04003	*C4BPA*	4	93.75	-0.127	0.076	-0.248	0.035
P00751	*CFB*	1	56.25	0.164	0.081	0.310	0.038
O43866	*CD5L*	5	75.00	-0.140	0.088	-0.288	0.028
P06727	*APOA4*	6	56.25	-0.144	0.115	-0.389	0.010
Q03591	*CFHR1*	8	87.50	0.155	0.178	0.483	0.007
P02647	*APOA1*	5	75.00	-0.101	0.229	-0.263	0.046
P01700	n/a	8	68.75	-0.081	0.378	-0.372	0.005
O43866	*CD5L*	6	56.25	0.077	0.400	0.347	0.022
P25311	*AZGP1*	7	62.50	0.076	0.461	0.327	0.021
P01023	*A2M*	3	100	0.048	0.497	0.290	0.010
P01768	n/a	9	68.75	0.054	0.600	0.291	0.031
P02679	*FGG*	6	62.50	0.044	0.613	-0.331	0.021

Table 3-9: Protein group MW isoforms measured by LC-MS/MS significantly associated with NAB groups (PiB-, PiB+) when applying a "median of all peptides" method. For regressions age, gender and presence of *APOE* ε4 was used as covariates. Protein group MW isoforms that passed a significance of *P* = <0.05 are highlighted (green). All multiple testing corrections = *Q* > 0.75.

				Median over all peptides mapping to protein			
				Logistic Regression		**Mann-Whitney U**	
UniProt ID	**Gene Name**	**1DGE Fraction**	**Samples Present (%)**	**Beta**	***P* value**	**Median difference**	***P* value**
P00738	*HP*	8	81.25	-1.048	0.018	-0.190	0.030
P01860	*IGHG3*	1	93.75	-0.715	0.018	-0.234	0.041
Q06033	*ITIH3*	2	56.25	1.267	0.019	0.422	0.013
P01876	*IGHA1*	8	100	-0.683	0.020	-0.411	0.109
P04196	*HRG*	3	68.75	1.149	0.024	0.611	0.030

P01700	n/a	7	81.25	-0.747	0.024	-0.195	0.050
P02647	*APOA1*	10	68.75	-0.872	0.025	-0.087	0.087
P04196	*HRG*	5	62.50	-0.996	0.031	-0.093	0.150
P00450	*CP*	6	75.00	-2.088	0.032	-0.222	0.019
P01768	n/a	6	56.25	-1.561	0.043	-0.178	0.137
P02747	*C1QC*	2	56.25	-0.746	0.043	-0.460	0.095
P00747	*PLG*	1	62.50	0.786	0.049	0.409	0.102
P0C0L4	*C4A*	7	100	-0.592	0.049	-0.224	0.037
P01876	*IGHA1*	4	93.75	-0.559	0.050	-0.224	0.253
P01860	*IGHG3*	2	81.25	-0.623	0.050	-0.555	0.042
P08519	*LPA*	1	62.50	0.869	0.064	0.222	0.045
O43866	*CD5L*	5	75.00	-0.596	0.080	-0.307	0.015
O14791	*APOL1*	5	81.25	0.578	0.091	0.795	0.007
P07357	*C8A*	5	75.00	-0.539	0.104	-0.474	0.032
P04003	*C4BPA*	4	93.75	-0.466	0.106	-0.473	0.038
P01860	*IGHG3*	6	81.25	-0.508	0.116	-0.325	0.049
P02768	*ALB*	1	100	0.499	0.128	0.229	0.011
P13671	*C6*	2	81.25	-0.430	0.145	-0.662	0.048
P01023	*A2M*	1	100	0.340	0.181	0.469	0.046
Q03591	*CFHR1*	8	87.50	1.414	0.187	0.186	0.019
P06396	*GSN*	5	75.00	1.149	0.202	0.151	0.042
Q92620	*DHX38*	2	87.50	-0.380	0.351	0.046	0.031
P02787	*TF*	1	87.50	0.249	0.372	0.352	0.040
P08603	*CFH*	6	87.50	0.190	0.490	0.243	0.041
P01700	n/a	8	68.75	-0.218	0.510	-0.366	0.002
P02768	*ALB*	8	100	0.144	0.565	0.420	0.025
P25311	*AZGP1*	7	62.50	0.140	0.681	0.327	0.043
P01762	n/a	4	68.75	0.018	0.952	-0.273	0.042

Table 3-10: Protein group MW isoforms measured by LC-MS/MS significantly associated with NAB as continuous measure, using a "median of all peptides" method. For regressions age, gender and presence of *APOE* ε4 was used as covariates. Protein group MW isoforms that passed a significance of *P* = <0.05 are highlighted (green). All multiple testing corrections = *Q* > 0.75.

				Median over all peptides mapping to protein			
				Linear regression		**Spearman's Rank Correlation (SRC)**	
UniProt ID	**Gene Name**	**1DGE Fraction**	**Samples Present (%)**	**Beta**	***P* value**	**Rho**	***P* value**
P04196	*HRG*	5	62.50	-0.228	0.011	-0.238	0.096
P02675	*FGB*	6	87.50	-0.172	0.016	-0.188	0.125
P00739	*HPR*	5	62.50	0.209	0.016	0.232	0.104

P02679	*FGG*	6	62.50	-0.191	0.021	-0.298	0.039
P0CG04	*IGLC1*	6	68.75	-0.188	0.021	-0.141	0.313
P01876	*IGHA1*	6	100	-0.160	0.022	-0.090	0.435
P04003	*C4BPA*	7	100	-0.158	0.023	-0.150	0.189
P02747	*C1QC*	2	56.25	-0.201	0.024	-0.210	0.165
P01768	n/a	6	56.25	-0.200	0.024	-0.094	0.539
P01024	*C3*	6	100	-0.156	0.025	-0.119	0.300
P01860	*IGHG3*	1	93.75	-0.158	0.026	-0.237	0.043
P01876	*IGHA1*	4	93.75	-0.157	0.033	-0.087	0.465
P02647	*APOA1*	10	68.75	-0.183	0.035	-0.266	0.049
P01860	*IGHG3*	2	81.25	-0.161	0.037	-0.243	0.055
Q92620	*DHX38*	5	62.50	0.197	0.038	0.144	0.318
P02647	*APOA1*	6	100	-0.143	0.038	-0.236	0.038
P01860	*IGHG3*	6	81.25	-0.145	0.039	-0.139	0.277
P00738	*HP*	5	100	-0.149	0.041	-0.181	0.112
P00751	*CFB*	1	56.25	0.189	0.042	0.363	0.014
P0C0L4	*C4A*	7	100	-0.143	0.042	-0.229	0.044
O43866	*CD5L*	5	75.00	-0.165	0.042	-0.235	0.076
P00738	*HP*	8	81.25	-0.157	0.043	-0.226	0.070
P01700	n/a	3	68.75	0.177	0.044	0.377	0.005
P01700	n/a	7	81.25	-0.156	0.044	-0.191	0.134
O75636	*FCN3*	6	75.00	-0.152	0.044	0.034	0.798
P07357	*C8A*	5	75.00	-0.153	0.073	-0.261	0.048
P19827	*ITIH1*	8	62.50	-0.164	0.113	-0.313	0.030
P06727	*APOA4*	6	56.25	-0.139	0.128	-0.387	0.010
P02790	*HPX*	5	100.00	0.105	0.134	0.228	0.045
P04003	*C4BPA*	4	93.75	-0.105	0.154	-0.275	0.018
Q92620	*DHX38*	2	87.50	-0.095	0.208	0.243	0.046
Q03591	*CFHR1*	8	87.50	0.144	0.217	0.444	0.014
O43866	*CD5L*	6	56.25	0.090	0.313	0.369	0.015
P01700	n/a	8	68.75	-0.081	0.378	-0.372	0.005
P25311	*AZGP1*	7	62.50	0.076	0.461	0.327	0.021
P01023	*A2M*	2	100	0.048	0.495	0.237	0.037
P01023	*A2M*	3	100	0.042	0.559	0.254	0.025
P02768	*ALB*	9	100	0.033	0.644	0.242	0.033
P08603	*CFH*	6	87.50	-0.001	0.987	0.286	0.018

Table 3-11: A summary of protein group MW isoforms significantly associated with NAB, ranked by the highest number of statistical tests passed (*P* <0.05). Protein groups that are represented by four separate MW isoforms are highlighted in blue. Protein groups that are represented by three separate MW isoforms are highlighted in red.

UniProt ID	Protein Name	Gene Name	1DGE Fraction	Number of *P* value tests <0.05	MS/MS spectral evidence
P0C0L4	complement C4-A (C4α)	*C4A*	7	8	Fig 3-12 to 3-13
P00738	haptoglobin	*HP*	8	7	Fig 3-14
P01700	Ig lambda chain V-I region HA	n/a	7	6	n/a
P02647	apolipoprotein A-I (apoA1)	*APOA1*	10	5	Fig 3-15
O14791	apolipoprotein L1 (apoL1)	*APOL1*	5	5	Fig 3-16 to 3-17
P00738	haptoglobin	*HP*	5	5	Fig 3-18 to 3-20
P25311	zinc-alpha-2-glycoprotein	*AZGP1*	7	4	Appendix 2
P02747	complement C1q subcomponent subunit C	*C1QC*	2	4	Appendix 2
O43866	CD5 antigen-like	*CD5L*	5	4	Appendix 2
Q03591	complement factor H related protein 1 (FHR-1)	*CFHR1*	8	4	Fig 3-21 to 3-22
P00450	ceruloplasmin	*CP*	6	4	Appendix 2
P04196	histidine-rich glycoprotein (HRG)	*HRG*	5	4	n/a
P04196	histidine-rich glycoprotein (HRG)	*HRG*	3	4	Fig 3-22 to 3-23
P01876	Ig alpha-1 chain C region	*IGHA1*	4	4	n/a
P01860	Ig gamma-3 chain C region	*IGHG3*	1	4	n/a
P01768	Ig heavy chain V-III region CAM	n/a	6	4	n/a
P01700	Ig lambda chain V-I region HA	n/a	3	4	n/a
P01700	Ig lambda chain V-I region HA	n/a	8	4	n/a
P02647	apolipoprotein A-I (apoA1)	*APOA1*	6	3	Fig 3-24 to 3-29
P04003	C4b-binding protein alpha chain	*C4BPA*	4	3	Appendix 2
P00751	complement factor B (CFB)	*CFB*	1	3	Fig 3-30 to 3-31
Q92620	pre-mRNA-splicing factor	*DHX38*	2	3	Appendix 2
P02679	fibrinogen γ chain (FGγ)	*FGG*	6	3	Fig 3-32 to 3-33

Q06033	Inter-alpha-trypsin inhibitor heavy chain H3	*ITIH3*	2	3	Appendix 2
P04220	Ig mu heavy chain disease protein	n/a	4	3	n/a
P01023	alpha-2-Macroglobulin (α2m)	*A2M*	9	2	n/a
P01023	alpha-2-Macroglobulin (α2m)	*A2M*	3	2	Fig 3-34 to 3-40
P02768	albumin	*ALB*	1	2	n/a
P06727	apolipoprotein A-IV (ApoA4)	*APOA4*	6	2	Fig 3-41 to 3-42
P01024	complement C3 (CC3)	*C3*	6	2	Fig 3-43to 3-49
P04003	C4b-binding protein alpha chain	*C4BPA*	7	2	Appendix 2
P07357	complement component C8 alpha chain (CC8α)	*C8A*	5	2	Appendix 2
O43866	CD5 antigen-like	*CD5L*	6	2	Appendix 2
P08603	complement factor H (CFH)	*CFH*	6	2	Fig 3-50 to 3-52
Q92620	pre-mRNA-splicing factor	*DHX38*	5	2	Appendix 2
O75636	ficolin 3	*FCN3*	6	2	Appendix 2
P06396	gelsolin	*GSN*	5	2	Fig 3-53 to 3-54
P00739	haptoglobin-related protein	*HPR*	5	2	n/a
P01876	Ig alpha-1 chain C region	*IGHA1*	6	2	n/a
P01860	Ig gamma-3 chain C region	*IGHG3*	2	2	n/a
P01860	Ig gamma-3 chain C region	*IGHG3*	6	2	n/a
P0CG04	Ig lambda-1 chain C regions	*IGLC1*	6	2	n/a
P19823	Inter-alpha-trypsin inhibitor heavy chain H2	*ITIH2*	4	2	n/a
Q14624	Inter-alpha-trypsin inhibitor heavy chain H4	*ITIH4*	1	2	n/a
P08519	apolipoprotein(a) (apo(a))	*LPA*	1	2	Fig 3-55
P01762	Ig heavy chain V-III region TRO	n/a	4	2	n/a
P00747	plasminogen	*PLG*	1	2	n/a
P01023	alpha-2-Macroglobulin (α2m)	*A2M*	2	1	Fig 3-56 to 3-61
P01023	alpha-2-Macroglobulin (α2m)	*A2M*	1	1	Fig 3-62 to 3-64
P02768	albumin	*ALB*	8	1	n/a
P02768	albumin	*ALB*	9	1	n/a

P02647	apolipoprotein A-I (apoA1)	*APOA1*	5	1	Fig 3-65 to 3-66
P02647	apolipoprotein A-I (apoA1)	*APOA1*	9	1	Fig 3-67 to 3-69
P01024	complement C3 (CC3)	*C3*	8	1	Fig 3-70
P0C0L4	complement C4-A (C4α)	*C4A*	1	1	Fig 3-71
P13671	complement Component C6 (CC6)	*C6*	2	1	Appendix 2
P10909	clusterin	*CLU*	6	1	Fig 3-72 to 3-74
P00450	ceruloplasmin	*CP*	2	1	Appendix 2
P00734	prothrombin	*F2*	6	1	Appendix 2
P02671	fibrinogen α chain (FGα)	*FGA*	4	1	Fig 3-75 to 3-78
P02675	fibrinogen β chain (FGβ)	*FGB*	6	1	n/a
P02790	hemopexin	*HPX*	6	1	Appendix 2
P02790	hemopexin	*HPX*	5	1	Appendix 2
P04196	histidine-rich glycoprotein (HRG)	*HRG*	6	1	n/a
P01876	Ig alpha-1 chain C region	*IGHA1*	1	1	n/a
P01876	Ig alpha-1 chain C region	*IGHA1*	8	1	n/a
P19827	Inter-alpha-trypsin inhibitor heavy chain H1	*ITIH1*	8	1	n/a
P01768	Ig heavy chain V-III region CAM	n/a	9	1	n/a
P02787	serotransferrin (TF)	*TF*	1	1	Fig 3-79 to 3-80

A total of 69 protein group MW isoforms corresponding to 43 separate unique protein groups passed at least one statistical test (uncorrected $P < 0.05$) for association with ^{11}C-PiB retention in the AIBL-1 imaging cohort. One protein group MW isoform, from protein group C4α, passed all eight statistical tests (Table 3-11). The most represented protein groups found to be related with ^{11}C-PiB were α2m, apoA1 and Ig alpha-1 chain C region each having four separate protein group MW isoforms having statistical significance (highlighted in blue; Table 3-11). Further protein groups having three MW isoforms significant with NAB were histidine-rich glycoprotein (HRG), Ig gamma-3 chain C region and Ig lambda chain V-I region HA (highlighted in red; Table 3-11).

3.4.4 Pathway analysis

Pathway analysis revealed that these 43 protein groups (Table 3-11) were over-represented for involvement in the complement and coagulation cascades (P = 3.7 x10^{-22}, Q = 3.3 x 10^{-21}), systemic lupus erythematosus (P = 2.65 x 10^{-4}, Q = 0.15) and prion diseases (P = 5.9 x 10^{-3}, Q = 0.051).

3.4.5 Candidate selection for technical replication

We sought to translate our LC-MS/MS discovery findings to a simple-to-use commercially available immunoassay format more applicable to a clinical setting. A technical replication using an orthogonal approach would reduce the number of false positives and ensure robust targets for future independent validation. Technical replication, by ELISA, was performed on the same 78 AIBL-1 subjects as in discovery LC-MS/MS.

For a technical replication to be feasible, the LC-MS/MS candidate list of 43 unique protein groups needed to be prioritised (Figure 3-11). In addition to statistical evidence already displayed (summarised in Table 3-11), conformation of the LC-MS/MS identifications by manual examination of the assigned spectra was performed for each candidate (Figure 3-12 to 3-80 and Appendix 2). The identifications reported in this study are initially based on automated database searching with cut-offs defined by FDR. Routine practice recommends manual examination of assigned spectra for a protein group in question or of interest; the peptide sequence would typically be confirmed by the presence of a majority of *b* and *y* ions in a series (described in Chapter 2.4.6). This is of paramount importance in discovery experiments when considering protein groups identified by relaxed FDR's or limited PSMs. We also favoured candidates with previous evidence in relation with Aβ and/or AD GWAS results (Table 3-12).

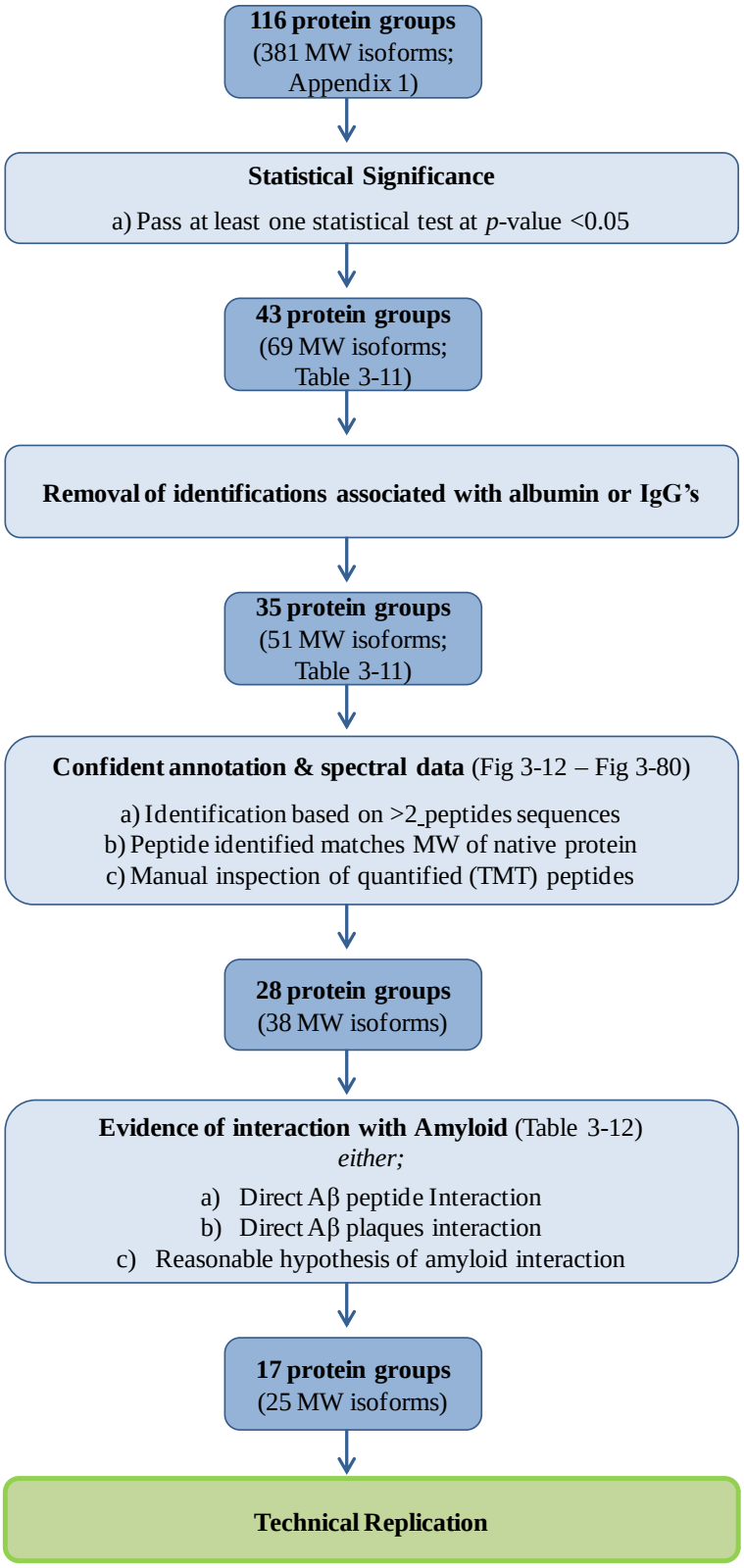

Figure 3-11: Schematic flow diagram to describe the process of prioritising LC-MS/MS candidates significantly associated with ^{11}C-PiB retention for technical replication.

Of the 43 protein groups associated with ^{11}C-PiB retention, 8 protein groups were associated with immunoglobins or albumin. A further 7 candidates were removed due poor quality TMT spectra. Of the remaining 28 candidates, which had confident TMT spectra, 17 protein groups had existing literature evidence of interacting with Aβ and/or highlighted in AD GWAS studies (Table 3-12). Spectral evidence for all the 25 MW isoforms for the 17 protein groups selected for technical replication are displayed from Figure 3-12 to Figure 3-80, with a figure reference for each protein group MW isoforms listed in Table 3-11. Spectral evidence for all other candidate protein group MW isoforms not chosen for technical replication can be found in Appendix 2.

Of the 17 candidates selected for technical replication, five protein groups had multiple MW isoforms significantly associated with ^{11}C-PiB (α2m, apoA1, haptoglobin, C4α and CC3; Table 3-11). In the most case, these isoforms were in gel fractions adjacent to each other, suggesting that the peptide sequences identified were common across these fractions. For α2m, TMT peptide sequences "*QKDNGCER*" and "*QLNYKHYDGSYSTFGER*" were observed in all significant α2m MW isoforms with "*TITKLSFVKVDSHFR*", "*GEAFTLKATVLNYLPKCIR*", "*TGKAAQVTIQSSGTFSSKFQVDNNNR*" and "*VVSMDENFHPLNELIPLVYIQDPKGNR*" being detected in 2/3 gel fractions. With common peptides quantified across these fractions, it is unsurprising the significant α2m peptides in gel fraction 1, 2 and 3 all showed an increased expression in the PiB+ group. In addition, apoA1 also had common peptides in adjacent fractions and all had a significant decrease in PiB+ group. Haptoglobin has a native MW of 18kDa and therefore its presence in gel fraction 8 is expected, however a significant peptide profile is also observed in gel fraction 5 (40 – 50kDa). Despite a differing location, haptoglobin in gel fraction 5 and 8 both demonstrated a decrease in the PiB+ group. C4α has a native MW of 190kDa (expected location gel fraction 1). C4α demonstrated significant MW isoforms in gel fractions 1 and 7, with both fractions showing a differing peptide profile. C4α in gel fraction 1 increased with PiB+, whereas C4α in gel fraction 7 decreased with PiB+. Peptide profiles for all MW isoforms used for protein group identification (No TMT) and quantitation (TMT) can be found in Appendix 3.

Table 3-12: LC-MS/MS candidate ranking based on Aβ interaction and/or AD GWAS results

UniProt ID	LC-MS/MS protein candidate	Gene Symbol	Score	Direct Aβ Peptide Interaction	Direct Aβ Plaques Interaction	AD GWAS & Variants	Reasonable Hypothesis	Comments, Interactions, Proposed Hypothesis
P10909	clusterin	*CLU*	4	1	1	1	1	Biochemical evidence of clusterin binding to Aβ. Binds to Aβ in CSF and found co-localised with Aβ plaques. Potential to modulate Aβ deposition and half-life.
P01023	α2m	*A2M*	3	1	0	1	1	Biochemical evidence shows that α2m can interact with Aβ thus maintaining its solubility. Shown to bind to Aβ with potential to increase or decrease its clearance.
P02647	apoA1	*APOA1*	3	1	0	1	1	Biochemical evidence of apoA1 binding to Aβ with potential to modulate Aβ deposition and half-life.
P02671	FGα	*FGA*	3	1	0	1	1	Fibrinogen can bind to Aβ and biochemical evidence showing fibrinogen may oligomerise in the presence of Aβ.
P06396	gelsolin	*GSN*	3	1	0	1	1	Biochemical data shows that gelsolin binds to Aβ and can modulate Aβ fibrillisation.
P08603	CFH	*CFH*	3	0	1	1	1	Evidence showing CFH binding to Aβ plaques. Possible involvement with Aβ plaques being recognized by microglia.
P00738	haptoglobin	*HP*	2	1	0	0	1	Biochemical evidence that haptoglobin can interact with prefibrillar Aβ thus maintaining its solubility.
P00751	CFB	*CFB*	2	0	0	1	1	Biochemical evidence shows that Aβ may indirectly modulate CFB expression with potential modulation of downstream markers MCP-1, IL-1β, TNF-α.
P01024	CC3	*C3*	2	1	0	0	1	Biochemical evidence that CC3 can accelerate Aβ fibrillisation. Some data showing CC3 mRNA concentrations increase between AD and age match controls.

P02679	FGγ	*FGG*	2	1	0	0	1	Fibrinogen can bind to Aβ and biochemical evidence showing fibrinogen may oligomerise in the presence of Aβ.
P02787	TF	*TF*	2	0	0	1	1	Biochemical binding to iron and transport into brain via TFR. Data showing the binding affinity of CP2 to the transferrin promoter was regulated by Aβ.
P06727	apoA4	*APOA4*	2	0	0	1	1	apoA4 is expressed in brain but intestines are higher.
P0C0L4	C4α	*C4A*	2	0	0	1	1	Biochemical evidence shows soluble Aβ can activate C4α
O14791	apoL1	*APOL1*	1	0	0	0	1	apoL1 is expressed in brain and it is a minor apoprotein component of HDL.
P08519	apo(a)	*LPA*	1	0	0	1	0	apo(a) concentrations can vary significantly between individuals and changes may be impacted by inflammatory response.
Q03591	FHR-1	*CFHR1*	1	0	0	0	1	Possible involvement with Aβ plaques being recognised by microglia.
P04196	HRG	*HRG*	1	0	0	0	1	HRG is a ligand for LRP1b involved in lipoprotein metabolism. Note that other ligands include Aβ precursor protein, fibrinogen, clusterin, serum amyloid P-component, and immunoglobulins.
O43866	CD5 antigen-like	*CD5L*	0	0	0	0	0	Did not find any biochemical studies directly linking protein to Aβ.
O75636	ficolin-3	*FCN3*	0	0	0	0	0	Did not find any biochemical studies directly linking protein to Aβ.
P00450	ceruloplasmin	*CP*	0	0	0	0	0	Did not find any biochemical studies directly linking protein to Aβ.
P00734	prothrombin	*F2*	0	0	0	0	0	Did not find any biochemical studies directly linking protein to Aβ.
P02747	C1QC	*C1QC*	0	0	0	0	0	Did not find any biochemical studies directly linking protein to Aβ.
P02790	hemopexin	*HPX*	0	0	0	0	0	Did not find any biochemical studies directly linking protein to Aβ.
P04003	C4b-binding protein alpha chain	*C4BPA*	0	0	0	0	0	Did not find any biochemical studies directly linking protein to Aβ.
P07357	CC8α	*C8A*	0	0	0	0	0	Did not find any biochemical studies directly linking protein to Aβ.
P13671	CC6	*C6*	0	0	0	0	0	Did not find any biochemical studies directly linking protein to Aβ.
P25311	zinc-alpha-2-glycoprotein	*AZGP1*	0	0	0	0	0	Did not find any biochemical studies directly linking protein to Aβ.
Q92620	pre-mRNA-splicing factor	*DHX38*	0	0	0	0	0	Did not find any biochemical studies directly linking protein to Aβ.

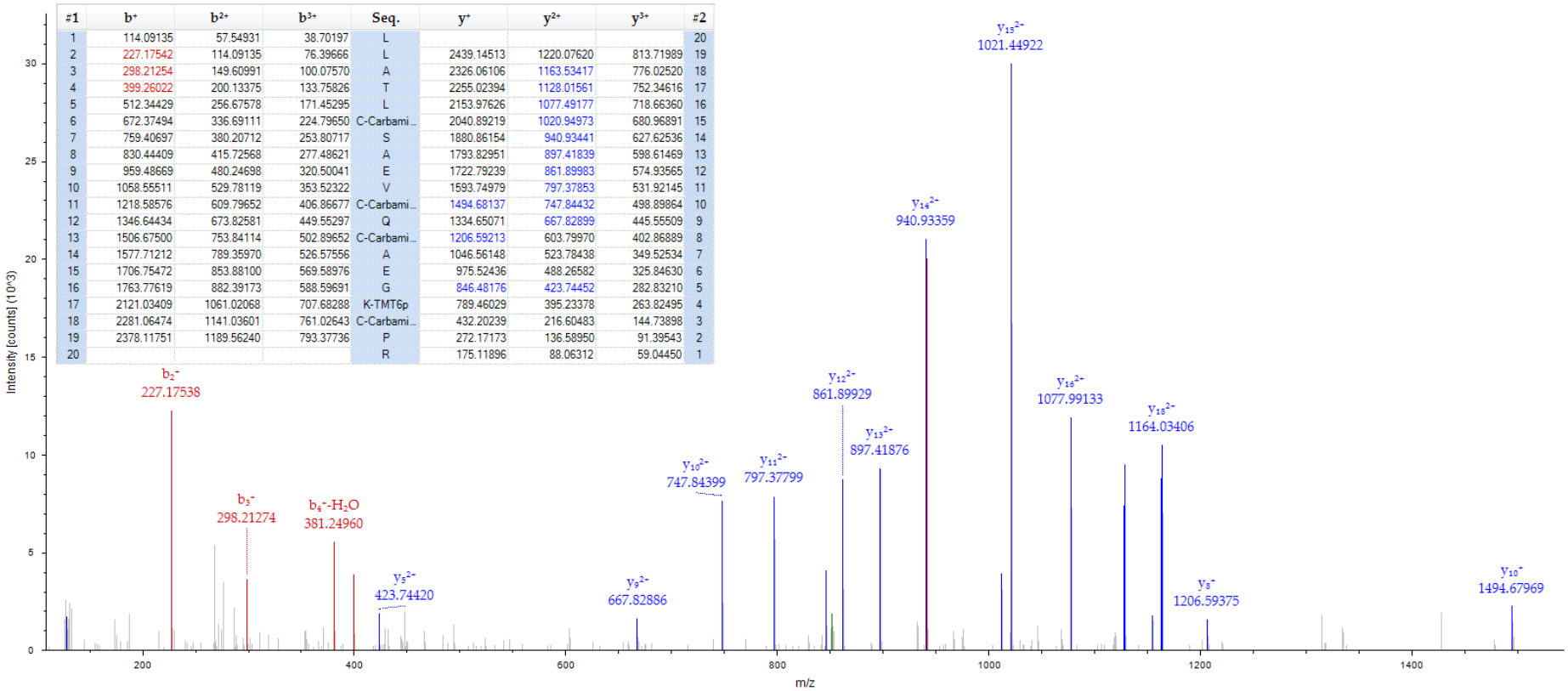

Figure 3-12: MS/MS spectrum of m/z 851.41the $[M+3H]^{3}+$ molecular ion for a peptide of 2552.23 Da with corresponding sequence LLATLCSAEVCQCAEGKCPR unique to C4α identified in 1DGE fraction 7 as significant (P value <0.05) between PiB+ and PiB- groups.

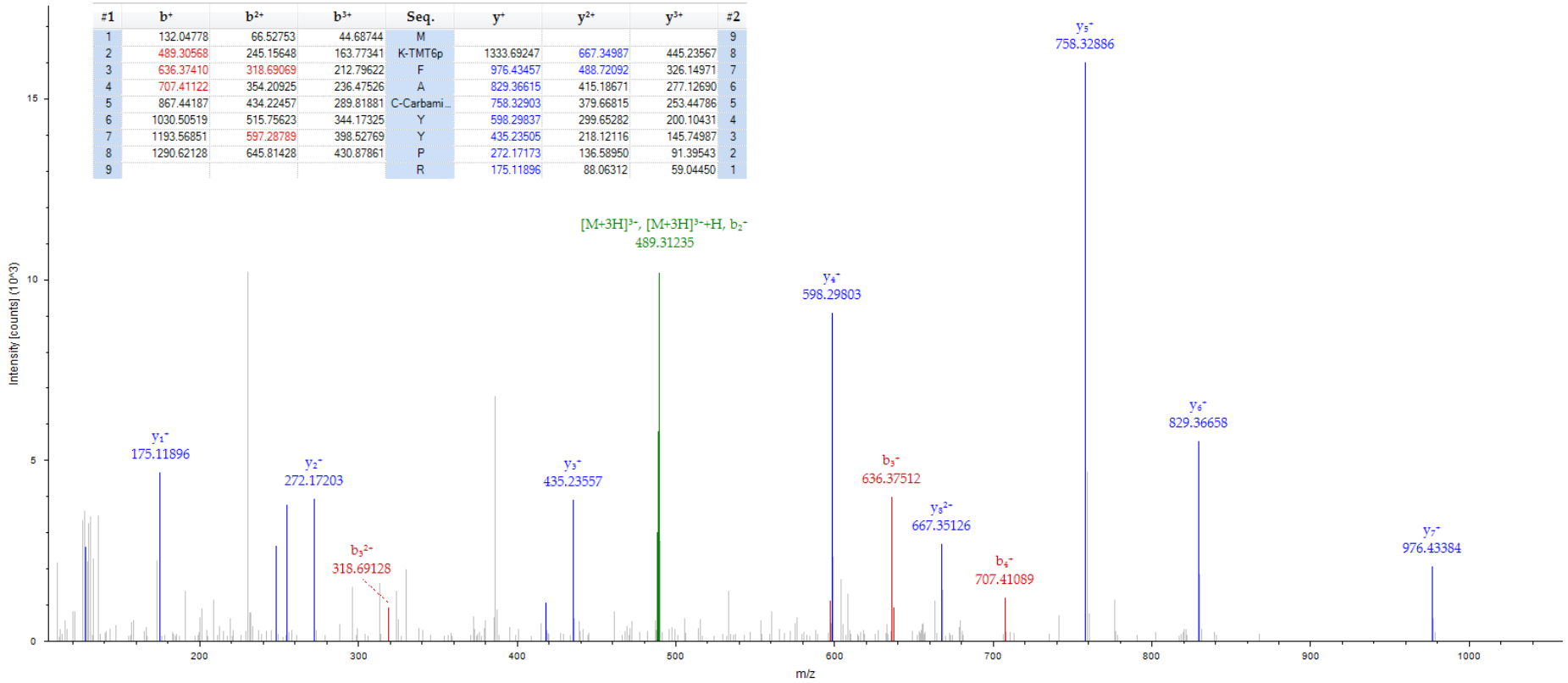

Figure 3-13: MS/MS spectrum of m/z 488.91 the $[M+3H]^{3}$+ molecular ion for a peptide of 1464.73 Da with corresponding sequence MKFACYYPR unique to C4α identified in 1DGE fraction 7 as significant (P value <0.05) between PiB+ and PiB- groups.

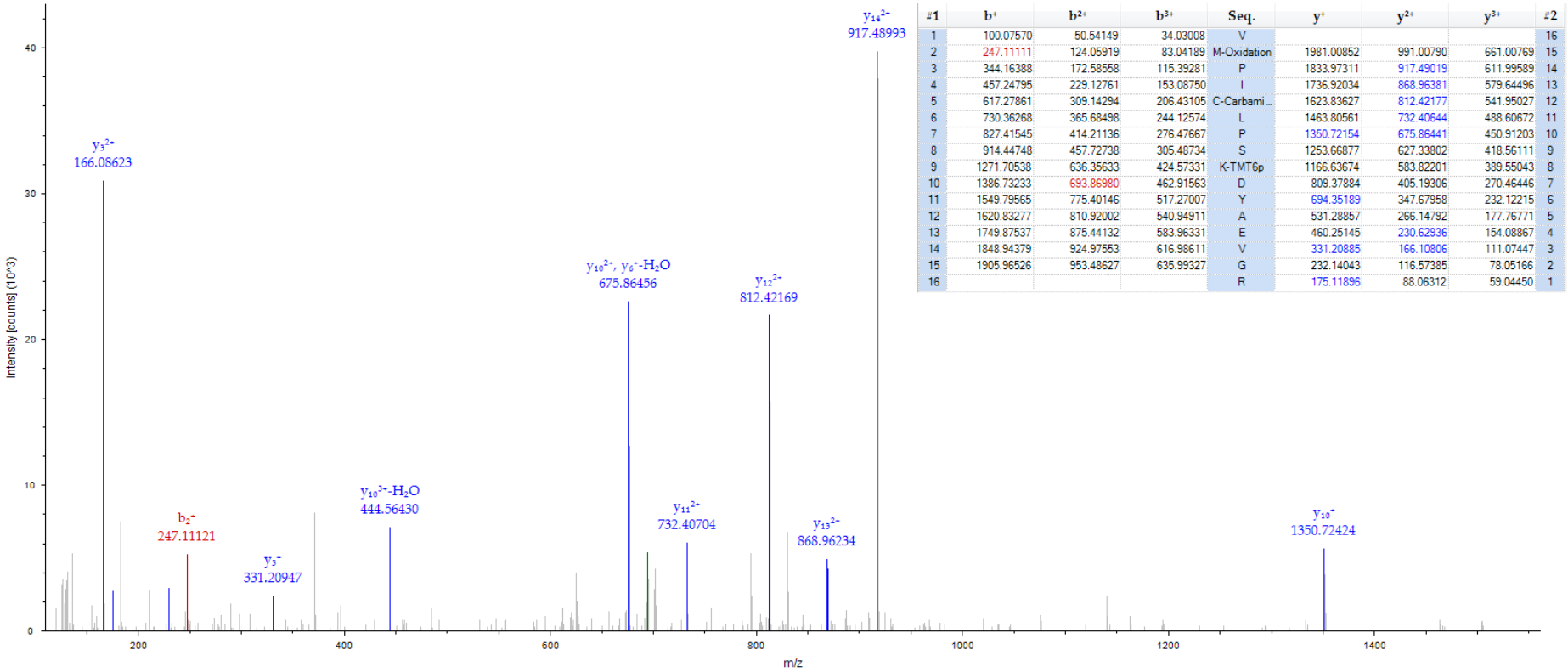

#1	b^+	b^{2+}	b^{3+}	Seq.	y^+	y^{2+}	y^{3+}	#2
1	100.07570	50.54149	34.03008	V				16
2	247.11111	124.05919	83.04189	M-Oxidation	1981.00852	991.00790	661.00769	15
3	344.16388	172.58558	115.39281	P	1833.97311	917.49019	611.99589	14
4	457.24795	229.12761	153.08750	I	1736.92034	868.96381	579.64496	13
5	617.27861	309.14294	206.43105	C-Carbami...	1623.83627	812.42177	541.95027	12
6	730.36268	365.68498	244.12574	L	1463.80561	732.40644	488.60672	11
7	827.41545	414.21136	276.47667	P	1350.72154	675.86441	450.91203	10
8	914.44748	457.72738	305.48734	S	1253.66877	627.33802	418.56111	9
9	1271.70538	636.35633	424.57331	K-TMT6p	1166.63674	583.82201	389.55043	8
10	1386.73233	693.86980	462.91563	D	809.37884	405.19306	270.46446	7
11	1549.79565	775.40146	517.27007	Y	694.35189	347.67958	232.12215	6
12	1620.83277	810.92002	540.94911	A	531.28857	266.14792	177.76771	5
13	1749.87537	875.44132	583.96331	E	460.25145	230.62936	154.08867	4
14	1848.94379	924.97553	616.98611	V	331.20885	166.10806	111.07447	3
15	1905.96526	953.48627	635.99327	G	232.14043	116.57385	78.05166	2
16				R	175.11896	88.06312	59.04450	1

Figure 3-14: MS/MS spectrum of *m/z* 694.03 the $[M+3H]^{3+}$ molecular ion for a peptide of 2080.07 Da with corresponding sequence VMPICLPSKDYAEVGR unique to haptoglobin identified in 1DGE fraction 8 as significant (*P* value <0.05) between PiB+ and PiB- groups.

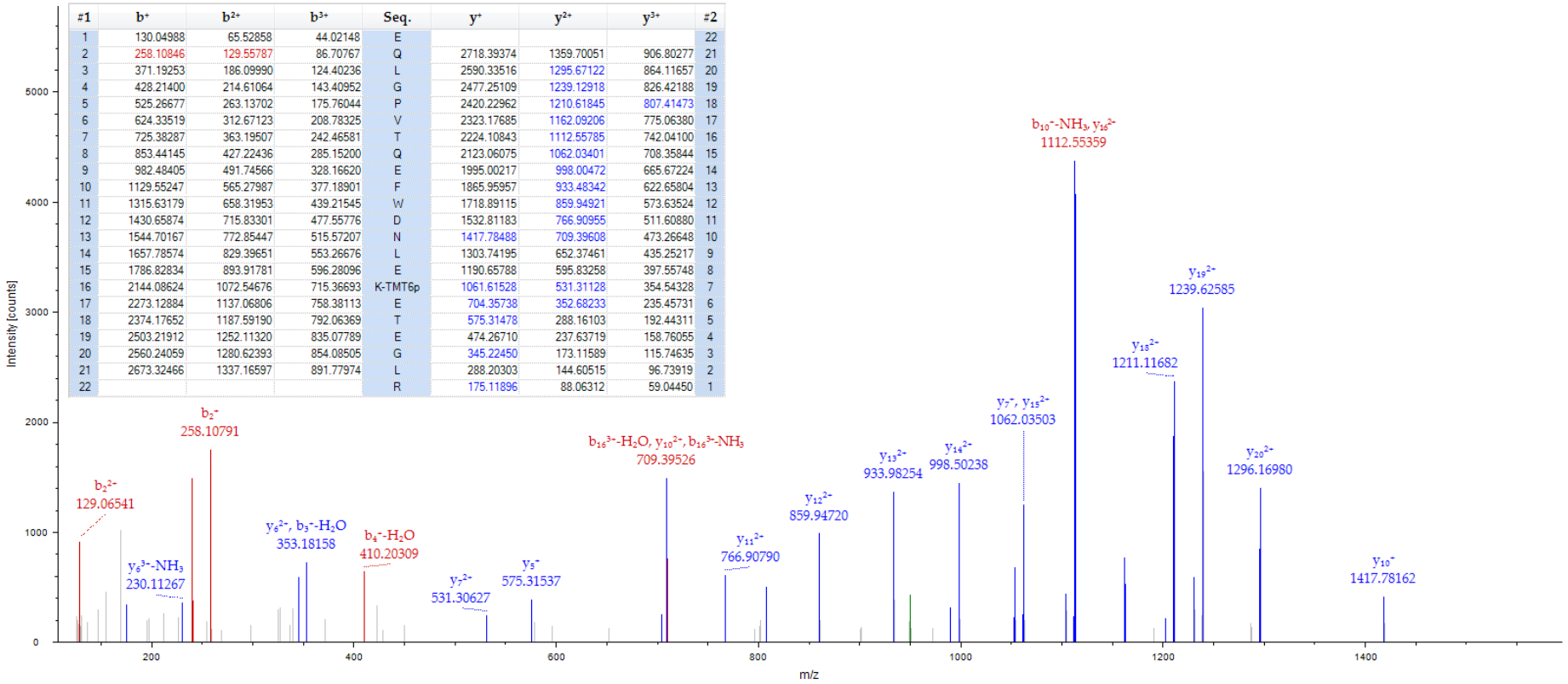

#1	b+	b2+	b3+	Seq.	y+	y2+	y3+	#2
1	130.04988	65.52858	44.02148	E				22
2	258.10846	129.55787	86.70767	Q	2718.39374	1359.70051	906.80277	21
3	371.19253	186.09990	124.40236	L	2590.33516	1295.67122	864.11657	20
4	428.21400	214.61064	143.40952	G	2477.25109	1239.12918	826.42188	19
5	525.26677	263.13702	175.76044	P	2420.22962	1210.61845	807.41473	18
6	624.33519	312.67123	208.78325	V	2323.17685	1162.09206	775.06380	17
7	725.38287	363.19507	242.46581	T	2224.10843	1112.55785	742.04100	16
8	853.44145	427.22436	285.15200	Q	2123.06075	1062.03401	708.35844	15
9	982.48405	491.74566	328.16620	E	1995.00217	998.00472	665.67224	14
10	1129.55247	565.27987	377.18901	F	1865.95957	933.48342	622.65804	13
11	1315.63179	658.31953	439.21545	W	1718.89115	859.94921	573.63524	12
12	1430.65874	715.83301	477.55776	D	1532.81183	766.90955	511.60880	11
13	1544.70167	772.85447	515.57207	N	1417.78488	709.39608	473.26648	10
14	1657.78574	829.39651	553.26676	L	1303.74195	652.37461	435.25217	9
15	1786.82834	893.91781	596.28096	E	1190.65788	595.83258	397.55748	8
16	2144.08624	1072.54676	715.36693	K-TMT6p	1061.61528	531.31128	354.54328	7
17	2273.12884	1137.06806	758.38113	E	704.35738	352.68233	235.45731	6
18	2374.17652	1187.59190	792.06369	T	575.31478	288.16103	192.44311	5
19	2503.21912	1252.11320	835.07789	E	474.26710	237.63719	158.76055	4
20	2560.24059	1280.62393	854.08505	G	345.22450	173.11589	115.74635	3
21	2673.32466	1337.16597	891.77974	L	288.20303	144.60515	96.73919	2
22				R	175.11896	88.06312	59.04450	1

Figure 3-15: MS/MS spectrum of *m/z* 949.82 the $[M+3H]^{3+}$ molecular ion for a peptide of 2847.43 Da with corresponding sequence EQLGPVTQEFWDNLEKETEGLR unique to apoA1 identified in 1DGE fraction 10 as significant (*P* value <0.05) between PiB+ and PiB- groups.

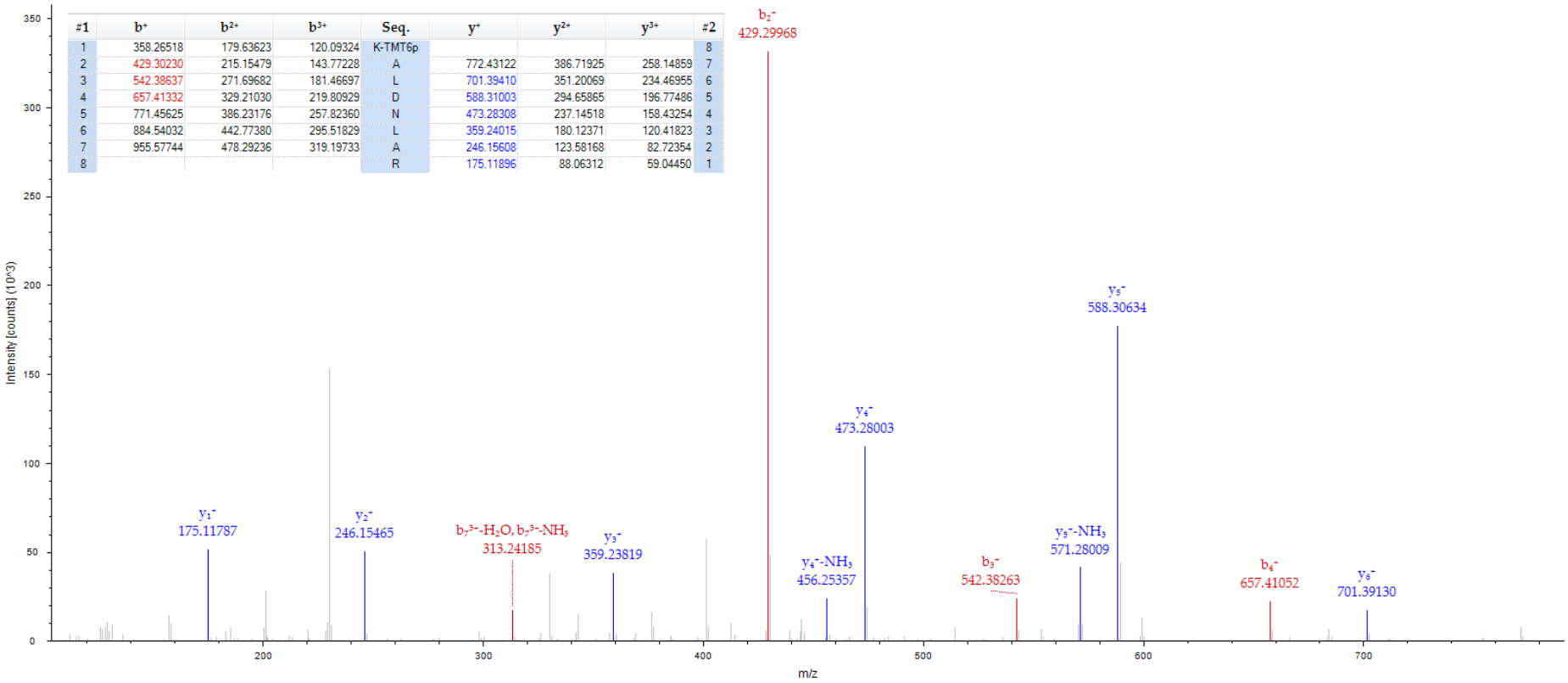

Figure 3-16: MS/MS spectrum of *m/z* 377.23 the $[M+3H]^{3+}$ molecular ion for a peptide of 1129.68 Da with corresponding sequence KALDNLAR unique to apoL1 identified in 1DGE fraction 5 as significant (*P* value <0.05) between PiB+ and PiB- groups.

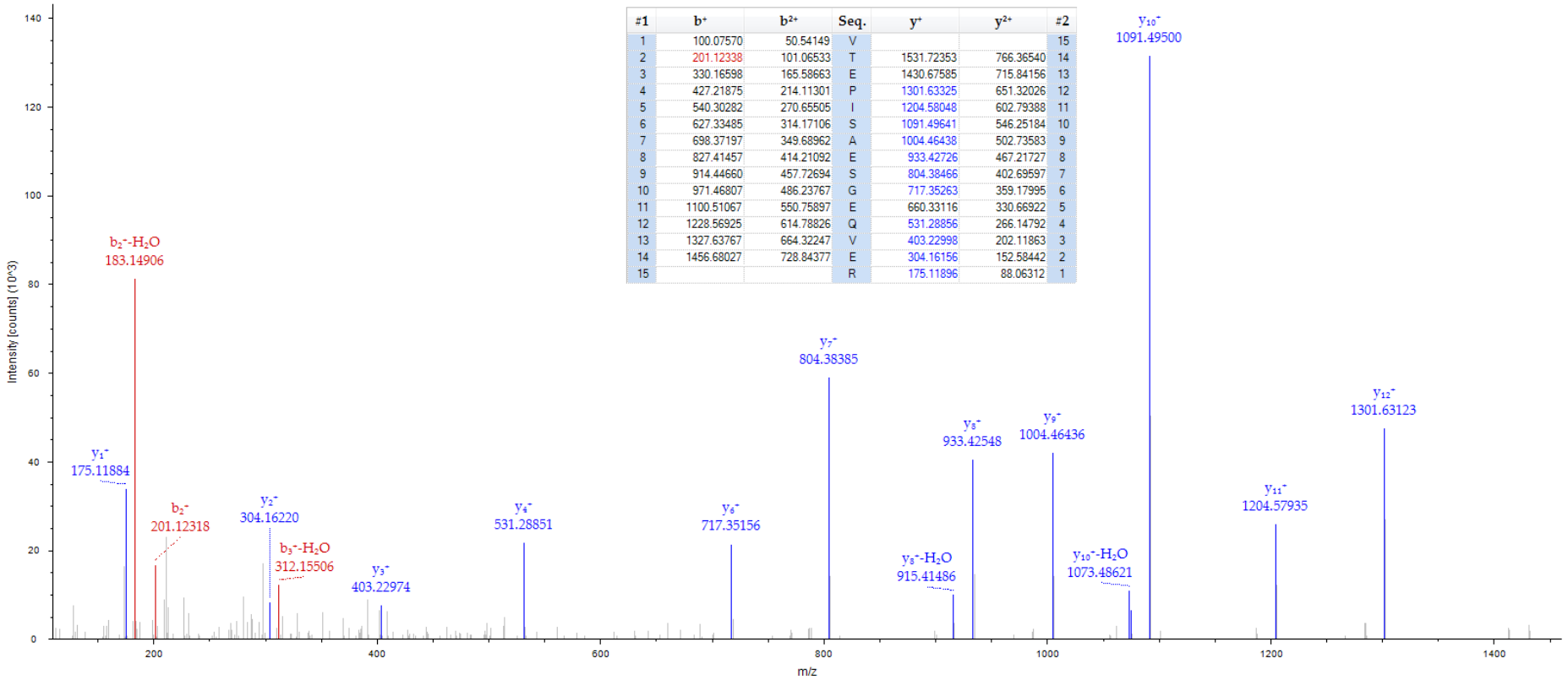

Figure 3-17: MS/MS spectrum of *m/z* 815.90 the $[M+2H]^{2+}$ molecular ion for a peptide of 1630.79 Da with corresponding sequence VTEPISAESGEQVER unique to apoL1 identified in 1DGE fraction 5 as significant (*P* value <0.05) between PiB+ and PiB- groups.

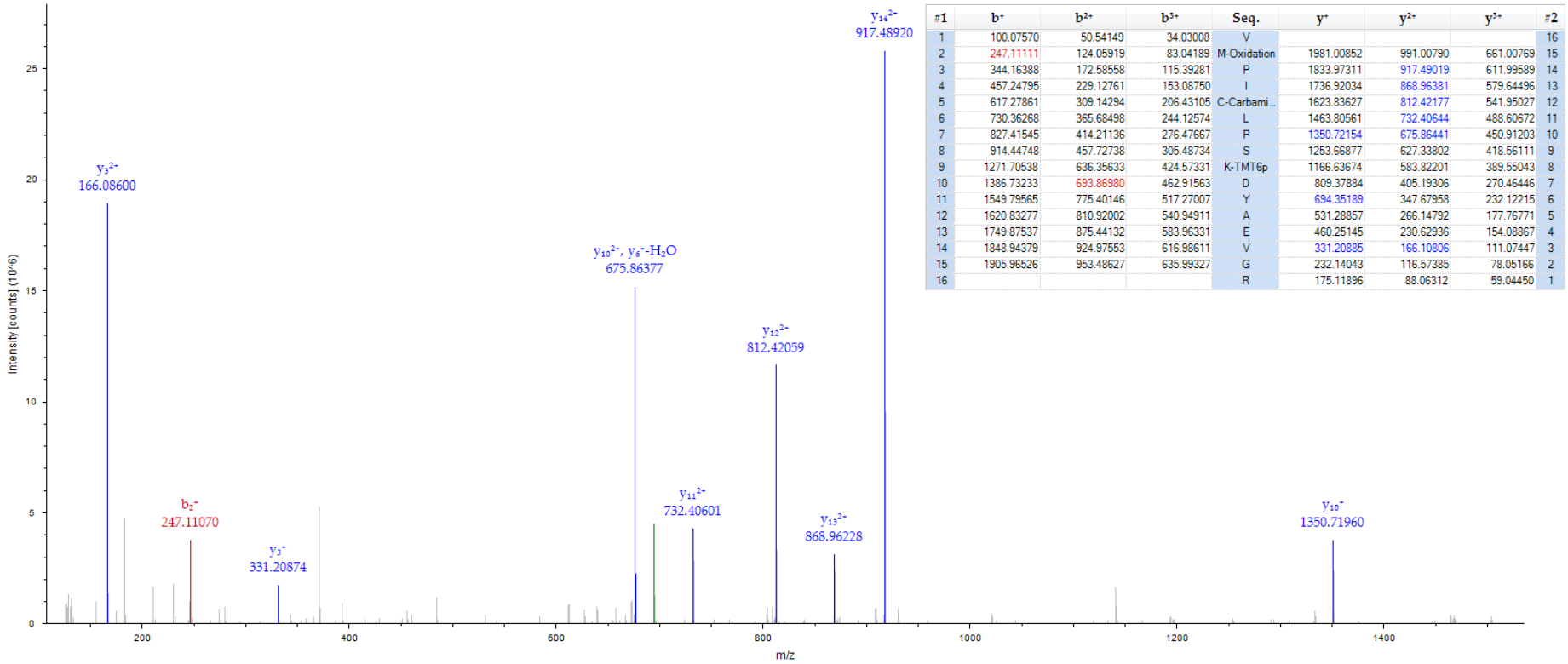

#1	b+	b2+	b3+	Seq.	y+	y2+	y3+	#2
1	100.07570	50.54149	34.03008	V				16
2	247.11111	124.05919	83.04189	M-Oxidation	1981.00852	991.00790	661.00769	15
3	344.16388	172.58558	115.39281	P	1833.97311	917.49019	611.99589	14
4	457.24795	229.12761	153.08750	I	1736.92034	868.96381	579.64496	13
5	617.27861	309.14294	206.43105	C-Carbami...	1623.83627	812.42177	541.95027	12
6	730.36268	365.68498	244.12574	L	1463.80561	732.40644	488.60672	11
7	827.41545	414.21136	276.47667	P	1350.72154	675.86441	450.91203	10
8	914.44748	457.72738	305.48734	S	1253.66877	627.33802	418.56111	9
9	1271.70538	636.35633	424.57331	K-TMT6p	1166.63674	583.82201	389.55043	8
10	1386.73233	693.86980	462.91563	D	809.37884	405.19306	270.46446	7
11	1549.79565	775.40146	517.27007	Y	694.35189	347.67958	232.12215	6
12	1620.83277	810.92002	540.94911	A	531.28857	266.14792	177.76771	5
13	1749.87537	875.44132	583.96331	E	460.25145	230.62936	154.08867	4
14	1848.94379	924.97553	616.98611	V	331.20885	166.10806	111.07447	3
15	1905.96526	953.48627	635.99327	G	232.14043	116.57385	78.05166	2
16				R	175.11896	88.06312	59.04450	1

Figure 3-18: MS/MS spectrum of *m/z* 694.03 the $[M+3H]^{3+}$ molecular ion for a peptide of 2080.08 Da with corresponding sequence VMPICLPSKDYAEVGR unique to haptoglobin identified in 1DGE fraction 5 as significant (*P* value <0.05) between PiB+ and PiB- groups.

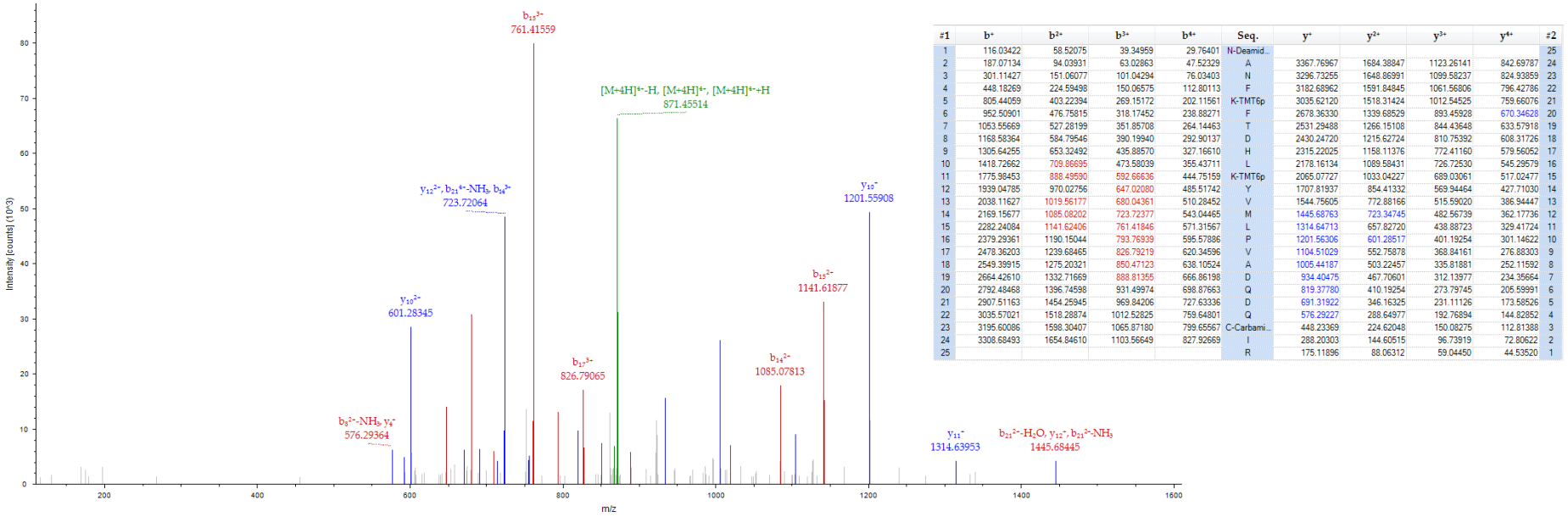

#1	b⁺	b²⁺	b³⁺	b⁴⁺	Seq.	y⁺	y²⁺	y³⁺	y⁴⁺	#2
1	116.03422	58.52075	39.34959	29.76401	N-Deamid...					25
2	187.07134	94.03931	63.02863	47.52329	A	3367.76967	1684.38847	1123.26141	842.69787	24
3	301.11427	151.06077	101.04294	76.03403	N	3296.73255	1648.86991	1099.58237	824.93859	23
4	448.18269	224.59498	150.06575	112.80113	F	3182.68962	1591.84845	1061.56806	796.42786	22
5	805.44059	403.22394	269.15172	202.11561	K-TMT6p	3035.62120	1518.31424	1012.54525	759.66076	21
6	952.50901	476.75815	318.17452	238.88271	F	2678.36330	1339.68529	893.45928	670.34628	20
7	1053.55669	527.28199	351.85708	264.14463	T	2531.29488	1266.15108	844.43648	633.57918	19
8	1168.58364	584.79546	390.19940	292.90137	D	2430.24720	1215.62724	810.75392	608.31726	18
9	1305.64255	653.32492	435.88570	327.16610	H	2315.22025	1158.11376	772.41160	579.56052	17
10	1418.72662	709.86695	473.58039	355.43711	L	2178.16134	1089.58431	726.72530	545.29579	16
11	1775.98453	888.49590	592.66636	444.75159	K-TMT6p	2065.07727	1033.04227	689.03061	517.02477	15
12	1939.04785	970.02756	647.02080	485.51742	Y	1707.81937	854.41332	569.94464	427.71030	14
13	2038.11627	1019.56177	680.04361	510.28452	V	1544.75605	772.88166	515.59020	386.94447	13
14	2169.15677	1085.08202	723.72377	543.04465	M	1445.68763	723.34745	482.56739	362.17736	12
15	2282.24084	1141.62406	761.41846	571.31567	L	1314.64713	657.82720	438.88723	329.41724	11
16	2379.29361	1190.15044	793.76939	595.57886	P	1201.56306	601.28517	401.19254	301.14622	10
17	2478.36203	1239.68465	826.79219	620.34596	V	1104.51029	552.75878	368.84161	276.88303	9
18	2549.39915	1275.20321	850.47123	638.10524	A	1005.44187	503.22457	335.81881	252.11592	8
19	2664.42610	1332.71669	888.81355	666.86198	D	934.40475	467.70601	312.13977	234.35664	7
20	2792.48468	1396.74598	931.49974	698.87663	Q	819.37780	410.19254	273.79745	205.59991	6
21	2907.51163	1454.25945	969.84206	727.63336	D	691.31922	346.16325	231.11126	173.58526	5
22	3035.57021	1518.28874	1012.52825	759.64801	Q	576.29227	288.64977	192.76894	144.82852	4
23	3195.60086	1598.30407	1065.87180	799.65567	C-Carbami...	448.23369	224.62048	150.08275	112.81388	3
24	3308.68493	1654.84610	1103.56649	827.92669	I	288.20303	144.60515	96.73919	72.80622	2
25					R	175.11896	88.06312	59.04450	44.53520	1

Figure 3-19: MS/MS spectrum of *m/z* 871.45 the $[M+4H]^{4+}$ molecular ion for a peptide of 3482.78 Da with corresponding sequence NANFKFTDHLKYVMLPVADQDQCIR unique to haptoglobin identified in 1DGE fraction 5 as significant (*P* value <0.05) between PiB+ and PiB- groups.

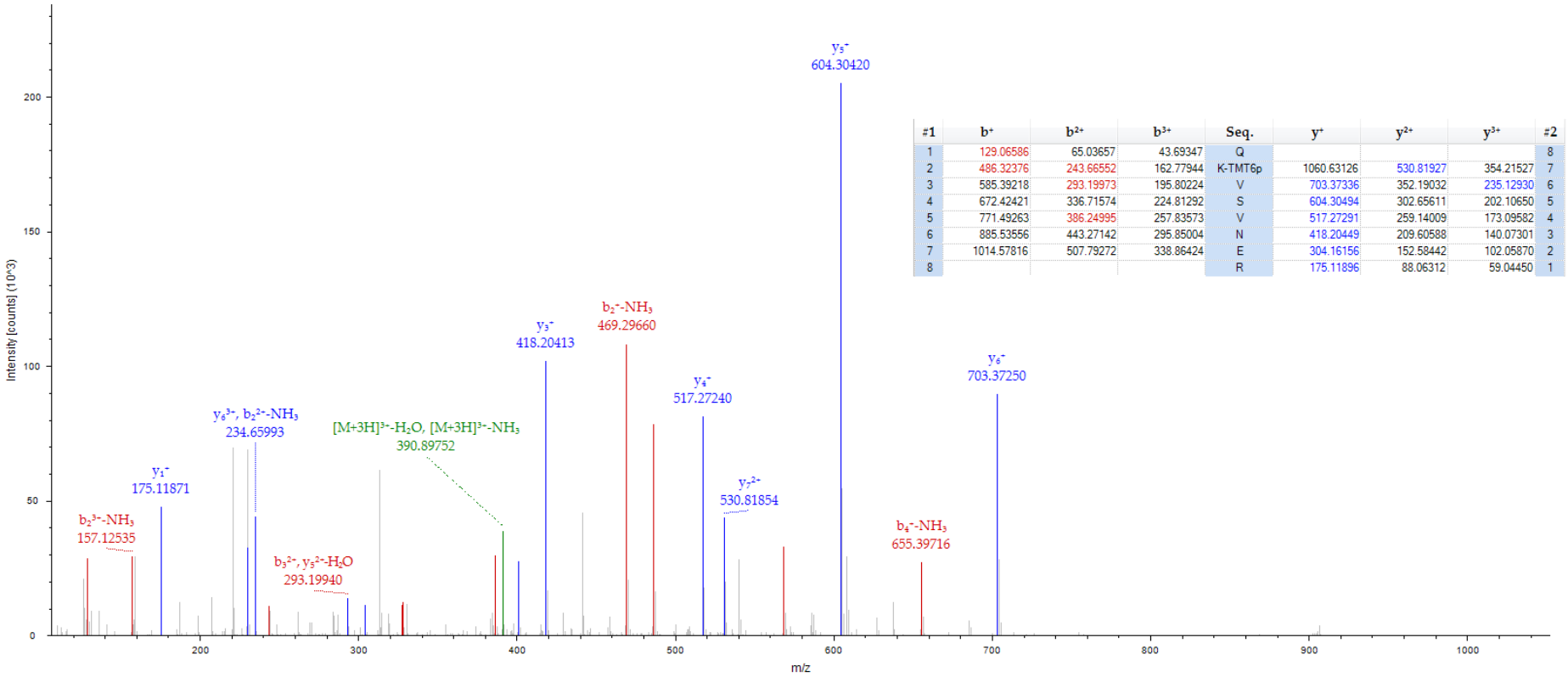

#1	b+	b2+	b3+	Seq.	y+	y2+	y3+	#2
1	129.06586	65.03657	43.69347	Q				8
2	486.32376	243.66552	162.77944	K-TMT6p	1060.63126	530.81927	354.21527	7
3	585.39218	293.19973	195.80224	V	703.37336	352.19032	235.12930	6
4	672.42421	336.71574	224.81292	S	604.30494	302.65611	202.10650	5
5	771.49263	386.24995	257.83573	V	517.27291	259.14009	173.09582	4
6	885.53556	443.27142	295.85004	N	418.20449	209.60588	140.07301	3
7	1014.57816	507.79272	338.86424	E	304.16156	152.58442	102.05870	2
8				R	175.11896	88.06312	59.04450	1

Figure 3-20: MS/MS spectrum of *m/z* 396.90 the $[M+3H]^{3+}$ molecular ion for a peptide of 1188.69 Da with corresponding sequence QKVSVNER unique to haptoglobin identified in 1DGE fraction 5 as significant (*P* value <0.05) between PiB+ and PiB- groups.

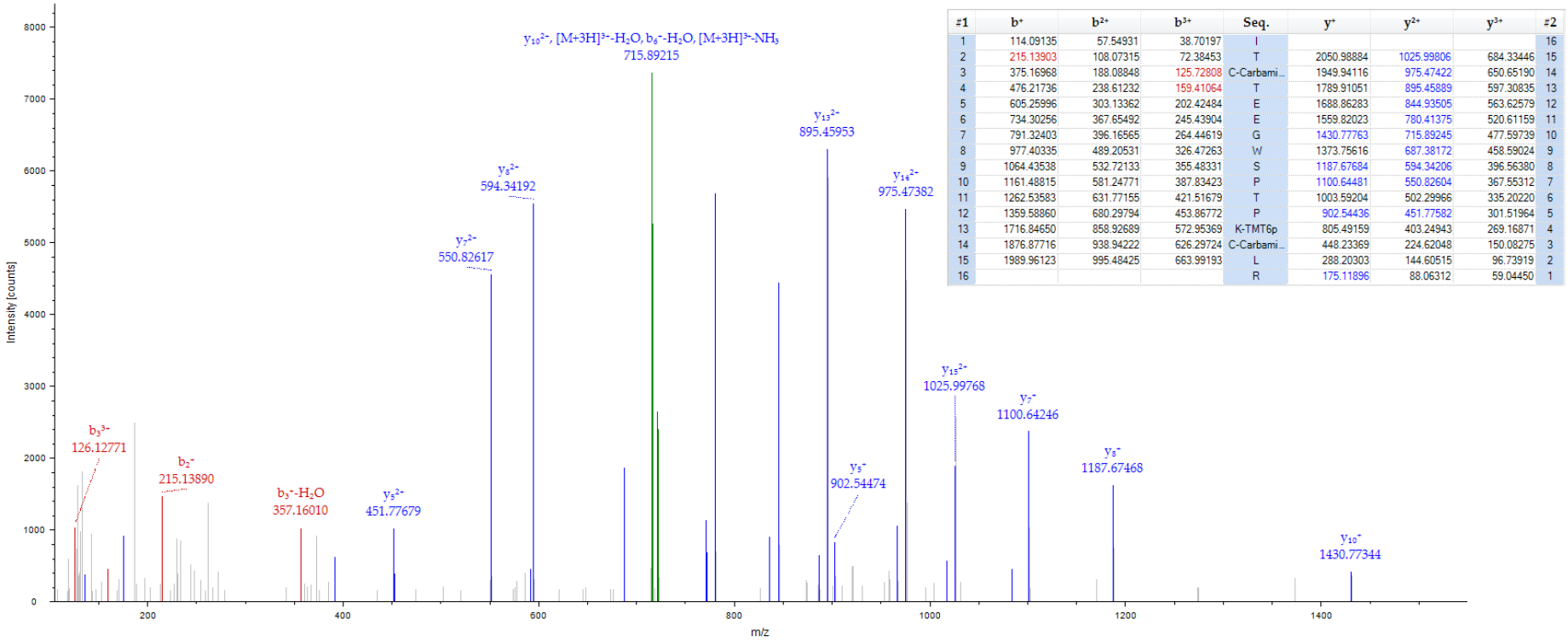

#1	b+	b2+	b3+	Seq.	y+	y2+	y3+	#2
1	114.09135	57.54931	38.70197	I				16
2	215.13903	108.07315	72.38453	T	2050.98884	1025.99806	684.33446	15
3	375.16968	188.08848	125.72808	C-Carbami...	1949.94116	975.47422	650.65190	14
4	476.21736	238.61232	159.41064	T	1789.91051	895.45889	597.30835	13
5	605.25996	303.13362	202.42484	E	1688.86283	844.93505	563.62579	12
6	734.30256	367.65492	245.43904	E	1559.82023	780.41375	520.61159	11
7	791.32403	396.16565	264.44619	G	1430.77763	715.89245	477.59739	10
8	977.40335	489.20531	326.47263	W	1373.75616	687.38172	458.59024	9
9	1064.43538	532.72133	355.48331	S	1187.67684	594.34206	396.56380	8
10	1161.48815	581.24771	387.83423	P	1100.64481	550.82604	367.55312	7
11	1262.53583	631.77155	421.51679	T	1003.59204	502.29966	335.20220	6
12	1359.58860	680.29794	453.86772	P	902.54436	451.77582	301.51964	5
13	1716.84650	858.92689	572.95369	K-TMT6p	805.49159	403.24943	269.16871	4
14	1876.87716	938.94222	626.29724	C-Carbami...	448.23369	224.62048	150.08275	3
15	1989.96123	995.48425	663.99193	L	288.20303	144.60515	96.73919	2
16				R	175.11896	88.06312	59.04450	1

Figure 3-21: MS/MS spectrum of *m/z* 722.03 the $[M+3H]^{3+}$ molecular ion for a peptide of 2164.07 Da with corresponding sequence ITCTEEGWSPTPKCLR unique to FHR-1 identified in 1DGE fraction 8 as significant (*P* value <0.05) between PiB+ and PiB- groups.

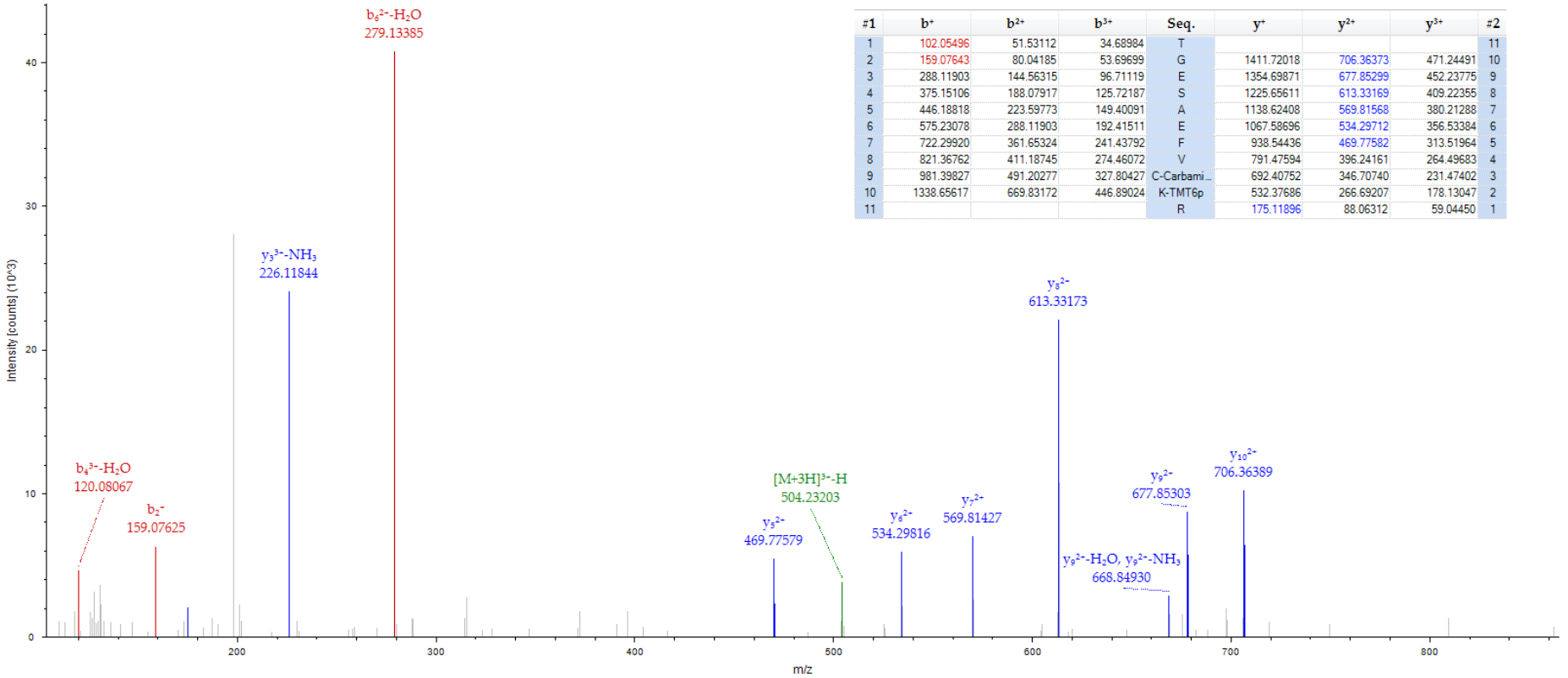

#1	b⁺	b²⁺	b³⁺	Seq.	y⁺	y²⁺	y³⁺	#2
1	102.05496	51.53112	34.68984	T				11
2	159.07643	80.04185	53.69699	G	1411.72018	706.36373	471.24491	10
3	288.11903	144.56315	96.71119	E	1354.69871	677.85299	452.23775	9
4	375.15106	188.07917	125.72187	S	1225.65611	613.33169	409.22355	8
5	446.18818	223.59773	149.40091	A	1138.62408	569.81568	380.21288	7
6	575.23078	288.11903	192.41511	E	1067.58696	534.29712	356.53384	6
7	722.29920	361.65324	241.43792	F	938.54436	469.77582	313.51964	5
8	821.36762	411.18745	274.46072	V	791.47594	396.24161	264.49683	4
9	981.39827	491.20277	327.80427	C-Carbami...	692.40752	346.70740	231.47402	3
10	1338.65617	669.83172	446.89024	K-TMT6p	532.37686	266.69207	178.13047	2
11				R	175.11896	88.06312	59.04450	1

Figure 3-22: MS/MS spectrum of m/z 504.93 the $[M+3H]^{3}$+ molecular ion for a peptide of 1512.77 Da with corresponding sequence TGESAEFVCKR unique to FHR-1 identified in 1DGE fraction 8 as significant (*P* value <0.05) between PiB+ and PiB- groups.

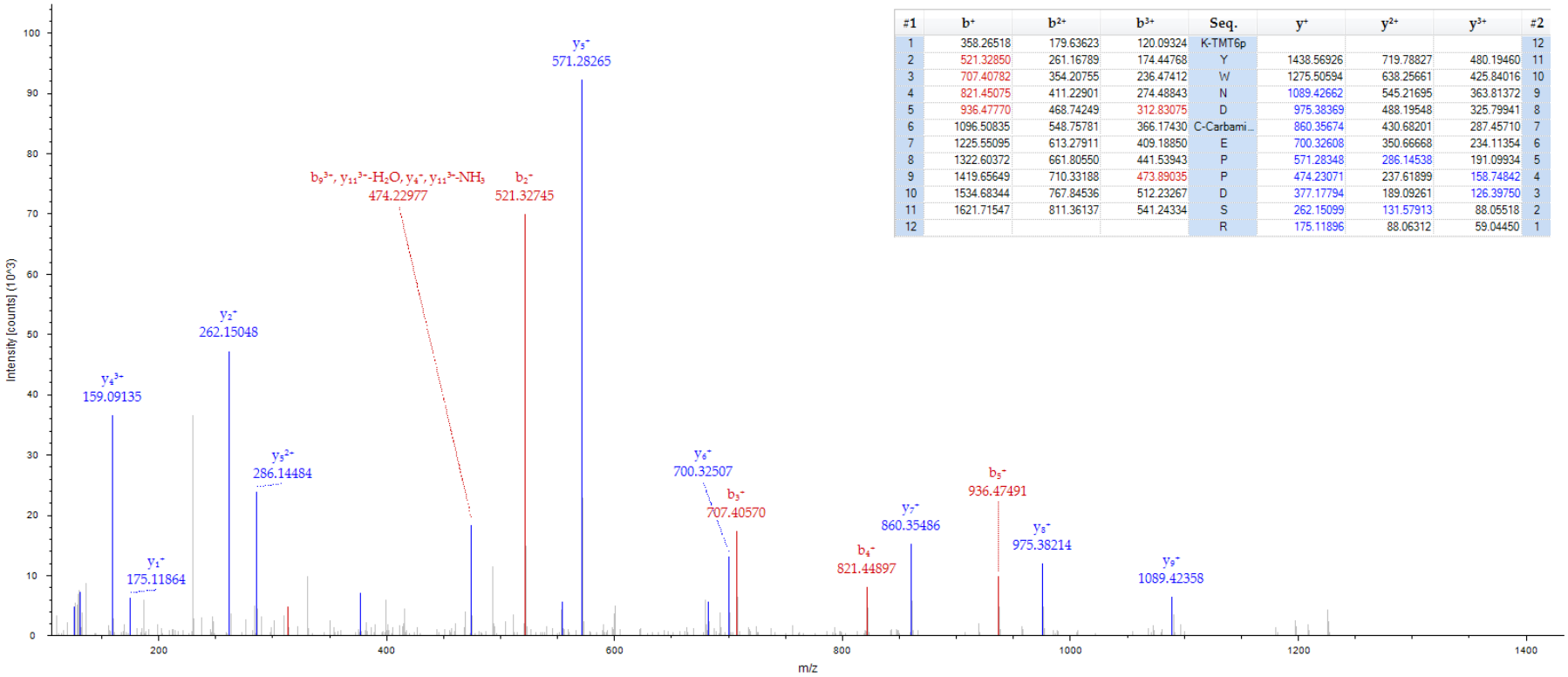

#1	b+	b2+	b3+	Seq.	y+	y2+	y3+	#2
1	358.26518	179.63623	120.09324	K-TMT6p				12
2	521.32850	261.16789	174.44768	Y	1438.56926	719.78827	480.19460	11
3	707.40782	354.20755	236.47412	W	1275.50594	638.25661	425.84016	10
4	821.45075	411.22901	274.48843	N	1089.42662	545.21695	363.81372	9
5	936.47770	468.74249	312.83075	D	975.38369	488.19548	325.79941	8
6	1096.50835	548.75781	366.17430	C-Carbami...	860.35674	430.68201	287.45710	7
7	1225.55095	613.27911	409.18850	E	700.32608	350.66668	234.11354	6
8	1322.60372	661.80550	441.53943	P	571.28348	286.14538	191.09934	5
9	1419.65649	710.33188	473.89035	P	474.23071	237.61899	158.74842	4
10	1534.68344	767.84536	512.23267	D	377.17794	189.09261	126.39750	3
11	1621.71547	811.36137	541.24334	S	262.15099	131.57913	88.05518	2
12				R	175.11896	88.06312	59.04450	1

Figure 3-23: MS/MS spectrum of m/z 599.28 the $[M+3H]^{3}+$ molecular ion for a peptide of 1795.83 Da with corresponding sequence KYWNDCEPPDSR unique to HRG identified in 1DGE fraction 3 as significant (*P* value <0.05) between PiB+ and PiB- groups.

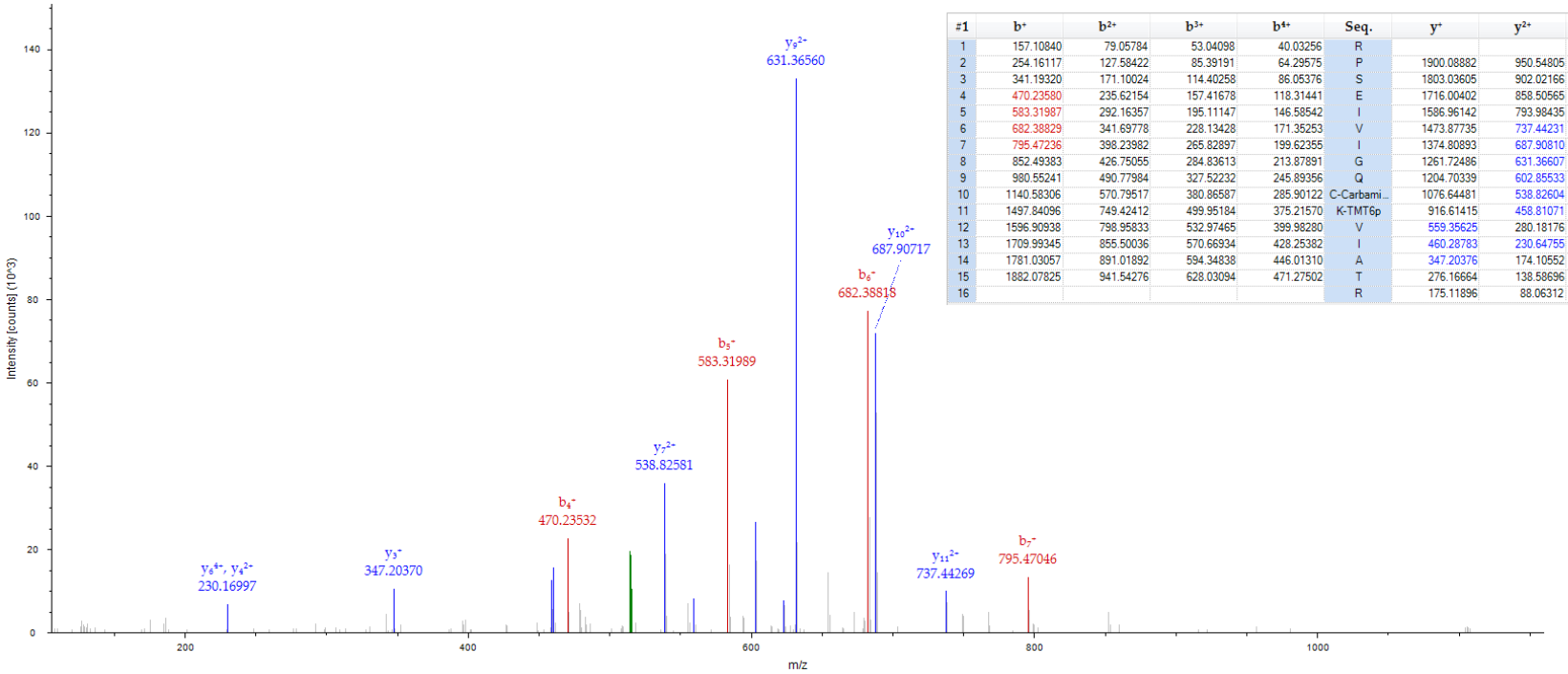

#1	b+	b2+	b3+	b4+	Seq.	y+	y2+	y3+	y4+	#2
1	157.10840	79.05784	53.04098	40.03256	R					16
2	254.16117	127.58422	85.39191	64.29575	P	1900.08882	950.54805	634.03446	475.77766	15
3	341.19320	171.10024	114.40258	86.05376	S	1803.03605	902.02166	601.68353	451.51447	14
4	470.23580	235.62154	157.41678	118.31441	E	1716.00402	858.50565	572.67286	429.75646	13
5	583.31987	292.16357	195.11147	146.58542	I	1586.96142	793.98435	529.65866	397.49581	12
6	682.38829	341.69778	228.13428	171.35253	V	1473.87735	737.44231	491.96397	369.22479	11
7	795.47236	398.23982	265.82897	199.62355	I	1374.80893	687.90810	458.94116	344.45769	10
8	852.49383	426.75055	284.83613	213.87891	G	1261.72486	631.36607	421.24647	316.18667	9
9	980.55241	490.77984	327.52232	245.89356	Q	1204.70339	602.85533	402.23931	301.93130	8
10	1140.58306	570.79517	380.86587	285.90122	C-Carbami...	1076.64481	538.82604	359.55312	269.91666	7
11	1497.84096	749.42412	499.95184	375.21570	K-TMT6p	916.61415	458.81071	306.20957	229.90900	6
12	1596.90938	798.95833	532.97465	399.98280	V	559.35625	280.18176	187.12360	140.59452	5
13	1709.99345	855.50036	570.66934	428.25382	I	460.28783	230.64755	154.10079	115.82742	4
14	1781.03057	891.01892	594.34838	446.01310	A	347.20376	174.10552	116.40610	87.55640	3
15	1882.07825	941.54276	628.03094	471.27502	T	276.16664	138.58696	92.72706	69.79712	2
16					R	175.11896	88.06312	59.04450	44.53520	1

Figure 3-24: MS/MS spectrum of m/z 514.80 the $[M+4H]^{4}+$ molecular ion for a peptide of 2056.18 Da with corresponding sequence RPSEIVIGQCKVIATR unique to HRG identified in 1DGE fraction 3 as significant (*P* value <0.05) between PiB+ and PiB- groups.

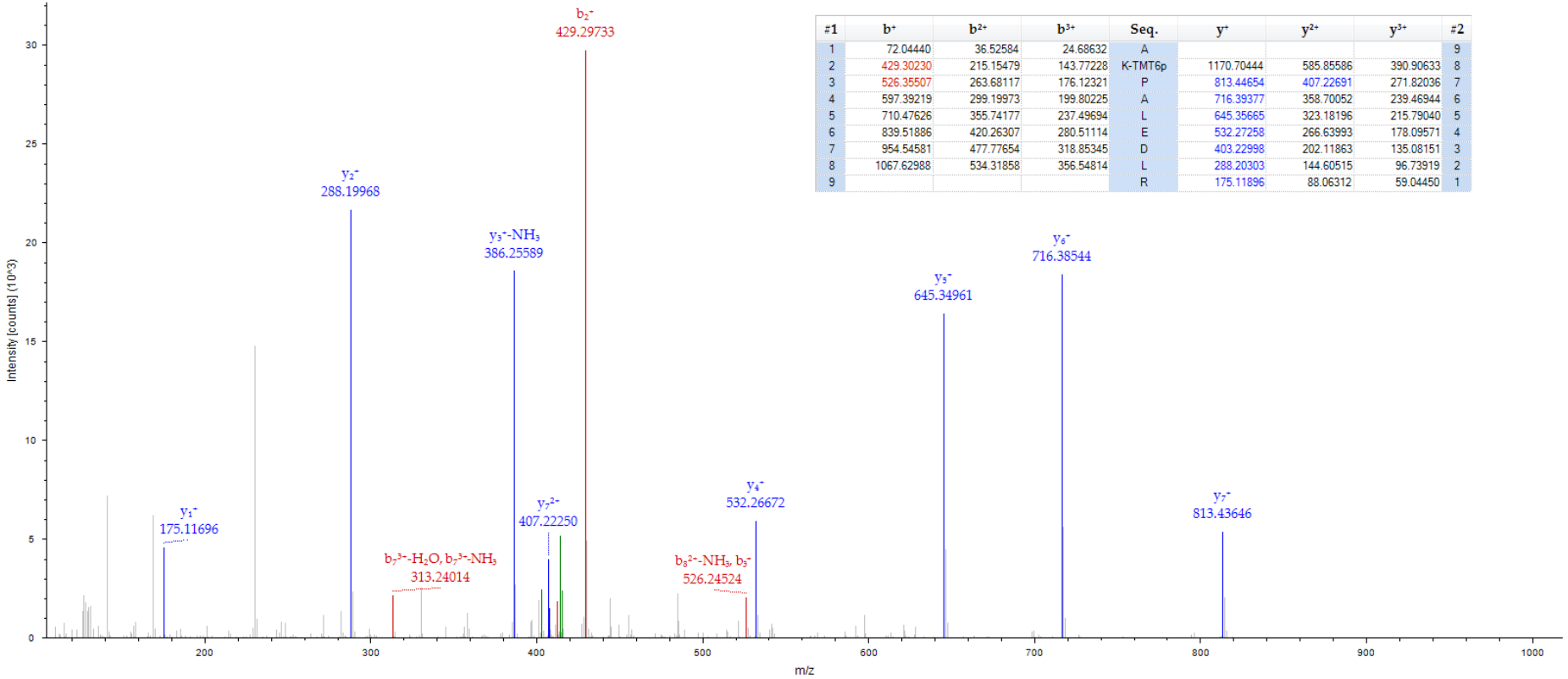

#1	b+	b2+	b3+	Seq.	y+	y2+	y3+	#2
1	72.04440	36.52584	24.68632	A				9
2	429.30230	215.15479	143.77228	K-TMT6p	1170.70444	585.85586	390.90633	8
3	526.35507	263.68117	176.12321	P	813.44654	407.22691	271.82036	7
4	597.39219	299.19973	199.80225	A	716.39377	358.70052	239.46944	6
5	710.47626	355.74177	237.49694	L	645.35665	323.18196	215.79040	5
6	839.51886	420.26307	280.51114	E	532.27258	266.63993	178.09571	4
7	954.54581	477.77654	318.85345	D	403.22998	202.11863	135.08151	3
8	1067.62988	534.31858	356.54814	L	288.20303	144.60515	96.73919	2
9				R	175.11896	88.06312	59.04450	1

Figure 3-25: MS/MS spectrum of m/z 414.59 the $[M+3H]^{3}+$ molecular ion for a peptide of 1241.74 Da with corresponding sequence AKPALEDLR unique to apoA1 identified in 1DGE fraction 6 as significant (*P* value <0.05) between PiB+ and PiB- groups.

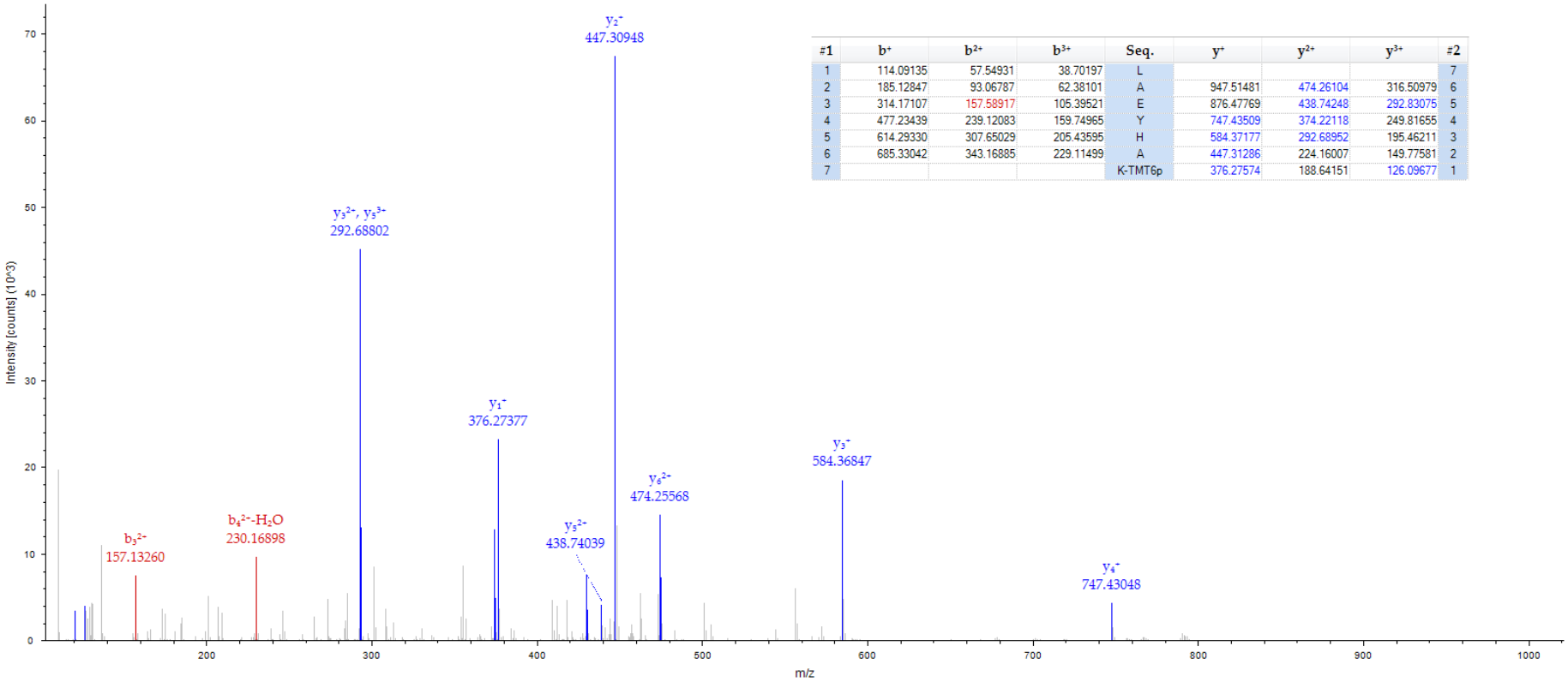

#1	b+	b2+	b3+	Seq.	y+	y2+	y3+	#2
1	114.09135	57.54931	38.70197	L				7
2	185.12847	93.06787	62.38101	A	947.51481	474.26104	316.50979	6
3	314.17107	157.58917	105.39521	E	876.47769	438.74248	292.83075	5
4	477.23439	239.12083	159.74965	Y	747.43509	374.22118	249.81655	4
5	614.29330	307.65029	205.43595	H	584.37177	292.68952	195.46211	3
6	685.33042	343.16885	229.11499	A	447.31286	224.16007	149.77581	2
7				K-TMT6p	376.27574	188.64151	126.09677	1

Figure 3-26: MS/MS spectrum of m/z 354.20 the $[M+3H]^{3}+$ molecular ion for a peptide of 1060.50 Da with corresponding sequence LAEYHAK unique to apoA1 identified in 1DGE fraction 6 as significant (*P* value <0.05) between PiB+ and PiB- groups.

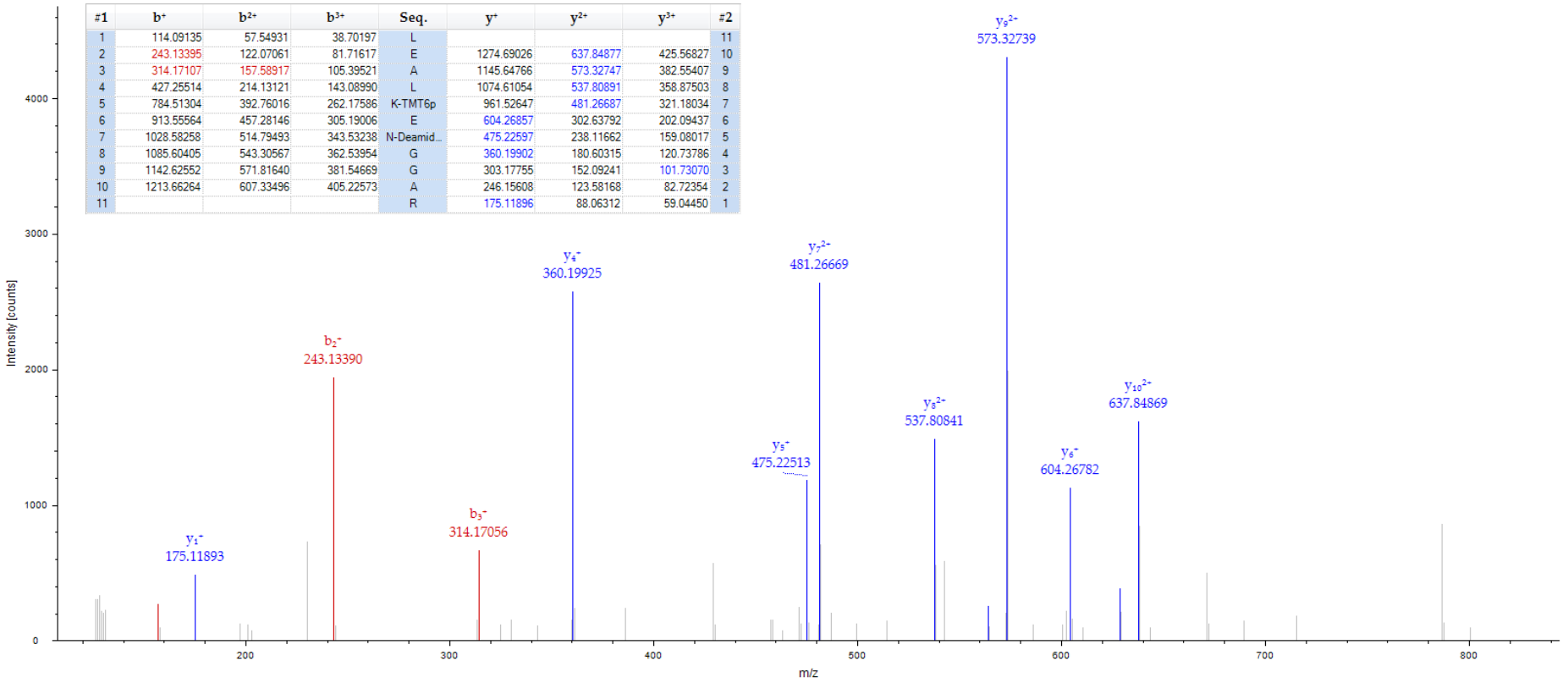

Figure 3-27: MS/MS spectrum of m/z 463.26 the $[M+3H]^{3}+$ molecular ion for a peptide of 1387.77 Da with corresponding sequence LEALKENGGAR unique to apoA1 identified in 1DGE fraction 6 as significant (*P* value <0.05) between PiB+ and PiB- groups.

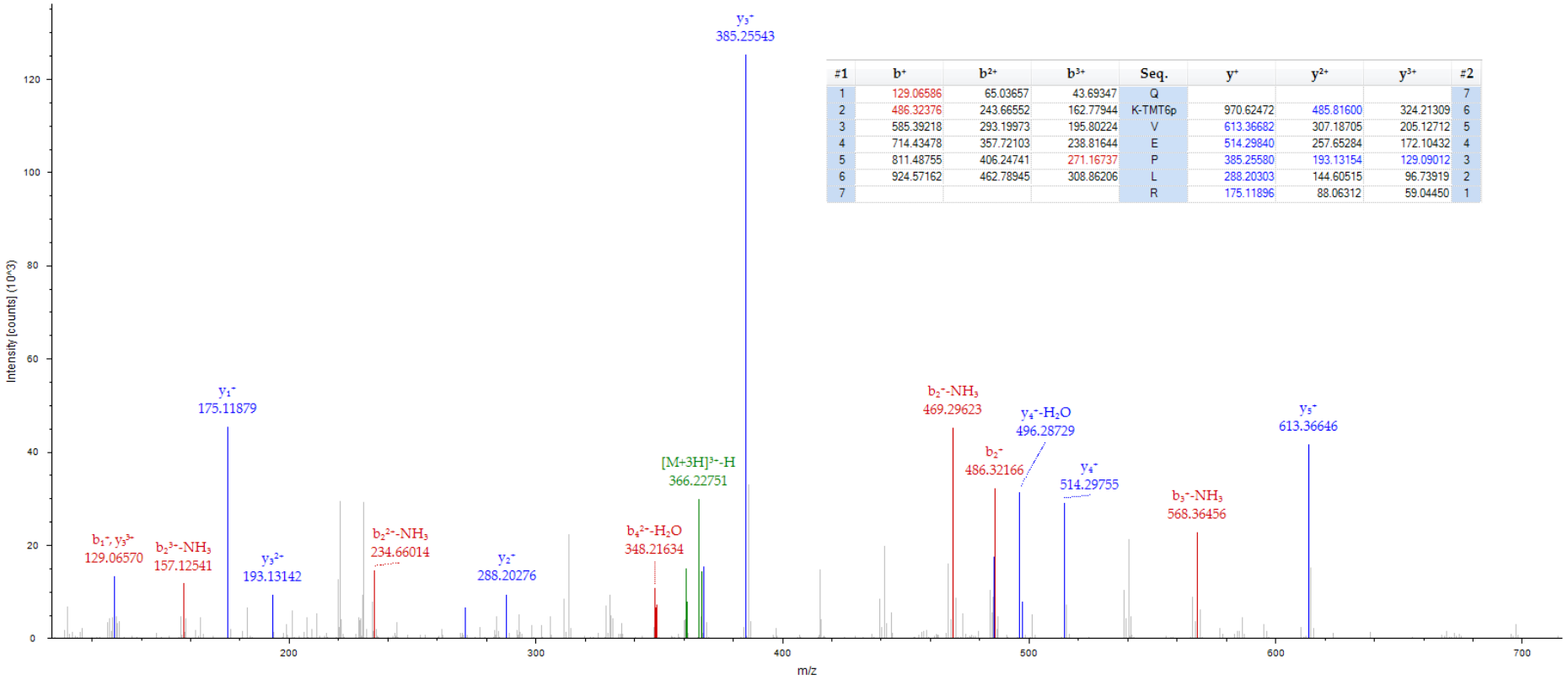

Figure 3-28: MS/MS spectrum of m/z 366.90 the $[M+3H]^{3}+$ molecular ion for a peptide of 1098.68 Da with corresponding sequence QKVEPLR unique to apoA1 identified in 1DGE fraction 6 as significant (*P* value <0.05) between PiB+ and PiB- groups.

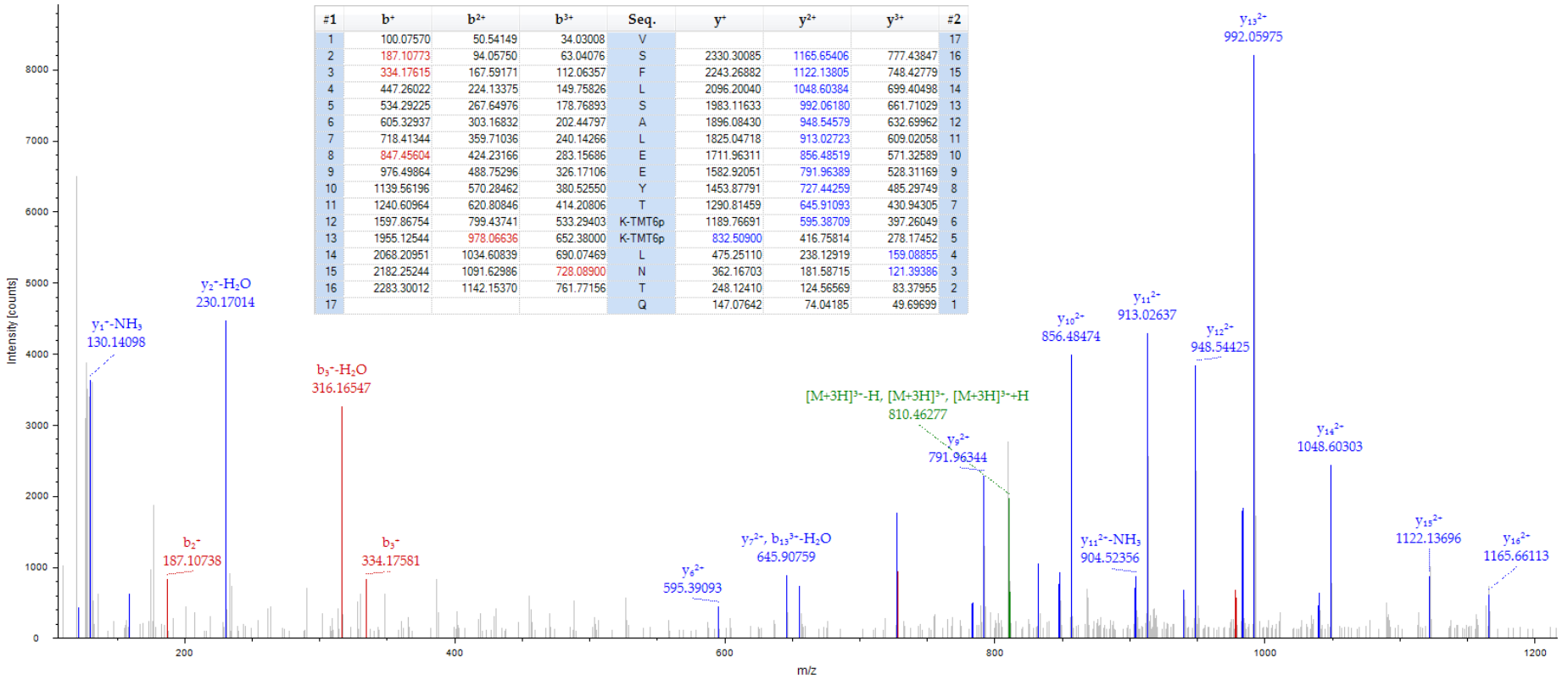

Figure 3-29: MS/MS spectrum of m/z 810.46 the $[M+3H]^{3}$+ molecular ion for a peptide of 2429.37 Da with corresponding sequence VSFLSALEEYTKKLNTQ unique to apoA1 identified in 1DGE fraction 6 as significant (*P* value <0.05) between PiB+ and PiB- groups.

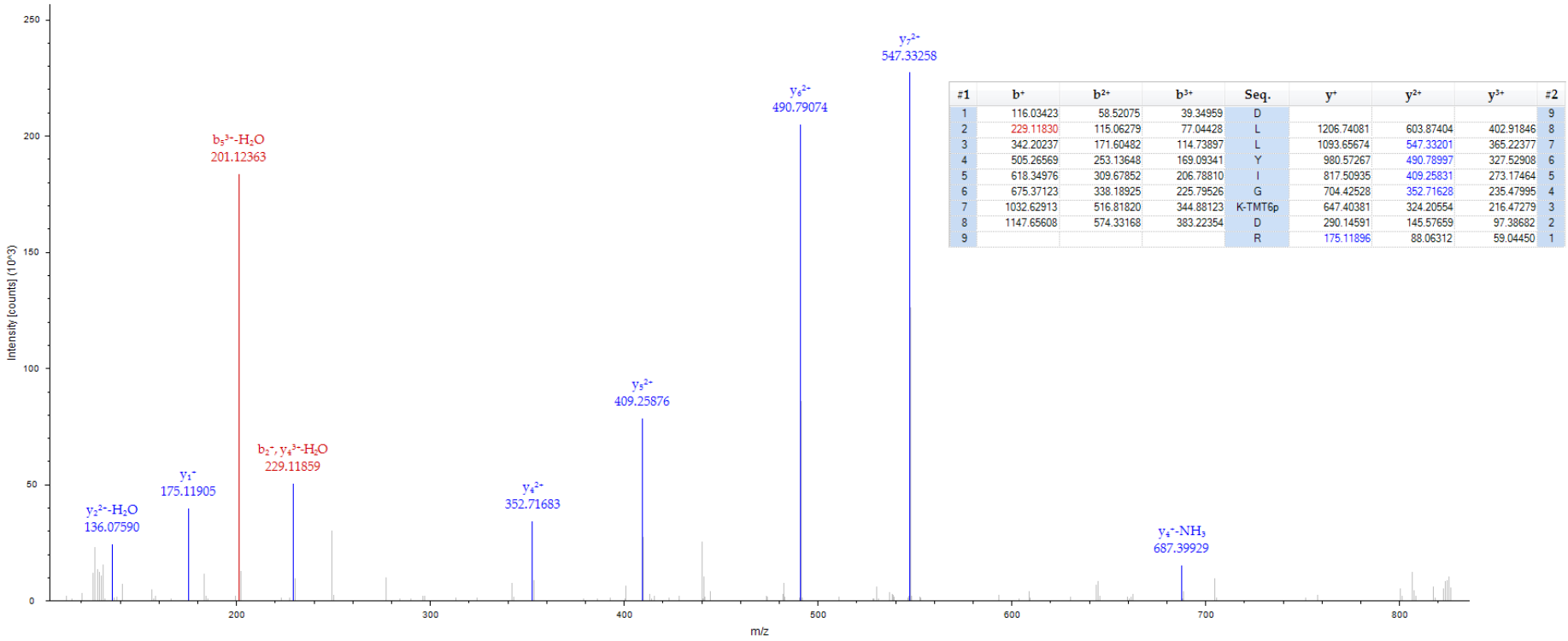

#1	b+	b2+	b3+	Seq.	y+	y2+	y3+	#2
1	116.03423	58.52075	39.34959	D				9
2	229.11830	115.06279	77.04428	L	1206.74081	603.87404	402.91846	8
3	342.20237	171.60482	114.73897	L	1093.65674	547.33201	365.22377	7
4	505.26569	253.13648	169.09341	Y	980.57267	490.78997	327.52908	6
5	618.34976	309.67852	206.78810	I	817.50935	409.25831	273.17464	5
6	675.37123	338.18925	225.79526	G	704.42528	352.71628	235.47995	4
7	1032.62913	516.81820	344.88123	K-TMT6p	647.40381	324.20554	216.47279	3
8	1147.65608	574.33168	383.22354	D	290.14591	145.57659	97.38682	2
9				R	175.11896	88.06312	59.04450	1

Figure 3-30: MS/MS spectrum of m/z 441.26 the $[M+3H]^{3}+$ molecular ion for a peptide of 1321.77 Da with corresponding sequence DLLYIGKDR unique to CFB identified in 1DGE fraction 1 as significant (*P* value <0.05) between PiB+ and PiB- groups.

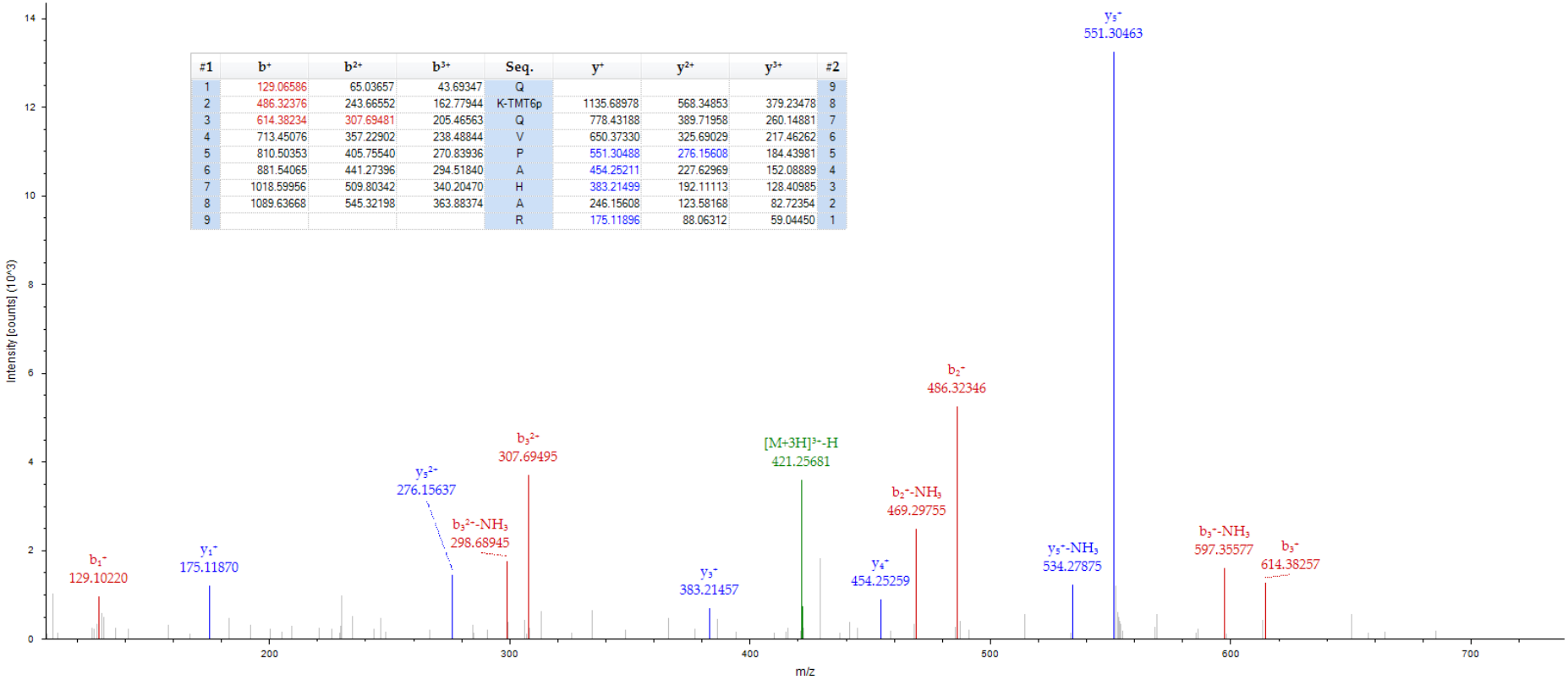

Figure 3-31: MS/MS spectrum of *m/z* 421.92 the $[M+3H]^{3+}$ molecular ion for a peptide of 1263.75 Da with corresponding sequence QKQVPAHAR unique to CFB identified in 1DGE fraction 1 as significant (*P* value <0.05) between PiB+ and PiB- groups.

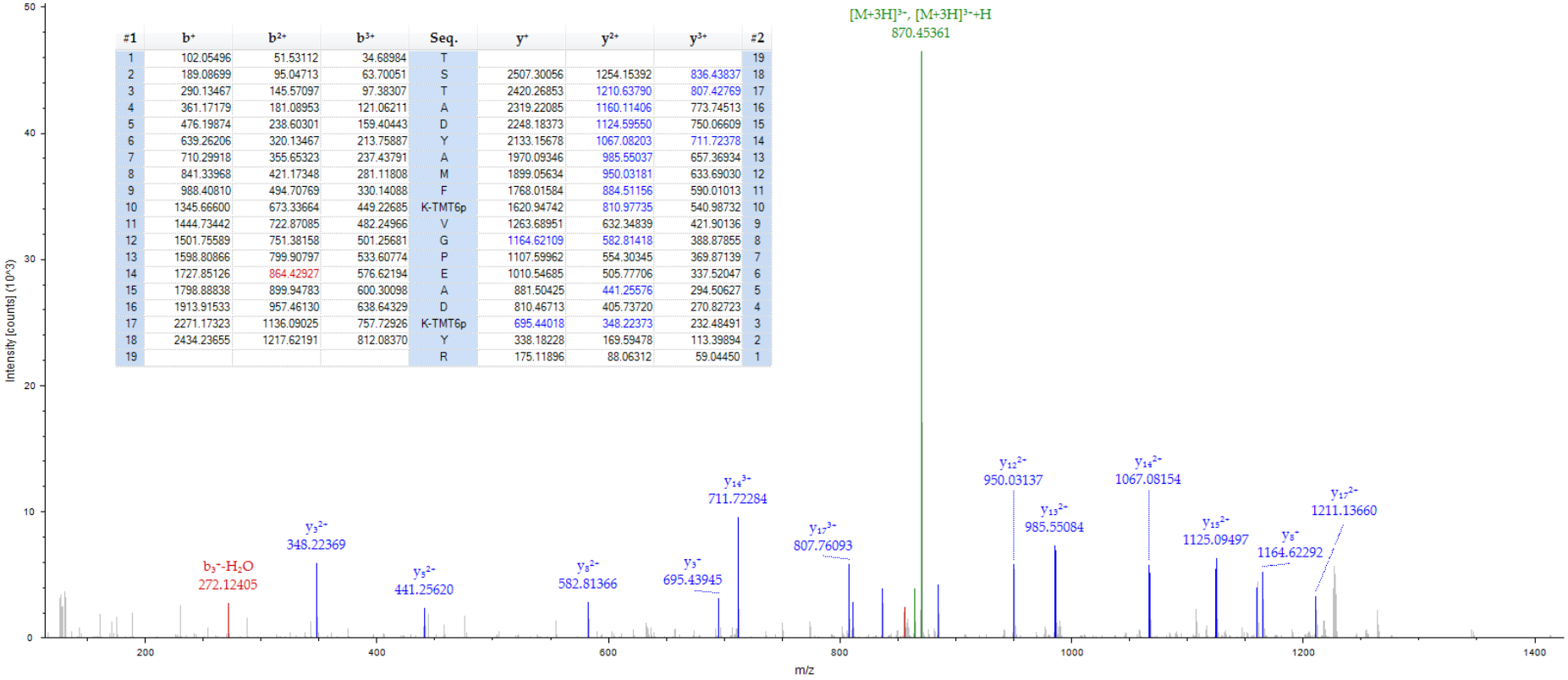

#1	b+	b2+	b3+	Seq.	y+	y2+	y3+	#2
1	102.05496	51.53112	34.68984	T				19
2	189.08699	95.04713	63.70051	S	2507.30056	1254.15392	836.43837	18
3	290.13467	145.57097	97.38307	T	2420.26853	1210.63790	807.42769	17
4	361.17179	181.08953	121.06211	A	2319.22085	1160.11406	773.74513	16
5	476.19874	238.60301	159.40443	D	2248.18373	1124.59550	750.06609	15
6	639.26206	320.13467	213.75887	Y	2133.15678	1067.08203	711.72378	14
7	710.29918	355.65323	237.43791	A	1970.09346	985.55037	657.36934	13
8	841.33968	421.17348	281.11808	M	1899.05634	950.03181	633.69030	12
9	988.40810	494.70769	330.14088	F	1768.01584	884.51156	590.01013	11
10	1345.66600	673.33664	449.22685	K-TMT6p	1620.94742	810.97735	540.98732	10
11	1444.73442	722.87085	482.24966	V	1263.68951	632.34839	421.90136	9
12	1501.75589	751.38158	501.25681	G	1164.62109	582.81418	388.87855	8
13	1598.80866	799.90797	533.60774	P	1107.59962	554.30345	369.87139	7
14	1727.85126	864.42927	576.62194	E	1010.54685	505.77706	337.52047	6
15	1798.88838	899.94783	600.30098	A	881.50425	441.25576	294.50627	5
16	1913.91533	957.46130	638.64329	D	810.46713	405.73720	270.82723	4
17	2271.17323	1136.09025	757.72926	K-TMT6p	695.44018	348.22373	232.48491	3
18	2434.23655	1217.62191	812.08370	Y	338.18228	169.59478	113.39894	2
19				R	175.11896	88.06312	59.04450	1

Figure 3-32: MS/MS spectrum of *m/z* 870.12 the $[M+3H]^{3+}$ molecular ion for a peptide of 2608.35 Da with corresponding sequence TSTADYAMFKVGPEADKY unique to FGγ identified in 1DGE fraction 6 as significant (*P* value <0.05) between PiB+ and PiB- groups.

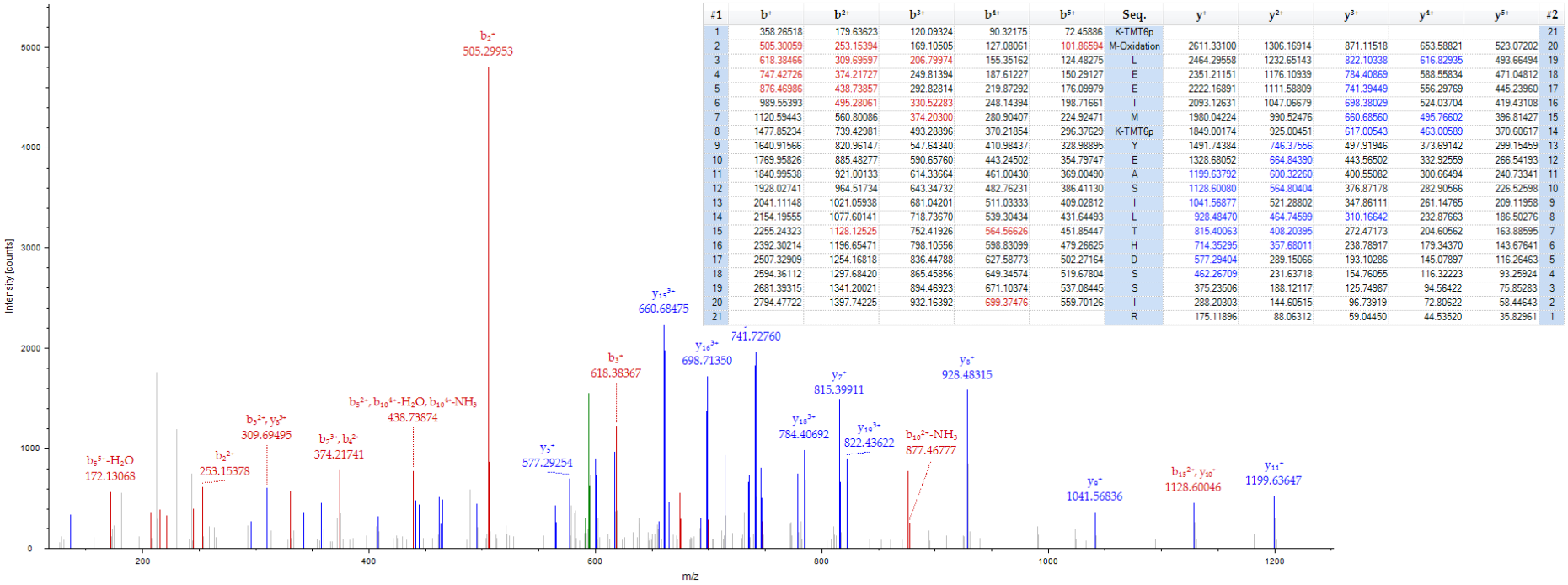

#1	b+	b2+	b3+	b4+	b5+	Seq.	y+	y2+	y3+	y4+	y5+	#2
1	358.26518	179.63623	120.09324	90.32175	72.45886	K-TMT6p						21
2	505.30059	253.15394	169.10505	127.08061	101.86594	M-Oxidation	2611.33100	1306.16914	871.11518	653.58821	523.07202	20
3	618.38466	309.69597	206.79974	155.35162	124.48275	L	2464.29558	1232.65143	822.10338	616.82935	493.66494	19
4	747.42726	374.21727	249.81394	187.61227	150.29127	E	2351.21151	1176.10939	784.40869	588.55834	471.04812	18
5	876.46986	438.73857	292.82814	219.87292	176.09979	E	2222.16891	1111.58809	741.39449	556.29769	445.23960	17
6	989.55393	495.28061	330.52283	248.14394	198.71661	I	2093.12631	1047.06679	698.38029	524.03704	419.43108	16
7	1120.59443	560.80086	374.20300	280.90407	224.92471	M	1980.04224	990.52476	660.68560	495.76602	396.81427	15
8	1477.85234	739.42981	493.28896	370.21854	296.37629	K-TMT6p	1849.00174	925.00451	617.00543	463.00589	370.60617	14
9	1640.91566	820.96147	547.64340	410.98437	328.98895	Y	1491.74384	746.37556	497.91946	373.69142	299.15459	13
10	1769.95826	885.48277	590.65760	443.24502	354.79747	E	1328.68052	664.84390	443.56502	332.92559	266.54193	12
11	1840.99538	921.00133	614.33664	461.00430	369.00490	A	1199.63792	600.32260	400.55082	300.66494	240.73341	11
12	1928.02741	964.51734	643.34732	482.76231	386.41130	S	1128.60080	564.80404	376.87178	282.90566	226.52598	10
13	2041.11148	1021.05938	681.04201	511.03333	409.02812	I	1041.56877	521.28802	347.86111	261.14765	209.11958	9
14	2154.19555	1077.60141	718.73670	539.30434	431.64493	L	928.48470	464.74599	310.16642	232.87663	186.50276	8
15	2255.24323	1128.12525	752.41926	564.56626	451.85447	T	815.40063	408.20395	272.47173	204.60562	163.88595	7
16	2392.30214	1196.65471	798.10556	598.83099	479.26625	H	714.35295	357.68011	238.78917	179.34370	143.67641	6
17	2507.32909	1254.16818	836.44788	627.58773	502.27164	D	577.29404	289.15066	193.10286	145.07897	116.26463	5
18	2594.36112	1297.68420	865.45856	649.34574	519.67804	S	462.26709	231.63718	154.76055	116.32223	93.25924	4
19	2681.39315	1341.20021	894.46923	671.10374	537.08445	S	375.23506	188.12117	125.74987	94.56422	75.85283	3
20	2794.47722	1397.74225	932.16392	699.37476	559.70126	I	288.20303	144.60515	96.73919	72.80622	58.44643	2
21						R	175.11896	88.06312	59.04450	44.53520	35.82961	1

Figure 3-33: MS/MS spectrum of *m/z* 594.52 the $[M+3H]^{3+}$ molecular ion for a peptide of 2968.59 Da with corresponding sequence KMLEEIMKYEASILTHDSSIR unique to FGγ identified in 1DGE fraction 6 as significant (*P* value <0.05) between PiB+ and PiB- groups.

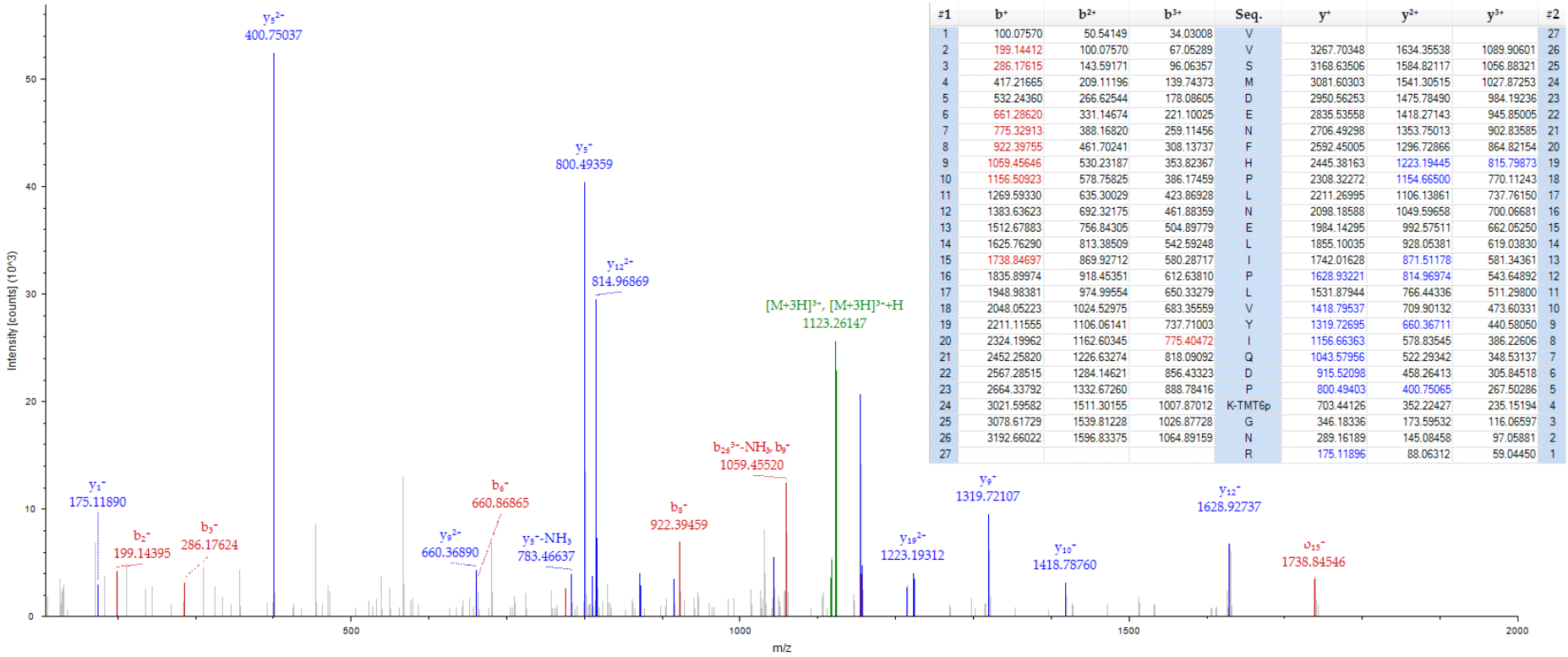

#1	b+	b2+	b3+	Seq.	y+	y2+	y3+	#2
1	100.07570	50.54149	34.03008	V				27
2	199.14412	100.07570	67.05289	V	3267.70348	1634.35538	1089.90601	26
3	286.17615	143.59171	96.06357	S	3168.63506	1584.82117	1056.88321	25
4	417.21665	209.11196	139.74373	M	3081.60303	1541.30515	1027.87253	24
5	532.24360	266.62544	178.08605	D	2950.56253	1475.78490	984.19236	23
6	661.28620	331.14674	221.10025	E	2835.53558	1418.27143	945.85005	22
7	775.32913	388.16820	259.11456	N	2706.49298	1353.75013	902.83585	21
8	922.39755	461.70241	308.13737	F	2592.45005	1296.72866	864.82154	20
9	1059.45646	530.23187	353.82367	H	2445.38163	1223.19445	815.79873	19
10	1156.50923	578.75825	386.17459	P	2308.32272	1154.66500	770.11243	18
11	1269.59330	635.30029	423.86928	L	2211.26995	1106.13861	737.76150	17
12	1383.63623	692.32175	461.88359	N	2098.18588	1049.59658	700.06681	16
13	1512.67883	756.84305	504.89779	E	1984.14295	992.57511	662.05250	15
14	1625.76290	813.38509	542.59248	L	1855.10035	928.05381	619.03830	14
15	1738.84697	869.92712	580.28717	I	1742.01628	871.51178	581.34361	13
16	1835.89974	918.45351	612.63810	P	1628.93221	814.96974	543.64892	12
17	1948.98381	974.99554	650.33279	L	1531.87944	766.44336	511.29800	11
18	2048.05223	1024.52975	683.35559	V	1418.79537	709.90132	473.60331	10
19	2211.11555	1106.06141	737.71003	Y	1319.72695	660.36711	440.58050	9
20	2324.19962	1162.60345	775.40472	I	1156.66363	578.83545	386.22606	8
21	2452.25820	1226.63274	818.09092	Q	1043.57956	522.29342	348.53137	7
22	2567.28515	1284.14621	856.43323	D	915.52098	458.26413	305.84518	6
23	2664.33792	1332.67260	888.78416	P	800.49403	400.75065	267.50286	5
24	3021.59582	1511.30155	1007.87012	K-TMT6p	703.44126	352.22427	235.15194	4
25	3078.61729	1539.81228	1026.87728	G	346.18336	173.59532	116.06597	3
26	3192.66022	1596.83375	1064.89159	N	289.16189	145.08458	97.05881	2
27				R	175.11896	88.06312	59.04450	1

Figure 3-34: MS/MS spectrum of *m/z* 1122.92 the $[M+3H]^{3+}$ molecular ion for a peptide of 3366.77 Da with corresponding sequence VVSMDENFHPLNELIPLVYIQDPKGNR unique to α2M identified in 1DGE fraction 3 as significant (*P* value <0.05) between PiB+ and PiB- groups.

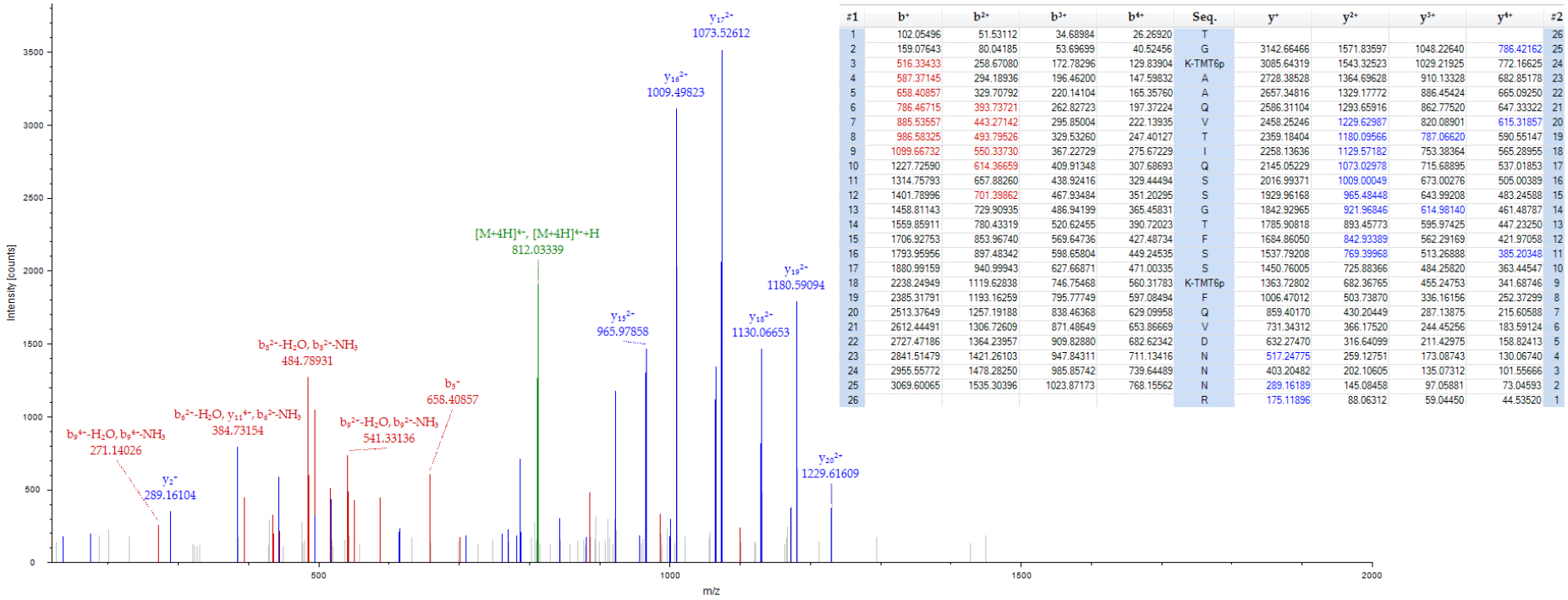

#1	b⁺	b²⁺	b³⁺	b⁴⁺	Seq.	y⁺	y²⁺	y³⁺	y⁴⁺	#2
1	102.05496	51.53112	34.68984	26.26920	T					26
2	159.07643	80.04185	53.69699	40.52456	G	3142.66466	1571.83597	1048.22640	786.42162	25
3	516.33433	258.67080	172.78296	129.83904	K-TMT6p	3085.64319	1543.32523	1029.21925	772.16625	24
4	587.37145	294.18936	196.46200	147.59832	A	2728.38528	1364.69628	910.13328	682.85178	23
5	658.40857	329.70792	220.14104	165.35760	A	2657.34816	1329.17772	886.45424	665.09250	22
6	786.46715	393.73721	262.82723	197.37224	Q	2586.31104	1293.65916	862.77520	647.33322	21
7	885.53557	443.27142	295.85004	222.13935	V	2458.25246	1229.62987	820.08901	615.31857	20
8	986.58325	493.79526	329.53260	247.40127	T	2359.18404	1180.09566	787.06620	590.55147	19
9	1099.66732	550.33730	367.22729	275.67229	I	2258.13636	1129.57182	753.38364	565.28955	18
10	1227.72590	614.36659	409.91348	307.68693	Q	2145.05229	1073.02978	715.68895	537.01853	17
11	1314.75793	657.88260	438.92416	329.44494	S	2016.99371	1009.00049	673.00276	505.00389	16
12	1401.78996	701.39862	467.93484	351.20295	S	1929.96168	965.48448	643.99208	483.24588	15
13	1458.81143	729.90935	486.94199	365.45831	G	1842.92965	921.96846	614.98140	461.48787	14
14	1559.85911	780.43319	520.62455	390.72023	T	1785.90818	893.45773	595.97425	447.23250	13
15	1706.92753	853.96740	569.64736	427.48734	F	1684.86050	842.93389	562.29169	421.97058	12
16	1793.95956	897.48342	598.65804	449.24535	S	1537.79208	769.39968	513.26888	385.20348	11
17	1880.99159	940.99943	627.66871	471.00335	S	1450.76005	725.88366	484.25820	363.44547	10
18	2238.24949	1119.62838	746.75468	560.31783	K-TMT6p	1363.72802	682.36765	455.24753	341.68746	9
19	2385.31791	1193.16259	795.77749	597.08494	F	1006.47012	503.73870	336.16156	252.37299	8
20	2513.37649	1257.19188	838.46368	629.09958	Q	859.40170	430.20449	287.13875	215.60588	7
21	2612.44491	1306.72609	871.48649	653.86669	V	731.34312	366.17520	244.45256	183.59124	6
22	2727.47186	1364.23957	909.82880	682.62342	D	632.27470	316.64099	211.42975	158.82413	5
23	2841.51479	1421.26103	947.84311	711.13416	N	517.24775	259.12751	173.08743	130.06740	4
24	2955.55772	1478.28250	985.85742	739.64489	N	403.20482	202.10605	135.07312	101.55666	3
25	3069.60065	1535.30396	1023.87173	768.15562	N	289.16189	145.08458	97.05881	73.04593	2
26					R	175.11896	88.06312	59.04450	44.53520	1

Figure 3-35: MS/MS spectrum of *m/z* 811.68 the $[M+4H]^{4+}$ molecular ion for a peptide of 3243.72 Da with corresponding sequence TGKAAQVTIQSSGTFSSKFQVDNNNR unique to α2M identified in 1DGE fraction 3 as significant (*P* value <0.05) between PiB+ and PiB- groups.

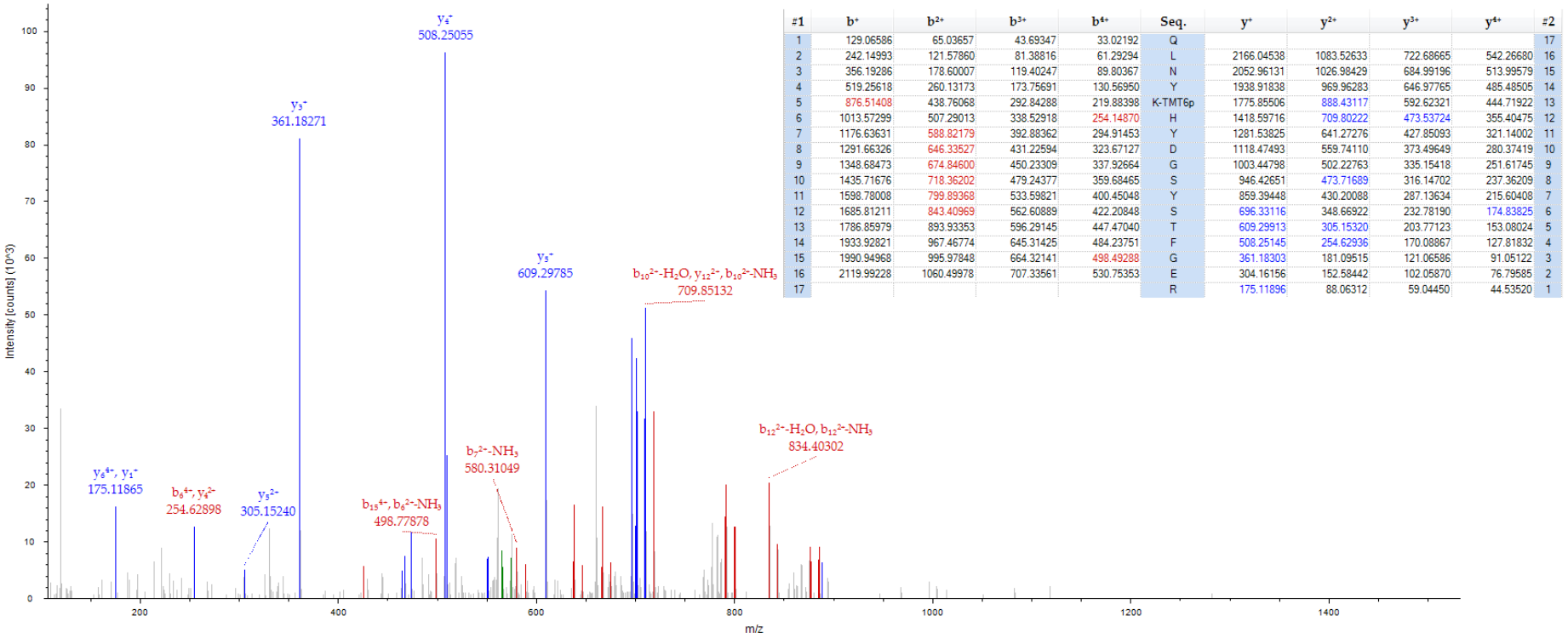

#1	b+	b2+	b3+	b4+	Seq.	y+	y2+	y3+	y4+	#2
1	129.06586	65.03657	43.69347	33.02192	Q					17
2	242.14993	121.57860	81.38816	61.29294	L	2166.04538	1083.52633	722.68665	542.26680	16
3	356.19286	178.60007	119.40247	89.80367	N	2052.96131	1026.98429	684.99196	513.99579	15
4	519.25618	260.13173	173.75691	130.56950	Y	1938.91838	969.96283	646.97765	485.48505	14
5	876.51408	438.76068	292.84288	219.88398	K-TMT6p	1775.85506	888.43117	592.62321	444.71922	13
6	1013.57299	507.29013	338.52918	254.14870	H	1418.59716	709.80222	473.53724	355.40475	12
7	1176.63631	588.82179	392.88362	294.91453	Y	1281.53825	641.27276	427.85093	321.14002	11
8	1291.66326	646.33527	431.22594	323.67127	D	1118.47493	559.74110	373.49649	280.37419	10
9	1348.68473	674.84600	450.23309	337.92664	G	1003.44798	502.22763	335.15418	251.61745	9
10	1435.71676	718.36202	479.24377	359.68465	S	946.42651	473.71689	316.14702	237.36209	8
11	1598.78008	799.89368	533.59821	400.45048	Y	859.39448	430.20088	287.13634	215.60408	7
12	1685.81211	843.40969	562.60889	422.20848	S	696.33116	348.66922	232.78190	174.83825	6
13	1786.85979	893.93353	596.29145	447.47040	T	609.29913	305.15320	203.77123	153.08024	5
14	1933.92821	967.46774	645.31425	484.23751	F	508.25145	254.62936	170.08867	127.81832	4
15	1990.94968	995.97848	664.32141	498.49288	G	361.18303	181.09515	121.06586	91.05122	3
16	2119.99228	1060.49978	707.33561	530.75353	E	304.16156	152.58442	102.05870	76.79585	2
17					R	175.11896	88.06312	59.04450	44.53520	1

Figure 3-36: MS/MS spectrum of *m/z* 574.28 the $[M+4H]^{4+}$ molecular ion for a peptide of 2294.10 Da with corresponding sequence QLNYKHYDGSYSTFGER unique to *α*2M identified in 1DGE fraction 3 as significant (*P* value <0.05) between PiB+ and PiB- groups.

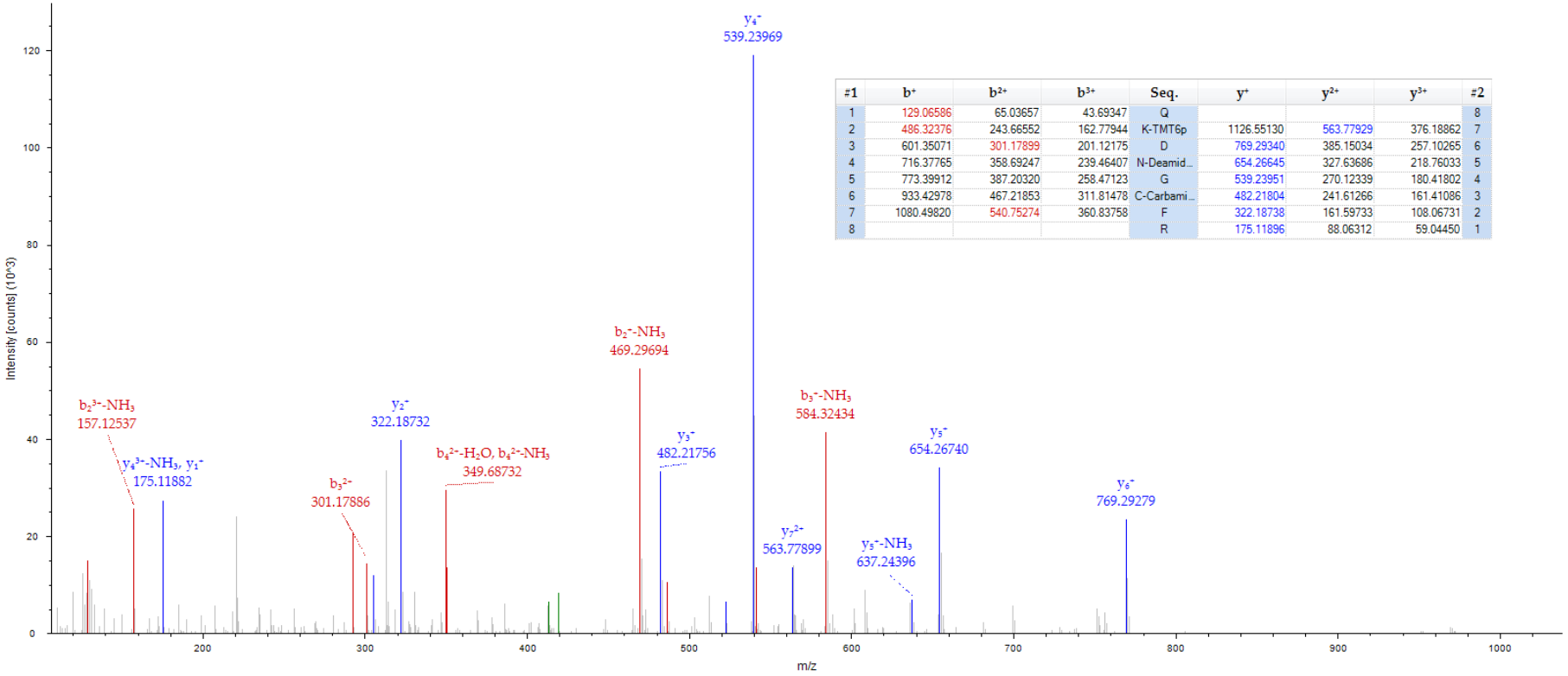

#1	b+	b2+	b3+	Seq.	y+	y2+	y3+	#2
1	129.06586	65.03657	43.69347	Q				8
2	486.32376	243.66552	162.77944	K-TMT6p	1126.55130	563.77929	376.18862	7
3	601.35071	301.17899	201.12175	D	769.29340	385.15034	257.10265	6
4	716.37765	358.69247	239.46407	N-Deamid...	654.26645	327.63686	218.76033	5
5	773.39912	387.20320	258.47123	G	539.23951	270.12339	180.41802	4
6	933.42978	467.21853	311.81478	C-Carbami...	482.21804	241.61266	161.41086	3
7	1080.49820	540.75274	360.83758	F	322.18738	161.59733	108.06731	2
8				R	175.11896	88.06312	59.04450	1

Figure 3-37: MS/MS spectrum of *m/z* 418.54 the $[M+3H]^{3+}$ molecular ion for a peptide of 1253.62 Da with corresponding sequence QKDNGCFR unique to α2M identified in 1DGE fraction 3 as significant (*P* value <0.05) between PiB+ and PiB- groups.

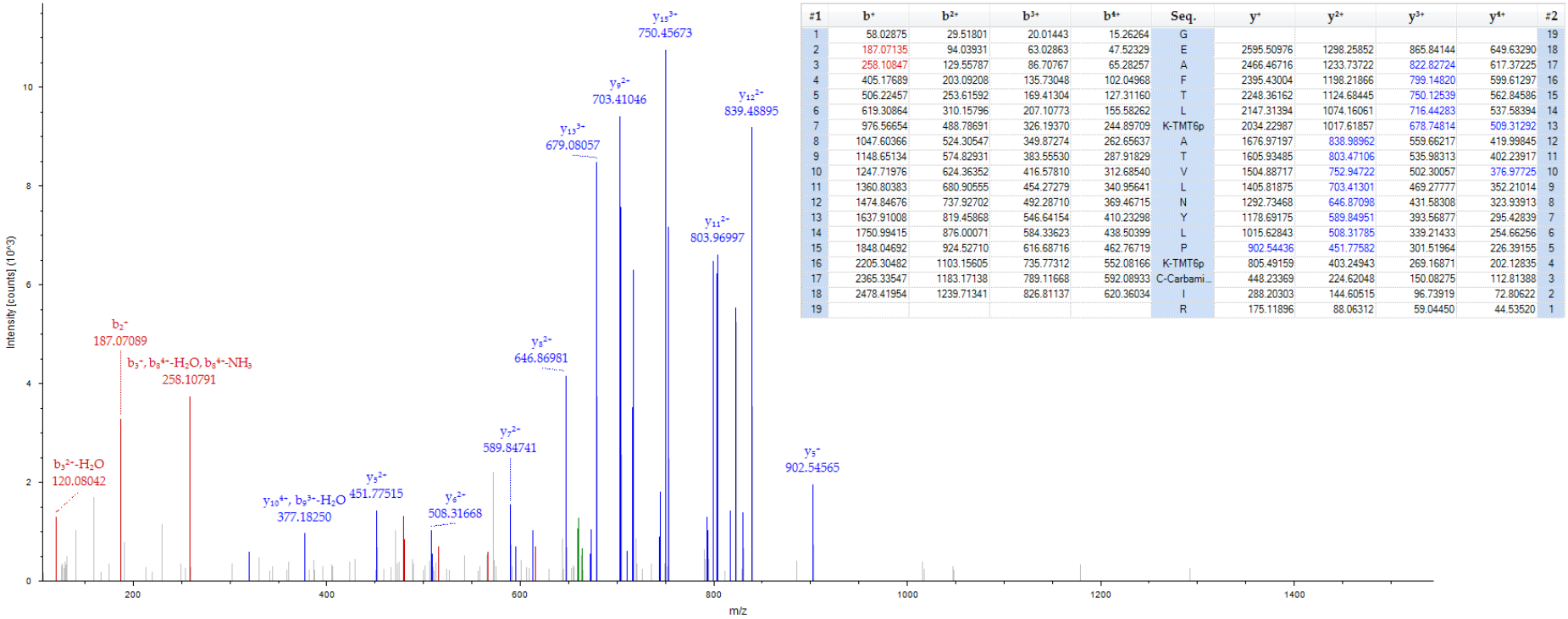

#1	b+	b2+	b3+	b4+	Seq.	y+	y2+	y3+	y4+	#2
1	58.02875	29.51801	20.01443	15.26264	G					19
2	187.07135	94.03931	63.02863	47.52329	E	2595.50976	1298.25852	865.84144	649.63290	18
3	258.10847	129.55787	86.70767	65.28257	A	2466.46716	1233.73722	822.82724	617.37225	17
4	405.17689	203.09208	135.73048	102.04968	F	2395.43004	1198.21866	799.14820	599.61297	16
5	506.22457	253.61592	169.41304	127.31160	T	2248.36162	1124.68445	750.12539	562.84586	15
6	619.30864	310.15796	207.10773	155.58262	L	2147.31394	1074.16061	716.44283	537.58394	14
7	976.56654	488.78691	326.19370	244.89709	K-TMT6p	2034.22987	1017.61857	678.74814	509.31292	13
8	1047.60366	524.30547	349.87274	262.65637	A	1676.97197	838.98962	559.66217	419.99845	12
9	1148.65134	574.82931	383.55530	287.91829	T	1605.93485	803.47106	535.98313	402.23917	11
10	1247.71976	624.36352	416.57810	312.68540	V	1504.88717	752.94722	502.30057	376.97725	10
11	1360.80383	680.90555	454.27279	340.95641	L	1405.81875	703.41301	469.27777	352.21014	9
12	1474.84676	737.92702	492.28710	369.46715	N	1292.73468	646.87098	431.58308	323.93913	8
13	1637.91008	819.45868	546.64154	410.23298	Y	1178.69175	589.84951	393.56877	295.42839	7
14	1750.99415	876.00071	584.33623	438.50399	L	1015.62843	508.31785	339.21433	254.66256	6
15	1848.04692	924.52710	616.68716	462.76719	P	902.54436	451.77582	301.51964	226.39155	5
16	2205.30482	1103.15605	735.77312	552.08166	K-TMT6p	805.49159	403.24943	269.16871	202.12835	4
17	2365.33547	1183.17138	789.11668	592.08933	C-Carbami...	448.23369	224.62048	150.08275	112.81388	3
18	2478.41954	1239.71341	826.81137	620.36034	I	288.20303	144.60515	96.73919	72.80622	2
19					R	175.11896	88.06312	59.04450	44.53520	1

Figure 3-38: MS/MS spectrum of *m/z* 663.89 the $[M+4H]^{4+}$ molecular ion for a peptide of 2652.52 Da with corresponding sequence GEAFTLKATVLNYLPKCIR unique to *α*2M identified in 1DGE fraction 3 as significant (*P* value <0.05) between PiB+ and PiB- groups.

#1	b+	b2+	b3+	b4+	b5+	Seq.	y+	y2+	y3+	y4+	y5+	#2
1	102.05496	51.53112	34.68984	26.26920	21.21681	T						15
2	215.13903	108.07315	72.38453	54.54021	43.83363	I	2135.27419	1068.14073	712.42958	534.57400	427.86066	14
3	316.18671	158.59699	106.06709	79.80213	64.04316	T	2022.19012	1011.59870	674.73489	506.30299	405.24384	13
4	673.44461	337.22594	225.15305	169.11661	135.49474	K-TMT6p	1921.14244	961.07486	641.05233	481.04107	385.03431	12
5	786.52868	393.76798	262.84774	197.38763	158.11156	L	1563.88453	782.44590	521.96636	391.72659	313.58273	11
6	873.56071	437.28399	291.85842	219.14563	175.51796	S	1450.80046	725.90387	484.27167	363.45557	290.96591	10
7	1020.62913	510.81820	340.88123	255.91274	204.93165	F	1363.76843	682.38785	455.26100	341.69757	273.55951	9
8	1119.69755	560.35241	373.90403	280.67984	224.74533	V	1216.70001	608.85364	406.23819	304.93046	244.14582	8
9	1476.95545	738.98136	492.99000	369.99432	296.19691	K-TMT6p	1117.63159	559.31943	373.21538	280.16336	224.33214	7
10	1576.02387	788.51557	526.01281	394.76143	316.01060	V	760.37369	380.69048	254.12941	190.84888	152.88056	6
11	1691.05082	846.02905	564.35512	423.51816	339.01599	D	661.30527	331.15627	221.10661	166.08178	133.06688	5
12	1778.08285	889.54506	593.36580	445.27617	356.42239	S	546.27832	273.64280	182.76429	137.32504	110.06149	4
13	1915.14176	958.07452	639.05210	479.54090	383.83417	H	459.24629	230.12678	153.75361	115.56703	92.65508	3
14	2062.21018	1031.60873	688.07491	516.30800	413.24786	F	322.18738	161.59733	108.06731	81.30230	65.24330	2
15						R	175.11896	88.06312	59.04450	44.53520	35.82961	1

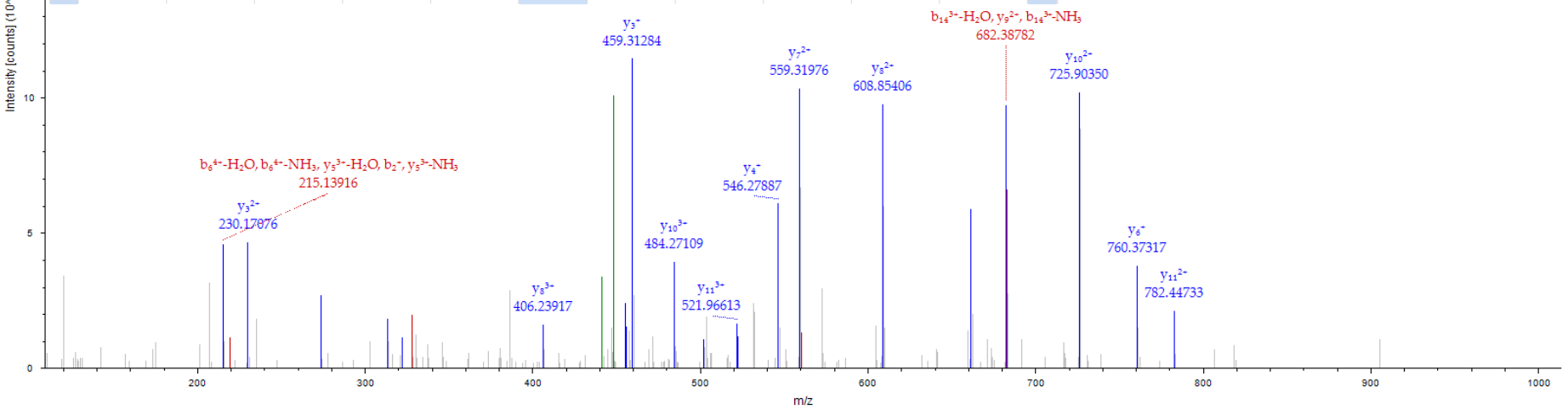

Figure 3-39: MS/MS spectrum of *m/z* 448.70 the $[M+5H]^{5+}$ molecular ion for a peptide of 2236.32 Da with corresponding sequence TITKLSFVKVDSHFR unique to α2M identified in 1DGE fraction 3 as significant (*P* value <0.05) between PiB+ and PiB- groups.

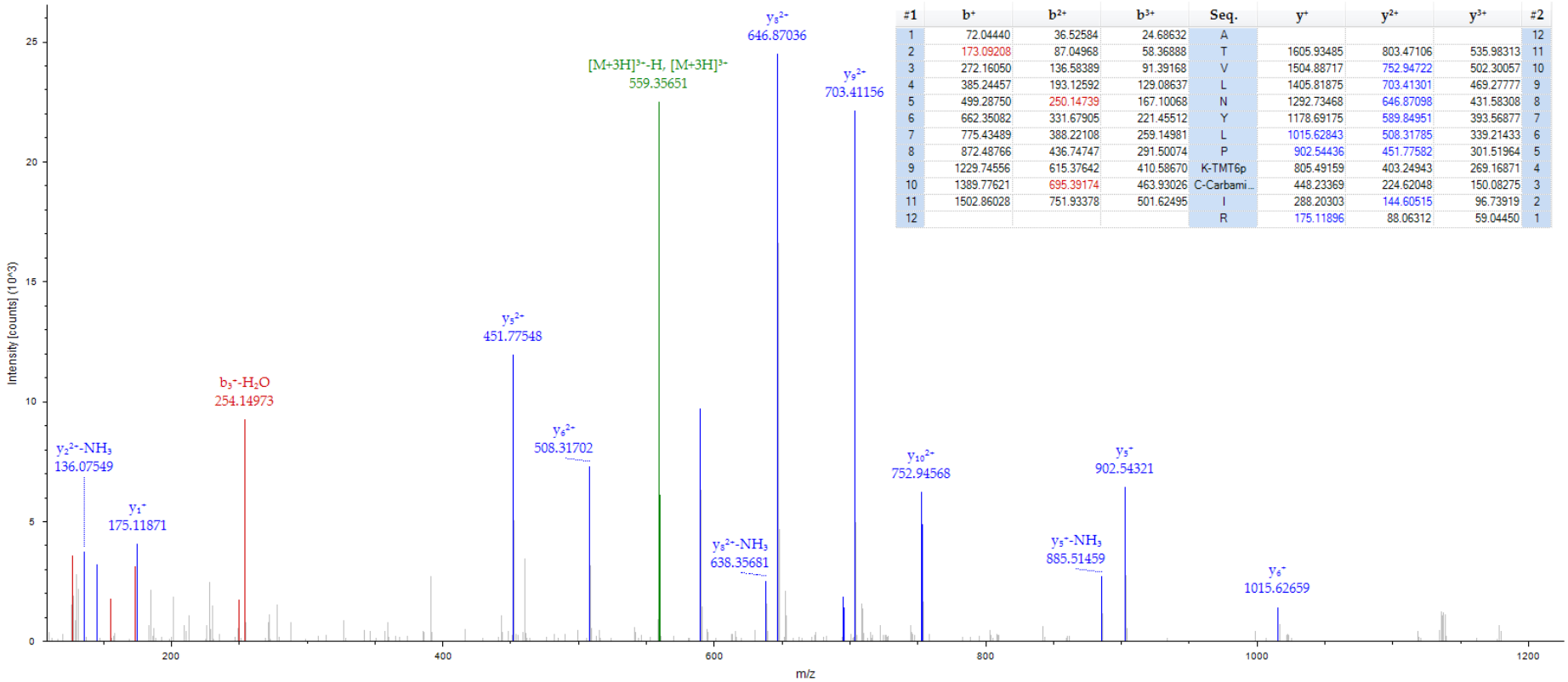

#1	b$^+$	b^{2+}	b^{3+}	Seq.	y$^+$	y^{2+}	y^{3+}	#2
1	72.04440	36.52584	24.68632	A				12
2	173.09208	87.04968	58.36888	T	1605.93485	803.47106	535.98313	11
3	272.16050	136.58389	91.39168	V	1504.88717	752.94722	502.30057	10
4	385.24457	193.12592	129.08637	L	1405.81875	703.41301	469.27777	9
5	499.28750	250.14739	167.10068	N	1292.73468	646.87098	431.58308	8
6	662.35082	331.67905	221.45512	Y	1178.69175	589.84951	393.56877	7
7	775.43489	388.22108	259.14981	L	1015.62843	508.31785	339.21433	6
8	872.48766	436.74747	291.50074	P	902.54436	451.77582	301.51964	5
9	1229.74556	615.37642	410.58670	K-TMT6p	805.49159	403.24943	269.16871	4
10	1389.77621	695.39174	463.93026	C-Carbami...	448.23369	224.62048	150.08275	3
11	1502.86028	751.93378	501.62495	I	288.20303	144.60515	96.73919	2
12				R	175.11896	88.06312	59.04450	1

Figure 3-40: MS/MS spectrum of *m/z* 559.66 the [M+3H]$^{3+}$ molecular ion for a peptide of 1676.97 Da with corresponding sequence ATVLNYLPKCIR unique to α2M identified in 1DGE fraction 3 as significant (*P* value <0.05) between PiB+ and PiB- groups.

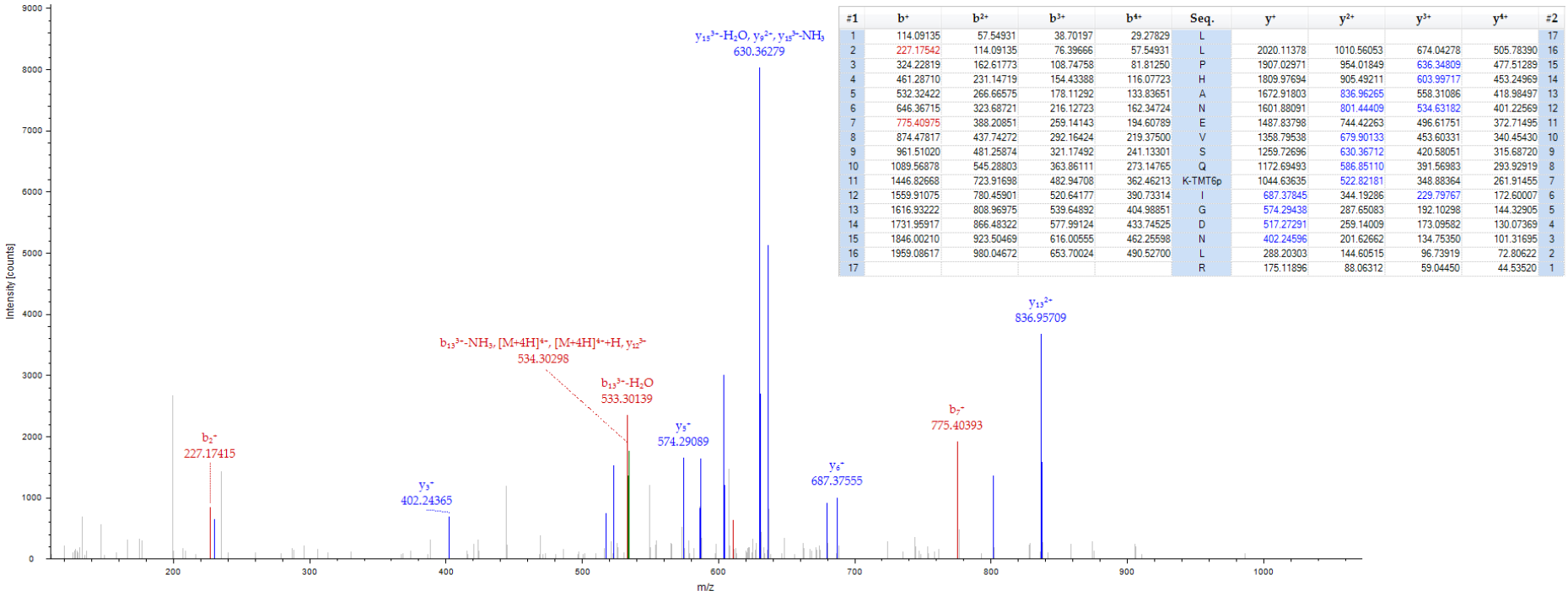

#1	b^+	b^{2+}	b^{3+}	b^{4+}	Seq.	y^+	y^{2+}	y^{3+}	y^{4+}	#2
1	114.09135	57.54931	38.70197	29.27829	L					17
2	227.17542	114.09135	76.39666	57.54931	L	2020.11378	1010.56053	674.04278	505.78390	16
3	324.22819	162.61773	108.74758	81.81250	P	1907.02971	954.01849	636.34809	477.51289	15
4	461.28710	231.14719	154.43388	116.07723	H	1809.97694	905.49211	603.99717	453.24969	14
5	532.32422	266.66575	178.11292	133.83651	A	1672.91803	836.96265	558.31086	418.98497	13
6	646.36715	323.68721	216.12723	162.34724	N	1601.88091	801.44409	534.63182	401.22569	12
7	775.40975	388.20851	259.14143	194.60789	E	1487.83798	744.42263	496.61751	372.71495	11
8	874.47817	437.74272	292.16424	219.37500	V	1358.79538	679.90133	453.60331	340.45430	10
9	961.51020	481.25874	321.17492	241.13301	S	1259.72696	630.36712	420.58051	315.68720	9
10	1089.56878	545.28803	363.86111	273.14765	Q	1172.69493	586.85110	391.56983	293.92919	8
11	1446.82668	723.91698	482.94708	362.46213	K-TMT6p	1044.63635	522.82181	348.88364	261.91455	7
12	1559.91075	780.45901	520.64177	390.73314	I	687.37845	344.19286	229.79767	172.60007	6
13	1616.93222	808.96975	539.64892	404.98851	G	574.29438	287.65083	192.10298	144.32905	5
14	1731.95917	866.48322	577.99124	433.74525	D	517.27291	259.14009	173.09582	130.07369	4
15	1846.00210	923.50469	616.00555	462.25598	N	402.24596	201.62662	134.75350	101.31695	3
16	1959.08617	980.04672	653.70024	490.52700	L	288.20303	144.60515	96.73919	72.80622	2
17					R	175.11896	88.06312	59.04450	44.53520	1

Figure 3-41: MS/MS spectrum of *m/z* 534.05 the $[M+4H]^{4+}$ molecular ion for a peptide of 2133.19 Da with corresponding sequence LLPHANEVSQKIGDNLR unique to apoA4 identified in 1DGE fraction 6 as significant (*P* value <0.05) between PiB+ and PiB- groups.

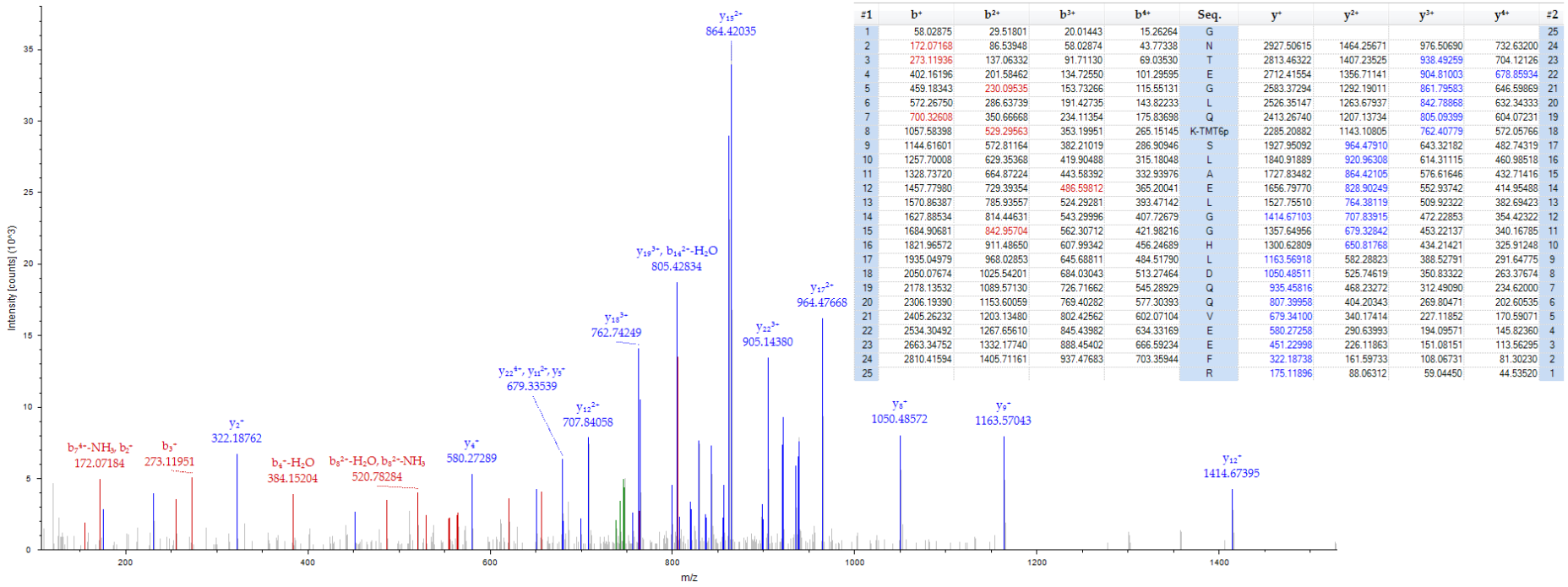

#1	b+	b2+	b3+	b4+	Seq.	y+	y2+	y3+	y4+	#2
1	58.02875	29.51801	20.01443	15.26264	G					25
2	172.07168	86.53948	58.02874	43.77338	N	2927.50615	1464.25671	976.50690	732.63200	24
3	273.11936	137.06332	91.71130	69.03530	T	2813.46322	1407.23525	938.49259	704.12126	23
4	402.16196	201.58462	134.72550	101.29595	E	2712.41554	1356.71141	904.81003	678.85934	22
5	459.18343	230.09535	153.73266	115.55131	G	2583.37294	1292.19011	861.79583	646.59869	21
6	572.26750	286.63739	191.42735	143.82233	L	2526.35147	1263.67937	842.78868	632.34333	20
7	700.32608	350.66668	234.11354	175.83698	Q	2413.26740	1207.13734	805.09399	604.07231	19
8	1057.58398	529.29563	353.19951	265.15145	K-TMT6p	2285.20882	1143.10805	762.40779	572.05766	18
9	1144.61601	572.81164	382.21019	286.90946	S	1927.95092	964.47910	643.32182	482.74319	17
10	1257.70008	629.35368	419.90488	315.18048	L	1840.91889	920.96308	614.31115	460.98518	16
11	1328.73720	664.87224	443.58392	332.93976	A	1727.83482	864.42105	576.61646	432.71416	15
12	1457.77980	729.39354	486.59812	365.20041	E	1656.79770	828.90249	552.93742	414.95488	14
13	1570.86387	785.93557	524.29281	393.47142	L	1527.75510	764.38119	509.92322	382.69423	13
14	1627.88534	814.44631	543.29996	407.72679	G	1414.67103	707.83915	472.22853	354.42322	12
15	1684.90681	842.95704	562.30712	421.98216	G	1357.64956	679.32842	453.22137	340.16785	11
16	1821.96572	911.48650	607.99342	456.24689	H	1300.62809	650.81768	434.21421	325.91248	10
17	1935.04979	968.02853	645.68811	484.51790	L	1163.56918	582.28823	388.52791	291.64775	9
18	2050.07674	1025.54201	684.03043	513.27464	D	1050.48511	525.74619	350.83322	263.37674	8
19	2178.13532	1089.57130	726.71662	545.28929	Q	935.45816	468.23272	312.49090	234.62000	7
20	2306.19390	1153.60059	769.40282	577.30393	Q	807.39958	404.20343	269.80471	202.60535	6
21	2405.26232	1203.13480	802.42562	602.07104	V	679.34100	340.17414	227.11852	170.59071	5
22	2534.30492	1267.65610	845.43982	634.33169	E	580.27258	290.63993	194.09571	145.82360	4
23	2663.34752	1332.17740	888.45402	666.59234	E	451.22998	226.11863	151.08151	113.56295	3
24	2810.41594	1405.71161	937.47683	703.35944	F	322.18738	161.59733	108.06731	81.30230	2
25					R	175.11896	88.06312	59.04450	44.53520	1

Figure 3-42: MS/MS spectrum of *m/z* 746.89 the $[M+4H]^{4+}$ molecular ion for a peptide of 2984.53 Da with corresponding sequence GNTEGLQKSLAELGGHLDQQVEEFR unique to apoA4 identified in 1DGE fraction 6 as significant (*P* value <0.05) between PiB+ and PiB- groups.

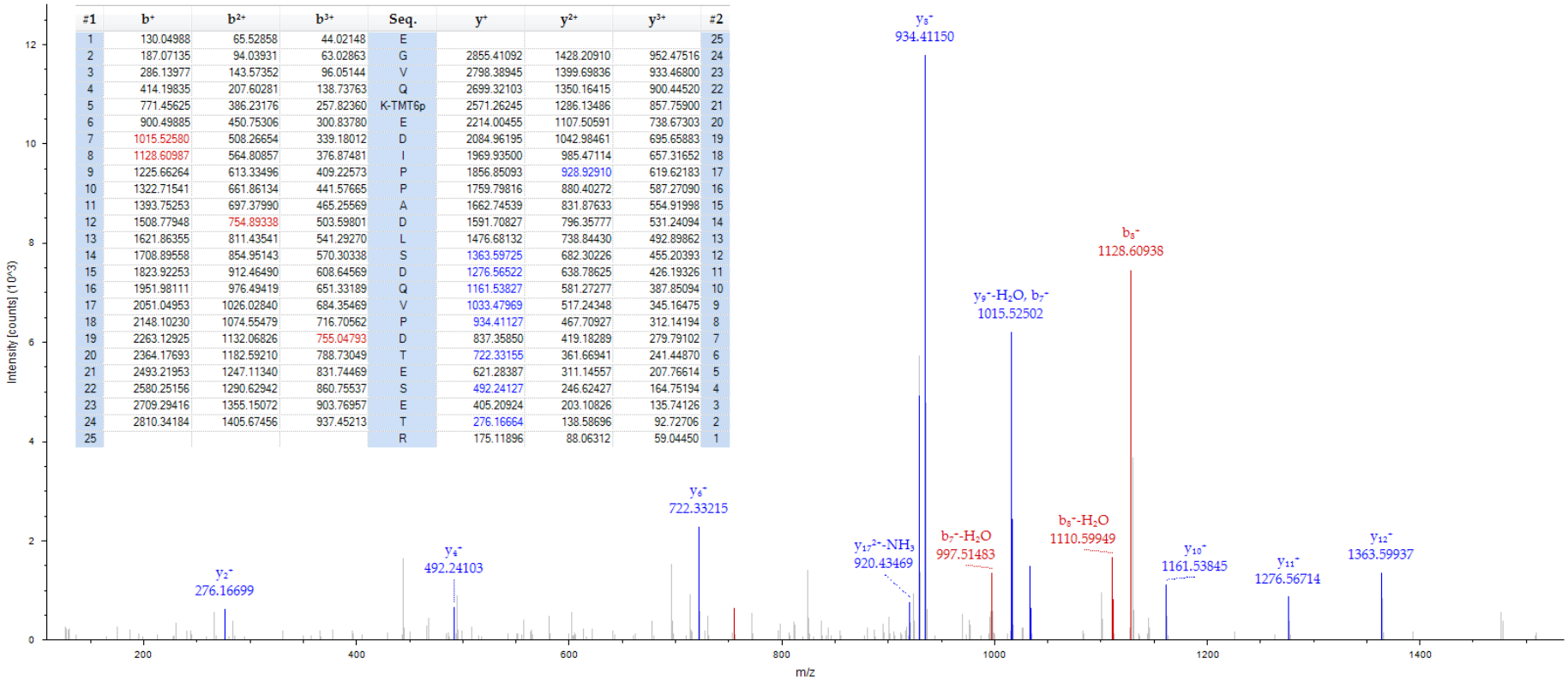

Figure 3-43: MS/MS spectrum of *m/z* 995.49 the $[M+4H]^{4+}$ molecular ion for a peptide of 2984.45 Da with corresponding sequence EGVQKEDIPPADLSDQVPDTESETR unique to CC3 identified in 1DGE fraction 6 as significant (*P* value <0.05) between PiB+ and PiB- groups.

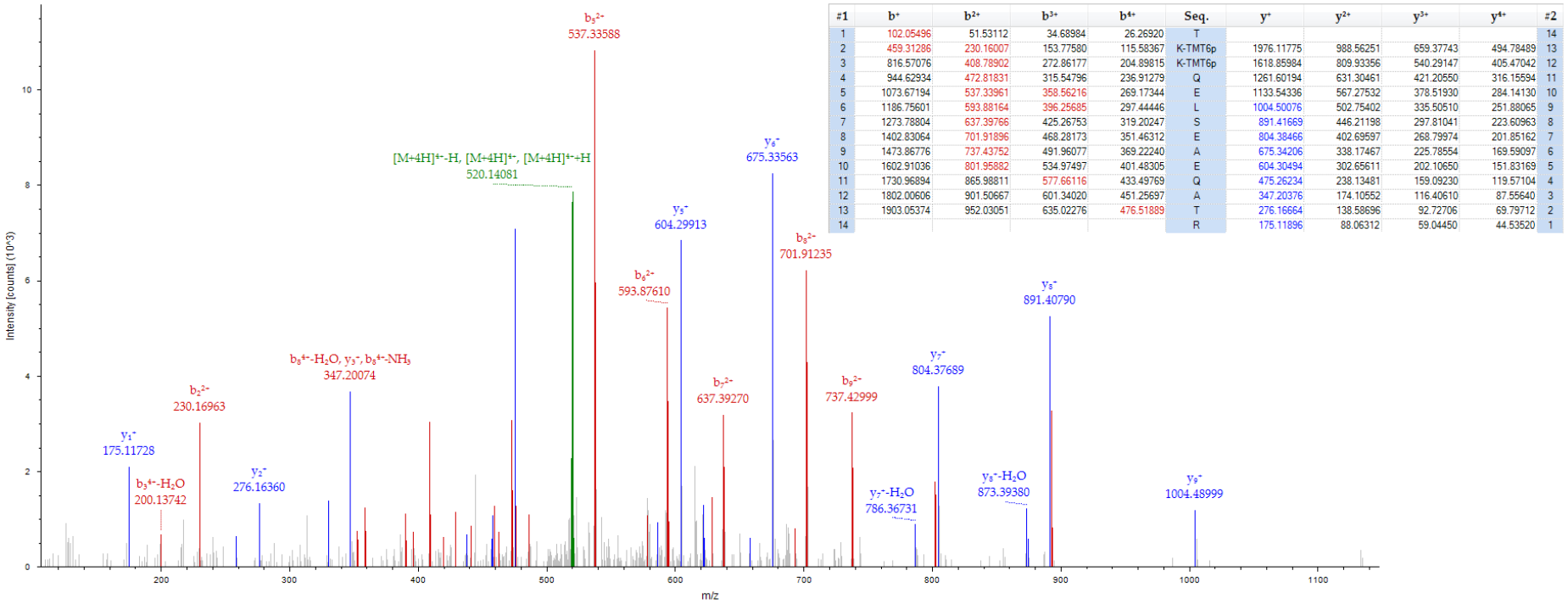

#1	b⁺	b²⁺	b³⁺	b⁴⁺	Seq.	y⁺	y²⁺	y³⁺	y⁴⁺	#2
1	102.05496	51.53112	34.68984	26.26920	T					14
2	459.31286	230.16007	153.77580	115.58367	K-TMT6p	1976.11775	988.56251	659.37743	494.78489	13
3	816.57076	408.78902	272.86177	204.89815	K-TMT6p	1618.85984	809.93356	540.29147	405.47042	12
4	944.62934	472.81831	315.54796	236.91279	Q	1261.60194	631.30461	421.20550	316.15594	11
5	1073.67194	537.33961	358.56216	269.17344	E	1133.54336	567.27532	378.51930	284.14130	10
6	1186.75601	593.88164	396.25685	297.44446	L	1004.50076	502.75402	335.50510	251.88065	9
7	1273.78804	637.39766	425.26753	319.20247	S	891.41669	446.21198	297.81041	223.60963	8
8	1402.83064	701.91896	468.28173	351.46312	E	804.38466	402.69597	268.79974	201.85162	7
9	1473.86776	737.43752	491.96077	369.22240	A	675.34206	338.17467	225.78554	169.59097	6
10	1602.91036	801.95882	534.97497	401.48305	E	604.30494	302.65611	202.10650	151.83169	5
11	1730.96894	865.98811	577.66116	433.49769	Q	475.26234	238.13481	159.09230	119.57104	4
12	1802.00606	901.50667	601.34020	451.25697	A	347.20376	174.10552	116.40610	87.55640	3
13	1903.05374	952.03051	635.02276	476.51889	T	276.16664	138.58696	92.72706	69.79712	2
14					R	175.11896	88.06312	59.04450	44.53520	1

Figure 3-44: MS/MS spectrum of *m/z* 520.05 the $[M+4H]^{4+}$ molecular ion for a peptide of 2077.17 Da with corresponding sequence TKKQELSEAEQATR unique to CC3 identified in 1DGE fraction 6 as significant (*P* value <0.05) between PiB+ and PiB- groups.

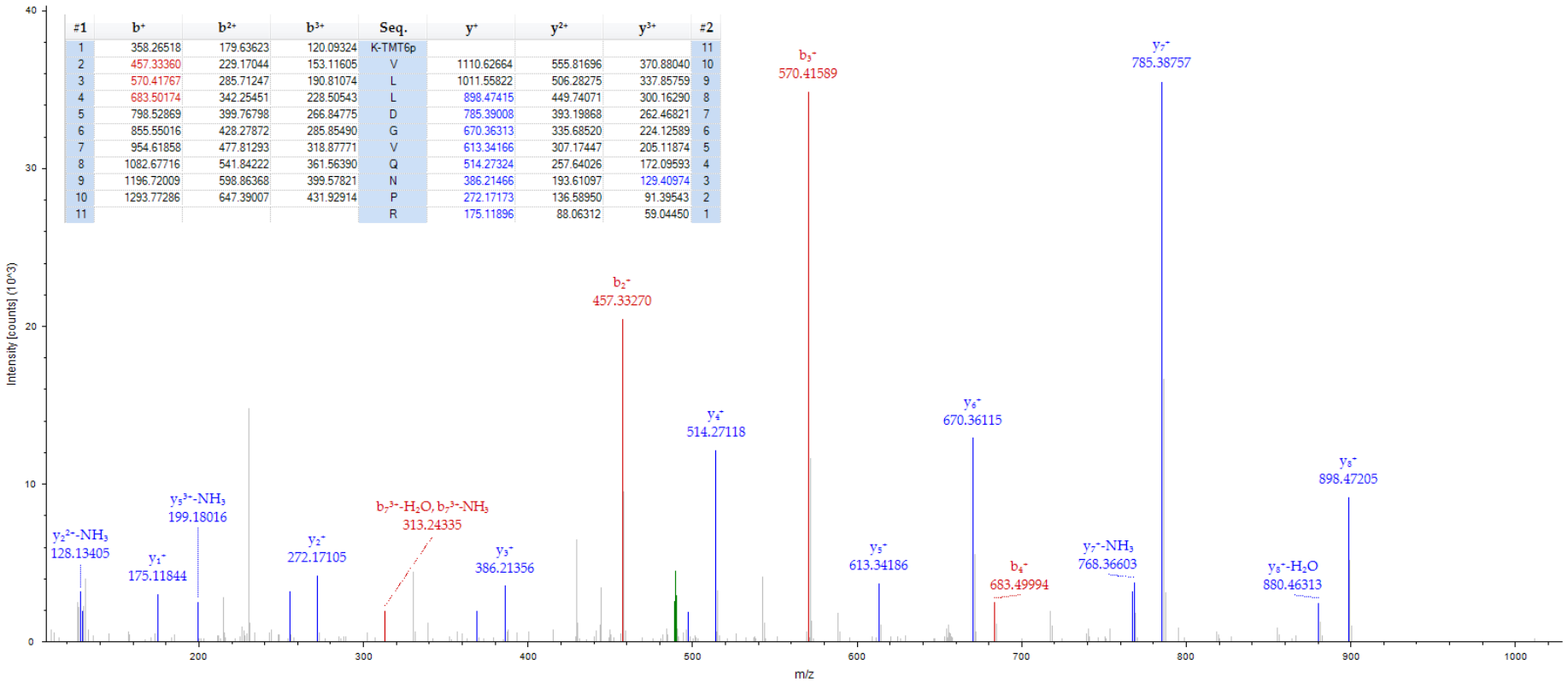

Figure 3-45: MS/MS spectrum of *m/z* 489.97 the $[M+3H]^{3+}$ molecular ion for a peptide of 1467.88 Da with corresponding sequence KVLLDGVQNPR unique to CC3 identified in 1DGE fraction 6 as significant (*P* value <0.05) between PiB+ and PiB- groups.

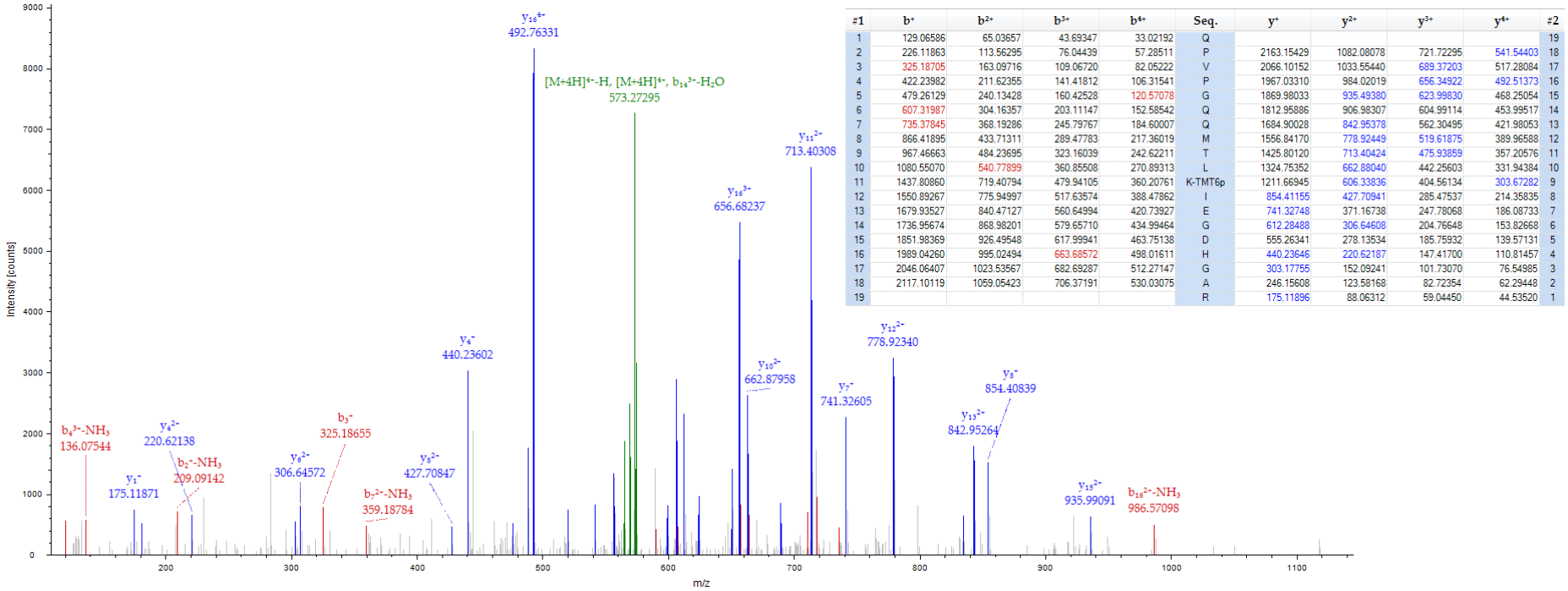

#1	b^+	b^{2+}	b^{3+}	b^{4+}	Seq.	y^+	y^{2+}	y^{3+}	y^{4+}	#2
1	129.06586	65.03657	43.69347	33.02192	Q					19
2	226.11863	113.56295	76.04439	57.28511	P	2163.15429	1082.08078	721.72295	541.54403	18
3	325.18705	163.09716	109.06720	82.05222	V	2066.10152	1033.55440	689.37203	517.28084	17
4	422.23982	211.62355	141.41812	106.31541	P	1967.03310	984.02019	656.34922	492.51373	16
5	479.26129	240.13428	160.42528	120.57078	G	1869.98033	935.49380	623.99830	468.25054	15
6	607.31987	304.16357	203.11147	152.58542	Q	1812.95886	906.98307	604.99114	453.99517	14
7	735.37845	368.19286	245.79767	184.60007	Q	1684.90028	842.95378	562.30495	421.98053	13
8	866.41895	433.71311	289.47783	217.36019	M	1556.84170	778.92449	519.61875	389.96588	12
9	967.46663	484.23695	323.16039	242.62211	T	1425.80120	713.40424	475.93859	357.20576	11
10	1080.55070	540.77899	360.85508	270.89313	L	1324.75352	662.88040	442.25603	331.94384	10
11	1437.80860	719.40794	479.94105	360.20761	K-TMT6p	1211.66945	606.33836	404.56134	303.67282	9
12	1550.89267	775.94997	517.63574	388.47862	I	854.41155	427.70941	285.47537	214.35835	8
13	1679.93527	840.47127	560.64994	420.73927	E	741.32748	371.16738	247.78068	186.08733	7
14	1736.95674	868.98201	579.65710	434.99464	G	612.28488	306.64608	204.76648	153.82668	6
15	1851.98369	926.49548	617.99941	463.75138	D	555.26341	278.13534	185.75932	139.57131	5
16	1989.04260	995.02494	663.68572	498.01611	H	440.23646	220.62187	147.41700	110.81457	4
17	2046.06407	1023.53567	682.69287	512.27147	G	303.17755	152.09241	101.73070	76.54985	3
18	2117.10119	1059.05423	706.37191	530.03075	A	246.15608	123.58168	82.72354	62.29448	2
19					R	175.11896	88.06312	59.04450	44.53520	1

Figure 3-46: MS/MS spectrum of *m/z* 573.56 the $[M+4H]^{4+}$ molecular ion for a peptide of 2291.21 Da with corresponding sequence QPVPGQQMTLKIEGDHGAR unique to CC3 identified in 1DGE fraction 6 as significant (*P* value <0.05) between PiB+ and PiB- groups.

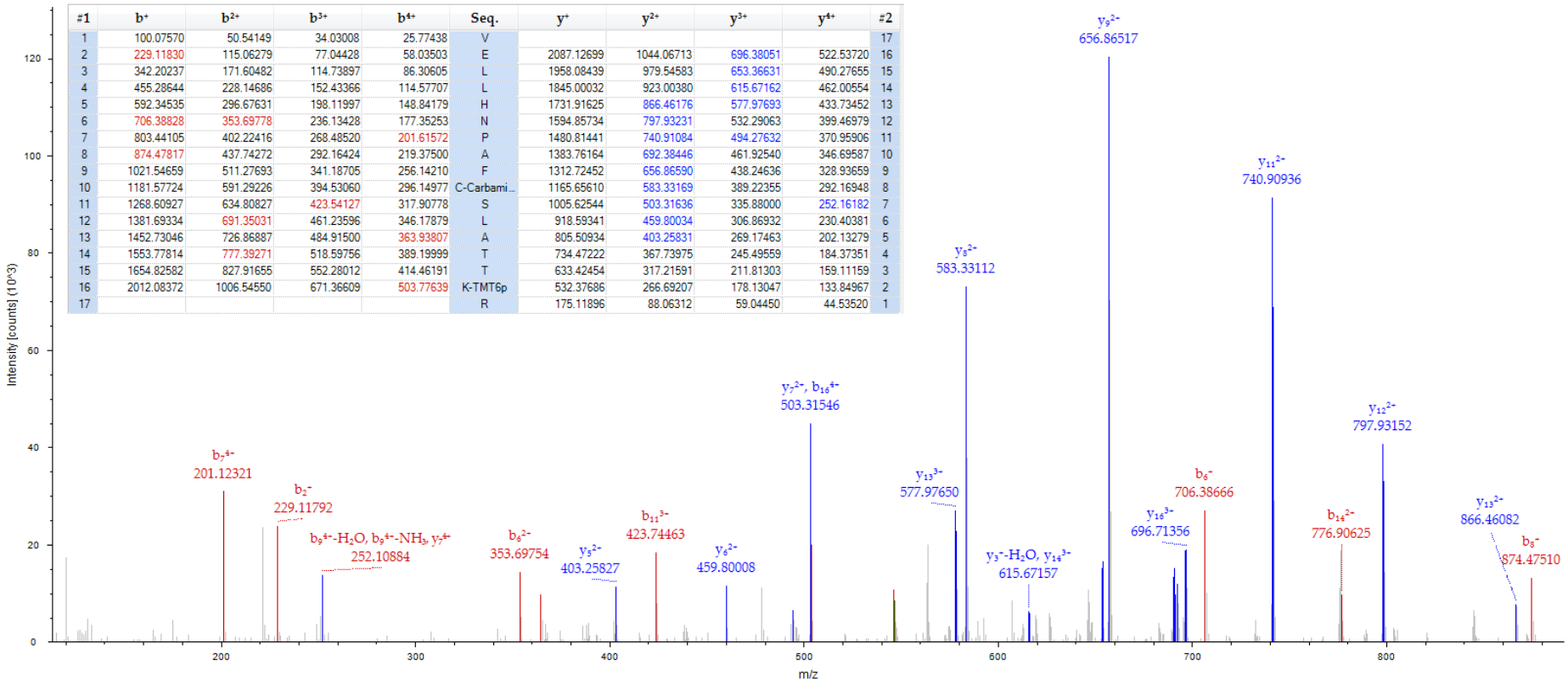

Figure 3-47: MS/MS spectrum of *m/z* 547.30 the $[M+4H]^{4+}$ molecular ion for a peptide of 2186.19 Da with corresponding sequence VELLHNPAFCSLATTKR unique to CC3 identified in 1DGE fraction 6 as significant (*P* value <0.05) between PiB+ and PiB- groups.

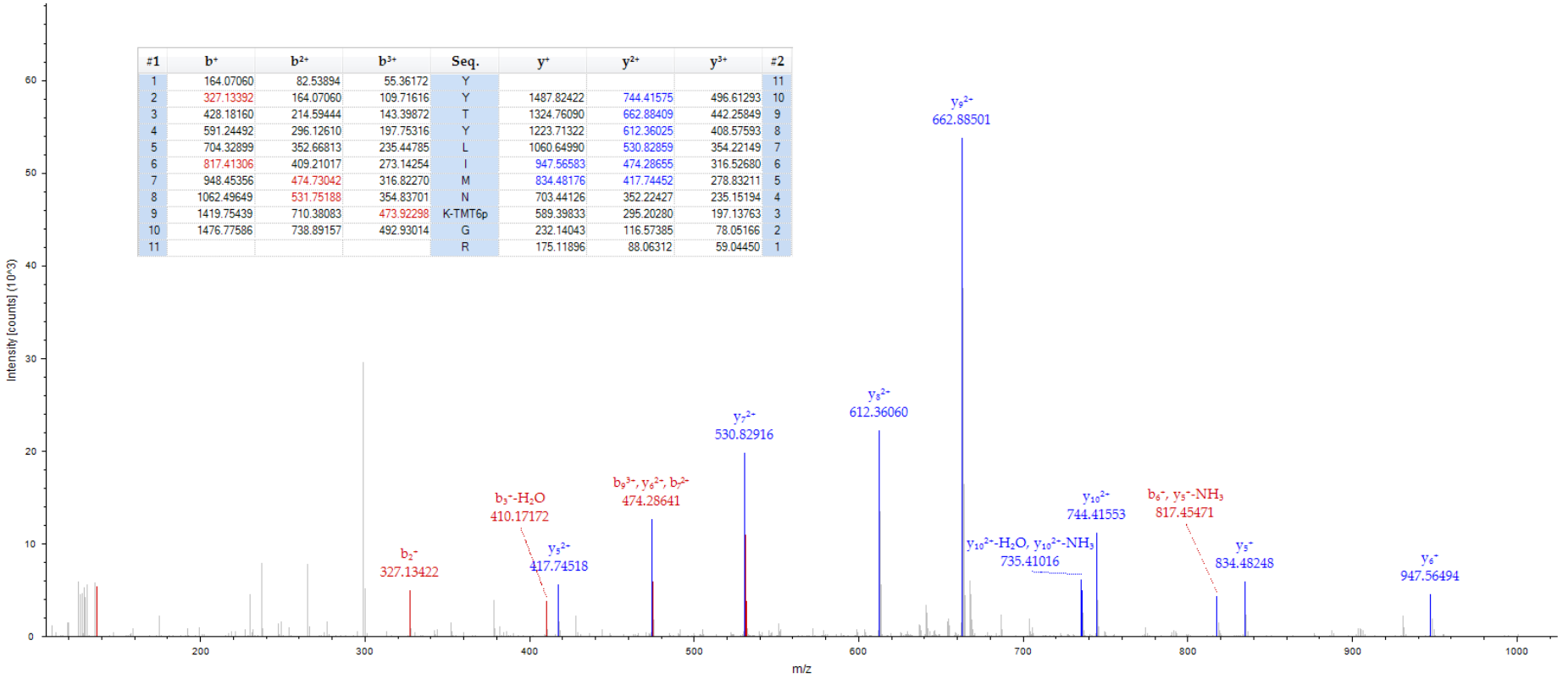

Figure 3-48: MS/MS spectrum of *m/z* 550.97 the $[M+3H]^{3+}$ molecular ion for a peptide of 1650.89 Da with corresponding sequence YYTYLIMNKGR unique to CC3 identified in 1DGE fraction 6 as significant (*P* value <0.05) between PiB+ and PiB- groups.

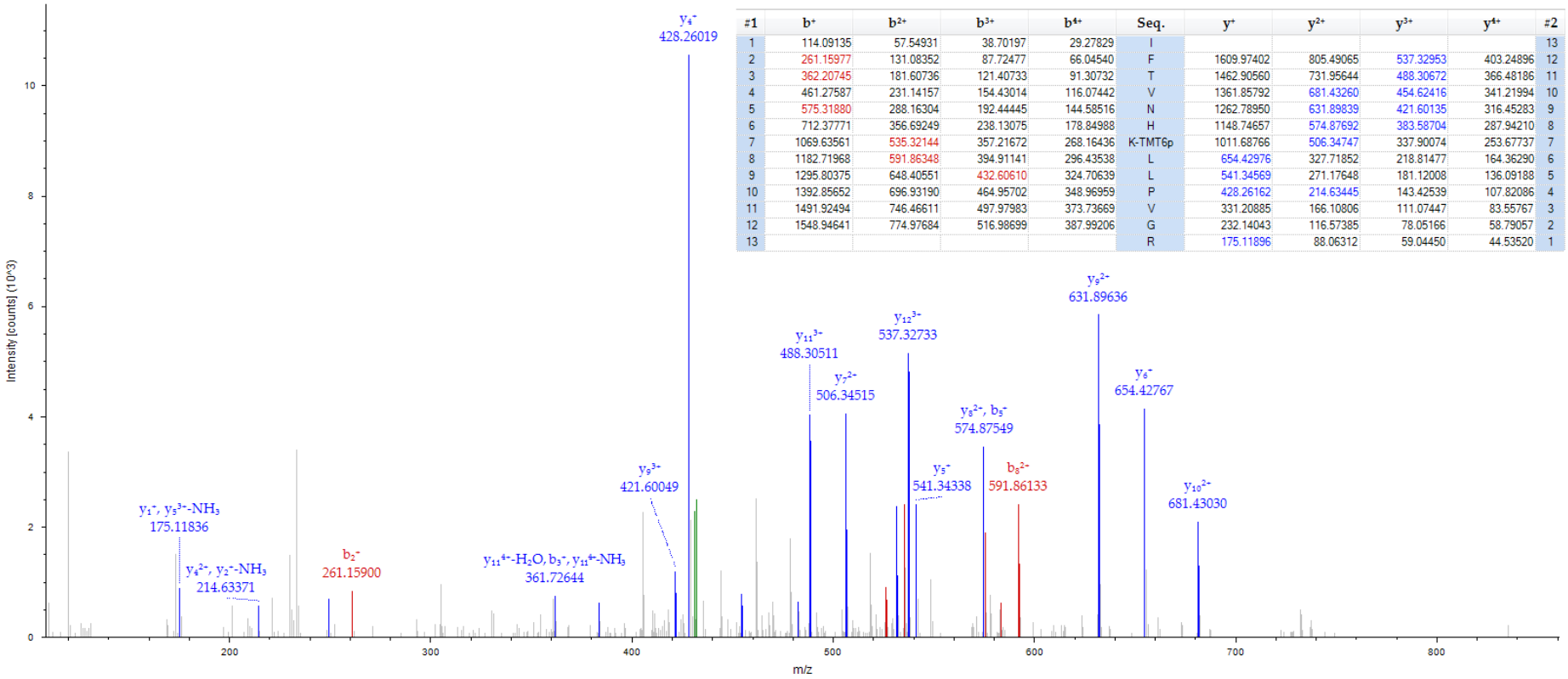

#1	b+	b2+	b3+	b4+	Seq.	y+	y2+	y3+	y4+	#2
1	114.09135	57.54931	38.70197	29.27829	I					13
2	261.15977	131.08352	87.72477	66.04540	F	1609.97402	805.49065	537.32953	403.24896	12
3	362.20745	181.60736	121.40733	91.30732	T	1462.90560	731.95644	488.30672	366.48186	11
4	461.27587	231.14157	154.43014	116.07442	V	1361.85792	681.43260	454.62416	341.21994	10
5	575.31880	288.16304	192.44445	144.58516	N	1262.78950	631.89839	421.60135	316.45283	9
6	712.37771	356.69249	238.13075	178.84988	H	1148.74657	574.87692	383.58704	287.94210	8
7	1069.63561	535.32144	357.21672	268.16436	K-TMT6p	1011.68766	506.34747	337.90074	253.67737	7
8	1182.71968	591.86348	394.91141	296.43538	L	654.42976	327.71852	218.81477	164.36290	6
9	1295.80375	648.40551	432.60610	324.70639	L	541.34569	271.17648	181.12008	136.09188	5
10	1392.85652	696.93190	464.95702	348.96959	P	428.26162	214.63445	143.42539	107.82086	4
11	1491.92494	746.46611	497.97983	373.73669	V	331.20885	166.10806	111.07447	83.55767	3
12	1548.94641	774.97684	516.98699	387.99206	G	232.14043	116.57385	78.05166	58.79057	2
13					R	175.11896	88.06312	59.04450	44.53520	1

Figure 3-49: MS/MS spectrum of *m/z* 431.52 the $[M+4H]^{4+}$ molecular ion for a peptide of 1723.06 Da with corresponding sequence IFTVNHKLLPVGR unique to CC3 identified in 1DGE fraction 6 as significant (*P* value <0.05) between PiB+ and PiB- groups.

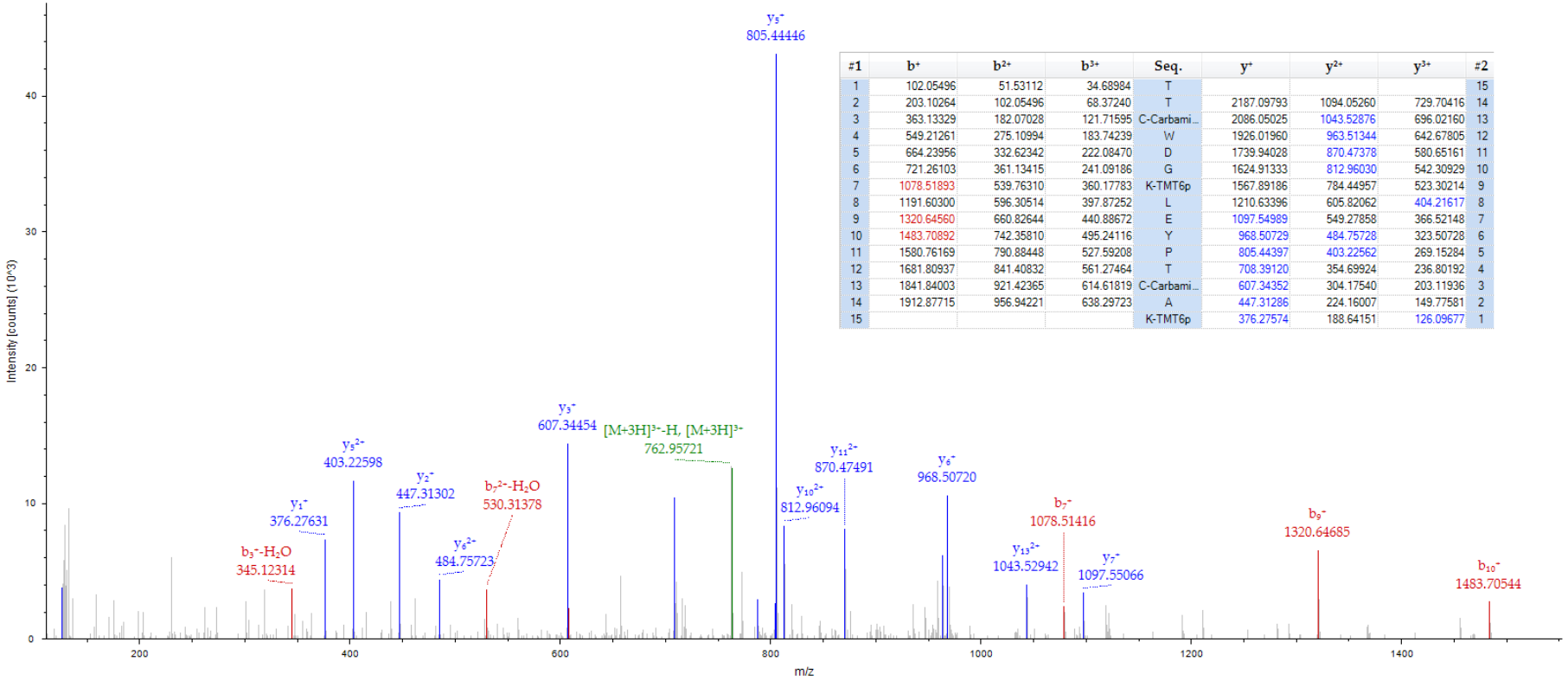

#1	b+	b2+	b3+	Seq.	y+	y2+	y3+	#2
1	102.05496	51.53112	34.68984	T				15
2	203.10264	102.05496	68.37240	T	2187.09793	1094.05260	729.70416	14
3	363.13329	182.07028	121.71595	C-Carbami...	2086.05025	1043.52876	696.02160	13
4	549.21261	275.10994	183.74239	W	1926.01960	963.51344	642.67805	12
5	664.23956	332.62342	222.08470	D	1739.94028	870.47378	580.65161	11
6	721.26103	361.13415	241.09186	G	1624.91333	812.96030	542.30929	10
7	1078.51893	539.76310	360.17783	K-TMT6p	1567.89186	784.44957	523.30214	9
8	1191.60300	596.30514	397.87252	L	1210.63396	605.82062	404.21617	8
9	1320.64560	660.82644	440.88672	E	1097.54989	549.27858	366.52148	7
10	1483.70892	742.35810	495.24116	Y	968.50729	484.75728	323.50728	6
11	1580.76169	790.88448	527.59208	P	805.44397	403.22562	269.15284	5
12	1681.80937	841.40832	561.27464	T	708.39120	354.69924	236.80192	4
13	1841.84003	921.42365	614.61819	C-Carbami...	607.34352	304.17540	203.11936	3
14	1912.87715	956.94221	638.29723	A	447.31286	224.16007	149.77581	2
15				K-TMT6p	376.27574	188.64151	126.09677	1

Figure 3-50: MS/MS spectrum of *m/z* 763.39 the $[M+3H]^{3+}$ molecular ion for a peptide of 2288.14 Da with corresponding sequence TTCWDGKLEYPTCAK unique to CFH identified in 1DGE fraction 6 as significant (*P* value <0.05) between PiB+ and PiB- groups.

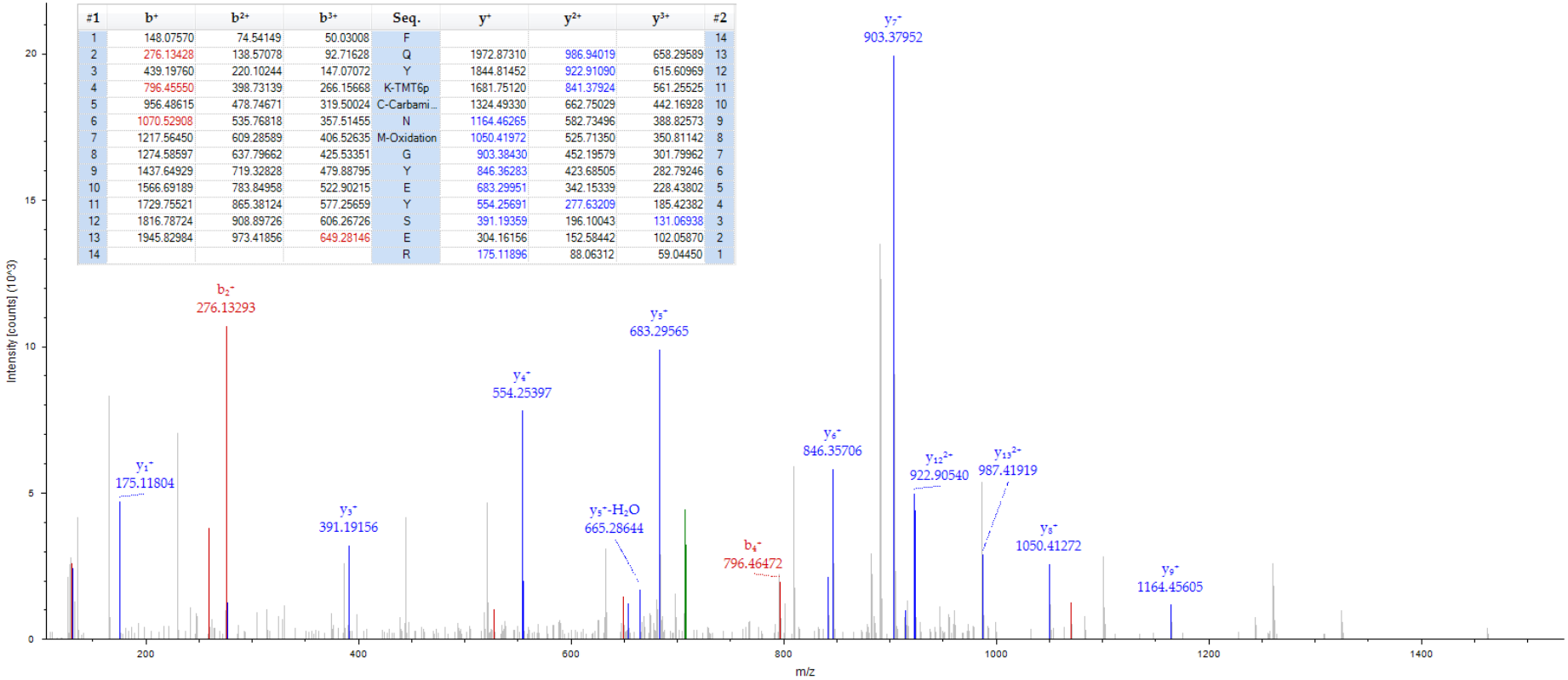

Figure 3-51: MS/MS spectrum of *m/z* 707.32 the $[M+3H]^{3+}$ molecular ion for a peptide of 2119.94 Da with corresponding sequence FQYKCNMGYEYSER unique to CFH identified in 1DGE fraction 6 as significant (*P* value <0.05) between PiB+ and PiB- groups.

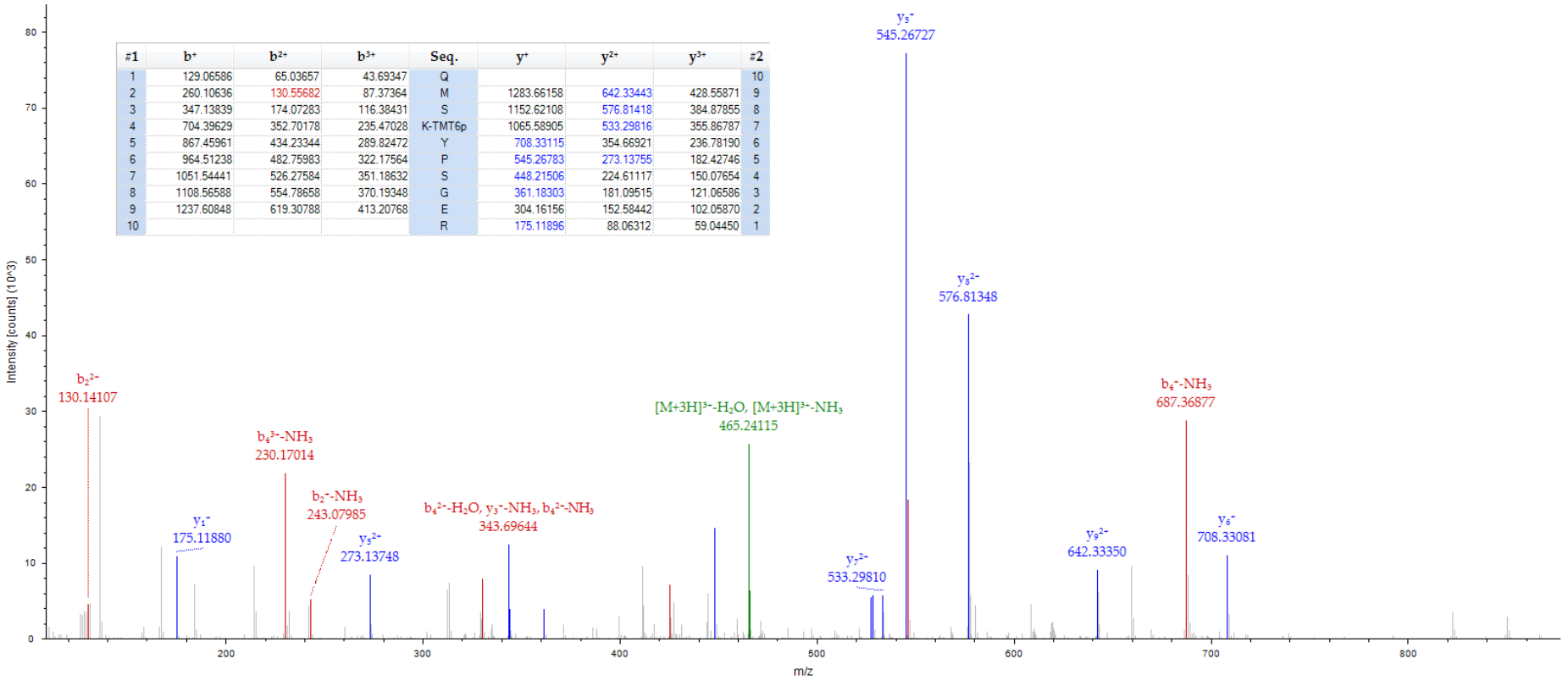

Figure 3-52: MS/MS spectrum of *m/z* 471.24 the $[M+3H]^{3+}$ molecular ion for a peptide of 1411.72 Da with corresponding sequence QMSKYPSGER unique to CFH identified in 1DGE fraction 6 as significant (*P* value <0.05) between PiB+ and PiB- groups.

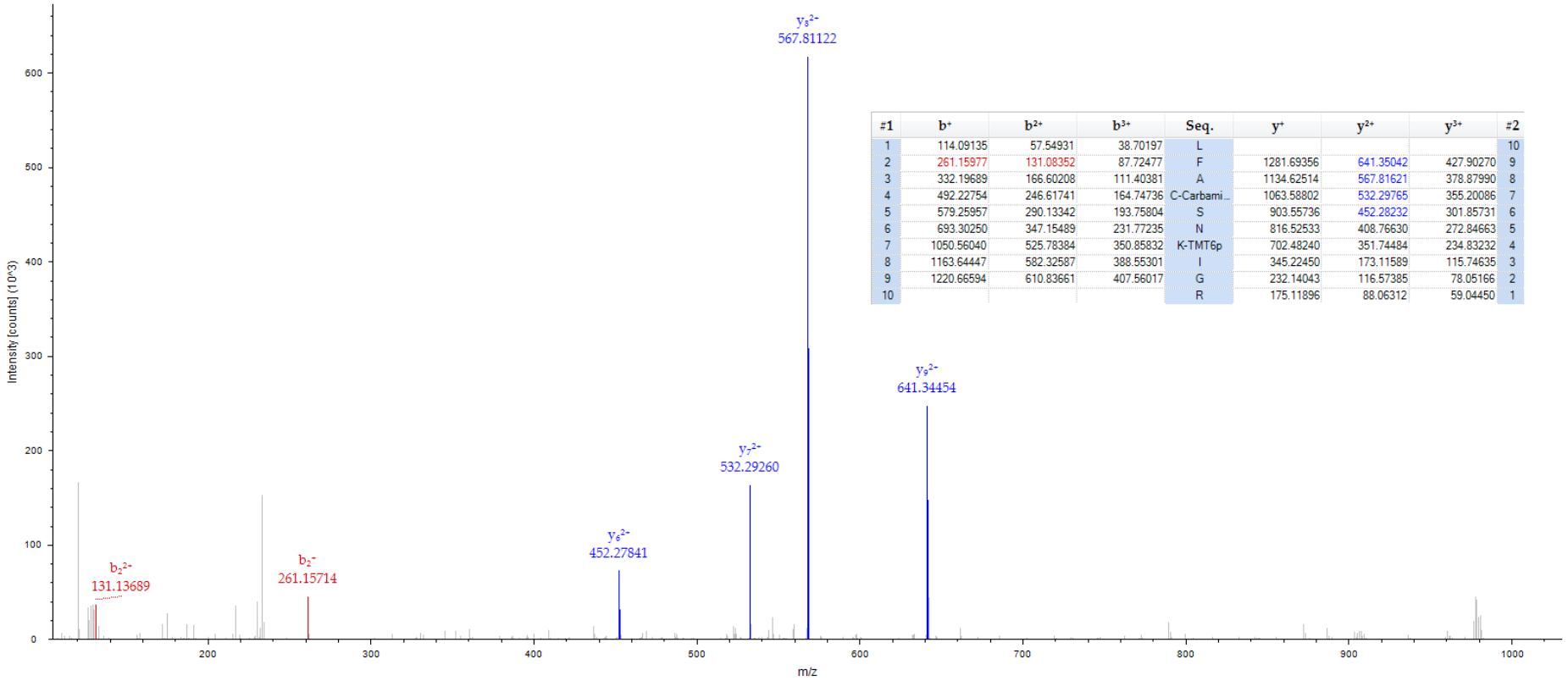

#1	b^+	b^{2+}	b^{3+}	Seq.	y^+	y^{2+}	y^{3+}	#2
1	114.09135	57.54931	38.70197	L				10
2	261.15977	131.08352	87.72477	F	1281.69356	641.35042	427.90270	9
3	332.19689	166.60208	111.40381	A	1134.62514	567.81621	378.87990	8
4	492.22754	246.61741	164.74736	C-Carbami...	1063.58802	532.29765	355.20086	7
5	579.25957	290.13342	193.75804	S	903.55736	452.28232	301.85731	6
6	693.30250	347.15489	231.77235	N	816.52533	408.76630	272.84663	5
7	1050.56040	525.78384	350.85832	K-TMT6p	702.48240	351.74484	234.83232	4
8	1163.64447	582.32587	388.55301	I	345.22450	173.11589	115.74635	3
9	1220.66594	610.83661	407.56017	G	232.14043	116.57385	78.05166	2
10				R	175.11896	88.06312	59.04450	1

Figure 3-53: MS/MS spectrum of *m/z* 465.60 the $[M+3H]^{3+}$ molecular ion for a peptide of 1394.78 Da with corresponding sequence LFACSNKIGR unique to gelsolin identified in 1DGE fraction 5 as significant (*P* value <0.05) between PiB+ and PiB- groups.

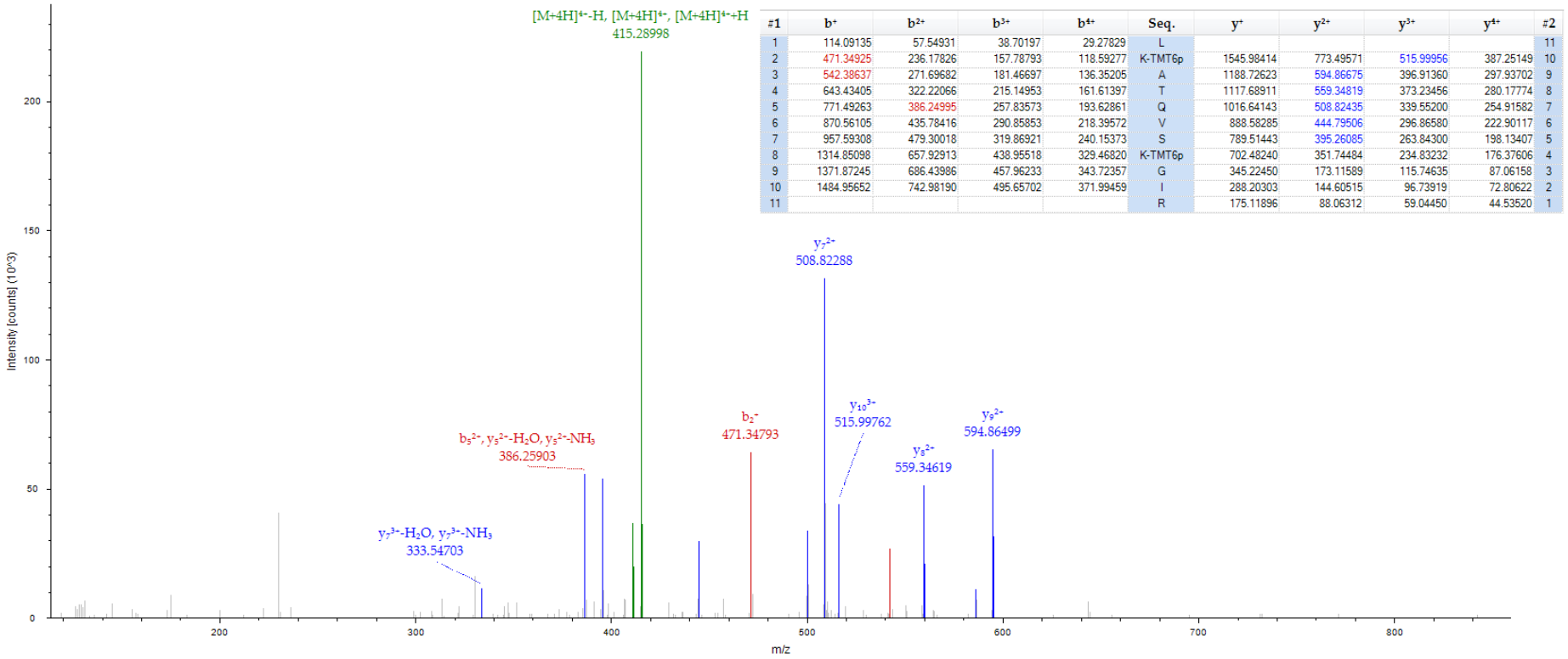

#1	b⁺	b²⁺	b³⁺	b⁴⁺	Seq.	y⁺	y²⁺	y³⁺	y⁴⁺	#2
1	114.09135	57.54931	38.70197	29.27829	L					11
2	471.34925	236.17826	157.78793	118.59277	K-TMT6p	1545.98414	773.49571	515.99956	387.25149	10
3	542.38637	271.69682	181.46697	136.35205	A	1188.72623	594.86675	396.91360	297.93702	9
4	643.43405	322.22066	215.14953	161.61397	T	1117.68911	559.34819	373.23456	280.17774	8
5	771.49263	386.24995	257.83573	193.62861	Q	1016.64143	508.82435	339.55200	254.91582	7
6	870.56105	435.78416	290.85853	218.39572	V	888.58285	444.79506	296.86580	222.90117	6
7	957.59308	479.30018	319.86921	240.15373	S	789.51443	395.26085	263.84300	198.13407	5
8	1314.85098	657.92913	438.95518	329.46820	K-TMT6p	702.48240	351.74484	234.83232	176.37606	4
9	1371.87245	686.43986	457.96233	343.72357	G	345.22450	173.11589	115.74635	87.06158	3
10	1484.95652	742.98190	495.65702	371.99459	I	288.20303	144.60515	96.73919	72.80622	2
11					R	175.11896	88.06312	59.04450	44.53520	1

Figure 3-54: MS/MS spectrum of *m/z* 415.52 the $[M+4H]^{4+}$ molecular ion for a peptide of 1659.06 Da with corresponding sequence LKATQVSKGIR unique to gelsolin identified in 1DGE fraction 5 as significant (*P* value <0.05) between PiB+ and PiB- groups.

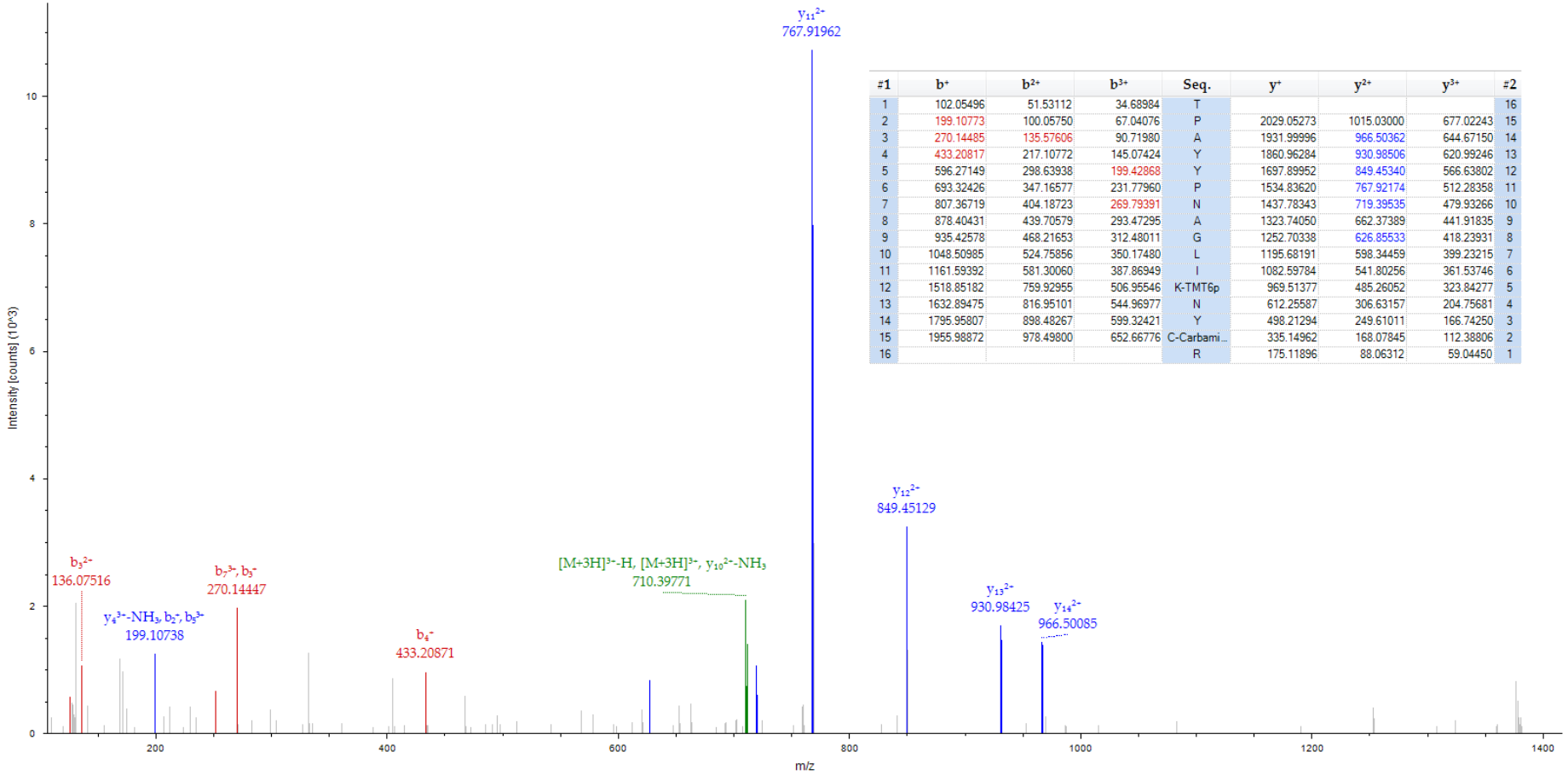

#1	b^{+}	b^{2+}	b^{3+}	Seq.	y^{+}	y^{2+}	y^{3+}	#2
1	102.05496	51.53112	34.68984	T				16
2	199.10773	100.05750	67.04076	P	2029.05273	1015.03000	677.02243	15
3	270.14485	135.57606	90.71980	A	1931.99996	966.50362	644.67150	14
4	433.20817	217.10772	145.07424	Y	1860.96284	930.98506	620.99246	13
5	596.27149	298.63938	199.42868	Y	1697.89952	849.45340	566.63802	12
6	693.32426	347.16577	231.77960	P	1534.83620	767.92174	512.28358	11
7	807.36719	404.18723	269.79391	N	1437.78343	719.39535	479.93266	10
8	878.40431	439.70579	293.47295	A	1323.74050	662.37389	441.91835	9
9	935.42578	468.21653	312.48011	G	1252.70338	626.85533	418.23931	8
10	1048.50985	524.75856	350.17480	L	1195.68191	598.34459	399.23215	7
11	1161.59392	581.30060	387.86949	I	1082.59784	541.80256	361.53746	6
12	1518.85182	759.92955	506.95546	K-TMT6p	969.51377	485.26052	323.84277	5
13	1632.89475	816.95101	544.96977	N	612.25587	306.63157	204.75681	4
14	1795.95807	898.48267	599.32421	Y	498.21294	249.61011	166.74250	3
15	1955.98872	978.49800	652.66776	C-Carbami...	335.14962	168.07845	112.38806	2
16				R	175.11896	88.06312	59.04450	1

Figure 3-55: MS/MS spectrum of *m/z* 710.70 the $[M+3H]^{3+}$ molecular ion for a peptide of 2130.10 Da with corresponding sequence TPAYYPNAGLIKNYCR unique to apo(a) identified in 1DGE fraction 1 as significant (*P* value <0.05) between PiB+ and PiB- groups.

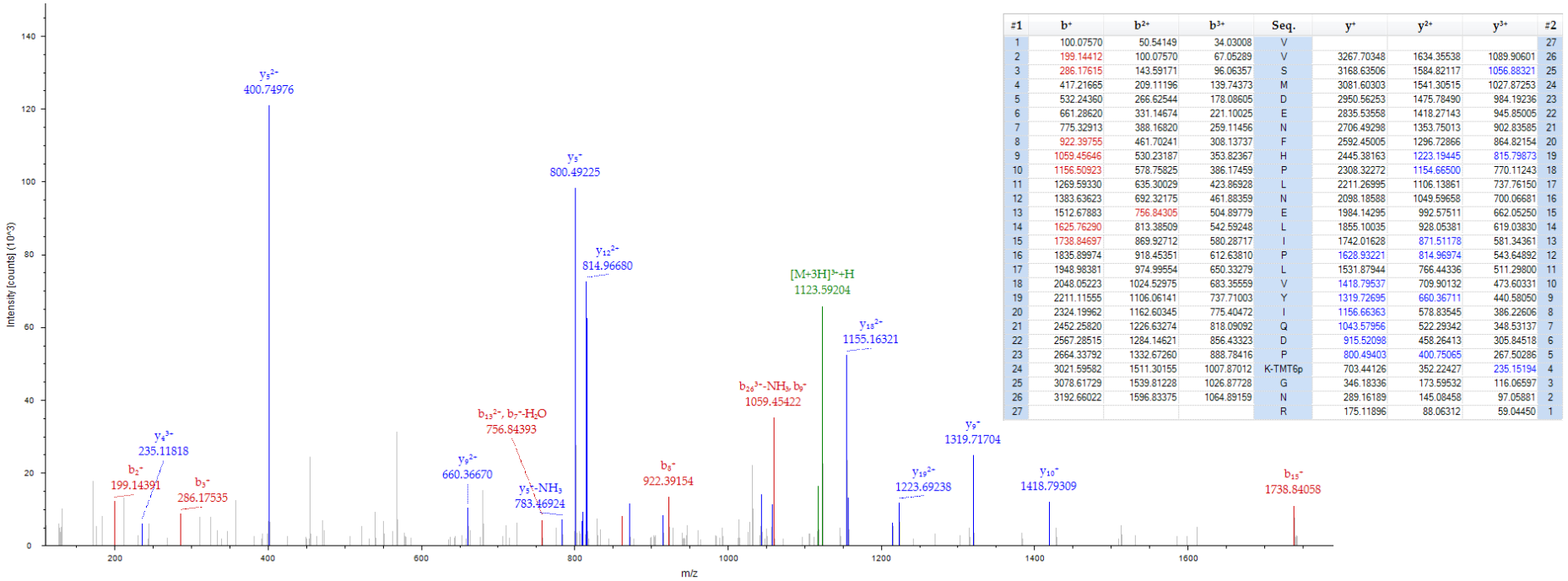

#1	b+	b2+	b3+	Seq.	y+	y2+	y3+	#2
1	100.07570	50.54149	34.03008	V				27
2	199.14412	100.07570	67.05289	V	3267.70348	1634.35538	1089.90601	26
3	286.17615	143.59171	96.06357	S	3168.63506	1584.82117	1056.88321	25
4	417.21665	209.11196	139.74373	M	3081.60303	1541.30515	1027.87253	24
5	532.24360	266.62544	178.08605	D	2950.56253	1475.78490	984.19236	23
6	661.28620	331.14674	221.10025	E	2835.53558	1418.27143	945.85005	22
7	775.32913	388.16820	259.11456	N	2706.49298	1353.75013	902.83585	21
8	922.39755	461.70241	308.13737	F	2592.45005	1296.72866	864.82154	20
9	1059.45646	530.23187	353.82367	H	2445.38163	1223.19445	815.79873	19
10	1156.50923	578.75825	386.17459	P	2308.32272	1154.66500	770.11243	18
11	1269.59330	635.30029	423.86928	L	2211.26995	1106.13861	737.76150	17
12	1383.63623	692.32175	461.88359	N	2098.18588	1049.59658	700.06681	16
13	1512.67883	756.84305	504.89779	E	1984.14295	992.57511	662.05250	15
14	1625.76290	813.38509	542.59248	L	1855.10035	928.05381	619.03830	14
15	1738.84697	869.92712	580.28717	I	1742.01628	871.51178	581.34361	13
16	1835.89974	918.45351	612.63810	P	1628.93221	814.96974	543.64892	12
17	1948.98381	974.99554	650.33279	L	1531.87944	766.44336	511.29800	11
18	2048.05223	1024.52975	683.35559	V	1418.79537	709.90132	473.60331	10
19	2211.11555	1106.06141	737.71003	Y	1319.72695	660.36711	440.58050	9
20	2324.19962	1162.60345	775.40472	I	1156.66363	578.83545	386.22606	8
21	2452.25820	1226.63274	818.09092	Q	1043.57956	522.29342	348.53137	7
22	2567.28515	1284.14621	856.43323	D	915.52098	458.26413	305.84518	6
23	2664.33792	1332.67260	888.78416	P	800.49403	400.75065	267.50286	5
24	3021.59582	1511.30155	1007.87012	K-TMT6p	703.44126	352.22427	235.15194	4
25	3078.61729	1539.81228	1026.87728	G	346.18336	173.59532	116.06597	3
26	3192.66022	1596.83375	1064.89159	N	289.16189	145.08458	97.05881	2
27				R	175.11896	88.06312	59.04450	1

Figure 3-56: MS/MS spectrum of *m/z* 1122.93 the $[M+3H]^{3+}$ molecular ion for a peptide of 3366.77 Da with corresponding sequence VVSMDENFHPLNELIPLVYIQDPKGNR unique to α2M identified in 1DGE fraction 2 as significant (*P* value <0.05) between PiB+ and PiB- groups.

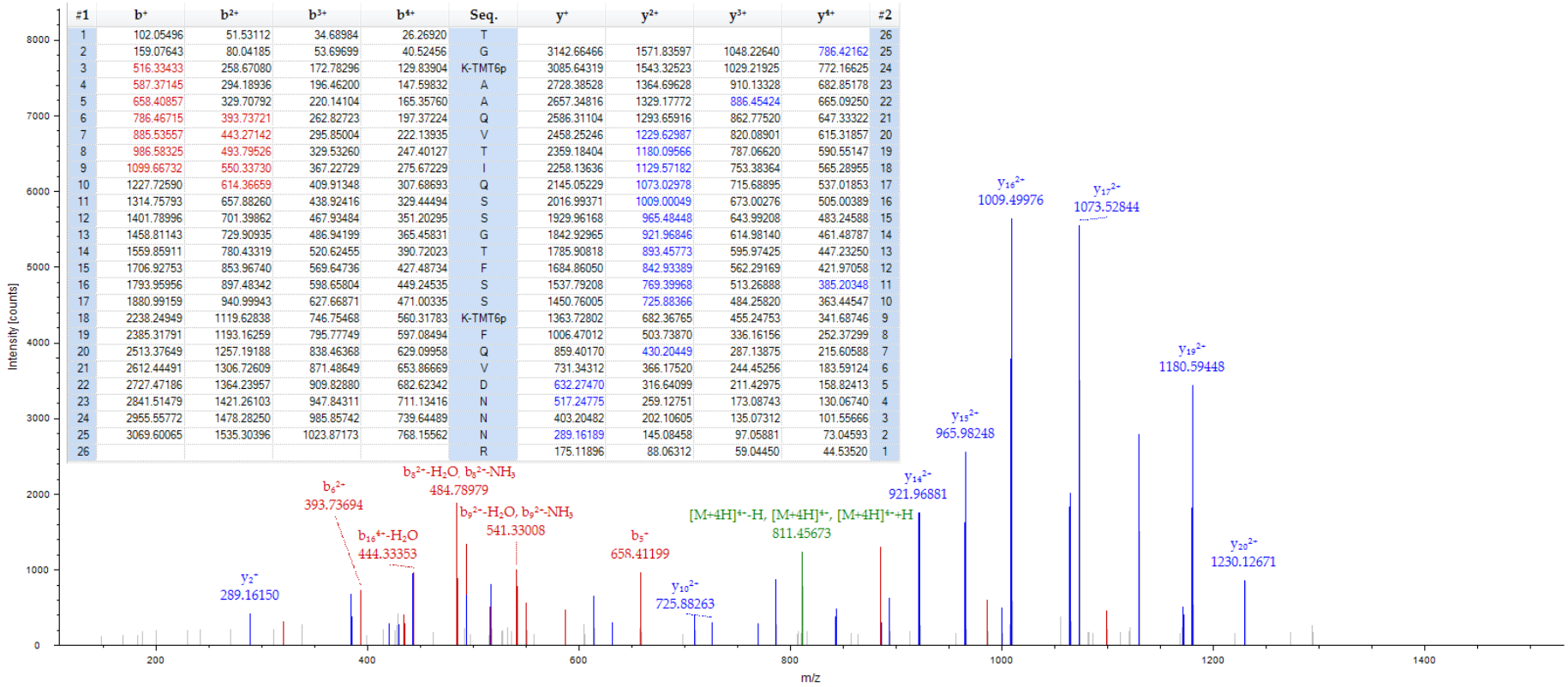

Figure 3-57: MS/MS spectrum of *m/z* 811.69 the $[M+4H]^{4+}$ molecular ion for a peptide of 3243.72 Da with corresponding sequence TGKAAQVTIQSSGTFSSKFQVDNNNR unique to α2M identified in 1DGE fraction 2 as significant (*P* value <0.05) between PiB+ and PiB- groups.

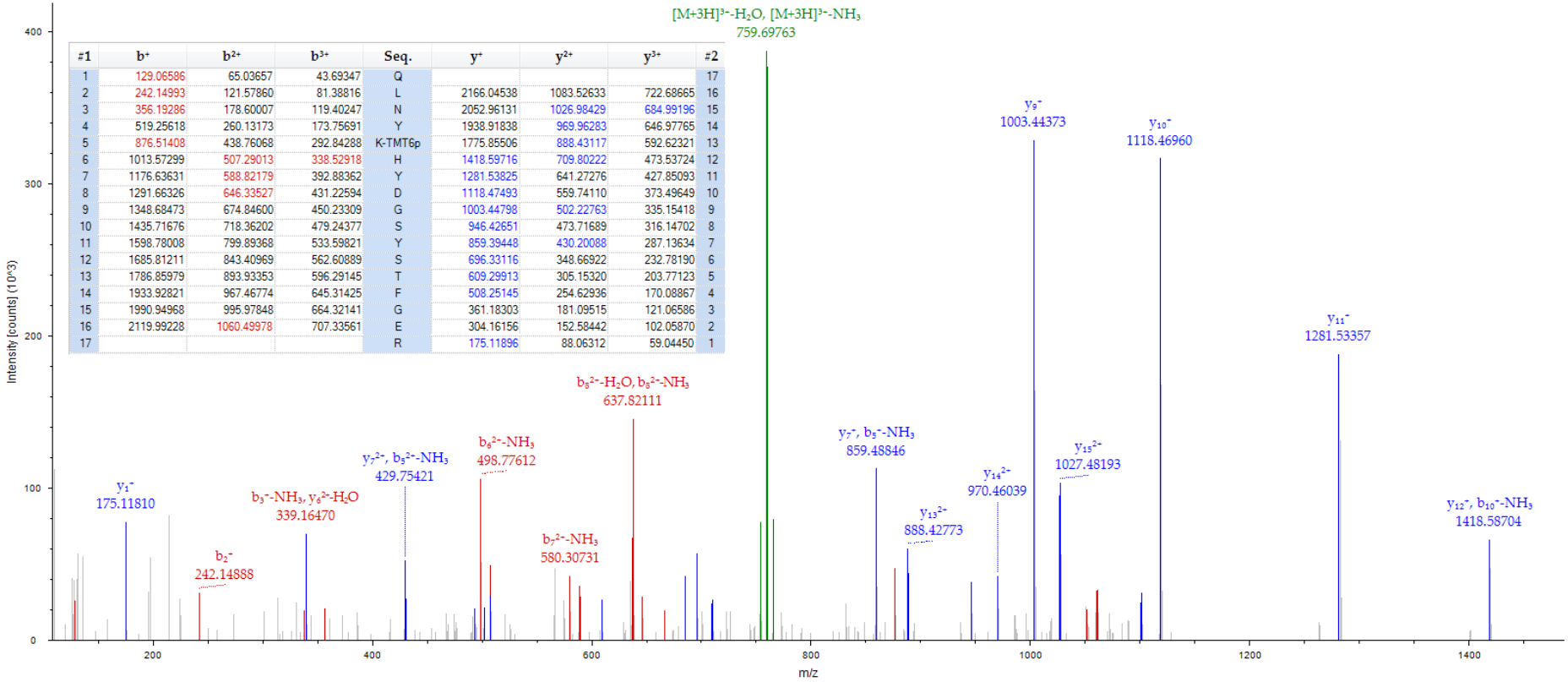

#1	b⁺	b²⁺	b³⁺	Seq.	y⁺	y²⁺	y³⁺	#2
1	129.06586	65.03657	43.69347	Q				17
2	242.14993	121.57860	81.38816	L	2166.04538	1083.52633	722.68665	16
3	356.19286	178.60007	119.40247	N	2052.96131	1026.98429	684.99196	15
4	519.25618	260.13173	173.75691	Y	1938.91838	969.96283	646.97765	14
5	876.51408	438.76068	292.84288	K-TMT6p	1775.85506	888.43117	592.62321	13
6	1013.57299	507.29013	338.52918	H	1418.59716	709.80222	473.53724	12
7	1176.63631	588.82179	392.88362	Y	1281.53825	641.27276	427.85093	11
8	1291.66326	646.33527	431.22594	D	1118.47493	559.74110	373.49649	10
9	1348.68473	674.84600	450.23309	G	1003.44798	502.22763	335.15418	9
10	1435.71676	718.36202	479.24377	S	946.42651	473.71689	316.14702	8
11	1598.78008	799.89368	533.59821	Y	859.39448	430.20088	287.13634	7
12	1685.81211	843.40969	562.60889	S	696.33116	348.66922	232.78190	6
13	1786.85979	893.93353	596.29145	T	609.29913	305.15320	203.77123	5
14	1933.92821	967.46774	645.31425	F	508.25145	254.62936	170.08867	4
15	1990.94968	995.97848	664.32141	G	361.18303	181.09515	121.06586	3
16	2119.99228	1060.49978	707.33561	E	304.16156	152.58442	102.05870	2
17				R	175.11896	88.06312	59.04450	1

Figure 3-58: MS/MS spectrum of *m/z* 765.37 the $[M+3H]^{3+}$ molecular ion for a peptide of 2294.10 Da with corresponding sequence QLNYKHYDGSYSTFGER unique to *α*2M identified in 1DGE fraction 2 as significant (*P* value <0.05) between PiB+ and PiB- groups.

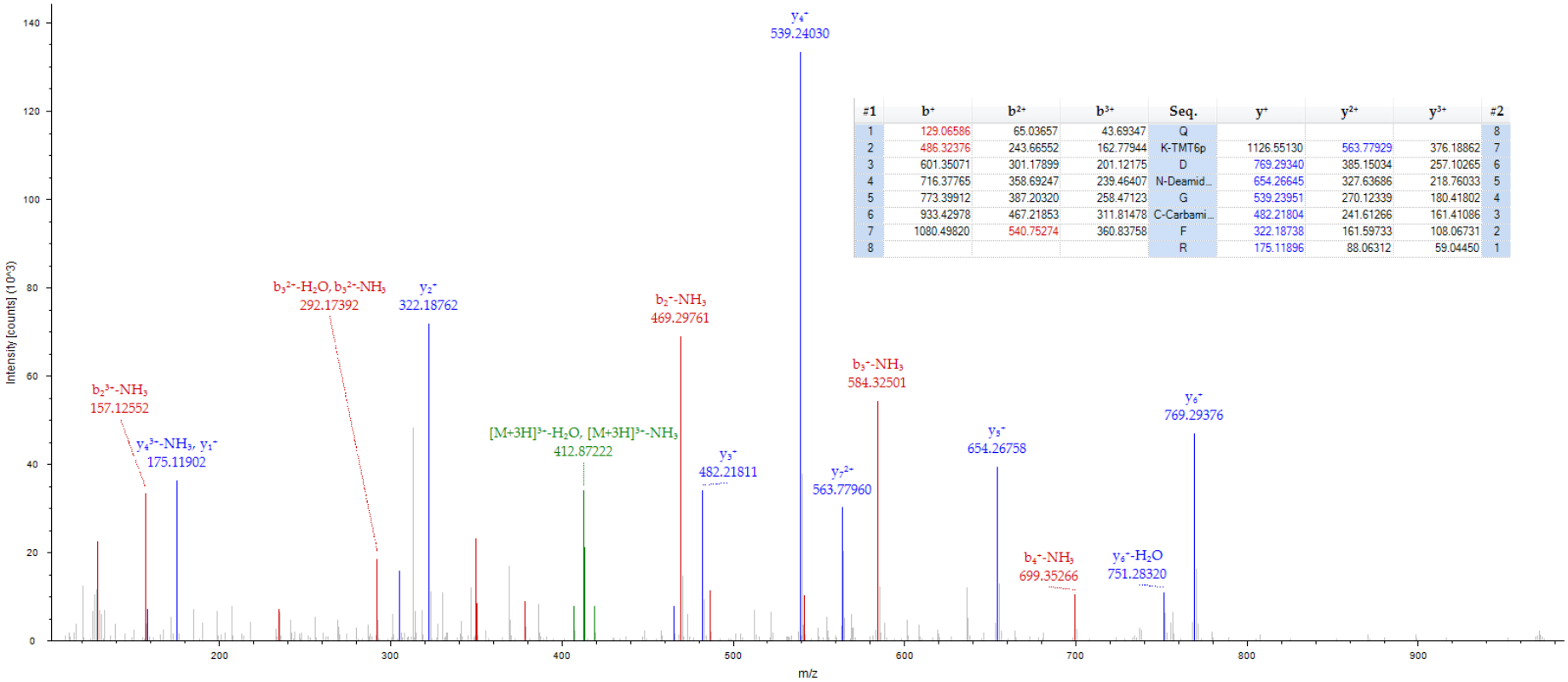

#1	b+	b2+	b3+	Seq.	y+	y2+	y3+	#2
1	129.06586	65.03657	43.69347	Q				8
2	486.32376	243.66552	162.77944	K-TMT6p	1126.55130	563.77929	376.18862	7
3	601.35071	301.17899	201.12175	D	769.29340	385.15034	257.10265	6
4	716.37765	358.69247	239.46407	N-Deamid...	654.26645	327.63686	218.76033	5
5	773.39912	387.20320	258.47123	G	539.23951	270.12339	180.41802	4
6	933.42978	467.21853	311.81478	C-Carbami...	482.21804	241.61266	161.41086	3
7	1080.49820	540.75274	360.83758	F	322.18738	161.59733	108.06731	2
8				R	175.11896	88.06312	59.04450	1

Figure 3-59: MS/MS spectrum of *m/z* 418.87 the [M+3H]3^{+} molecular ion for a peptide of 1254.61 Da with corresponding sequence QKDNGCFR unique to α2M identified in 1DGE fraction 2 as significant (*P* value <0.05) between PiB+ and PiB- groups.

#1	b^{+}	b^{2+}	b^{3+}	b^{4+}	b^{5+}	Seq.	y^{+}	y^{2+}	y^{3+}	y^{4+}	y^{5+}	#2
1	102.05496	51.53112	34.68984	26.26920	21.21681	T						15
2	215.13903	108.07315	72.38453	54.54021	43.83363	I	2135.27419	1068.14073	712.42958	534.57400	427.86066	14
3	316.18671	158.59699	106.06709	79.80213	64.04316	T	2022.19012	1011.59870	674.73489	506.30299	405.24384	13
4	673.44461	337.22594	225.15305	169.11661	135.49474	K-TMT6p	1921.14244	961.07486	641.05233	481.04107	385.03431	12
5	786.52868	393.76798	262.84774	197.38763	158.11156	L	1563.88453	782.44590	521.96636	391.72659	313.58273	11
6	873.56071	437.28399	291.85842	219.14563	175.51796	S	1450.80046	725.90387	484.27167	363.45557	290.96591	10
7	1020.62913	510.81820	340.88123	255.91274	204.93165	F	1363.76843	682.38785	455.26100	341.69757	273.55951	9
8	1119.69755	560.35241	373.90403	280.67984	224.74533	V	1216.70001	608.85364	406.23819	304.93046	244.14582	8
9	1476.95545	738.98136	492.99000	369.99432	296.19691	K-TMT6p	1117.63159	559.31943	373.21538	280.16336	224.33214	7
10	1576.02387	788.51557	526.01281	394.76143	316.01060	V	760.37369	380.69048	254.12941	190.84888	152.88056	6
11	1691.05082	846.02905	564.35512	423.51816	339.01599	D	661.30527	331.15627	221.10661	166.08178	133.06688	5
12	1778.08285	889.54506	593.36580	445.27617	356.42239	S	546.27832	273.64280	182.76429	137.32504	110.06149	4
13	1915.14176	958.07452	639.05210	479.54090	383.83417	H	459.24629	230.12678	153.75361	115.56703	92.65508	3
14	2062.21018	1031.60873	688.07491	516.30800	413.24786	F	322.18738	161.59733	108.06731	81.30230	65.24330	2
15						R	175.11896	88.06312	59.04450	44.53520	35.82961	1

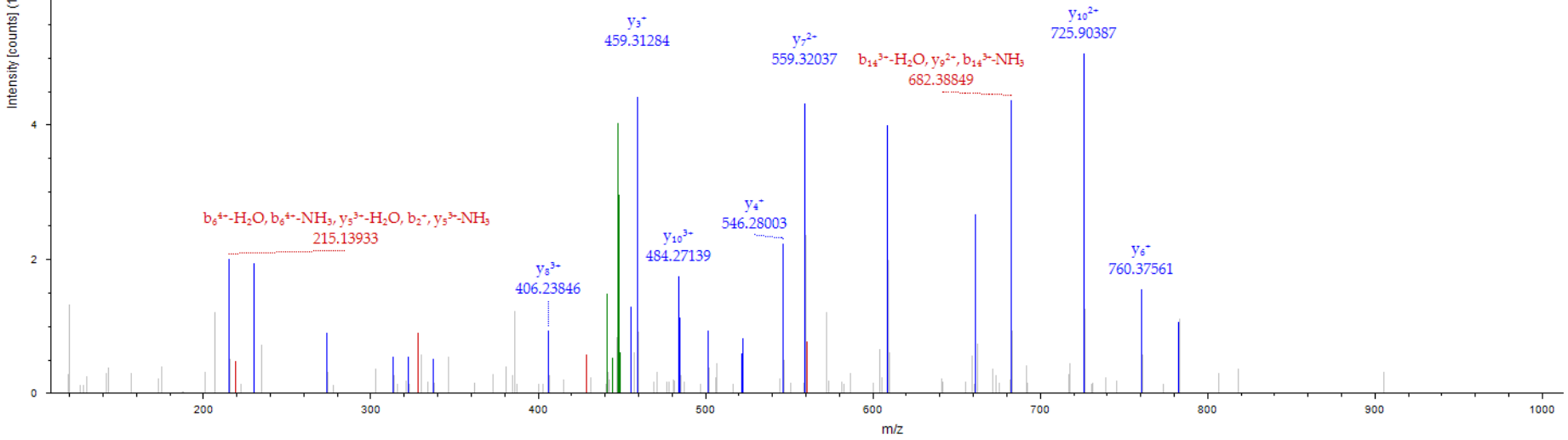

Figure 3-60: MS/MS spectrum of *m/z* 448.10 the $[M+5H]5^{+}$ molecular ion for a peptide of 2236.32 Da with corresponding sequence TITLKLSFVKVDSHFR unique to α2M identified in 1DGE fraction 2 as significant (*P* value <0.05) between PiB+ and PiB- groups.

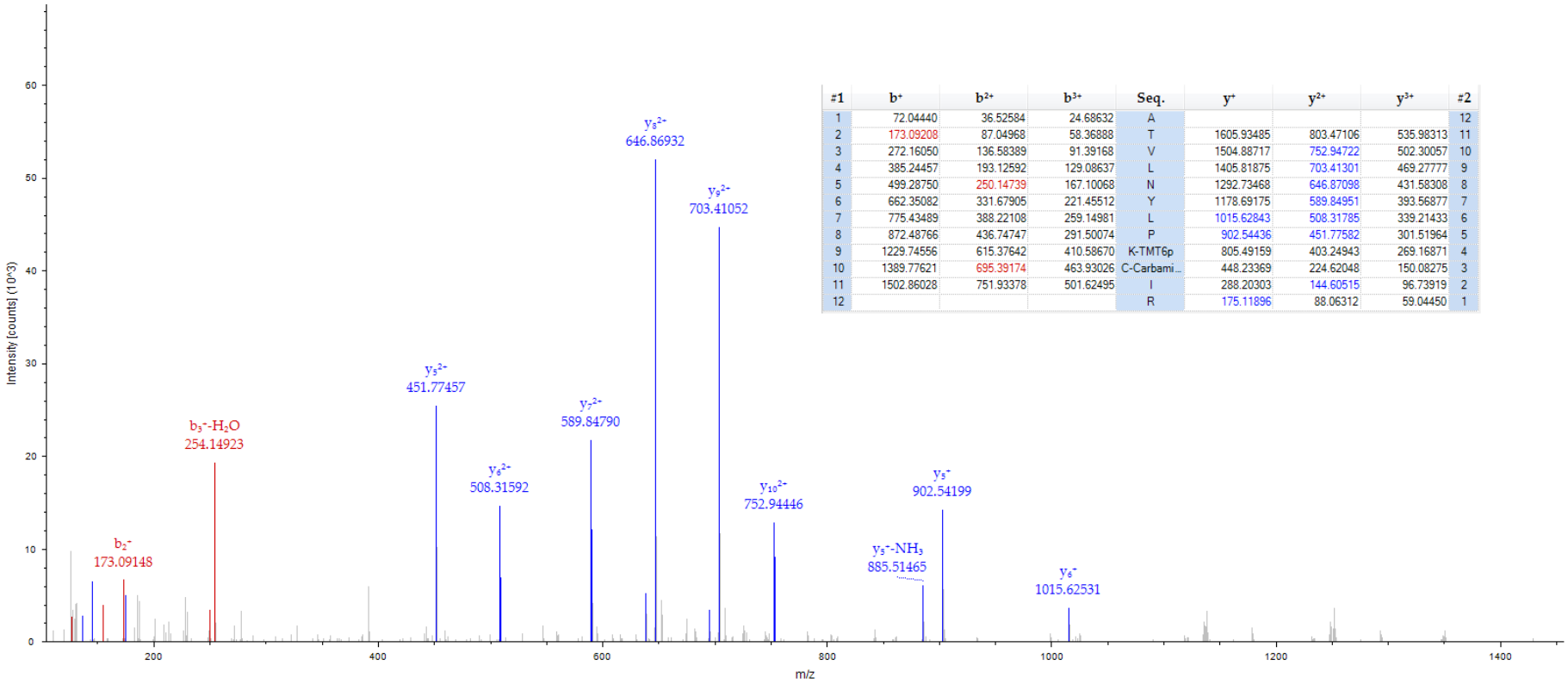

#1	b+	b2+	b3+	Seq.	y+	y2+	y3+	#2
1	72.04440	36.52584	24.68632	A				12
2	173.09208	87.04968	58.36888	T	1605.93485	803.47106	535.98313	11
3	272.16050	136.58389	91.39168	V	1504.88717	752.94722	502.30057	10
4	385.24457	193.12592	129.08637	L	1405.81875	703.41301	469.27777	9
5	499.28750	250.14739	167.10068	N	1292.73468	646.87098	431.58308	8
6	662.35082	331.67905	221.45512	Y	1178.69175	589.84951	393.56877	7
7	775.43489	388.22108	259.14981	L	1015.62843	508.31785	339.21433	6
8	872.48766	436.74747	291.50074	P	902.54436	451.77582	301.51964	5
9	1229.74556	615.37642	410.58670	K-TMT6p	805.49159	403.24943	269.16871	4
10	1389.77621	695.39174	463.93026	C-Carbami...	448.23369	224.62048	150.08275	3
11	1502.86028	751.93378	501.62495	I	288.20303	144.60515	96.73919	2
12				R	175.11896	88.06312	59.04450	1

Figure 3-61: MS/MS spectrum of *m/z* 559.66 the $[M+3H]^{3+}$ molecular ion for a peptide of 1676.97 Da with corresponding sequence ATVLNYLPKCIR unique to α2M identified in 1DGE fraction 2 as significant (*P* value <0.05) between PiB+ and PiB- groups.

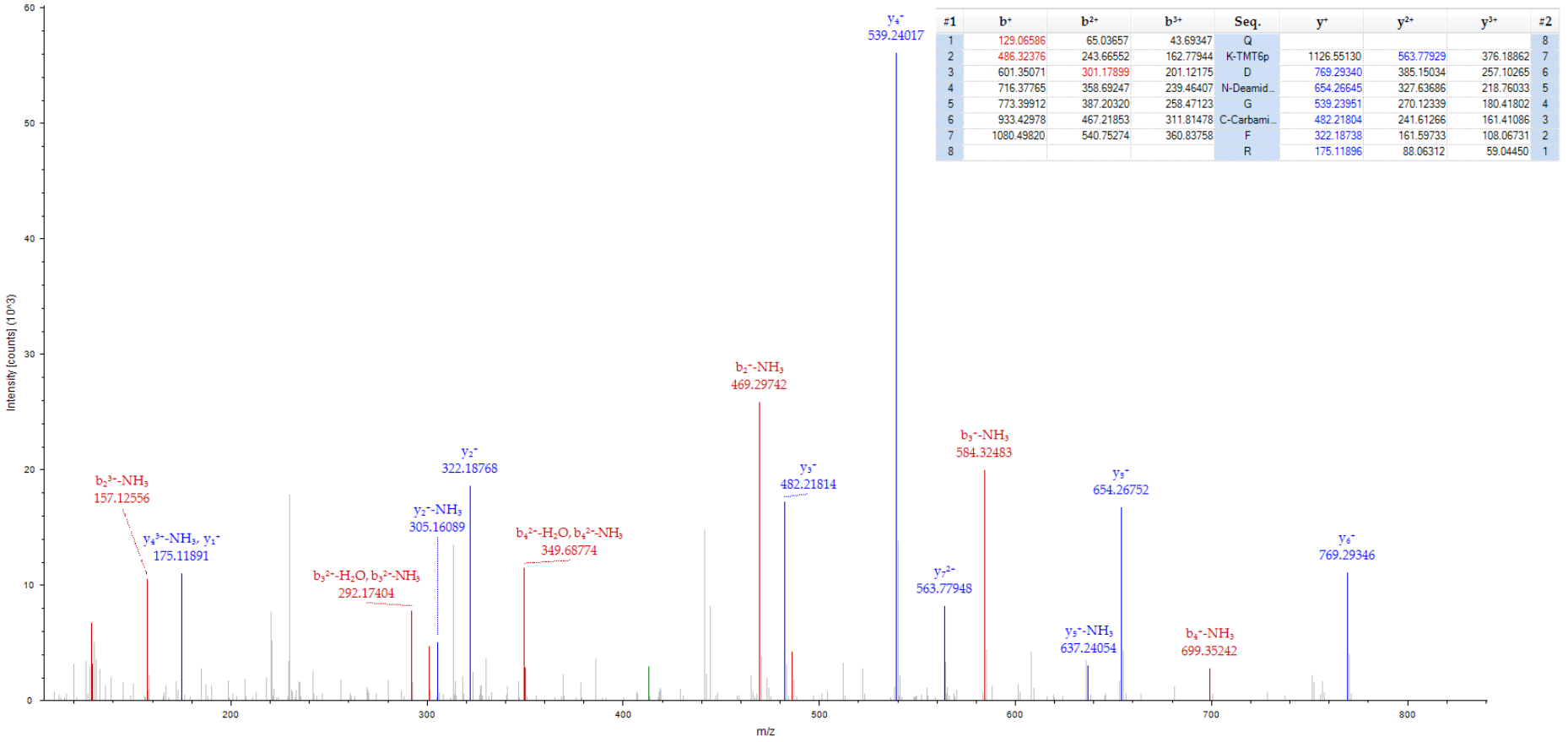

#1	b+	b2+	b3+	Seq.	y+	y2+	y3+	#2
1	129.06586	65.03657	43.69347	Q				8
2	486.32376	243.66552	162.77944	K-TMT6p	1126.55130	563.77929	376.18862	7
3	601.35071	301.17899	201.12175	D	769.29340	385.15034	257.10265	6
4	716.37765	358.69247	239.46407	N-Deamid...	654.26645	327.63686	218.76033	5
5	773.39912	387.20320	258.47123	G	539.23951	270.12339	180.41802	4
6	933.42978	467.21853	311.81478	C-Carbami...	482.21804	241.61266	161.41086	3
7	1080.49820	540.75274	360.83758	F	322.18738	161.59733	108.06731	2
8				R	175.11896	88.06312	59.04450	1

Figure 3-62: MS/MS spectrum of *m/z* 418.88 the $[M+3H]^{3+}$ molecular ion for a peptide of 1240.61 Da with corresponding sequence QKDNGCFR unique to α2M identified in 1DGE fraction 1 as significant (*P* value <0.05) between PiB+ and PiB- groups.

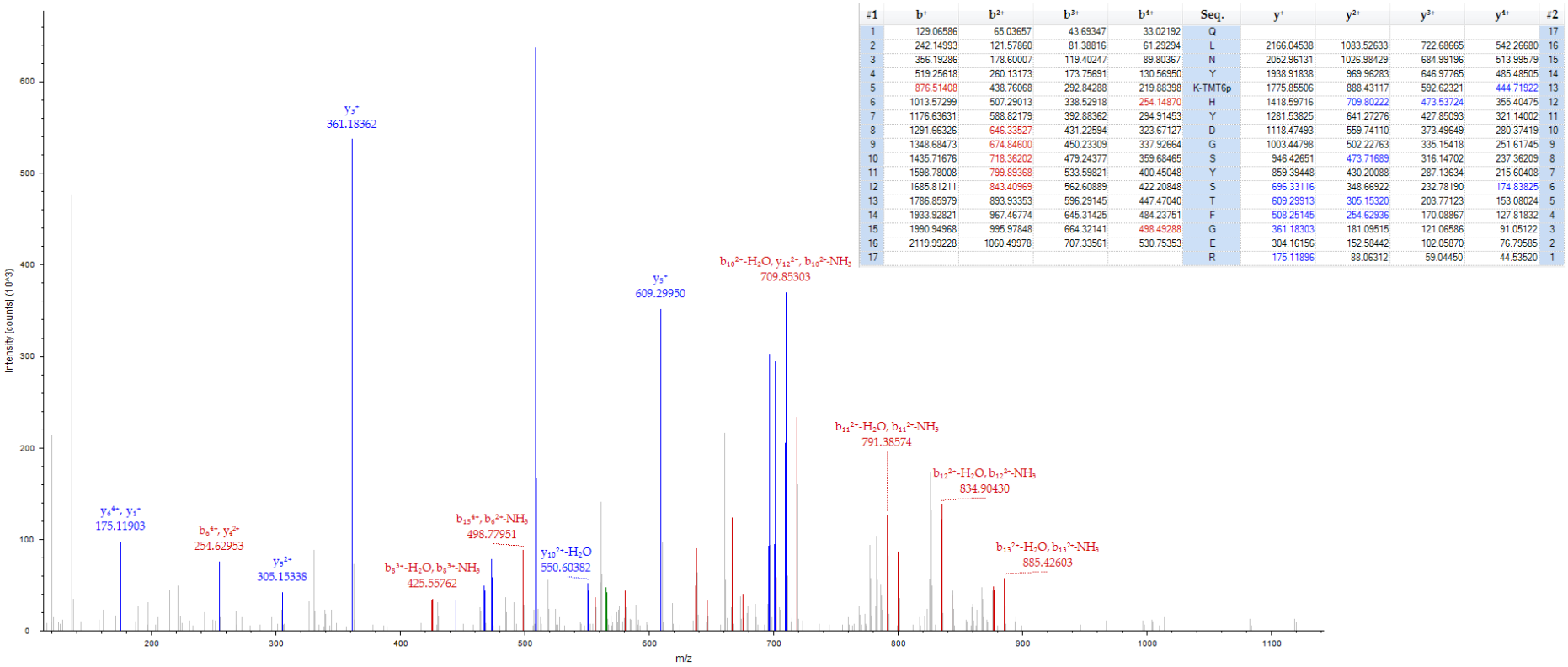

#1	b+	b2+	b3+	b4+	Seq.	y+	y2+	y3+	y4+	#2
1	129.06586	65.03657	43.69347	33.02192	Q					17
2	242.14993	121.57860	81.38816	61.29294	L	2166.04538	1083.52633	722.68665	542.26680	16
3	356.19286	178.60007	119.40247	89.80367	N	2052.96131	1026.98429	684.99196	513.99579	15
4	519.25618	260.13173	173.75691	130.56950	Y	1938.91838	969.96283	646.97765	485.48505	14
5	876.51408	438.76068	292.84288	219.88398	K-TMT6p	1775.85506	888.43117	592.62321	444.71922	13
6	1013.57299	507.29013	338.52918	254.14870	H	1418.59716	709.80222	473.53724	355.40475	12
7	1176.63631	588.82179	392.88362	294.91453	Y	1281.53825	641.27276	427.85093	321.14002	11
8	1291.66326	646.33527	431.22594	323.67127	D	1118.47493	559.74110	373.49649	280.37419	10
9	1348.68473	674.84600	450.23309	337.92664	G	1003.44798	502.22763	335.15418	251.61745	9
10	1435.71676	718.36202	479.24377	359.68465	S	946.42651	473.71689	316.14702	237.36209	8
11	1598.78008	799.89368	533.59821	400.45048	Y	859.39448	430.20088	287.13634	215.60408	7
12	1685.81211	843.40969	562.60889	422.20848	S	696.33116	348.66922	232.78190	174.83825	6
13	1786.85979	893.93353	596.29145	447.47040	T	609.29913	305.15320	203.77123	153.08024	5
14	1933.92821	967.46774	645.31425	484.23751	F	508.25145	254.62936	170.08867	127.81832	4
15	1990.94968	995.97848	664.32141	498.49288	G	361.18303	181.09515	121.06586	91.05122	3
16	2119.99228	1060.49978	707.33561	530.75353	E	304.16156	152.58442	102.05870	76.79585	2
17					R	175.11896	88.06312	59.04450	44.53520	1

Figure 3-63: MS/MS spectrum of *m/z* 574.28 the $[M+4H]^{4+}$ molecular ion for a peptide of 2294.11 Da with corresponding sequence QLNYKHYDGSYSTFGER unique to *α*2M identified in 1DGE fraction 1 as significant (*P* value <0.05) between PiB+ and PiB- groups.

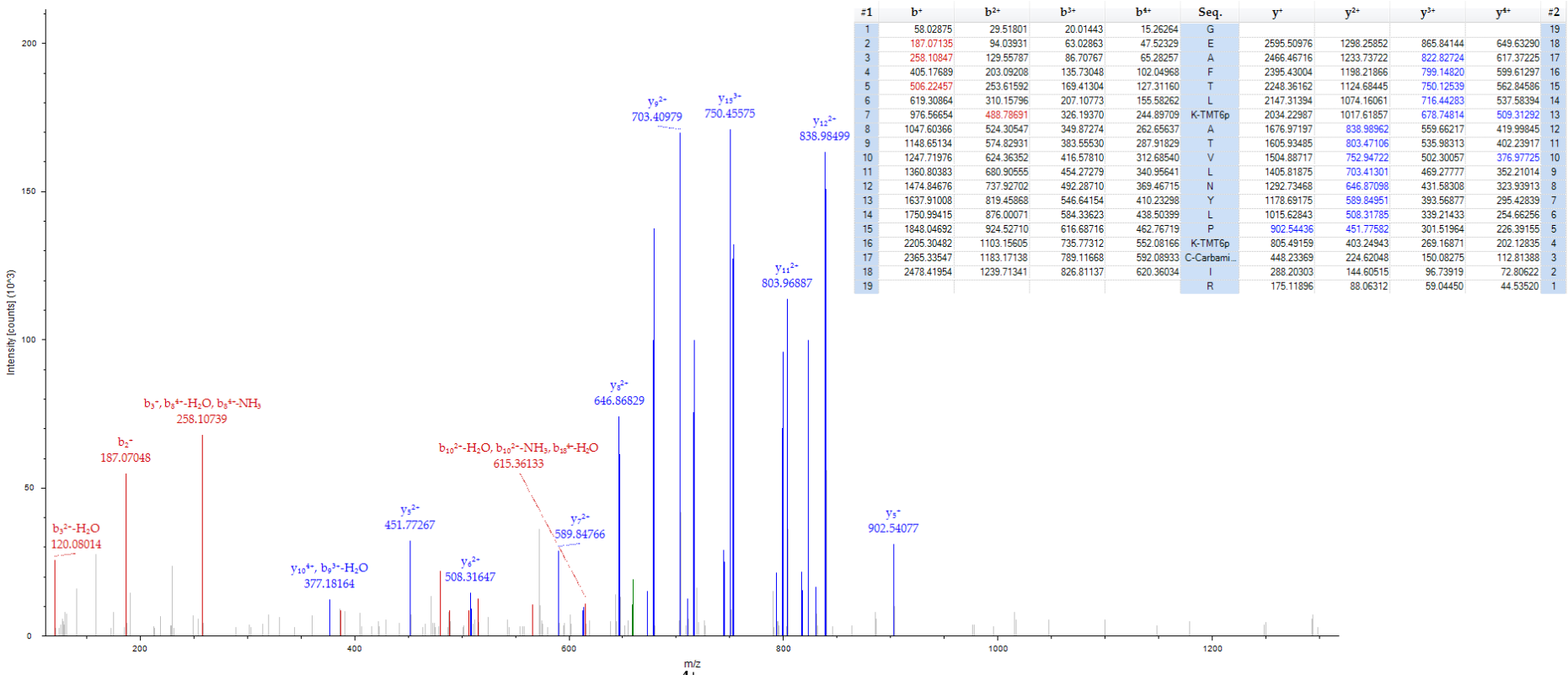

#1	b+	b2+	b3+	b4+	Seq.	y+	y2+	y3+	y4+	#2
1	58.02875	29.51801	20.01443	15.26264	G					19
2	187.07135	94.03931	63.02863	47.52329	E	2595.50976	1298.25852	865.84144	649.63290	18
3	258.10847	129.55787	86.70767	65.28257	A	2466.46716	1233.73722	822.82724	617.37225	17
4	405.17689	203.09208	135.73048	102.04968	F	2395.43004	1198.21866	799.14820	599.61297	16
5	506.22457	253.61592	169.41304	127.31160	T	2248.36162	1124.68445	750.12539	562.84586	15
6	619.30864	310.15796	207.10773	155.58262	L	2147.31394	1074.16061	716.44283	537.58394	14
7	976.56654	488.78691	326.19370	244.89709	K-TMT6p	2034.22987	1017.61857	678.74814	509.31292	13
8	1047.60366	524.30547	349.87274	262.65637	A	1676.97197	838.98962	559.66217	419.99845	12
9	1148.65134	574.82931	383.55530	287.91829	T	1605.93485	803.47106	535.98313	402.23917	11
10	1247.71976	624.36352	416.57810	312.68540	V	1504.88717	752.94722	502.30057	376.97725	10
11	1360.80383	680.90555	454.27279	340.95641	L	1405.81875	703.41301	469.27777	352.21014	9
12	1474.84676	737.92702	492.28710	369.46715	N	1292.73468	646.87098	431.58308	323.93913	8
13	1637.91008	819.45868	546.64154	410.23298	Y	1178.69175	589.84951	393.56877	295.42839	7
14	1750.99415	876.00071	584.33623	438.50399	L	1015.62843	508.31785	339.21433	254.66256	6
15	1848.04692	924.52710	616.68716	462.76719	P	902.54436	451.77582	301.51964	226.39155	5
16	2205.30482	1103.15605	735.77312	552.08166	K-TMT6p	805.49159	403.24943	269.16871	202.12835	4
17	2365.33547	1183.17138	789.11668	592.08933	C-Carbami...	448.23369	224.62048	150.08275	112.81388	3
18	2478.41954	1239.71341	826.81137	620.36034	I	288.20303	144.60515	96.73919	72.80622	2
19					R	175.11896	88.06312	59.04450	44.53520	1

Figure 3-64: MS/MS spectrum of *m/z* 663.89 the $[M+4H]^{4+}$ molecular ion for a peptide of 2652.53 Da with corresponding sequence GEAFTLKATVLNYLPKCIR unique to *α*2M identified in 1DGE fraction 1 as significant (*P* value <0.05) between PiB+ and PiB- groups.

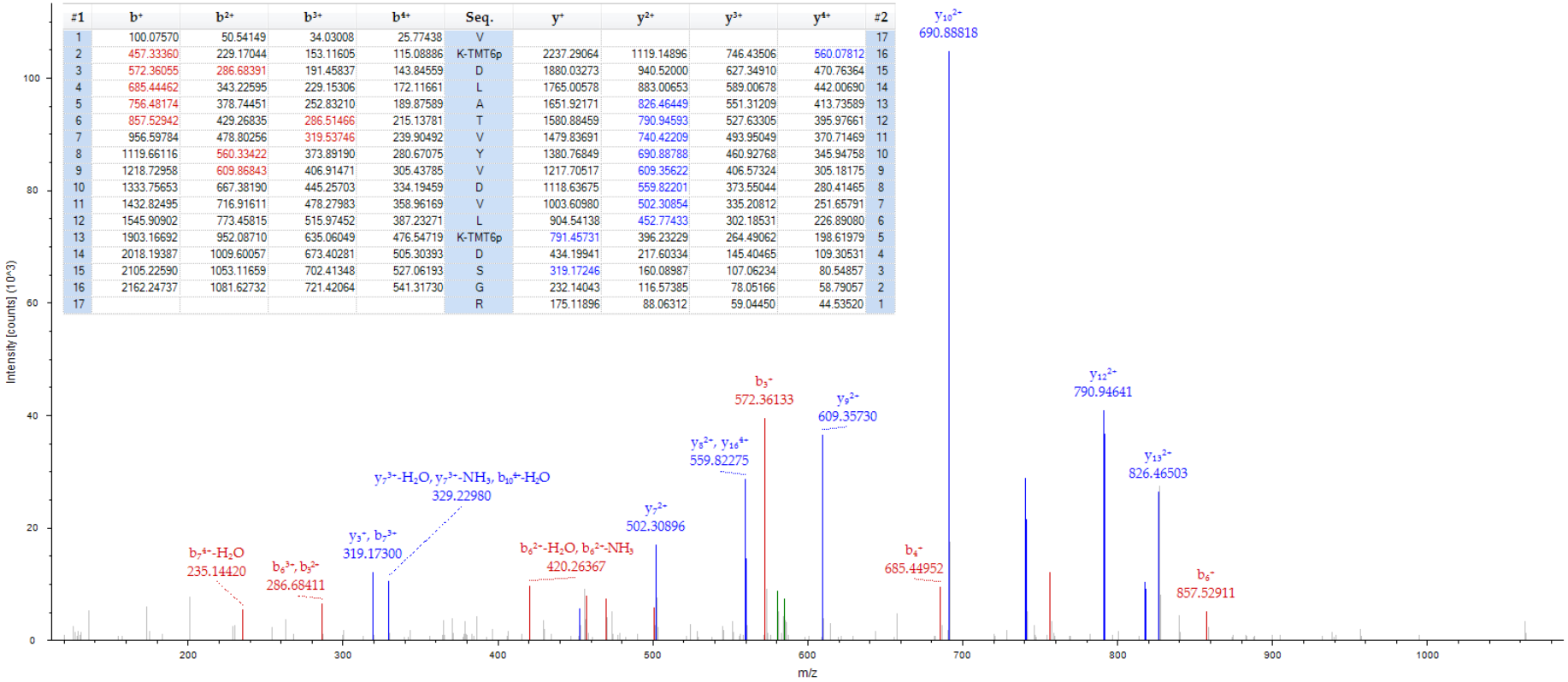

Figure 3-65: MS/MS spectrum of *m/z* 584.85 the $[M+3H]^{3+}$ molecular ion for a peptide of 2336.36 Da with corresponding sequence VKDLATVYVDVLKDSGR unique to apoA1 identified in 1DGE fraction 5 as significant (*P* value <0.05) between PiB+ and PiB- groups.

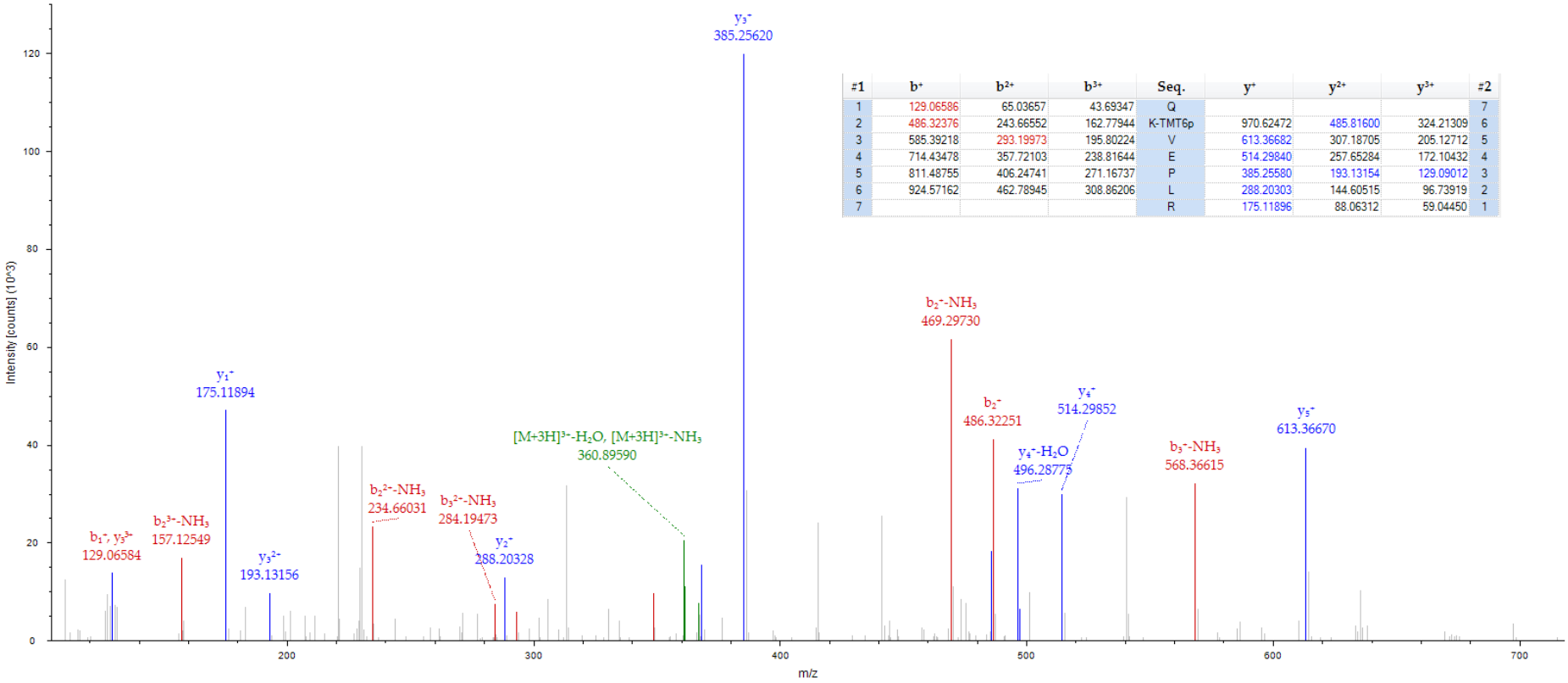

#1	b⁺	b²⁺	b³⁺	Seq.	y⁺	y²⁺	y³⁺	#2
1	129.06586	65.03657	43.69347	Q				7
2	486.32376	243.66552	162.77944	K-TMT6p	970.62472	485.81600	324.21309	6
3	585.39218	293.19973	195.80224	V	613.36682	307.18705	205.12712	5
4	714.43478	357.72103	238.81644	E	514.29840	257.65284	172.10432	4
5	811.48755	406.24741	271.16737	P	385.25580	193.13154	129.09012	3
6	924.57162	462.78945	308.86206	L	288.20303	144.60515	96.73919	2
7				R	175.11896	88.06312	59.04450	1

Figure 3-66: MS/MS spectrum of *m/z* 366.90 the $[M+3H]^{3+}$ molecular ion for a peptide of 1098.68 Da with corresponding sequence QKVEPLR unique to apoA1 identified in 1DGE fraction 5 as significant (*P* value <0.05) between PiB+ and PiB- groups.

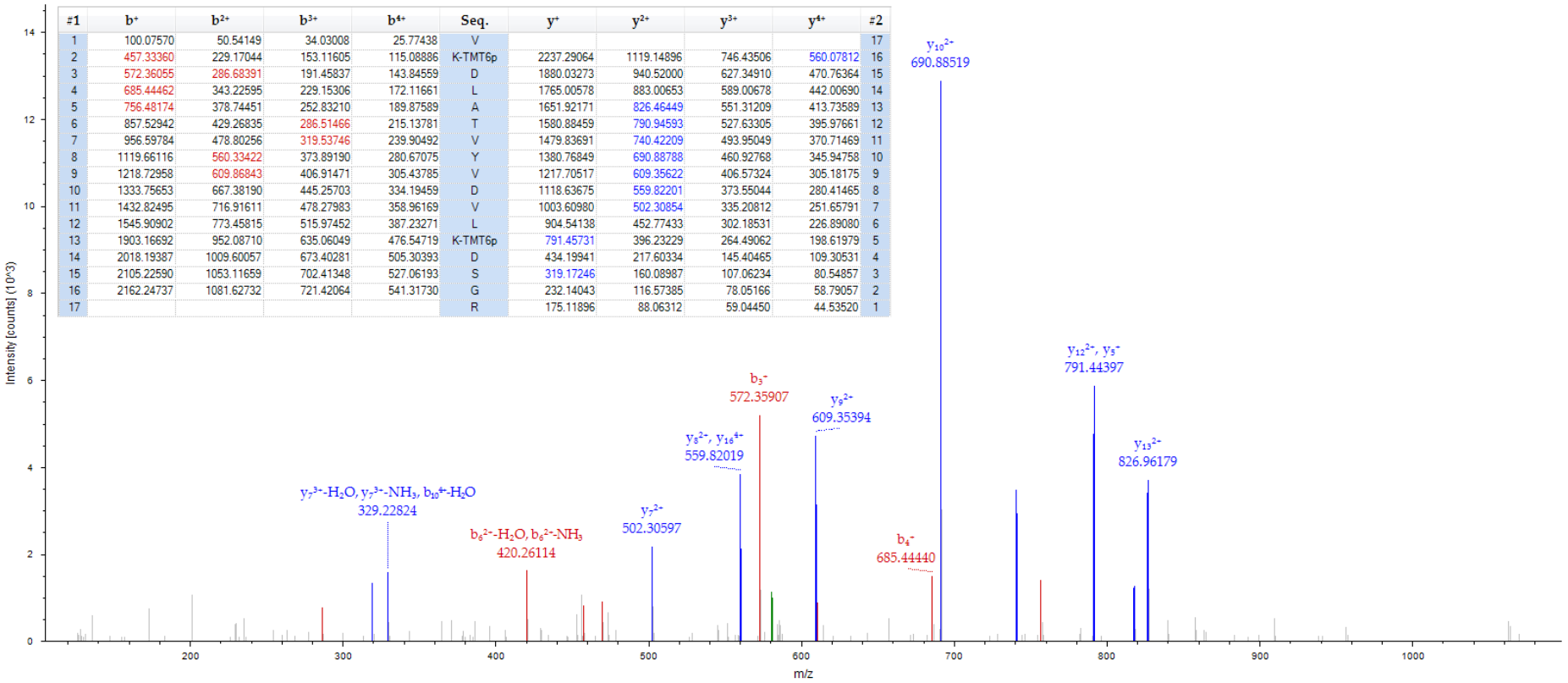

#1	b^+	b^{2+}	b^{3+}	b^{4+}	Seq.	y^+	y^{2+}	y^{3+}	y^{4+}	#2
1	100.07570	50.54149	34.03008	25.77438	V					17
2	457.33360	229.17044	153.11605	115.08886	K-TMT6p	2237.29064	1119.14896	746.43506	560.07812	16
3	572.36055	286.68391	191.45837	143.84559	D	1880.03273	940.52000	627.34910	470.76364	15
4	685.44462	343.22595	229.15306	172.11661	L	1765.00578	883.00653	589.00678	442.00690	14
5	756.48174	378.74451	252.83210	189.87589	A	1651.92171	826.46449	551.31209	413.73589	13
6	857.52942	429.26835	286.51466	215.13781	T	1580.88459	790.94593	527.63305	395.97661	12
7	956.59784	478.80256	319.53746	239.90492	V	1479.83691	740.42209	493.95049	370.71469	11
8	1119.66116	560.33422	373.89190	280.67075	Y	1380.76849	690.88788	460.92768	345.94758	10
9	1218.72958	609.86843	406.91471	305.43785	V	1217.70517	609.35622	406.57324	305.18175	9
10	1333.75653	667.38190	445.25703	334.19459	D	1118.63675	559.82201	373.55044	280.41465	8
11	1432.82495	716.91611	478.27983	358.96169	V	1003.60980	502.30854	335.20812	251.65791	7
12	1545.90902	773.45815	515.97452	387.23271	L	904.54138	452.77433	302.18531	226.89080	6
13	1903.16692	952.08710	635.06049	476.54719	K-TMT6p	791.45731	396.23229	264.49062	198.61979	5
14	2018.19387	1009.60057	673.40281	505.30393	D	434.19941	217.60334	145.40465	109.30531	4
15	2105.22590	1053.11659	702.41348	527.06193	S	319.17246	160.08987	107.06234	80.54857	3
16	2162.24737	1081.62732	721.42064	541.31730	G	232.14043	116.57385	78.05166	58.79057	2
17					R	175.11896	88.06312	59.04450	44.53520	1

Figure 3-67: MS/MS spectrum of *m/z* 584.85 the $[M+4H]^{4+}$ molecular ion for a peptide of 2336.36 Da with corresponding sequence VKDLATVYVDVLKDSGR unique to apoA1 identified in 1DGE fraction 9 as significant (*P* value <0.05) between PiB+ and PiB- groups.

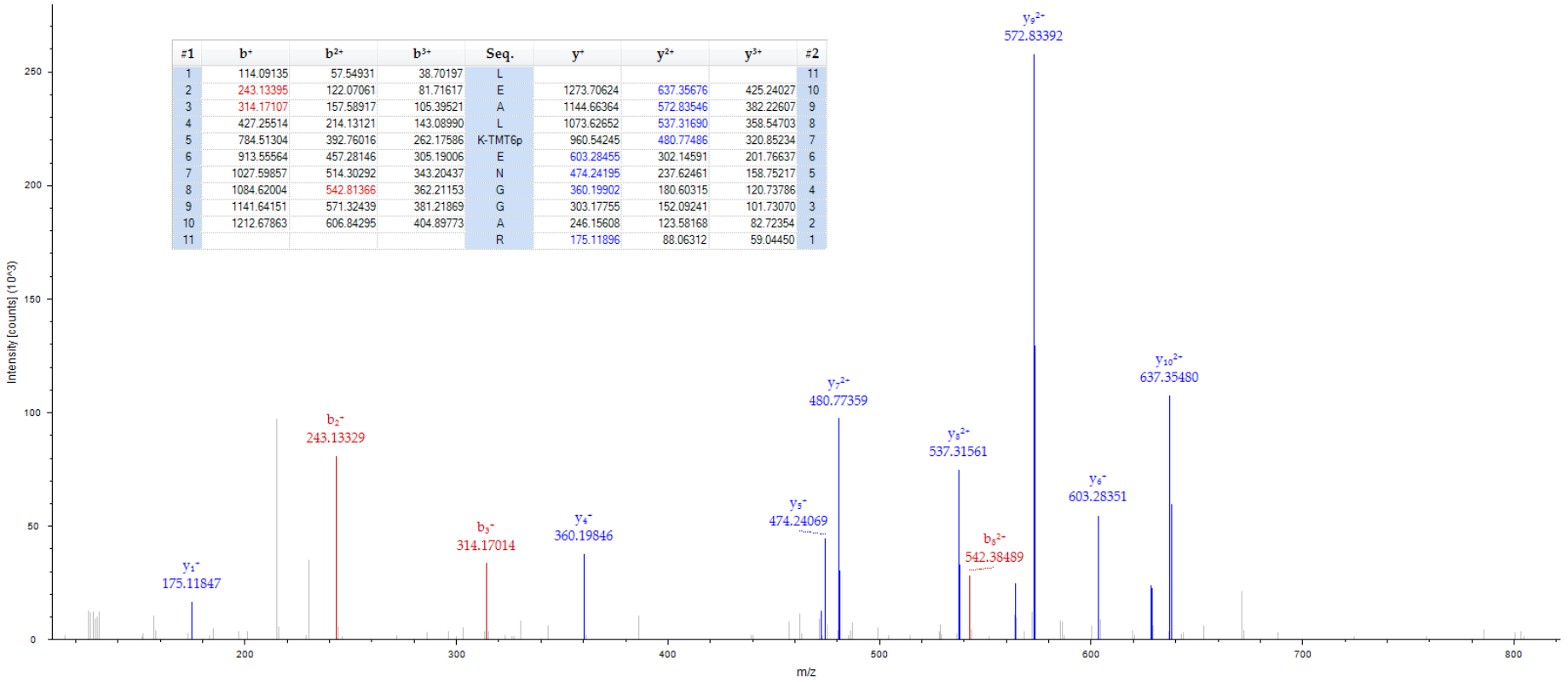

Figure 3-68: MS/MS spectrum of *m/z* 462.93 the $[M+3H]^{3+}$ molecular ion for a peptide of 1386.79 Da with corresponding sequence LEALKENGGAR unique to apoA1 identified in 1DGE fraction 9 as significant (*P* value <0.05) between PiB+ and PiB- groups.

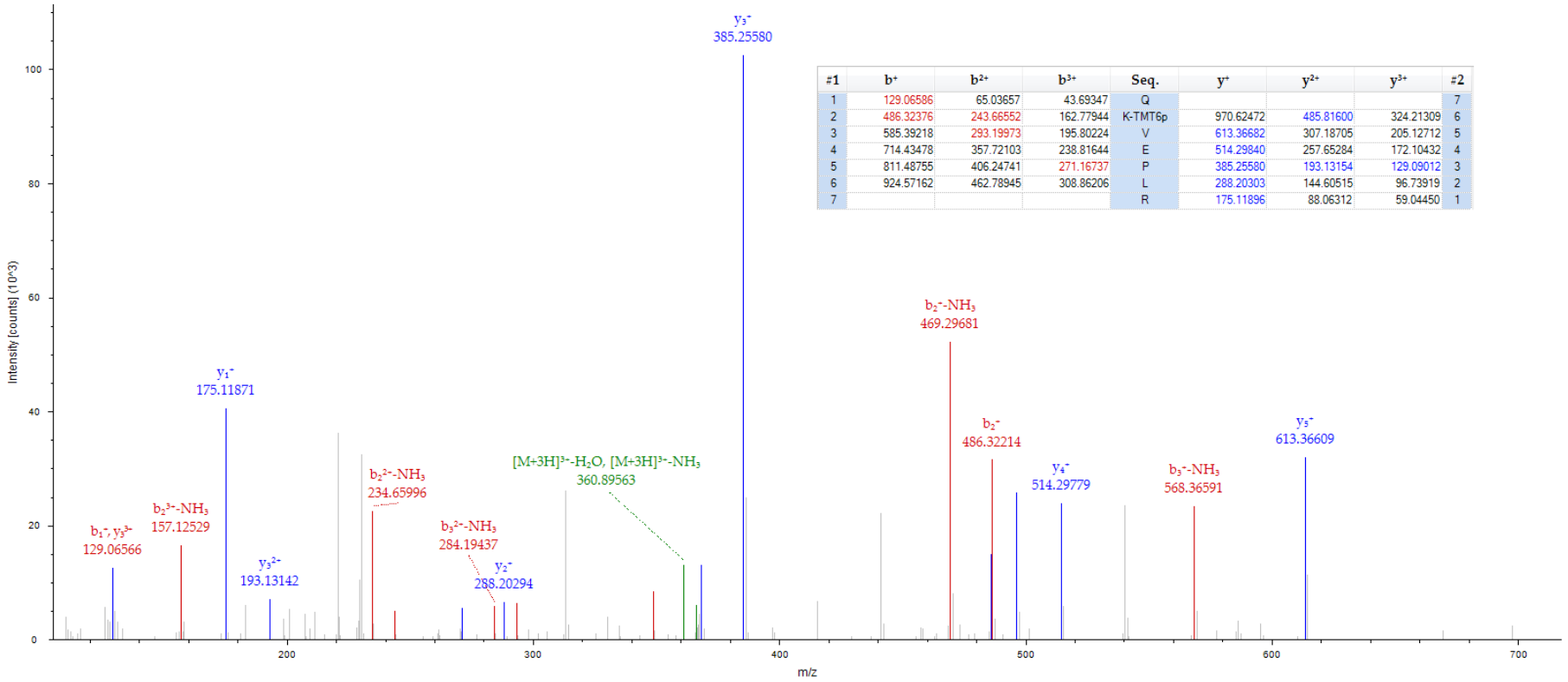

#1	b⁺	b²⁺	b³⁺	Seq.	y⁺	y²⁺	y³⁺	#2
1	129.06586	65.03657	43.69347	Q				7
2	486.32376	243.66552	162.77944	K-TMT6p	970.62472	485.81600	324.21309	6
3	585.39218	293.19973	195.80224	V	613.36682	307.18705	205.12712	5
4	714.43478	357.72103	238.81644	E	514.29840	257.65284	172.10432	4
5	811.48755	406.24741	271.16737	P	385.25580	193.13154	129.09012	3
6	924.57162	462.78945	308.86206	L	288.20303	144.60515	96.73919	2
7				R	175.11896	88.06312	59.04450	1

Figure 3-69: MS/MS spectrum of *m/z* 366.90 the $[M+3H]^{3+}$ molecular ion for a peptide of 1098.68 Da with corresponding sequence QKVEPLR unique to apoA1 identified in 1DGE fraction 9 as significant (*P* value <0.05) between PiB+ and PiB- groups.

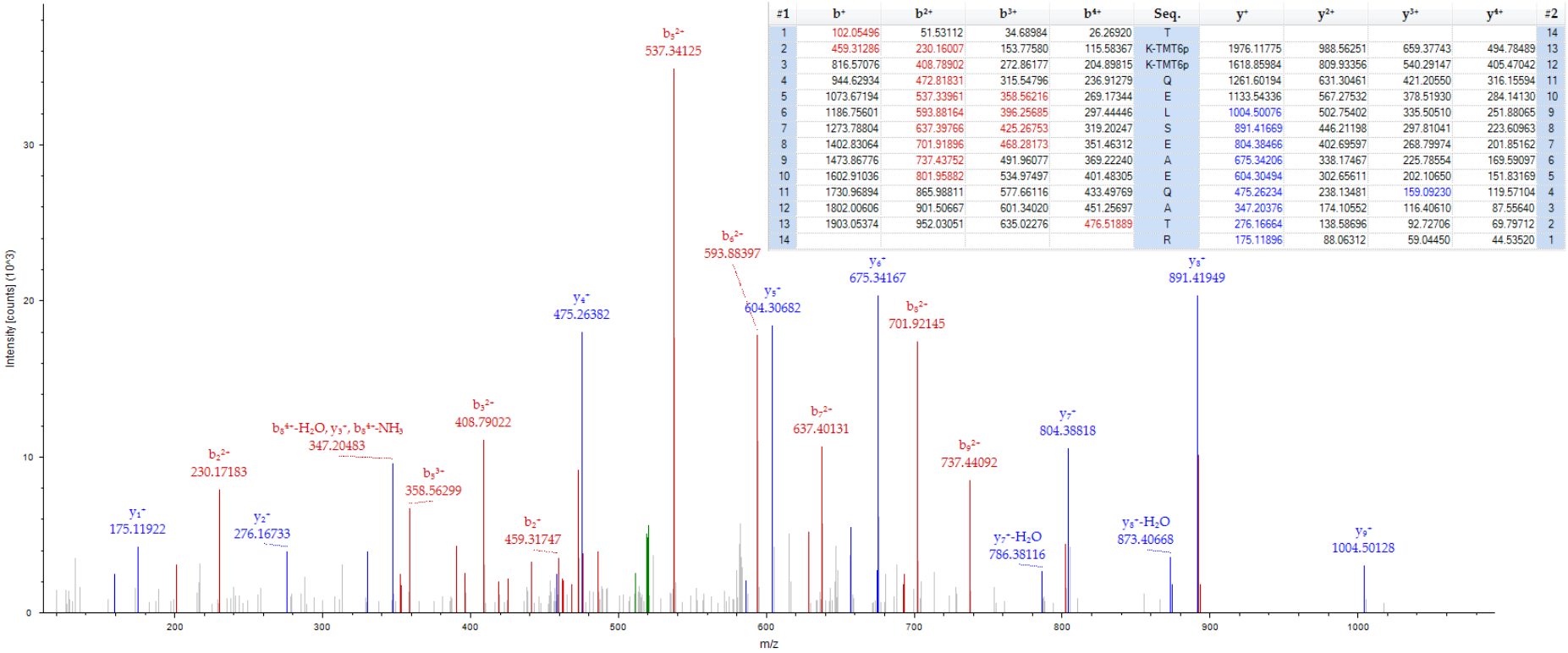

#1	b+	b2+	b3+	b4+	Seq.	y+	y2+	y3+	y4+	#2
1	102.05496	51.53112	34.68984	26.26920	T					14
2	459.31286	230.16007	153.77580	115.58367	K-TMT6p	1976.11775	988.56251	659.37743	494.78489	13
3	816.57076	408.78902	272.86177	204.89815	K-TMT6p	1618.85984	809.93356	540.29147	405.47042	12
4	944.62934	472.81831	315.54796	236.91279	Q	1261.60194	631.30461	421.20550	316.15594	11
5	1073.67194	537.33961	358.56216	269.17344	E	1133.54336	567.27532	378.51930	284.14130	10
6	1186.75601	593.88164	396.25685	297.44446	L	1004.50076	502.75402	335.50510	251.88065	9
7	1273.78804	637.39766	425.26753	319.20247	S	891.41669	446.21198	297.81041	223.60963	8
8	1402.83064	701.91896	468.28173	351.46312	E	804.38466	402.69597	268.79974	201.85162	7
9	1473.86776	737.43752	491.96077	369.22240	A	675.34206	338.17467	225.78554	169.59097	6
10	1602.91036	801.95882	534.97497	401.48305	E	604.30494	302.65611	202.10650	151.83169	5
11	1730.96894	865.98811	577.66116	433.49769	Q	475.26234	238.13481	159.09230	119.57104	4
12	1802.00606	901.50667	601.34020	451.25697	A	347.20376	174.10552	116.40610	87.55640	3
13	1903.05374	952.03051	635.02276	476.51889	T	276.16664	138.58696	92.72706	69.79712	2
14					R	175.11896	88.06312	59.04450	44.53520	1

Figure 3-70: MS/MS spectrum of *m/z* 520.06 the $[M+4H]^{4+}$ molecular ion for a peptide of 2077.17 Da with corresponding sequence TKKQELSEAEQATR unique to CC3 identified in 1DGE fraction 9 as significant (*P* value <0.05) between PiB+ and PiB- groups.

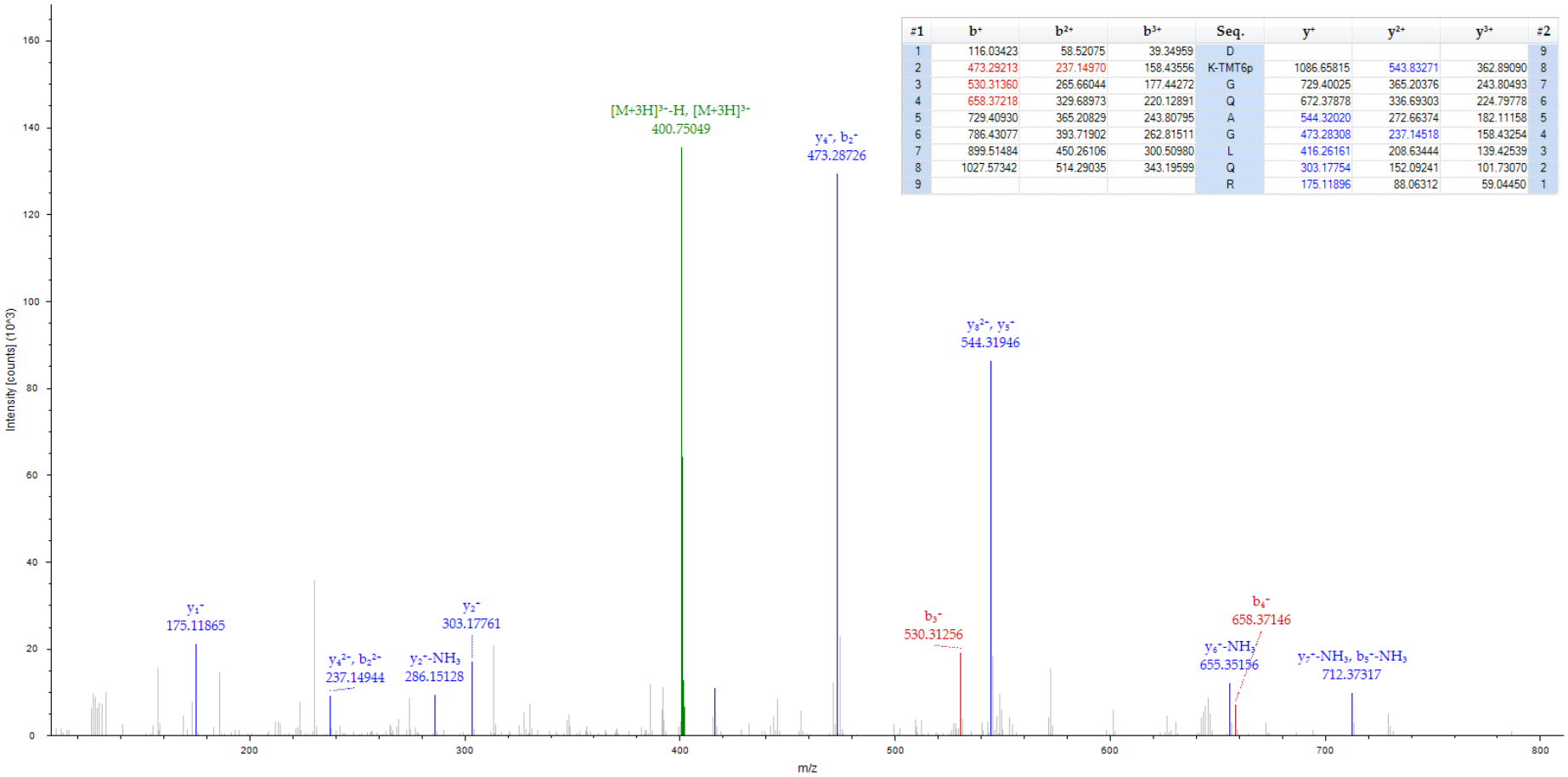

Figure 3-71: MS/MS spectrum of *m/z* 401.23 the $[M+3H]^{3+}$ molecular ion for a peptide of 1208.61 Da with corresponding sequence DKGQAGLQR unique to C4*α* identified in 1DGE fraction 1 as significant (*P* value <0.05) between PiB+ and PiB- groups.

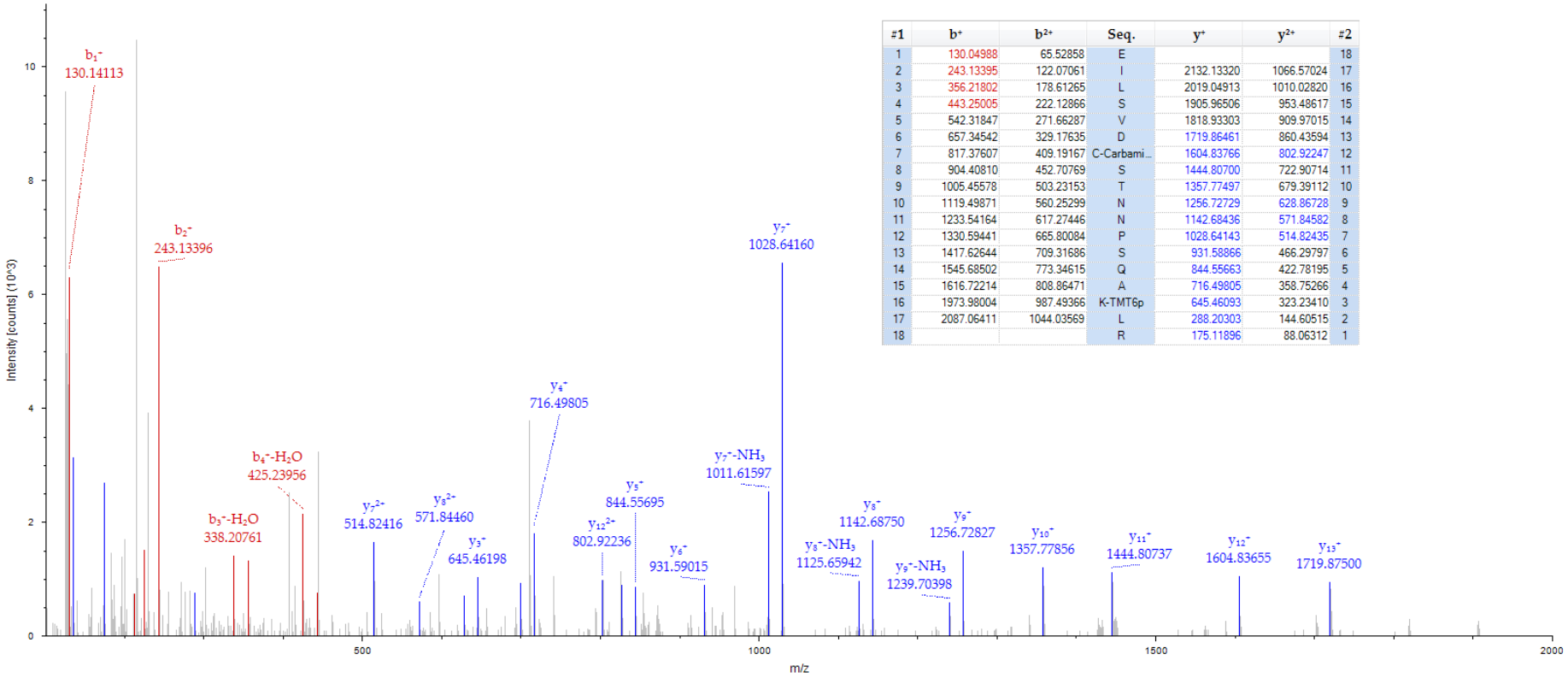

#1	b+	b2+	Seq.	y+	y2+	#2
1	130.04988	65.52858	E			18
2	243.13395	122.07061	I	2132.13320	1066.57024	17
3	356.21802	178.61265	L	2019.04913	1010.02820	16
4	443.25005	222.12866	S	1905.96506	953.48617	15
5	542.31847	271.66287	V	1818.93303	909.97015	14
6	657.34542	329.17635	D	1719.86461	860.43594	13
7	817.37607	409.19167	C-Carbami...	1604.83766	802.92247	12
8	904.40810	452.70769	S	1444.80700	722.90714	11
9	1005.45578	503.23153	T	1357.77497	679.39112	10
10	1119.49871	560.25299	N	1256.72729	628.86728	9
11	1233.54164	617.27446	N	1142.68436	571.84582	8
12	1330.59441	665.80084	P	1028.64143	514.82435	7
13	1417.62644	709.31686	S	931.58866	466.29797	6
14	1545.68502	773.34615	Q	844.55663	422.78195	5
15	1616.72214	808.86471	A	716.49805	358.75266	4
16	1973.98004	987.49366	K-TMT6p	645.46093	323.23410	3
17	2087.06411	1044.03569	L	288.20303	144.60515	2
18			R	175.11896	88.06312	1

Figure 3-72: MS/MS spectrum of *m/z* 1131.09 the $[M+2H]^{2+}$ molecular ion for a peptide of 2261.17 Da with corresponding sequence EILSVDCSTNNPSQAKLR unique to clusterin identified in 1DGE fraction 6 as significant (*P* value <0.05) between PiB+ and PiB- groups.

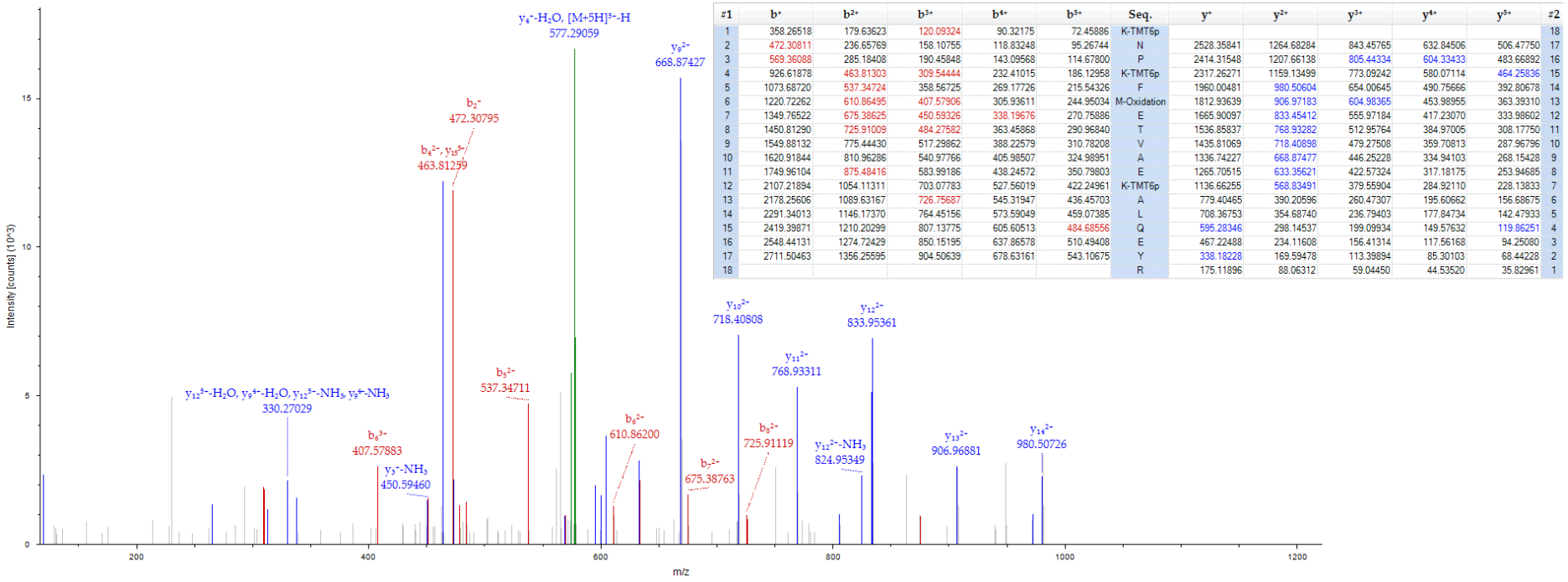

#1	b+	b2+	b3+	b4+	b5+	Seq.	y+	y2+	y3+	y4+	y5+	#2
1	358.26518	179.63623	120.09324	90.32175	72.45886	K-TMT6p						18
2	472.30811	236.65769	158.10755	118.83248	95.26744	N	2528.35841	1264.68284	843.45765	632.84506	506.47750	17
3	569.36088	285.18408	190.45848	143.09568	114.67800	P	2414.31548	1207.66138	805.44334	604.33433	483.66892	16
4	926.61878	463.81303	309.54444	232.41015	186.12958	K-TMT6p	2317.26271	1159.13499	773.09242	580.07114	464.25836	15
5	1073.68720	537.34724	358.56725	269.17726	215.54326	F	1960.00481	980.50604	654.00645	490.75666	392.80678	14
6	1220.72262	610.86495	407.57906	305.93611	244.95034	M-Oxidation	1812.93639	906.97183	604.98365	453.98955	363.39310	13
7	1349.76522	675.38625	450.59326	338.19676	270.75886	E	1665.90097	833.45412	555.97184	417.23070	333.98602	12
8	1450.81290	725.91009	484.27582	363.45868	290.96840	T	1536.85837	768.93282	512.95764	384.97005	308.17750	11
9	1549.88132	775.44430	517.29862	388.22579	310.78208	V	1435.81069	718.40898	479.27508	359.70813	287.96796	10
10	1620.91844	810.96286	540.97766	405.98507	324.98951	A	1336.74227	668.87477	446.25228	334.94103	268.15428	9
11	1749.96104	875.48416	583.99186	438.24572	350.79803	E	1265.70515	633.35621	422.57324	317.18175	253.94685	8
12	2107.21894	1054.11311	703.07783	527.56019	422.24961	K-TMT6p	1136.66255	568.83491	379.55904	284.92110	228.13833	7
13	2178.25606	1089.63167	726.75687	545.31947	436.45703	A	779.40465	390.20596	260.47307	195.60662	156.68675	6
14	2291.34013	1146.17370	764.45156	573.59049	459.07385	L	708.36753	354.68740	236.79403	177.84734	142.47933	5
15	2419.39871	1210.20299	807.13775	605.60513	484.68556	Q	595.28346	298.14537	199.09934	149.57632	119.86251	4
16	2548.44131	1274.72429	850.15195	637.86578	510.49408	E	467.22488	234.11608	156.41314	117.56168	94.25080	3
17	2711.50463	1356.25595	904.50639	678.63161	543.10675	Y	338.18228	169.59478	113.39894	85.30103	68.44228	2
18						R	175.11896	88.06312	59.04450	44.53520	35.82961	1

Figure 3-73: MS/MS spectrum of *m/z* 577.93 the $[M+4H]^{4+}$ molecular ion for a peptide of 2885.62 Da with corresponding sequence KNPKFMETVAEKALQEYR unique to clusterin identified in 1DGE fraction 6 as significant (*P* value <0.05) between PiB+ and PiB- groups.

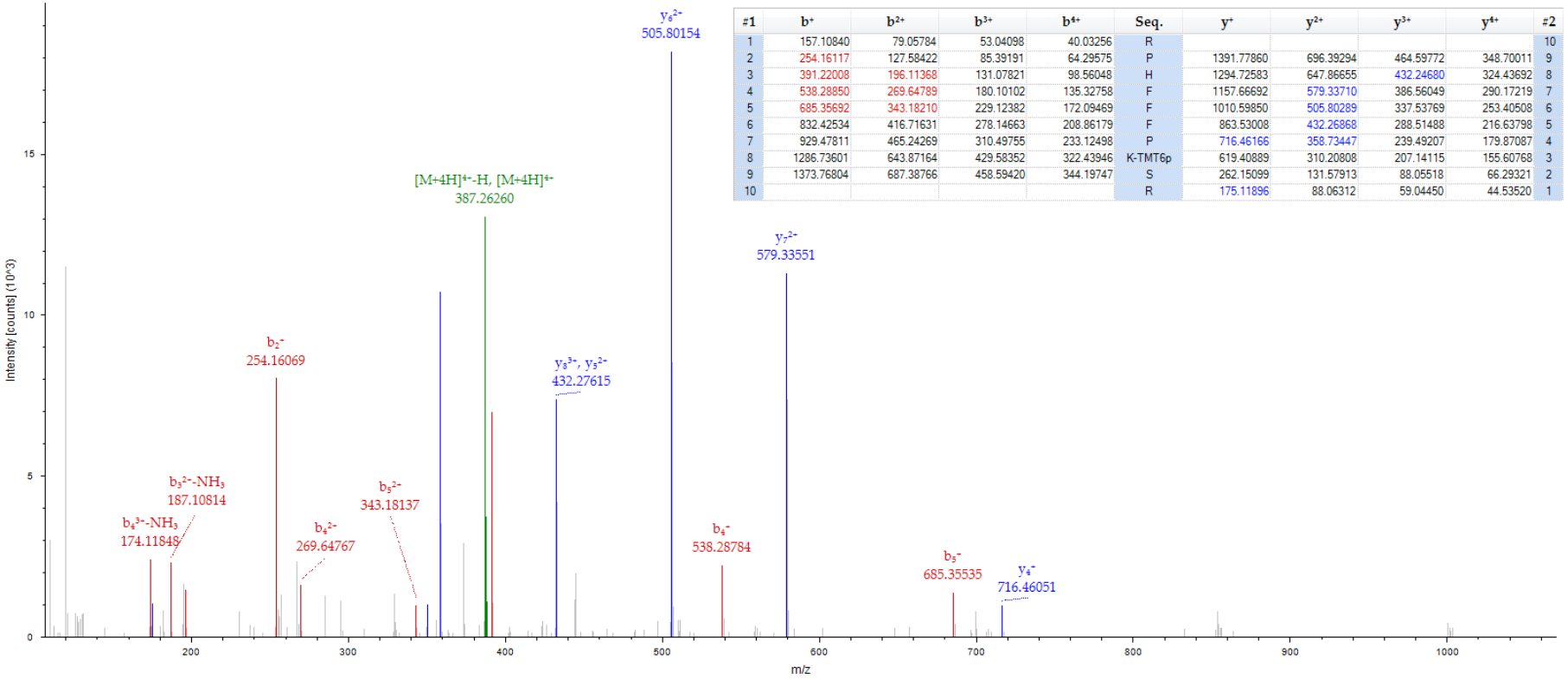

#1	b+	b2+	b3+	b4+	Seq.	y+	y2+	y3+	y4+	#2
1	157.10840	79.05784	53.04098	40.03256	R					10
2	254.16117	127.58422	85.39191	64.29575	P	1391.77860	696.39294	464.59772	348.70011	9
3	391.22008	196.11368	131.07821	98.56048	H	1294.72583	647.86655	432.24680	324.43692	8
4	538.28850	269.64789	180.10102	135.32758	F	1157.66692	579.33710	386.56049	290.17219	7
5	685.35692	343.18210	229.12382	172.09469	F	1010.59850	505.80289	337.53769	253.40508	6
6	832.42534	416.71631	278.14663	208.86179	F	863.53008	432.26868	288.51488	216.63798	5
7	929.47811	465.24269	310.49755	233.12498	P	716.46166	358.73447	239.49207	179.87087	4
8	1286.73601	643.87164	429.58352	322.43946	K-TMT6p	619.40889	310.20808	207.14115	155.60768	3
9	1373.76804	687.38766	458.59420	344.19747	S	262.15099	131.57913	88.05518	66.29321	2
10					R	175.11896	88.06312	59.04450	44.53520	1

Figure 3-74: MS/MS spectrum of *m/z* 387.72552 the $[M+4H]^{4+}$ molecular ion for a peptide of 1547.882 Da with corresponding sequence RPHFFFPKSR unique to clusterin identified in 1DGE fraction 6 as significant (*P* value <0.05) between PiB+ and PiB- groups.

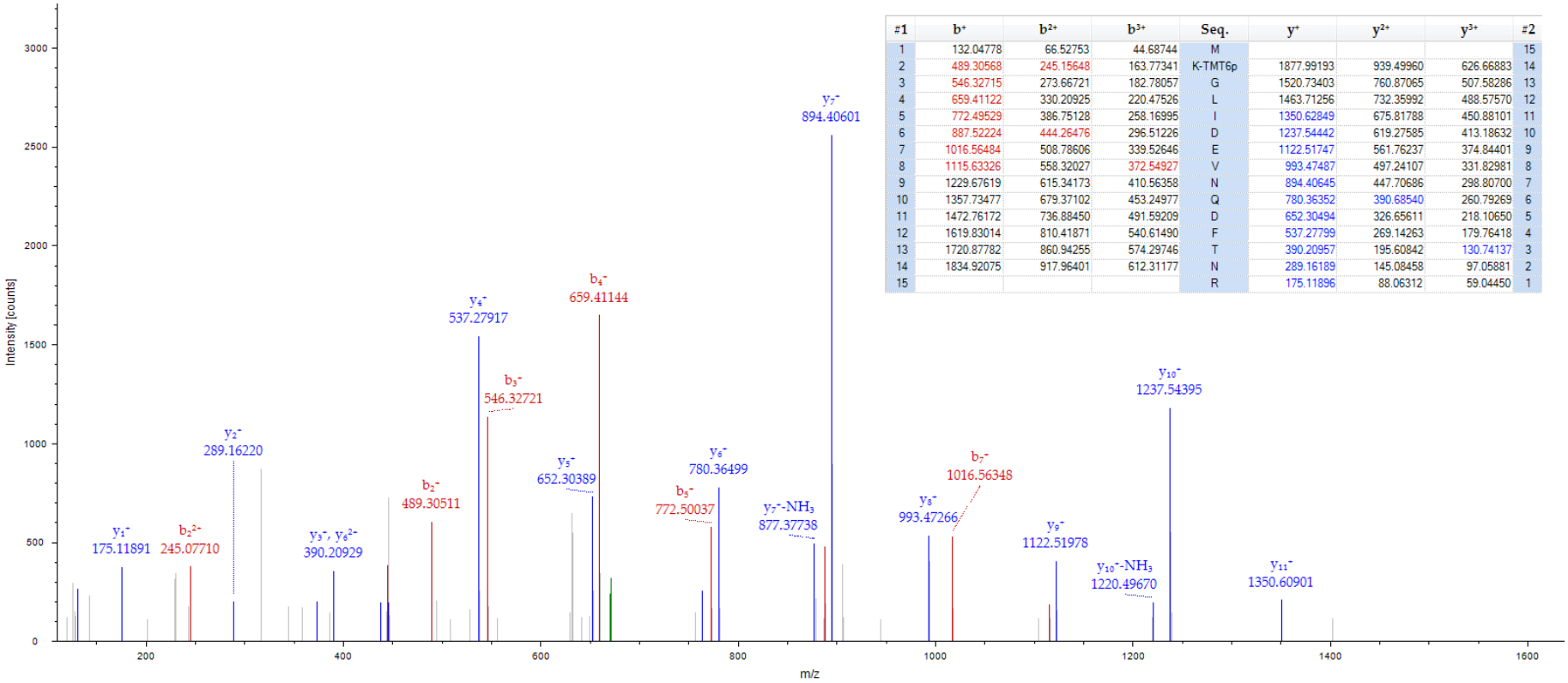

#1	b+	b2+	b3+	Seq.	y+	y2+	y3+	#2
1	132.04778	66.52753	44.68744	M				15
2	489.30568	245.15648	163.77341	K-TMT6p	1877.99193	939.49960	626.66883	14
3	546.32715	273.66721	182.78057	G	1520.73403	760.87065	507.58286	13
4	659.41122	330.20925	220.47526	L	1463.71256	732.35992	488.57570	12
5	772.49529	386.75128	258.16995	I	1350.62849	675.81788	450.88101	11
6	887.52224	444.26476	296.51226	D	1237.54442	619.27585	413.18632	10
7	1016.56484	508.78606	339.52646	E	1122.51747	561.76237	374.84401	9
8	1115.63326	558.32027	372.54927	V	993.47487	497.24107	331.82981	8
9	1229.67619	615.34173	410.56358	N	894.40645	447.70686	298.80700	7
10	1357.73477	679.37102	453.24977	Q	780.36352	390.68540	260.79269	6
11	1472.76172	736.88450	491.59209	D	652.30494	326.65611	218.10650	5
12	1619.83014	810.41871	540.61490	F	537.27799	269.14263	179.76418	4
13	1720.87782	860.94255	574.29746	T	390.20957	195.60842	130.74137	3
14	1834.92075	917.96401	612.31177	N	289.16189	145.08458	97.05881	2
15				R	175.11896	88.06312	59.04450	1

Figure 3-75: MS/MS spectrum of *m/z* 670.40 the $[M+3H]^{3+}$ molecular ion for a peptide of 2009.03 Da with corresponding sequence MKGLIDEVNQDFTNR unique to FG*α* identified in 1DGE fraction 4 as significant (*P* value <0.05) between PiB+ and PiB- groups.

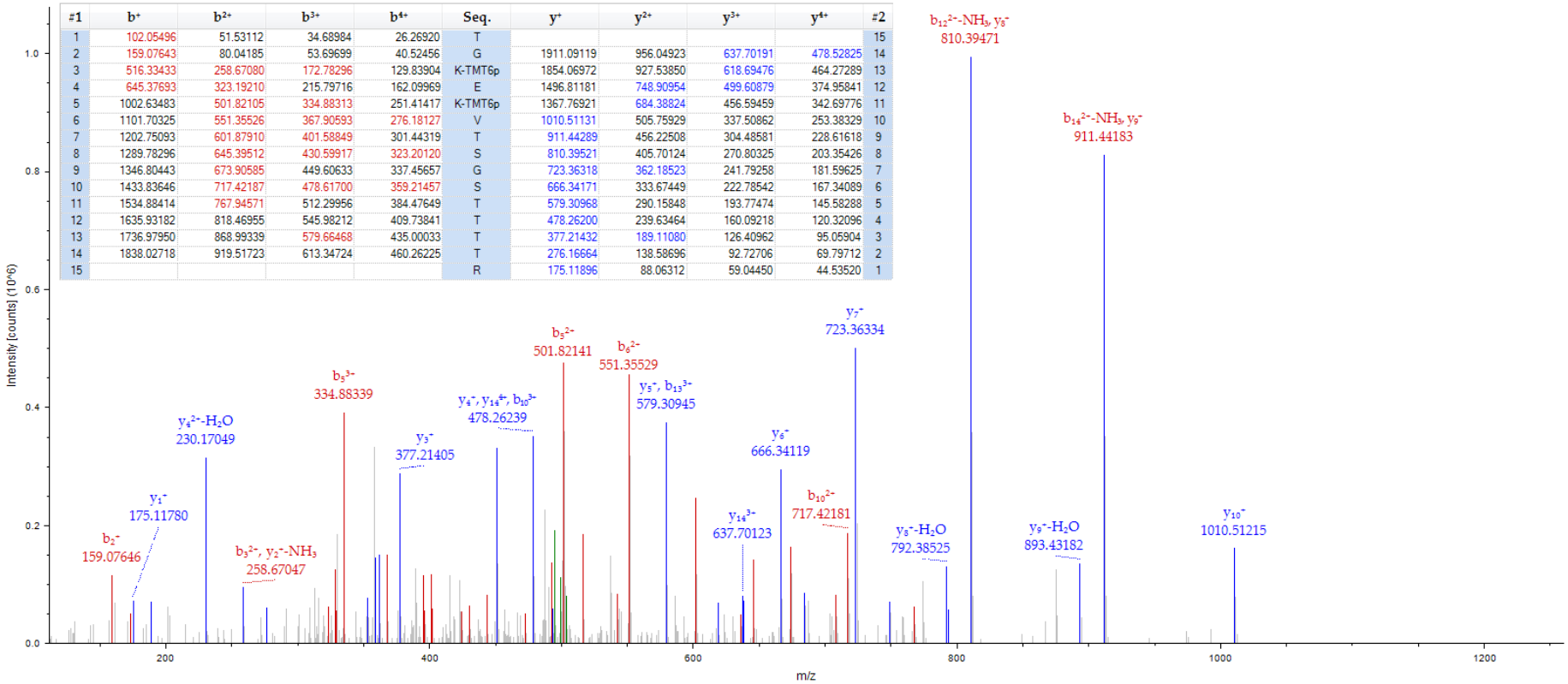

Figure 3-76: MS/MS spectrum of *m/z* 503.79 the $[M+4H]^{4+}$ molecular ion for a peptide of 2012.14 Da with corresponding sequence TGKEKVTSGSTTTTR unique to FGα identified in 1DGE fraction 4 as significant (*P* value <0.05) between PiB+ and PiB- groups.

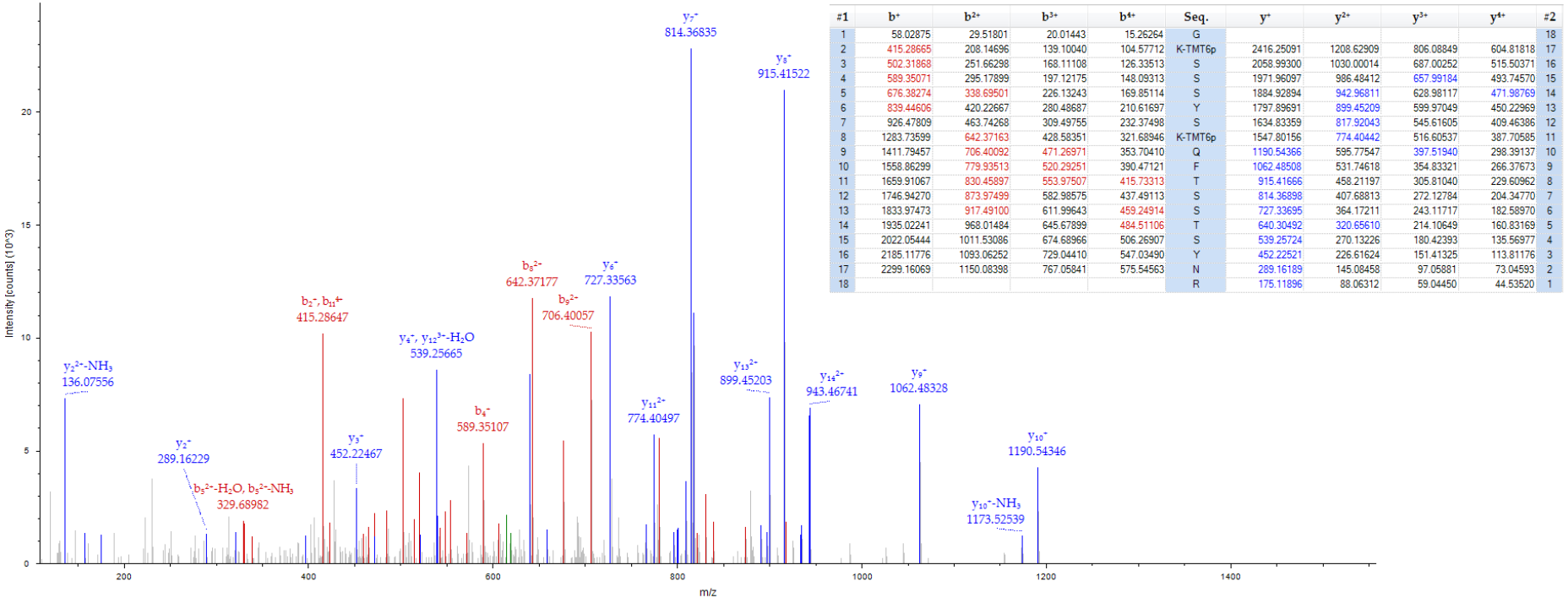

#1	b+	b2+	b3+	b4+	Seq.	y+	y2+	y3+	y4+	#2
1	58.02875	29.51801	20.01443	15.26264	G					18
2	415.28665	208.14696	139.10040	104.57712	K-TMT6p	2416.25091	1208.62909	806.08849	604.81818	17
3	502.31868	251.66298	168.11108	126.33513	S	2058.99300	1030.00014	687.00252	515.50371	16
4	589.35071	295.17899	197.12175	148.09313	S	1971.96097	986.48412	657.99184	493.74570	15
5	676.38274	338.69501	226.13243	169.85114	S	1884.92894	942.96811	628.98117	471.98769	14
6	839.44606	420.22667	280.48687	210.61697	Y	1797.89691	899.45209	599.97049	450.22969	13
7	926.47809	463.74268	309.49755	232.37498	S	1634.83359	817.92043	545.61605	409.46386	12
8	1283.73599	642.37163	428.58351	321.68946	K-TMT6p	1547.80156	774.40442	516.60537	387.70585	11
9	1411.79457	706.40092	471.26971	353.70410	Q	1190.54366	595.77547	397.51940	298.39137	10
10	1558.86299	779.93513	520.29251	390.47121	F	1062.48508	531.74618	354.83321	266.37673	9
11	1659.91067	830.45897	553.97507	415.73313	T	915.41666	458.21197	305.81040	229.60962	8
12	1746.94270	873.97499	582.98575	437.49113	S	814.36898	407.68813	272.12784	204.34770	7
13	1833.97473	917.49100	611.99643	459.24914	S	727.33695	364.17211	243.11717	182.58970	6
14	1935.02241	968.01484	645.67899	484.51106	T	640.30492	320.65610	214.10649	160.83169	5
15	2022.05444	1011.53086	674.68966	506.26907	S	539.25724	270.13226	180.42393	135.56977	4
16	2185.11776	1093.06252	729.04410	547.03490	Y	452.22521	226.61624	151.41325	113.81176	3
17	2299.16069	1150.08398	767.05841	575.54563	N	289.16189	145.08458	97.05881	73.04593	2
18					R	175.11896	88.06312	59.04450	44.53520	1

Figure 3-77: MS/MS spectrum of *m/z* 619.07 the $[M+4H]^{4+}$ molecular ion for a peptide of 2473.27 Da with corresponding sequence GKSSSYSKQFTSSTSYNR unique to FGα identified in 1DGE fraction 4 as significant (*P* value <0.05) between PiB+ and PiB- groups.

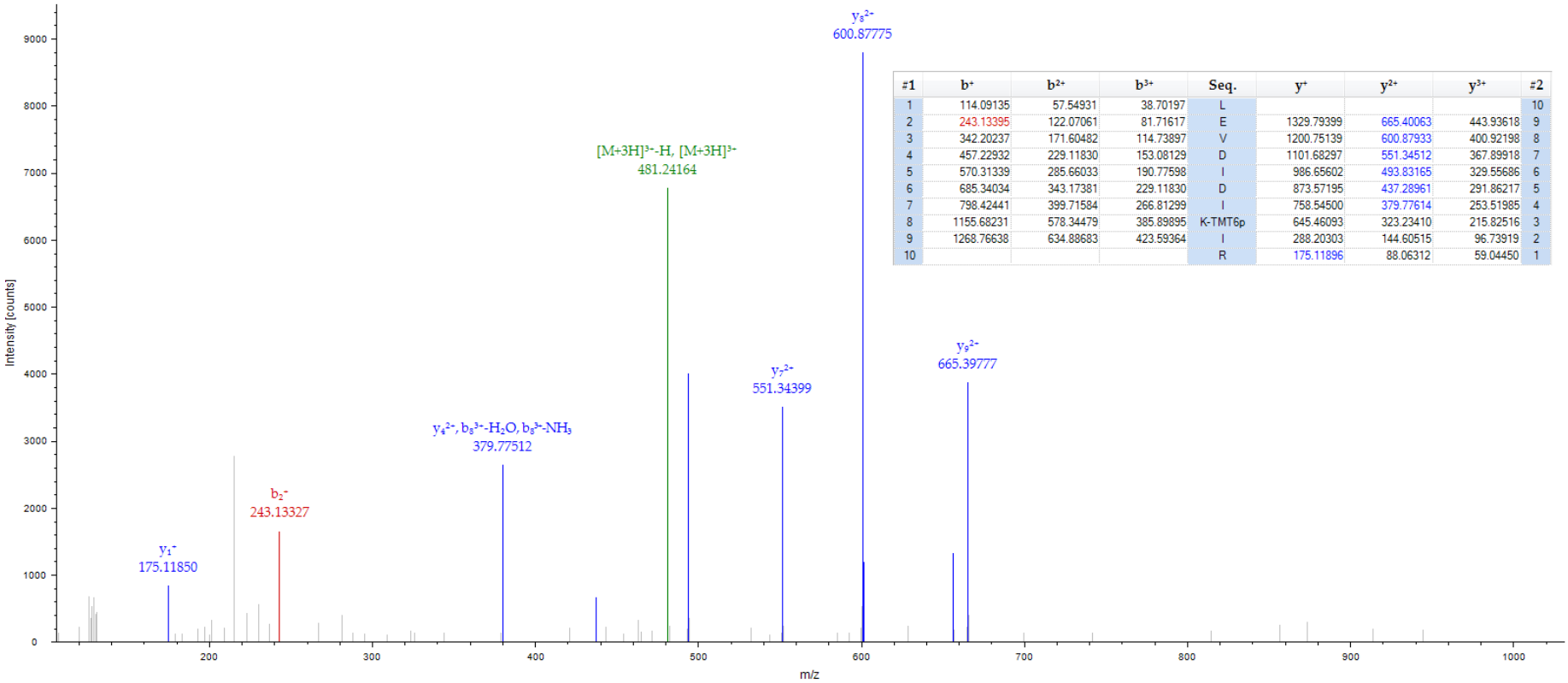

#1	b$^+$	b^{2+}	b^{3+}	Seq.	y$^+$	y^{2+}	y^{3+}	#2
1	114.09135	57.54931	38.70197	L				10
2	243.13395	122.07061	81.71617	E	1329.79399	665.40063	443.93618	9
3	342.20237	171.60482	114.73897	V	1200.75139	600.87933	400.92198	8
4	457.22932	229.11830	153.08129	D	1101.68297	551.34512	367.89918	7
5	570.31339	285.66033	190.77598	I	986.65602	493.83165	329.55686	6
6	685.34034	343.17381	229.11830	D	873.57195	437.28961	291.86217	5
7	798.42441	399.71584	266.81299	I	758.54500	379.77614	253.51985	4
8	1155.68231	578.34479	385.89895	K-TMT6p	645.46093	323.23410	215.82516	3
9	1268.76638	634.88683	423.59364	I	288.20303	144.60515	96.73919	2
10				R	175.11896	88.06312	59.04450	1

Figure 3-78: MS/MS spectrum of *m/z* 481.63 the [M+3H]$^{3+}$ molecular ion for a peptide of 1442.88 Da with corresponding sequence LEVDIDIKIR unique to FGα identified in 1DGE fraction 4 as significant (*P* value <0.05) between PiB+ and PiB- groups.

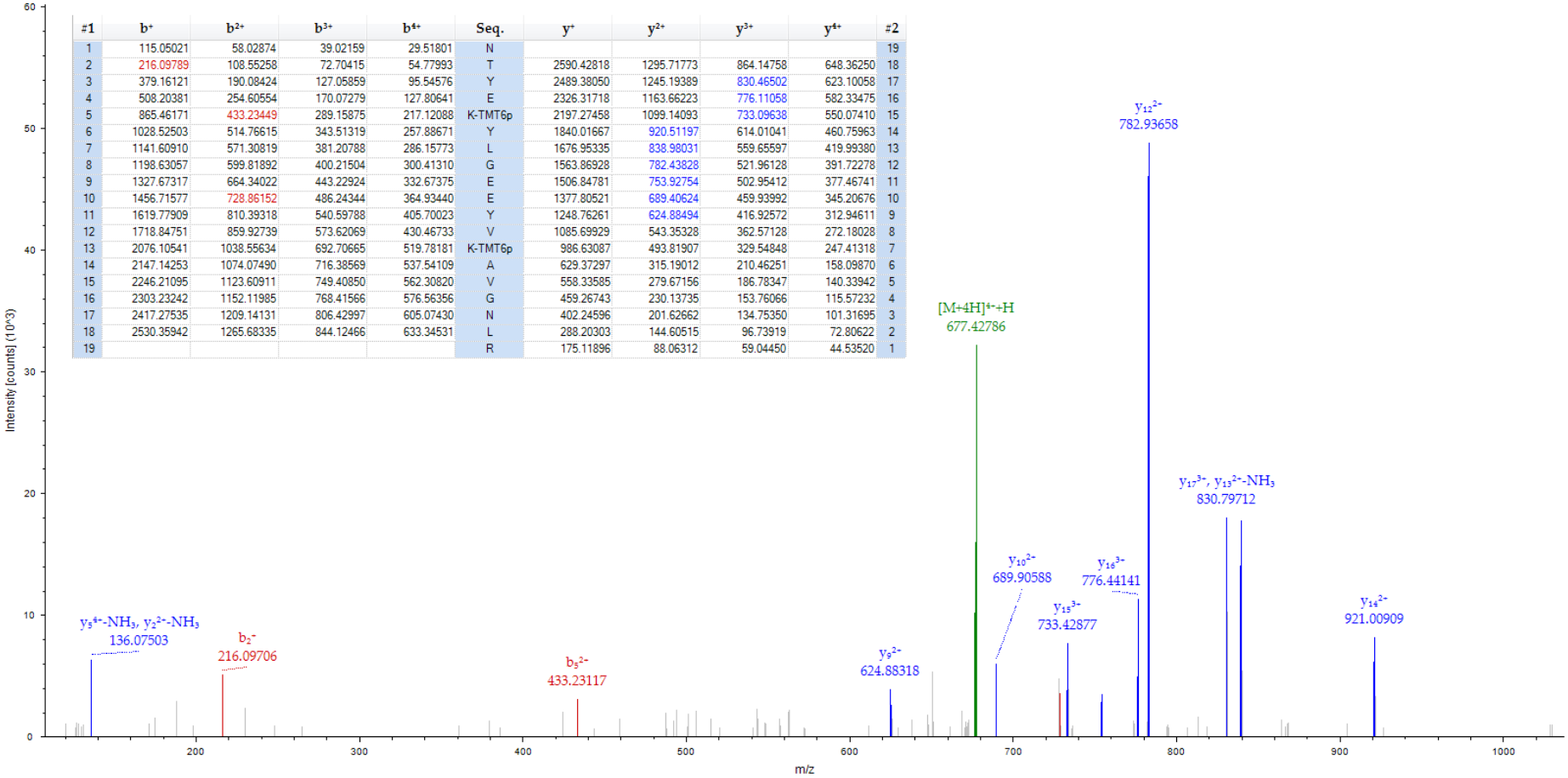

Figure 3-79: MS/MS spectrum of *m/z* 676.87 the $[M+4H]^{4+}$ molecular ion for a peptide of 2704.46 Da with corresponding sequence NTYEKYLGEEYVKAVGNLR unique to TF identified in 1DGE fraction 1 as significant (*P* value <0.05) between PiB+ and PiB- groups.

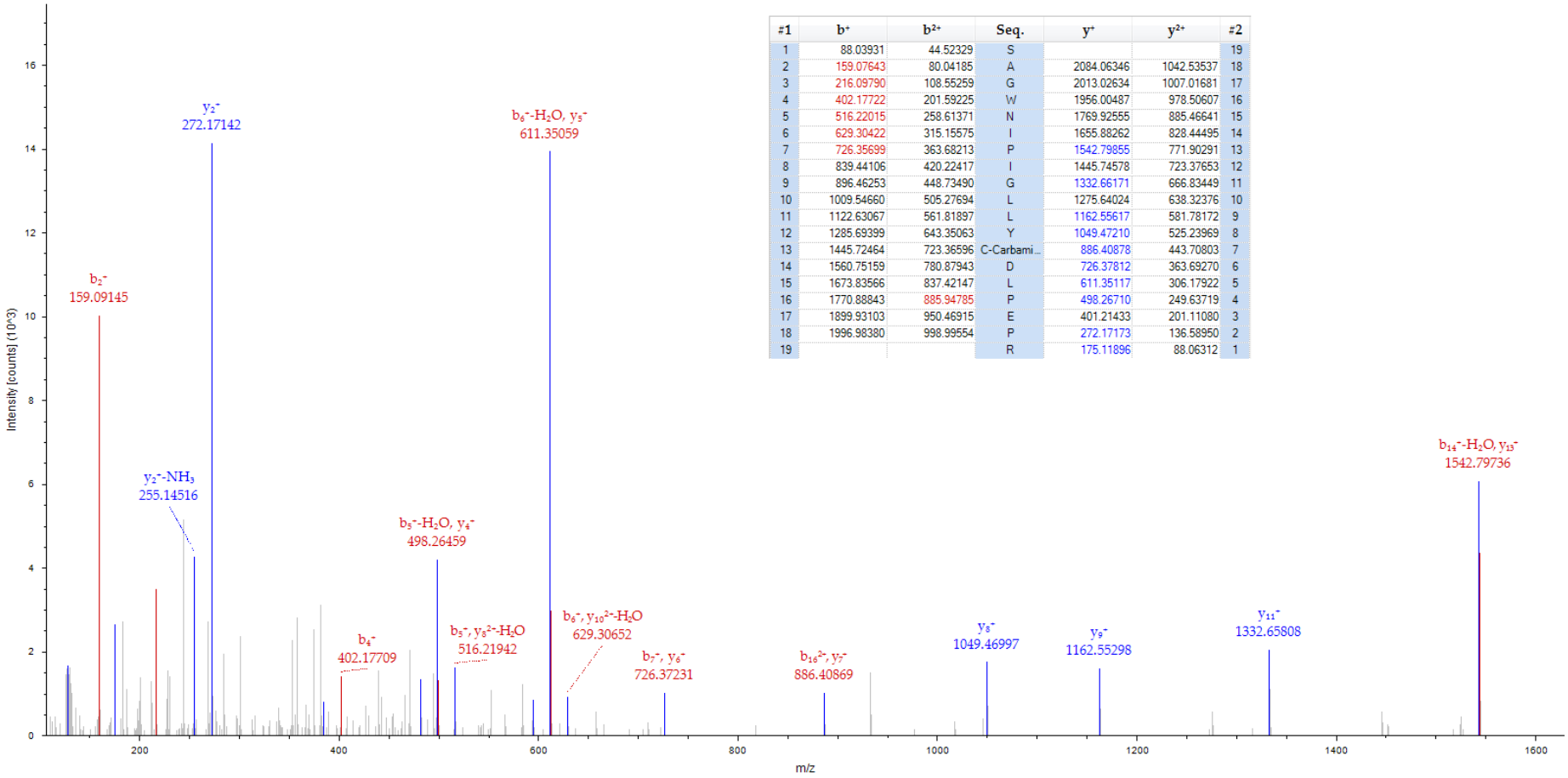

#1	b+	b2+	Seq.	y+	y2+	#2
1	88.03931	44.52329	S			19
2	159.07643	80.04185	A	2084.06346	1042.53537	18
3	216.09790	108.55259	G	2013.02634	1007.01681	17
4	402.17722	201.59225	W	1956.00487	978.50607	16
5	516.22015	258.61371	N	1769.92555	885.46641	15
6	629.30422	315.15575	I	1655.88262	828.44495	14
7	726.35699	363.68213	P	1542.79855	771.90291	13
8	839.44106	420.22417	I	1445.74578	723.37653	12
9	896.46253	448.73490	G	1332.66171	666.83449	11
10	1009.54660	505.27694	L	1275.64024	638.32376	10
11	1122.63067	561.81897	L	1162.55617	581.78172	9
12	1285.69399	643.35063	Y	1049.47210	525.23969	8
13	1445.72464	723.36596	C-Carbami...	886.40878	443.70803	7
14	1560.75159	780.87943	D	726.37812	363.69270	6
15	1673.83566	837.42147	L	611.35117	306.17922	5
16	1770.88843	885.94785	P	498.26710	249.63719	4
17	1899.93103	950.46915	E	401.21433	201.11080	3
18	1996.98380	998.99554	P	272.17173	136.58950	2
19			R	175.11896	88.06312	1

Figure 3-80: MS/MS spectrum of *m/z* 1086.05 the $[M+2H]^{2+}$ molecular ion for a peptide of 2171.10 Da with corresponding sequence SAGWNIPIGILLYCDLPEPR unique to TF identified in 1DGE fraction 1 as significant (*P* value <0.05) between PiB+ and PiB- groups.

3.4.6 Technical replication of LC-MS/MS candidates by immunoassay

The 17 candidate proteins from the LC-MS/MS discovery were measured in plasma samples from the same 78 AIBL-1 discovery cohort subjects using commercially available ELISA kits (Table 2-1). Using Logistic and Linear Regression models (including age, gender, *APOE* status, ELISA assay plate as covariates) we found that two proteins – α2m (Figure 3-81) and FGγ (Figure 3-83), replicated our findings from the LC-MS/MS discovery study (Table 3-13).

Table 3-13: Technical replication of plasma protein candidates discovered by LC-MS/MS in AIBL-1. For regressions age, gender, presence of *APOE* ε4 and ELISA plate were used as covariates.

		Logistic regression with SUVR >1.5			Linear regression with SUVR		
UniProt ID	**Protein Name**	**Beta**	***P* value**	***Q* value**	**Beta**	***P* value**	***Q* value**
P01023	α2m	1.000	0.009	0.076	0.200	0.008	0.068
Q03591	FHR-1	-1.000	0.005	0.076	-0.220	0.006	0.068
P02679	FGγ	-0.700	0.041	0.230	-0.200	0.014	0.081
P08519	apo(a)	0.480	0.130	0.340	0.180	0.051	0.180
P06396	gelsolin	-0.480	0.110	0.340	-0.140	0.068	0.190
P00738	haptoglobin	-0.380	0.180	0.390	-0.130	0.089	0.190
P04196	HRG	0.480	0.140	0.340	0.140	0.081	0.190
P06727	apoA4	-0.630	0.083	0.340	-0.170	0.067	0.190
P01024	CC3	-0.610	0.250	0.470	-0.210	0.130	0.250
P0C0L4	C4α	-0.550	0.510	0.660	-0.270	0.220	0.380
P10909	clusterin	-0.270	0.360	0.510	-0.091	0.270	0.410
P02647	apoA1	0.340	0.290	0.470	0.088	0.320	0.460
P02671	FGα	-0.280	0.300	0.470	-0.064	0.390	0.520
P02787	TF	-0.013	0.960	0.960	-0.041	0.600	0.730
O14791	apoL1	-0.090	0.740	0.890	-0.026	0.730	0.770
P08603	CFH	0.066	0.800	0.890	0.027	0.700	0.770
P00751	CFB	0.053	0.840	0.890	0.018	0.810	0.810

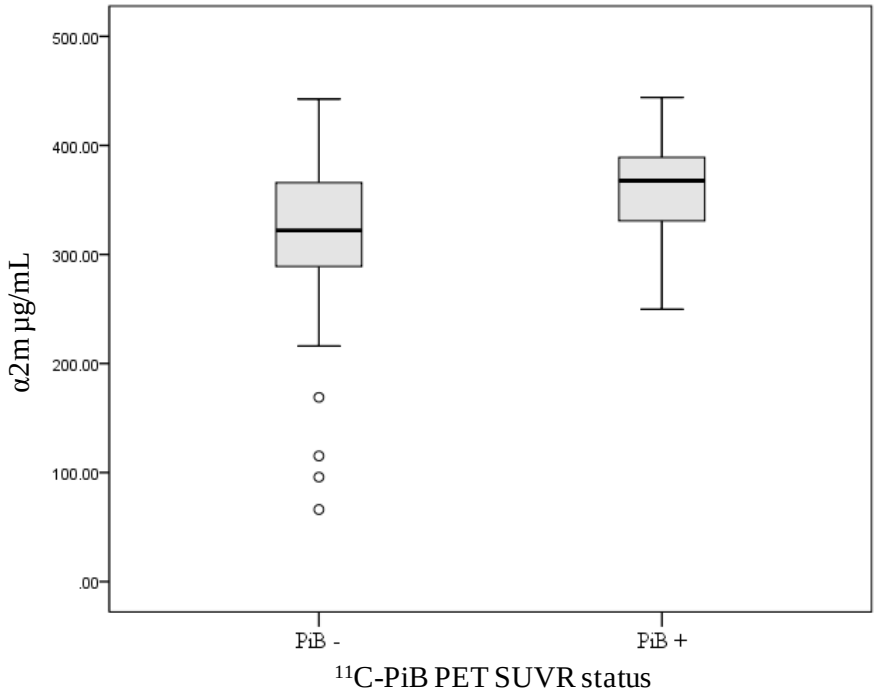

Figure 3-81: Box and whisker plot to show the *α*2m group differences (*P* = 0.009) between PiB- and PiB+ in the AIBL-1 cohort as a technical replication.

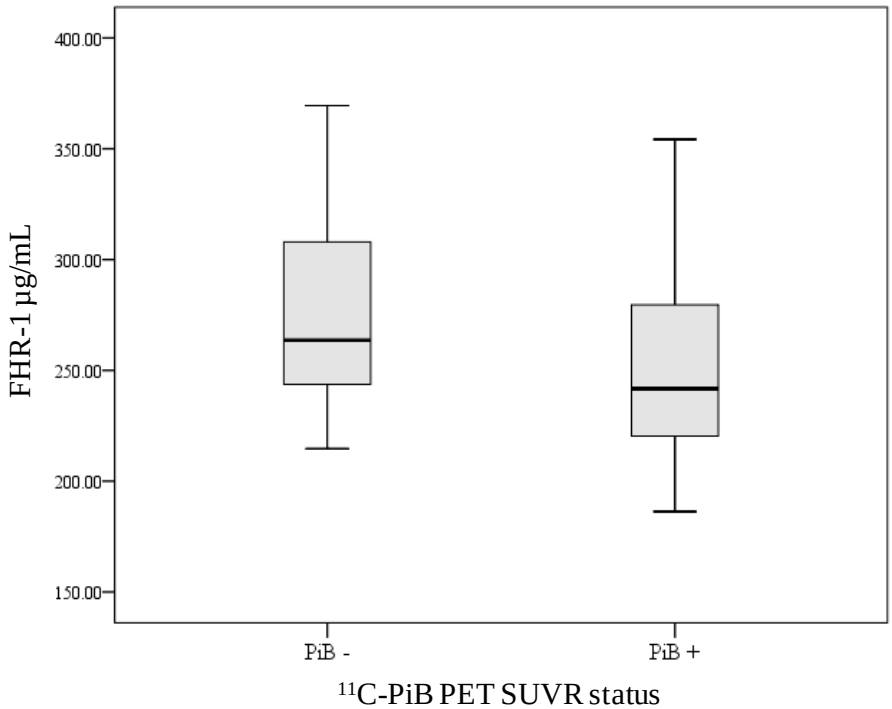

Figure 3-82: Box and whisker plot to show the FHR-1 group differences (*P* = 0.005) between PiB- and PiB+ in the AIBL-1 cohort as a technical replication.

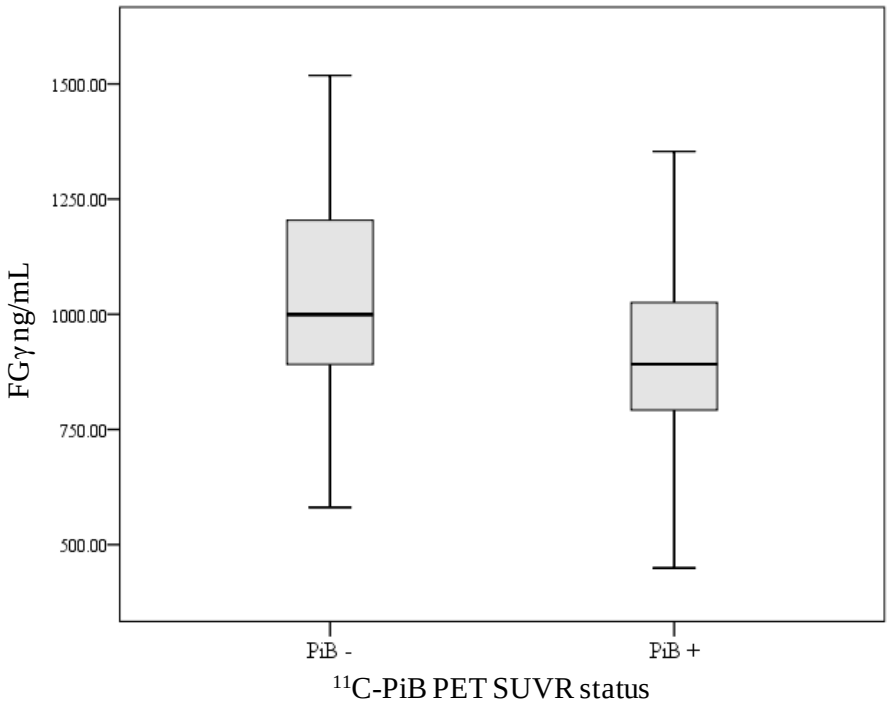

Figure 3-83: Box and whisker plot to show the FGγ group differences (*P* = 0.041) between PiB- and PiB+ in the AIBL-1 cohort as a technical replication.

After multiple testing comparisons, α2m, FHR-1 and FGγ remained associated with NAB (*Q* value = <0.1). In the LC-MS/MS discovery study, FHR-1 was increased in the PiB+ group. Even though FHR-1 was associated with NAB in the technical replication (Table 3-13), an opposite trend was observed (Figure 3-82). Furthermore, apo(a), haptoglobin, HRG, apoA4, CC3, C4α, clusterin, FGα, CFH and CFB all showed the same directional change as in the LC-MS/MS discovery, although not significant at the uncorrected *P* <0.05 level (Table 3-13). The similarities and differences with regards to directional protein change within the PiB+ group between LC-MS/MS discovery and technical replication can be observed in Table 3-14.

Table 3-14: A comparison of directional change in the PiB+ group between LC-MS/MS discovery and ELISA technical replication. For LC-MS/MS results one arrow represents one MW protein isoform, of which 25 were represent for 17 protein groups.

Protein Name	Direction of change in PiB+		Protein Name	Direction of change in PiB+	
	LC-MS/MS	ELISA		LC-MS/MS	ELISA
α2m≠	↑↑↑	↑	C4α	↓↑	↓
FHR-1†	↑	↓	clusterin	↓	↓
FGγ≠	↑	↑	apoA1	↓↓↓↓	↑
apo(a)	↑	↑	FGα	↓	↓
gelsolin	↑	↓	TF	↑	↓
haptoglobin	↓↓	↓	apoL1	↑	↓
HRG	↑	↑	CFH	↑	↑
apoA4	↓	↓	CFB	↑	↑
CC3	↓↓	↓			

≠ Statistically significant (uncorrected P <0.05 level) in technical replication with the same directional change as discovery; † Statistically significant (uncorrected P <0.05) level in technical replication with an opposite directional change as discovery.

3.4.7 Independent replication by immunoassay in the UCSF cohort

To verify the results from the AIBL-1 cohort (discovery and technical replication), the levels of the three proteins significantly associated with NAB in the technical replication (α2m, FGγ and FHR-1) were measured using samples from an independent cohort with Aβ measures. These proteins were measured by ELISA in 79 samples from the UCSF cohort (Table 3-2; Figure 3-3). Logistic and Linear Regression models were built using the same confounding factors as AIBL-1 technical replication, with the added variable of PET scanner type.

FGγ was found to be significantly associated with ^{11}C-PiB positivity, as determined both by visual examination of ^{11}C-PiB PET scans (Table 3-15, Figure 3-84; P = 0.002, Q = 0.006) and by applying a threshold of >1.5 to SUVRs (Table 3-16, Figure 3-85; P = 0.017, Q = 0.051). Assessing ^{11}C-PiB PET as a continuous measure there was a statistically significant correlation between FGγ and NAB (Table 3-16, Figure

3-86; *P* = <0.001, *Q* = 0.001). As with LC-MS/MS discovery and technical replication, lower plasma FGγ were associated with increased NAB. Despite not being significantly associated with NAB, α2m correlated with SUVR positivity in the same direction as in the discovery study and technical replication (Table 3-16). There was no association found for FHR-1.

Table 3-15: Independent replication in UCSF of plasma protein candidates discovered by LC-MS/MS and technically verified by immunoassay (Visual read to Aβ). For regressions age, gender, presence of *APOE* ε4, ELISA assay plate and PET scanner type were used as covariates.

		Logistic Regression to visual read		
UniProt ID	**Protein Name**	**Beta**	***P* value**	***Q* value**
P01023	α2m	-0.013	0.960	0.960
P02679	FGγ	-1.000	0.002	0.006
Q03591	FHR-1	-0.066	0.790	0.960

Table 3-16: Independent replication in UCSF of plasma protein candidates discovered by LC-MS/MS and technical verified by immunoassay (SUVR to Aβ). For regressions age, gender, presence of *APOE* ε4, ELISA assay plate and PET scanner type were used as covariates.

		Logistic Regression to SUVR > 1.5			Linear Regression to SUVR		
UniProt ID	**Protein Name**	**Beta**	***P* value**	***Q* value**	**Beta**	***P* value**	***Q* value**
P01023	α2m	0.270	0.290	0.440	0.075	0.22	0.33
P02679	FGγ	-0.740	0.017	0.051	-0.210	<0.001	0.001
Q03591	FHR-1	0.011	0.970	0.970	0.002	0.98	0.98

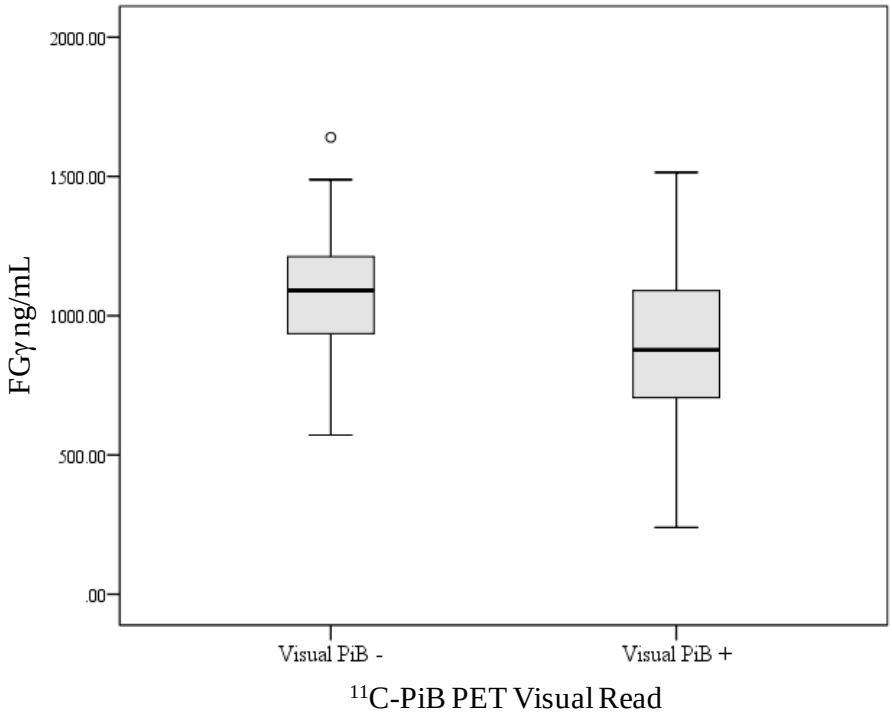

Figure 3-84: Box and whisker plot to show the FGγ group differences (*P* = 0.002; *Q* = 0.006) between PiB- and PiB+ according to visual examination of ^{11}C-PiB PET in the UCSF cohort.

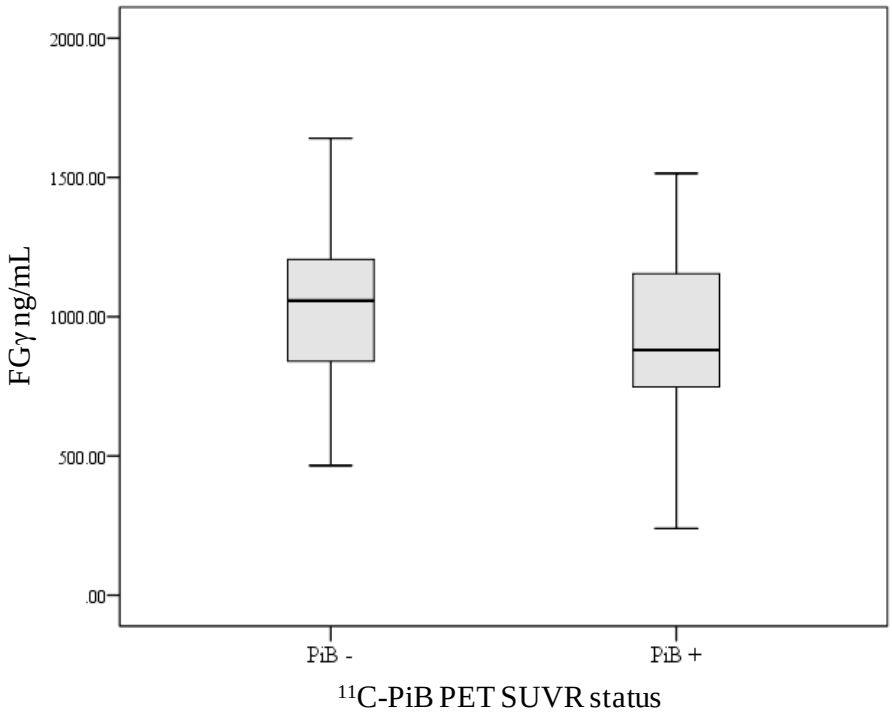

Figure 3-85: Box and whisker plot to show the FGγ group differences (*P* = 0.017; *Q* = 0.051) between PiB- and PiB+ according to an ^{11}C-PiB PET SUVR cut-off of >1.5 in the UCSF cohort.

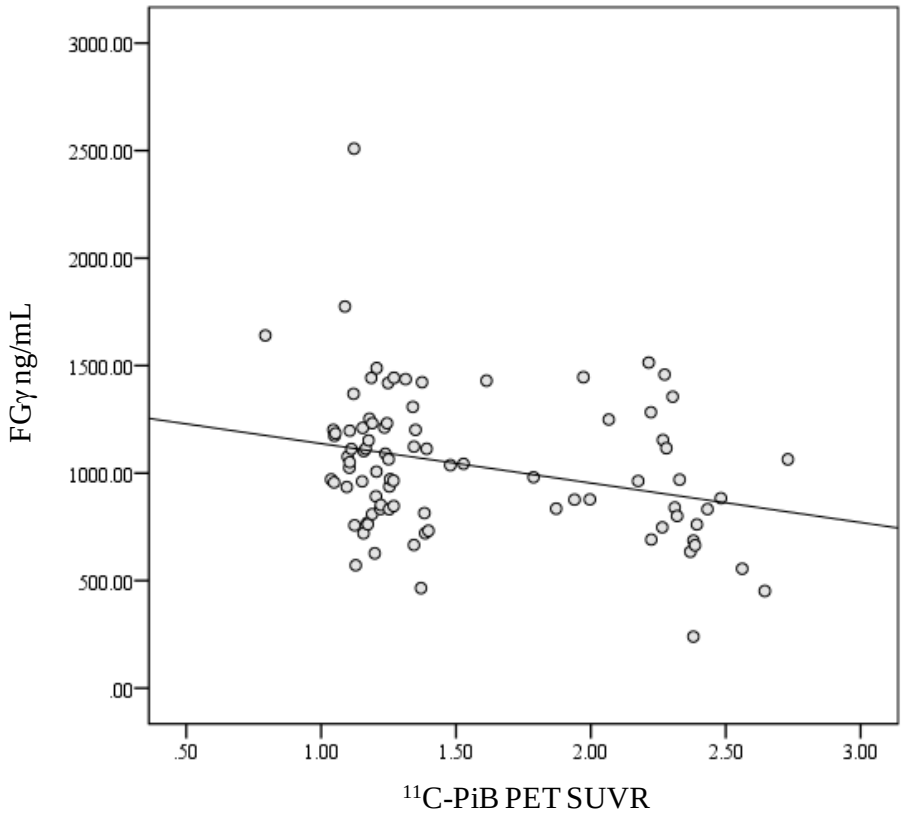

Figure 3-86: Scatter plot to show the FGγ correlation (*P* = <0.001; *Q* = 0.001) with ^{11}C-PiB PET SUVR in the UCSF cohort.

3.4.8 Multivariate analysis

It is unlikely that a single marker alone will be able to explain heterogeneity demonstrated in AD and elevated Aβ. Therefore, a multimodal prediction model was attempted to be trained and tested (ELISA data only). Subjects with any missing covariates or protein measurements were excluded from the multivariate analysis, leaving 70 subjects from AIBL-1 (34 PiB-, 36 PiB+ based on SUVR cut-off >1.3) and 78 subjects from UCSF (46 PiB-, 32 PiB+ based on visual inspection). Classification models were trained in the AIBL-1 ELISA data to predict SUVR positivity (>1.3) and tested in the UCSF ELISA data to predict ^{11}C-PiB positivity determined by visual inspection (more robust across multiple PET scanners). A 'basic' model (age/gender/*APOE* ε4) was compared to a 'basic + proteins' model which used the plasma concentrations of FGγ, α2m and FHR-1. Figure 3-87a and 3-87b shows a Receiver Operator Characteristic (ROC) analysis, where an Area Under the Curve (AUC) was shown to be higher for the 'basic + protein' model than for the 'basic' model in the test datasets. The highest test AUC was found using the Random

Forest approach, where the 'basic + protein' model (AUC = 0.70) outperformed the 'basic' model (AUC = 0.46) in the test dataset. The Random Forest 'basic + proteins' model gave a test set sensitivity of 50% and specificity of 85%.

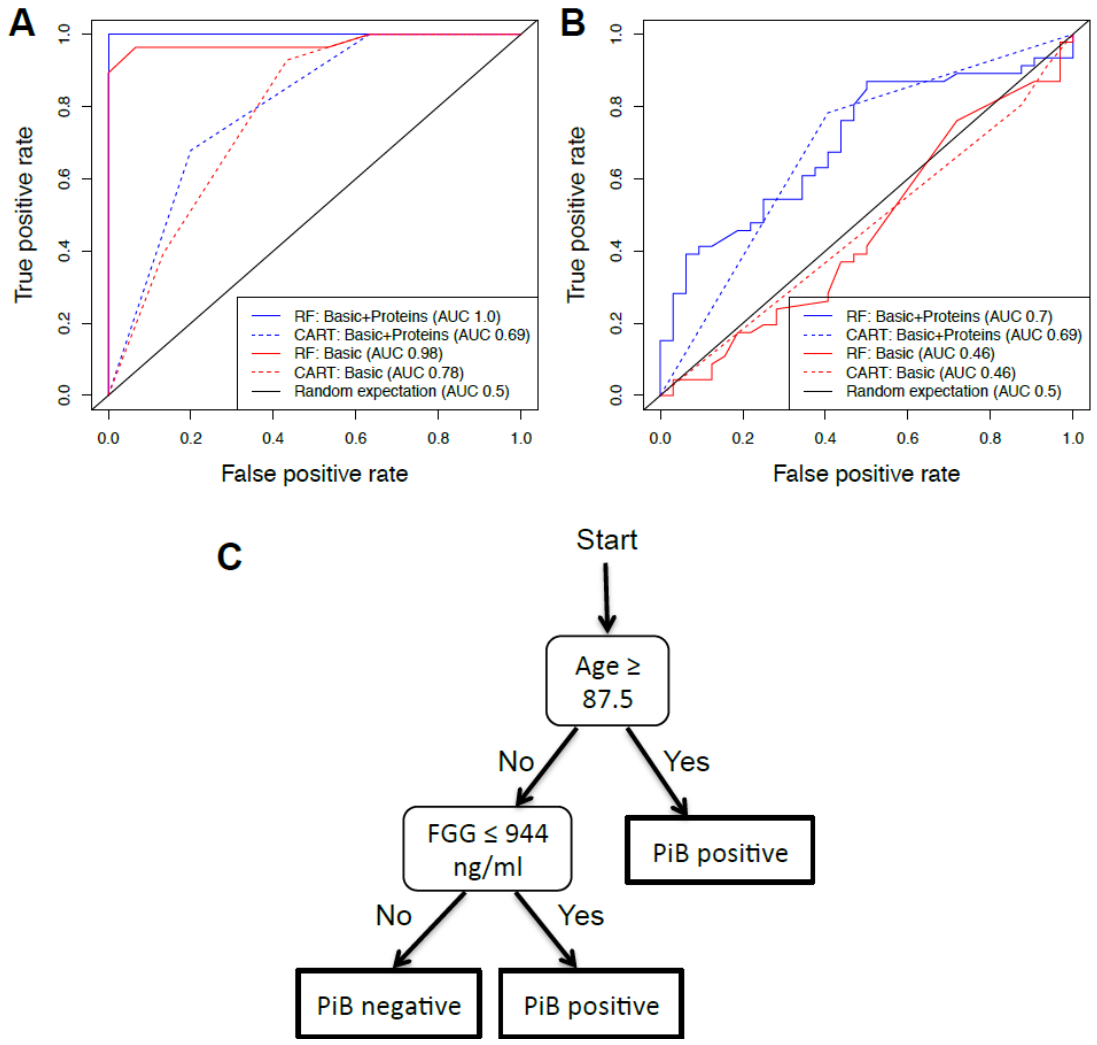

Figure 3-87: Receiver Operator Characteristic (ROC) for the prediction of ^{11}C-PiB positivity. A 'basic' model (age/gender/APOE4 presence) is compared to a 'basic + proteins' model also including the ELISA plasma levels of FGγ, α2M and FHR-1. Random Forest and Classification and Regression Trees (CART) were used to fit models in CARET using default parameters. Area Under the Curve (AUC) is given for each model. ROC curves are shown comparing predictive accuracy of models in (A) the training dataset (AIBL-1), and (B) the test dataset (UCSF). Classification tree trained on AIBL-1 ELISA data to predict NAB positivity and estimated cut-off (C).

Furthermore, a classification tree was fitted to the 'basic + proteins' model, to provide a simpler alternative with clear thresholds. The resulting classification tree

used just two variables (age/plasma FGγ level; Figure 3-87c) and achieved a comparable AUC to the Random Forest model (AUC 0.69, sensitivity 59%, specificity 78%).

3.4.9 The association of plasma FGγ with core CSF biomarkers

Previous studies have shown a good inverse relationship between ^{11}C-PiB PET SUVR and CSF $A\beta_{1-42}$ [474-476] as well as other Aβ imaging tracers [477]. Given this, a plasma marker that demonstrates altered ^{11}C-PiB should also reflect altered CSF $A\beta_{1-42.}$ There has been evidence to support that CSF Aβ biomarkers are altered before a global ^{11}C-PiB SUVR threshold is reached in affect individual [242, 246, 478-479]. Consequently, surrogate measures of CSF $A\beta_{1-42}$ maybe a more sensitive measure of for preclinical Aβ accumulation and therefore AD. We investigated the association of plasma FGγ with CSF $A\beta_{1-42}$ measures from 489 subjects in the EMIF-AD cohort (Table 3-3). We also explored the relationship of plasma FGγ with p-tau, t-tau and a CSF $A\beta_{1-42}$ /tau algorithm [480].

Given the reported inverse relationship of ^{11}C-PiB SUVR and CSF $A\beta_{1-42}$ in AD and the negative correlation observed between FGγ and ^{11}C-PiB SUVR, we would expect to see a positive correlation between plasma FGγ levels and CSF $A\beta_{1-42}$ where low CSF $A\beta_{1-42}$- (indicative of PiB+) is associated with reduced FGγ.

FGγ levels were affected by multi-cohort centres included in the EMIF-AD study (P = 0.049, F = 2.165) and ELISA assay plate (P = 9.205 x10^{-5}; F = 9.394), therefore values were adjusted using a GLM. There was no association between FGγ with age or gender. No data was available for time of plasma sample storage. All subsequent analysis was performed on the GLM adjusted data. We observed a significant association between FGγ and *APOE* ε4 (P = 0.028), therefore we looked at the association of FGγ and core CSF biomarkers with and without adjusting for *APOE* genotype.

We observed a statistically significant positive relationship between FGγ and CSF $A\beta_{1-42}$ (Table 3-17; Figure 3-88a). When accounting for the effect of *APOE* (by partial correlation), a postivie relationship between FGγ and CSF $A\beta_{1-42}$ remained (Table 3-17; Figure 3-88b). When CSF $A\beta_{1-42}$ was treated as categorical measure

there was again a significant association between FGγ and CSF $A\beta_{1-42}$ which was less significant that then correlation analysis (Table 3-17). However, this became non-significant when co-varying for *APOE* genotype (Table 3-17).

Table 3-17: The association of FGγ with CSF $A\beta_{1-42}$ in the EMIF-AD cohort. Associations were made using CSF $A\beta_{1-42}$ as discrete and continuous measures as well as investigating the effect *APOE* genotype. A basic GLM co-varying for cohort centre and ELISA assay was applied in both analysis.

	CSF $A\beta_{1-42}$			
	Spearman Rank Correlation		Mann Whitney U	
	Rho	*P* value	Mean Difference	*P* value
FGγ	0.151	<0.001	-2.518	0.012
FGγ (Adjusted for *APOE* ε4)	0.121	0.008	-1.909	0.056

As CSF $A\beta_{1-42}$ measures correlate greatly with the CSF algorithm values (Figure 3-8) it was unsurprising to finding FGγ significantly associated with the CSF algorithm (Table 3-18). However, this was not as significant as the association of FGγ with CSF $A\beta_{1-42}$ alone and this is likely to be confounded by the inclusion of CSF t-tau in the algorithm (Table 3-19).

Table 3-18: The association of FGγ with CSF algorithm in the EMIF-AD cohort. Associations were made using CSF algorithm as discrete and continuous measures as well as investigating the effect *APOE* genotype. A basic GLM co-varying for cohort centre and ELISA assay was applied in both analysis.

	CSF Algorithm			
	Spearman Rank Correlation		Mann Whitney U	
	Rho	*P* value	Mean Difference	*P* value
FGγ	-0.096	0.034	-2.210	0.027
FGγ (Adjusted for *APOE* ε4)	-0.099	0.028	-1.538	0.107

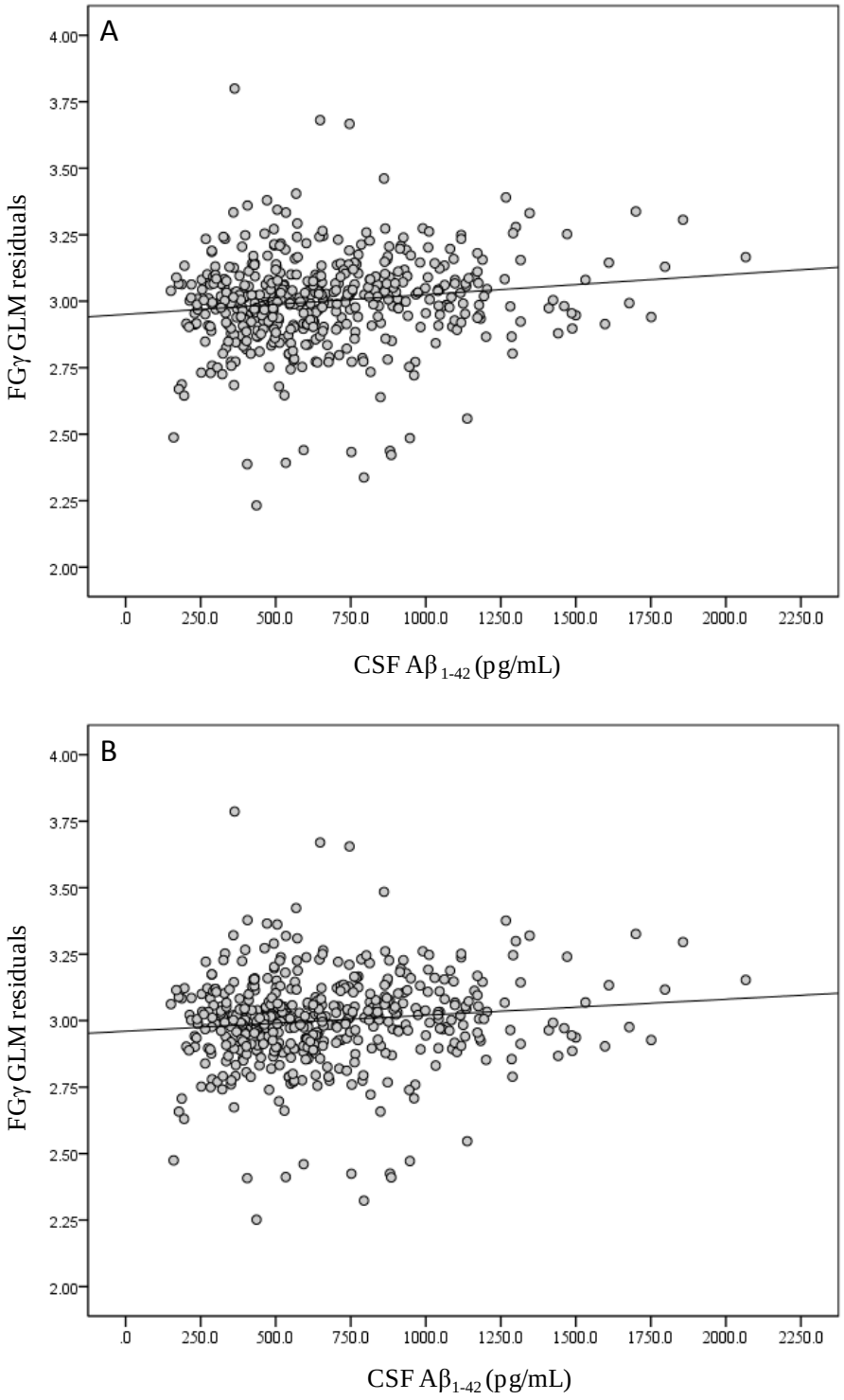

Figure 3-88: Scatter plots demonstrating the correlations of CSF $A\beta_{1-42}$ with FGγ co-varying with *APOE* genotype (B) and without (A). A basic GLM co-varying for cohort centre and ELISA assay was applied in both analysis.

When examining tau measures individually, a statistically significant but weak negative correlation was found between FGγ and CSF p-tau, which was effected by

APOE genotype (Table 3-19). There was no association between FGγ and CSF t-tau although a negative trend was observed (Table 3-19).

Table 3-19: The association of FGγ with CSF t-tau and p-tau in the EMIF-AD cohort. Associations were made using CSF t-tau and p-tau as discrete and continuous measures as well as investigating the effect *APOE* genotype. A basic GLM co-varying for cohort centre and ELISA assay was applied in both analysis.

	CSF t-tau			
	Spearman Rank Correlation		**Mann Whitney *U***	
	Rho	***P* value**	**Mean Difference**	***P* value**
FGγ	-0.090	0.046	-1.586	0.113
FGγ (Adjusted for *APOE*)	-0.071	0.115	-1.212	0.225
	CSF p-tau			
	Spearman Rank Correlation		**Mann Whitney *U***	
	Rho	***P* value**	**Mean Difference**	***P* value**
FGγ	-0.130	0.005	-2.170	0.030
FGγ (Adjusted for *APOE*)	-0.110	0.017	-1.181	0.069

3.4.10 Plasma FGγ to predict elevated NAB for therapeutic trials

Recent studies have shown that Aβ begins to accumulate ~15 years before the clinical onset of AD, leading many to suggest that anti-Aβ trials should begin in asymptomatic older individuals with elevated brain Aβ levels. This has led to the development of AD prevention trials, such as A4, GAP, TOMORROW and EPAD [470]. There is some tentative evidence to suggest that anti-Aβ treatments may be more affective if given in preclinical or prodromal AD [481]. These trials will require the identification of large populations of Aβ positive asymptomatic individuals, which is currently challenging. One of the key challenges is the low prevalence of NAB in asymptomatic individuals (~30%), which means that screening is necessary. We have found that measuring a single plasma protein – FGγ – with age could allow the prediction of individuals with NAB with a sensitivity of 59% and a specificity of

78% (Figure 3-87). Here we test the ability of the described cut-off concentrations of FGγ to predict elevated Aβ in cohort that included a large number of asymptomatic individuals (EMIF-AD).

Firstly, we compared the raw EMIF-AD FGγ concentrations against the immunoassay results from AIBL-1 and UCSF. This demonstrated that there was a very consistent measurement of FGγ across all cohorts, with no significant differences between the three groups (*P* = 0.172; Figure 3-89). The largest mean difference was between AIBL-1 and EMIF-AD (*P* = 0.089; Mean difference = 109.28 ng/mL), however this may be due to the greater variability in the substantially larger EMIF-AD cohort. When comparing cohorts of a similar size (AIBL-1 versus UCSF), the mean difference was considerably smaller (*P* = 0.498; Mean difference 67.34 ng/mL). This is evidence to show that the classifier and FGγ concentration cut-offs built in AIBL-1 and tested in UCSF should be applicable to EMIF-AD.

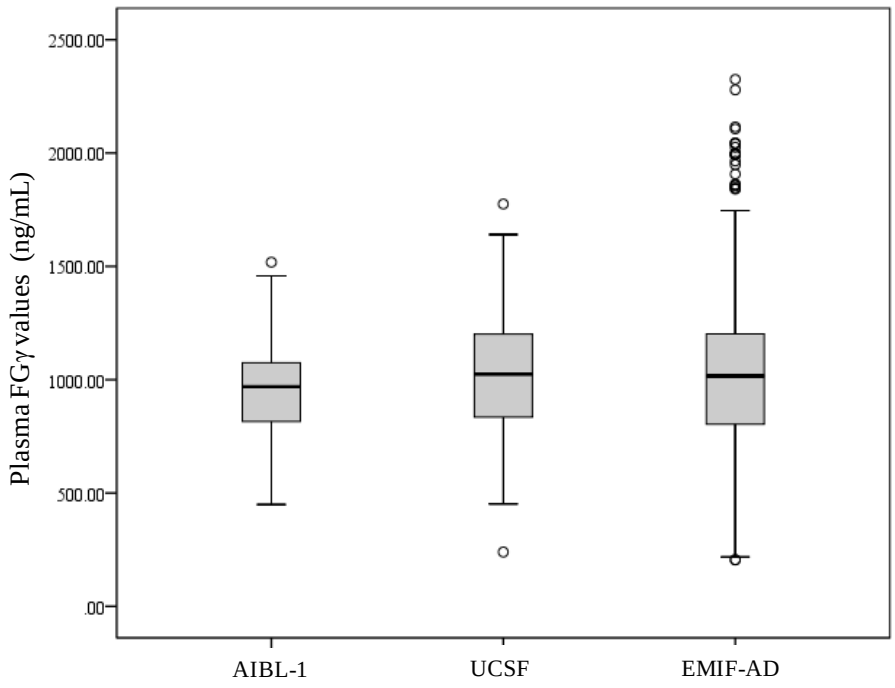

Figure 3-89: Box and whisker plots demonstrating the concentration ranges of FGγ (ng/mL) across three independent cohorts; AIBL-1, UCSF and EMIF-AD.

The classifier was tested in 489 subjects from the EMIF-AD cohort (Table 3-3). The EMIF-AD replication data achieved lower sensitivity (44% vs. 59%) and specificity

(59% vs. 78%) for predicting elevated Aβ in all subjects than in UCSF. When participants were divided into diagnostic groups, the classifier was seen to perform best in HEC (i.e. asymptomatic) individuals with a sensitivity of 50% and a specificity of 61% (Table 3-20). As the prevalence of elevated Aβ in EMIF-AD control individuals was lower than typical asymptomatic AD trial participants (12% vs. 30%), we adjusted positive (PPV) and negative predictive values (NPV) to be more representative. At a prevalence of 0.3 (as observed in the A4 trial), our classifier leads to a PPV of 0.35 but a NPV of 0.74.

Table 3-20: Accuracy, sensitivity and specificity of the FGγ classifier (Figure 3-82) to predict NAB in the EMIF-AD cohort and by diagnostic group.

	Diagnostic groups			
	All (*n* = 489)	**HEC** (*n* = 94)	**MCI** (*n* = 234)	**AD** (*n* = 161)
Accuracy	53%	59%	52%	50%
Sensitivity	44%	50%	37%	48%
Specificity	59%	61%	59%	57%

Abbreviations: HEC, Healthy elderly control; MCI, Mild cognitive impairment; AD, Alzheimer's disease.

3.5 Discussion

With the serial failure of Aβ based therapeutics in clinical trials compromised by the inclusion of substantial numbers of participants without the target pathology the need for biomarkers markers of NAB is an essential step in the search for a global prevention strategy. Blood-based biomarkers could be used to screen large numbers of potential participants, and those predicted to have abnormally high NAB would be retested using CSF assays or PET scans, reducing screen failure rates. This could reduce recruitment time and costs, as well as allowing eligible subjects to be identified more readily, for example from bio-banks with permission for re-contact.

This work has demonstrated that a blood test consisting of FGγ plasma levels along with age could have some potential for predicting NAB, achieving a test set sensitivity, specificity and AUC of 59%, 78% and 69% respectively, highlighting its potential use in stratifying patients for anti-Aβ trials. The initial replication was performed in a mixed dementia cohort (UCSF) with Aβ measures, suggesting that FGγ and age may also have utility for distinguishing between Aβ and non-Aβ dementias. Additionally, because the classification model was trained in a subset of the AIBL-1 cohort containing very few AD subjects, it is more likely that FGγ will be able to predict Aβ positivity in the earlier stage of AD. As the UCSF cohort contained only few cognitively normal individuals we further examined FGγ in a larger cohort, with additional cognitively normal individuals (EMIF-AD). This study initially verified that FGγ positively correlates with CSF $A\beta_{1-42}$. As CSF levels of $A\beta_{1-42}$ are negatively correlated to brain NAB it is encouraging to see this relationship and reinforces the connection between FGγ and NAB. The association of FGγ with p-tau and not t-tau is also encouraging and links FGγ to a biomarker that reflects neuronal degeneration, with a greater sensitivity for AD. There was also a significant association of FGγ and a CSF algorithm however this did not outperform CSF $A\beta_{1-42}$. Given the individual associations of FGγ with CSF $A\beta_{1-42}$ and CSF p-tau but not CSF t-tau an algorithm of $A\beta_{1-42}$ and p-tau may yield greater results.

Next, we aimed to replicate the classifier trained and tested in AIBL-1 and UCSF, in EMIF-AD. We demonstrated that FGγ was consistently measured across these three differing cohorts. As these assays were performed within the same laboratory, inter

laboratory variability could not be tested. The FGγ classifier was shown to predict NAB best in HEC and out perform a demographic model. However, it is worth noting that in larger studies, using demographics models reach an accuracy of ~0.6 across all individuals. While the specificity and sensitivity was lower in EMIF-AD than in our previous investigations and lower than a blood test developed by Burnham and colleagues [437] this is the only blood test whose predictive ability has been tested in an asymptomatic population relevant to AD prevention trials. Additionally, as it requires the measurement of a single protein, using a commercially available ELISA, it could be affordably combined with other markers to produce a more accurate test.

APOE status is a substantial risk factor for AD [482] and Aβ [253]. While we took *APOE* ε4 status into account during our analyses we were not surprised to find that *APOE* genotype markers did not improve our initial classification model as the study was designed to be independent of this effect. However, in EMIF-AD *APOE* ε4 did have an effect on the data and in a general population sample *APOE* genotype is likely to contribute to the prediction of NAB.

FGγ has been previously associated with NAB [373] [436]. However, in the study by Burnham and colleagues [437] total fibrinogen was not found to associate with NAB, whereas Kiddle and colleagues [436] showed it was negatively associated with NAB. Additionally, complementary work to our study demonstrated that plasma measures of FGγ considerably improved the predictive ability of a 5 metabolite panel for elevated NAB [445]. Further to this, decreased levels of plasma FGγ have been shown to be associated with a smaller whole brain volume in AD subjects [428] whereas measures of whole fibrinogen in plasma have shown an increase [404, 483]. Discrepancies in these findings may be due to the platform used to measure total fibrinogen or highlight the importance of looking at specific fibrinogen chains. FGγ is normally rejected from the brain by the blood-brain barrier (BBB), yet has still been detected in mice and human brain tissue [484-485]. This could be due to the reported dysfunction of the BBB in mice [486] and humans in AD [487]. However, the movement of fibrinogen across a defected BBB seems to be molecule-specific, as smaller molecules are not BBB-permeable in AD [488]. Fibrinogen has been shown to accumulate over time as AD pathology progresses [489] and co-deposits with Aβ in

brain tissue [490]. Ahn and colleagues [491] demonstrated that fibrinogen binds to toxic Aβ, which enhances aggregation and increases Aβ fibrillisation. Further to this FGγ-A chain precursor was found to be increased in the CSF in both MCI and AD patients compared to normal controls [492].

After FGγ, plasma α2m was the second most promising candidate, shown for the first time to associate with NAB, and more recently by Westwood and colleagues [375]. This is noteworthy because, α2m has been found to be one of the most replicable markers of other AD-related phenotypes including diagnosis, hippocampal metabolism and response to treatment with sodium divalproex. Furthermore, α2m has been shown to be present in senile plaques [493], binds to $A\beta_{1-42}$ [494-495] and prevents fibrillogensis and Aβ toxicity [494-495]. However, the role of α2m in the neurodegenerative process is not clear, given that α2m has been shown to exert both neuroprotective and neurotoxic effects on cultured neurons [496]. Furthermore, several polymorphisms in the *A2M* gene have been associated with AD and result in significantly increased accumulation of Aβ plaques [497]. It has also been suggested that α2m is strongly correlated with AD progression in females and not males [426].

Technical replication was performed to reduce the number of false positives and to ensure robust translation of LC/MS-MS findings using a platform more applicable to clinical setting. Using commercially available ELISAs, we confirmed that α2m, FGγ and FHR-1 significantly predicted NAB with a 0.1 *Q*-value significance level. In addition to FGγ and α2m a further nine proteins (apo(a), haptoglobin, HRG, apoA4, CC3, C4α, clusterin, FGα, CFH and CFB) technically replicated the trend observed in the LC-MS/MS discovery without reaching statistical significance. Immunoassays cannot always distinguish between sequence variants, proteins modified with different PTM, or different truncated forms of a same protein seen by LC/MS-MS. It is also possible that the LC-MS/MS peptides used for quantification do not match the epitope measured by immunoassay. This could also explain the differences seen in significance, association and trend (e.g. FHR-1) between discovery and replication in some cases; therefore these candidates should not necessarily be discounted.

Furthermore, the confounding influence of non-analyte specific interference also needs to be considered when immunoassays are the platform of choice. Heterophilic

antibodies (HAs) are found in upto 40% of healthy and diseased patient samples [498] and have the ability to bridge between the capture and the detection antibodies in the immunometric assay creating a false signal. The influence of heterophilic antibodies on the immunoassays utilised in this study was not examined and could be another factor in we observed a poor replication between an MS-based discovery and ELISA-based replication. Approaches can be taken in sample pre-treatemnt (IgG depletion and heat shocking) and assay modification (replacement of monoclonal antibodies or HA blocking buffers) to reduce the interaction of HAs [499]. The concentration of HAs is higher in blood samples than in CSF [392] and for low abundant proteins such as Aβ oligomers, positive signals are eliminated in plasma or reduced in CSF when immunoassays are repeated in the presence of heterophilic antibodies-blocking factors [500].

In addition to these confounding factors, spike and recovery assessments were not performed on commercial ELISAs in this study and therefore the absolute accuracy of measuring an analyte in a complex sample matrix was not determined. This could be contributing to the poor replication from MS to ELISA. The immunoassay replication was reliant on an LC-MS/MS discovery phase and there are some limitations to this initial technique that needs to be considered. There was clear restriction on the number of protein group measured and a restriction dynamic range, with only classical plasma proteome targets being analysed. This is likely to due to the method of isobaric labelling employed and/or the pre-fractionation for LC-MS/MS acquisition. These caveats will be discussed further in Chapter 4.

3.5.1 Conclusions

Using a well established discovery proteomic technique, this current study indentifies numerous cross-sectional candidate biomarkers of NAB. Many of these candidates have been previously been reported as AD putative biomarkers in "case versus control" cohorts, and this provides further evidence for utility as biomarkers in disease. In translation to quantitative assays we further demonstrated a potential blood test (plasma FGγ with age) having some ability to predict NAB. This was replicated in two independent sample cohorts of ^{11}C-PiB imaging and CSF $A\beta_{1-42}$ measures. Plasma FGγ was also shown to have utility in preclinical disease by

illustrating a modest prediction of elevated NAB in asymptomatic individuals. We also demonstrated that plasma FGγ has an association with CSF p-tau but not t-tau. This study adds further evidence that differences in the plasma proteome in relation to AD and its pathology do exist, and therefore such changes could be used to stratify patients for anti-Aβ treatment trials.

Statement of collaborative work

Dr. Steven Kiddle (King's College London) wrote the code for PRQ-1. Dr. Kiddle also contributed to the multivariate analysis in this Chapter.

CHAPTER 4

IN-DEPTH PROTEOMIC PROFILING OF PLASMA: AN APPLICATION FOR THE DISCOVERY OF PERIPHERAL BIOMARKERS OF NEUROLOGICAL DISEASE

4.1 Introduction

Protein markers for early detection, accurate diagnosis and prognosis are in great demand for a number of diseases, including neurodegeneration. Routine clinical practices are utilising blood as their first port of call, due to its minimally invasive nature, availability and relatively minimal cost. Moreover, blood is a good indicator of an individual's overall function as it perfuses all body tissues and organs [501] and changes in the levels of blood proteins reflect most physical conditions [502]. Immunoassays are frequently the method of choice in a clinical and research setting however they pose particular limitations e.g. inability to perform unbiased biomarker discovery, sample multiplexing and to detect protein isoforms/modifications. Futhermore, immunoassays are susepctible to non-analyte specific interference. In contrast a proteomic strategy that utilises Mass Spectrometry (MS) as a discovery platform would be able to address these limitations.

Proteomic analysis of blood (plasma/serum) for the discovery and validation of disease related biomarkers by MS is a challenging task. While improving instrumentation has been important in advancing the development of shotgun proteomics, sample preparation still remains the critical factor. The high complexity and large dynamic range of plasma proteins ($>10^{10}$-fold) [501] causes difficulties in deep profiling of the plasma proteome. In addition plasma is comprised of 20 highly abundant proteins including albumin, immunoglobulins, transferrin and haptoglobin, which make up 99% of the total protein content [369]. When considering an unbiased shotgun proteomics method, peptides derived from highly abundant proteins dominate the focus of the analysis. This leads to the 'masking' of lower abundant proteins or they simply fall below the detection limits of MS instrumentation because

the abundant proteins dictate the volume of plasma that can be injected and analysed [503]. More recently, the removal of the most abundant proteins (Top2, 6, 12, 14 or 20) is employed in shotgun proteomics. By using these strategies it has been shown that analytes of low abundance (<100ng/mL) are readily detectable in the plasma proteome [504-505]. A potential concern with immunodepletion strategies, particularly in non-denaturing conditions, is the removal of several proteins associated with immunocaptured targets that are known to function as carrier proteins [506-507]. For example, the "albuminome" is the term given to intact proteins and fragments that are bound to *anti*-albumin resin during immunocapture process [508]. This unwanted removal of proteome content is only likely to increase when depleting multiple analytes.

The removal of albumin alone has been described as inadequate to achieve the sensitivity required to measure the much desired "tissue leakage" portion of the plasma proteome [509]. While improving the coverage of medium abundant proteins, other studies have confirmed that the removal of several targets, in addition to albumin, does little to improve detection of proteins at low abundance [142, 507]. Furthermore, increasing the number of depletion targets has minimal benefit given the additional expenditure [510]. Importantly, proteins routinely included in multi-immunocapture columns have been highlighted to be of major importance in several disease processes, in particular plasma biomarkers of neurodegeneration[357, 372, 374, 429]. This is further supported by the observed association of FGγ, α2m, apoA1 and haptoglobin with NAB in Chapter 3. Even with the inclusion of a depletion strategy the issue of high complexity in plasma remains. This can be overcome by the combination of depletion and upstream protein or peptide level fractionation before LC-MS/MS. Strong cation exchange or SCX chromatography and 1DGE are highly compatible with immunodepletion and LC-MS/MS for peptide and protein separation respectively. However, one of the main disadvantages of SCX is the very strict buffer requirements needed to get optimal separation; a consistent column set up is also required. On the other hand a gel-based approach with 1DGE is robust and a popular technique for fractionating proteins based on molecular weight, as demonstrated in Chapter 3. However, gel-based techniques are still limited to the amount of protein that can be separated and a laborious process of peptide extraction from gel for MS analysis is required.

The development of the OFFGEL approach that fractionates proteins/peptides based on their isoelectric point (pI) has demonstrated superior performance in terms of protein identifications [511-514] and specifically peptide OFFGEL has been shown to be a greater separation technique than SCX [515] and 1DGE [503, 516] in complex matrices. Although in some instances, reports have demonstrated that gel-based separation can be superior to OFFGEL in less complex materials [517-518]. A major drawback of having any upstream fractionation in a discovery methodology is the time and cost involved in performing the MS acquisition in order to be able to identify targets. This cost can be reduced by using multiplex isobaric labelling (TMT or iTRAQ) at the protein or peptide level. Protein separation utilising TMT6plex protein labelling has already been utilised in Chapter 3. With the recent development of TMT10plex, up to nine samples and one study reference can be measured in a single MS acquisition with relative quantification.

The ideal goal of a MS-based plasma discovery would be to capture a wide dynamic range of low abundant proteins without losing the coverage of high/medium abundances, whilst keeping cost to a manageable level. However, if one is purely after the absolute maximum coverage, several studies have performed extensive MS approaches to detect total plasma protein numbers [463, 509]. These studies in effect are an excellent reference tool and a valuable source for identifying detectable targets in the plasma proteome. However, these approaches could be deemed unrealistic to apply in a typical biomarker discovery project; firstly, they are often performed on a single sample with multiple techniques and huge number of technical repeats. Secondly, the cost, time and effort to apply such strategies is beyond the scope of a typical biomarker study in an research setting, which are generally conducted in a multi-disciplinary facility, examining >100 biological samples.

Chapter 3 "*Blood protein predictors of neocortical amyloid pathology for enrichment in therapeutic trials*" presented results using a typical proteomic approach utilising 1DGE, TMT protein labelling without immunodepletion. Although it was shown to be an extremely useful proteomic technique, this methodology does have limitations that need to be addressed when aiming to conduct a thorough analysis of the plasma proteome. The main limitation in this method places on our biomarker discovery investigation is its restriction on dynamic

range, with only classical plasma proteome targets being analysed. Low abundant proteins play important roles in major biological processes such as cell cycle control and stress response. More recently, CNS proteins have been described in plasma as markers of neuronal injury and BBB dysfunction [519]. Low abundant analytes were under represented in the dataset presented in Chapter 3 but are also under represented in the wider plasma proteomic literature, particularly for neurodegeneration. Highly abundant targets, such as FGγ and α2m, which were discovered in relation to NAB have also been attributed to number of other diseases. This would mean that alone their disease/phenotype accuracy is unlikely reach a level of clinical utility. However, if combined within a multi-analyte model alongside novel protein groups of lower abundance, this may foster greater sensitivity and specificity to the disease phenotype.

In this study we have focused only on applying a number of common and widely used proteomic approaches to assess the optimum strategy to maximum proteome coverage, dynamic range and increase sample cohort size all within a manageable cost effective pipeline for typical plasma biomarker research. We also aim to examine these datasets for protein groups related to the CNS or neurodegeneration. Therefore, we have focused on plasma obtained from elderly subjects with differing disease classifications. However, in this Chapter we do not aim to investigate differential expression between clinical phenotypes but principally describe the limit of detectable content within using various methodologies.

4.2 Aims

To investigate a number of plasma proteomic strategies that can be coupled to LC-MS/MS for the greater detection of lower abundance plasma protein groups. Methodologies will investigate immunodepletion, pre-fractionation and isobaric quantitation at the protein and peptide level. The plasma protein datasets and MS/MS spectra produced will be specifically interrogated for protein groups of low abundance (<100ng/mL), brain-specific protein groups and proteins related to neurodegenerative pathogenesis.

4.3 Methodological overview

The proteomic workflows investigated in this study are outlined in Figure 4-1. The detailed methodological protocols for each procedure are outlined in Chapter 2.6.

All methods utilised TMT10plex isobaric tagging at the protein or peptide level for LC–MS/MS based quantification. This was applied to increase sample throughput and achieve relative quantification against a study reference. Either a gel-based method (1DGE) or isoelectric focusing method (OFFGEL (OGE)) of 10 or 20 fractions was utilised for upfront separation of proteins and peptides respectively. This was compared alongside non-fractionated (NF) strategies. All 1DGE methods incorporated TMT protein labelling (1DGE-4, 1DGE-5, 1DGE-7 and 1DGE-8) whereas OGE (OGE-6 and OGE-9) and NF strategies used TMT peptide labelling (NF-1, NF-2 and NF-3). Furthermore, six strategies incorporated an initial immunodepletion step. ProteoPrep® Immunoaffinity removal of albumin and IgG's was applied to methods NF-2, 1DGE-5, OGE-6, 1DGE-8 and OGE-9 whereas Pierce™ Top12 depletion was only applied to method NF-3. No depletion strategy was applied to methods NF-1, 1DGE-4 and 1DGE-7. The resulting peptide fractions for each proteomic methodology were analysed in an identical manner. Peptides were resolved using a linear gradient for 115 minutes through a C18 analytical column and mass spectra were acquired on a Thermo Scientific LTQ Orbitrap Velos instrument. Two different computational MS approaches in Proteome Discoverer 1.4 for protein group/peptide identification and quantification were performed; sequential searching and MudPIT.

Plasma samples were obtained from the multicentre European study, AddNeuroMed (ANM). For each methodology, pools of clinically confirmed healthy elderly (HEC), mild cognitive impairment (MCI) and Alzheimer's disease (AD) plasma occupied isobaric labels in each TMT10plex analysis. Each pool consisted of differing HEC, MCI and AD participants to allow for subject variability.

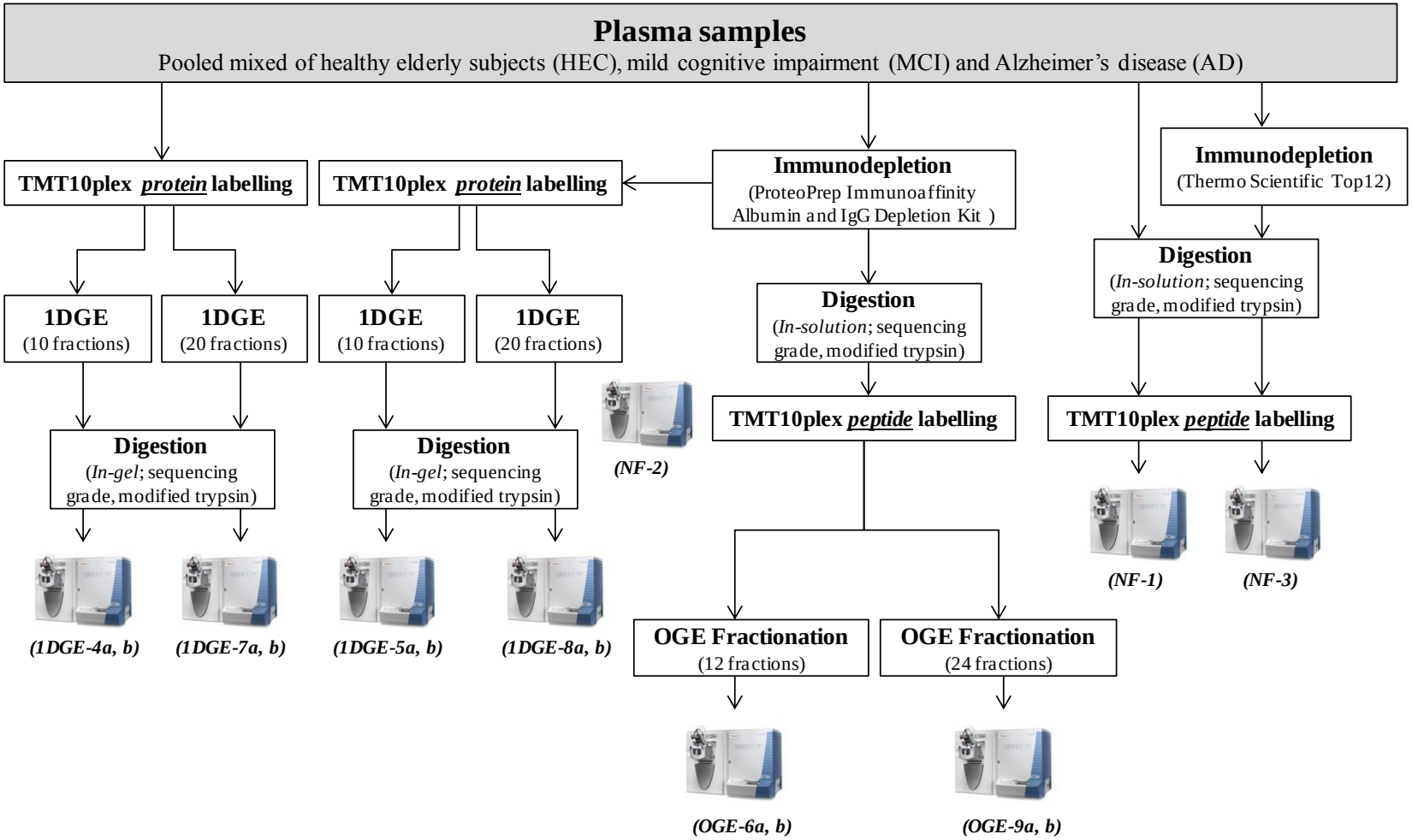

Figure 4-1: Schematic flow diagram represents the 15 proteomic workflows investigated in Chapter 4.

Abbreviations: 1DGE, One dimensional gel electrophoresis; NF, non-fractionated, OGE, OFFGEL; TMT, Tandem mass tag.

4.4 Results

4.4.1 Protein/peptide metrics

In total 7,439 unique proteins groups at 5% FDR have been identified across all methodologies (Supplementary Material 4), of which only 62.25% have been previously reported by the plasma proteome database (PPD; www.plasmaproteomedatabse.com) [369]. A total of 4,404 protein groups were identified based on ≥2 peptides of which 23 were identified as "contaminant protein groups" (i.e. trypsin and human epidermal keratins). We also examined the protein groups, peptides, PSMs and spectral yield rates of each methodology at 1% FDR and contrasted this to 5% FDR (Table 4-1). Typically gel-based methods gave a spectral yield of between 45-55% whereas OGE methods returned a yield of between 35-45% at 5% FDR. As expected there was a reduction in protein groups, peptides, PSMs and spectral yield performance when applying a 1% FDR, this was more detrimental in methods with a greater number of fractions. For all further analysis 5% FDR was applied.

Our initial analysis was to evaluate the total number of protein groups (Figure 4-2a), peptides (Figure 4-2b) and peptide spectral matches (PSMs; Figure 4-2c) that were detectable with each proteomic methodology. The number of protein groups identified using LC–MS/MS exponentially increased with greater pre-fractionation of complex matrices. OGE-9 (20 fractions) consistently yielded the greatest number of protein group identifications (Mean = 1202, SD = 122.92) whereas the equivalent gel-based method (1DGE-8) was significantly lower (Mean = 1049, SD = 91.12). However, it was interesting that gel-based method 1DGE-5 (Mean = 720, SD = 68.8) outperformed the OGE equivalent (OGE-6, Mean = 672, SD = 54.8). In our hands non-fractionated (NF) methodologies yielded between 201-319 protein group identifications depending on depletion strategy employed (Figure 4-2).

Table 4-1: The performance of each proteomic methodology by number of protein groups, peptides, PSM, and spectral yield at false discovery rates (FDR) of 5% and 1%. The mean of 3 biological repeats has been shown for each method.

		5% FDR				1% FDR			
Proteomic Method	**MS/MS events**	**Protein Groups (mean)**	**Peptides (mean)**	**PSM (mean)**	**Spectral Yield (%)**	**Protein Groups (mean)**	**Peptides (mean)**	**PSM (mean)**	**Spectral Yield (%)**
NF-1	21256	220	969	6741	31.71%	163	942	6629	31.19%
NF-2	19565	271	975	7504	38.35%	200	946	7145	36.52%
NF-3	14555	280	1114	7117	48.89%	213	880	6687	45.94%
1DGE-4a	75180	487	2033	35759	47.56%	442	1967	25146	33.45%
1DGE-4b	75180	542	2349	36438	48.47%	422	1972	26167	34.81%
1DGE-5a	88206	709	3714	48322	54.78%	587	3475	43451	49.26%
1DGE-5b	88206	730	4031	48433	54.91%	554	3442	48908	55.45%
OGE-6a	82020	713	2257	30700	37.43%	517	1683	19524	23.80%
OGE-6b	82020	620	2354	33596	40.96%	425	1648	19855	24.21%
1DGE-7a	157126	802	4230	72620	46.22%	487	2109	69209	44.05%
1DGE-7b	157126	874	4321	72110	45.89%	410	2076	69234	44.06%
1DGE-8a	184943	1058	5699	76055	41.12%	754	4304	69364	37.51%
1DGE-8b	184943	1041	5478	76736	41.49%	675	4203	70278	38.00%
OGE-9a	194650	1359	5103	67913	34.89%	739	3872	57239	29.41%
OGE-9b	194650	1045	4540	66960	34.40%	787	3797	56883	29.22%

Abbreviations:NF-1, non-fractionated, TMT peptide labelling; NF-2, non-fractionated, Top2 depletion, TMT peptide labelling; NF-3, non-fractionated, Top12 depletion, TMT peptide labelling; 1DGE-4a, One dimensional gel electrophoresis, 10 fractions, Top2 depletion, TMT protein labelling, sequential database searching; 1DGE-4b, One dimensional gel electrophoresis, 10 fractions, Top2 depletion, TMT protein labelling, MudPIT database searching; 1DGE-5a, One dimensional gel electrophoresis, 20 fractions, Top2 depletion, TMT protein labelling, sequential database searching; 1DGE-5b, One dimensional gel electrophoresis, 20 fractions, Top2 depletion, TMT protein labelling, MudPIT database searching; OGE-6a, OFFGEL fractionation, 10 fractions, Top2 depletion, TMT peptide labelling, sequential database searching; OGE-6b, OFFGEL fractionation, 10 fractions, Top2 depletion, TMT peptide labelling, MudPIT database searching; 1DGE-7a , One dimensional gel electrophoresis, 20 fractions, TMT protein labelling, sequential database searching; 1DGE-7b , One dimensional gel electrophoresis, 20 fractions, TMT protein labelling, MudPIT database searching; 1DGE-8a, One dimensional gel electrophoresis, 20 fractions, Top2 depletion, TMT protein labelling, sequential database searching; 1DGE-8b, One dimensional gel electrophoresis, 20 fractions, Top2 depletion, TMT protein labelling, MudPIT database searching; OGE-9a, OFFGEL fractionation, 20 fractions, Top2 depletion, TMT peptide labelling, sequential database searching; OGE-9b, OFFGEL fractionation, 20 fractions, Top2 depletion, TMT peptide labelling, MudPIT database searching.

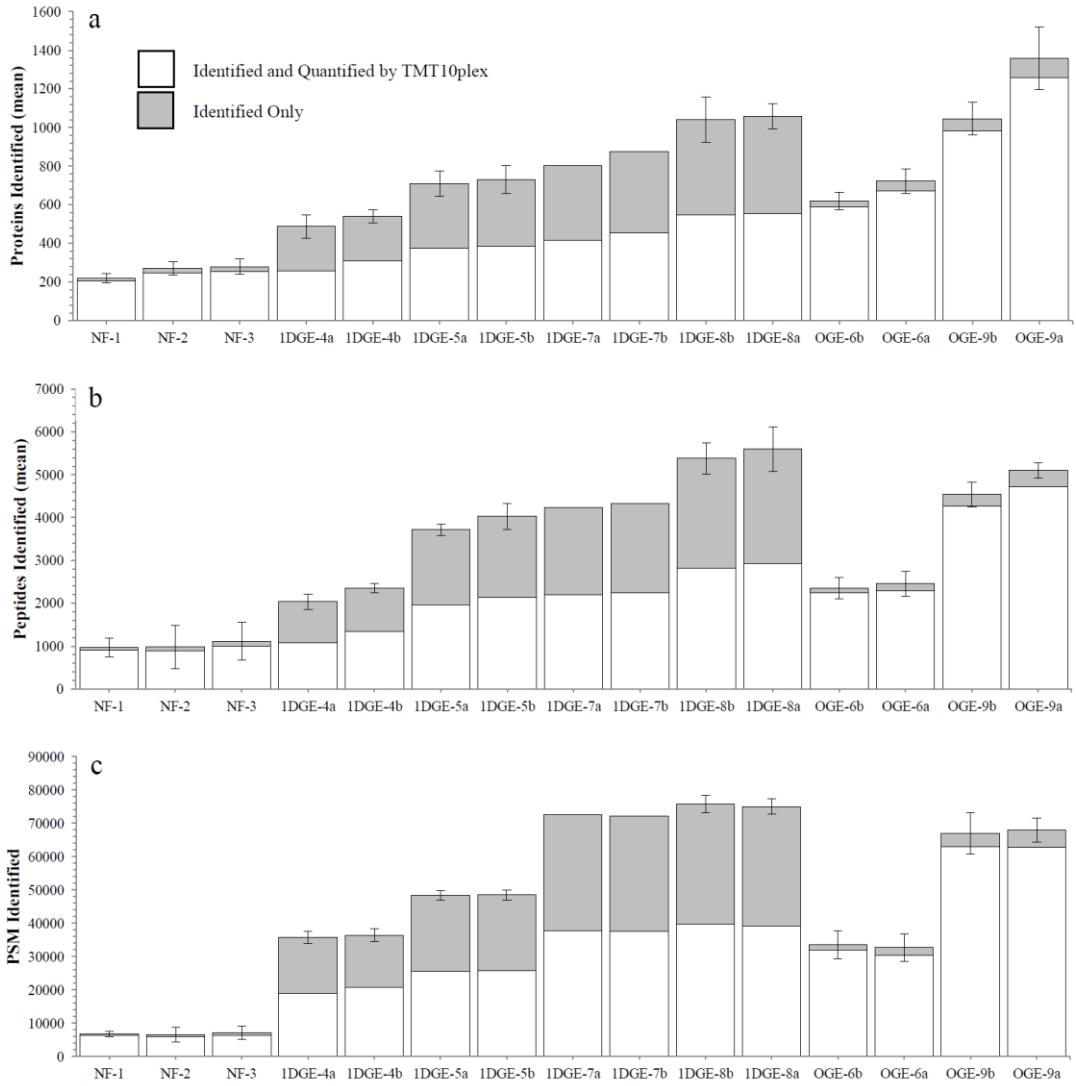

Figure 4-2: The number of (a) protein groups (b) unique peptides and (c) peptide spectral matches (PSM) identified in plasma for 15 proteomic methodologies. White shading of the bars illustrates number of entities that can quantify by TMT10plex whereas grey shading represents identified protein groups only. The error bars shown are the standard deviation of 3 biological repeats. Identification is based on an FDR of 5%. All 1DGE methods (10 fractions [4a, 4b, 5a, 5b] or 20 fractions [7a, 7b, 8a, 8b]) incorporated TMT10plex protein labelling whereas OGE (10 fractions [6a, 6b] or 20 fractions [9a or 9b]) and NF strategies used TMT10plex peptide labelling. Furthermore, 6 strategies incorporated an initial immuodepletion step (2, 3, 5, 6, 8 and 9). No depletion strategy was applied to methods 1, 4 and 7. For 1DGE-7a and 1DGE-7b only 1 experimental repeat was performed.

Despite a decreased number of protein group identifications, all gel-based techniques yielded a greater number of peptides and PSM compared with OGE. To assess if this increase in peptide/PSM features equated to greater protein group sequence coverage we assessed the protein sequence coverage of several protein groups at differing concentrations (Figure 4-3). Protein group sequence coverage improved with greater fractionation however this analysis demonstrated that gel-based techniques produced marginally greater coverage of proteins at higher concentrations (>1µg/ml) whereas method OGE-9 revealed greater sequence coverage of proteins of lower abundance (<1ng/ml).

Despite having a fewer number of total PSMs than 1DGE-8, OGE-9 produced a 1.25-fold increase in unique PSM sequences. Since gel-based proteomics is only compatible with TMT protein labelling all OGE methods resulted in a significantly higher number of quantified protein groups, peptides and PSMs. All TMT protein labelling methods were able to quantify between 52-57% of protein groups whereas TMT peptide methods ranged between 91-94% efficiency (white shading; Figure 4-2).

In addition, we also performed two different computational MS approaches for protein group/peptide identification; sequential searching (1DGE-4a, 1DGE-5a, OGE-6a, 1DGE-7a, 1DGE-8a and OGE-9a) and MudPIT (1DGE-4b, 1DGE-5b, OGE-6b, 1DGE-7b, 1DGE-8b and OGE-9b). For the most part sequential searching yielded a greater number of features, although OGE methods demonstrated a noticeable reduction in protein group and peptide identifications in the MudPIT methodology (Table 4-1, Figure 4-2). This is likely due to the robust identification in MudPIT searching which applies FDR's across the whole dataset rather than within one fraction. Despite this difference both sequential and MudPIT performed equally in the protein sequence coverage assessment (Figure 4-3).

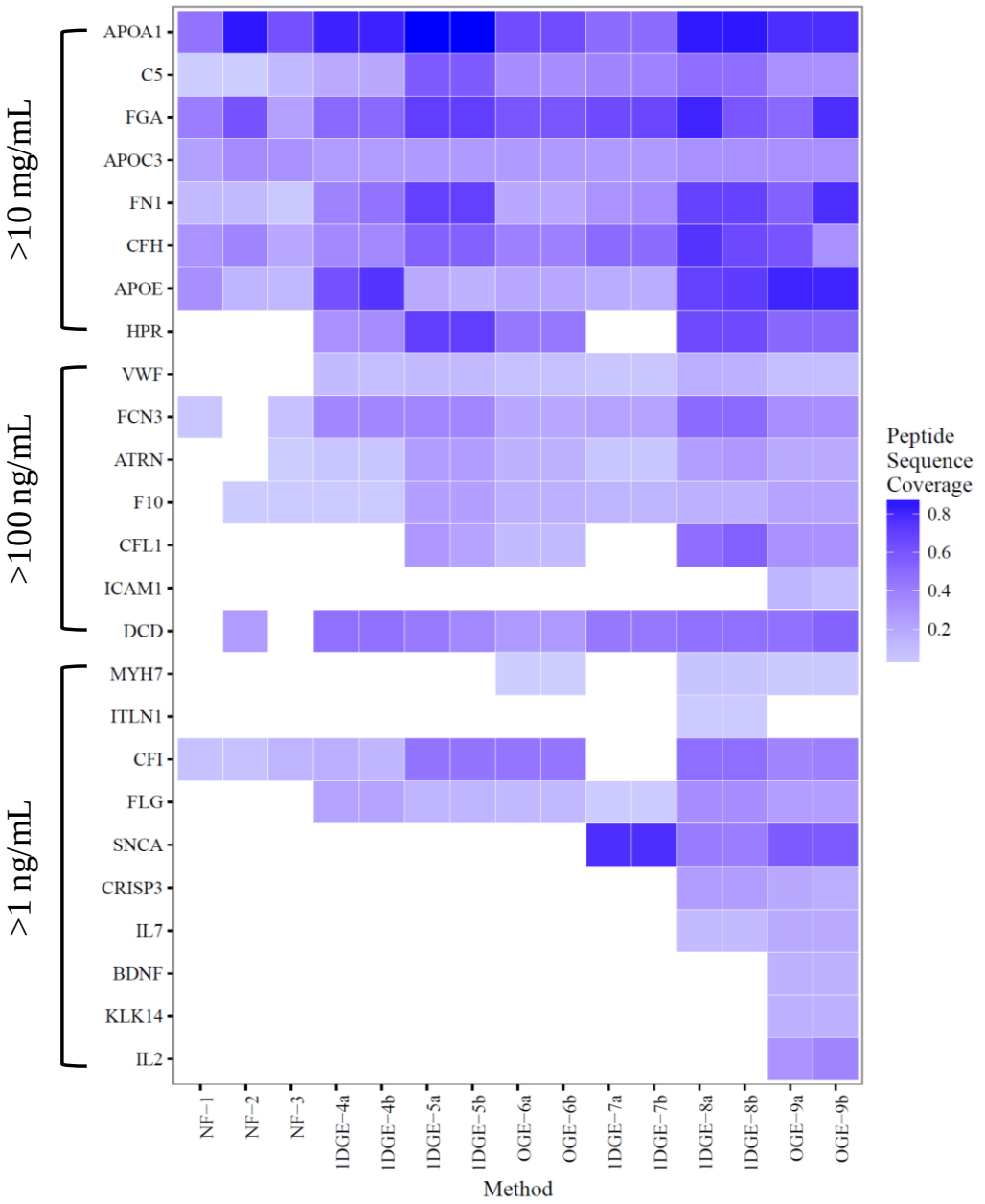

Figure 4-3: **Heat map to demonstrate the percentage of protein group sequence coverage for each proteomic methodology at three concentration levels; high abundance (>10mg/mL), medium abundance (>100ng/mL) and low abundance (<1ng/mL). Peptide sequence coverage colour gradient is shown as a percentage of the protein coverage identified in each method.Protein concentrations were estimated by the plasma proteome database (PPD).**

Gene identifications: APOA1, apoA1; C5, complement C5; FGA, FGα; APOC3, apolipoprotein C-III; FN1, fibronectin 1; APOE, ApoE; HPR, haptoglobin-related; VWF, von Willebrand factor; FCN3, ficolin-3; ATRN, attractin; F10, factor X; CFL1, cofilin 1; ICAM1, Intercellular Adhesion Molecule 1; DCD, dermcidin; MYH7, myosin-7; ITLN1, Intelectin-1; CFI, complement factor I; FLG, filaggrin; SNCA, α-synuclein; CRISP3, cysteine-rich secretory protein 3; IL7, Interleukin-7; BDNF, brain-derived neurotrophic factor; KLK14; kallikrein-14; IL2, Interleukin-2.

4.4.2 Assessment of proteomic dynamic range

In order to measure the depth of coverage achieved with the different workflows we compared our findings with the Plasma Proteome Database (PPD) that has reported the concentrations of >1,200 proteins [463]. Only 12% of the protein groups observed in our data had reported concentration in PPD. The protein concentration ranges for each methodology are $\log_2$ transformed and are displayed as box and whisker plots in Figure 4-4.

Highly significant mean differences were found between OGE-9 methods and all other methods (P = 8.7 x10^{-10}). OGE-9a achieved the lowest level of detection (LOD, multiple epidermal growth factor-like domains protein 8 [4.3pg/ml]) whereas methods 1DGE-8a, 1DGE-8b and OGE-9b achieved an equivalent lowest LOD (cysteine-rich secretory protein 3 [6.4pg/ml]). OGE-9a also achieved the lowest median level of detection (66ng/ml) compared with OGE-9b (92ng/ml), 8a (120ng/ml) and 8b (175ng/ml). Although these methods accomplished a marked improvement in lowest LOD, full annotation of protein groups at all concentration levels was achieved (Figure 4-4). NF methods (NF-1, NF-2 and NF-3) all showed the same lowest LOD (apo(a) [1.4ng/ml]) however NF-1, despite having no depletion strategy, surprisingly achieved the lower median concentration (5.2ug/ml). Gel-based methods with 10 fractions (1DGE-4 and 1DGE-5) performed similarly regardless of depletion (Lowest LOD = kallikrein-10 [440pg/ml], Median = 210ng/ml) or without depletion (Lowest LOD = kallikrein-10 [440pg/ml], Median = 290ng/ml). OGE-6 performed poorly in this analysis (Median = 1.28 ug/ml) compared with all other fractionated methods despite having a lower LOD of 90pg/ml (S100 calcium-binding B).

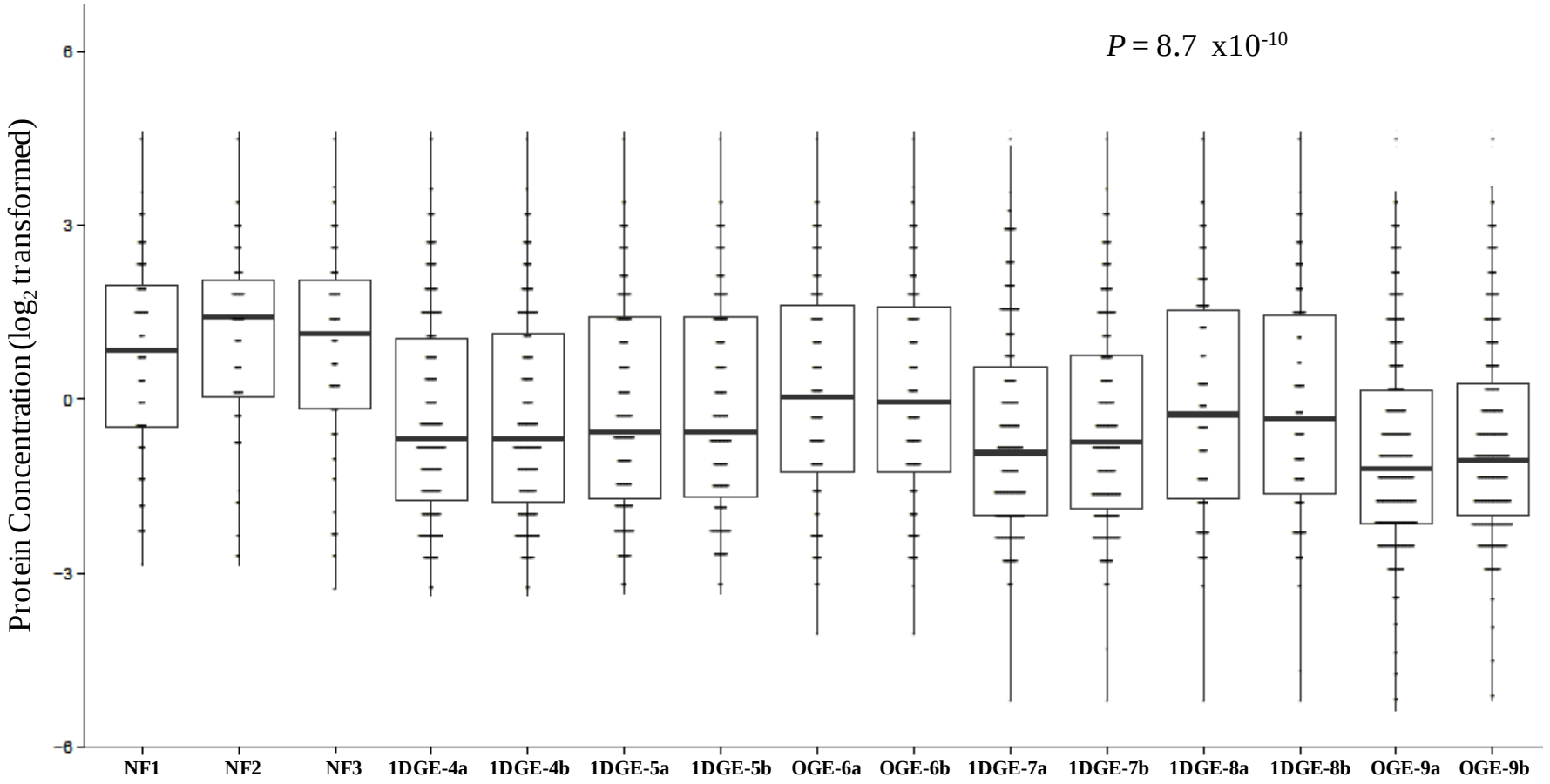

Figure 4-4: **Assessment of dynamic range achieved by each proteomic methodology. Box and whisker plots demonstrate the range of concentration (log_2 transformed) identified in all 15 proteomic methods. Vertical bars within each box plot illustrate the frequency of proteins identified at a particular concentration level.**

To highlight the improved proteomic coverage, we compared protein groups identified (not quantified) in the LC-MS/MS discovery study in Chapter 3 with the best performing methodology (OGE-9a) presented in this Chapter (Figure 4-5).

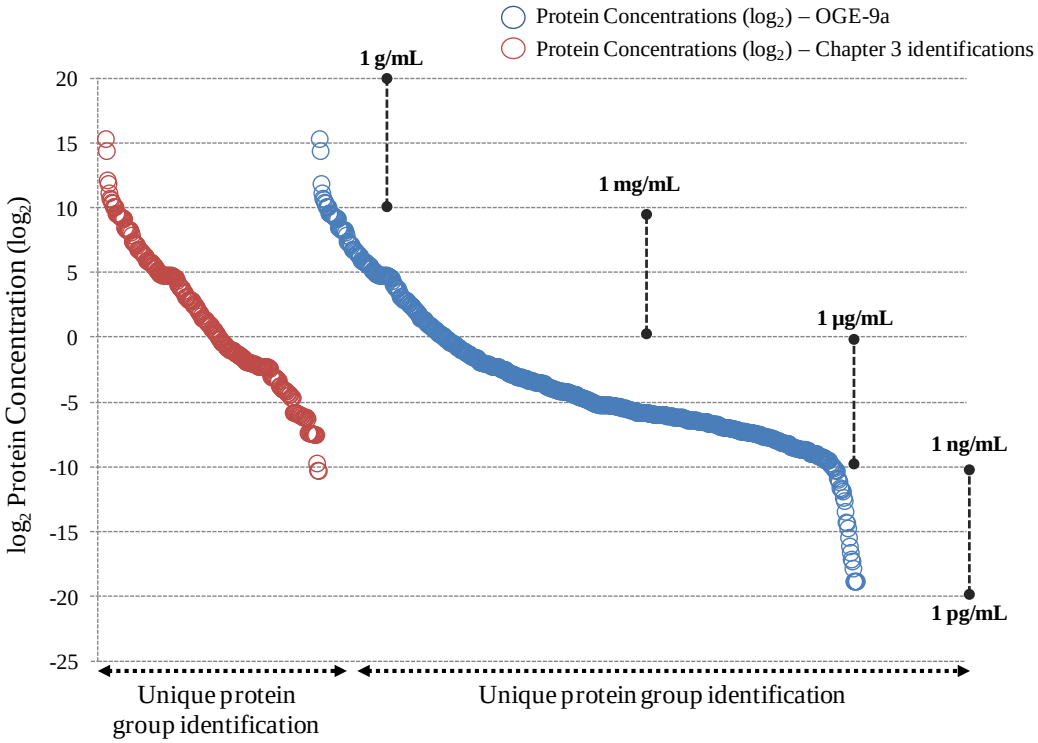

Figure 4-5: A proteomic coverage comparison between protein groups identified in Chapter 3 (red) and the best performing proteomic methodology in Chapter 4 (OGE-9a; blue). Each circle represents an individual protein group. Concentrations from the plasma proteome database (PPD) have been log_2 transformed with an indication (dashed line) of calculated concentration level given.

Identical coverage of the milligram and microgram concentration ranges was observed between the two methods (Figure 4-5). However, OGE-9a demonstrated comprehensive coverage of the nanogram concentration level of the plasma proteome despite only 12% of protein groups being matched to the PPD database. Protein groups at the picogram level were also identified, which was not observed in protein groups from the results in Chapter 3. This comparison reveals the ability of the OGE-9a to identify a larger proportion of low abundance protein groups without losing the coverage of the "classical plasma proteome".

4.4.3 Immunodepletion

Immunodepletion played a considerable role in the improvement of protein group identification and three approaches were investigated in this study; non-depleted, Top2 depleted and Top12 depleted plasma. A statistically significant increase in protein groups between non-depleted (NF-1) and Top2 depletion (NF-2) was observed (P = 0.027; Figure 4-6). The addition of an immunodepletion strategy was the only difference between these two methodologies and therefore would be the principal cause of the significant increase in protein groups. Conversely, a Top12 depletion method (NF-3) did not significantly improve the number of observed proteins groups compared to NF-2 (P = 0.701; Figure 4-6) although a marginal mean increase was observed (Table 4-1; Figure 4-6). This small increase in protein groups was no greater than the experimental variation between replicates and therefore it was concluded that the Top12 depletion strategy had no further benefit than Top2 depletion. In addition, other non-depleted methods that were compared to Top2 depleted method, which included a fractionation step, also demonstrated a significant increase in the number of protein groups; 1DGE-4 versus 1DGE-5 (P = 0.012) and 1DGE-7 versus 1DGE-8 (P = 0.023). This confirms the notable advantage of Top2 depletion. Top12 depletion was not performed on fractionated samples.

It was apparent that the target proteins for Top12 immunocapture (NF-3 only) were still identified among the most highly abundant proteins groups identified in plasma. Table 4-2 demonstrates that 8/12 protein groups targeted for removal by Top12 depletion still remain as the 25 most abundant protein groups when analysed by LC-MS/MS. This is a concern for MS-based discoveries as highly abundant peptides, which are thought to be significantly reduced in the sample, still dominate the focus of analysis. The direct comparison of the abundance of immunocapture proteins from NF-3 to their abundance in a non-depleted sample (NF-1) is evident that the Top12 depletion column is not optimal in removal of specific analytes (Figure 4-7). The Top12 depletion column has been successful in a modest reduction in albumin, total fibrinogen, TF, haptoglobin and α2m with almost complete removal of IgA, IgG and IgM. On the other hand abundances of apoA2 remained constant with apoA1 and α1AT abundances increasing.

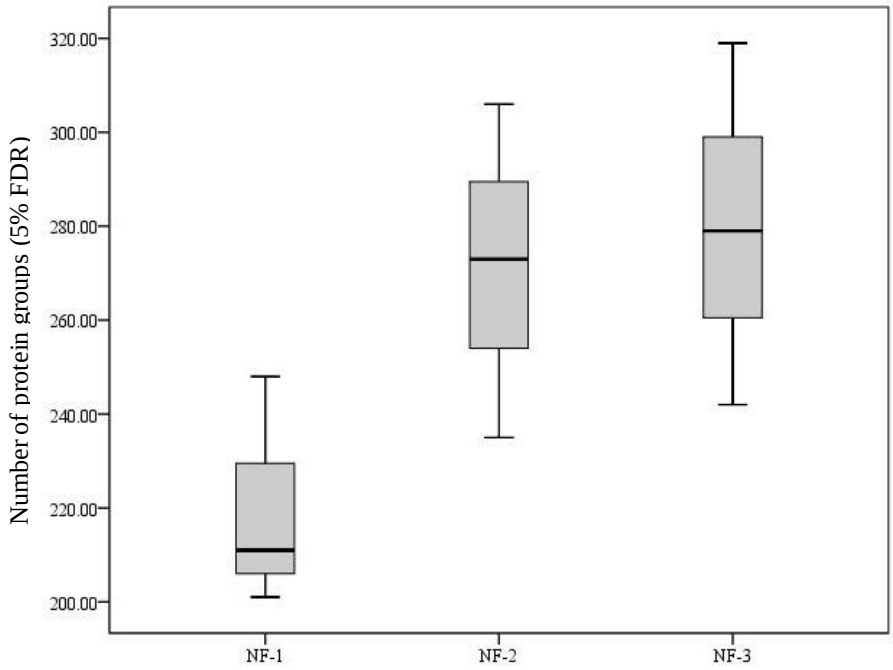

Figure 4-6: Box plot to illustrate the number of protein groups identified with each non-fractionated methodology. A significant increase between non-depleted (NF-1) and Top2 depleted (NF-2) plasma was observed (*P* = 0.027). No significant increase was seen in employing Top12 depletion (NF-3) method. Each method was a result of three technical repeats.

Table 4-2: The top 25 abundant proteins in non-fractionated Top12 depleted plasma (NF-3) based on the sum of PSMs of 3 technical repeats. Observed are 8/12 protein groups (highlighted in green) targeted for immunodepletion that remain as the most abundant proteins.

UniProt ID	Protein Name	Gene Name	Sum of peptides (*n* = 3)	Sum of PSMs (*n* = 3)
P02768	albumin	*ALB*	56	2630
P01024	CC3	*C3*	108	1893
P02790	hemopexin	*HPX*	29	1456
P02675	fibrinogen (α,β,γ)	*FGA* *FGB* *FGG*	38	1392
P01009	α1-antitrypsin (A1AT)	*SERPINA1*	46	1130
P02766	transthyretin	*TTR*	18	1102
P02647	apoA1	*APOA1*	40	569
P02765	α2-HS-glycoprotein	*AHSG*	13	565
P00450	ceruloplasmin	*CP*	39	536
P02774	vitamin D-binding protein	*VDBP*	32	531
Q14624	Inter-alpha-trypsin inhibitor heavy chain H4	*ITIH4*	31	474
P02753	retinol-binding protein 4	*RBP4*	9	408
P00738	haptoglobin	*HP*	24	356
P08603	CFH	*CFH*	43	316
P01008	antithrombin-III	*SERPINC1*	24	307
P02652	apoA2	*APOA2*	10	291
P02787	TF	*TF*	31	286
P01011	α1-antichymotrypsin	*SERPINA3*	19	283
P19827	Inter-alpha-trypsin inhibitor heavy chain H1	*ITIH1*	21	272
P19823	Inter-alpha-trypsin inhibitor heavy chain H2	*ITIH2*	21	267
P01042	kininogen-1	*KNG1*	21	256
P0C0L5	complement C4-B	*C4B*	62	250
P0C0L4	C4α	*C4A*	60	248
P04217	α1B-glycoprotein	*A1BG*	15	245
P01023	α2m	*A2M*	41	223

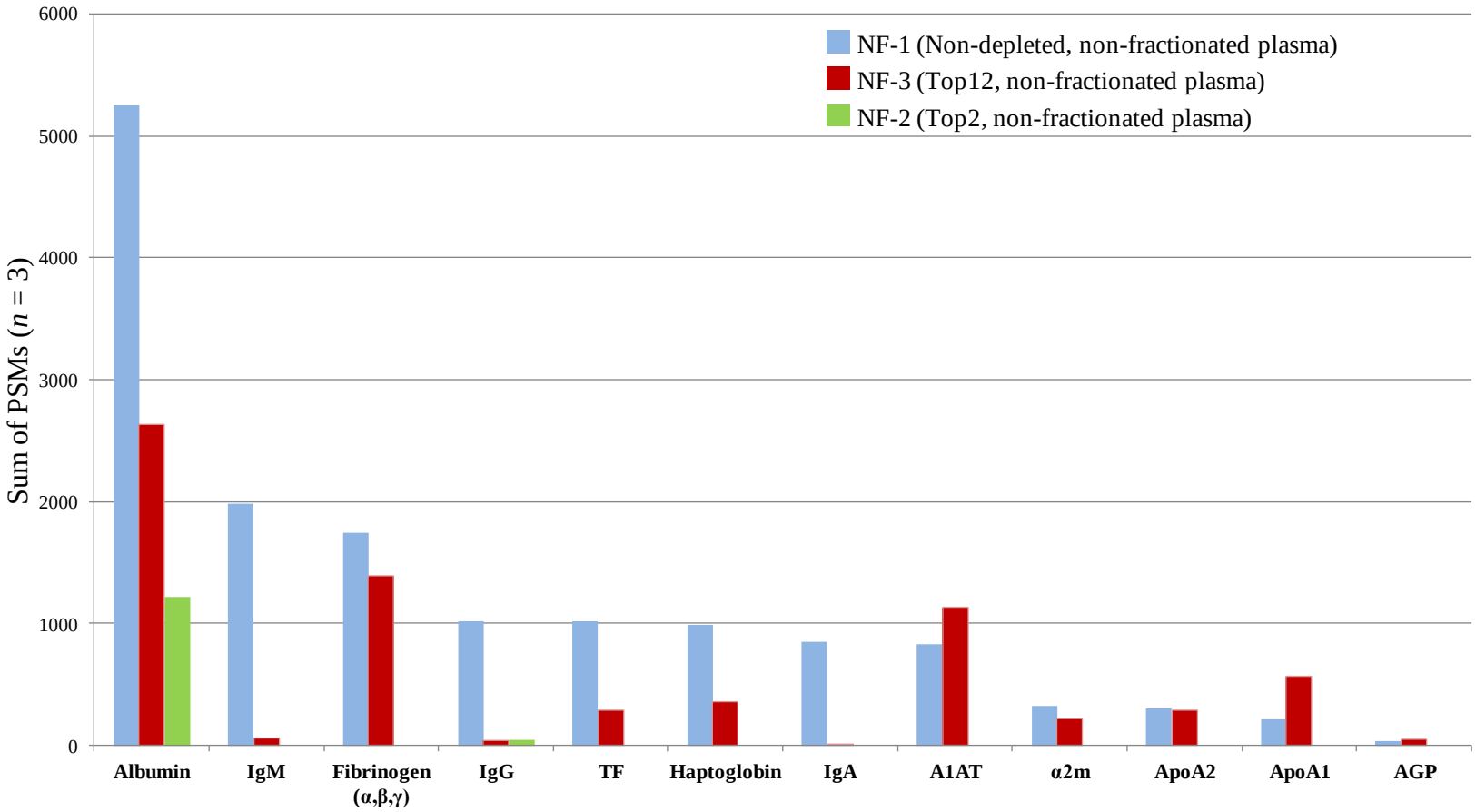

Figure 4-7: Bar chart demonstrating the change in the sum total of PSMs between NF-1 (blue) and NF-3 (red). A reduction was observed for IgA (98.1%), IgM (96.9%), IgG (95.2%), TF (71.8%), haptoglobin (64%), albumin (49.8%), α2m (30.3%), total fibrinogen (21.8%) and apoA2 (3.9%). An increase in PSMs was observed for apoA1 (57.2%), α1AT (26.6%), AGP (3%). Sum PSMs for NF-2 have also been included (green).

Top2 immunodepletion was successful in decreasing the albumin and IgG content by 76.80% and 95.08% respectively (Table 4-3). Even with this large reduction in PSMs, albumin was still the 3rd most abundant protein group in non-fractionated Top2 depleted plasma; however this was not the case when examining fractionated plasma (Table 4-4). It was also apparent that Top2 depletion was more efficient in the removal of albumin whereas IgG removal was comparable across both depletion methods (Figure 4-7).

Table 4-3: Showing the sum of PSMs, rank of abundance and % reduction for both albumin and IgG for methods NF-1 and NF-2. A 76.8% and 95.1% reduction in albumin and IgG PSMs is observed between non-depleted plasma (NF-1) and Top2 depleted plasma (NF-2).

Protein Name	NF-1 (non-depleted plasma)		NF-2 (Top2 depleted plasma)		% Reduction
	Sum of PSMs (n = 3)	Rank	Sum of PSMs (n = 3)	Rank	
albumin	5247	1	1219	3	76.80%
IgG	1017	3	50	60	95.08%

Unsurprisingly, the addition or increase in fractionation resulted in an increase in the number of PSMs attributed to albumin and IgG. At the non-depleted level, 13,521 and 2,644 total PSMs were observed for albumin and IgG's respectively for method 1DGE-4 (non-depleted, 10 fractions). In contrast, 1DGE-7 (non-depleted, 20 fractions) demonstrated a substantial increase; 30,216 and 3,086 PSMs observed for albumin and IgG's respectively.

Fractionation had a large influence on immunodepletion performance. Top2 depletion with both 10 fractions (1DGE-5) and 20 fractions (1DGE-8) demonstrated greater "removal percentage" in albumin and IgG content than non-fractionated methods (Table 4-4). A reduction in of 82.70% in albumin PSMs was observed in 1DGE-5 whereas a 93% reduction was measured in 1DGE-8. This is compared to 76.80% reduction in non-fractionated methods (Table 4-3). A reduction in IgG content was also observed (Table 4-4; Figure 4-8). It was also observed that the

overall abundance rank of albumin and IgG fell exponentially with increasing fractionation (Table 4-4). Top2 depleted non-fractionated (NF-2) plasma ranked albumin and IgG 3rd and 60th most abundant respectively (Table 4-3). However, Top2 10 fraction (1DGE-5) plasma ranked albumin 25th and IgG 115th with Top2 20 fraction (1DGE-8) plasma ranked albumin 40th and IgG 141st respectively (Table 4-4). This demonstrates that the reduction of highly abundant proteins is not solely dependent on the immunocapture strategy employed and that a complementary fractionation step will enhance the impact of immunodepletion further.

Table 4-4: Showing the sum of PSMs, rank of abundance and % reduction for both albumin and IgG for methods 1DGE-4, 1DGE-5, 1DGE-7 and 1DGE-8. An 82.70% and 98.30% reduction in albumin and IgG PSMs was observed between non-depleted 10 fraction plasma (1DGE-4) and Top2 depleted 10 fraction plasma (1DGE-5). A 93% and 97.85% reduction in albumin and IgG content was observed between non-depleted 20 fraction plasma (1DGE-7) and Top2 depleted 20 fraction plasma (1DGE-8). This is an improvement on non-fractionated methods (Table 4-3).

Protein Name	1DGE-4		1DGE-5		% Reduction
	Sum of PSMs (*n* = 3)	Rank	Sum of PSMs (*n* = 3)	Rank	
albumin	13521	1	2330	25	82.70%
IgG	2644	6	45	115	98.30%
Protein Name	**1DGE-7**		**1DGE-8**		**% Reduction**
	Sum of PSMs (*n* = 3)	**Rank**	**Sum of PSMs (*n* = 3)**	**Rank**	
albumin	30216	1	2127	40	93.00%
IgG	3086	5	157	141	97.85%

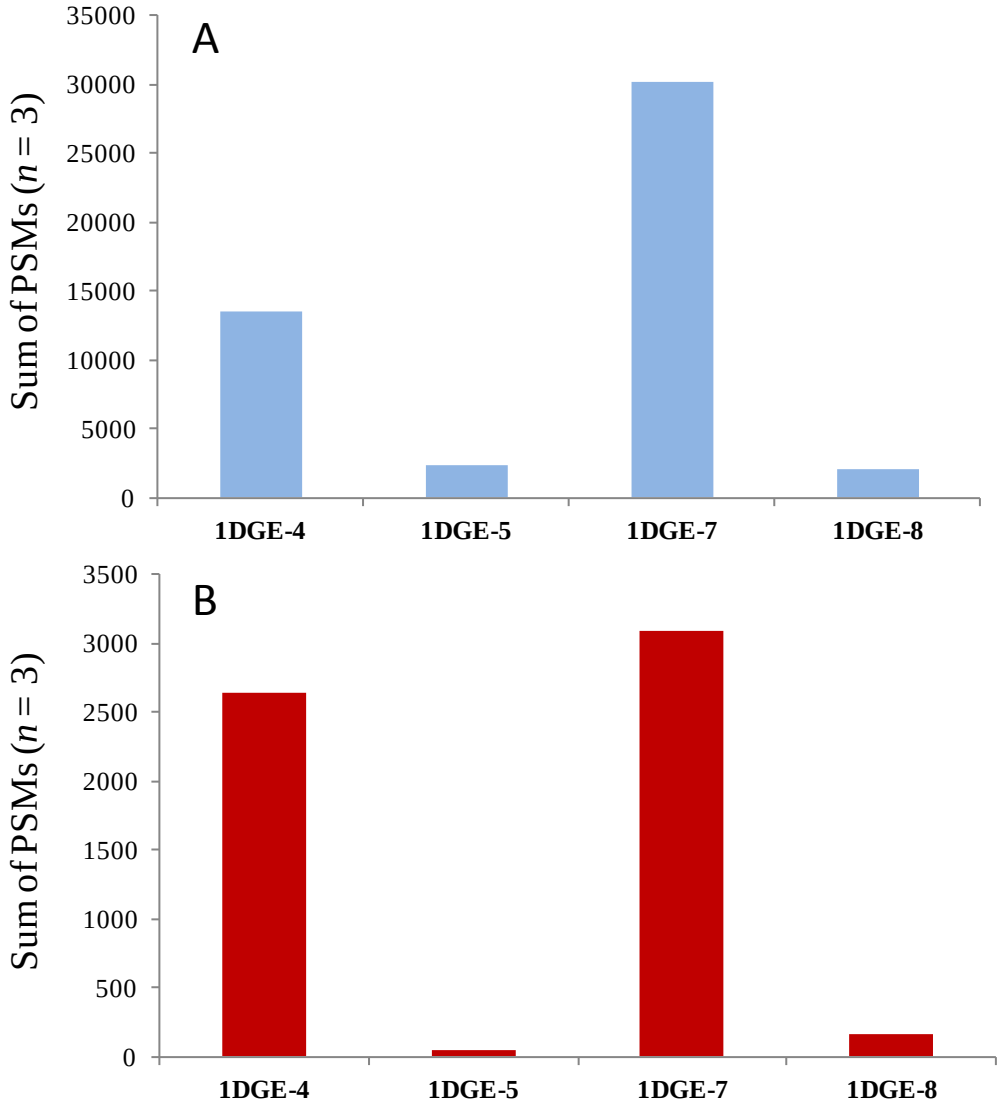

Figure 4-8: Bar charts representing of the performance of (A) albumin and (B) IgG removal between non-depleted fractionated methods (1DGE-4 and 1DGE-7) and Top2 depleted fractionated methods (1DGE-5 and 1DGE-8).

The "albuminome" is a term given to proteins that bind or interact with albumin. Experimental evidence has shown that, together with albumin, a number of proteins are bound to, and may be released from, an anti-albumin resin after plasma/serum immunodepletion. Therefore, we investigated the albumin bound portion of the immunodepletion process to identify any significant removal of albumin bound proteins (Figure 4-9). Proteins significantly observed in the albumin bound portion would have to be discounted as potential biomarkers.

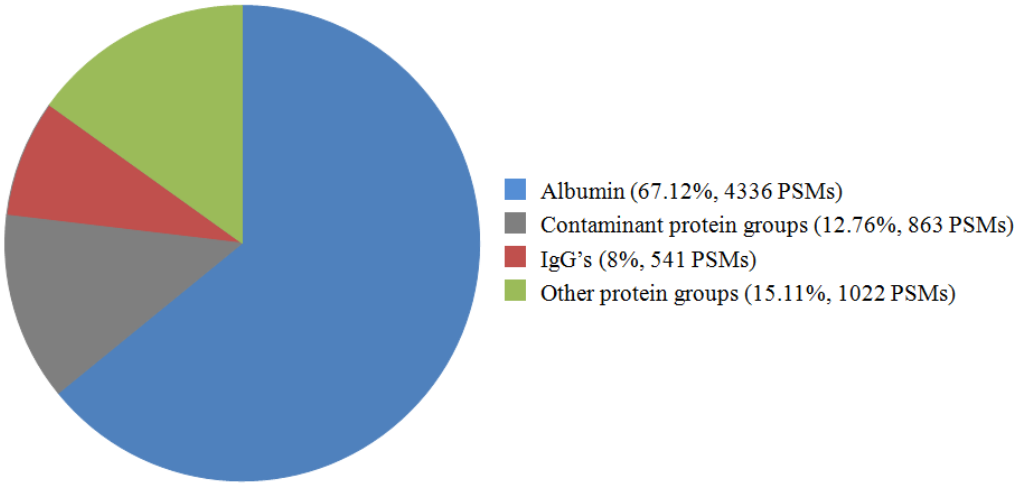

Figure 4-9: Pie chart to demonstrate the content of the albumin bound portion ("albuminome") of the immunodepletion process (Top2 only).

As expected albumin dominated the analysis in the albumin bound portion (67.12%, Figure 4-9). A large portion of contaminant protein groups (trypsin and human epidermal keratins) are also found within the albumin bound portion (12.76%, Figure 4-9). Furthermore, 15.11% of the albumin bound portion was occupied by 34 other plasma protein groups (Table 4-5).

The plasma protein groups found within the albumin bound fraction are displayed in Table 4-5 and are compared to the unbound fraction as a ratio. The majority of protein groups observed in the albumin bound fraction are a small proportion of the total PSMs in unbound fraction (<0.12). However, some protein groups do have a higher abundance in the albumin bound compared with the unbound fraction suggesting that they are significantly bound to albumin or albumin resin in the immunodepletion process (Table 4-5; dermcidin, Immunoglobulin lambda-like polypeptide 5, krev interaction trapped protein 1, probable G-protein coupled receptor 115, Ig kappa chain V-I region DEE and Ig kappa chain C region). Other protein groups have a considerable proportion (>0.40) of PSMs in the albumin bound fraction (Table 4-5; Ig lambda-2 chain C regions, Ig lambda-3 chain C regions, Ig kappa chain V-III region B6, Ig lambda-1 chain C regions). These protein groups should not be considered as disease related biomarkers when analysing plasma that has been through a Top2 depletion process as a considerable quantity of the PSMs will not be present in the unbound fraction.

Table 4-5: Protein groups observed in the albumin bound fraction ("albuminome") when utilising Top2 immunodepletion. Protein groups are ranked by a PSM ratio (albuminome (bound)/unbound). Unbound PSMs are calculated from NF-2 analysis.

UniProt ID	Protein Name	Unbound (PSMs)	"albuminome" (PSMs)	Ratio (albuminome/ unbound)
P81605	dermcidin	1	27	27.00
B9A064	Immunoglobulin lambda-like polypeptide 5	2	40	20.00
O00522	krev interaction trapped protein 1	2	22	11.00
Q8IZF3	probable G-protein coupled receptor 115	4	14	3.50
P01597	Ig kappa chain V-I region DEE	6	20	3.33
P01834	Ig kappa chain C region	130	194	1.49
P0CG05	Ig lambda-2 chain C regions	99	64	0.65
P0CG06	Ig lambda-3 chain C regions	100	64	0.64
P01619	Ig kappa chain V-III region B6	51	32	0.63
P0CG04	Ig lambda-1 chain C regions	99	40	0.40
P69905	hemoglobin subunit alpha	24	3	0.12
P01876	Ig alpha-1 chain C region	161	19	0.12
P01871	Ig mu chain C region	218	22	0.10
P68871	hemoglobin subunit beta	70	7	0.10
P02647	apoA1	595	59	0.10
P01023	α2m	534	47	0.09
P08603	CFH	265	24	0.09
P02671	FGα	510	37	0.07
P00747	plasminogen	149	10	0.07
P02787	TF	1271	72	0.06
P02753	retinol-binding protein 4	237	13	0.05
P02751	fibronectin	111	6	0.05
P0C0L4	C4α	140	7	0.05
P0C0L5	C4β	142	7	0.05
P00751	CFB	111	5	0.05
P02679	FGγ	641	24	0.04
P00738	haptoglobin	485	15	0.03
P01024	CC3	853	25	0.03
P02675	FGβ	815	23	0.03
Q14624	Inter-alpha-trypsin inhibitor heavy chain H4	337	5	0.01
Q86YZ3	hornerin	488	6	0.01
P02766	transthyretin	546	4	0.01
P02652	apoA2	292	2	0.01
P02790	hemopexin	1014	6	0.01

4.4.4 Pathway analysis

Pathway analysis (KEGG and BIOCARTA) was performed on the protein groups identified by each proteomic methodology. This was done to see which pathways, in plasma, could be enriched and if this differed depending on which proteomic methodology was employed. Highly significant over-represented pathways were common between all methodologies (Table 4-6). This included anticipated pathways for blood analysis; complement, metabolic and coagulation pathways as well as protein groups related to cardiovascular diseases, inflammation and autoimmune diseases (Table 4-6).

Table 4-6: DAVID pathway analysis of over-represented KEGG and BIOCARTA terms common to all plasma proteomic methodologies.

KEGG pathway term	BIOCARTA pathway term
Complement and coagulation cascades	Complement Pathway
Staphylococcus aureus infection	Classical Complement Pathway
Systemic lupus erythematosus	Lectin Induced Complement Pathway
Prion diseases	Extrinsic Prothrombin Activation Pathway
Glycolysis / Gluconeogenesis	Alternative Complement Pathway
	Intrinsic Prothrombin Activation Pathway
	Acute Myocardial Infarction
	Fibrinolysis Pathway

The number of unique protein groups detected in OGE-9 method demonstrated significant over-expression (uncorrected *P* value level <0.05) of pathways related to AD, Huntington's disease (HD), neurotrophin signalling, MAPK signalling and GnRH signalling which were not enriched in any other methodology (KEGG pathway analysis, Table 4-7). Furthermore, BIOCARTA pathway analysis demonstrated over-representation for synaptic junction proteins (Table 4-8), highlighting the sensitivity and potential of OGE-9 over other methods to explore the protein groups, within plasma, involved in neurodegenerative disease or CNS processes.

Table 4-7: DAVID pathway analysis of over-represented KEGG terms in a list of protein groups detected by method OGE-9 only.

KEGG term	Protein Group Count	*P* value	*Q* value
Complement and coagulation cascades	54	7.77×10^{-30}	1.49×10^{-27}
Glycolysis / Gluconeogenesis	26	1.14×10^{-06}	1.10×10^{-04}
Pathogenic Escherichia coli infection	24	5.93×10^{-06}	3.79×10^{-04}
Prion diseases	15	4.49×10^{-04}	0.021
Systemic lupus erythematosus	29	9.42×10^{-04}	0.035
Focal adhesion	48	0.002	0.075
Fatty acid elongation in mitochondria	6	0.003	0.091
Butanoate metabolism	13	0.004	0.091
Viral myocarditis	21	0.005	n/s
Alzheimer's disease	33	0.006	n/s
Gap junction	23	0.007	n/s
Neurotrophin signaling pathway	31	0.008	n/s
Pentose phosphate pathway	10	0.011	n/s
Fructose and mannose metabolism	12	0.013	n/s
Citrate cycle (TCA cycle)	11	0.017	n/s
MAPK signaling pathway	47	0.019	n/s
Propanoate metabolism	11	0.021	n/s
GnRH signaling pathway	20	0.025	n/s
Adherens junction	20	0.027	n/s
Huntington's disease	37	0.032	n/s
Cell adhesion molecules (CAMs)	30	0.035	n/s
Regulation of actin cytoskeleton	45	0.039	n/s
Lysine degradation	13	0.034	n/s
Fatty acid metabolism	12	0.039	n/s

Table 4-8: DAVID analysis of over-represented BIOCARTA terms in list of protein groups detected by method OGE-9 only.

BIOCART term	Protein Group Count	*P* value	*Q* value
Complement Pathway	17	5.36×10^{-11}	1.39×10^{-08}
Classical Complement Pathway	12	1.52×10^{-07}	1.97×10^{-05}
Lectin Induced Complement Pathway	12	1.52×10^{-07}	1.97×10^{-05}
Alternative Complement Pathway	10	3.43×10^{-06}	2.96×10^{-04}
Intrinsic Prothrombin Activation Pathway	13	6.91×10^{-06}	4.47×10^{-04}
Extrinsic Prothrombin Activation Pathway	8	0.002	0.086
Glycolysis Pathway	8	0.002	0.086
Acute Myocardial Infarction	8	0.006	n/s
Platelet Amyloid Precursor Protein Pathway	6	0.018	n/s
Synaptic Proteins at the Synaptic Junction	8	0.047	n/s
Monocyte and its Surface Molecules	6	0.047	n/s
Fibrinolysis Pathway	6	0.047	n/s
Neutrophil and Its Surface Molecules	5	0.047	n/s

4.4.5 The detection of brain-derived proteins and the plasma expression of neurodegeneration and CNS injury.

With a focus on neurodegeneration and CNS injury with the added indication from the pathway analyses (Table 4-7 and Table 4-8), we were interested in assessing if brain-derived proteins (BDP) could be measured in plasma. To address this we utilised the Human Protein Atlas (HPA) (http://www.proteinatlas.org/) which illustrates 1,223 genes with elevated protein expression in the cerebral cortex compared with all other tissues [520] (download date from HPA 20/10/2016). We also chose to only cross-reference this HPA list with protein groups that were only detected by methodology OGE-9. OGE-9 was shown to detect a superior number of protein groups and quantified protein groups (Figure 4-2), increased plasma proteome coverage to include the pg/mL range (Figure 4-4 and 4-5) and have pathways over-represented for neurodegeneration and/or CNS processes (Table 4-7 and 4-8). Therefore this methodology would be the most likely to be utilised for

future plasma biomarker studies, compared with the others investigated. OGE-9 alone (OGE-9a and OGE-9b) detected 3,175 unique protein groups (Supplementary Material 4) across three technique repeats and this dataset was mined for suspected BDPs highlighted by HPA.

The OGE-9 plasma dataset demonstrated spectral evidence for 468/1,223 of these highly expressed cerebral cortex proteins (Supplementary Material 5) however a large percentage of these proteins do show evidence of significant peripheral expression. A total of 311/468 proteins have been described as "Group Enriched" (*n* = 88) or "Tissue Enhanced" (*n* = 223) by HPA (Supplementary Material 5). These are proteins that have five-fold higher expression in cerebral cortex but also exhibit substantial expression in other tissues. Therefore these protein groups cannot be exclusively deemed as a BDP.

The "Tissue Enriched" category in HPA (>five-fold increased expression in the cerebral cortex compared with all other tissues) was used as an indication of a BDP candidate, due to high expression in the brain and minimal/no expression in other tissues. In this enriched dataset, which contained 381 cerebral cortex proteins, 157 (99 with $\geq$2 PSMs) had detectable expression in our plasma protein list using automated database searches (Table 4-9). After manual inspection of the assigned spectra, 31 protein groups did not have sufficient *b* and *y* ion evidence to be considered as a confident identification (Table 4-9, highlighted in red). Glial fibrillary acidic protein (GFAP) and oligodendrocytic myelin paranodal and inner loop protein (OPALIN) are the highest scoring cerebral cortex specific proteins in HPA (download version date 20/10/2016). There is adequate support to suggest that these proteins are present within our plasma dataset and MS/MS spectrum are shown (Figure 4-10, 4-11, 4-12 and 4-13). Furthermore, spectral evidence for other high scoring cerebral cortex specific proteins in HPA (myelin-oligodendrocyte glycoprotein (MOG) and β-synuclein (SNCB)) are also displayed (Figure 4-14 and 4-15). Evidence for all other candidate BDPs observed in our plasma dataset is shown by the number PSMs (Table 4-9).

Table 4-9: Protein groups classified as "Tissue Enriched" by HPA that are detected in OGE-9 plasma dataset. The "Tissue Enriched" category in HPA (>five-fold increased expression in the cerebral cortex compared with all other tissues) was used as an indication of a candidate BDP due to high expression in the brain and minimal/none expression in other tissues. In this enriched dataset, which contained 381 cerebral cortex proteins, 157 had detectable expression in the OGE-9 plasma protein list. All MS/MS spectra were manually examined and protein groups that did pass automated database criteria but not manual MS/MS spectra validation (*n* = 31) are highlighted in red.

Gene symbol	Plasma evidence (OGE-9)		Human Protein Atlas (HPA) evidence			
	PPD ID	Number of plasma PSMs	HPA tissue category (Cerebral Cortex)	HPA Rank (Cerebral Cortex)	HPA TS (calculated as the fold change to the 2nd highest tissue)	Cerebral Cortex TS score
GFAP	HPRD_00675	160	Tissue enriched	1	1262	cerebral cortex: 1983.8
OPALIN	HPRD_15521	8	Tissue enriched	2	447	cerebral cortex: 44.7
OMG	HPRD_01257	2	Tissue enriched	6	168	cerebral cortex: 72.2
MOG	HPRD_11831	2	Tissue enriched	17	83	cerebral cortex: 103.3
NCAN	HPRD_02897	5	Tissue enriched	18	82	cerebral cortex: 87.4
SNCB	HPRD_03980	10	Tissue enriched	23	62	cerebral cortex: 146.2
POU3F2	HPRD_02734	1	Tissue enriched	24	60	cerebral cortex: 10.2
FEZF2		1	Tissue enriched	29	54	cerebral cortex: 5.3
PLP1	HPRD_02321	26	Tissue enriched	30	49	cerebral cortex: 1662.8
SLC12A5	HPRD_09469	1	Tissue enriched	33	49	cerebral cortex: 36.6
CSPG5		1	Tissue enriched	34	48	cerebral cortex: 73.7
GPR37L1	HPRD_13603	1	Tissue enriched	37	45	cerebral cortex: 17.6
CACNG8	HPRD_06063	1	Tissue enriched	39	44	cerebral cortex: 12.1
GABRA1	HPRD_00662	1	Tissue enriched	40	44	cerebral cortex: 60.7
HPCA	HPRD_00811	2	Tissue enriched	41	44	cerebral cortex: 75.9
SEZ6		1	Tissue enriched	46	40	cerebral cortex: 28.2
ELAVL3	HPRD_16024	1	Tissue enriched	47	39	cerebral cortex: 31.9

MBP	HPRD_01158	214	Tissue enriched	48	37	cerebral cortex: 1427.5
PCDHGC5	HPRD_07318	1	Tissue enriched	49	37	cerebral cortex: 25.4
GAP43	HPRD_01198	4	Tissue enriched	59	30	cerebral cortex: 188.8
GPM6B		2	Tissue enriched	62	29	cerebral cortex: 439.1
SYN2		1	Tissue enriched	64	29	cerebral cortex: 98.6
TNR		1	Tissue enriched	69	27	cerebral cortex: 36.8
CASKIN1	HPRD_10809	2	Tissue enriched	77	24	cerebral cortex: 8.4
GRIN2B	HPRD_00697	6	Tissue enriched	78	24	cerebral cortex: 5.8
SYN1	HPRD_02433	12	Tissue enriched	82	24	cerebral cortex: 115.5
SNAP25	HPRD_02637	10	Tissue enriched	85	23	cerebral cortex: 916.5
CNTNAP4	HPRD_13079	2	Tissue enriched	91	21	cerebral cortex: 18.2
NRXN1	HPRD_11858	3	Tissue enriched	95	20	cerebral cortex: 65.1
TRIM67		1	Tissue enriched	98	20	cerebral cortex: 4.9
JPH3	HPRD_05589	2	Tissue enriched	107	18	cerebral cortex: 20.0
SCN2A	HPRD_03133	1	Tissue enriched	110	18	cerebral cortex: 31.4
SHANK1	HPRD_05413	9	Tissue enriched	111	18	cerebral cortex: 14.6
SLC4A10		1	Tissue enriched	112	18	cerebral cortex: 31.7
SV2B		3	Tissue enriched	113	18	cerebral cortex: 23.6
AK5	HPRD_10472	2	Tissue enriched	115	17	cerebral cortex: 112.6
LRRTM4		1	Tissue enriched	119	17	cerebral cortex: 10.0
OLFM1	HPRD_09249	5	Tissue enriched	121	17	cerebral cortex: 346.0
RPH3A	HPRD_15273	4	Tissue enriched	123	17	cerebral cortex: 44.8
APC2	HPRD_09802	2	Tissue enriched	126	16	cerebral cortex: 24.2
CTNND2	HPRD_09181	1	Tissue enriched	127	16	cerebral cortex: 67.6
SLC1A2	HPRD_02625	3	Tissue enriched	134	16	cerebral cortex: 195.0
ERC2	HPRD_10810	1	Tissue enriched	137	15	cerebral cortex: 14.3
ACTL6B	HPRD_12419	3	Tissue enriched	144	14	cerebral cortex: 21.1
GABRG1	HPRD_15923	1	Tissue enriched	163	13	cerebral cortex: 13.8

HRH3	HPRD_05162	2	Tissue enriched	167	13	cerebral cortex: 4.8
KIAA1549L		1	Tissue enriched	170	13	cerebral cortex: 16.0
PCDH9	HPRD_04661	1	Tissue enriched	173	13	cerebral cortex: 36.2
SLC1A3	HPRD_02523	10	Tissue enriched	175	13	cerebral cortex: 269.2
CYP46A1	HPRD_04970	5	Tissue enriched	190	12	cerebral cortex: 30.0
DNM1	HPRD_03851	2	Tissue enriched	191	12	cerebral cortex: 162.5
PTPN5	HPRD_01472	1	Tissue enriched	198	12	cerebral cortex: 26.5
C1QL2		1	Tissue enriched	210	11	cerebral cortex: 1.0
CHN1	HPRD_00319	2	Tissue enriched	211	11	cerebral cortex: 327.1
CMTM5	HPRD_06986	1	Tissue enriched	213	11	cerebral cortex: 39.5
GAD2	HPRD_11817	1	Tissue enriched	218	11	cerebral cortex: 11.2
MYT1L		12	Tissue enriched	223	11	cerebral cortex: 30.8
NETO1	HPRD_16264	1	Tissue enriched	225	11	cerebral cortex: 28.0
PCDHA5	HPRD_07323	3	Tissue enriched	229	11	cerebral cortex: 2.0
SV2A		1	Tissue enriched	234	11	cerebral cortex: 83.1
APLP1	HPRD_00102	1	Tissue enriched	236	10	cerebral cortex: 198.0
DSCAM	HPRD_03953	2	Tissue enriched	245	10	cerebral cortex: 6.0
KIF3C	HPRD_04164	17	Tissue enriched	253	10	cerebral cortex: 68.9
NRGN	HPRD_03828	43	Tissue enriched	255	10	cerebral cortex: 429.0
PRKCG	HPRD_01502	8	Tissue enriched	256	10	cerebral cortex: 19.6
RAB3A		1	Tissue enriched	258	10	cerebral cortex: 111.7
SERPINI1	HPRD_03901	1	Tissue enriched	259	10	cerebral cortex: 172.9
SLIT1	HPRD_04773	4	Tissue enriched	262	10	cerebral cortex: 28.0
AMPH	HPRD_02687	3	Tissue enriched	267	9	cerebral cortex: 42.4
ATCAY	HPRD_10491	1	Tissue enriched	269	9	cerebral cortex: 56.9
B4GALNT1	HPRD_03525	2	Tissue enriched	271	9	cerebral cortex: 12.6
BRINP1		3	Tissue enriched	272	9	cerebral cortex: 30.7
CNTNAP2	HPRD_05197	3	Tissue enriched	275	9	cerebral cortex: 15.8

CPNE6	HPRD_05748	1	Tissue enriched	276	9	cerebral cortex: 41.0
KIRREL3	HPRD_09679	4	Tissue enriched	287	9	cerebral cortex: 9.6
LPPR4		5	Tissue enriched	290	9	cerebral cortex: 47.2
MAP2	HPRD_01140	3	Tissue enriched	292	9	cerebral cortex: 157.0
PCDHGB1	HPRD_09389	2	Tissue enriched	294	9	cerebral cortex: 9.6
PRMT8	HPRD_11029	2	Tissue enriched	296	9	cerebral cortex: 9.7
RLBP1	HPRD_01572	2	Tissue enriched	298	9	cerebral cortex: 2.9
SCG3	HPRD_11538	3	Tissue enriched	299	9	cerebral cortex: 144.0
SH3GL2	HPRD_05125	2	Tissue enriched	301	9	cerebral cortex: 89.5
SHISA7		4	Tissue enriched	302	9	cerebral cortex: 8.8
SYP	HPRD_02435	2	Tissue enriched	306	9	cerebral cortex: 264.6
TRIM9	HPRD_05947	4	Tissue enriched	307	9	cerebral cortex: 39.5
ELFN2		2	Tissue enriched	320	8	cerebral cortex: 11.0
FAM155A		1	Tissue enriched	322	8	cerebral cortex: 7.7
GRIN3A	HPRD_09443	1	Tissue enriched	327	8	cerebral cortex: 6.3
NEFL	HPRD_01206	13	Tissue enriched	336	8	cerebral cortex: 151.6
PGM2L1		3	Tissue enriched	339	8	cerebral cortex: 35.4
UNC13A	HPRD_19058	1	Tissue enriched	350	8	cerebral cortex: 16.1
AMER3	HPRD_08241	1	Tissue enriched	352	7	cerebral cortex: 3.5
AP3B2	HPRD_03699	1	Tissue enriched	353	7	cerebral cortex: 17.7
C1QL1	HPRD_12712	2	Tissue enriched	357	7	cerebral cortex: 15.5
CDH10	HPRD_05187	2	Tissue enriched	362	7	cerebral cortex: 18.1
CNKSR2	HPRD_06473	1	Tissue enriched	369	7	cerebral cortex: 28.3
CNP	HPRD_00448	27	Tissue enriched	370	7	cerebral cortex: 294.9
FGFBP3		2	Tissue enriched	375	7	cerebral cortex: 8.7
LHFPL4		1	Tissue enriched	390	7	cerebral cortex: 11.1
MAP1A	HPRD_02549	7	Tissue enriched	392	7	cerebral cortex: 82.9
NAPB	HPRD_17627	1	Tissue enriched	395	7	cerebral cortex: 156.1

PTPRZ1	HPRD_01481	4	Tissue enriched	405	7	cerebral cortex: 135.2
RUNDC3A	HPRD_16106	6	Tissue enriched	410	7	cerebral cortex: 91.3
SCN8A	HPRD_09006	2	Tissue enriched	412	7	cerebral cortex: 11.2
SMIM18		6	Tissue enriched	418	7	cerebral cortex: 4.7
SOGA3		1	Tissue enriched	420	7	cerebral cortex: 1.3
STXBP1	HPRD_04235	3	Tissue enriched	426	7	cerebral cortex: 193.7
TAGLN3	HPRD_12136	1	Tissue enriched	427	7	cerebral cortex: 179.4
TPPP	HPRD_18522	9	Tissue enriched	428	7	cerebral cortex: 74.9
TUBB2A		133	Tissue enriched	429	7	cerebral cortex: 234.6
ANKS1B		4	Tissue enriched	435	6	cerebral cortex: 53.9
ASIC4		5	Tissue enriched	440	6	cerebral cortex: 4.8
BAI1	HPRD_04062	4	Tissue enriched	443	6	cerebral cortex: 9.2
BAI3	HPRD_04064	2	Tissue enriched	444	6	cerebral cortex: 30.0
CAMK2A	HPRD_06532	9	Tissue enriched	450	6	cerebral cortex: 136.1
CHD5	HPRD_10828	7	Tissue enriched	453	6	cerebral cortex: 20.6
DCLK2		1	Tissue enriched	456	6	cerebral cortex: 46.1
DLG4	HPRD_04199	1	Tissue enriched	459	6	cerebral cortex: 82.7
DLGAP1	HPRD_09260	1	Tissue enriched	460	6	cerebral cortex: 46.8
EFR3B	HPRD_13824	1	Tissue enriched	463	6	cerebral cortex: 16.2
ENO2	HPRD_00573	16	Tissue enriched	464	6	cerebral cortex: 215.7
FEZ1		1	Tissue enriched	469	6	cerebral cortex: 200.4
FMN2	HPRD_10449	2	Tissue enriched	471	6	cerebral cortex: 29.8
GABRA3	HPRD_02375	1	Tissue enriched	473	6	cerebral cortex: 15.2
GABRA4	HPRD_08839	1	Tissue enriched	474	6	cerebral cortex: 8.0
GNAO1	HPRD_00757	11	Tissue enriched	476	6	cerebral cortex: 209.4
GRIK3	HPRD_00691	2	Tissue enriched	481	6	cerebral cortex: 9.7
GRIN2A	HPRD_00698	8	Tissue enriched	482	6	cerebral cortex: 14.2
GRM2	HPRD_04977	1	Tissue enriched	484	6	cerebral cortex: 2.0

HCN1	HPRD_09099	12	Tissue enriched	485	6	cerebral cortex: 10.0
JAKMIP2	HPRD_11090	1	Tissue enriched	488	6	cerebral cortex: 16.7
KCNC1	HPRD_15936	3	Tissue enriched	489	6	cerebral cortex: 7.6
KIAA0513		2	Tissue enriched	496	6	cerebral cortex: 51.8
LRRC4C	HPRD_12303	1	Tissue enriched	503	6	cerebral cortex: 17.2
NECAB1		2	Tissue enriched	508	6	cerebral cortex: 41.6
NLGN3	HPRD_02275	3	Tissue enriched	510	6	cerebral cortex: 29.7
NRXN2	HPRD_11859	3	Tissue enriched	512	6	cerebral cortex: 64.2
NSF	HPRD_03380	1	Tissue enriched	513	6	cerebral cortex: 117.5
POU3F4		5	Tissue enriched	520	6	cerebral cortex: 3.5
RAB6B		2	Tissue enriched	526	6	cerebral cortex: 106.1
SYT16		1	Tissue enriched	536	6	cerebral cortex: 7.2
VSNL1	HPRD_02890	1	Tissue enriched	545	6	cerebral cortex: 382.8
YWHAH	HPRD_00215	38	Tissue enriched	547	6	cerebral cortex: 462.5
BEND6		1	Tissue enriched	556	5	cerebral cortex: 18.9
BSN	HPRD_04933	5	Tissue enriched	557	5	cerebral cortex: 14.0
CELF5		1	Tissue enriched	560	5	cerebral cortex: 17.2
GAREML		3	Tissue enriched	578	5	cerebral cortex: 10.9
IBSP		6	Tissue enriched	585	5	cerebral cortex: 0.8
IDS	HPRD_02402	1	Tissue enriched	586	5	cerebral cortex: 233.3
KIF5C	HPRD_18371	2	Tissue enriched	593	5	cerebral cortex: 111.0
MEGF10		1	Tissue enriched	598	5	cerebral cortex: 7.9
PPFIA2	HPRD_04392	4	Tissue enriched	607	5	cerebral cortex: 30.2
SEZ6L	HPRD_08449	2	Tissue enriched	613	5	cerebral cortex: 43.3
SLC24A2		2	Tissue enriched	614	5	cerebral cortex: 27.2
SPTBN4	HPRD_09372	8	Tissue enriched	617	5	cerebral cortex: 8.4
UCHL1	HPRD_01877	9	Tissue enriched	625	5	cerebral cortex: 212.5
BDNF	HPRD_00214	18	Tissue enriched	665	5	cerebral cortex: 10.0

Abbreviations: PPD, plasma protein database; HPA, Human protein atlas; TS, Tissue score,

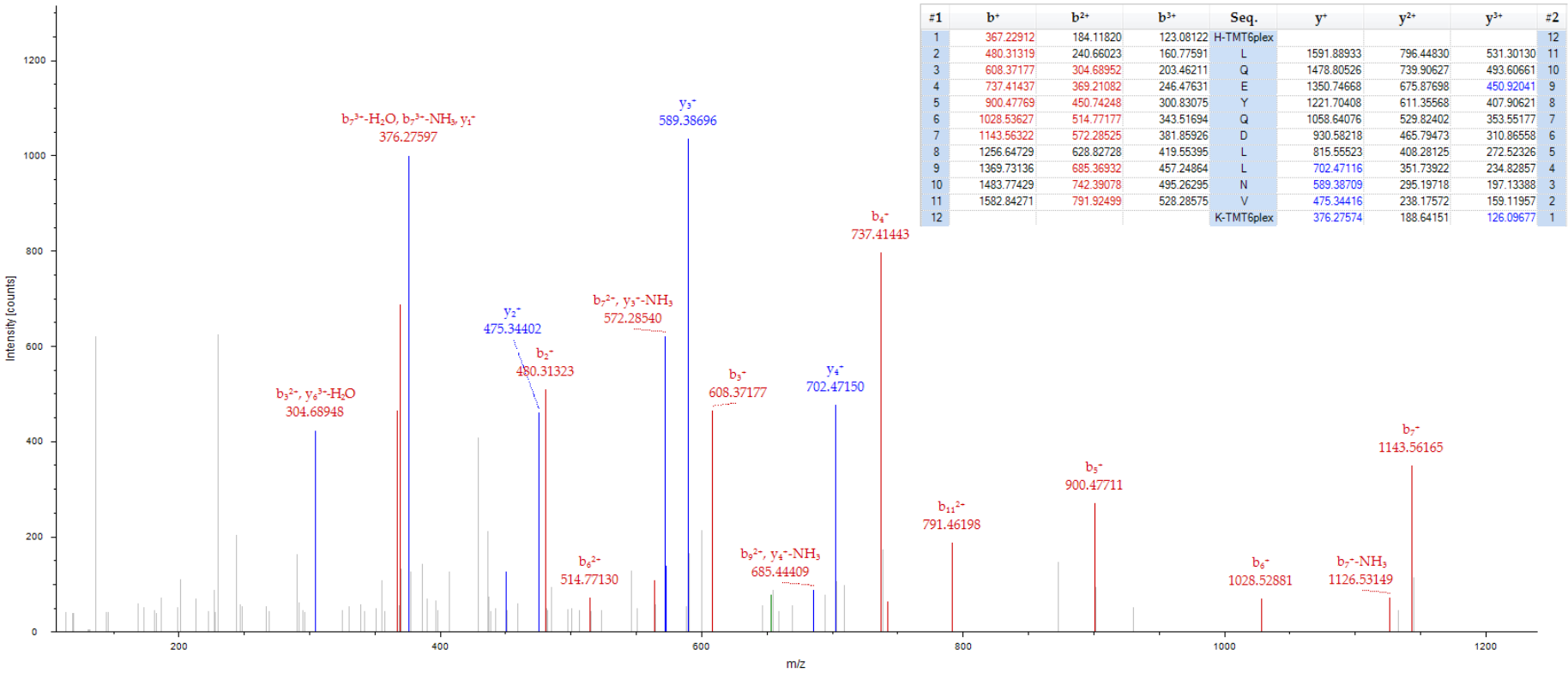

#1	b⁺	b²⁺	b³⁺	Seq.	y⁺	y²⁺	y³⁺	#2
1	367.22912	184.11820	123.08122	H-TMT6plex				12
2	480.31319	240.66023	160.77591	L	1591.88933	796.44830	531.30130	11
3	608.37177	304.68952	203.46211	Q	1478.80526	739.90627	493.60661	10
4	737.41437	369.21082	246.47631	E	1350.74668	675.87698	450.92041	9
5	900.47769	450.74248	300.83075	Y	1221.70408	611.35568	407.90621	8
6	1028.53627	514.77177	343.51694	Q	1058.64076	529.82402	353.55177	7
7	1143.56322	572.28525	381.85926	D	930.58218	465.79473	310.86558	6
8	1256.64729	628.82728	419.55395	L	815.55523	408.28125	272.52326	5
9	1369.73136	685.36932	457.24864	L	702.47116	351.73922	234.82857	4
10	1483.77429	742.39078	495.26295	N	589.38709	295.19718	197.13388	3
11	1582.84271	791.92499	528.28575	V	475.34416	238.17572	159.11957	2
12				K-TMT6plex	376.27574	188.64151	126.09677	1

Figure 4-10: MS/MS spectrum of *m/z* 653.37 the $[M+3H]^{3+}$ molecular ion for a peptide of 1958.11 Da with corresponding sequence HLQEYQDLLNVK unique to GFAP.

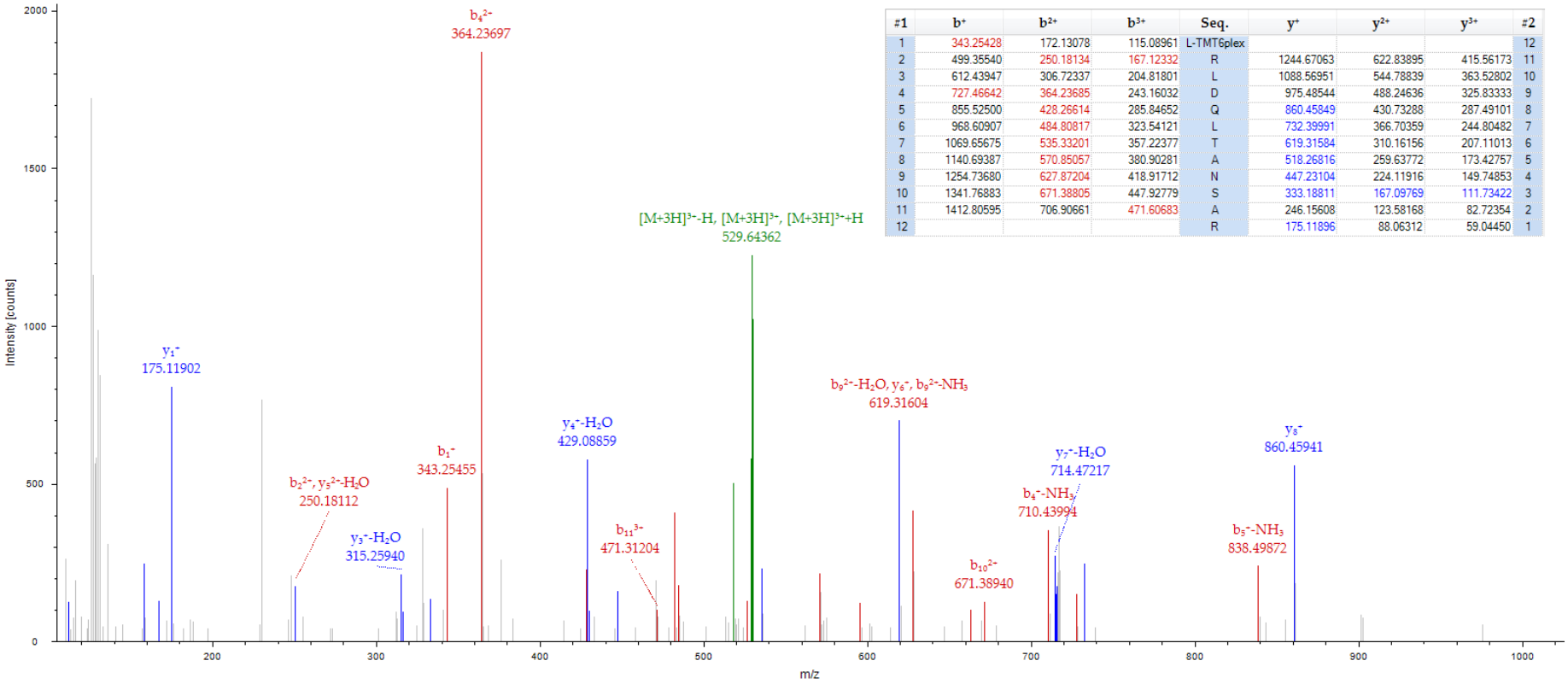

#1	b⁺	b²⁺	b³⁺	Seq.	y⁺	y²⁺	y³⁺	#2
1	343.25428	172.13078	115.08961	L-TMT6plex				12
2	499.35540	250.18134	167.12332	R	1244.67063	622.83895	415.56173	11
3	612.43947	306.72337	204.81801	L	1088.56951	544.78839	363.52802	10
4	727.46642	364.23685	243.16032	D	975.48544	488.24636	325.83333	9
5	855.52500	428.26614	285.84652	Q	860.45849	430.73288	287.49101	8
6	968.60907	484.80817	323.54121	L	732.39991	366.70359	244.80482	7
7	1069.65675	535.33201	357.22377	T	619.31584	310.16156	207.11013	6
8	1140.69387	570.85057	380.90281	A	518.26816	259.63772	173.42757	5
9	1254.73680	627.87204	418.91712	N	447.23104	224.11916	149.74853	4
10	1341.76883	671.38805	447.92779	S	333.18811	167.09769	111.73422	3
11	1412.80595	706.90661	471.60683	A	246.15608	123.58168	82.72354	2
12				R	175.11896	88.06312	59.04450	1

Figure 4-11: MS/MS spectrum of *m/z* 529.64 the $[M+3H]^{3+}$ molecular ion for a peptide of 1586.91 Da with corresponding sequence LRLDQLTANSAR unique to GFAP.

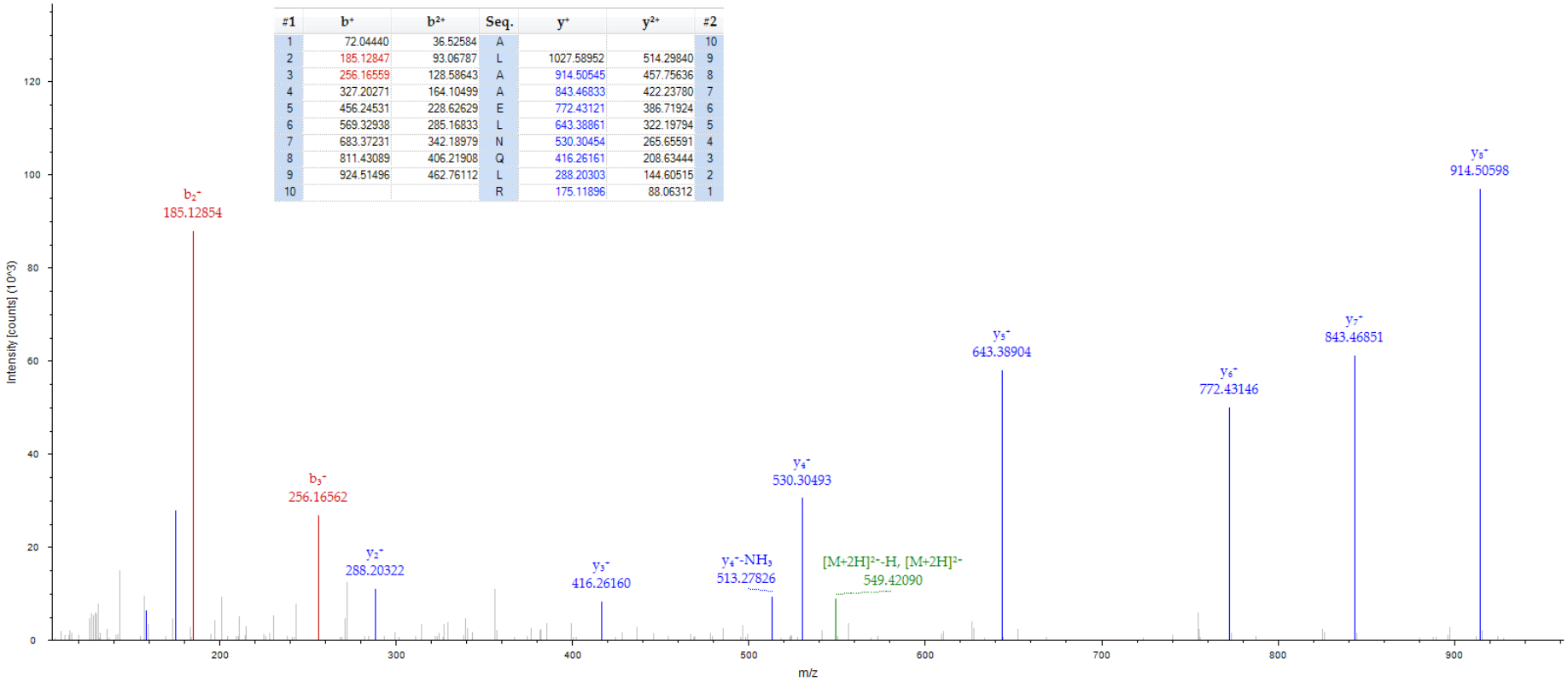

Figure 4-12: MS/MS spectrum of m/z 549.81 the $[M+2H]^{2}$+ molecular ion for a peptide of 1098.62 Da with corresponding sequence ALAAELNQLR unique to GFAP.

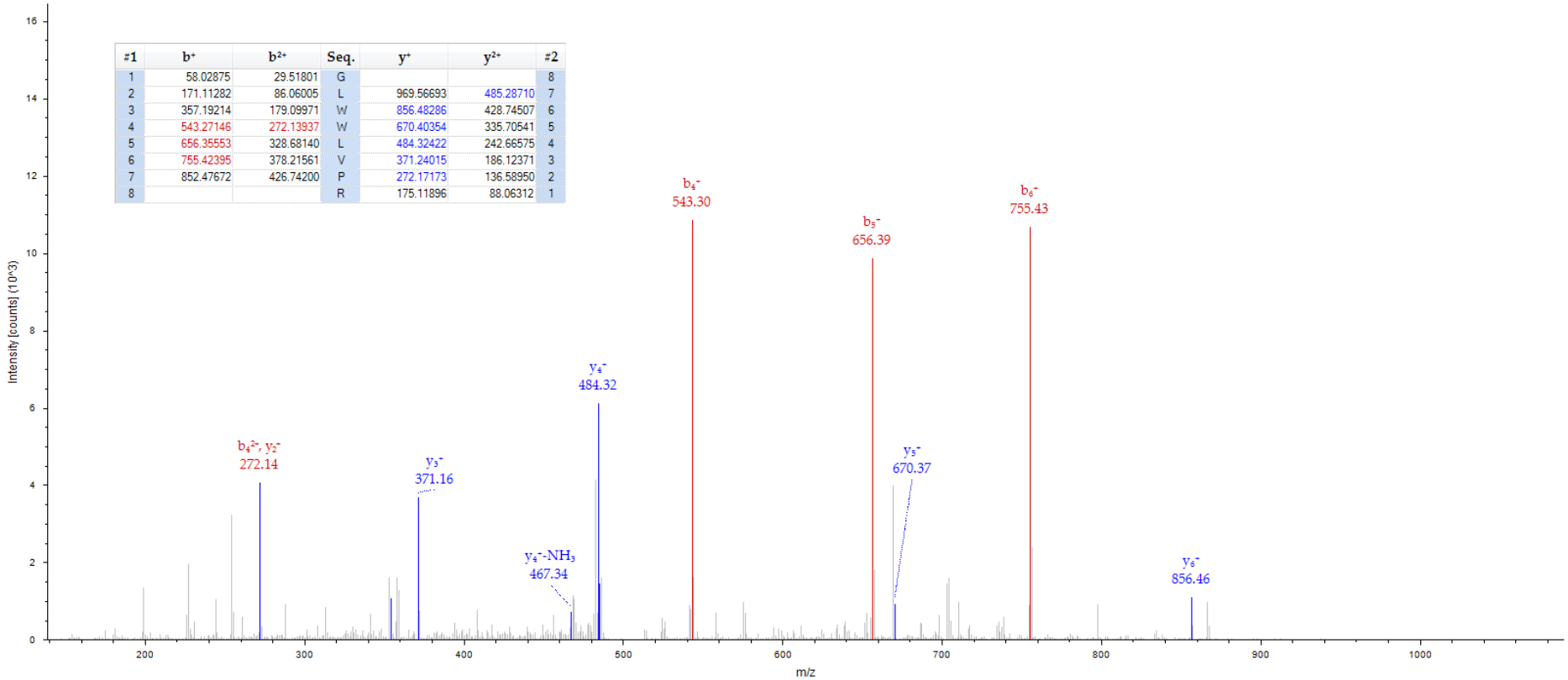

Figure 4-13: MS/MS spectrum of m/z 513.80 the $[M+2H]^{2}$+ molecular ion for a peptide of 1026.59 Da with corresponding sequence GLWWLVPR unique to OPALIN.

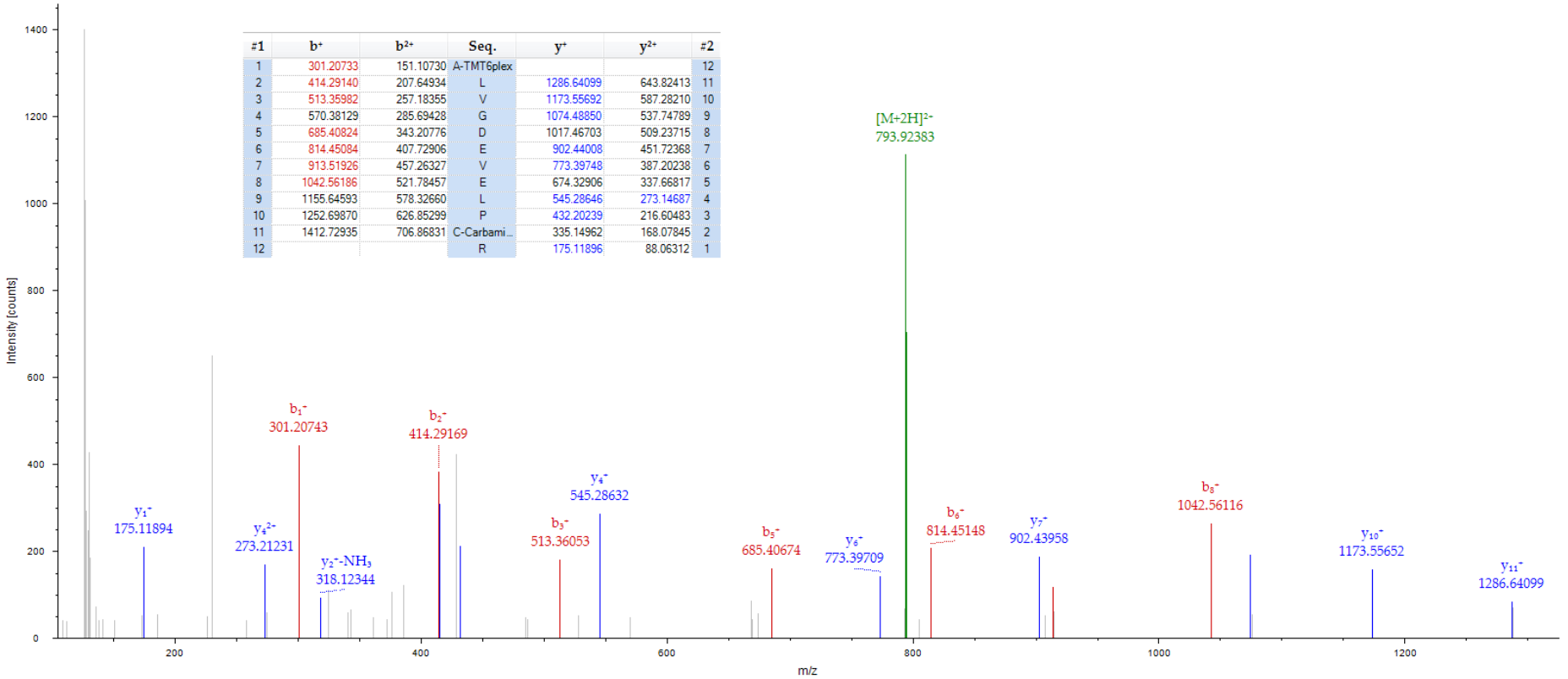

Figure 4-14: MS/MS spectrum of m/z 793.92 the $[M+2H]^{2}$+ molecular ion for a peptide of 1586.83 Da with corresponding sequence ALVGDEVELPCR unique to MOG.

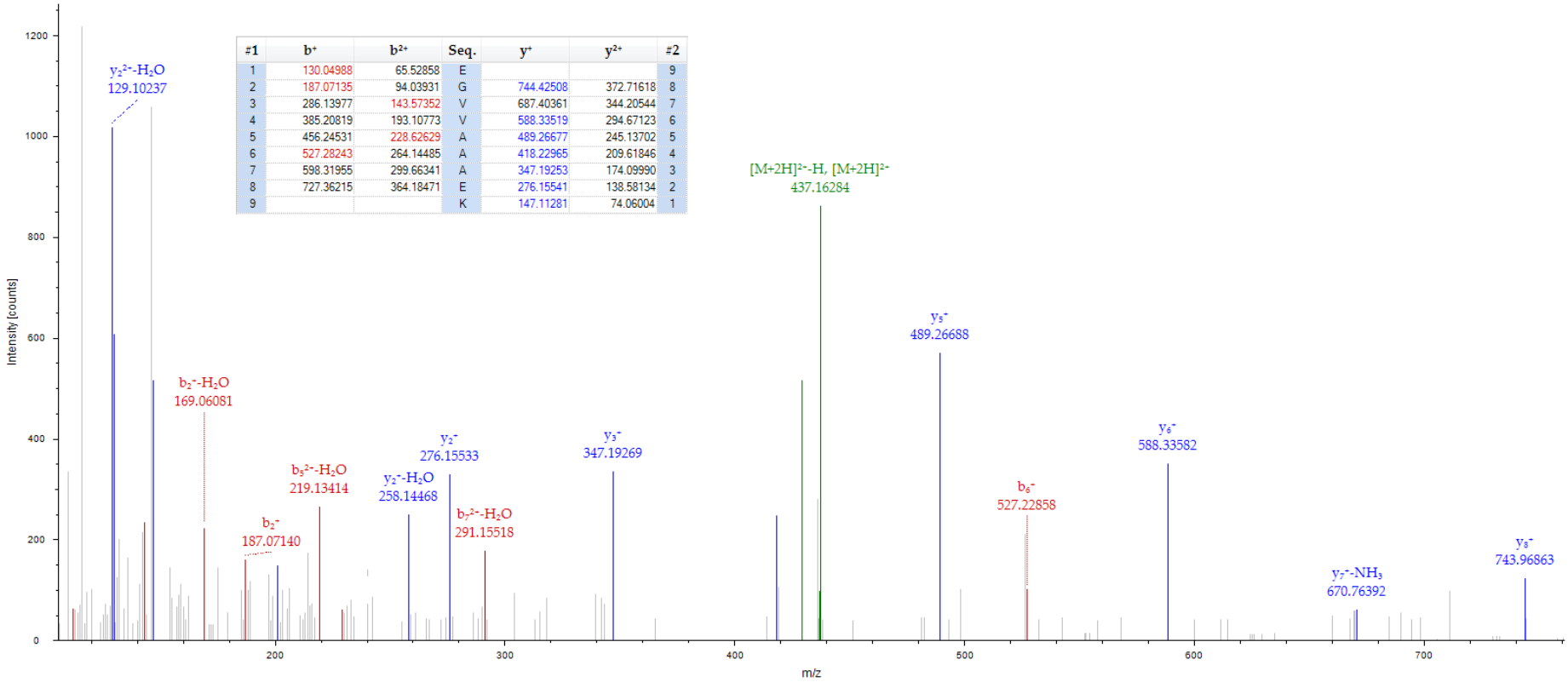

Figure 4-15: MS/MS spectrum of m/z 437.23 the $[M+2H]^{2}$+ molecular ion for a peptide of 873.46 Da with corresponding sequence EGVVAAAEK unique to SNCB.

Additionally, mining the OGE-9 plasma dataset revealed evidence for protein groups implicated in neurodegenerative pathogenesis. A number of proteins that have significant involvement in AD, DLB, PD, other tauopathies, Amyotrophic lateral sclerosis (ALS) and Polyglutamine diseases were identified (Table 4-10). Furthermore, proteins that been highlighted to have roles in neuronal injury, dendritic spines, post/pre-synaptic function as well as blood-brain barrier (BBB) breakdown also have been detected (Table 4-10). The spectral MS/MS evidence for these protein group identifications are shown from Figure 4-16 to Figure 4-29.

Table 4-10: Proteins detected in the OGE-9 plasma dataset that are involved in neurodegenerative pathogenesis or CNS injury/damage. All MS/MS spectra were manually examined and protein groups that did pass automated database criteria but not manual MS/MS spectra validation (*n* = 6) are highlighted in red.

Protein Description	Total PSMs	MS/MS evidence	Action/Disease
α-synuclein (SNCA)	218	Good (Fig 4-16, 4-17)	Protein aggregation in AD, PD, DLB and MSA. Preparation of synaptic vesicles in pre-synaptic terminals.
amyloid beta A4 protein (Aβ)	57	Good (Fig 4-18, 4-20)	Protein aggregation in AD, amyloidopathies and DLB. CSF biomarker for NAB. Processing generates the Aβ peptides deposited in Aβ plaques.
β-secretase 1 (BACE1)	8	Poor (n/a)	Proteolytic processing of APP.
glial fibrillary acidic protein (GFAP)	160	Good (Fig 4-10, 4-11, 4-12)	Implicated in TBI and BBB dysfunction and acute astroglial injury.
microtubule-associated protein tau (MAPT)	13	Poor (n/a)	Protein aggregation in AD, FTD, PD and tauopathies. Hyperphosphorylated tau aggregated in neurons.
neurogranin (NRGN)	43	Moderate (Fig 4-20)	Implicated in Schizophrenia (SZ). A CSF biomarker for AD and synaptic loss. Post-synaptic protein that binds to calcium calmodulin and that may regulate calcium influx when neurons fire; a substrate for protein kinase C, an enzyme that phosphorylates proteins.

neurofilament light polypeptide (NEFL)	13	Good/Moderate (Fig 4-21, 4-22)	CSF biomarker in AD and FTD. Neuroaxonal injury.
neuromodulin (GAP43)	4	Moderate (Fig 4-23)	Implicated in AD and FTD. Pre-synaptic neuronal growth membrane protein that is important for axonal growth and synaptic plasticity.
neuron specific enolase (ENO2)	10	Moderate (Fig 4-24)	Marker of BBB dysfunction.
protein DJ-1 (PARK7)	26	Moderate (Fig 4-25, 4-26)	Autosomal recessive early onset Parkinson's disease. PARK7 inhibits the aggregation of α-synuclein.
ras-related protein Rab-3A (RAB3A)	2	Moderate (Fig 4-27)	Synaptic vesicle protein that directs membrane trafficking and docking.
S100B	25	Moderate (Fig 4-29)	Astroglial injury and marker BBB dysfunction
superoxide dismutase [Cu-Zn] (SOD1)	3	Moderate (Fig 4-28)	Protein aggregation in ALS. SOD1 provides a defence against oxygen toxicity.
synapsin-1 (SYN1)	12	Good (Fig 4-30)	Regulation of neurotransmitter release.
synaptosomal-associated protein 25 (SNAP25)	10	Poor (n/a)	Marker of functional synapses. A component of the SNARE complex.
synaptophysin (STP)	2	Poor (n/a)	Pre-synaptic vesicle protein involved in the release and accumulation docking of synaptic proteins.
synaptotagmin (SYT1)	5	Poor (n/a)	Synaptic membrane protein that triggers synaptic vesicle fusion.
TAR DNA-binding protein 43 (TDP43)	2	Poor (n/a)	Protein aggregation in ALS.

Abbreviations: PD, Parkinson's disease; DLB, Dementia with Lewy Bodies; MSA, Multiple system atrophy; SZ, Schizophrenia; *TBI, Traumatic brain injury; BBB, Blood-brain barrier; FTD, Frontotemporal dementia; ALS, Amyotrophic lateral* sclerosis*; SNARE, Soluble NSF attachment Protein Receptor.*

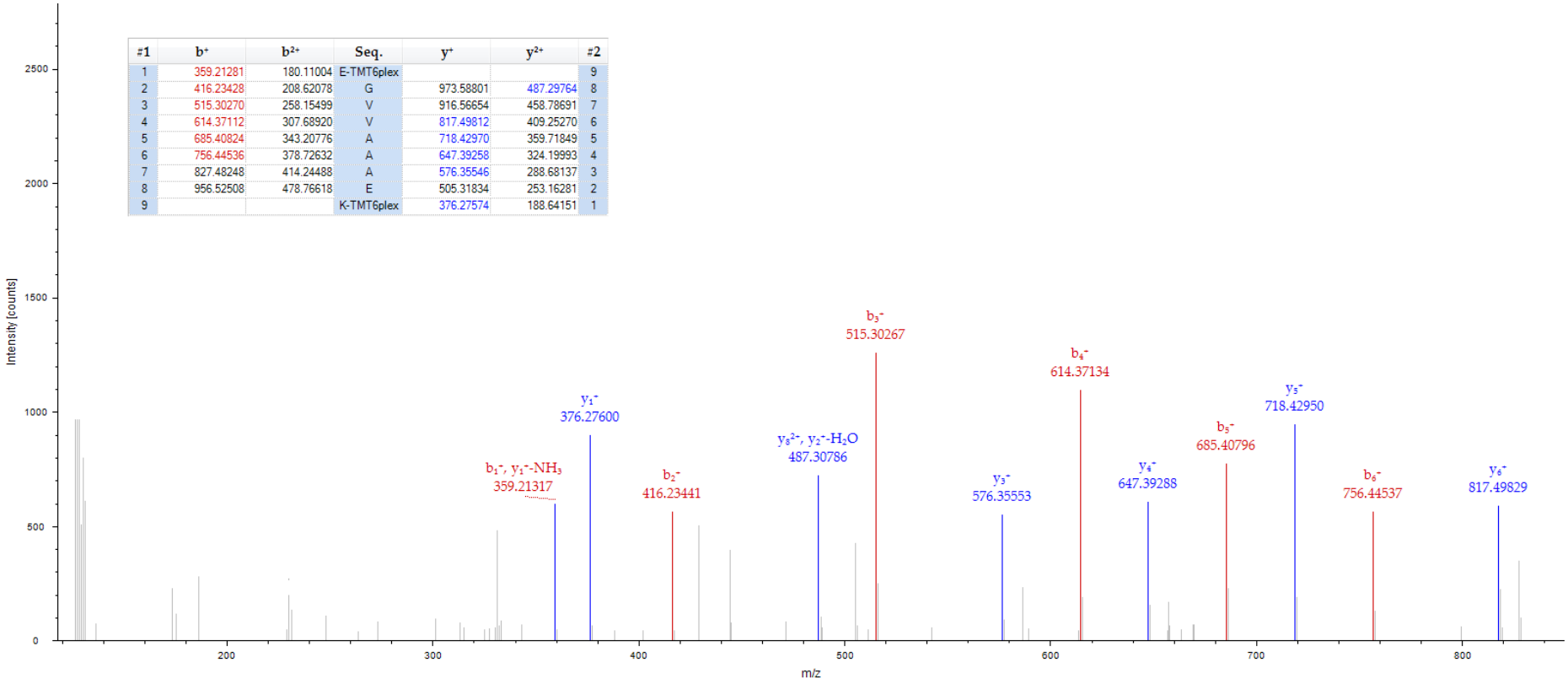

Figure 4-16: MS/MS spectrum of m/z 666.39 the $[M+2H]^{2+}$ molecular ion for a peptide of 1331.79 Da with corresponding sequence EGVVAAAEK unique to SNCA.

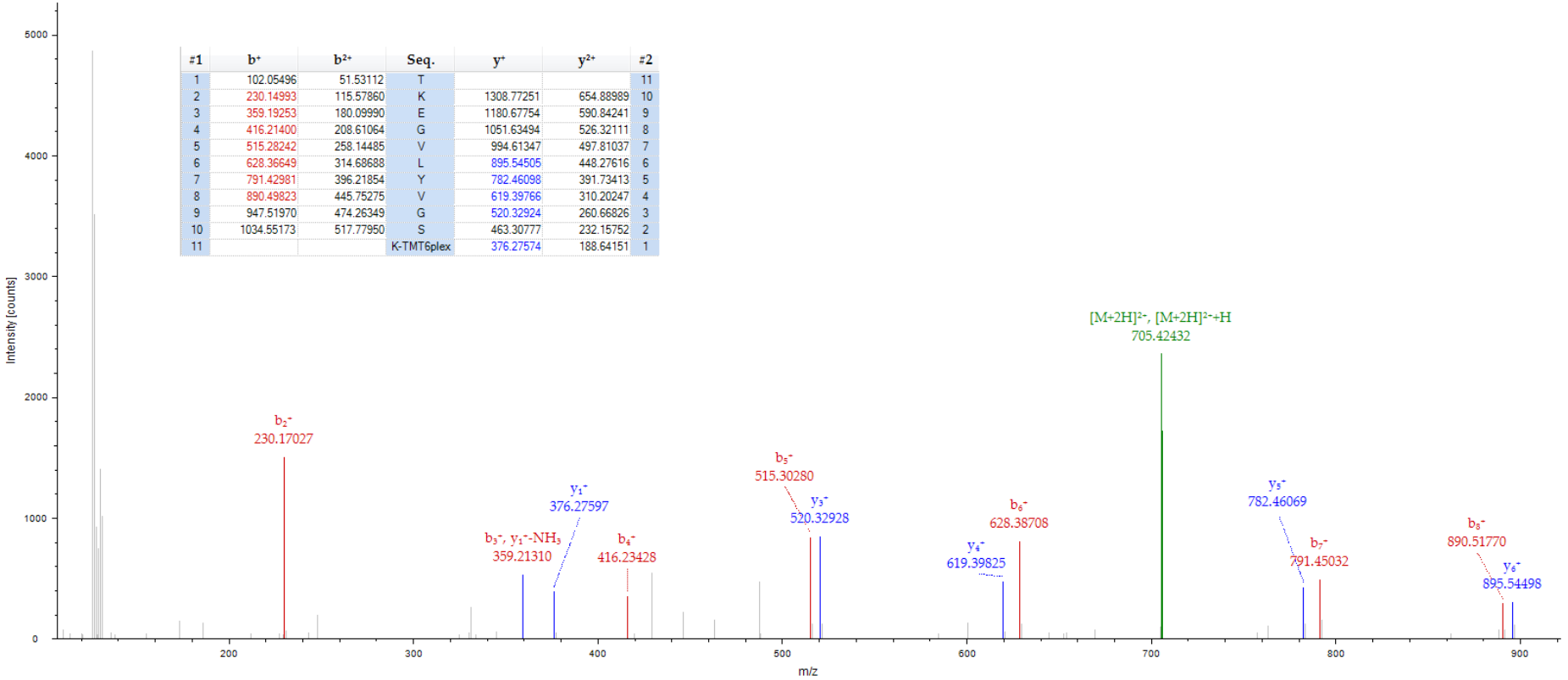

Figure 4-17: MS/MS spectrum of m/z 705.42 the $[M+2H]^{2+}$ molecular ion for a peptide of 1409.83 Da with corresponding sequence TKEGVLYVGSK unique to SNCA

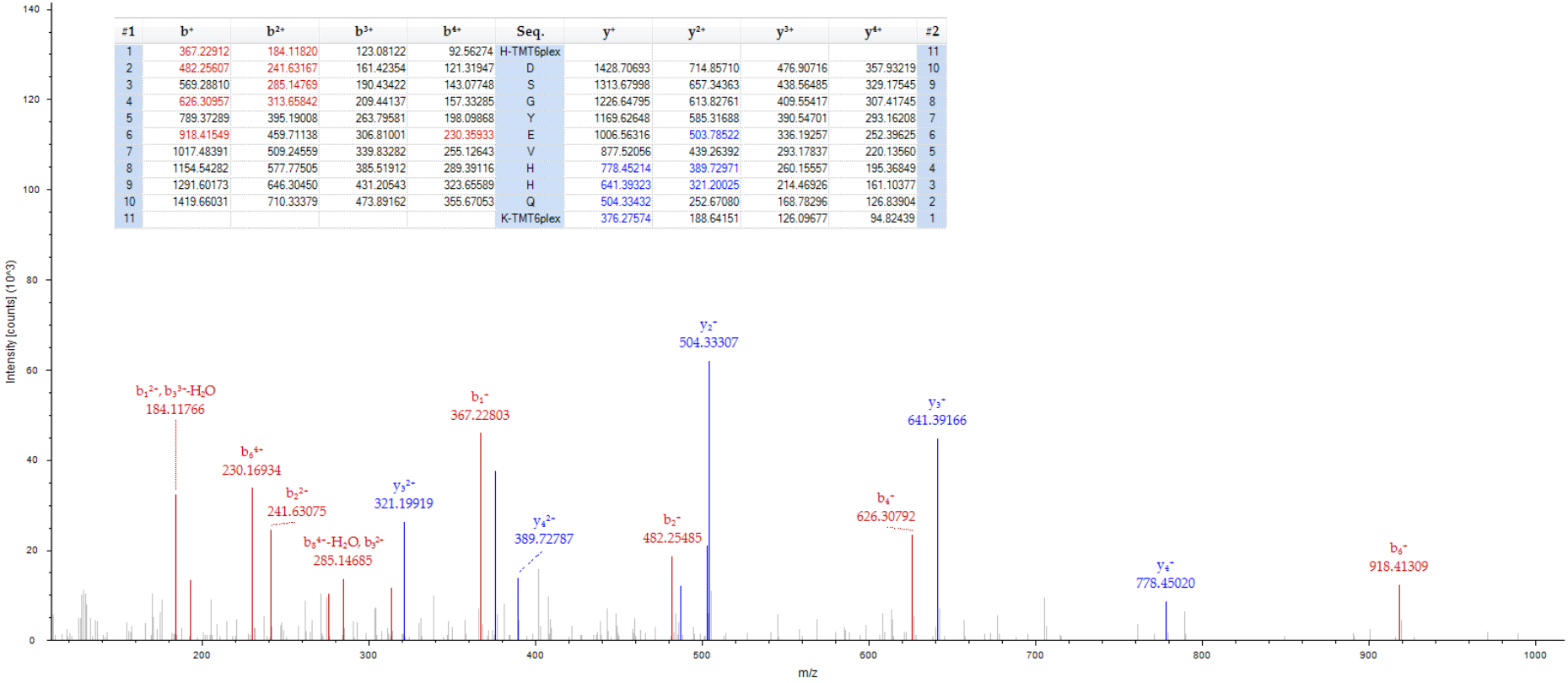

Figure 4-18: MS/MS spectrum of m/z 449.48 the $[M+4H]^{4+}$ molecular ion for a peptide of 1794.92 Da with corresponding sequence HDSGYEVHHQK unique to Aβ.

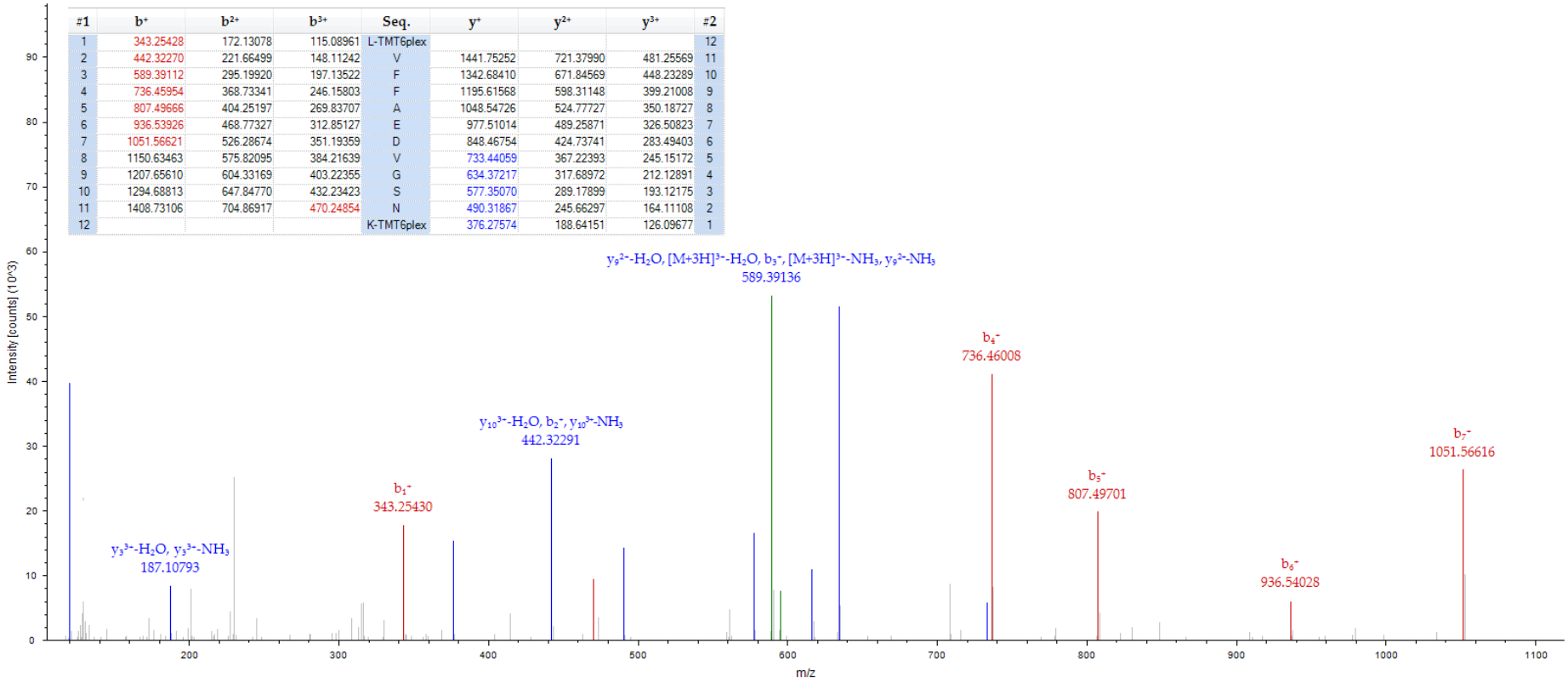

Figure 4-19: MS/MS spectrum of m/z 595.33 the $[M+3H]^{3+}$ molecular ion for a peptide of 1783.99 Da with corresponding sequence LVFFAEDVGSNK unique to Aβ.

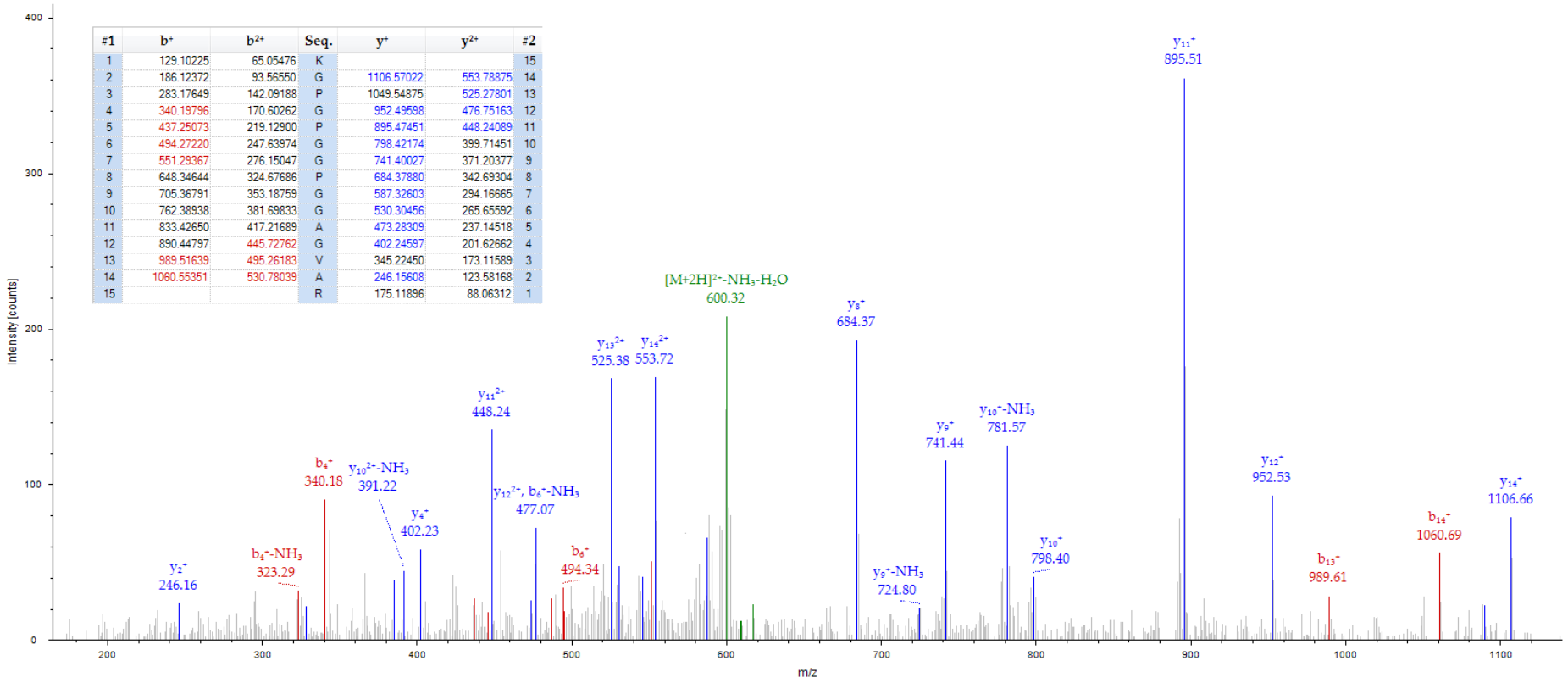

Figure 4-20: MS/MS spectrum of m/z 617.83 the $[M+2H]^{2+}$ molecular ion for a peptide of 1234.66 Da with corresponding sequence KGPGPGGPGGAGVAR unique to NRGN.

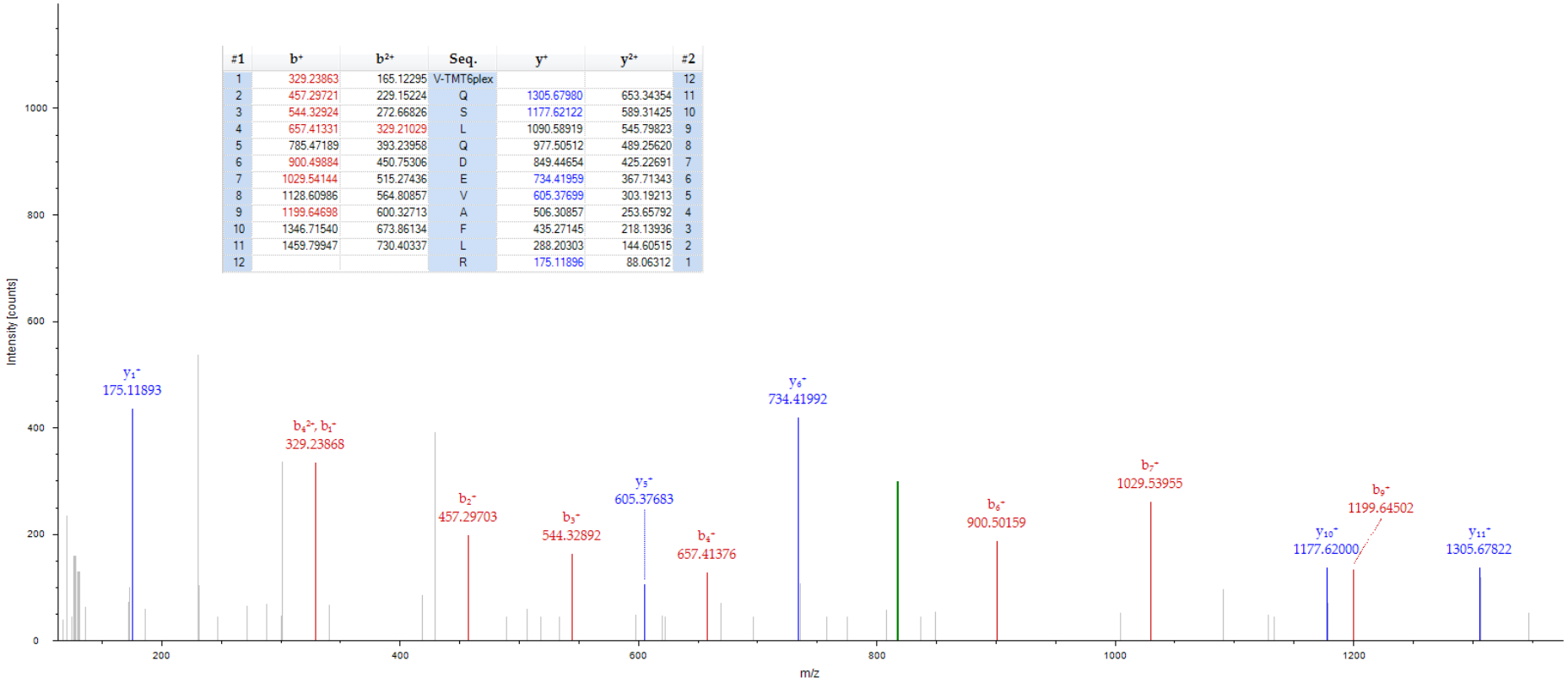

Figure 4-21: MS/MS spectrum of m/z 817.45 the $[M+2H]^{2+}$ molecular ion for a peptide of 1633.90 Da with corresponding sequence VQSLQDEVAFLR unique to NEFL.

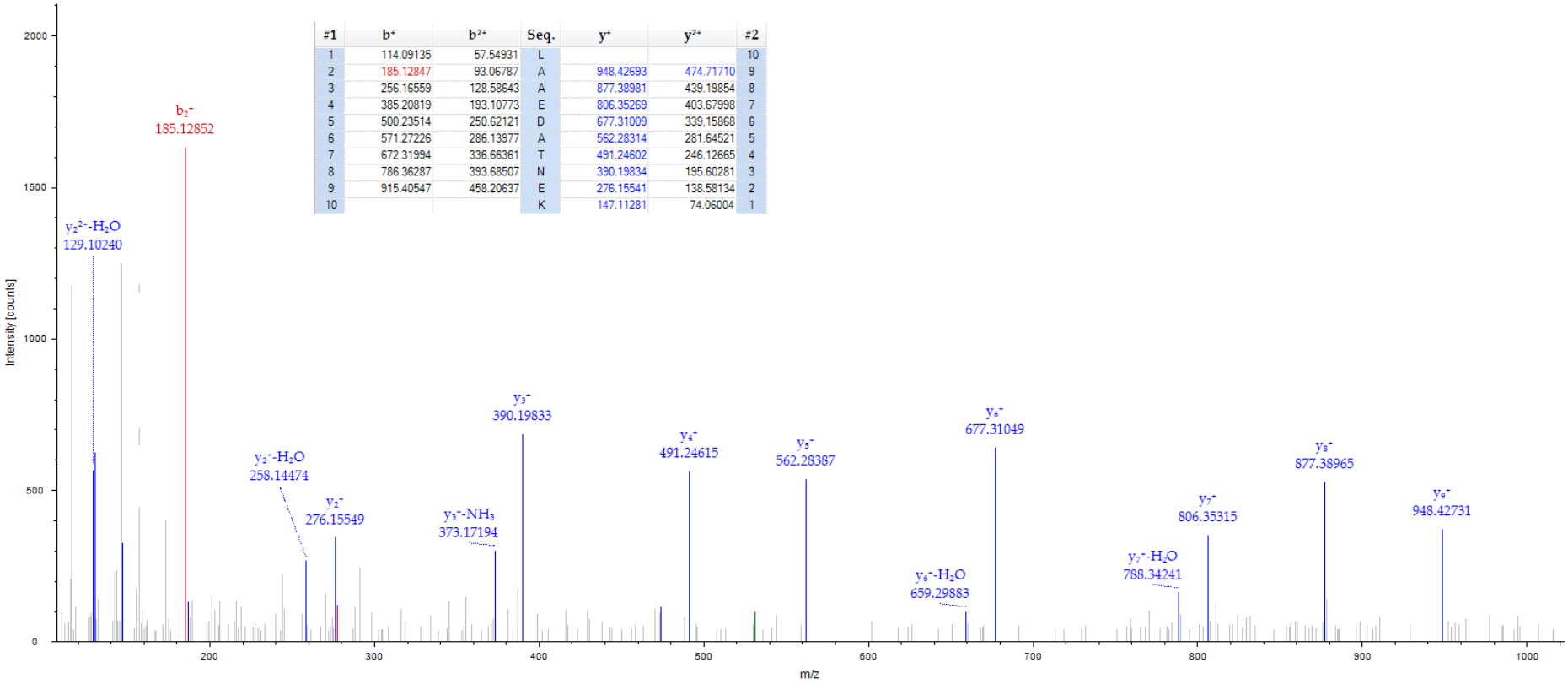

Figure 4-22: MS/MS spectrum of m/z 531.25 the $[M+2H]^{2+}$ molecular ion for a peptide of 1061.51 Da with corresponding sequence LAAEDATNEK unique to NEFL.

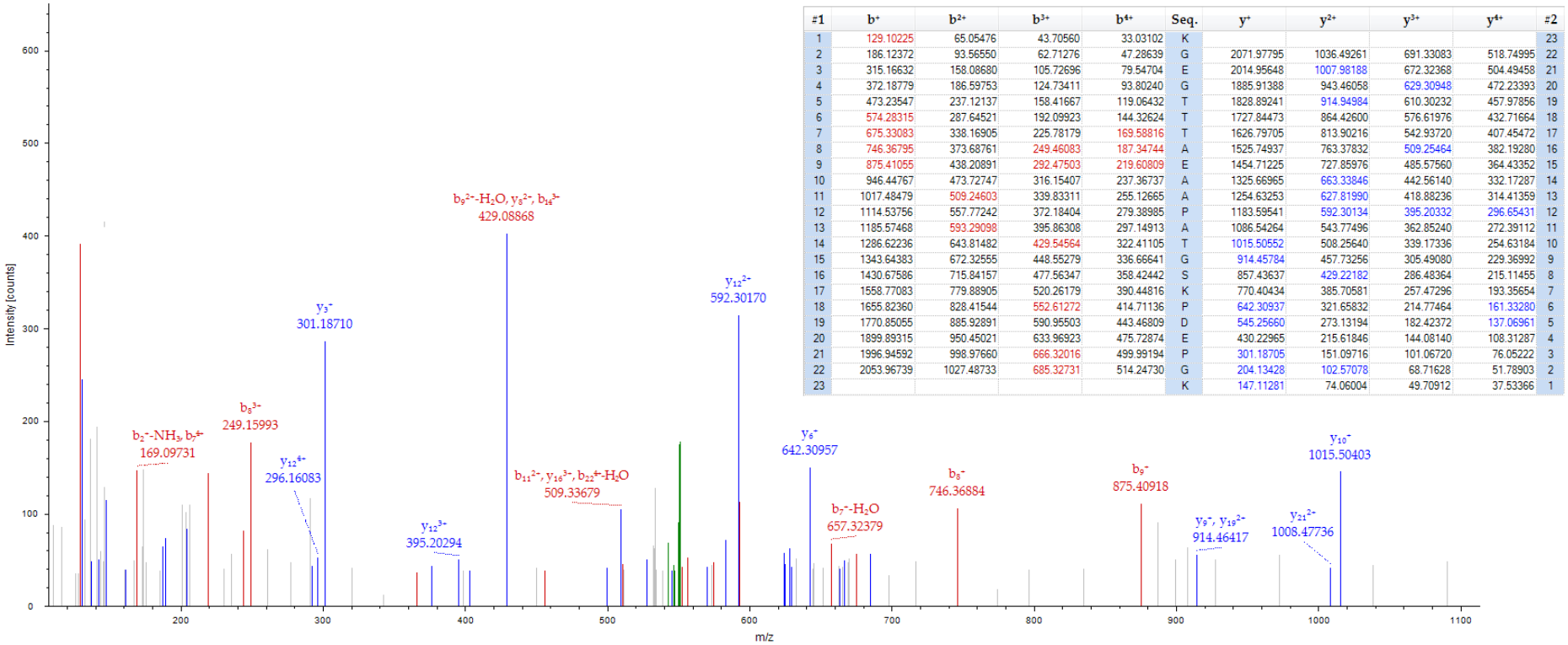

#1	b+	b2+	b3+	b4+	Seq.	y+	y2+	y3+	y4+	#2
1	129.10225	65.05476	43.70560	33.03102	K					23
2	186.12372	93.56550	62.71276	47.28639	G	2071.97795	1036.49261	691.33083	518.74995	22
3	315.16632	158.08680	105.72696	79.54704	E	2014.95648	1007.98188	672.32368	504.49458	21
4	372.18779	186.59753	124.73411	93.80240	G	1885.91388	943.46058	629.30948	472.23393	20
5	473.23547	237.12137	158.41667	119.06432	T	1828.89241	914.94984	610.30232	457.97856	19
6	574.28315	287.64521	192.09923	144.32624	T	1727.84473	864.42600	576.61976	432.71664	18
7	675.33083	338.16905	225.78179	169.58816	T	1626.79705	813.90216	542.93720	407.45472	17
8	746.36795	373.68761	249.46083	187.34744	A	1525.74937	763.37832	509.25464	382.19280	16
9	875.41055	438.20891	292.47503	219.60809	E	1454.71225	727.85976	485.57560	364.43352	15
10	946.44767	473.72747	316.15407	237.36737	A	1325.66965	663.33846	442.56140	332.17287	14
11	1017.48479	509.24603	339.83311	255.12665	A	1254.63253	627.81990	418.88236	314.41359	13
12	1114.53756	557.77242	372.18404	279.38985	P	1183.59541	592.30134	395.20332	296.65431	12
13	1185.57468	593.29098	395.86308	297.14913	A	1086.54264	543.77496	362.85240	272.39112	11
14	1286.62236	643.81482	429.54564	322.41105	T	1015.50552	508.25640	339.17336	254.63184	10
15	1343.64383	672.32555	448.55279	336.66641	G	914.45784	457.73256	305.49080	229.36992	9
16	1430.67586	715.84157	477.56347	358.42442	S	857.43637	429.22182	286.48364	215.11455	8
17	1558.77083	779.88905	520.26179	390.44816	K	770.40434	385.70581	257.47296	193.35654	7
18	1655.82360	828.41544	552.61272	414.71136	P	642.30937	321.65832	214.77464	161.33280	6
19	1770.85055	885.92891	590.95503	443.46809	D	545.25660	273.13194	182.42372	137.06961	5
20	1899.89315	950.45021	633.96923	475.72874	E	430.22965	215.61846	144.08140	108.31287	4
21	1996.94592	998.97660	666.32016	499.99194	P	301.18705	151.09716	101.06720	76.05222	3
22	2053.96739	1027.48733	685.32731	514.24730	G	204.13428	102.57078	68.71628	51.78903	2
23					K	147.11281	74.06004	49.70912	37.53366	1

Figure 4-23: MS/MS spectrum of m/z 550.77 the $[M+4H]^{4+}$ molecular ion for a peptide of 2200.07 Da with corresponding sequence KGEGTTTAEAAPATGSKPDEPGK unique to GAP43.

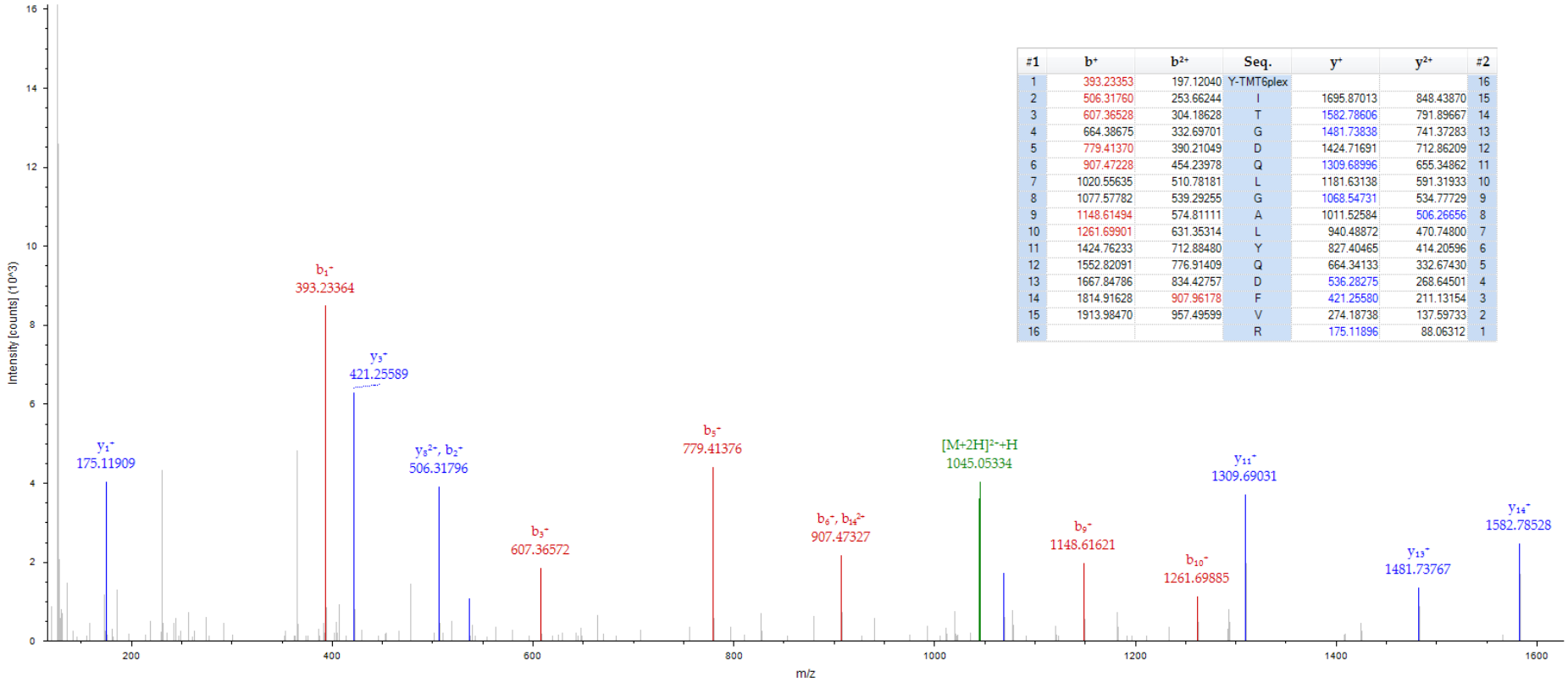

#1	b⁺	b²⁺	Seq.	y⁺	y²⁺	#2
1	393.23353	197.12040	Y-TMT6plex			16
2	506.31760	253.66244	I	1695.87013	848.43870	15
3	607.36528	304.18628	T	1582.78606	791.89667	14
4	664.38675	332.69701	G	1481.73838	741.37283	13
5	779.41370	390.21049	D	1424.71691	712.86209	12
6	907.47228	454.23978	Q	1309.68996	655.34862	11
7	1020.55635	510.78181	L	1181.63138	591.31933	10
8	1077.57782	539.29255	G	1068.54731	534.77729	9
9	1148.61494	574.81111	A	1011.52584	506.26656	8
10	1261.69901	631.35314	L	940.48872	470.74800	7
11	1424.76233	712.88480	Y	827.40465	414.20596	6
12	1552.82091	776.91409	Q	664.34133	332.67430	5
13	1667.84786	834.42757	D	536.28275	268.64501	4
14	1814.91628	907.96178	F	421.25580	211.13154	3
15	1913.98470	957.49599	V	274.18738	137.59733	2
16			R	175.11896	88.06312	1

Figure 4-24: MS/MS spectrum of m/z 1044.55 the $[M+2H]^{2+}$ molecular ion for a peptide of 2088.09 Da with corresponding sequence YITGDQLGALYQDFVR unique to ENO2.

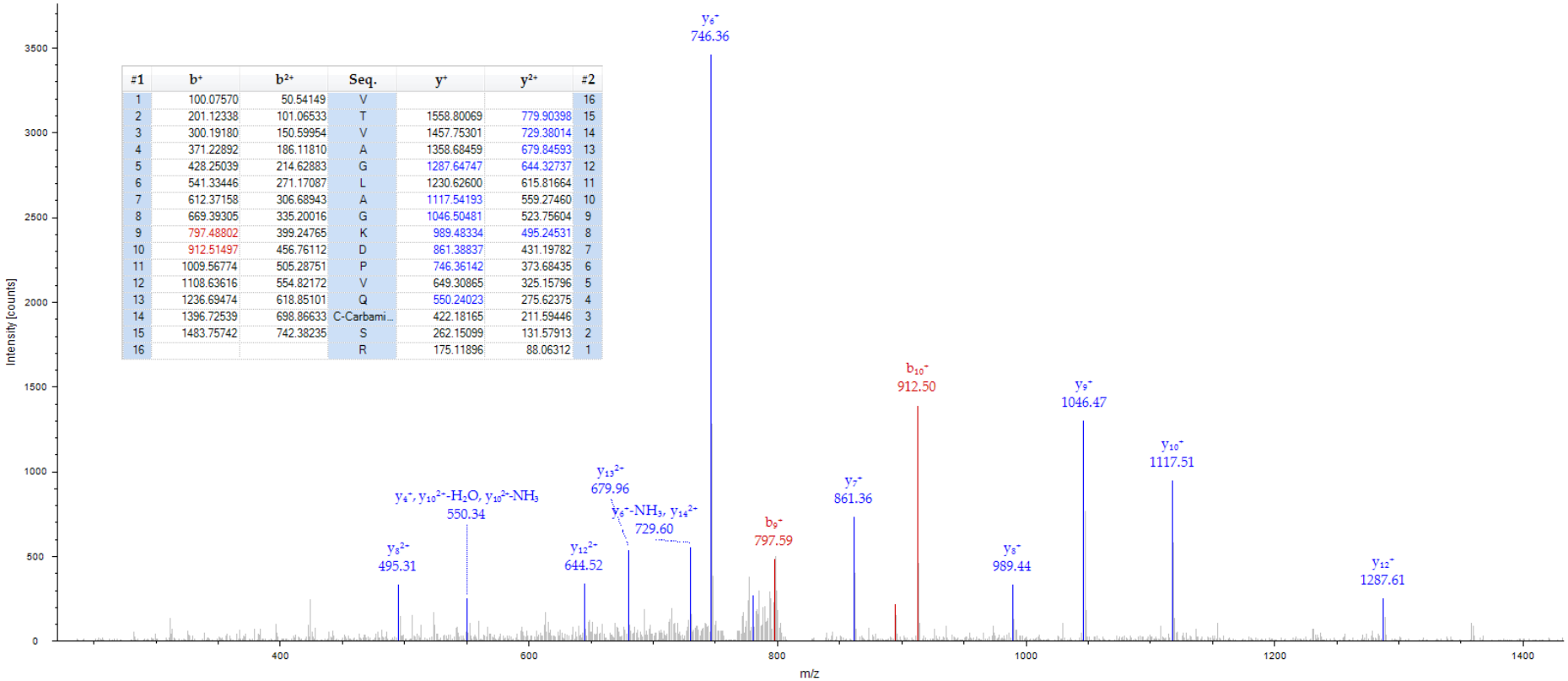

Figure 4-25: MS/MS spectrum of m/z 829.43 the $[M+2H]^{2+}$ molecular ion for a peptide of 1657.86 Da with corresponding sequence VTVAGLAGKDPVQCSR unique to PARK7.

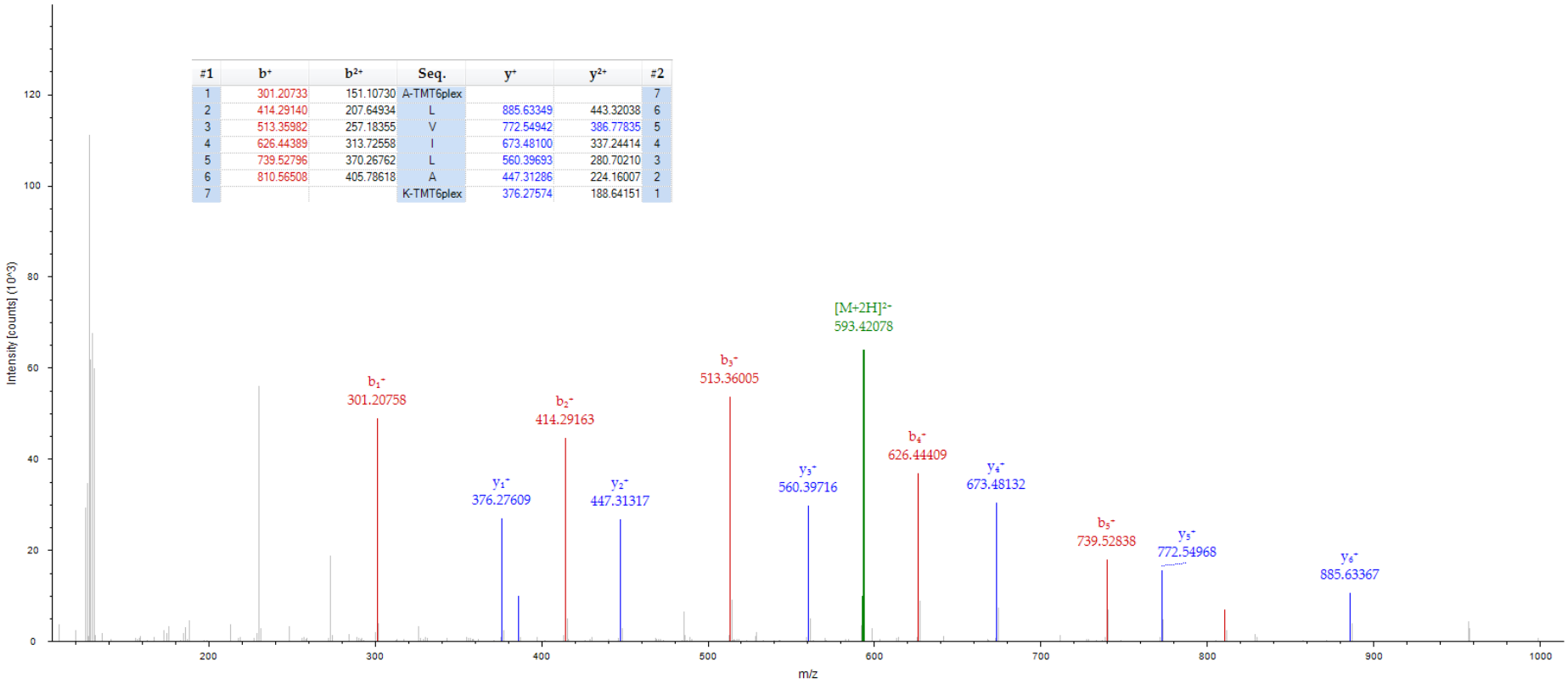

Figure 4-26: MS/MS spectrum of m/z 593.42 the $[M+2H]^{2+}$ molecular ion for a peptide of 1185.836 Da with corresponding sequence ALVILAK unique to PARK7.

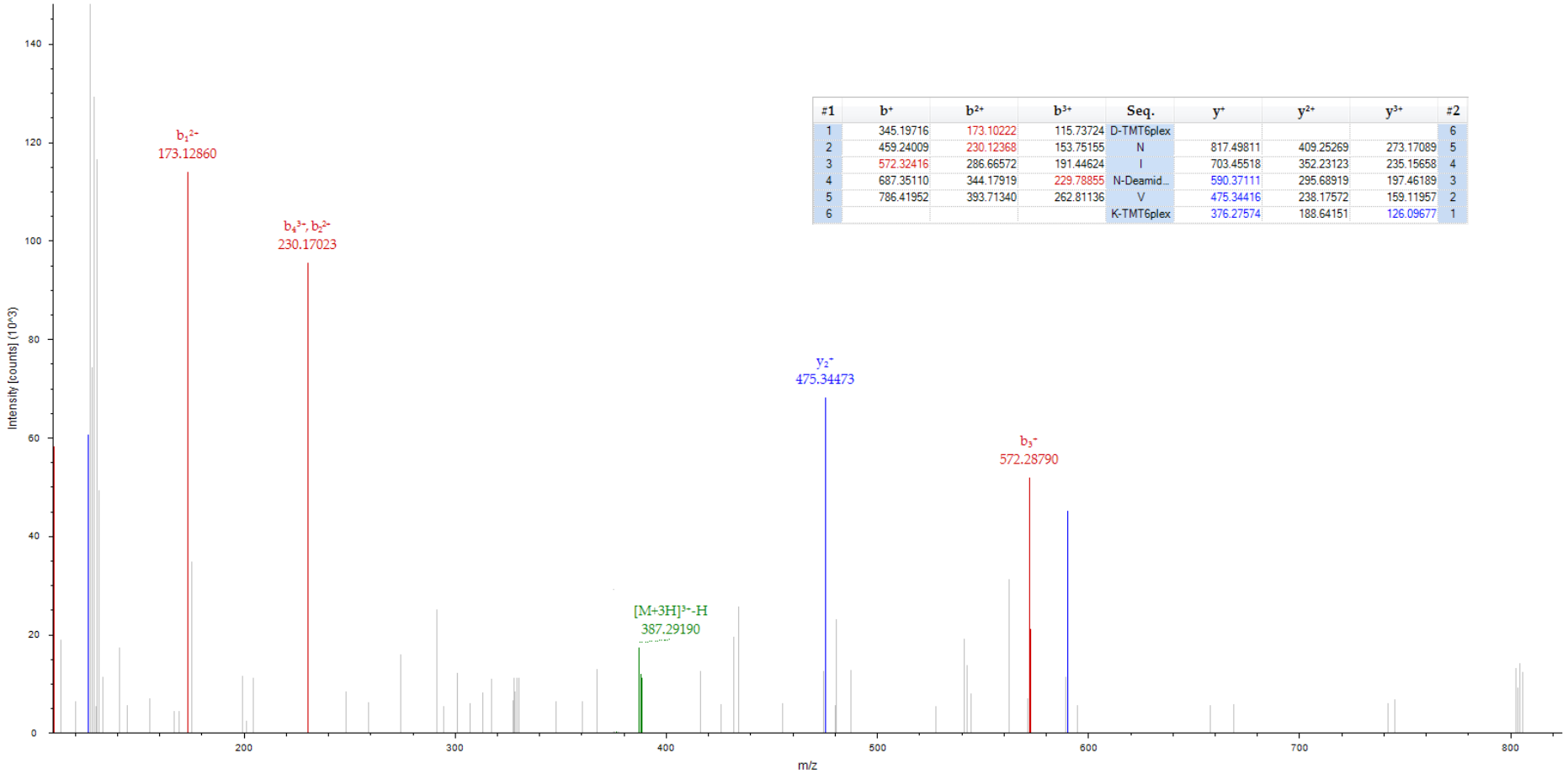

#1	b+	b2+	b3+	Seq.	y+	y2+	y3+	#2
1	345.19716	173.10222	115.73724	D-TMT6plex				6
2	459.24009	230.12368	153.75155	N	817.49811	409.25269	273.17089	5
3	572.32416	286.66572	191.44624	I	703.45518	352.23123	235.15658	4
4	687.35110	344.17919	229.78855	N-Deamid...	590.37111	295.68919	197.46189	3
5	786.41952	393.71340	262.81136	V	475.34416	238.17572	159.11957	2
6				K-TMT6plex	376.27574	188.64151	126.09677	1

Figure 4-27: MS/MS spectrum of m/z 387.90 the $[M+3H]^{3+}$ molecular ion for a peptide of 1161.69Da with corresponding sequence DNINVK unique to RAB3A.

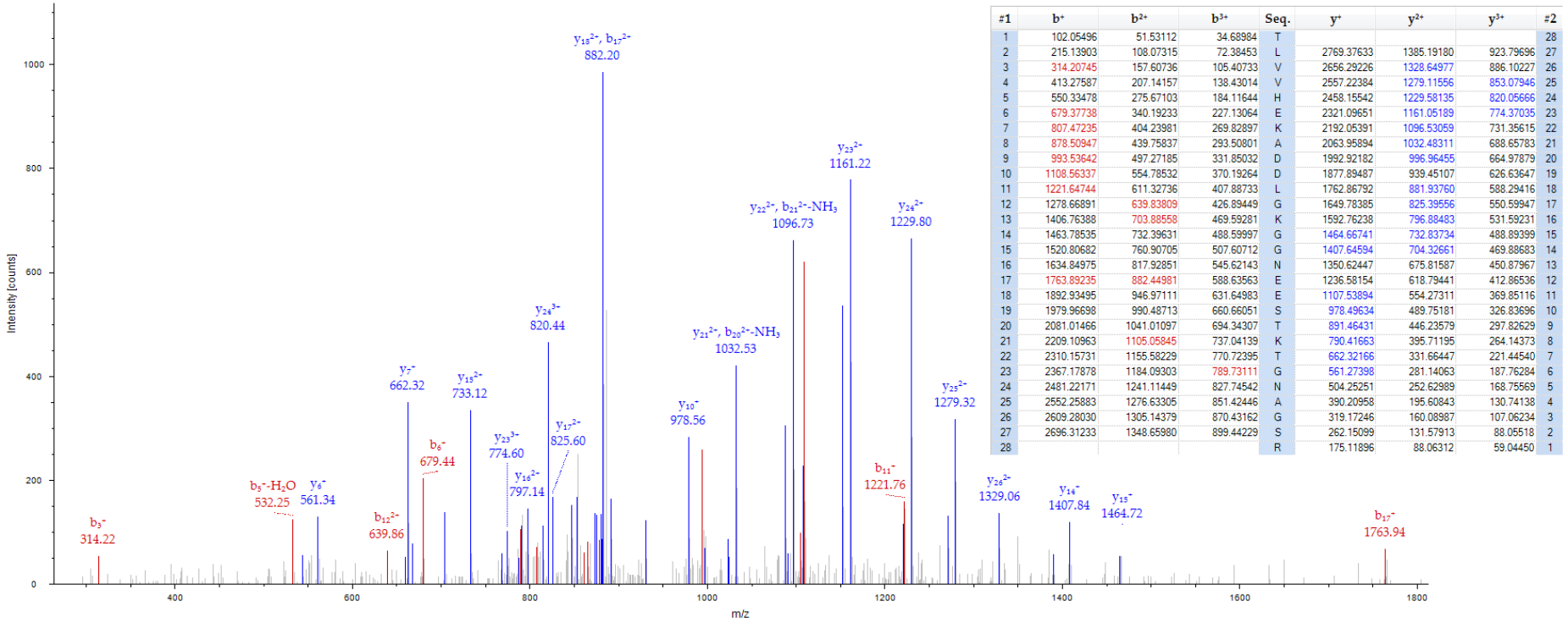

#1	b^{+}	b^{2+}	b^{3+}	Seq.	y^{+}	y^{2+}	y^{3+}	#2
1	102.05496	51.53112	34.68984	T				28
2	215.13903	108.07315	72.38453	L	2769.37633	1385.19180	923.79696	27
3	314.20745	157.60736	105.40733	V	2656.29226	1328.64977	886.10227	26
4	413.27587	207.14157	138.43014	V	2557.22384	1279.11556	853.07946	25
5	550.33478	275.67103	184.11644	H	2458.15542	1229.58135	820.05666	24
6	679.37738	340.19233	227.13064	E	2321.09651	1161.05189	774.37035	23
7	807.47235	404.23981	269.82897	K	2192.05391	1096.53059	731.35615	22
8	878.50947	439.75837	293.50801	A	2063.95894	1032.48311	688.65783	21
9	993.53642	497.27185	331.85032	D	1992.92182	996.96455	664.97879	20
10	1108.56337	554.78532	370.19264	D	1877.89487	939.45107	626.63647	19
11	1221.64744	611.32736	407.88733	L	1762.86792	881.93760	588.29416	18
12	1278.66891	639.83809	426.89449	G	1649.78385	825.39556	550.59947	17
13	1406.76388	703.88558	469.59281	K	1592.76238	796.88483	531.59231	16
14	1463.78535	732.39631	488.59997	G	1464.66741	732.83734	488.89399	15
15	1520.80682	760.90705	507.60712	G	1407.64594	704.32661	469.88683	14
16	1634.84975	817.92851	545.62143	N	1350.62447	675.81587	450.87967	13
17	1763.89235	882.44981	588.63563	E	1236.58154	618.79441	412.86536	12
18	1892.93495	946.97111	631.64983	E	1107.53894	554.27311	369.85116	11
19	1979.96698	990.48713	660.66051	S	978.49634	489.75181	326.83696	10
20	2081.01466	1041.01097	694.34307	T	891.46431	446.23579	297.82629	9
21	2209.10963	1105.05845	737.04139	K	790.41663	395.71195	264.14373	8
22	2310.15731	1155.58229	770.72395	T	662.32166	331.66447	221.44540	7
23	2367.17878	1184.09303	789.73111	G	561.27398	281.14063	187.76284	6
24	2481.22171	1241.11449	827.74542	N	504.25251	252.62989	168.75569	5
25	2552.25883	1276.63305	851.42446	A	390.20958	195.60843	130.74138	4
26	2609.28030	1305.14379	870.43162	G	319.17246	160.08987	107.06234	3
27	2696.31233	1348.65980	899.44229	S	262.15099	131.57913	88.05518	2
28				R	175.11896	88.06312	59.04450	1

Figure 4-28: MS/MS spectrum of m/z 957.47 the $[M+3H]^{3+}$ molecular ion for a peptide of 2870.42 Da with corresponding sequence TLVVHEKADDLGKGGNEESTKTGNAGSR unique to SOD1.

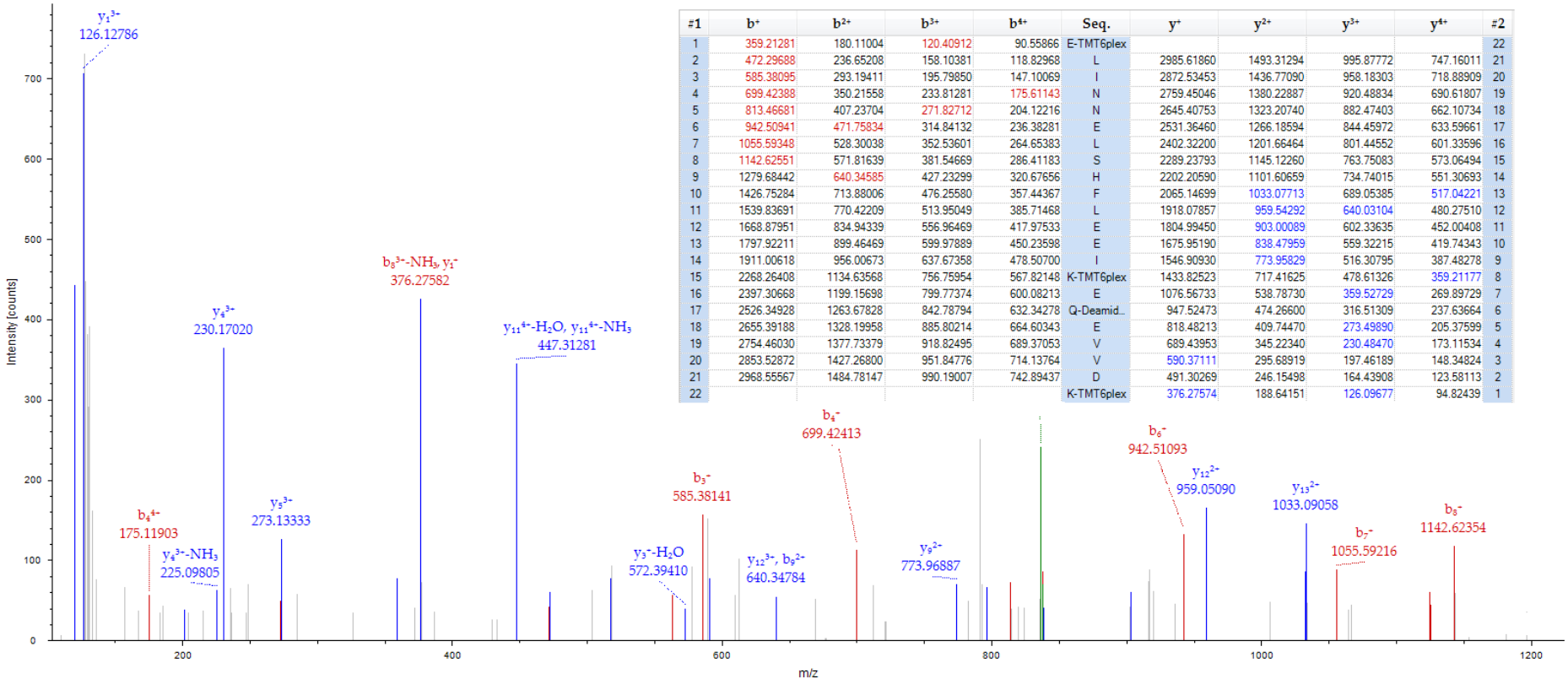

#1	b+	b2+	b3+	b4+	Seq.	y+	y2+	y3+	y4+	#2
1	359.21281	180.11004	120.40912	90.55866	E-TMT6plex					22
2	472.29688	236.65208	158.10381	118.82968	L	2985.61860	1493.31294	995.87772	747.16011	21
3	585.38095	293.19411	195.79850	147.10069	I	2872.53453	1436.77090	958.18303	718.88909	20
4	699.42388	350.21558	233.81281	175.61143	N	2759.45046	1380.22887	920.48834	690.61807	19
5	813.46681	407.23704	271.82712	204.12216	N	2645.40753	1323.20740	882.47403	662.10734	18
6	942.50941	471.75834	314.84132	236.38281	E	2531.36460	1266.18594	844.45972	633.59661	17
7	1055.59348	528.30038	352.53601	264.65383	L	2402.32200	1201.66464	801.44552	601.33596	16
8	1142.62551	571.81639	381.54669	286.41183	S	2289.23793	1145.12260	763.75083	573.06494	15
9	1279.68442	640.34585	427.23299	320.67656	H	2202.20590	1101.60659	734.74015	551.30693	14
10	1426.75284	713.88006	476.25580	357.44367	F	2065.14699	1033.07713	689.05385	517.04221	13
11	1539.83691	770.42209	513.95049	385.71468	L	1918.07857	959.54292	640.03104	480.27510	12
12	1668.87951	834.94339	556.96469	417.97533	E	1804.99450	903.00089	602.33635	452.00408	11
13	1797.92211	899.46469	599.97889	450.23598	E	1675.95190	838.47959	559.32215	419.74343	10
14	1911.00618	956.00673	637.67358	478.50700	I	1546.90930	773.95829	516.30795	387.48278	9
15	2268.26408	1134.63568	756.75954	567.82148	K-TMT6plex	1433.82523	717.41625	478.61326	359.21177	8
16	2397.30668	1199.15698	799.77374	600.08213	E	1076.56733	538.78730	359.52729	269.89729	7
17	2526.34928	1263.67828	842.78794	632.34278	Q-Deamid...	947.52473	474.26600	316.51309	237.63664	6
18	2655.39188	1328.19958	885.80214	664.60343	E	818.48213	409.74470	273.49890	205.37599	5
19	2754.46030	1377.73379	918.82495	689.37053	V	689.43953	345.22340	230.48470	173.11534	4
20	2853.52872	1427.26800	951.84776	714.13764	V	590.37111	295.68919	197.46189	148.34824	3
21	2968.55567	1484.78147	990.19007	742.89437	D	491.30269	246.15498	164.43908	123.58113	2
22					K-TMT6plex	376.27574	188.64151	126.09677	94.82439	1

Figure 4-29: MS/MS spectrum of m/z 836.71 the $[M+4H]^{4+}$ molecular ion for a peptide of 3343.83 Da with corresponding sequence ELINNELSHFLEEIKEQEVVDK unique to S100B.

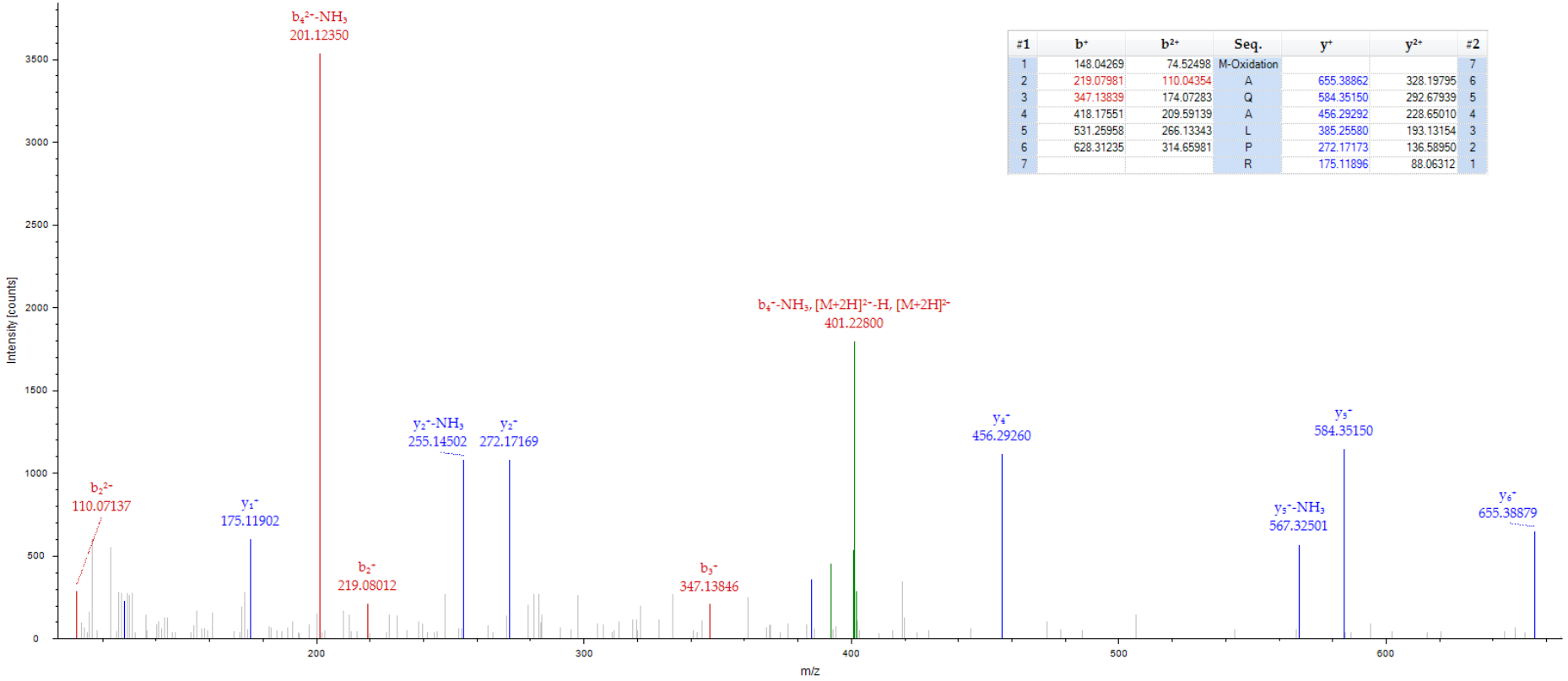

#1	b⁺	b²⁺	Seq.	y⁺	y²⁺	#2
1	148.04269	74.52498	M-Oxidation			7
2	219.07981	110.04354	A	655.38862	328.19795	6
3	347.13839	174.07283	Q	584.35150	292.67939	5
4	418.17551	209.59139	A	456.29292	228.65010	4
5	531.25958	266.13343	L	385.25580	193.13154	3
6	628.31235	314.65981	P	272.17173	136.58950	2
7			R	175.11896	88.06312	1

Figure 4-30: MS/MS spectrum of m/z 401.71 the $[M+2H]^{2+}$ molecular ion for a peptide of 802.42 Da with corresponding sequence MAQALPR unique to SYN1.

4.5 Discussion

In this study our aim was to investigate proteomic workflows to identify a suitable approach for deep profiling of human plasma for a biomarker discovery setting. By using a combination of immunodepletion, isobaric labelling and fractionation, we optimised a strategy that obtains reproducible metrics, wider proteome coverage and wider dynamic range (mg/mL – pg/mL) as well as relative quantification (OGE-9). This was designed all within a manageable cost effective pipeline for typical plasma biomarker research and could span across several research disciplines. This Chapter primarily focused on the content observed by each proteomic technique and the aim was not to investigate differential expression between clinical groups (this is explored further in Chapter 5). With a focus on neurological disease, we found evidence for brain-derived proteins (BDP) circulating in plasma as well as key proteins implicated in disease pathogenesis and CNS processes.

We firstly demonstrated that the inclusion of an upfront immunodepletion step improves proteome coverage in complex matrices, which is in agreement with the majority of studies in the field [504, 507, 521]. A commercially available immunoaffinity column for the depletion of albumin and IgG (Top2) has been previously shown to be reproducible in human plasma [375]. In all non-fractionated and fractionated methodologies the Top2 depletion significantly improved protein group identifications compared with non-depleted samples. As expected from previous studies, immunodepletion methods did not fully remove their targeted proteins; however, this was more apparent in the Top12 depletion strategy. In our hands, a Top12 immunodepletion approach had little benefit in increasing protein group numbers in non-fractionated samples. It is possible that if greater separation was applied to the Top12 method the benefits could have been more apparent but this was not investigated. Furthermore, multi-immunocapture columns (including Top12) do include analytes of disease interest. Using neurodegenerative disorders as an example α2m [372, 374], FGγ [374, 428], CC3 [436], α1-acid glycoprotein [357], apoA1 [357] and transthyretin [357, 429] have all been implicated as plasma biomarkers of AD and routinely captured in all commercially available multi-immunocapture strategies.

Without pre-fractionation, protein groups in the µg/mL range are well annotated with sporadic sampling of the ng/mL concentration level. As with all methodologies this would be improved with extended liquid chromatography (LC) gradients and the implementation of the newest generation of MS technology [522].

As expected the greater pre-fractionation of complex matrices exponentially increased the number of protein groups identified and therefore a lower LOD is achieved. On average greater fractionation demonstrated a 1.5-fold increase in protein identifications and a wider concentration range. Thus methodologies with Top2 depletion and 20 fractions were superior (1DGE-8 and OGE-9). Method OGE-9a, outperformed 1DGE-8 at the protein level consistently identifying ~1,200 proteins, a median protein concentration of 66ng/mL and a lower LOD of 4.3pg/mL. It is important to note that protein concentrations extracted from the plasma protein database (PPD) only represent 12% of the protein groups identified in this study. Therefore it is possible that protein groups of lower concentrations have been identified but remain unreported in terms of their level of abundance. OGE methods exhibited a lower spectral yield than gel-based methods. In addition, OGE demonstrated a more dramatic reduction in protein group identifications when applying a more stringent FDR to the dataset. This was seen to be driven by a large number of protein groups being identified with only PSM. Despite this, even at 1% FDR, OGE-9 returned greater number of protein group identifications with relative quantification than gel-based methods.

Isobaric labelling is now a critical step in MS biomarker discovery primarily because of its application in measuring multiple samples in a single acquisition. This is fundamental to drive down cost, reduce analytical time, reduce technical variability and increase sample size. In addition, an experimental reference can be added for relative quantification and global normalisation across several experiments. An increase from TMT6plex to TMT10plex has been made in this study. An isobaric labelling strategy is less variable than other MS quantification techniques such as label-free, metabolic-labelling and other MS1-based quantification [523]. When each sample is run individually or with limited multiplexing, an ion selected for fragmentation on one analytical run may not be selected consistently in subsequent acquisitions. This will result in inconsistent observations, affecting identification and

quantification. Isobaric labelling overcomes this variability as a common precursor ion is fragmented that corresponds to the same peptide species present in all of the labelled samples. Quantification is based upon the intensity of unique reporter ions generated for each channel (sample) and these are simultaneously measured.

Here, two variations of isobaric labelling (peptide and protein TMT10plex) were investigated and a marked difference in labelling efficiency was observed. TMT peptide labelling efficiency quantified between 91-94% of acquired peptides whereas TMT protein labelling ranged between 52-57%. This under labelling at the protein level has been previously reported [524] and was also noted as a limitation in Chapter 3. TMT protein labelling is thought to reduce sample variability and have a more physico-chemically diverse separation than the derived peptides but is limited to labelling of lysine amino acid residues. This restricts protein digestion as well as quantitative coverage. Peptide spectra identified in MS/MS acquisition without lysine residues will be without quantitative TMT information. Therefore, without TMT information these peptides cannot be assigned to individual clinical sample, effectively making these peptide identifications irrelevant. Conversely, TMT peptide labelling is not restricted to a particular class of peptide and is reactive toward the free amino-terminus, allowing quantification of almost all peptide sequences and this is evident in our data. The choice of isobaric labelling therefore dictates the choice of fractionation that can be used. For TMT peptide labelling, fractionation commences after digestion and therefore gel-based techniques (1DGE and 2DGE) are unsuitable. Separation at the peptide level would require separation by SCX or Isoelectric Focusing (IEF) – IEF by OFFGEL (OGE) as investigated in this study.

Within the plasma protein group indentifications generated by method OGE-9 we observed a number of analytes that are shown to be highly or exclusively expressed in the cerebral cortex. Protein groups that are thought to have an origin within the CNS are of particular interest as they may indicate loss of blood-brain barrier integrity [519, 525], neuronal injury [363, 526-527], protein aggregation or on-going neurodegeneration [528-529]. It has also recently been shown that CNS or brain-derived proteins can be transported into the periphery by neuronally-derived exosomes [530-531]. The denaturing conditions of sample preparation required for LC-MS/MS methodologies would ensure that any cargo derived from these vesicles would be

released and detected, another key advantage over immunoassays. We demonstrated automated database evidence for 157 BDPs within our plasma dataset. Of the top 30 most exclusively expressed proteins in the cerebral cortex nine were observed in our plasma proteomic dataset; GFAP, OPALIN, oligodendrocyte-myelin glycoprotein (OMG), myelin oligodendrocyte glycoprotein (MOG), neurocan (NCAN), β-synuclein (SNCB), brain-specific homeobox/POU domain protein 2 (POU3F2), FEZ family zinc finger 2 (FEZF2) and proteolipid protein 1 (PLP1). GFAP is a CNS specific protein that is almost entirely expressed in astroglia and has been highlighted as a marker of acute injury in Traumatic Brain Injury (TBI) [532-533]. Injury to astroglial cells lead to release of GFAP into the extracellular matrix, which might increase levels in both cerebrospinal fluid and blood [526], this would be in parallel with S100B and a panel of interleukins [534-535] also observed within our plasma dataset, demonstrating the potential ability of this methodology to assess CNS insults. However, limited investigations into GFAP in blood have found no association with neurological disease or damage [536]. OPALIN, OMG, MOG and PLP1 are proteins involved in the structure and integrity of the myelin sheath where as NCAN is reported to play a role in axon guidance and neurite growth [537]. SNCB is found predominately in the pre-synaptic terminals. Highly homologous to α-synuclein (SNCA), SNCB is thought to inhibit SNCA aggregation and therefore may protect the CNS from the toxic effects of SNCA. To our knowledge, these markers (not GFAP) have yet to be described in blood however replication in an independent dataset is of importance due to low number of matched PSMs. However, after manual inspection of the MS/MS spectra, OMG, NCAN and FEZF2 were seen to be not of sufficient quality for a positive identification. Additionally, a further 29/157 BDPs database matched in our plasma dataset were classified as falsely identified after manual MS/MS inspection. Other protein groups hypothesised to reflect brain injury are ENO2 [538], synaptophysin [539], neuromodulin [539], synaptotagmin [539], SNAP-25 [540], UCH-L1 [532, 534], and NEFL [363, 526] are all observed within our plasma dataset. Proteins implicated in neurodegenerative pathogenesis have also been detected in this study. Although plasma expression of Aβ, MAPT, SNCA, SOD1 and others have been observed in plasma previously by immunoassay or MS studies we demonstrate a methodology that will simultaneously detect peptides from these protein groups in the same subjects in the same experiment. Further to this, pathway analysis of the best performing proteomic methodology (OGE-9) revealed over-

representation of protein groups related to specific neurodegenerative diseases and CNS pathways. The neurotrophin signalling pathway is involved in differentiation and survival of neural cells plus a significant role in high-order functions such as learning and memory. This pathway is regulated by the MAPK signalling pathway, which is also over-represented in OGE-9 plasma protein group dataset. Although this analysis does not identify a change in plasma protein expression between two differing phenotypes it does indicate that CNS specific protein groups and pathways can be measured in plasma if the correct methodology is applied.

The use of OFFGEL (OGE) fractionation, combined with immunodepletion and TMT10plex peptide labelling has shown to be a sensitive workflow for comprehensive plasma exploration. Proteins of medium and high abundance have excellent protein coverage and reproducibility. This method also demonstrates peptides derived from proteins of low abundance (<100 pg/mL) and although consistent in their measurement across biological repeats, this method may not reflect an accurate plasma expression due to variable sequence coverage. Nonetheless, this dataset is an indication that low abundant BDPs are circulating in plasma with a significant number related to synaptic processes and neuronal injury. These proteins would be prime targets to predict CNS insults in the periphery and should be further validated and then investigated by an ultra-sensitive targeted assay.

The identifications reported in this study are largely based on automated database searching with cut-offs defined by false discovery rates. Routine practice recommends manual examination of assigned spectra for a protein in question or of interest; the peptide sequence would typically be confirmed by the presence of an overlapping series of *b* and *y* ions. This is of paramount importance in discovery experiments when considering protein groups identified by relaxed FDR's or limited PSMs. The results reported here are all at 5% FDR and this does increase the chances of falsely assigned spectra. However a more stringent biomarker discovery, particularly when subtle changes in novel candidates are anticipated, has the potential to overlook disease related changes. Manual MS/MS spectra interrogation, replication in multiple samples, cohorts and targeted assays are essential to confirm identification and expression change.

TMT10plex labelling requires a superior level of MS resolution than TMT6plex labelling. This is needed to identify TMT reporter channels with only 0.0006 Da mass differences, which currently increases MS and MS/MS survey scanning. Further developments in mass spectrometer technology continue to improve sensitivity and scan rates thereby increasing MS/MS events in a defined period of time. This will lead to the detection of more PSMs so that overall experimental coverage of a sample is enhanced. This is important in relation to this study because sequence coverage of each protein, particularly those of low abundance of 1-2 PSMs, can be improved giving more accurate expression levels in relation to disease.

4.5.1 Conclusions

In this study, we have highlighted a methodology for plasma protein profiling that utilises isobaric TMT10plex peptide labelling, simple immunodepletion and OFFGEL fractionation coupled to LC-MS/MS (OGE-9; Figure 4-1). The main aim was to maximise proteome coverage, increase concentration range and increase cost effective throughput for plasma biomarker research and this has been achieved. Using this technique, we can identify >1200 proteins at 5% FDR within a single TMT10plex experiment, with relative quantification of >92%. OGE-9 also demonstrates a broad dynamic range covering the "classic proteome" with coverage of protein proteins within ng/mL and pg/mL region. We have highlighted the potential of this method in a neurological setting by identifying a number of brain-derived proteins, some of which are established markers of neuronal and synaptic injury, as well as proteins involved in the pathogenesis of neurodegenerative disease circulating within blood. This technique has utility for a range of disease conditions and even differing bio-fluids. It could also serve as a "point of interest" reference set of what is present in blood for future targeted investigations

The application of this in-depth profiling methodology will determine if further observations can be made between disease phenotypes of AD risk within blood (Chapter 5).

Statement of collaborative work

I am grateful to Dr. Roman Fischer (Target Discovery Institute; Oxford University), Steve Lynham (King's College London), Dr. Malcolm Ward (King's College London) and the Centre of Excellence for Mass Spectrometry at King's College London for access to the instrumentation needed to carry out this work.

CHAPTER 5

A MASS SPECTROMETRY-BASED DISCOVERY AND REPLICATION OF A MULTI-ANALYTE CLASSIFIER FOR NEOCORTICAL AMYLOID PATHOLOGY

5.1 Introduction

Chapter 3 outlined a typical LC-MS/MS proteomic approach that was shown to be a particularly useful discovery tool in highlighting plasma biomarkers that are related to NAB. Whilst the study produced replicated candidates for predicting Aβ, there were limitations that restricted this initial discovery from having further impact. Firstly, almost up to 50% of protein groups indentified using this technique could not be quantified due the nature of isobaric protein labelling. Even if this was addressed, the sensitivity of the workflow could still only report coverage of the "classical plasma proteome". Current hypotheses indicates that biomarkers of disease relevance in plasma, particularly of CNS disorders, would mostly be located at the "tissue leakage" level (pg/mL – ng/mL) [501]. Indeed, levels of $A\beta_{1-42}$ and p-tau reported by immunoassays are estimated to be at picogram level in blood [359, 377]. More recently, CNS proteins (e.g. S100B) have been described at the picogram level in plasma as a hypothesised response to BBB impairment [519, 541].

A methodological review of the latest LC-MS/MS proteomic pipelines in Chapter 4 highlighted a strategy that incorporated high-resolution peptide separation, immunodepletion and isobaric peptide labelling (OGE-9). This workflow was shown to dramatically increase the number of quantifiable targets and widen plasma proteome coverage over all other strategies. Furthermore, it was shown that a subset of protein groups identified in plasma had considerable, in some cases exclusive, cerebral cortex expression or involvement in neurodegenerative pathogenesis. Given these results it is essential to utilise this approach in independent and well characterised cohorts, not only to validate findings from Chapter 3 but also to discover novel candidates relating to NAB given the improved sensitivity.

Chapter 3 also demonstrated the difficulty of translating findings from MS-based platform to an orthogonal immunoassay approach. Only 3/17 targets replicated from an MS platform to an ELISA approach and it cannot be determined if this was because of a false association in the LC-MS/MS discovery or simply the difference in proteomic platform. It is inevitable that an immunoassay, similar to an ELISA platform, will be at the basis for any future biomarker clinical testing for AD. However, in this study, to minimise candidate rejection due to platform variation we choose to use an identical LC-MS/MS platform in discovery and replication. As previously, this approach was applied to plasma samples from individuals with concurrent Aβ PET imaging; discovery (AIBL-2; ^{11}C-PiB) and replication (KARVIAH; ^{18}FBB). Given the recent focus towards therapeutic intervention at the preclinical stages [218, 470] the cohorts utilised in this study were more focused toward cognitively healthy individuals with elevated NAB.

5.2 Aims

To investigate further plasma proteins predictive of Aβ burden using the improved proteomic strategy established in Chapter 4 (Figure 5-1). Furthermore, our dataset will be mined to replicate the plasma expression of brain-derived proteins than have been previously described, and where possible, relate to Aβ burden. Lastly, we will attempt to relate this generated data to further replicate LC-MS/MS candidates highlighted in Chapter 3.

Univariate analysis will be performed to describe single plasma proteins that are associated with "high Aβ (Aβ+)" or "low Aβ (Aβ-)", as measured by ^{11}C-PiB and ^{18}F-Florbetaben (^{18}FBB), and confounding variables by either correlation or a binary endophenotype approach. Multivariate analysis will include least absolute shrinkage and selection operator (LASSO) as a variable reduction tool and support vector machine learning to build a predictive model of elevated Aβ in a discovery cohort (AIBL-2) that will be tested in an independent cohort (KARVIAH).

5.3 Methodology Overview

The proteomic workflow utilised in this Chapter is outlined in detail in Figure 5-1. This method has been shown to produce a superior coverage of the plasma proteome over other conventional proteomic methodologies (Chapter 4). This was in terms of protein group numbers and identification of low abundant proteins with almost complete relative quantification. The detailed methodological protocols for each procedure are outlined in Chapter 2.6.

Plasma samples (30µL) were immunodepleted of albumin and IgG's prior to enzymatic digestion of 100µg of protein from each depleted sample. Increased sample throughput and relative quantification was achieved by TMT10plex peptide labelling, using a dynamic global study reference. Each TMT10plex was randomly assigned to nine clinical samples, which was a mixture of both cohorts utilised in this study (AIBL-2 and KARVIAH). Unlike previous studies the study reference was assigned a random TMT label within each TMT10plex. Peptide based fractionation was achieved by isoelectric focusing using the OFFGEL system (OGE). A total of 1mg of digested protein material from the combined clinical samples was separated by the OGE system. TMT10plex labelled peptide fractions were focused for 50 kwh and collected in 24 fractions. Peripheral fractions were combined to create 20 peptide fractions for LC-MS/MS acquisition. This was repeated for 32 TMT10plex's which comprised 284 plasma samples. The resulting peptide fractions were analysed separately on a Thermo Scientific LTQ Orbitrap Velos instrument for 115 minutes. Raw data acquired was processed in Proteome Discoverer (ver. 1.4) for protein group/peptide identification and quantification using Mascot and Sequest sequentially.

Plasma samples were obtained from the Australian Imaging, Biomarkers and Lifestyle Flagship Study of Ageing imaging sub-cohort (AIBL-2) and McCusker Kerr Anglican Retirement Village Initiative in Ageing Health Research Centre (KARVIAH).

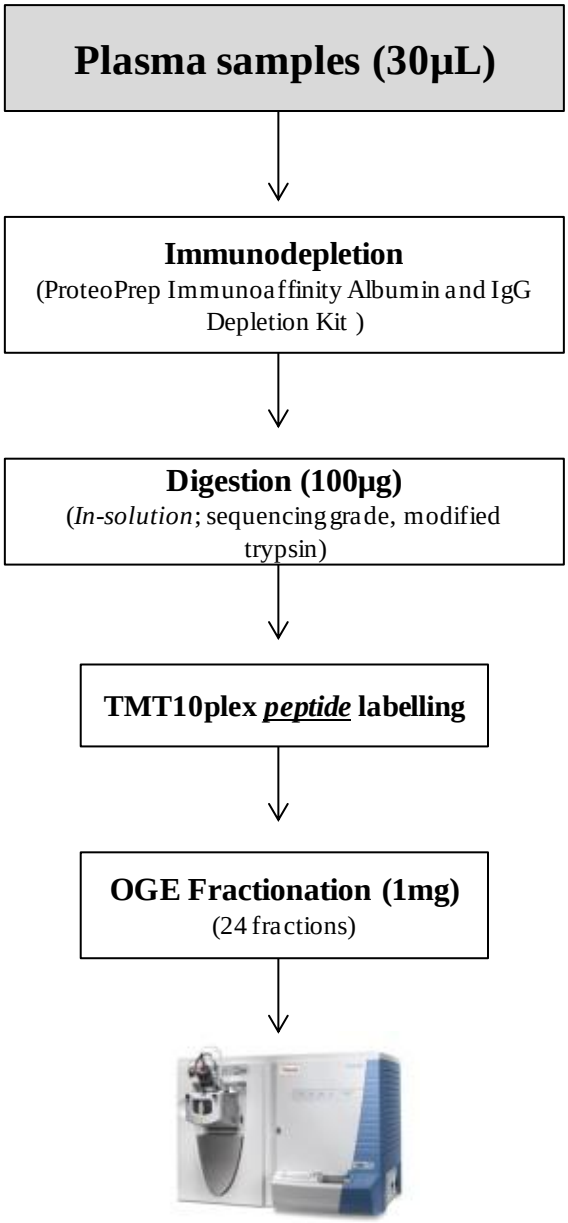

Figure 5-1: Methodological Overview: Schematic flow diagram represents the proteomic workflow applied to the AIBL-2 and KARVIAH cohorts in Chapter 5.

5.4 Results

5.4.1 Demographic characteristics (AIBL-2 and KARVIAH)

In this study, participants were selected from the Australian Imaging, Biomarkers and Lifestyle Flagship Study of Ageing imaging sub-cohort (AIBL-2). AIBL-2 subjects are different from the AIBL-1 cohort examined in Chapter 3. Furthermore, participants from the McCusker Kerr Anglican Retirement Village Initiative in Ageing Health Research Centre (KARVIAH) were also utilised. Individuals from both cohorts must have undergone Aβ PET at baseline, cognitive assessment (MMSE) and *APOE* genotyping to be included in the study. Furthermore, the AIBL-2 cohort had longitudinal Aβ PET and cognitive information. To classify NAB as positive (Aβ+) or NAB negative (Aβ-) individuals, a study specific SUVR cut-off of >1.5 was set for Aβ+ in the AIBL-2 cohort whereas an SUVR cut-off of >1.35 was used for Aβ+ the KARVIAH cohort. The difference in SUVR cut-offs is due to the KARVIAH cohort utilising an F^{18}-Florbetapen (^{18}FBB) tracer whereas the AIBL-2 participants were imaged using the "gold standard" ^{11}C-PiB. ^{18}FBB and ^{11}C-PiB have an excellent linear correlation and the same pattern of cortical distribution [271, 465]. ^{18}FBB has been shown to be more sensitive in discriminating other dementias from AD [233, 465].

The distribution of SUVR's can be seen in Figure 5-2. In contrast to Chapter 3, an extreme endophenotype approach was not employed but a more continuous assessment of SUVR was examined. Consistent with Chapter 3, the greater variability in SUVR was found in the Aβ+ group (range = 1.35 – 3.18) whereas the Aβ- SUVR ranged from 0.97 – 1.44. Given the overlap in SUVR ranges, due to Aβ PET differences, a binary Aβ- versus Aβ+ will be the primary focus of this analysis.

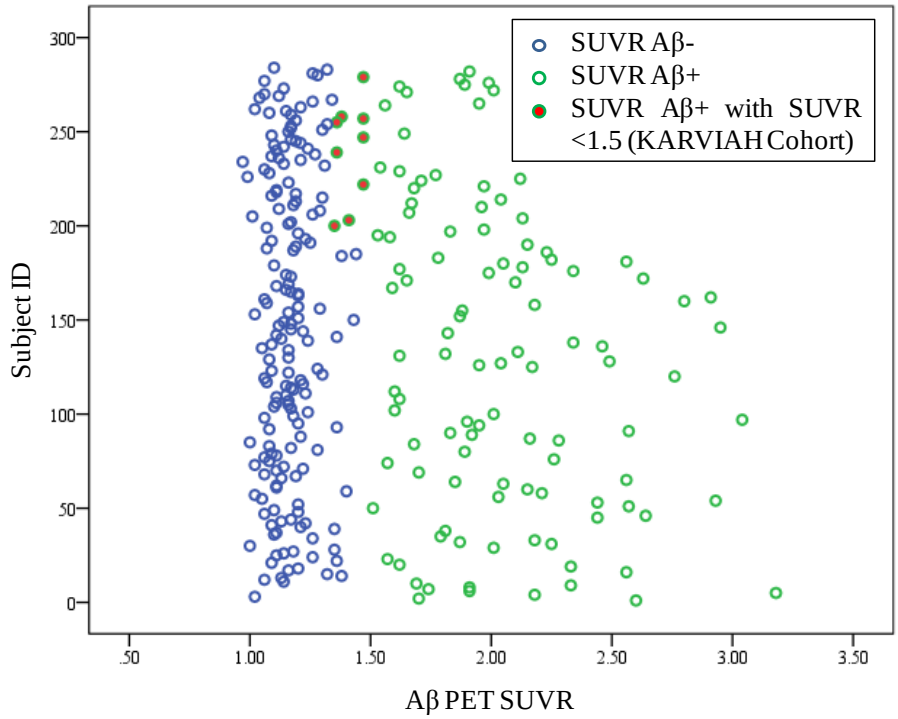

Figure 5-2: Scatter plot demonstrating the distribution of PET SUVR for the AIBL-2 and KARVIAH imaging cohorts. The individual SUVR values are coded by Aβ classification; Aβ- (blue) or Aβ+ (green). KARVIAH subjects underwent ^{18}FBB imaging rather than ^{11}C-PiB. KARVIAH subjects classified as Aβ+ but are below the ^{11}C-PiB threshold for Aβ+ (>1.5) are displayed in red.

AIBL-2 and KARVIAH individuals were enriched for cognitively healthy individuals (83.5%) for the investigation of preclinical NAB. Although a small variation in MMSE, the KARVIAH cohort (n = 94) is clinically defined as cognitively normal (HEC). A small proportion of participants from AIBL-2, defined clinically as MCI (7.5%) or AD (8.9%), were also included in the study (Figure 5-3). The demographic information for the 284 subjects examined in this study is displayed in Table 5.1.

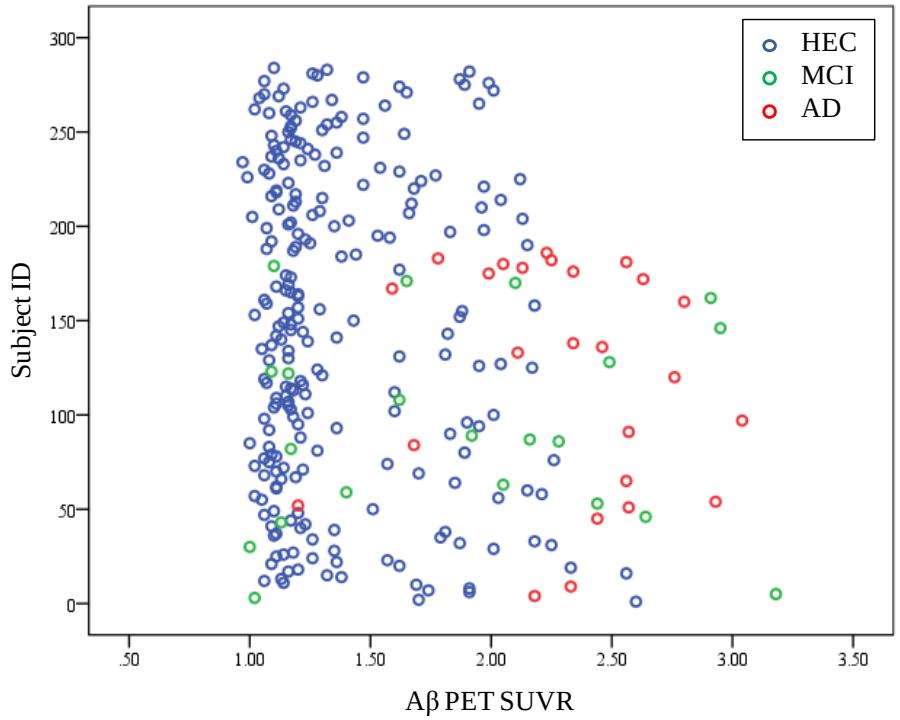

Figure 5-3: Scatter plot demonstrating the distribution of PET SUVR for the AIBL-2 and KARVIAH imaging cohorts. The individual SUVR values are coded by clinical diagnosis; HEC (Healthy elderly controls, blue), MCI (green) and AD (red).

Table 5-1: Subject demographics for participant's classified as Aβ+ or Aβ- by PET SUVR measures in the AIBL-2 and KARVIAH cohorts.

	Low Neocortical SUVR (Aβ-)	High Neocortical SUVR (Aβ+)	*P* value
Number of subjects (*n*)	170	114	
Aβ PET SUVR (mean (S.D))	1.16 (0.09)	1.99 (0.41)	9.30×10^{-76}
Gender; females (*n* (%))	95 (56.5)	60 (53.5)	0.624
Age in years (mean (S.D))	73.73 (6.94)	75.79 (7.54)	0.036
Clinical diagnosis (*n* (%))	HEC: 161 (94.7) MCI: 8 (4.7) AD: 1 (0.6)	HEC: 77 (67.5) MCI: 13 (11.2) AD: 24 (21.3)	1.36×10^{-5}
APOE ε4 carrier (*n* (%))	45 (26.5)	68 (59.6)	4.56×10^{-4}
MMSE (mean (S.D))	28.26 (1.42)	26.79 (3.63)	9.30×10^{-4}

Abbreviations: HEC, Healthy elderly control; MCI, Mild cognitive impairment; AD, Alzheimer's disease; SUVR, Standardized uptake values ratio; S.D; Standard deviation; MMSE, Mini mental state examination.

All subjects were matched for gender but were significantly different in age (P = 0.036, Table 5-1). As expected, there was a bias towards an AD clinical diagnosis in the Aβ+ group (Table 5-1, Figure 5-3). With a larger number of AD subjects present in the Aβ+ group, it is expected that a significantly lower MMSE (P = 9.30 x10^{-4}) and a greater number *APOE* ε4 carriers (P = 4.56 x10^{-4}) would be observed (Table 5-1). However, when examining the HEC group separately (Table 5-2) there is no difference between MMSE when comparing Aβ+ and Aβ- groups (P = 0.261) but still a highly significant difference in *APOE* ε4 carriers remains (P = 3.34 x10^{-4}). This difference between the two groups needs to be accounted for when interpreting the results of the study.

Table 5-2: Subject demographics for healthy elderly controls (HEC) only participant's classified as Aβ+ or Aβ- by PET SUVR measures in the AIBL-2 and KARVIAH cohorts.

	Low Neocortical SUVR (Aβ-)	**High Neocortical SUVR (Aβ+)**	***P* value**
Number of subjects (*n*)	161	77	
Aβ PET SUVR (mean (S.D))	1.16 (0.09)	1.82 (0.27)	9.30 x10^{-54}
Gender; females (*n* (%))	91 (56.5)	42 (54.4)	0.522
Age in years (mean (S.D))	73.3	77.3	0.008
APOE ε4 carrier (*n* (%))	34 (21.1)	41 (53.2)	3.34 x10^{-4}
MMSE (mean (S.D))	29.2	28.9	0.261

Abbreviations: HEC, Healthy elderly control; SUVR, Standardized uptake values ratio; S.D; Standard deviation; MMSE, Mini mental state examination.

There is a significantly higher Aβ SUVR in the AIBL-2 cohort (P = 0.001) and a significantly lower MMSE in AIBL-2 (P = 0.017; Table 5-3). This is likely due to all AD and MCI individuals being from AIBL-2 and a higher percentage of *APOE* ε4 carriers in AIBL-2 (Table 5-3). Despite this, there was no statistical difference in the proportion of Aβ+ subjects recruited into this study between the two cohorts (P = 0.445). The subjects in the KARVIAH cohort were seen to be substantially older than AIBL-2 (P = 1.07 x10^{-7}). Once more, these cohort differences need to be considered when looking for protein differences between Aβ+ and Aβ- subjects.

Table 5-3: Subject demographics for participants separated by cohorts; AIBL-2 (*n* = 190) and KARVIAH (*n* = 94) imaging cohorts.

	AIBL-2 (^{11}C-PiB)	KARVIAH (^{18}FBB)	*P* value
Number of subjects (*n*)	190	94	
Aβ Classification; Aβ+ (*n* (%))	79 (41.58)	35 (37.24)	0.445
Aβ PET SUVR (mean (S.D))	1.60 (0.54)	1.36 (0.31)	0.001
Gender; females (*n* (%))	94 (49.49)	61 (64.89)	0.022
Age in years (mean (S.D))	72.41 (7.35)	78.26 (5.47)	1.07×10^{-7}
Clinical diagnosis (*n* (%))	HEC: 144 MCI: 21 AD: 25	HEC: 94 MCI: 0 AD: 0	n/a
APOE ε4 carrier (*n* (%))	82 (43.15)	21 (22.34)	0.001
MMSE (mean (S.D))	27.62 (3.10)	28.43 (1.48)	0.017

Abbreviations: HEC, Healthy elderly control; MCI, Mild cognitive impairment; AD, Alzheimer's disease; SUVR, Standardized uptake values ratio; S.D; Standard deviation; MMSE, Mini mental state examination.

5.4.2 Protein/peptide metrics

Our refined plasma proteomic methodology and subsequent LC-MS/MS acquisition (Figure 5-1) was performed on plasma samples from 284 subjects from the AIBL-2 and KARVIAH imaging cohorts, whose full demographics are shown in Table 5-1 and Table 5-3. Thus each sample followed a proteomic methodology which incorporated immunodepletion, TMT10plex peptide labelling and fractionation by isoelectric focusing (OGE). The 284 plasma samples were measured in 32 "TMT10plex groups" (9 clinical samples and 1 study reference). Each TMT10plex was fractionated into 20 peptide fractions which were individually analysed by an LTQ Orbitrap MS. The number of MS/MS events demonstrated in Table 5-4 indicates that sample preparation and instrument performance was consistent across all experiments.

Table 5-4: The number of MS/MS events acquired for each TMT10plex group. Each TMT10plex included 9 clinical samples from the AIBL-2 or KARVIAH imaging cohorts plus a study reference.

TMT10plex #	MS/MS events		
TMT1	189476	TMT17	170045
TMT2	148265	TMT18	152142
TMT3	158778	TMT19	166534
TMT4	220465	TMT20	166408
TMT5	186761	TMT21	166851
TMT6	186761	TMT22	166851
TMT7	158968	TMT23	180740
TMT8	159488	TMT24	158102
TMT9	162580	TMT25	184533
TMT10	167061	TMT26	165384
TMT11	161896	TMT27	169418
TMT12	166723	TMT28	173620
TMT13	170909	TMT29	174372
TMT14	144403	TMT30	168967
TMT15	169559	TMT31	174206
TMT16	171406	TMT32	169470

Mean	Standard Dev.	Coefficient of Variation (CV %)
169723.2	13934	8.21

We also examined the number of protein groups, peptides, PSMs and spectral yield rates of each TMT10plex group at 5% FDR (Table 5-5). In contrast to Chapter 3, due to peptide fractionation and not protein fractionation being utilised, each peptide identified for a unique protein group was combined to create one protein group score regardless of the fraction it was obtained from. On average 1,711 protein groups were measured per TMT10plex group and this was moderately consistent across all 10plex's (CV = 16.04%, Table 5-5). There was considerable variation in the number of PSMs measured and this was also reflected in the spectral yield. TMT10plex groups 4, 30, 31 and 32 demonstrated PSMs >70,000 and spectral yields of >3.5, this was significantly greater than the mean of the data (Table 5-5). However, this greater number of PSMs and spectral yield did not translate to a significantly greater number of protein groups.

Table 5-5: The performance of each TMT10plex by number of protein groups, peptides, PSM and spectral yield at FDR of 5%.

TMT10plex #	Protein Groups	Peptides	Peptide Spectral Matches (PSM)	Spectral Yield
TMT1	1615	4556	52218	0.28
TMT2	1377	3536	28520	0.19
TMT3	1665	3964	33026	0.21
TMT4	2164	6667	76239	0.35
TMT5	1510	3814	30408	0.16
TMT6	1510	3814	32897	0.18
TMT7	1472	3586	29408	0.18
TMT8	1941	4981	30064	0.19
TMT9	1933	4800	29897	0.18
TMT10	2170	5656	36044	0.22
TMT11	1763	4081	33443	0.21
TMT12	1757	4257	33137	0.2
TMT13	1852	4292	39375	0.23
TMT14	2117	5355	34059	0.24
TMT15	1906	4673	38994	0.23
TMT16	2244	5690	36694	0.21
TMT17	2055	5102	33468	0.2
TMT18	1969	4835	31666	0.21
TMT19	1560	3899	34744	0.21
TMT20	1823	4626	36320	0.22
TMT21	1913	4636	31135	0.19
TMT22	1276	4008	48451	0.29
TMT23	1315	4635	41456	0.23
TMT24	1445	4953	42180	0.27
TMT25	1810	4451	37490	0.2
TMT26	1316	4699	45321	0.27
TMT27	1480	4242	47360	0.28
TMT28	1443	4288	43682	0.25
TMT29	1451	4801	49144	0.28
TMT30	1865	5543	74788	0.44
TMT31	1919	5526	79463	0.46
TMT32	1860	5578	75008	0.44
Mean	1734.25	4673.71	41830.25	0.25
Standard Dev.	278.82	712.26	14847.88	0.08
Coefficient of Variation (CV %)	16.04%	15.24%	35.50%	31.17%

In total, 12,572 unique proteins groups at 5% FDR were identified across all 32 TMT10plex's. However, these protein groups were not observed across all TMT10plex groups. With the increased numbers of samples analysed in this study compared with the method development phase (Chapter 4), it was shown that a large proportion of protein groups were identified in <50% of subjects (Figure 5-4).

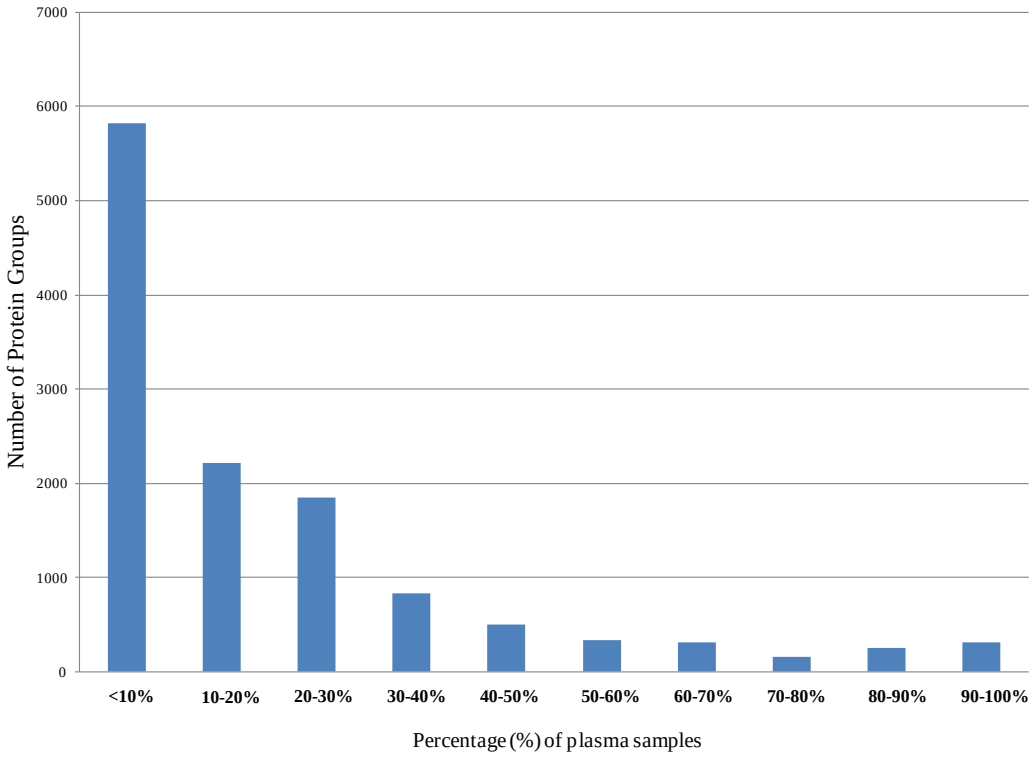

Figure 5-4: Bar chart to represent the frequency of identified protein groups in this study.

For the association of plasma proteins with NAB, only protein groups observed in >50% of the data (n = 1,085) were taken forward for further investigation. The full list of proteins groups investigated (shown as gene names) are listed in Appendix 4.

5.4.3 Generation of protein residuals by a generalised linear model (GLM)

All protein group ratios were $\log_{10}$ transformed to achieve normal distribution. Shaprio-Wilks normality tests (P >0.05) and a visual inspection of their histograms with Q-Q plots demonstrated that a large majority of the 1,085 protein groups still maintained a non-normal distribution. Therefore, further analyses utilised non-parametric statistical tests.

Covariates investigated included age, gender, cohort and technical variance. Firstly, before investigating covariates associated with the sample demographics, technical variation was investigated by principle component analysis (PCA). Scatter plot (Figure 5-5) demonstrated a clustering of TMT10plex groups, which would have a significant effect on protein ratios. A number of experimental factors are connected with TMT10plex group; OGE fractionation date, TMT labelling date and date of MS acquisition which are subject to significant variation. Therefore, an initial GLM correcting for only TMT10plex group was performed before investigating the effect of other covariates on protein group ratios (Figure 5-6).

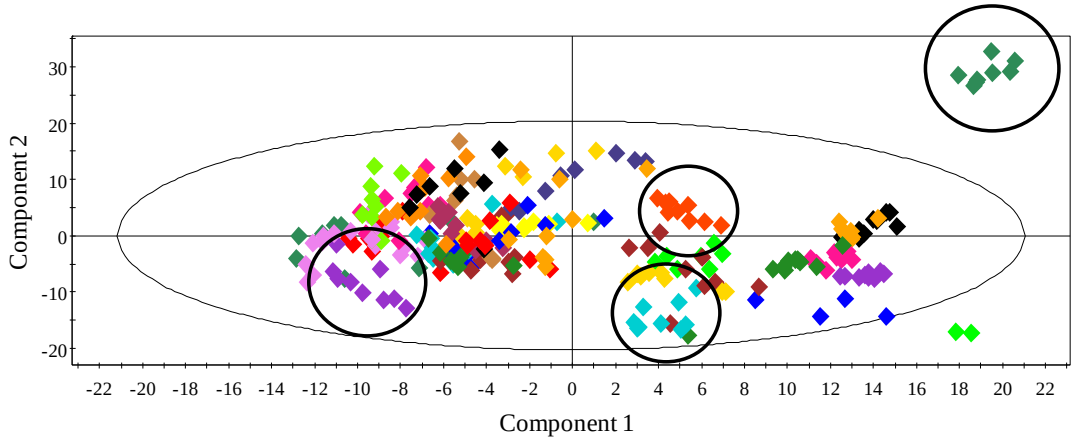

Figure 5-5: PCA analysis demonstrating the association of protein ratios with TMT10plex groups. Four examples of TMT10plex clusters are highlighted; TMT group 27 (green), TMT group 13 (orange), TMT group 25 (blue) and TMT group 11 (purple).

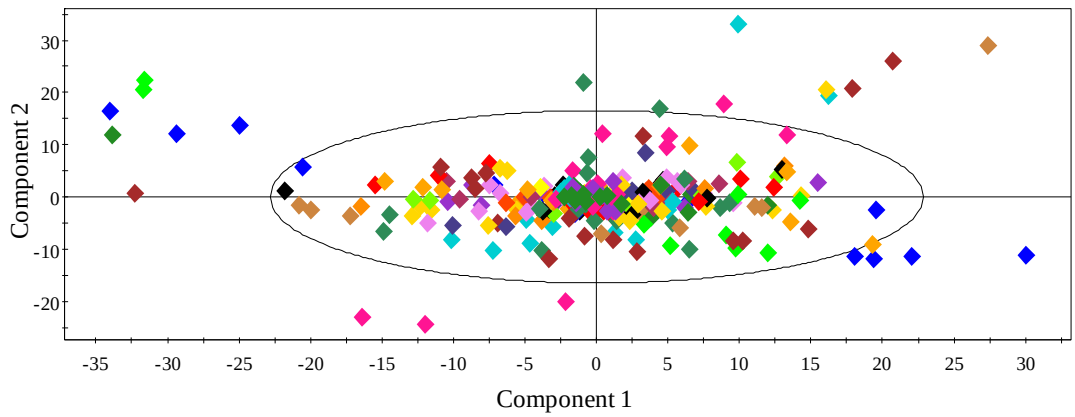

Figure 5-6: PCA analysis demonstrating the association of protein ratios with TMT10plex groups after GLM correction.

Residuals generated from the GLM (correcting for TMT10plex group variance; Figure 5-6) were then used to investigate other potential covariates. Table 5-6 shows the number protein groups that were significantly associated (uncorrected *P* value <0.05) with gender, age and cohort. We found that a substantial number of protein groups were significantly affected by these covariates. Using a Mann Whitney-U test, sample cohort (Table 5-7) and gender (Table 5-7) were associated with 17.06% and 15.86% of all protein groups respectively. Participant age (Table 5-9) was correlated with 9.85% of the total protein groups with a Spearman Rank Correlation. Therefore, a GLM model was reapplied to the original ratios to adjust the data for TMT10plex group with the addition of gender, age and sample cohort.

Table 5-6: The number of protein groups (*n*) associated with covariates (gender, age and cohort) at the uncorrected *P* value <0.05. A percentage (%) of the total number protein groups (*n* = 1,085) associated with covariates is also shown.

Covariate	*n*	%
Gender	172	15.86%
Age	104	9.85%
Sample cohort	191	17.06%

Table 5-7: Protein groups ranked by significance (shown as gene names) associated with sample cohort differences at the uncorrected *P* value <0.05.

Gene Name	*t*	*df*	*P* value				
ACTB	-4.611	282	6.00×10^{-06}	*ABHD10*	2.447	178	0.015
AK	-3.651	185	4.57×10^{-05}	*HOXD3*	-2.431	210	0.016
FN1	-5.373	282	4.20×10^{-04}	*MAP3K7*	2.433	184	0.016
STXBP3	4.028	185	4.70×10^{-04}	*MST1*	2.431	238	0.016
TPM3	-4.96	239	5.20×10^{-04}	*TARBP1*	2.418	220	0.016
TPM4	-3.742	211	9.85×10^{-04}	*UACA*	2.423	164	0.016
CDKL2	-3.441	185	0.001	*CFHR1*	2.401	282	0.017
NRGN	-3.312	274	0.001	*MFN1*	-2.408	150	0.017
THG1L	3.256	213	0.001	*MICALL2*	-2.407	190	0.017
CFD	3.16	282	0.002	*CENPF*	-2.384	208	0.018
KRT13	-3.137	210	0.002	*FGA*	-2.334	282	0.02
F9	3.038	282	0.003	*PON3*	-2.321	273	0.021
RAB3GAP2	-2.995	238	0.003	*GSE1*	-2.271	157	0.024
EPRS	-2.867	265	0.004	*IGHG2*	-2.252	282	0.025
KIAA1731	-2.882	168	0.004	*C1QB*	2.237	282	0.026
AMBP	2.822	282	0.005	*IGFBP3*	2.244	239	0.026
CDH13	-2.844	158	0.005	*PPFIBP2*	-2.246	172	0.026
CFP	2.854	264	0.005	*FUT8*	2.224	185	0.027
RELA	-2.82	177	0.005	*PROS1*	2.215	282	0.028
C4BPB	2.764	228	0.006	*CDH5*	-2.209	167	0.029
RIMS2	-2.783	211	0.006	*CEP290*	2.182	176	0.03
ZNF93	-2.761	158	0.006	*RFC4*	-2.186	178	0.03
FCN2	-2.746	141	0.007	*PON1*	-2.156	282	0.032
HSP90AA5P	-2.729	282	0.007	*ANKRD36B*	2.145	150	0.034
KIF4B	2.712	247	0.007	*ASH1L*	2.141	176	0.034
MTFMT	-2.724	248	0.007	*APOB*	-2.121	282	0.035
EPPK1	-2.673	238	0.008	*IGLC3*	2.109	273	0.036
FGG	-2.652	282	0.008	*FGB*	-2.099	282	0.037
EPB41	-2.631	168	0.009	*SHBG*	-2.091	269	0.037
RBP4	2.645	282	0.009	*SLC16A10*	-2.088	175	0.038
KIAA0753	-2.594	161	0.01	*SNX15*	-2.09	218	0.038
NDUFAF6	2.597	165	0.01	*SYTL2*	-2.089	150	0.038
APOH	2.569	282	0.011	*APOC4*	2.065	220	0.04
RLTPR	-2.572	167	0.011	*C1orf222*	-2.074	167	0.04
SRRM1	2.566	239	0.011	*PCNX*	-2.048	238	0.042
ULK2	-2.573	141	0.011	*C1S*	2.029	282	0.043
C1R	2.5	282	0.013	*FARSB*	2.017	141	0.046
HECTD4	2.508	175	0.013	*SYNE2*	2.001	259	0.046
PPBP	2.499	282	0.013	*FAM186A*	1.981	205	0.049
VEZT	-2.491	175	0.014				

Abbreviations: df, degree of freedom.

Table 5-8: Protein groups ranked by significance (shown as gene names) associated with participant gender at the uncorrected *P* value <0.05.

Gene Name	*t*	*df*	*P* value				
STX11	-3.929	274	1.08 x10^{-04}	*KIF16B*	-2.22	256	0.027
CDK1	3.313	255	0.001	*SERPING1*	2.222	282	0.027
KRT222	3.431	213	0.001	*KIF21B*	2.215	141	0.028
TRRAP	-2.96	176	0.003	*BIRC6*	-2.195	214	0.029
CD5L	2.942	282	0.004	*LRP1B*	-2.193	167	0.03
NPY5R	-2.862	248	0.005	*TPM4*	-2.181	211	0.03
RB1CC1	-2.836	141	0.005	*APOA2*	2.162	282	0.031
FAM81A	-2.771	221	0.006	*D2*	-2.171	204	0.031
VTN	-2.786	282	0.006	*ZFC3H1*	-2.178	186	0.031
SIPA1L1	-2.727	164	0.007	*DKFZp571N1833*	-2.151	203	0.033
CFHR5	2.681	203	0.008	*FCN3*	2.128	282	0.034
MAP2	-2.691	264	0.008	*GPSM2*	2.136	169	0.034
TPM3	-2.69	239	0.008	*DZIP3*	2.114	273	0.035
HCN2	2.614	168	0.01	*GC*	2.12	282	0.035
NCOR2	-2.592	220	0.01	*ANK3*	-2.118	155	0.036
DEFA1	-2.569	282	0.011	*GFAP*	-2.102	282	0.036
RELA	-2.586	177	0.011	*LRSAM1*	-2.114	173	0.036
IGHM	2.527	282	0.012	*SERPI3*	2.104	282	0.036
RG2	-2.534	157	0.012	*EIF5B*	-2.102	163	0.037
TRAK1	-2.491	221	0.013	*CHD5*	2.084	194	0.038
INTS3	2.464	282	0.014	*SLC16A10*	2.087	175	0.038
FGA	-2.421	282	0.016	*VIPAS39*	2.094	158	0.038
NEK3	2.399	274	0.017	*DST*	-2.075	264	0.039
PIBF1	2.387	282	0.018	*NRAP*	2.08	247	0.039
IGKC	2.353	282	0.019	*CROCC*	2.057	237	0.041
BLOC1S6	2.352	211	0.02	*RAB3GAP2*	-2.039	238	0.043
LRP12	-2.349	264	0.02	*C1QC*	2.027	221	0.044
MASP2	-2.356	151	0.02	*SCN2A*	-2.016	168	0.045
APOB	2.329	282	0.021	*ATRN*	2.006	282	0.046
GMFG	-2.327	282	0.021	*BAZ2B*	-2.007	195	0.046
CNNM4	2.305	165	0.022	*DAPK1*	-2.012	168	0.046
FN1	-2.255	282	0.025	*REST*	-1.991	282	0.047
TRIL	-2.259	150	0.025	*ORM2*	1.987	282	0.048
TTC7B	-2.265	176	0.025	*PCDHB15*	-1.967	222	0.05
C2	2.229	280	0.027	*SNCA*	-1.97	274	0.05
HMBOX1	2.24	140	0.027				

Abbreviations: df, degree of freedom.

Table 5-9: Protein groups ranked by significance (shown as gene names) correlating with participant age at the uncorrected *P* value <0.05.

Gene Name	Spearman Rank Correlation (Rho)	*P* value			
APOL1	-0.209	2.31 x10^{-4}	*SLC16A10*	-0.175	0.02
C7	0.215	2.59 x10^{-4}	*VEZT*	-0.175	0.02
ABHD10	0.271	3.83 x10^{-4}	*ZC3H13*	-0.166	0.021
CFD	0.187	0.002	*MUC12*	0.172	0.021
AMBP	0.177	0.003	*ACTB*	-0.136	0.022
EPB41	-0.226	0.003	*EPRS*	-0.139	0.023
CDH13	-0.231	0.003	*KRT20*	-0.133	0.025
CASC2	0.201	0.006	*ZNF106*	-0.166	0.025
HECTD4	0.201	0.007	*APOC3*	-0.13	0.029
KIAA0753	-0.206	0.008	*TPM3*	-0.141	0.029
DENND3	-0.199	0.01	*RELA*	-0.163	0.029
ULK2	-0.216	0.01	*SERPI6*	-0.128	0.031
MAPK9	-0.18	0.013	*TPM4*	-0.146	0.033
KRT18	0.2	0.013	*HAUS3*	-0.172	0.034
TXLNG	-0.209	0.013	*APOB*	-0.125	0.036
GSE1	-0.195	0.014	*CA5A*	-0.142	0.037
SERPINF2	-0.144	0.015	*FN1*	-0.123	0.039
IGKC	0.144	0.015	*CD163*	0.172	0.041
SPHKAP	-0.174	0.015	*APOH*	0.117	0.048
FMN2	0.159	0.016	*IGLC3*	0.119	0.049
RIMS3	0.144	0.017	*CADPS2*	-0.116	0.05
LRSAM1	0.178	0.019			

Abbreviations: df, degree of freedom.

We also examined our GLM adjusted protein group data for association with *APOE* status. As *APOE* genotype is itself highly correlated with AD and *APOE* ε4 variants influence the clearance of Aβ, it is possible that differences can be entirely or largely due to differences in *APOE* genotype. It was found that 46 protein groups were associated with *APOE* genotype (Table 5-10). This included proteins related to Aβ (Amyloid beta A4 protein (Aβ) and amyloid beta A4 precursor protein-binding family B member 3 (APBB3)) and the apoE protein itself. ApoE was found to be significantly lower in ε4 carriers (P = 0.013). *APOE* genotype was not included in the GLM model because of its contribution in AD. However protein groups found to be associated with *APOE* genotype (Table 5-10) were separately investigated with *APOE* genotype as a covariate.

Table 5-10: Protein groups ranked by significance (shown as gene names) associated with *APOE* genotype at the uncorrected *P* value <0.05.

Gene name	*t*	*df*	*P* value				
NEFL	-3.755	256	0.001	*BROMI*	2.416	194	0.017
NBEA	3.766	150	0.001	*ASPM*	2.393	229	0.018
APP	-3.253	282	0.001	*TBC1D32*	2.389	194	0.018
APBB3	-3.389	273	0.001	*B2M*	2.342	247	0.02
EPPK1	3.277	238	0.001	*ABCA6*	2.345	174	0.02
SYTL2	3.28	150	0.001	*CEP250*	-2.346	167	0.02
HECTD3	3.276	148	0.001	*FGB*	2.315	282	0.021
HABP2	3.039	282	0.003	*STXBP3*	-2.263	185	0.025
TMEM131	2.969	155	0.003	*DNM3*	2.213	159	0.028
SLBP	2.936	193	0.004	*KANSL1*	2.207	146	0.029
KRT1	-2.858	282	0.005	*FN1*	2.108	282	0.036
DYNC1H1	-2.724	220	0.007	*IL18RAP*	-2.109	273	0.036
TRIP11	2.716	194	0.007	*HLTF*	2.111	168	0.036
CSDE1	-2.642	256	0.009	*KLKB1*	2.094	282	0.037
APOE	2.489	282	0.013	*STX11*	-2.102	274	0.037
OBSCN	2.51	202	0.013	*AKNA*	2.102	185	0.037
NEUROG2	-2.469	273	0.014	*ANKRD36B*	2.054	150	0.042
NEK3	2.44	274	0.015	*ATRN*	2.03	282	0.043
KRT9	-2.449	189	0.015	*FAN1*	2.044	173	0.043
EPRS	2.435	265	0.016	*REV3L*	-2.046	147	0.043
KRT8	-2.428	150	0.016	*A2M*	1.996	282	0.047
LGALS3BP	2.412	282	0.017	*BLOC1S6*	1.978	211	0.049
KRT10	-2.407	282	0.017	*FUT8*	-1.985	185	0.049

Abbreviations: df, degree of freedom.

5.4.4 Plasma proteins correlating with Aβ SUVR as continuous measure

Spearman Rank Correlations were performed to associate the GLM adjusted values of 1,085 protein groups with Aβ SUVR as a continuous measure. A total of 57 protein groups were found to be significantly associated with SUVR at the uncorrected *P* value of <0.05 (Table 5-11). After multiple testing correction (FDR), seven protein groups demonstrated a *Q* value of <0.1 (amyloid beta A4 protein (Aβ), neurofilament light polypeptide (NEFL), neurogenin-2 (NEUROG2), amyloid beta A4 precursor protein-binding family B member 3 (APBB3), V-type proton ATPase 116 kDa subunit (ATP6V0A2), rootletin (CROCC) and isoform 4 of RE1-silencing transcription factor (REST). A positive correlation with Aβ SUVR was observed for

Aβ, NEFL, NEUROG2, APBB3 and ATP6V0A2 with negative association with observed for CROCC and REST (Table 5-11).

A partial correlation, adjusting for *APOE* genotype, was only performed on protein groups associated with Aβ SUVR that were also previously seen to be influenced by *APOE* genotype (Table 5-10). After adjustment for *APOE*, seven protein groups remained significantly correlated at the uncorrected *P* value <0.05 with Aβ, NEFL and NEUROG2 remaining significant after FDR multiple testing correction. A total of eight protein groups found to be associated with Aβ SUVR lost significance at the uncorrected *P* value <0.05 suggesting that their significance with Aβ was driven by *APOE* (Table 5-11).

Table 5-11: Protein groups significantly associated with Aβ SUVR as a continuous measure (using a Spearman's Rank Correlation). GLM residuals were adjusted for TMT10plex group, age, gender and sample cohort. A partial correlation co-varying for *APOE* genotype for *APOE* associated protein groups (Table 5-10) was also investigated. Benjamini-Hochberg *Q* values were calculated for multiple testing correction.

				Spearman Rank Correlation with SUVR			Partial Correlation with SUVR (adjusting for *APOE* status)		
UniProt ID	**Protein Description**	**Gene Name**	***n***	**Rho**	***P* value**	***Q* value**	**Partial Correlation**	***P* value**	***Q* value**
P05067	amyloid beta A4 protein (Aβ)	*APP*	284	0.286	1.05×10^{-06}	5.87×10^{-04}	0.233	7.50×10^{-05}	0.024
P07196	neurofilament light polypeptide (NEFL)	*NEFL*	258	0.29	2.46×10^{-06}	6.88×10^{-04}	0.223	3.15×10^{-04}	0.059
Q9H2A3	neurogenin-2 (NEUROG2)	*NEUROG2*	275	0.272	5.28×10^{-06}	9.84×10^{-04}	0.235	8.63×10^{-05}	0.024
O95704	amyloid beta A4 precursor protein-binding family B member 3 (APBB))	*APBB3*	275	0.24	6.59×10^{-05}	9.21×10^{-03}	0.177	0.003	0.152
Q9Y487	V-type proton ATPase 116 kDa subunit (ATP6V0A2)	*ATP6V0A2*	143	0.292	3.19×10^{-04}	3.57×10^{-02}			
Q5TZA2	rootletin (CROCC)	*CROCC*	239	-0.216	0.001	0.080			
Q13127	isoform 4 of RE1-silencing transcription factor (REST)	*REST*	284	-0.19	0.001	0.080			
Q14520	hyaluronan-binding protein 2	*HABP2*	284	-0.188	0.002	0.124	-0.129	0.030	>0.200
Q8IVF4	dynein heavy chain 10, axonemal	*DNAH10*	240	0.202	0.002	0.124			
P29597	non-receptor tyrosine-protein kinase	*TYK2*	239	-0.188	0.004	0.186			
P42356	phosphatidylinositol 4-kinase alpha	*PI4KA*	160	-0.228	0.004	0.186			
P15924	desmoplakin	*DSP*	231	0.188	0.004	0.186			
O60841	eukaryotic translation initiation factor 5B	*EIF5B*	165	-0.216	0.006	>0.200			
Q6ZUS6	coiled-coil domain-containing protein 149	*CCDC149*	151	0.221	0.007	>0.200			

Q6P2H3	centrosomal protein of 85 kDa	*CEP85*	169	0.203	0.007	>0.200			
A2RUS2	DENN domain-containing protein 3	*DENND3*	167	-0.211	0.007	>0.200			
Q9UQ16	dynamin-3	*DNM3*	161	-0.212	0.008	>0.200	-0.158	0.046	>0.200
Q9UKN1	mucin-12	*MUC12*	179	-0.198	0.009	>0.200			
Q13103	secreted phosphoprotein 24	*SPP2*	179	-0.199	0.009	>0.200			
P03952	plasma kallikrein	*KLKB1*	284	-0.155	0.009	>0.200	-0.116	0.052	>0.200
Q8IWV7	E3 ubiquitin-protein ligase	*UBR1*	149	0.212	0.010	>0.200	0.172	0.037	>0.200
Q8IZ81	ELMO domain-containing protein 2	*ELMOD2*	213	-0.177	0.011	>0.200			
O60674	tyrosine-protein kinase JAK2	*JAK2*	143	0.215	0.012	>0.200			
P00734	prothrombin	*F2*	284	-0.15	0.012	>0.200			
Q9Y2M0	fanconi-associated nuclease 1	*FAN1*	175	-0.191	0.012	>0.200	-0.143	0.060	>0.200
P01861	Ig gamma-4 chain C region	*IGHG4*	284	0.149	0.013	>0.200			
B1AJZ9	forkhead-associated domain-containing protein 1	*FHAD1*	184	0.18	0.013	>0.200			
Q15485	ficolin-2	*FCN2*	143	-0.206	0.013	>0.200			
Q9NSD9	phenylalanine--tRNA ligase beta subunit	*FARSB*	143	0.214	0.013	>0.200			
P0DJI8	serum amyloid A-1 protein	*SAA1*	284	0.148	0.013	>0.200			
Q92686	neurogranin	*NRGN*	276	0.147	0.015	>0.200			
Q15047	histone-lysine N-methyltransferase SETDB1	*SETDB1*	160	0.195	0.015	>0.200			
P51956	serine/threonine-protein kinase	*NEK3*	276	-0.147	0.015	>0.200	-0.098	0.104	>0.200
Q8TDY2	RB1-inducible coiled-coil protein 1	*RB1CC1*	143	0.202	0.017	>0.200			
Q8N139	ATP-binding cassette sub-family A member 6	*ABCA6*	176	-0.179	0.019	>0.200	-0.121	0.110	>0.200
Q09666	neuroblast differentiation-associated protein	*AHNAK*	230	-0.154	0.021	>0.200			
P35249	replication factor C subunit 4	*RFC4*	180	-0.173	0.022	>0.200			

P49454	centromere protein F	*CENPF*	210	-0.162	0.022	>0.200			
Q12830	nucleosome-remodeling factor subunit BPTF	*BPTF*	142	-0.186	0.025	>0.200			
Q5T447	E3 ubiquitin-protein ligase	*HECTD3*	150	-0.181	0.026	>0.200	-0.087	0.293	>0.200
Q9NTJ3	structural maintenance of chromosomes protein 4	*SMC4*	169	0.171	0.027	>0.200			
Q14624	Inter-alpha-trypsin inhibitor heavy chain H4	*ITIH4*	284	0.13	0.029	>0.200			
P81274	G-protein-signaling modulator 2	*GPSM2*	171	-0.171	0.030	>0.200			
P35542	serum amyloid A-4 protein	*SAA4*	284	0.128	0.032	>0.200			
Q6RI45	bromodomain and WD repeat-containing protein 3	*BRWD3*	195	-0.154	0.034	>0.200			
Q9NQW8	cyclic nucleotide-gated cation channel beta-3	*CNGB3*	239	-0.137	0.037	>0.200			
Q8TBY8	polyamine-modulated factor 1-binding protein 1	*PMFBP1*	196	0.148	0.037	>0.200			
P08571	monocyte differentiation antigen CD14	*CD14*	263	0.129	0.037	>0.200			
P02647	apoA1	*APOA1*	284	-0.124	0.037	>0.200			
P17936	insulin-like growth factor-binding protein 3	*IGFBP3*	241	-0.134	0.038	>0.200			
P21549	serine-pyruvate aminotransferase	*AGT*	284	0.123	0.039	>0.200			
O95256	interleukin-18 receptor accessory protein	*IL18RAP*	275	0.123	0.041	>0.200	0.08	0.188	>0.200
P23142	fibulin-1	*FBLN1*	275	0.123	0.042	>0.200			
Q8IX21	SMC5-SMC6 complex localization factor protein 2	*FAM178A*	182	-0.15	0.042	>0.200			
P05787	keratin, type II cytoskeletal 8	*KRT8*	152	0.166	0.043	>0.200	0.098	0.232	>0.200
Q8N7X0	androglobin	*ADGB*	198	-0.139	0.045	>0.200			
P02751	fibronectin	*FN1*	284	-0.118	0.049	>0.200	-0.075	0.211	>0.200

Among our 284 subjects, a proportion had received a diagnosis of either MCI or AD (n = 46). With the pressing need for a biomarker at the preclinical stage of disease, we decided to investigate Aβ SUVR correlations in the cognitively normal individuals only. Demographics of the cognitively normal individuals (HEC) can be found in Table 5-2. In removing MCI and AD individuals from the analysis we found that 25 protein groups lost statistical association with Aβ at the uncorrected P <0.05 (Table 5-12). It is possible that these proteins are more associated with an MCI/AD diagnosis than Aβ SUVR. However, it is more likely the reduction in significance is due to loss of statistical power as 95% of AD and 61% MCI individuals are found in the Aβ+ group.

Table 5-12: Protein groups (shown as gene names) that lost statistical significance (at the uncorrected *P* <0.05) when removing individuals with a clinical diagnosis of MCI and AD.

Gene Name		
CROCC	*APOA1*	*HECTD3*
IL18RAP	*FCN2*	*NEK3*
ELMOD2	*AGT*	*CENPF*
SETDB1	*DSP*	*TYK2*
EIF5B	*UBR1*	*FARSB*
AHNAK	*RB1CC1*	*MUC12*
FAM178A	*IGHG4*	*KRT8*
ITIH4	*SAA4*	*FN1*
IGFBP3		

In addition, a further 19 protein groups became significantly correlated with Aβ SUVR when examining just the cognitively normal group (Table 5-13, highlighted green), most notably brain mitochondrial carrier protein 1 (SLC25A14). None of these 19 protein groups passed multiple testing corrections or were seen to be associated with *APOE* genotype. It was also apparent that Aβ (Figure 5-7), NEUROG2 (Figure 5-8) and NEFL (Figure 5-9) were more associated with Aβ SUVR in the cognitively normal group (Table 5-13) whereas APBB3, REST, CROCC and ATP6V0A2 became less significant. DENN domain-containing protein 3 (DENND3) became highly significant with Aβ SUVR when removing AD and MCI subjects and also passed multiple testing correction (Q = 0.004).

Table 5-13: Protein groups significantly associated with Aβ SUVR as a continuous measure (using a Spearman's Rank correlation) in cognitively normal subjects only. A total of 25 protein groups lost association with Aβ at the uncorrected *P* <0.05. An additional 19 protein groups became significantly correlated with Aβ SUVR in the cognitively normal group (highlighted in green). GLM residuals adjusted for TMT10plex group, age, gender and sample cohort. Benjamini-Hochberg *Q* values were calculated for multiple testing correction.

Uniprot ID	Protein Description	Gene Name	*n*	Rho	*P* value	*Q* value
P05067	amyloid beta A4 protein (Aβ)	*APP*	238	0.336	1.09×10^{-07}	3.84×10^{-05}
Q9H2A3	neurogenin-2 (NEUROG2)	*NEUROG2*	230	0.339	1.37×10^{-07}	3.84×10^{-05}
P07196	neurofilament light polypeptide (NEFL)	*NEFL*	215	0.327	9.73×10^{-07}	1.82×10^{-04}
A2RUS2	DENN domain-containing protein 3 (DENND3)	*DENND3*	143	-0.343	2.70×10^{-05}	0.004
O95704	amyloid beta A4 precursor protein-binding family B member 3 (APBB3)	*APBB3*	230	0.249	1.35×10^{-04}	0.02
Q8IVF4	dynein heavy chain 10, axonemal	*DNAH10*	202	0.213	0.002	0.16
Q9UQ16	dynamin-3	*DNM3*	134	-0.267	0.002	0.16
Q13127	isoform 4 of RE1-silencing transcription factor (REST)	*REST*	238	-0.179	0.006	>0.200
Q6ZUS6	coiled-coil domain-containing protein 149	*CCDC149*	128	0.237	0.007	>0.200
Q8TBY8	polyamine-modulated factor 1-binding protein 1	*PMFBP1*	168	0.209	0.007	>0.200
O95258	brain Mitochondrial Carrier Protein 1 (SLC25A14)	*SLC25A14*	223	0.177	0.008	>0.200
Q12830	nucleosome-remodeling factor subunit BPTF	*BPTF*	113	-0.242	0.01	>0.200
Q9Y487	V-type proton ATPase 116 kDa subunit (ATP6V0A2)	*ATP6V0A2*	120	0.231	0.011	>0.200
P00734	prothrombin	*F2*	238	-0.165	0.011	>0.200
Q9Y2M0	fanconi-associated nuclease 1	*FAN1*	152	-0.207	0.011	>0.200

P23142	fibulin-1	*FBLN1*	230	0.168	0.011	>0.200
Q6P2H3	centrosomal protein of 85 kDa	*CEP85*	144	0.204	0.014	>0.200
P08571	monocyte differentiation antigen CD14	*CD14*	222	0.163	0.015	>0.200
P0CF74	Ig lambda-6 chain C region	*IGLC6*	183	0.18	0.015	>0.200
Q92686	neurogranin	*NRGN*	231	0.158	0.016	>0.200
Q9NQW8	cyclic nucleotide-gated cation channel beta-3	*CNGB3*	199	-0.168	0.018	>0.200
P20742	pregnancy zone protein	*PZP*	238	0.152	0.019	>0.200
B1AJZ9	forkhead-associated domain-containing protein 1	*FHAD1*	163	0.181	0.021	>0.200
Q14520	hyaluronan-binding protein 2	*HABP2*	238	-0.149	0.021	>0.200
Q6RI45	bromodomain and WD repeat-containing protein 3	*BRWD3*	171	-0.173	0.024	>0.200
P32189	glycerol kinase	*GK*	164	0.175	0.025	>0.200
Q659A1	little elongation complex subunit 2	*NARG2*	131	-0.195	0.026	>0.200
P35249	replication factor C subunit 4	*RFC4*	146	-0.185	0.026	>0.200
Q8N139	ATP-binding cassette sub-family A member 6	*ABCA6*	154	-0.177	0.028	>0.200
Q08379	golgin subfamily A member 2	*GOLGA2*	186	-0.161	0.029	>0.200
P03952	plasma kallikrein	*KLKB1*	238	-0.142	0.029	>0.200
Q9BQG0	myb-binding protein 1A	*MYBBP1A*	149	-0.179	0.029	>0.200
Q8IYT8	serine/threonine-protein kinase ULK2	*ULK2*	123	0.196	0.03	>0.200
P02765	alpha-2-HS-glycoprotein	*AHSG*	238	-0.138	0.033	>0.200
Q8NDH2	coiled-coil domain-containing protein 168	*CCDC168*	140	-0.177	0.036	>0.200

Q9NTJ3	structural maintenance of chromosomes protein 4	*SMC4*	141	0.175	0.038	>0.200
P31483	nucleolysin TIA-1 isoform p40	*TIA1*	134	-0.179	0.038	>0.200
O60674	tyrosine-protein kinase JAK2	*JAK2*	118	0.19	0.039	>0.200
Q8IVF2	protein AHNAK2	*AHNAK2*	136	0.176	0.041	>0.200
Q96RV3	pecanex-like protein	*PCNX*	203	0.143	0.042	>0.200
Q9NQ66	1-phosphatidylinositol 4,5-bisphosphate phosphodiesterase beta-1	*PLCB1*	117	-0.187	0.043	>0.200
P42356	phosphatidylinositol 4-kinase alpha	*PI4KA*	134	-0.174	0.044	>0.200
Q13103	secreted phosphoprotein 24	*SPP2*	153	-0.163	0.044	>0.200
O15078	centrosomal protein of 290 kDa	*CEP290*	151	-0.163	0.045	>0.200
Q0VDD8	dynein heavy chain 14, axonemal	*DNAH14*	137	-0.172	0.045	>0.200
P27816	microtubule-associated protein 4	*MAP4*	162	-0.156	0.048	>0.200
Q14524	sodium channel protein type 5 subunit alpha	*NAV1*	231	0.13	0.049	>0.200
Q8IYB3	serine/arginine repetitive matrix protein 1	*SRRM1*	204	-0.138	0.049	>0.200

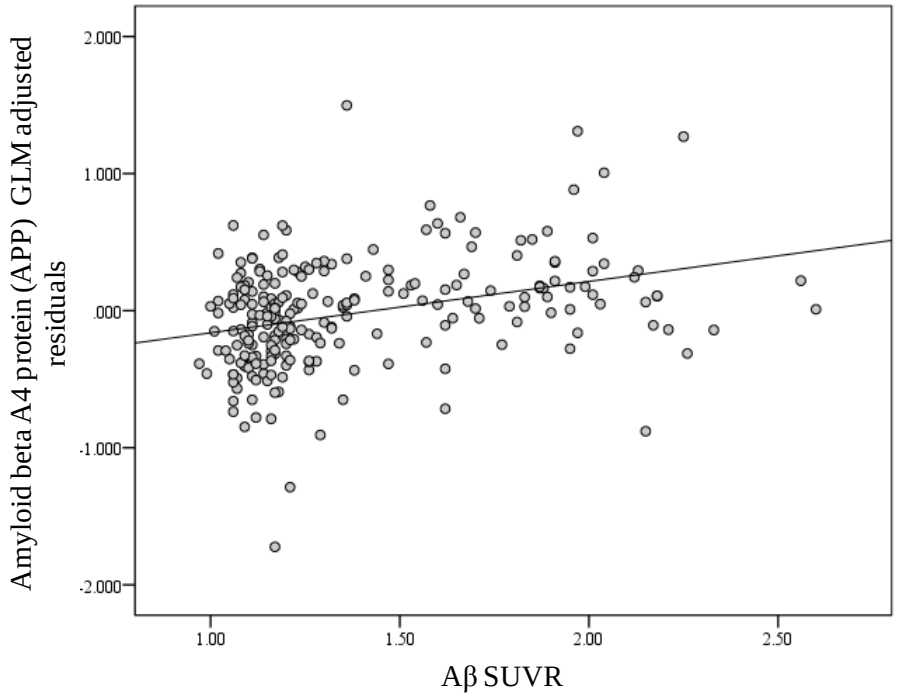

Figure 5-7: Scatter plot to show the correlation between amyloid beta A4 protein (Aβ) and Aβ SUVR in cognitively normal individuals (P = 1.09 x10^{-07}; Q = 3.84 x10^{-05}).

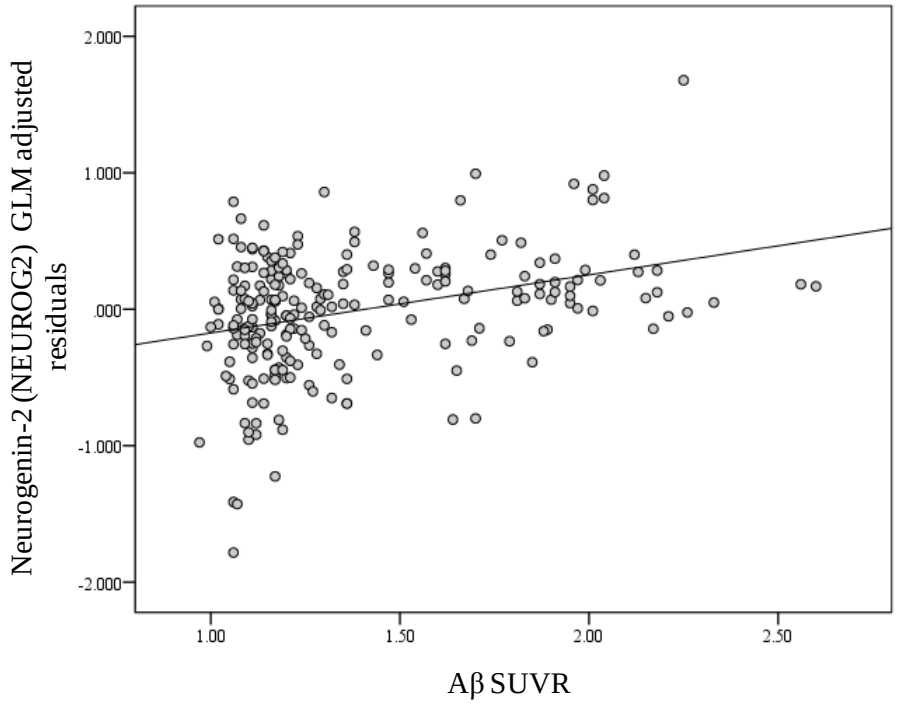

Figure 5-8: Scatter plot to show the correlation between neurogenin-2 (NEUROG2) and Aβ SUVR in cognitively normal individuals (P = 1.37 x10^{-07}; Q = 3.84 x10^{-05}).

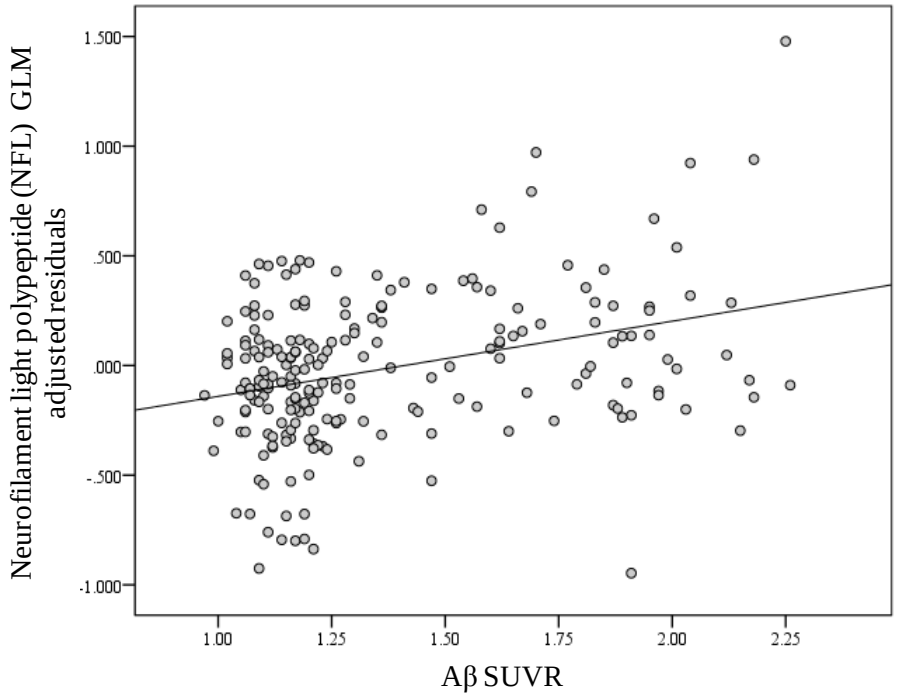

Figure 5-9: Scatter plot to show the correlation between neurofilament light polypeptide (NEFL) and Aβ SUVR in cognitively normal individuals (*P* = 9.73 x10^{-07}; *Q* = 1.82 x10^{-04}).

5.4.5 Plasma proteins associated with Aβ classification

Aβ SUVR measures from the 284 individuals were categorised as Aβ- or Aβ+. The AIBL-2 cohort underwent ^{11}C-PiB PET neuroimaging and an Aβ+ cut-off was defined as ≥1.5. The KARVIAH cohort underwent ^{18}FBB PET imaging and Aβ+ cut-off was defined as ≥1.35. The distribution of Aβ- or Aβ+ individuals is shown in Figure 5-2. The 1,085 GLM adjusted protein groups were analysed for their association with pathology endophenotypes (Aβ- versus Aβ+) using a Mann Whitney-U test. A total of 57 protein groups were found be statistically different between Aβ- and Aβ+ groups at the uncorrected *P* value <0.05 (Table 5-14). After correction for multiple testing nine protein groups remained associated with Aβ classification (*Q* = <0.1, Table 5-14). Once more Aβ (Figure 5-10), NEUROG2 (Figure 5-11), NEFL (Figure 5-12), APBB3 (Figure 5-13) and REST (Figure 5-14) were the most significant protein groups associated NAB classification.

Unsurprisingly, there was a large overlap (43/57) between the candidate protein groups correlating with Aβ SUVR and those associated with Aβ classification. The

protein group that was most associated with Aβ classification without being associated with Aβ SUVR was serotransferrin (TF; *P* = 0.0009, Figure 5-15). Furthermore, protein groups previously associated with *APOE* genotype (Table 5-10) were further investigated with *APOE* being added to the GLM model and subsequent Mann Whitney-U analysis performed. This demonstrated consistent findings with Table 5-11 with a number of protein groups association with Aβ attributed to *APOE* genotype. Aβ, NEUROG2, NEFL and APBB3 still passed FDR multiple testing corrections after adjustment for *APOE* genotype.

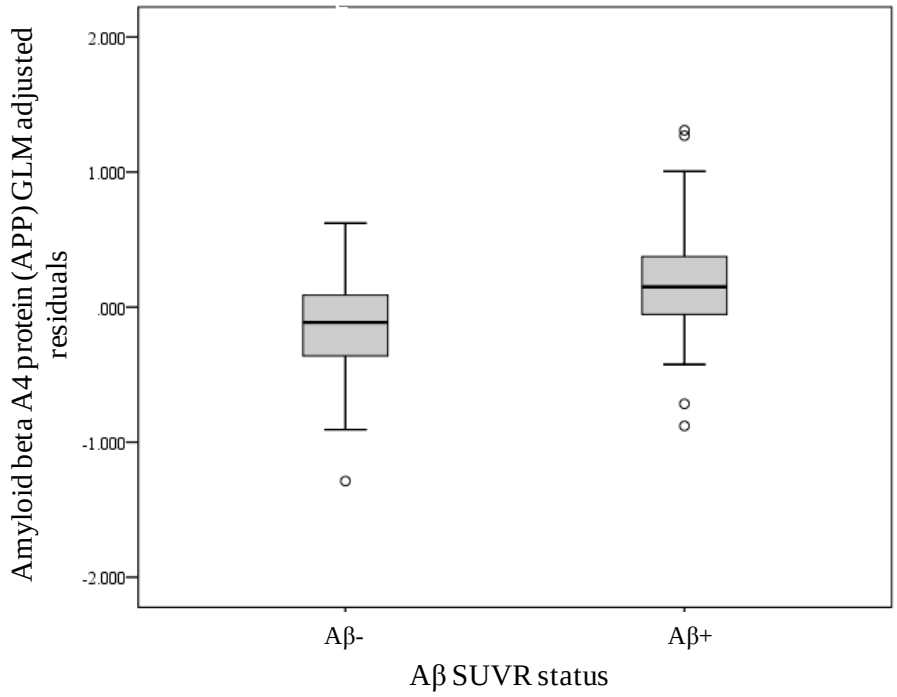

Figure 5-10: Box and whisker diagram to show the amyloid beta A4 (Aβ) protein group differences (*P* = 1.26 x10^{-08}; *Q* = 7.06 x10^{-06}) between Aβ- and Aβ+ groups.

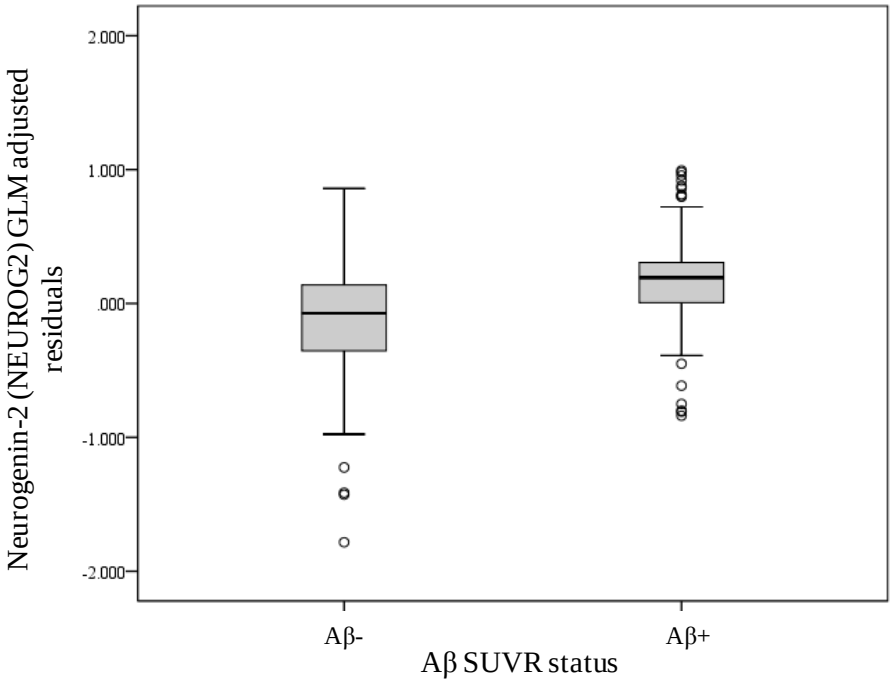

Figure 5-11: Box and whisker diagram to show the neurogenin-2 (NEUROG2) protein group differences (P = 1.20 x10^{-07}; Q = 3.36 x10^{-05}) between Aβ- and Aβ+ groups.

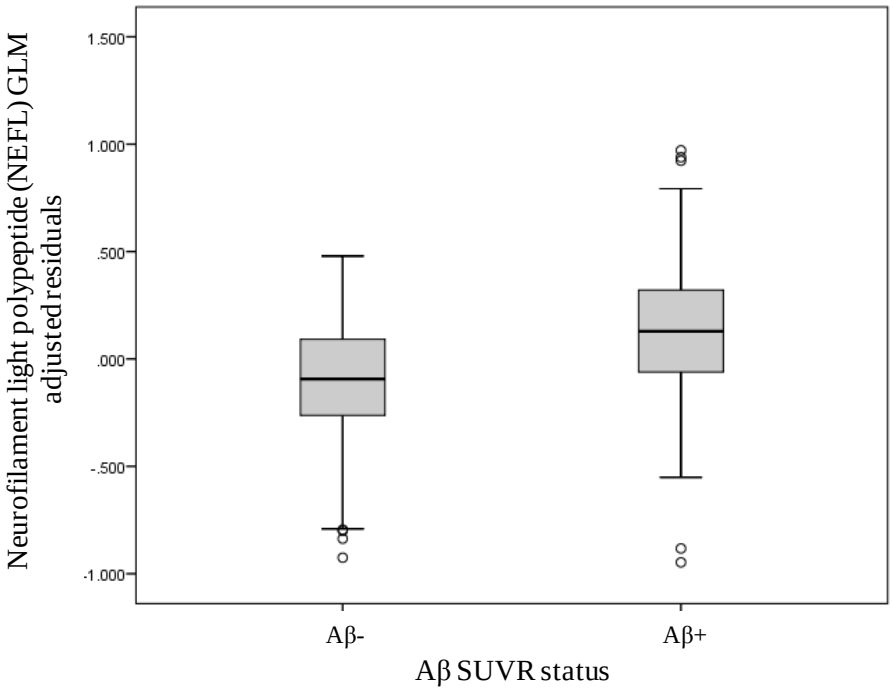

Figure 5-12: Box and whisker diagram to show the neurofilament light polypeptide (NEFL) protein group differences (P = 2.26 x10^{-07}; Q = 4.22 x10^{-05}) between Aβ- and Aβ+ groups.

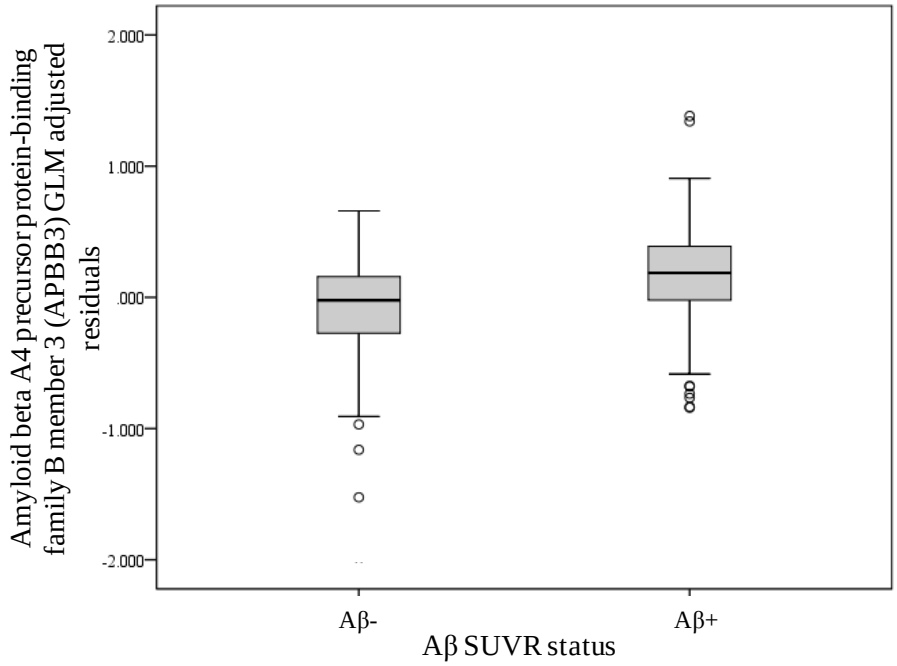

Figure 5-13: Box and whisker diagram to show the amyloid beta A4 precursor protein-binding family B member 3 (APBB3) protein group differences (*P* = 1.54 x10^{-06}; *Q* = 2.16 x10^{-04}) between Aβ- and Aβ+ groups.

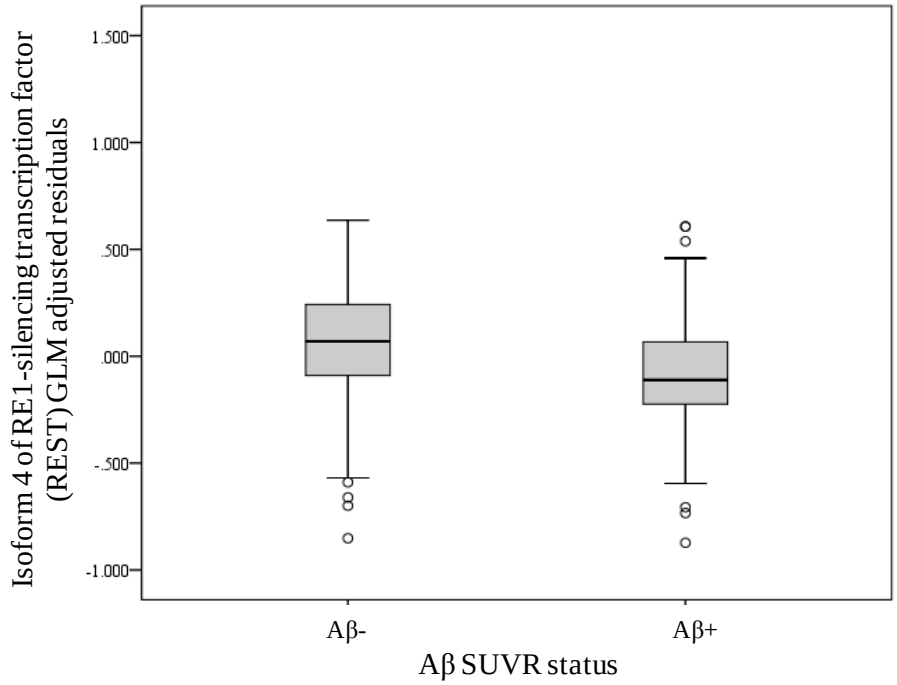

Figure 5-14: Box and whisker diagram to show the RE1-silencing transcription factor (REST) protein group differences (P = 8.03 x10-05; Q = 0.009) between Aβ- and Aβ+ groups.

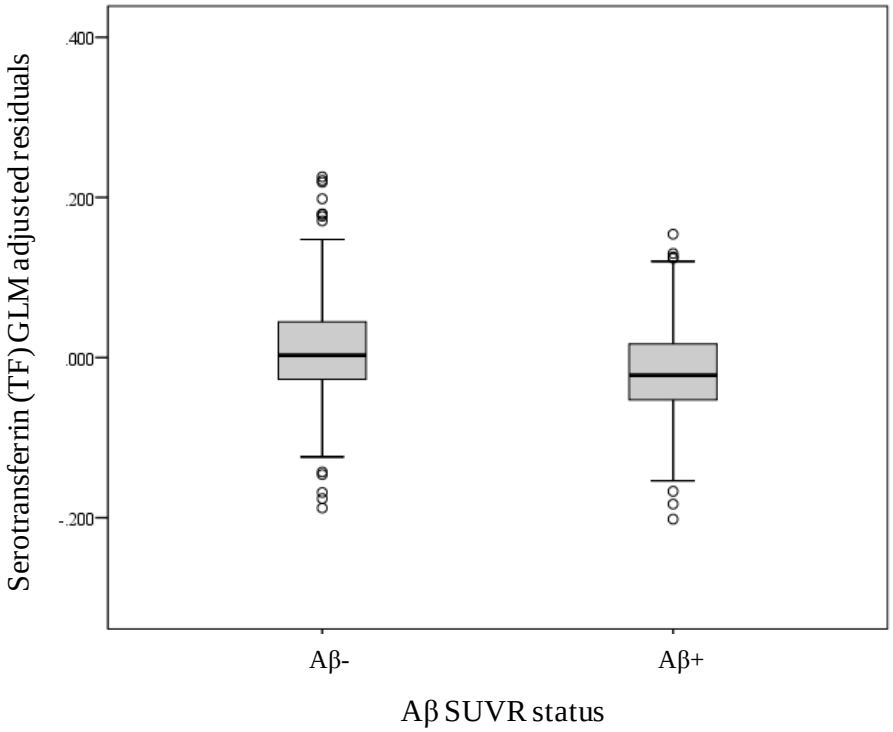

Figure 5-15: Box and whisker diagram to show the serotransferrin (TF) protein group differences (P = 0.0009) between Aβ- and Aβ+ groups.

In cognitively normal subjects we demonstrated a reduced group of 32 protein groups being associated with Aβ classification (Table 5-15). A total of eight protein groups were exclusively associated with Aβ classification when excluding MCI and AD participants. These protein groups were probable methyltransferase (TARBP1), proline-glutamic acid-leucine-rich protein 1 (PLEP1), ninein (NIN), pecanex-like protein 1 (PCNX), CC5, dickkopf-like protein 1 (DKKL1), nucleolysin TIA-1 isoform p40 (TIA1) and cilia- and flagella-associated protein 43 (WDR96). None of these protein groups were associated with *APOE* genotype not did they pass FDR correction. There seemed to be little change in the association of Aβ classification and Aβ, NEUROG2, NEFL, APBB3 and REST whereas TF, cyclic nucleotide-gated cation channel beta-3 (CNGB3), neurogranin (NRGN) and DENN3 all passed multiple testing correction (Q = <0.100) in the cognitively normal group (Table 5-15).

Table 5-14: Protein groups significantly associated with Aβ classification (Aβ- or Aβ+) using a Mann Whitne-U test. GLM residuals adjusted for TMT10plex group, age, gender and sample cohort. An additional GLM was performed adjusting for *APOE* genotype. Benjamini-Hochberg *Q* values were calculated for multiple testing correction.

			Mann Whitney-U for group differences (Aβ- versus Aβ+)			Mann Whitney-U for group differences (Aβ- versus Aβ+) adjusted for *APOE* genotype		
UniProt ID	**Protein Description**	**Gene Name**	**Z**	***P* value**	***Q* value**	**Z**	***P* value**	***Q* value**
P05067	amyloid beta A4 protein (Aβ)	*APP*	-6.319	1.26×10^{-08}	7.06×10^{-06}	-4.866	1.00×10^{-06}	1.20×10^{-05}
Q9H2A3	neurogenin-2 (NEUROG2)	*NEUROG2*	-5.668	1.20×10^{-07}	3.36×10^{-05}	-4.564	5.00×10^{-06}	3.00×10^{-05}
P07196	neurofilament light polypeptide (NEFL)	*NEFL*	-5.717	2.26×10^{-07}	4.22×10^{-05}	-4.33	1.50×10^{-05}	6.00×10^{-05}
O95704	amyloid beta A4 precursor protein-binding family B member 3 (APBB3)	*APBB3*	-5.338	1.54×10^{-06}	2.16×10^{-04}	-3.513	4.42×10^{-04}	0.001
Q13127	Isoform 4 of RE1-silencing transcription factor (REST)	*REST*	-4.670	8.03×10^{-05}	0.009			
Q9Y487	V-type proton ATPase 116 kDa subunit (ATP6V0A2)	*ATP6V0A2*	-3.544	0.001	0.055			
B1AJZ9	forkhead-associated domain-containing protein 1	*FHAD1*	-3.815	0.001	0.076			
Q14520	hyaluronan-binding protein 2	*HABP2*	-2.495	0.001	0.076	-0.96	0.337	>0.200
Q8IVF4	dynein heavy chain 10, axonemal	*DNAH10*	-2.643	0.001	0.076			
Q92686	neurogranin	*NRGN*	-3.600	0.003	0.135			
O60674	tyrosine-protein kinase JAK2	*JAK2*	-2.374	0.003	0.135			
Q13103	secreted phosphoprotein 24	*SPP2*	-2.827	0.003	0.135			
Q15485	ficolin-2	*FCN2*	-2.841	0.003	0.137			
Q6ZUS6	coiled-coil domain-containing protein 149	*CCDC149*	-2.597	0.004	0.176			

Q8IWV7	E3 ubiquitin-protein ligase	*UBR1*	-1.957	0.005	0.178	-1.164	0.244	>0.200
P81274	G-protein-signaling modulator 2	*GPSM2*	-2.373	0.005	0.178			
P51956	serine/threonine-protein kinase	*NEK3*	-2.807	0.006	0.195	-1.572	0.116	0.199
Q5TZA2	rootletin (CROCC)	*CROCC*	-2.617	0.007	>0.200			
Q8TBY8	polyamine-modulated factor 1-binding protein 1	*PMFBP1*	-2.239	0.007	>0.200			
O95256	interleukin-18 receptor accessory protein	*IL18RAP*	-2.019	0.008	>0.200	-1.031	0.303	>0.200
Q9Y2M0	fanconi-associated nuclease 1	*FAN1*	-2.362	0.009	>0.200	-1.773	0.076	0.152
P02787	serotransferrin (TF)	*TF*	-3.301	0.009	>0.200			
P42356	phosphatidylinositol 4-kinase alpha	*PI4KA*	-2.038	0.009	>0.200			
Q6P2H3	centrosomal protein of 85 kDa	*CEP85*	-1.845	0.010	>0.200			
Q9UQ16	dynamin-3	*DNM3*	-2.808	0.010	>0.200	-1.78	0.075	0.152
Q8N7X0	androglobin	*ADGB*	-2.279	0.011	>0.200			
Q5T447	E3 ubiquitin-protein ligase	*HECTD3*	-1.965	0.011	>0.200	-0.687	0.492	>0.200
P15924	desmoplakin	*DSP*	-1.793	0.011	>0.200			
A2RUS2	DENN domain-containing protein 3 (DENN3)	*DENND3*	-2.640	0.012	>0.200			
Q8IZ81	ELMO domain-containing protein 2	*ELMOD2*	-2.348	0.012	>0.200			
O60292	signal-induced proliferation-associated 1-like protein 3	*SIPA1L3*	-1.997	0.012	>0.200			
O60841	eukaryotic translation initiation factor 5B	*EIF5B*	-2.041	0.013	>0.200			
P08571	monocyte differentiation antigen CD14	*CD14*	-1.985	0.013	>0.200			
P03952	plasma kallikrein	*KLKB1*	-2.084	0.013	>0.200	-1.135	0.256	>0.200
Q9UKN1	mucin-12	*MUC12*	-2.349	0.017	>0.200			
P0DJI8	serum amyloid A-1 protein	*SAA1*	-1.763	0.019	>0.200			

P00488	coagulation factor XIII	*F13A1*	-2.035	0.020	>0.200			
Q12830	nucleosome-remodeling factor subunit BPTF	*BPTF*	-1.923	0.021	>0.200			
P00734	prothrombin	*F2*	-2.068	0.022	>0.200			
Q14624	Inter-alpha-trypsin inhibitor heavy chain H4	*ITIH4*	-1.685	0.027	>0.200			
Q8TDY2	RB1-inducible coiled-coil protein 1	*RB1CC1*	-2.567	0.031	>0.200			
P09871	complement C1s subcomponent	*C1S*	-2.167	0.032	>0.200			
Q9NQW8	cyclic nucleotide-gated cation channel beta-3	*CNGB3*	-3.174	0.033	>0.200			
Q86TU7	histone-lysine N-methyltransferase SETD3	*SETD3*	-2.421	0.036	>0.200			
Q8N139	ATP-binding cassette sub-family A member 6	*ABCA6*	-2.655	0.036	>0.200	-1.874	0.061	0.141
P00742	coagulation factor X	*F10*	-1.950	0.037	>0.200			
Q15047	Histone-lysine N-methyltransferase SETDB1	*SETDB1*	-1.515	0.037	>0.200			
Q5VTT5	myomesin-3	*MYOM3*	-1.630	0.038	>0.200			
Q9NTJ3	structural maintenance of chromosomes protein 4	*SMC4*	-1.022	0.040	>0.200			
Q6RI45	bromodomain and WD repeat-containing protein 3	*BRWD3*	-1.460	0.040	>0.200			
Q14493	histone RNA hairpin-binding protein	*SLBP*	-1.173	0.041	>0.200			
P0DJI9	serum amyloid A-2 protein	*SAA2*	-1.477	0.042	>0.200			
Q9UGM5	fetuin-B	*FETUB*	-2.504	0.042	>0.200			
P08185	corticosteroid-binding globulin	*SERPINA6*	-2.222	0.042	>0.200			
P35353	corticotropin-releasing factor receptor 1	*CRHR1*	-2.296	0.045	>0.200			
P02765	alpha-2-HS-glycoprotein	*AHSG*	-1.481	0.045	>0.200			
Q13651	interleukin-10 receptor subunit alpha	*IL10RA*	-1.829	0.047	>0.200			

Table 5-15: Protein groups significantly associated with Aβ classification (Aβ- or Aβ+) in the cognitively normal individuals only. An additional 8 protein groups became significantly associated with Aβ classification in the cognitively normal group (highlighted in green). GLM residuals adjusted for TMT10plex group, age, gender and sample cohort. Benjamini-Hochberg *Q* values were calculated for multiple testing correction.

UniProt ID	Protein Description	Gene Name	Z	*P* value	*Q* value
P05067	amyloid beta A4 protein (Aβ)	*APP*	-5.686	1.30×10^{-08}	7.28×10^{-06}
Q9H2A3	neurogenin-2 (NEUROG2)	*NEUROG2*	-5.305	1.12×10^{-07}	3.14×10^{-05}
P07196	neurofilament light polypeptide (NEFL)	*NEFL*	-4.706	3.00×10^{-06}	5.60×10^{-04}
O95704	amyloid beta A4 precursor protein-binding family B member 3 (APPB3)	*APBB3*	-4.451	9.00×10^{-06}	0.001
Q13127-4	isoform 4 of RE1-silencing transcription factor (REST)	*REST*	-3.935	8.30×10^{-05}	0.009
P02787	serotransferrin (TF)	*TF*	-3.55	3.85×10^{-04}	0.037
Q92686	neurogranin (NRGN)	*NRGN*	-3.266	0.001	0.062
Q9NQW8	cyclic nucleotide-gated cation channel beta-3 (CNGB3)	*CNGB3*	-3.425	0.001	0.062
A2RUS2	DENN domain-containing protein 3 (DENN3)	*DENND3*	-3.329	0.001	0.062
B1AJZ9	forkhead-associated domain-containing protein 1	*FHAD1*	-3.009	0.003	0.168
Q9Y487	V-type proton ATPase 116 kDa subunit (ATP6V0A2)	*ATP6V0A2*	-2.827	0.005	>0.200
Q9UQ16	dynamin-3	*DNM3*	-2.595	0.009	>0.200
Q8IVF4	dynein heavy chain 10, axonemal	*DNAH10*	-2.504	0.012	>0.200
Q9UGM5	fetuin-B	*FETUB*	-2.471	0.013	>0.200
P51956	serine/threonine-protein kinase	*NEK3*	-2.408	0.016	>0.200

Q8TBY8	polyamine-modulated factor 1-binding protein 1	*PMFBP1*	-2.399	0.016	>0.200
Q86TU7	histone-lysine N-methyltransferase SETD3	*SETD3*	-2.359	0.018	>0.200
Q13395	probable methyltransferase (TARBP1)	*TARBP1*	-2.349	0.019	>0.200
Q8N139	ATP-binding cassette sub-family A member 6	*ABCA6*	-2.35	0.019	>0.200
Q6ZUS6	coiled-coil domain-containing protein 149	*CCDC149*	-2.278	0.023	>0.200
Q8IZL8	proline-, glutamic acid- and leucine-rich protein 1 (PELP1)	*PELP1*	-2.259	0.024	>0.200
Q8N4C6	ninein (NIN)	*NIN*	-2.237	0.025	>0.200
Q8N7X0	androglobin	*ADGB*	-2.223	0.026	>0.200
Q96RV3	pecanex-like protein 1 (PCNX)	*PCNX*	-2.217	0.027	>0.200
Q15485	ficolin-2	*FCN2*	-2.151	0.031	>0.200
Q8TDY2	RB1-inducible coiled-coil protein 1	*RB1CC1*	-2.068	0.039	>0.200
O95256	interleukin-18 receptor accessory protein	*IL18RAP*	-2.057	0.04	>0.200
P01031	complement C5 (CC5)	*C5*	-2.005	0.045	>0.200
Q9UK85	dickkopf-like protein 1 (DKKL1)	*DKKL1*	-2.00	0.045	>0.200
P81274	G-protein-signaling modulator 2	*GPSM2*	-1.988	0.047	>0.200
P31483	nucleolysin TIA-1 isoform p40 (TIA1)	*TIA1*	-1.983	0.047	>0.200
Q8NDM7	cilia- and flagella-associated protein 43 (WDR96)	*WDR96*	-1.976	0.048	>0.200

5.4.6 Summary of protein groups related to Aβ SUVR and Aβ classification

A total of 95 unique protein groups have been associated with Aβ (Table 5-16). This has been examined as a correlation or a group-wise difference. Furthermore, we have also examined the full dataset (including MCI and AD individuals) and the cognitively normal subjects alone in regards to Aβ SUVR and classification. Table 5-16 summarises these findings by displaying the protein group and its association with an endophenotype (shown as *P* value). We have also displayed any relationship found with *APOE* genotype (Table 5-16).

APBB3, Aβ, NEFL and NEUROG2 are highly associated with all SUVR variables and are also related to *APOE* genotype. When adjusting for *APOE* all four of these protein groups remain highly significant with Aβ and also after applying FDR. A further 11 protein groups were significantly associated with all four analysis, including REST and NRGN.

Interestingly, TIA1 and PCNX were the only protein groups exclusively associated with both analyses that included only cognitively normal individuals. A large number of protein groups were only associated with Aβ when MCI and AD individuals were included in the analysis. This suggests that these proteins are related to other AD processes and not necessarily a reflection of NAB.

Table 5-16: A summary of protein groups associated (uncorrected *P* value) with Aβ in this study. Association with *APOE* genotype is shown when significant.

	Correlation with Aβ SUVR (*P* value)		**Group-wise association with Aβ classification (*P* value)**		
Gene Name	**All Individuals**	**Cognitively Normal**	**All Individuals**	**Cognitively Normal**	***APOE* genotype**
APBB3	6.59×10^{-05}	1.35×10^{-04}	1.54×10^{-06}	9.00×10^{-06}	0.001
APP	1.05×10^{-06}	1.09×10^{-07}	1.26×10^{-08}	1.30×10^{-08}	0.001
ABCA6	0.019	0.028	0.036	0.019	0.02
CCDC149	0.007	0.007	0.004	0.023	n/s
CNGB3	0.037	0.018	0.033	0.001	n/s
DENND3	0.007	2.70×10^{-05}	0.012	0.001	n/s
DNM3	0.008	0.002	0.010	0.009	0.028
DNAH10	0.002	0.002	0.001	0.012	n/s

FHAD1	0.013	0.021	0.001	0.003	n/s
REST	0.001	0.006	8.03×10^{-05}	8.30×10^{-05}	n/s
NEFL	2.46×10^{-06}	9.73×10^{-07}	2.26×10^{-07}	3.00×10^{-06}	0.001
NEUROG2	5.28×10^{-06}	1.37×10^{-07}	1.20×10^{-07}	1.12×10^{-07}	0.014
NRGN	0.015	0.016	0.003	0.001	n/s
PMFBP1	0.037	0.007	0.007	0.016	n/s
ATP6V0A2	3.19×10^{-04}	0.011	0.001	0.005	n/s
ADGB	0.045	n/s	0.011	0.026	n/s
BRWD3	0.034	0.024	0.040	n/s	n/s
CEP85	0.007	0.014	0.010	n/s	n/s
FAN1	0.012	0.011	0.009	n/s	0.043
FCN2	0.013	n/s	0.003	0.031	n/s
GPSM2	0.030	n/s	0.005	0.047	n/s
HABP2	0.002	0.021	0.001	n/s	0.003
IL18RAP	0.041	n/s	0.008	0.04	0.036
CD14	0.037	0.015	0.013	n/s	n/s
BPTF	0.025	0.01	0.021	n/s	n/s
PI4KA	0.004	0.044	0.009	n/s	n/s
KLKB1	0.009	0.029	0.013	n/s	0.037
RB1CC1	0.017	n/s	0.031	0.039	n/s
SPP2	0.009	0.044	0.003	n/s	n/s
NEK3	0.015	n/s	0.006	0.016	0.015
SMC4	0.027	0.038	0.040	n/s	n/s
JAK2	0.012	0.039	0.003	n/s	n/s
AHSG	n/s	0.033	0.045	n/s	n/s
DSP	0.004	n/s	0.011	n/s	n/s
HECTD3	0.026	n/s	0.011	n/s	0.001
UBR1	0.010	n/s	0.005	n/s	n/s
ELMOD2	0.011	n/s	0.012	n/s	n/s
EIF5B	0.006	n/s	0.013	n/s	n/s
FETUB	n/s	n/s	0.042	0.013	n/s
FBLN1	0.042	0.011	n/s	n/s	n/s
SETD3	n/s	n/s	0.036	0.018	n/s
SETDB1	0.015	n/s	0.037	n/s	n/s
ITIH4	0.029	n/s	0.027	n/s	n/s
MUC12	0.009	n/s	0.017	n/s	n/s
TIA1	n/s	0.038	n/s	0.047	n/s
PCNX	n/s	0.042	n/s	0.027	n/s
F2	0.012	0.011	n/s	n/s	n/s

RFC4	0.022	0.026	n/s	n/s	n/s
CROCC	0.001	n/s	0.007	n/s	n/s
TF	n/s	n/s	0.009	3.85×10^{-04}	n/s
SAA1	0.013	n/s	0.019	n/s	n/s
PLCB1	n/s	0.043	n/s	n/s	n/s
APOA1	0.037	n/s	n/s	n/s	n/s
SLC25A14	n/s	0.008	n/s	n/s	n/s
CENPF	0.022	n/s	n/s	n/s	n/s
CEP290	n/s	0.045	n/s	n/s	n/s
WDR96	n/s	n/s	n/s	0.048	n/s
F10	n/s	n/s	0.037	n/s	n/s
F13A1	n/s	n/s	0.020	n/s	n/s
CCDC168	n/s	0.036	n/s	n/s	n/s
C1S	n/s	n/s	0.032	n/s	n/s
C5	n/s	n/s	n/s	0.045	n/s
SERPINA6	n/s	n/s	0.042	n/s	n/s
CRHR1	n/s	n/s	0.045	n/s	n/s
DKKL1	n/s	n/s	n/s	0.045	n/s
DNAH14	n/s	0.045	n/s	n/s	n/s
FN1	0.049	n/s	n/s	n/s	0.036
GK	n/s	0.025	n/s	n/s	n/s
GOLGA2	n/s	0.029	n/s	n/s	n/s
SLBP	n/s	n/s	0.041	n/s	0.004
IGHG4	0.013	n/s	n/s	n/s	n/s
IGLC6	n/s	0.015	n/s	n/s	n/s
IGFBP3	0.038	n/s	n/s	n/s	n/s
IL10RA	n/s	n/s	0.047	n/s	n/s
KRT8	0.043	n/s	n/s	n/s	0.016
NARG2	n/s	0.026	n/s	n/s	n/s
MAP4	n/s	0.048	n/s	n/s	n/s
MYBBP1A	n/s	0.029	n/s	n/s	n/s
MYOM3	n/s	n/s	0.038	n/s	n/s
AHNAK	0.021	n/s	n/s	n/s	n/s
NIN	n/s	n/s	n/s	0.025	n/s
TYK2	0.004	n/s	n/s	n/s	n/s
FARSB	0.013	n/s	n/s	n/s	n/s
PZP	n/s	0.019	n/s	n/s	n/s
TARBP1	n/s	n/s	n/s	0.019	n/s
PELP1	n/s	n/s	n/s	0.024	n/s

AHNAK2	n/s	0.041	n/s	n/s	n/s
SRRM1	n/s	0.049	n/s	n/s	n/s
ULK2	n/s	0.03	n/s	n/s	n/s
AGT	0.039	n/s	n/s	n/s	n/s
SAA2	n/s	n/s	0.042	n/s	n/s
SAA4	0.032	n/s	n/s	n/s	n/s
SIPA1L3	n/s	n/s	0.012	n/s	n/s
FAM178A	0.042	n/s	n/s	n/s	n/s
NAV1	n/s	0.049	n/s	n/s	n/s

5.4.7 Pathway analysis

Pathway analysis revealed that these 96 significantly associated protein groups (Table 5-16) were over-represented for involvement in complement and coagulation cascades (P = 2.9 x10^{-5}, Q = 0.032) and platelet degranulation (P = 7.2 x10^{-6}, Q = 0.012). Other pathways included the intrinsic prothrombin activation pathway (P = 0.028) and the Stat3 signalling pathway (P = 0.034) however these pathways did not pass multiple testing correction.

5.4.8 Comparisons with LC-MS/MS performed on AIBL-1 (Chapter 3)

In Chapter 3 "*Blood protein predictors for neocortical amyloid pathology for enrichment in therapeutic trials*" we presented an initial LC-MS/MS discovery that demonstrated 43 protein groups that were found to be significantly different between PiB+ and PiB- subjects (Table 3-11). Only 17 of these protein groups were taken forward for replication (Table 3-13) via immunoassay of which only α2m, FHR-1 and most prominently FGγ were replicated. Here, we have compared only the LC-MS/MS findings from Chapter 3 to the LC-MS/MS discovery performed in this Chapter as a way of independent validation (Table 5-17). Firstly, 42/43 protein groups from AIBL-1 were measured in AIBL-2 and KARVIAH with only pre-mRNA-splicing factor (DHX38) not being identified. We found that only four protein groups that were significantly associated with Aβ in the AIBL-1 cohort were significantly associated with Aβ in AIBL-2 and KARVIAH cohorts. It was shown that TF and prothrombin (F2) were related with Aβ in conflicting directions with AIBL-1 whereas apoA1 and Inter-alpha-trypsin inhibitor heavy chain 4 (ITIH4)

replicated the LC-MS/MS finding with AIBL-1. CD5 antigen-like (CD5L) was also approaching significance (*P* = 0.052) with the same direction of association. Ficolin-2 was found to be significantly reduced with Aβ+ individuals in AIBL-2/KARVIAH datasets whereas ficolin-3 was significantly reduced in AIBL-1. Ficolin-3 shares 50% amino acid homology with ficolin-2 [542] and therefore the small number of significant peptides identified as ficolin-3 in AIBL-1 could be attributed to ficolin-2. Albeit not significant, a number of protein groups did replicate the direction of association with Aβ+ groups (Table 5-17), this included FGγ and α2m. FGγ was found to be significantly reduced in AIBL-1, UCSF and EMIF-AD in Chapter 3. Here we show that FGγ is minimally reduced in Aβ+ group (Rho = -0.058, *P* = 0.382). α2m has been shown to be increased in AIBL-1, UCSF, EMIF-AD and now AIBL-2/KARVIAH. However, statistical significance was not achieved in AIBL-2 and KARVIAH cohorts (Rho = 0.028, *P* = 0.700). When examining HEC subjects only, α2m was found to be approaching statistical significance (Rho = 0.108, *P* = 0.082) and co-varying for *APOE* genotype became statistical significant (*P* = 0.042).

The poor overlap with the findings from Chapter 3 is unsurprising given the methodological differences. The method employed in this Chapter has been shown to have greater protein sequence coverage and therefore is likely to be a better reflection of overall protein expression. Furthermore, the study design that includes a continuum of Aβ SUVR rather than an extreme endophenotype, as in Chapter 3, is less likely to be biased towards markers of an AD diagnosis. However, as apoA1 and ITIH4 are replicated across these two methodologies, and given these differences, should be considered as robust indicators for NAB.

Table 5-17: Protein groups found to be significantly associated using LC-MS/MS in Chapter 3 and the association in Chapter 5. Directional change in relation to Aβ+ is shown.

UniProt ID	Protein Name	Gene Name	Chapter 3 directional change (Aβ+)	Chapter 5 directional change (Aβ+)
P02768	albumin†	*ALB*	↑	↑
P01023	α2m	*A2M*	↑	↑
P02647	apoA1	*APOA1*	↓	↓≠
P06727	apoA4	*APOA4*	↑	↑

O14791	apoL1	*APOL1*	↑	↓
P08519	apo(a)	*LPA*	↑	↑
P04003	C4b-binding protein alpha chain	*C4BPA*	↓	↓
O43866	CD5 antigen-like	*CD5L*	↓	↓^
P00450	ceruloplasmin	*CP*	↓↑	↑
P10909	clusterin	*CLU*	↓	↓
P02747	complement C1q subcomponent	*C1QC*	↓	↓
P01024	CC3	*C3*	↓	↑
P0C0L4	C4α	*C4A*	↑↓	↑
P13671	CC6	*C6*	↓	↓
P07357	C8α	*C8A*	↓	↓
P00751	CFB	*CFB*	↑	↓
P08603	CFH	*CFH*	↑	↓
Q03591	FHR-1	*CFHR1*	↑	↓
P02671	FGα	*FGA*	↓	↓
P02675	FGβ	*FGB*	↓	↓
P02679	FGγ	*FGG*	↓	↓
O75636	ficolin-3	*FCN3*	↓	↑
P06396	gelsolin	*GSN*	↑	-
P00738	haptoglobin	*HP*	↓	↓
P00739	haptoglobin-related protein	*HPR*	↑	↓
P02790	hemopexin	*HPX*	↑	↑
P04196	HRG	*HRG*	↑	-
P01876	Ig alpha-1 chain C region	*IGHA1*	↓	↑
P01860	Ig gamma-3 chain C region†	*IGHG3*	↓	↑
P01768	Ig heavy chain V-III region CAM	*n/a*	↓	↓
P01762	Ig heavy chain V-III region TRO	*n/a*	↓	↓
P01700	Ig lambda chain V-I region HA	*n/a*	↓	↓
P0CG04	Ig lambda-1 chain C regions	*IGLC1*	↓	↓
P04220	Ig mu heavy chain disease protein	*n/a*	↓	↑
P19827	Inter-alpha-trypsin inhibitor heavy chain H1	*ITIH1*	↓	↓
P19823	Inter-alpha-trypsin inhibitor heavy chain H2	*ITIH2*	↓	↑
Q06033	Inter-alpha-trypsin inhibitor heavy chain H3	*ITIH3*	↑	↑
Q14624	Inter-alpha-trypsin inhibitor heavy chain H4	*ITIH4*	↑	↑≠
P00747	plasminogen	*PLG*	↑	↓
Q92620	pre-mRNA-splicing factor	*DHX38*	↑	n/a
P00734	prothrombin (F2)	*F2*	↑	↓≠
P02787	TF	*TF*	↑	↓≠
P25311	zinc-alpha-2-glycoprotein	*AZGP1*	↑	↑

≠ Statistically significant (P = < 0.05) in one or more tests in Chapter 5; † Protein group deleted from Chapter 5 analysis; ^ Protein group approaching statistical significance.

5.4.9 Plasma protein classifier for Aβ positivity

Univariate analysis has shown that a number of single plasma protein groups have the ability to predict Aβ classification. However, it is unlikely that a single marker would achieve the sensitivity or specificity required for clinical implementation. Therefore, we have attempted to build a multi-analyte classifier that can accurately predict Aβ status.

The data was divided into a train (AIBL-2) and test (KARVIAH) sets. As the two cohorts were analysed separately, the covariate "cohort" was removed from the GLM model. This is also important to demonstrate how a plasma protein classifier will perform in an independent cohort. Missing values were imputed by using the average score of the protein group. Support Vector Machine (SVM) classifiers were built from $n = 2$ to $n = 560$ in the order they were ranked by LASSO. LASSO is a feature selection regression analysis that produces a simpler and more interpretable model by applying L1 regularisation. In practice, LASSO implicitly assesses the correlation between variables, removing from each correlated group those proteins that less significantly improve the accuracy of the prediction model. Performance of the classification method in the training set was assessed using a 100 repeats of a 5-fold cross validation (blue graph in Figure 5-16). While, in the training set, every repeat and fold of the cross validation may select a slightly different set of proteins when applying LASSO (each one of the 100 repeats, randomly divides the training set into 5 folds for cross-validation), sets of 10-20 proteins obtained the maximum Area Under the Curve (AUC), with an average of 90.0 ± 0.01 (s.d.). Meanwhile, training the model in the whole training set (all samples from AIBL-2) selected the panel of proteins shown in Table 5-18 with LASSO. When this already trained model was then tested in KAVIRAH, the panel of Table 5.18 produced the AUCs shown in Figure 5-16 (red graph), with maximum value at 14 protein groups (AUC 86.6).

Table 5-18: Protein groups (listed by feature number) included in the classifier model trained in AIBL-2 cohort.

Feature Number	UniProt ID	Protein description	Gene Name
1	P00734	prothrombin	*F2*
2	P07196	neurofilament light polypeptide	*NEFL*
3	Q9Y487	V-type proton ATPase 116 kDa subunit	*ATP6V0A2*
4	Q15485	ficolin-2	*FCN2*
5	P05067	amyloid beta A4 protein	*APP*
6	B1AJZ9	forkhead-associated domain-containing protein 1	*FHAD1*
7	Q9H2A3	neurogenin-2	*NEUROG2*
8	Q8IZ81	ELMO domain-containing protein 2	*ELMOD*
9	Q13127	isoform 4 of RE1-silencing transcription factor	*REST*
10	O95704	amyloid beta A4 precursor protein-binding family B member 3	*APBB3*
11	Q8IVF4	dynein heavy chain 10, axonemal	*DNAH10*
12	Q8IWV7	E3 ubiquitin-protein ligase	*UBR1*
13	Q8IZF3	adhesion G protein-coupled receptor F4	*GPR115*
14	P81274	G-protein-signaling modulator 2	*GPSM2*
15	Q13103	secreted phosphoprotein 24	*SPP2*
16	Q14520	hyaluronan-binding protein 2	*HABP2*
17	Q04206	transcription factor p65	*RELA*
18	Q5TZA2	rootletin	*CROCC*
19	Q14493	histone RNA hairpin-binding protein	*SLBP*
20	Q8NH67	olfactory receptor 52I2	*OR52I2*

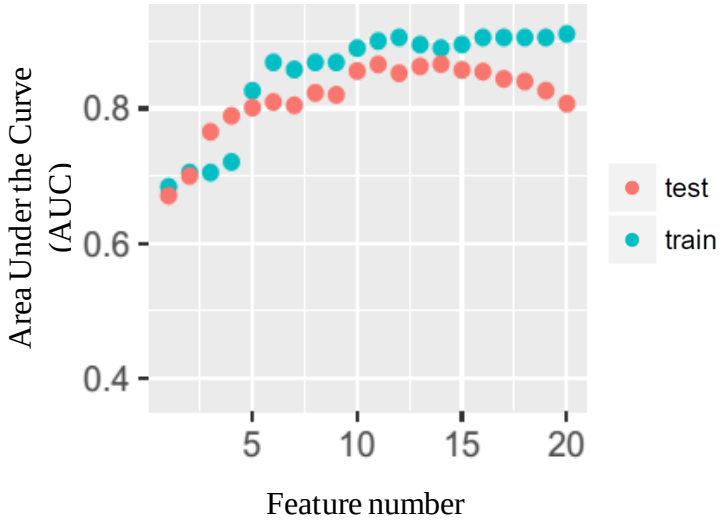

Figure 5-16: Plasma biomarker classifier for Aβ classification. A twenty-protein set with optimal AUC for classifying PET Aβ positivity was built in AIBL-2 with stability selection with LASSO and with 100 repeats of 5-fold cross validation. This classifier was tested in KARVIAH with a maximum AUC of 86.6.

As mentioned in previous Chapters, it is important to gather spectral evidence for automated database assignments in MS discovery projects. This is of particular importance here when an LC-MS/MS dataset has been used to train a prediction model, with an independent LC-MS/MS dataset used for testing. Peptides used to generate protein group scores for the classifier model are shown in Table 5-19. To our knowledge, this is the first time this has been done in the development of a biomarker model for AD or AD pathology.

Table 5-19: LC-MS/MS identified and matched peptides contributing to the overall score of each protein group included in the 20 plasma protein classifier for Aβ group prediction. Protein groups are ranked by their feature number in Table 5-18.

Feature Number	Protein Group	Gene Name	Peptide Sequence	Monoisotopic m/z (Da)	Number of *b* ions	Number of *y* ions
1	prothrombin	*F2*	ENLDRDIALMK	521.61	7	4
			YTACETAR	600.79	6	5
			ANTFLEEVR	654.36	7	5
			ELLESYIDGR	712.38	7	6
			RGDACEGDSGGPFVMK	714.35	12	8
			KSPQELLCGASLISDR	744.75	11	10
			TFGSGEADCGLRPLFEK	781.41	9	9
			NPDSSTTGPWCYTTDPTVR	795.37	8	8
			IVEGSDAEIGMSPWQVMLFR	832.09	12	14
			DKLAACLEGNCAEGLGTNYR	891.11	15	13
			TATSEYQTFFNPR	896.44	9	11
			GDACEGDSGGPFVMK	992.97	11	7
			SEGSSVNLSPPLEQCVPDR	1150.71	9	11
2	neurofilament light	*NEFL*	LAAEDATNEK	531.25	8	4
			ALYEQEIR	625.85	5	5
			QNADISAMQDTINK	688.1	6	5
			EYQDLLNVK	700.94	3	4
			LLEGEETR	712.32	3	3
			VQSLQDEVAFLR	817.45	4	4
3	V-type proton ATPase 116 kDa subunit	*ATP6V0A2*	FYVGAGTK	536.96	5	5
			ETPPTRIRTNK	591.23	7	4
			QSFLELTELK	718.23	2	5
			QDQIHSSIVSTLLALMDGLDSR	806.39	9	9
4	ficolin-2	*FCN2*	NCHVSNLNGR	467.56	5	5

			GEAGTNGK	596.83	4	4
			VADEAEK	610.35	3	4
			GTHGSFANGINWK	616.66	5	8
			MVGLEGSDKLTILR	664.06	3	3
			GYNYSYK	676.86	5	5
			VDLVDFEDNYQFAK	721.04	7	5
5	amyloid beta A4 protein	*APP*	HFEHVRMVDPKK			
			HDSGYEVHHQK	449.48	4	7
			LVFFAEDVGSNK	595.33	4	8
6	forkhead-associated domain-containing protein 1	*FHAD1*	SLHLPK	462.29	1	5
			EISESNIAYEK	504.59	4	4
			QHAQTIVSLEEK	537.96	5	2
			QKMELEQNVVLVQQQSK	565.8	3	7
			MTTEGGPPPAPLRR	570.32	3	2
7	neurogranin	*NRGN*	GGAGGGPSGD	480.37	2	5
			GRKGPGPGGPGGAGVARGGAGGP	698.58	5	4
8	ELMO domain-containing protein 2	*ELMOD2*	KRPYDSDNLQHEELLMKLWNLLMPTK	574.64	5	7
9	RE1-Silencing Transcription factor	*REST*	EPVQMELSPPMEVVQK	685.37	7	7
			LLNTGEGNKEAPLQK	691.39	7	4
			IKGDVAGKKNEKSVK	722.35	5	4
			QVHNGPKPLNCPHCDYK	841.76	5	5
10	amyloid beta A4 precursor protein-binding, family B, member 3	*APBB3*	CLVASAAR	359.53	3	4
			SRSQPPDGAWGEGQNMLMLLK	930.5	5	6
11	dynein heavy chain 10, axonemal	*DNAH10*	DCLSWPR	581.79	4	3
			SSQFWK	658.18	5	6
12	E3 ubiqutin-protein ligase	*UBR1*	KSQQAGPSYVQNCVK	481.99	5	2
			FDVNYAFGRVK	515.61	3	5

			QWIALLQRGNCTFKEK	613.83	6	9
			LLLKQNVDVEAEDK	692.07	8	4
13	adhesion G protein-coupled receptor F4	*GPR115*	QVNGLVLSVVLPER	508.95	8	8
			KTKSPSSESTKTTK	580.33	3	3
14	G-protein-signaling modulator 2	*GPSM2*	IGEGRACWSLGNAYTALGNHDQAMHFAEK	863.4	4	6
			VQNWNSEILAKQKPLIAKPSAK	631.18	9	8
15	secreted phosphoprotein 24	*SPP2*	VSAQQVQGVHAR	503.62	5	7
			VNSQSLSPYLFR	820.45	2	6
16	hyaluronan-binding protein 2	*HABP2*	TEIAER	474.27	4	2
			VVLGDQDLKKEEFHEQSFR	599.13	12	15
			HLKVVLGDQDLK	608.7	2	6
			VQNTCKDNPCGR	636.32	6	4
			LIANTLCNSR	695.88	6	4
			YSHYNERDEIPHNDIALLK	697.36	10	10
			LKPVDGHCALESK	714.4	11	11
			FTCACPDQFK	866.43	6	5
17	transcription factor p65	*RELA*	IQTNNNPFQGDSAGPIR	515.75	12	12
			DLEQAISQR	645.34	4	4
18	rootletin	*CROCC*	RAAEAQLGGLR	457.6	4	8
			ELQELR	509.29	4	4
			QQIIATQEK	530.28	5	4
			KTFPNSEANPLNAYYLK	607.84	9	8
19	histone RNA hairpin-binding protein	*SLBP*	QINYGK	590.85	4	4
			TESQKTKSK	374.72	5	4
			LVQHGLQVRLQLFK	636.73	6	7
20	olfactory receptor 52I2	*OR52I2*	CQQILR	410.2	6	4
			NKDVHVALK	494.96	4	7
			MLQNQDTMEILSNSTSK	729.35	4	5

5.4.10 Replication of brain-derived proteins observed within human plasma

In Chapter 4, we described a group of 157 (99 with >2 PSMs; Table 4-9) proteins (termed brain-derived proteins (BDPs)) observed and measured within human plasma. These proteins are described in the Human Protein Atlas (HPA, http://www.proteinatlas.org/) to have a >five-fold increased expression in the cerebral cortex compared with all other tissues. This was used as an indication of a BDP due to high expression in the brain and minimal/none expression in other tissues. These protein groups were identified based on 5% FDR with some protein groups such as GFAP, PLP1 and MBP having substantial PSMs evidence. Conversely, proteins such as POU3F2, FEZF2 and GPR37L1 were based upon <2 PSMs (Table 4-9). Manual inspection of the MS/MS spectra demonstrated that some protein group identifications were based upon moderate-to-poor quality spectra. Therefore, we utilised the AIBL-2 and KARVIAH cohorts to replicate the presence of these protein groups within plasma and where possible examine these BDPs relationship with NAB.

Mining the AIBL-2 cohort we demonstrated that 120/157 BDPs described in Chapter 4 were again identified at 5% FDR, with further confirmation of their occurrence in the KARVIAH cohort (Table 5-20). However, only 12 of these BDPs in Table 5-20 were included in the main analysis above. This was because a majority of BDPs in our dataset occur in <50% of the dataset and therefore were removed from further statistical analysis by our criteria. It was encouraging to observe that BDPs GFAP, BDNF, NEFL, NRGN, synaptosomal-associated protein, 25kDa (SNAP25) and formin 2 (FMN2) were measured in >80% of individuals included in this study. Of the BDPs that did not replicate in this dataset 15 protein groups were based upon 1 PSMs and 20 protein groups were grouped as “poor spectral evidence” in the discovery data (Table 4-9), this emphasises the importance of manual spectral interrogation to avoid false database identifications. Furthermore, we examined if additional cerebral cortex “Tissue Enriched” proteins, described in HPA, but not observed in our discovery data were present in the AIBL-2 and KARVIAH cohorts, given the larger cohort sizes. We demonstrated evidence that a further 52 cerebral cortex “Tissue Enriched” proteins were measured in AIBL-2 and then KARVIAH plasma samples (Table 5-21). As above, very few of these additional BDPs were

included in the main analysis and only amyloid beta (A4) precursor protein-binding, family A, member 2 (APBA2) and regulating synaptic membrane exocytosis 3 (RIMS3) being measured in >50% of subjects (Table 5-21).

Table 5-20: ID replication of 120/157 brain-derived proteins discovered in Chapter 4. The evidence generated from the discovery dataset is shown as PSMs with evidence of the identification in AIBL-2 and KARVIAH shown as a percentage of individuals the BDP was observed in. Protein groups that did not replicate (37) are shown in the table with 0% for both AIBL-2 and KARVIAH. The "Tissue Enriched" category in HPA (>five-fold increased expression in the cerebral cortex compared with all other tissues) was used as an indication of a candidate BDP due to high expression in the brain and minimal/none expression in other tissues.

Gene symbol	Protein description	HPA Rank (Cerebral Cortex)	Discovery MS/MS evidence (PSMs, Chapter 4)	AIBL-2 cohort (% of subjects identified, *n* = 190)	KARVIAH cohort (% of subjects identified, *n* = 94)
GFAP	glial fibrillary acidic protein	1	160	100.00%	100.00%
BDNF	brain-derived neurotrophic factor	665	18	98.95%	94.68%
NEFL	neurofilament, light polypeptide	336	13	90.53%	91.49%
NRGN	neurogranin	255	43	86.32%	89.36%
SNAP25	synaptosomal-associated protein, 25kDa	85	10	81.05%	75.53%
FMN2	formin 2	471	2	81.05%	80.85%
CHD5	chromodomain helicase DNA binding protein 5	453	7	68.95%	69.15%
MYT1L	myelin transcription factor 1-like	223	12	62.63%	62.77%
MAP2	microtubule-associated protein 2	292	3	62.11%	51.06%
SCN2A	sodium channel, voltage-gated, type II, alpha subunit	110	1	60.00%	59.57%
SYT16	synaptotagmin XVI	536	1	59.47%	59.57%
SHANK1	SH3 and multiple ankyrin repeat domains 1	111	9	51.58%	51.06%
DSCAM	down syndrome cell adhesion molecule	245	2	44.21%	44.68%

MBP	myelin basic protein	48	214	43.16%	22.34%
JPH3	junctophilin 3	107	2	41.05%	39.36%
PCDH9	protocadherin 9	173	1	34.21%	35.11%
BSN	bassoon presynaptic cytomatrix protein	557	5	34.21%	32.98%
SYN1	synapsin I	82	12	32.63%	31.91%
KIF5C	kinesin family member 5C	593	2	31.58%	29.79%
NRXN1	neurexin 1	95	3	31.05%	31.91%
NRXN2	neurexin 2	512	3	31.05%	31.91%
SOGA3	SOGA family member 3	420	1	28.95%	26.60%
KIRREL3	kin of IRRE like 3 (Drosophila)	287	4	28.42%	28.72%
SLC24A2	solute carrier family 24 (sodium/potassium/calcium exchanger), member 2	614	2	28.42%	28.72%
SPTBN4	spectrin, beta, non-erythrocytic 4	617	8	28.42%	28.72%
ERC2	ELKS/RAB6-interacting/CAST family member 2	137	1	25.26%	25.53%
CMTM5	CKLF-like MARVEL transmembrane domain containing 5	213	1	25.26%	24.47%
ANKS1B	ankyrin repeat and sterile alpha motif domain containing 1B	435	4	25.26%	25.53%
NSF	N-ethylmaleimide-sensitive factor	513	1	22.63%	21.28%
LRRTM4	leucine rich repeat transmembrane neuronal 4	119	1	22.11%	22.34%
MAP1A	microtubule-associated protein 1A	392	7	22.11%	21.28%
PTPRZ1	protein tyrosine phosphatase, receptor-type, Z polypeptide 1	405	4	22.11%	22.34%
ELAVL3	ELAV like neuron-specific RNA binding protein 3	47	1	21.58%	19.15%
CNTP4	contactin associated protein-like 4	91	2	21.58%	22.34%
CASKIN1	CASK interacting protein 1	77	2	21.05%	21.28%
SLIT1	slit homolog 1	262	4	20.00%	19.15%

CNKSR2	connector enhancer of kinase suppressor of Ras 2	369	1	20.00%	20.21%
SNCB	synuclein, beta	23	10	18.95%	19.15%
UNC13A	Unc-13 homolog A (C. elegans)	350	1	18.95%	12.77%
JAKMIP2	janus kinase and microtubule interacting protein 2	488	1	18.95%	18.09%
PPFIA2	protein tyrosine phosphatase, receptor type, f polypeptide (PTPRF), interacting protein (liprin), alpha 2	607	4	18.95%	19.15%
UCHL1	ubiquitin carboxyl-terminal esterase L1 (ubiquitin thiolesterase)	625	9	18.42%	19.15%
IDS	iduronate 2-sulfatase	586	1	17.89%	19.15%
KIAA1549L	KIAA1549-like	170	1	15.79%	15.96%
GRIK3	glutamate receptor, ionotropic, kainate 3	481	2	15.79%	15.96%
YWHAH	tyrosine 3-monooxygenase/tryptophan 5-monooxygenase activation protein, eta	547	38	15.79%	15.96%
APC2	adenomatosis polyposis coli 2	126	2	15.26%	15.96%
KIF3C	kinesin family member 3C	253	17	15.26%	14.89%
EFR3B	EFR3 homolog B (S. cerevisiae)	463	1	15.26%	13.83%
OMG	oligodendrocyte myelin glycoprotein	6	2	14.21%	19.15%
PLP1	proteolipid protein 1	31	26	14.21%	19.15%
SLC12A5	solute carrier family 12 (potassium/chloride transporter), member 5	33	1	14.21%	19.15%
ACTL6B	actin-like 6B	144	3	13.16%	11.70%
PGM2L1	phosphoglucomutase 2-like 1	339	3	12.63%	12.77%
CNP	2',3'-cyclic nucleotide 3' phosphodiesterase	370	27	12.63%	12.77%
LRRC4C	leucine rich repeat containing 4C	503	1	12.63%	11.70%
TRIM67	tripartite motif containing 67	98	1	12.11%	12.77%
DLG4	discs, large homolog 4 (Drosophila)	459	1	12.11%	12.77%

ENO2	enolase 2 (gamma, neuronal)	464	16	11.58%	8.51%
NETO1	neuropilin (NRP) and tolloid (TLL)-like 1	225	1	10.00%	9.57%
ELFN2	extracellular leucine-rich repeat and fibronectin type III domain containing 2	320	2	10.00%	8.51%
CSPG5	chondroitin sulfate proteoglycan 5 (neuroglycan C)	34	1	9.47%	9.57%
DNM1	dynamin 1	191	2	9.47%	9.57%
CHN1	chimerin 1	211	2	9.47%	9.57%
B4GALNT1	beta-1,4-N-acetyl-galactosaminyl transferase 1	271	2	9.47%	8.51%
LPPR4	lipid phosphate phosphatase-related protein type 4	290	5	9.47%	9.57%
PCDHGB1	protocadherin gamma subfamily B, 1	294	2	9.47%	9.57%
SCG3	secretogranin III	299	3	9.47%	9.57%
TPPP	tubulin polymerization promoting protein	428	9	9.47%	7.45%
TUBB2A	tubulin, beta 2A class IIa	429	133	9.47%	9.57%
SEZ6	seizure related 6 homolog (mouse)	46	1	8.95%	8.51%
BAI1	brain-specific angiogenesis inhibitor 1	443	4	8.95%	3.19%
DCLK2	doublecortin-like kinase 2	456	1	8.95%	9.57%
GABRA4	gamma-aminobutyric acid (GABA) A receptor, alpha 4	474	1	8.95%	9.57%
PRKCG	protein kinase C, gamma	256	8	7.37%	7.45%
CTNND2	catenin (cadherin-associated protein), delta 2	127	1	6.84%	5.32%
SEZ6L	seizure related 6 homolog (mouse)-like	613	2	6.84%	5.32%
OLFM1	olfactomedin 1	121	5	6.32%	6.38%
SLC1A3	solute carrier family 1 (glial high affinity glutamate transporter), member 3	175	10	6.32%	6.38%
RAB3A	RAB3A, member RAS oncogene family	258	1	6.32%	6.38%
GRIN3A	glutamate receptor, ionotropic, N-methyl-D-aspartate 3A	327	1	6.32%	6.38%

SCN8A	sodium channel, voltage gated, type VIII, alpha subunit	412	2	6.32%	6.38%
STXBP1	syntaxin binding protein 1	426	3	6.32%	6.38%
TAGLN3	transgelin 3	427	1	6.32%	6.38%
GABRA3	gamma-aminobutyric acid (GABA) A receptor, alpha 3	473	1	6.32%	6.38%
HCN1	hyperpolarization activated cyclic nucleotide-gated potassium channel 1	485	12	6.32%	6.38%
CELF5	CUGBP, Elav-like family member 5	560	1	6.32%	6.38%
GRIN2B	glutamate receptor, ionotropic, N-methyl D-aspartate 2B	78	6	5.79%	6.38%
PCDHA5	protocadherin alpha 5	229	3	5.79%	6.38%
CPNE6	copine VI (neuronal)	276	1	5.26%	5.32%
FEZ1	fasciculation and elongation protein zeta 1 (zygin I)	469	1	5.26%	6.38%
GAP43	growth associated protein 43	59	4	4.74%	3.19%
SH3GL2	SH3-domain GRB2-like 2	301	2	3.68%	1.06%
AP3B2	adaptor-related protein complex 3, beta 2 subunit	353	1	3.68%	3.19%
VSNL1	visinin-like 1	545	1	3.68%	6.38%
OPALIN	oligodendrocytic myelin paranodal and inner loop protein	2	8	3.16%	3.19%
MOG	myelin oligodendrocyte glycoprotein	17	2	3.16%	3.19%
POU3F2	POU class 3 homeobox 2	24	1	3.16%	3.19%
AK5	adenylate kinase 5	115	2	3.16%	3.19%
RPH3A	rabphilin 3A	123	4	3.16%	3.19%
PTPN5	protein tyrosine phosphatase, non-receptor type 5 (striatum-enriched)	198	1	3.16%	3.19%
SERPINI1	serpin peptidase inhibitor, clade I (neuroserpin), member 1	259	1	3.16%	2.13%
AMPH	amphiphysin	267	3	3.16%	3.19%
ATCAY	ataxia, cerebellar, Cayman type	269	1	3.16%	3.19%

PRMT8	protein arginine methyltransferase 8	296	2	3.16%	3.19%
RLBP1	retinaldehyde binding protein 1	298	2	3.16%	3.19%
TRIM9	tripartite motif containing 9	307	4	3.16%	3.19%
AMER3	APC membrane recruitment protein 3	352	1	3.16%	3.19%
C1QL1	complement component 1, q subcomponent-like 1	357	2	3.16%	3.19%
LHFPL4	lipoma HMGIC fusion partner-like 4	390	1	3.16%	3.19%
BAI3	brain-specific angiogenesis inhibitor 3	444	2	3.16%	3.19%
CAMK2A	calcium/calmodulin-dependent protein kinase II alpha	450	9	3.16%	3.19%
DLGAP1	discs, large homolog-associated protein 1	460	1	3.16%	3.19%
GRIN2A	glutamate receptor, ionotropic, N-methyl D-aspartate 2A	482	8	3.16%	3.19%
KCNC1	potassium voltage-gated channel, Shaw-related subfamily, member 1	489	3	3.16%	4.26%
GAREML	GRB2 associated, regulator of MAPK1-like	578	3	3.16%	3.19%
IBSP	integrin-binding sialoprotein	585	6	3.16%	3.19%
MEGF10	multiple EGF-like-domains 10	598	1	3.16%	3.19%
GABRG1	gamma-aminobutyric acid (GABA) A receptor, gamma 1	163	1	2.63%	1.06%
C1QL2	complement component 1, q subcomponent-like 2	210	1	2.63%	3.19%
NCAN	neurocan	18	5	0.00%	0.00%
FEZF2	FEZ family zinc finger 2	29	1	0.00%	0.00%
GPR37L1	G protein-coupled receptor 37 like 1	37	1	0.00%	0.00%
CACNG8	calcium channel, voltage-dependent, gamma subunit 8	39	1	0.00%	0.00%
GABRA1	gamma-aminobutyric acid (GABA) A receptor, alpha 1	40	1	0.00%	0.00%
HPCA	hippocalcin	41	2	0.00%	0.00%
PCDHGC5	protocadherin gamma subfamily C, 5	49	1	0.00%	0.00%

GPM6B	glycoprotein M6B	62	2	0.00%	0.00%
SYN2	synapsin II	64	1	0.00%	0.00%
TNR	tenascin R	69	1	0.00%	0.00%
SLC4A10	solute carrier family 4, sodium bicarbonate transporter, member 10	112	1	0.00%	0.00%
SV2B	synaptic vesicle glycoprotein 2B	113	3	0.00%	0.00%
SLC1A2	solute carrier family 1 (glial high affinity glutamate transporter), member 2	134	3	0.00%	0.00%
HRH3	histamine receptor H3	167	2	0.00%	0.00%
CYP46A1	cytochrome P450, family 46, subfamily A, polypeptide 1	190	5	0.00%	0.00%
GAD2	glutamate decarboxylase 2 (pancreatic islets and brain, 65kDa)	218	1	0.00%	0.00%
SV2A	synaptic vesicle glycoprotein 2A	234	1	0.00%	0.00%
APLP1	amyloid beta (A4) precursor-like protein 1	236	1	0.00%	0.00%
BRINP1	bone morphogenetic protein/retinoic acid inducible neural-specific 1	272	3	0.00%	0.00%
CNTNAP2	contactin associated protein-like 2	275	3	0.00%	0.00%
SHISA7	shisa family member 7	302	4	0.00%	0.00%
SYP	synaptophysin	306	2	0.00%	0.00%
FAM155A	family with sequence similarity 155, member A	322	1	0.00%	0.00%
CDH10	cadherin 10, type 2 (T2-cadherin)	362	2	0.00%	0.00%
FGFBP3	fibroblast growth factor binding protein 3	375	2	0.00%	0.00%
NAPB	N-ethylmaleimide-sensitive factor attachment protein, beta	395	1	0.00%	0.00%
RUNDC3A	RUN domain containing 3A	410	6	0.00%	0.00%
SMIM18	small integral membrane protein 18	418	6	0.00%	0.00%
ASIC4	acid-sensing (proton-gated) ion channel family member 4	440	5	0.00%	0.00%
GNAO1	guanine nucleotide binding protein (G protein), alpha activating activity	476	11	0.00%	0.00%

	polypeptide O				
GRM2	glutamate receptor, metabotropic 2	484	1	0.00%	0.00%
KIAA0513	KIAA0513	496	2	0.00%	0.00%
NECAB1	N-terminal EF-hand calcium binding protein 1	508	2	0.00%	0.00%
NLGN3	neuroligin 3	510	3	0.00%	0.00%
POU3F4	POU class 3 homeobox 4	520	5	0.00%	0.00%
RAB6B	RAB6B, member RAS oncogene family	526	2	0.00%	0.00%
BEND6	BEN domain containing 6	556	1	0.00%	0.00%

Table 5-21: ID discovery of an additional 52 BDPs in AIBL-2 and KARVIAH that were not initially observed in the discovery study in Chapter 4. Evidence of the identification in AIBL-2 and KARVIAH is shown as a percentage of individuals the BDP was observed in. The "Tissue Enriched" category in HPA (>five-fold increased expression in the cerebral cortex compared with all other tissues) was used as an indication of a candidate BDP due to high expression in the brain and minimal/none expression in other tissues.

Gene name	Protein description	Plasma Evidence		Human Protein Atlas (HPA) evidence
		AIBL (%)	KARVIAH (%)	Cerebral Cortex TS score
ADCY1	adenylate cyclase 1 (brain)	18.42%	17.78%	cerebral cortex: 17.8
APBA2	amyloid beta (A4) precursor protein-binding, family A, member 2	100.00%	100.00%	cerebral cortex: 32.6
ARNT2	aryl-hydrocarbon receptor nuclear translocator 2	8.42%	10.00%	cerebral cortex: 77.9
BAI2	brain-specific angiogenesis inhibitor 2	3.16%	3.33%	cerebral cortex: 33.7
C4orf50	chromosome 4 open reading frame 50	22.11%	23.33%	cerebral cortex: 1.5
CA10	carbonic anhydrase X	12.63%	13.33%	cerebral cortex: 33.2
CACNG2	calcium channel, voltage-dependent, gamma subunit 2	9.47%	10.00%	cerebral cortex: 7.1
CACNG3	calcium channel, voltage-dependent, gamma subunit 3	8.95%	10.00%	cerebral cortex: 22.2
CAMKV	caM kinase-like vesicle-associated	6.32%	6.67%	cerebral cortex: 44.6
CHRNB2	cholinergic receptor, nicotinic, beta 2 (neuronal)	5.79%	5.56%	cerebral cortex: 11.0
DRP2	dystrophin related protein 2	15.79%	16.67%	cerebral cortex: 6.1
ERMN	ermin, ERM-like protein	10.53%	10.00%	cerebral cortex: 116.4
FRMPD4	FERM and PDZ domain containing 4	22.11%	23.33%	cerebral cortex: 8.0
GABBR2	gamma-aminobutyric acid (GABA) B receptor, 2	14.21%	13.33%	cerebral cortex: 45.8
GABRA5	gamma-aminobutyric acid (GABA) A receptor, alpha 5	10.00%	7.78%	cerebral cortex: 43.1

GRIA2	glutamate receptor, ionotropic, AMPA 2	10.00%	8.89%	cerebral cortex: 98.2
GRIN1	glutamate receptor, ionotropic, N-methyl D-aspartate 1	18.95%	18.89%	cerebral cortex: 71.9
GRM3	glutamate receptor, metabotropic 3	9.47%	8.89%	cerebral cortex: 32.9
GRM5	glutamate receptor, metabotropic 5	12.63%	13.33%	cerebral cortex: 11.6
HTR2A	5-hydroxytryptamine (serotonin) receptor 2A, G protein-coupled	6.84%	5.56%	cerebral cortex: 16.9
IL1RAPL1	interleukin 1 receptor accessory protein-like 1	6.32%	6.67%	cerebral cortex: 2.9
KCNH1	potassium voltage-gated channel, subfamily H member 1	6.32%	6.67%	cerebral cortex: 5.6
KCNH7	potassium voltage-gated channel, subfamily H member 7	22.11%	22.22%	cerebral cortex: 2.4
KCNIP1	KV channel interacting protein 1	9.47%	10.00%	cerebral cortex: 22.0
KCNK12	potassium channel, subfamily K, member 12	24.74%	26.67%	cerebral cortex: 2.5
KIF1A	kinesin family member 1A	14.74%	15.56%	cerebral cortex: 136.1
KIF5A	kinesin family member 5A	22.11%	23.33%	cerebral cortex: 163.0
LGI1	leucine-rich, glioma inactivated 1	7.89%	10.00%	cerebral cortex: 23.0
LMTK3	lemur tyrosine kinase 3	9.47%	10.00%	cerebral cortex: 8.5
MAST1	microtubule associated serine/threonine kinase 1	6.32%	6.67%	cerebral cortex: 16.0
MEPE	matrix extracellular phosphoglycoprotein	12.63%	13.33%	cerebral cortex: 2.3
OLFM3	olfactomedin 3	14.74%	14.44%	cerebral cortex: 13.7
PAQR6	progestin and adipoQ receptor family member VI	12.63%	13.33%	cerebral cortex: 48.1
PDZD4	PDZ domain containing 4	9.47%	10.00%	cerebral cortex: 56.7
PMP2	peripheral myelin protein 2	8.95%	10.00%	cerebral cortex: 148.4
RIMS3	regulating synaptic membrane exocytosis 3	96.84%	101.11%	cerebral cortex: 30.4
RIT2	ras-like without CAAX 2	17.37%	18.89%	cerebral cortex: 11.3

RTN1	reticulon 1	9.47%	10.00%	cerebral cortex: 178.7
SLC17A7	solute carrier family 17 (vesicular glutamate transporter), member 7	9.47%	10.00%	cerebral cortex: 291.7
SLC35F1	solute carrier family 35, member F1	8.95%	10.00%	cerebral cortex: 24.7
SLC39A12	solute carrier family 39 (zinc transporter), member 12	12.63%	13.33%	cerebral cortex: 12.9
SLC7A14	solute carrier family 7, member 14	12.63%	13.33%	cerebral cortex: 13.8
SLCO1C1	solute carrier organic anion transporter family, member 1C1	11.58%	13.33%	cerebral cortex: 13.6
STX1A	syntaxin 1A (brain)	12.63%	13.33%	cerebral cortex: 83.6
STX1B	syntaxin 1B	10.00%	8.89%	cerebral cortex: 43.2
SYNGR3	synaptogyrin 3	9.47%	10.00%	cerebral cortex: 38.9
SYT1	synaptotagmin I	6.32%	6.67%	cerebral cortex: 272.2
SYT11	synaptotagmin XI	12.63%	12.22%	cerebral cortex: 209.7
TMEM132B	transmembrane protein 132B	12.63%	13.33%	cerebral cortex: 11.9
TMEM132D	transmembrane protein 132D	21.58%	21.11%	cerebral cortex: 6.7
TMOD2	tropomodulin 2 (neuronal)	21.58%	23.33%	cerebral cortex: 58.0

We have thus gathered strong evidence to suggest that suspected BDPs are circulating within human plasma. A total of 120 BDPs were discovered and then independently identified in two larger cohorts (AIBL-2 and KARVIAH). A large majority of the protein groups have moderate-to-good spectral evidence to support their identifications. In addition, a further 52 probable BDPs were discovered in AIBL-2 and then observed in KARVIAH. Despite their confirmation in multiple cohorts all but 14 BDP protein groups were excluded from the main analysis due to their inconsistent measurement in both cohorts. It is likely that the very low abundances of these protein groups, expected to be at the limit of sensitivity for MS analysis, are the cause for the inconsistent measurement. Furthermore, if these protein groups are truly "brain-derived" biological and disease state will influence their abundances within plasma. We have examined the association of these BDP with NAB as a continuous and binary measure.

Of the 172 replicated BDPs only 119 were investigated. We chose to examine only protein groups with data present in >18 participants. Furthermore, protein groups GFAP, BDNF, NEFL, NRGN, SNAP25, FMN2, SH3 and multiple ankyrin repeat domains 1 (SHANK1), sodium channel, voltage-gated, type II, alpha subunit (SCN2A), APBA2, chromodomain helicase DNA binding protein 5 (CHD5), microtubule-associated protein 2 (MAP2), RIMS3, synaptotagmin XVI (SYT16) and myelin transcription factor 1-like (MYT1L) were not examined here due to their inclusion in the main analysis. NEFL and NRGN (Table 5-11, Table 5-13, Table 5-14 and Table 5-15) were shown to have an associated with NAB. RIMSA and FMN2 were associated with age (Table 5-9) whereas SHANK1, CHD5 and MAP2 were associated with gender (Table 5-8). Using a Spearman Rank Correlation we found five BDPs to be nominally associated with Aβ SUVR at the uncorrected <0.05 *P* value (Table 5-22). No proteins groups were found to be statistically significant when applying a multiple testing correlation. Furthermore, only two protein groups demonstrated significance when adding *APOE* genotype as an additional covariate; TAGLN3 ($P = 0.026$) and SLC1A3 ($P = 0.006$). Additionally, seven protein groups were found to be associated with Aβ classification at the uncorrected <0.05 *P* value (Table 5-23). Box plots demonstrating the group separation of the most significant BDP protein groups (DLG4 and SNCB) are shown in Figure 5-17 and Figure 5-18. BDPs found to be associated with NAB in this study are underpowered with a

number of candidates found in <50 participants. Replication using an MS-MRM assay utilising the peptides discovered in study or an ultra-sensitive targeted assay would be necessary. However, from the initial discovery in Chapter 4 and identification in AIBL-2 and KARVIAH we have good evidence to conclude a number of potentially disease relevant BDPs are circulating and measurable in plasma.

Table 5-22: Protein groups termed as "brain-derived" associated with Aβ SUVR as continuous measure using Spearman's Rank correlation. GLM residuals were created by adjusted for TMT10plex group, age, gender and sample cohort. Benjamini-Hochberg *Q* values were all >0.3.

Protein Name	Gene name	Rho	*n*	*P* value
postsynaptic density protein 95	*DLG4*	-0.482	35	0.003
adenylyl cyclase type 1	*ADCY1*	0.574	18	0.013
ERC protein 2	*ERC2*	-0.295	71	0.013
mylein basic protein	*MBP*	0.520	118	0.027
DS Cell Adhesion Molecule	*DSCAM*	-0.168	126	0.049
neurexin 1	*NRXN1*	-0.195	89	0.067
CKLF Like MARVEL Transmembrane Domain Containing 5	*CMTM5*	-0.207	72	0.08
solute Carrier Family 1 Member 3	*SLC1A3*	-0.408	18	0.092
CASK Interacting Protein 1	*CASKIN1*	0.217	59	0.099
SNCB	*SNCB*	-0.248	44	0.099

Table 5-23: Protein groups termed as "brain-derived" associated with Aβ classification using Mann Whitney-U test. GLM residuals were created by adjusted for TMT10plex group, age, gender and sample cohort. Benjamini-Hochberg *Q* values were all >0.4.

	n				
Gene name	**Total**	**Aβ-**	**Aβ+**	**Z**	***P* value**
postsynaptic density protein 95	35	13	22	-2.868	0.004
SNCB	44	30	14	-2.621	0.009
ERC protein 2	71	37	34	-2.371	0.018
transgelin 3	18	9	9	-2.163	0.031
tubulin Beta 2A Class IIa	27	17	10	-2.159	0.031
kinesin Family Member 3C	44	29	15	-2.117	0.034
iduronate 2-Sulfatase	52	30	22	-2.037	0.042
adenylyl cyclase type 1	18	12	6	-1.873	0.061
RTN1	27	17	10	-1.707	0.088

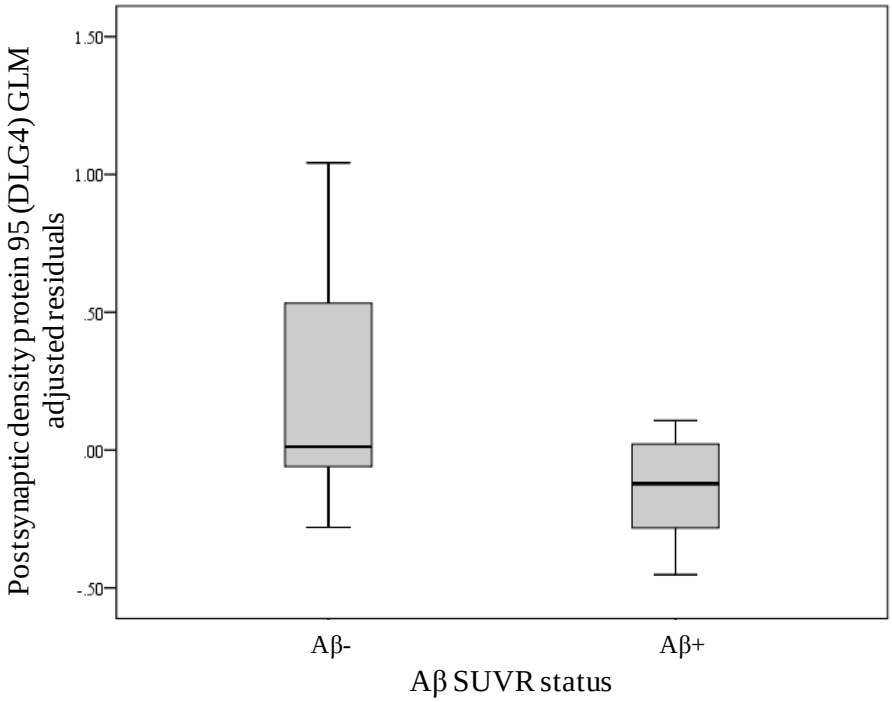

Figure 5-17: Box and whisker diagram to show the postsynaptic density protein 95 (DLR4) group differences (*P* = 0.004) between Aβ- and Aβ- (*n* = 35).

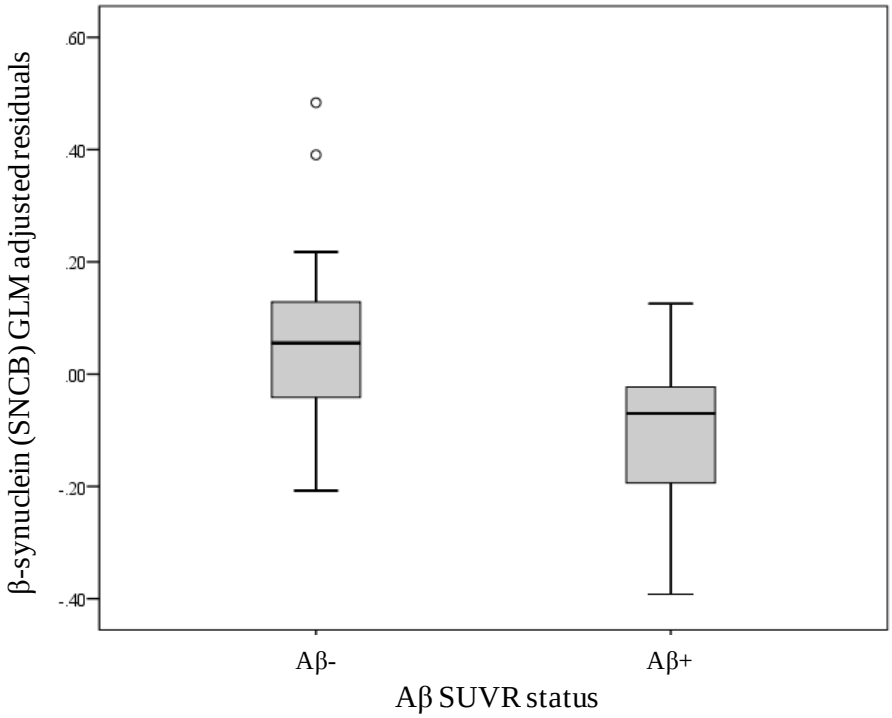

Figure 5-18: Box and whisker diagram to show the β-synuclein (SNCB) group differences (*P* = 0.009) between Aβ- and Aβ- (*n* = 44).

In Chapter 4, we also described a group of proteins that were implicated in neurodegenerative pathogenesis or CNS injury/damage (Table 4-10). Of the 18 protein groups highlighted in Table 4-10, a total of 14 were once again identified in AIBL-2 and KARVIAH. Protein groups that were not replicated in this study demonstrated poor spectral evidence in the discovery dataset. Seven of these protein groups were included in the main analysis with Aβ, NRGN and NEFL exhibiting an association with NAB. Eight other protein groups were not included in the main analysis due to being measured in only <50% of the dataset (BACE1, GAP43, ENO2, PARK7, RAB43, SOD1 and SYN1) therefore these protein groups were investigated for their association with NAB separately (Table 5-24). It was observed that only neuron specific enolase (ENO2 or NSE) demonstrated a significant but weak positive correlation with NAB (P = 0.036, Spearman's Rho = 0.346; Figure 5-19).

Table 5-24: Protein groups involved in neurodegenerative pathogenesis discovered in plasma in Chapter 4 and the replication of discovery in Chapter 5.

	MS/MS from Chapter 4 (Table 4-10)		AIBL-2 and KARVIAH
Protein Description (Gene symbol)	**Total PSMs**	**Spectral Classification**	***n***
alpha-synuclein	218	Good	44
amyloid beta A4 protein	57	Good	284
β-secretase 1	8	Poor	18
glial fibrillary acidic protein	160	Good	284
microtubule-associated protein tau	13	Poor	284
neurogranin	43	Moderate	276
neurofilament light polypeptide	13	Good/Moderate	257
neuromodulin	4	Moderate	12
neuron specific enolase	10	Moderate	30
protein DJ-1	26	Moderate	25
ras-related protein Rab-3A	2	Moderate	18
S100B	25	Moderate	n/a
superoxide dismutase [Cu-Zn]	3	Moderate	18
synapsin-1	12	Good	90
synaptosomal-associated protein 25	10	Poor	257
synaptophysin	2	Poor	n/a
synaptotagmin	5	Poor	n/a
TAR DNA-binding protein 43	2	Poor	n/a

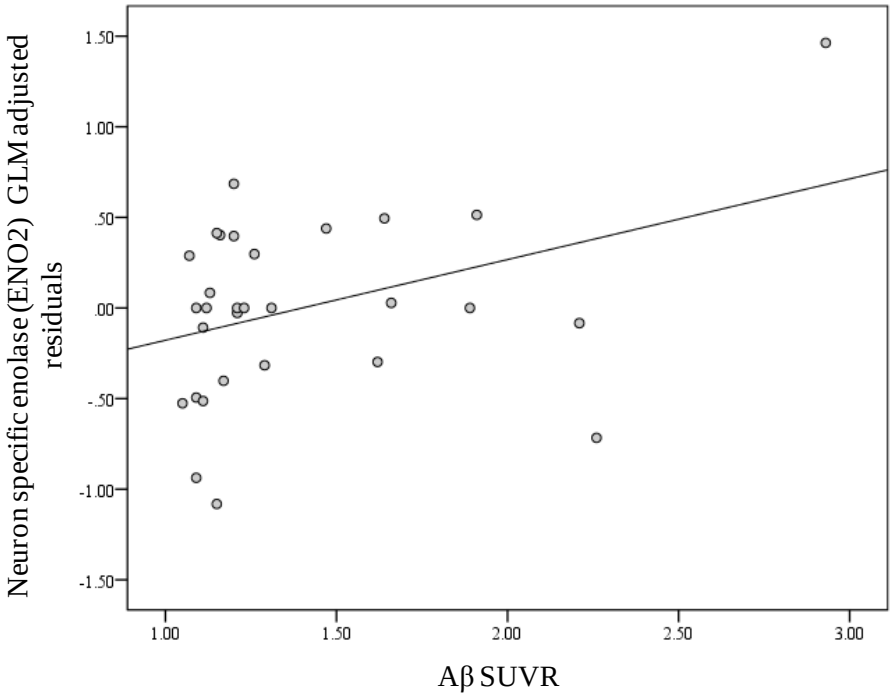

Figure 5-19: Scatter plot to show the correlation between neuron specific enolase (ENO2) and Aβ SUVR (*P* = 0.036).

5.5 Discussion

In this study we employed a deep proteomic profiling technique to discover, in some instances, novel plasma biomarkers of Aβ pathology assessed by either ^{11}C-PiB or ^{18}FBB PET imaging. Using an endophenotype design and an LC-MS/MS workflow we have described a substantial number of single plasma proteins significantly related to Aβ. Furthermore, we also detail a twenty-plasma protein panel, which was discovered and replicated by LC-MS/MS with 81% accuracy, increasing to 86.6%, in an independent cohort.

In previous blood-based biomarkers studies, we and others have first utilised LC-MS/MS as a hypothesis-generating tool to identify plasma protein biomarkers of AD pathology [372-375]. An attempt was then made to replicate these markers by an orthogonal platform, typically ELISA. In most cases, this translation has been disappointing and this is likely due to key platform differences. Mass spectrometry involves the analysis of peptides resulting from denatured protein, whilst ELISA measures native protein, or more precisely the region of the intact protein where the epitope recognized by the antibody resides. It is possible, therefore, that the measurement of different protein regions and the introduction of non-analyte interference in ELISAs will affect these results. To our knowledge, this is the first time a multi-analyte plasma biomarker for an AD related phenotype has been discovered and independently replicated by LC-MS/MS and the commonality in platform between discovery and replication has certainly aided this successful replication.

At the univariate level, a large number of protein groups were associated with Aβ pathology in correlation or group-wise analysis. Pathway analysis, as in Chapter 3, demonstrated that the coagulation and complement cascade pathways were overrepresented in this group. A total of 16 protein groups were associated with all statistical analysis in both the full dataset and cognitively normal individuals and 10 protein groups passed multiple testing corrections (Aβ, NEFL, NEUROG2, APBB3, ATPVOA2, CROCC, REST, DENND3, FHAD1, CNGB3 and NRGN (Table 5-16)). Of these highly associated protein groups, only three were not included in our multivariate classifier. DENN domain-containing protein 3 (DENND3) was found to

be decreased in relation to elevated NAB and interestingly was found to be more associated with elevated NAB in the cognitively normal individuals (Q = 0.004). In the same manner, cyclic nucleotide gated channel beta 3 (CNGB3) was found to have a more significant negative correlation in the cognitively normal individuals. DENND3 and CNGB3 have not been previously linked to AD although have been implicated to C9orf72 related ALS [543] and macular degeneration [544] respectively. On the other hand, the link between AD and neurogranin (NRGN) has been widely reported. NRGN is a post-synaptic protein thought to have a major role in synaptic plasticity and it is hypothesised that synaptic degradation releases NRGN into the CSF. Consequently, increased levels of CSF NRGN have been extensively reported in AD [528, 545-547] but more encouragingly are seen to be specific for AD [548]. Kvartsberg and colleagues [528], using MS, have been able to categorise NRGN peptides from CSF and plasma. While showing significant increases in NRGN CSF, that also correlate to $A\beta_{1-42}$, they report no difference in plasma NRGN related to AD phenotypes and this has been verified by others [549]. Furthermore, subgroups of NRGN peptides have been shown to be specific to plasma and not CSF as well as CSF specific peptides and those that are identified in both compartments [528]. Kvartsberg and colleagues found there to be no correlation between CSF and plasma NRGN peptides. In our data, peptides that make up our NRGN protein score correspond with plasma specific peptides reported by Kvartsberg and colleagues [528] and therefore confirming that our NRGN expression is exclusively peripheral. NRGN expression in the spleen, bone marrow, platelets and lung tissue has been previously reported [550] and this is our likely source. Nonetheless, in contrast to the studies mentioned, we report for the first time a highly significant positive correlation between plasma NRGN and Aβ SUVR. Increased levels of serum NRGN have been previously attributed to TBI [551].

We also attempted to use the LC-MS/MS discovery findings from Chapter 3. This was largely unsuccessful with only 2/43 protein groups replicating a significant directional change in the Aβ (apoA1 and ITIH4). Significant methodological differences could explain this poor replication. Firstly, in Chapter 3, upfront fractionation was performed at the protein level by 1DGE. IDGE gel fractions were analysed and statistically examined separately. Identical protein groups found in separate gel fractions were considered as differing protein group MW isoforms as

protein modifications or proteolytic cleavage seemingly have altered structure to the native molecular MW of the protein. Therefore, protein groups identified by this method are likely to be fragment specific. In contrast, the LC-MS/MS methodology applied in this Chapter incorporated enzymatic digestion prior to fractionation. All peptides from a protein group were merged together for analysis; therefore, this method is a more global representation of overall protein levels in plasma. Further to this, Chapter 3 employed TMT protein labelling to be compatible with 1DGE separation. As previously described TMT protein labelling can only quantify between 52-57% of the identified peptides as TMT protein labelling is limited to lysine residues. Conversely, TMT peptide labelling utilised in this Chapter chemically labels each peptide toward the free amino-terminus, allowing quantification of almost all peptide sequences. Again, this points towards the methodology applied in this Chapter being a more accurate and global estimation of plasma protein expression.

Many candidate biomarkers of AD pathology were identified in this study. Of these, 20 protein groups (Table 5-18) were found by a combination of variable reduction analysis and support vector machine learning together to accurately predict elevated NAB. This plasma protein model was trained in the full AIBL-2 cohort and tested in the KARVIAH cohort. It is encouraging that a model of NAB trained in a mixed diagnosis cohort (AIBL-2) has good predictability in a cognitively normal cohort (KARVIAH) and demonstrates potential use as population screening tool. Using the univarite analysis as a guide, a differing protein panel may have been observed if only cognitively normal individuals in AIBL-2 were used to build the classifier. This is based upon CROCC, UBR1, ELMOD2 and ficolin-2 being only associated with Aβ when MCI and AD subjects were included in the study. Furthermore, targets not included in the model such as CNGB3, TF, DENN3, TIA and PCNX were more associated with cognitively normal individuals at the univariate level. Nonetheless, the observed high accuracy of predicting NAB by this panel (AUC 86.6%; Figure 5-16) is of greater accuracy then previous blood-biomarker studies [374, 437, 552] and nearing the predictive ability of core CSF biomarkers.

It must be noted that although entirely independent cohorts, AIBL-2 and KARVIAH plasma samples were prepared and analysed concurrently with one another. This

reduces the technical variability between the cohorts and therefore may inflate the result of our replication. Furthermore, a key advantage of employing an isobaric labelling technique for sample multiplexing is that it overcomes analytical variability that is introduced by single sample acquisition. Quantitative TMT10plex reporter ions arise from a common fragmented precursor ion present in the sample. In most cases the precursor ion intensity will be a combined signal from all samples in a TMT10plex group. However, in our data, which has two different cohorts multiplexed together, it is possible that the precursor ion intensity maybe driven by one cohort of samples forcing a TMT reporter ion values in the other cohort.

The protein groups included in the predictive panel are included in Table 5-18 and are discussed below, in terms of their biological function and relation or possible link to AD and Aβ pathology.

5.5.1 APP processing

The most significant protein group in all univariate level analysis was amyloid beta A4 protein (Aβ). Here, we observed a positive correlation between plasma Aβ and Aβ PET SUVR as well as a highly significant increase of plasma Aβ in Aβ+ individuals (Table 5-16). This highly significant association remained when examining just the cognitively normal group.

The *APP* gene codes for a protein 770 amino acids in length. Alternative proteolysis in this protein group generates several fragments including Aβ peptides that are the principle composition of senile plaques in AD brains. The LC-MS/MS data presented here identified three unique Aβ peptides that were consistently measured in all subjects and were database matched to Aβ (Table 5-25). The sequences identified highlight peptides located within the C99 region (672-770) of the amyloid beta A4 protein. Proteolytic cleavage of C99 by γ-secretase results in the production of toxic $A\beta_{1-40}$ and $A\beta_{1-42}$. Peptide sequences "HDSGYEVHHQK" and "LVFFAEDVGSNK" fall within the region of $A\beta_{1-40}$ and $A\beta_{1-42}$ peptides (Table 5-25). However, without further supporting evidence it cannot be determined if these peptides are solely from toxic fragments or alternative processed fragments (Table 5-25).

Table 5-25: Peptide sequences and amino acid positions identified by LC-MS/MS matched to amyloid beta A4 protein.

Peptide Sequence	Amino acid positions	Possible molecular processing fragments
HFEHVRMVDPKK	510-522	sAPPα/ sAPPβ
HDSGYEVHHQK	676-687	sAPPα/C99/$Aβ_{1-40}$/$Aβ_{1-42}$
LVFFAEDVGSNK	688-699	C99/$Aβ_{1-40}$/$Aβ_{1-42}$/C83

Almost all of the investigations of Aβ in plasma have been performed by antibody-based immunoassays. Mass Spectrometry efforts for the detection of Aβ in plasma have been limited to selected reaction monitoring (SRM) studies [553-554] or immunoprecipitation MS (IP-MS) [555]. The difficulties in detecting Aβ variants in plasma are due to the concentrations of $Aβ_{1-40}$ and $Aβ_{1-42}$ in human plasma being approximately 50-fold lower than in human CSF but the total protein concentration being 100-fold higher in plasma [556]. We have shown that an unbiased and untargeted MS approach can be utilised to consistently measure Aβ peptides, although it is not as extensively measured as the aforementioned SRM and IP-MS studies. As previously discussed, the association of plasma Aβ peptides to AD and AD pathology has been inconclusive. $Aβ_{1-40}$ and $Aβ_{1-42}$ have been shown to be increased [376, 382 383], decreased [379-381, 384] or unchanged [350, 377, 379, 381, 384, 557] in relation to an AD diagnosis or elevated NAB. Rembach and colleagues [380] concluded that plasma Aβ species have limited diagnostic utility alone but do have utility as part of a peripheral panel, as Aβ is influenced by a number of peripheral age-related analytes [380]. Burnham and colleagues [437] have previously described the validity of including plasma $Aβ_{1-42}$ in a multi-analyte panel and our data, without being able to determine the species of Aβ, comes to a similar conclusion.

A hypothesised theory in the field suggests that the clearance of CSF Aβ into the blood gives the reasonable assumption that plasma Aβ levels would follow the same disease related trend as CSF. However, it is important to consider and not over simplify the source of circulating Aβ fragments. *APP* processing occurs in a wide variety of tissues in both the CNS and periphery [558] with skeletal muscle, platelets and vascular walls generating Aβ peptides in the heart, pancreas, liver and kidneys [559]. These compartments may allow for an active exchange of Aβ peptides between

the brain and periphery but undoubtedly contribute to the pool of circulating Aβ peptides [558]. Studies have demonstrated that Aβ processing in the periphery does differ from the CNS and therefore distinctions can be made [560]. Conversely, increased platelet Aβ peptide levels with associated reduced α-secretase and increased β-secretase activities indicates that blood platelet Aβ is processed by the same amyloidogenic and non-amyloidogenic pathways as the CNS [561]. An increased Aβ blood platelet levels associated with clinical AD have been previously shown [561-563] and is in concordance with the results we demonstrate.

We also reported the significant positive association of the amyloid beta A4 precursor protein-binding, family B, member 3 (APBB3) and Aβ SUVR. APBB3 is a member of the FE65 protein family (with APBB1 and APBB2), adaptor and scaffolding proteins that mediate complexes through a variety of protein interactions including Aβ [564]. FE65 proteins are highly expressed in the brain; however APBB2 and APBB3 have been shown to be expressed in a variety of tissues. All FE65 proteins have similar structures; however, they diverge in their N-termini. Peptides identified in our study show exclusivity to APBB3 and these exact peptides sequences have been previously identified in a large MS plasma study giving further validity to their assignment [565]. To our knowledge, APBB3 has not been shown to be differentially expressed in blood for any disease modality. In cellular models, APBB3 has been shown to promote Aβ production [566]. A polymorphism in the APBB3 gene was shown to be a risk factor for EOAD [567] whereas a deletion in the APBB1 gene has been reported to have a protective effect in individuals over 75 years [568]. However, the role for FE65 proteins in the adult brain is not fully understood, particularly with regard to their individual effects on *APP* processing. The presence of APBB3 in blood plasma, it's highly significant association with NAB and peripheral Aβ peptides revealed here suggest a mirrored role of alternative Aβ processing in blood.

5.5.2 Coagulation and complement pathways

Interestingly, prothrombin and hyaluronan-binding protein 2 (HABP2) were included in our protein classifier and at the univariate level were shown to be decreased in relation to elevated NAB. The identification of prothrombin and

HABP2 once again highlights the importance of fibrinogen production, fibrin cleavage products and the coagulation cascade in AD [484, 489]. It also supports the growing body of evidence for the physical interaction between coagulation factors, *APP* processing and Aβ peptides [484-485, 489]. The coagulation cascade activates a series of events that lead to the production of thrombin (a serine protease) from prothrombin; this mediates the conversion of fibrinogen to fibrin. In the brain, thrombin affects several processes that are directly relevant for AD. Thrombin (also code by the *F2* gene) *in vitro* can stimulate production of *APP* and cleavage of *APP* into fragments [569]. Furthermore, thrombin is also important for the proteolytic processing of tau [570]. On the other hand, HABP2 is another serine protease that does not act upon F2 but directly cleavages α and β chains of fibrinogen at multiple sites. This action prevents thrombin's action in creating cleavage products (fibrinopeptide A and B) and therefore disrupts the formation of clots pointing towards HABP2 being an inhibitor of coagulation [571]. In blood, AD subjects often show increased clot formation, decreased fibrinolysis, and elevated levels of thrombin, fibrinogen and coagulation factors [371, 404, 483, 572-576]. A decrease expression of an inhibitor of the coagulation process, such as HABP2, would be in line with this theory. However, we have extensively demonstrated the negative relationship of coagulation activators and products F2, factor Xa (F10), plasma kallikrein (KLKB1), factor XIII (F13A-1) and fibrinogen chains (Chapter 3) with NAB. An explanation for this observed decrease in response to AD pathology could be that coagulation factors also act upon the complement system [577-578]. An overactive complement system is often reported in AD and this would correspond to a reduction in complement inhibitors that include fibrinogen (α, β, γ) and F2.

In the brain, a bidirectional association between the complement and coagulation systems occurs. Complement proteins are the target for several coagulation factors and therefore the levels of coagulation factors present in the AD brain could enhance the activation of the complement cascade [484, 579]. On the other hand, complement activation might lead to coagulation and fibrin deposition [484]. Aβ and tau are potent activators of the complement pathway [580-581] and therefore in AD, after Aβ and tau activation, a complement response may induce a prothrombic state. With complement and coagulation factors prominent in blood it is likely that this interaction between these systems occurs in the periphery. This is supported by both

LC-MS/MS discovery investigations in this thesis demonstrating significant protein groups that were over-represented for involvement in complement and coagulation cascades simultaneously.

The complement system is critical in both the innate and adaptive immune system, and has been previously associated in the pathogenesis of many neurodegenerative diseases, including AD [582-583]. The complement system is divided into three main pathways (Figure 5-20). The classical pathway primarily acts to lyse cells and bacteria already recognised then signalling these cells for immunological clearance. The alternate pathway acts independently of plasma antibodies and binds to cells and bacteria that do not express complement decay accelerating factor (DAF). The mannose-binding lectin (MBL) pathway recognises lectins and ficolins, common bacterial surface proteins and acts primarily to lyse bacteria and target them for immunological clearance. Furthermore, in relation to coagulation, another complement activation pathway, named the extrinsic pathway that is driven by prothrombin and KLKB1 has been described [584].

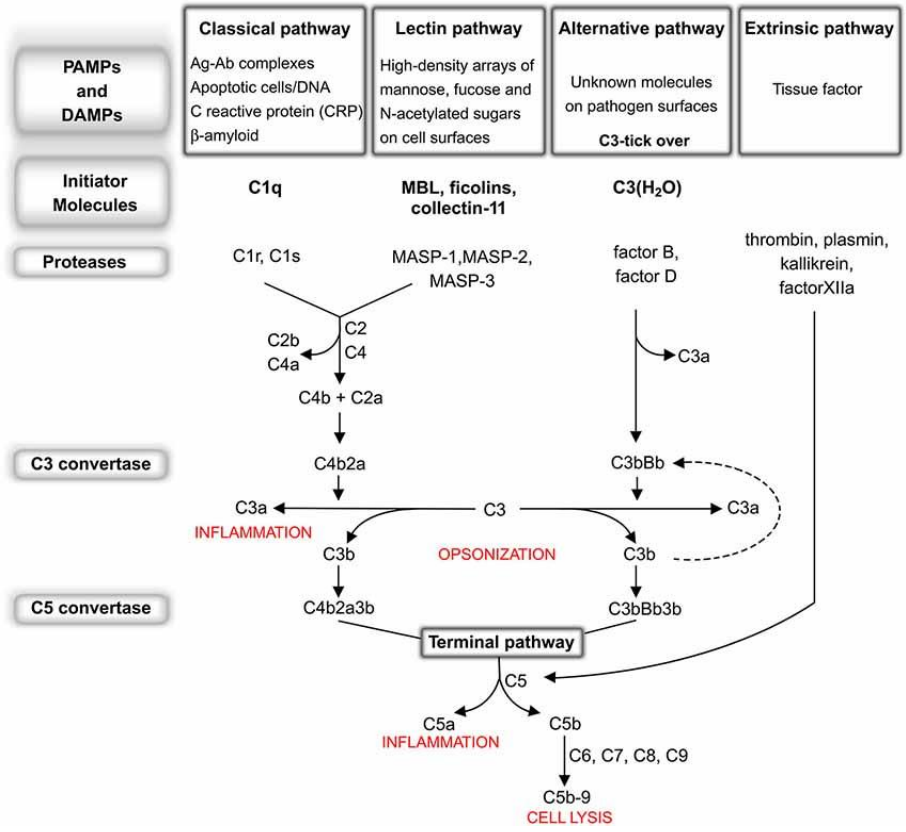

Figure 5-20: An overview of the complement pathway (Huber-Lang and colleagues 2006).

Complement C3 (CC3) is a central component in the complement system, where all three major pathways converge. CC3 is one of the most common plasma proteins to be reported as an AD biomarker (reviewed by [354, 552]) and Aβ pathology [373, 375, 436] but conflicting results suggested both a protective role and causal role for CC3. In Chapter 3, we found a significant decrease of CC3 (42% protein sequence coverage) in relation to elevated Aβ using LC-MS/MS however here we found a non-significance increase of CC3 with Aβ (87% protein sequence coverage). The differences in protein sequence coverage and directional change of CC3 between these studies suggest that CC3 isoform/fragment specific association with Aβ should be investigated. At the univariate level we have shown increased complement C1s (C1s) and CC5 are nominally associated with elevated NAB. CC5 is only associated with Aβ in the cognitively normal groups only, suggesting it is an early event in relation to Aβ deposition. However, our main finding in relation to the complement pathway is the highly significant association and inclusion of ficolin-2, an activator of the lectin complement pathway, in our twenty-plasma prediction model. ficolin-2 was found to be significantly negatively correlated with Aβ+ individuals and was more significant in an endophenotype approach. Ficolin-3 shares 50% amino acid homology with ficolin-2 [129] and was also found to be significantly reduced with Aβ+ subject in AIBL-1. Ficolin-2 has previously been associated with type 2 diabetes [585-586], diabetic peripheral neuropathy [146] and more recently plasma ficolin-2 was discovered to be associated with CSF $A\beta_{1-42}$ measures in an endophenotype LC-MS/MS study (Baird AL et al., under review).

5.5.3 Transcription factors

REST (Repressor Element 1-Silencing Transcription factor) is a protein that modulates neuronal differentiation and gene expression, and more recently been found to play an important role in AD [587]. Though highly expressed during development, REST was not thought to be expressed in the adult brain. However, recent observations indicate REST expression increases in the aging brain. REST expression has been shown to protect mature hippocampal neurons from toxic insults, e.g., hyperexcitation, and to play a key role in regulating the ageing brain's response to stress [588]. Furthermore, preclinical and clinical evidence demonstrate that reduced REST levels are associated with decreased hippocampal volume and

cognitive impairment [587]. Recently, the peripheral expression of REST, in relation to AD, has become of great interest. REST has been identified in neuronally-derived exosomes circulating in plasma and that levels are reduced in AD and MCI subjects [530, 589]. Furthermore, unpublished data has also demonstrates that reduce levels of REST is found in AD and converting MCI plasma using an immunoassay approach (Ashton NJ et al., under review). Here, we have also demonstrated a reduction in REST but for the first time in relation to Aβ pathology. It is possible that the denaturing conditions of LC-MS/MS methodologies would ensure that cargo from neuronally-derived exosomes and peripherally circulating REST would be measured as one entity. Commercial immunoassay analysis often does not allow for identification of protein epitopes measured. Database probability matching in this study has identified four peptide sequences to isoform 4 of REST (Table 5-26). Isoform 4 of REST differs to the canonical sequence by having amino acids 304-326 deleted from the sequence. However, sequence information obtained from our LC-MS/MS data cannot differentiate between isoform 1 or isoform 4 of REST. We can conclude that isoforms 2 and 3 of REST are not present in our sample as the peptide sequences identified are deleted from those isoforms sequences (Table 5-26).

Table 5-26: Peptide sequences and amino acid positions identified by LC-MS/MS matched to RE1-Silencing Transcription factor (REST).

Peptide Sequence	Amino acid positions
QVHNGPKPLNCPHCDYK	353-369
IKGDVAGKKNEKSVK	453-467
EPVQIELSPPMEVVQK	743-758
LLNTGEGNKEAPLQK	882-896

Neurogenins are a family of basic helix-loop-helix (bHLH) transcription factors involved in specifying neuronal differentiation [590]. In the developing cerebral cortex, neurogenin-1 and neurogenin-2 are expressed exclusively in the cortical ventricular zone during embryonic neurogenesis [591]. Contrasting to neurogenin-1, which is only expressed in the developing brain, neurogenin-2 (NEUROG2) is expressed in both embryonic brains as well as in adult hippocampal neural progenitor cells [592-593]. Hippocampal neurogenesis is thought to be essential in

maintaining hippocampus related cognitive abilities [594] and if impaired adds to the progression of AD [595]. In animal models of AD, the regeneration of hippocampal neurones is decreased in the presence of toxic Aβ peptides [596] supporting the notion that AD related pathology directly affects neurogenesis. Further to this, studies have shown that a potential normal function of APP regulates NEUROG2 to increase hippocampal neurogenesis [597]. In this study, we have identified two unique peptide sequences consistently measured in >94% of individuals that are unique to NEUROG2. Together these plasma peptides have highly significant correlations with Aβ and increases in Aβ+ individuals, even after statistical correction for multiple testing. We also demonstrate that NEUROG2 is more associated with Aβ in the cognitively normal group and is highly correlated with Aβ peptides that have been detected by the same approach. It is unclear if this increased expression of NEUROG2 is related to adult neurogenesis in response to NAB or even if these NEUROG2 peptides are brain-derived. However, NEUROG2 is a putative novel peripheral marker that has established mechanistic connections with cognitive decline and AD pathology. The presence of NEUROG2 in plasma has only been described in one large-scale plasma profiling study [565] despite having evidence of peripheral tissue expression. Interestingly, NEUROG2 was not identified in our proteomic profiling study in Chapter 4, even though the same methodology and analytical apparatus was applied. This would point towards cohort differences and analytical variation having an impact on the detection of NEUROG2.

Inflammation and oxidative stress is a well-documented event in ageing and AD (reviewed in [598-599]) and these processes have been shown to stimulate the NF-κB family. NF-κB transcriptionally regulates genes involved in cytokine expression, chemokine expression and adhesion molecules. In addition, NF-κB regulates both pro-apoptotic and anti-apoptotic genes [600]. The role of an abnormal NF-κB signalling system is well described in a number of age-associated diseases [601-602] that include neurodegeneration [603], osteoporosis [604], diabetes [605] and atherosclerosis [606-607]. We have identified a key member of the NF-κB family, transcription factor p65 (RELA), to be decreased in the plasma of individuals with elevated Aβ SUVR. Although nominally associated at the univariate level, RELA was highlighted by variable reduction analysis and included in our twenty-plasma protein panel. NF-κB, via RELA, regulates IL-1β and TNFα and these key inflammatory proteins are found at

increased levels in the brains of AD patients [608]. The decreased levels of RELA we observe could suggest an aberrant NF-κB modulation leading to increased peripheral inflammation. Evidence suggests that overstimulation and chronic activation of NF-κB plays not only a critical role in AD related inflammation and cytokine signalling but also senile plaque formation [609-610]. Further to this, in PD, a 70-fold increase in RELA activation is found in dopaminergic neurons [611] with NF-κB inhibitors improving motor function in PD animal models [612]. Many have postulated the NF-κB system as a possible therapeutic target for AD [613]. The peripheral measurement of NF-κB, by RELA, offers the opportunity to track NF-κB activation in relation to disease and in response to therapy, although, the connection of how plasma expression of RELA relates to CNS RELA needs to be determined.

5.5.4 Axonal injury

Neurofilaments (NF) are the most abundant neuronal cytoskeletal proteins in the CNS and are crucial to the structure of axons and transport. NF's are composed of three subunits based on the molecular weight; high (NFEH), medium (NFEM), and light (NFEL). NF subunits, mainly NEFL, are actively involved in the pathogenesis of axonal injury and degeneration both as causative agents and progression markers for a number of neurological diseases. NEFL is expressed in neurons in both the CNS and peripheral nervous system (PNS) [614] and therefore neuronal damage is seen to release into the extracellular compartment resulting in increased CSF NEFL levels [615]. High CSF levels of NEFL have been suggested to be consequence of normal ageing [348, 616-617]. However, higher levels have also shown to be associated with AD [346, 378, 618-620], FTD [347], ALS [349, 616, 621-622], progressive supranuclear palsy (PSP) [623] and multiple sclerosis [624]. More recently, CSF NEFL levels have been shown to be a marker of accelerated cognitive decline and shorter survival time across several neurodegenerative diseases [348]. The substantial overlap of CSF measures of NEFL across neurological disease has attributed this marker to one of disease integrity, progression and not to be disease specific marker [625]. NEFL is detectable and quantifiable in blood and shown to be more than 50-fold lower in concentration than in the CSF using an ultra-sensitive assay [363], although we have demonstrated NEFL measures using an untargeted MS approach. Similar findings have been described in plasma studies, with increased NEFL described in AD [626-627], ALS [628] and PSP [629].

An encouraging finding is that NEFL CSF and plasma concentrations seem to be correlated in a number of studies [363, 627-628] supporting the notion that plasma NEFL is a reflection of CNS damage.

We have identified six unique peptides that correspond to NEFL in plasma (Table 5-27); although two peptide sequences cannot be distinguished from NEFM we believe that there is good supporting evidence to conclude they are peptides from NEFL (Table 5-27). NEFL, after Aβ, was the most statistically significant finding in our study. We demonstrate that a highly significant correlation exists between NEFL and Aβ, which reveals increased NEFL with Aβ+ individuals.

Table 5-27: Peptide sequences and amino acid positions identified by LC-MS/MS matched to neurofilament light chain (NEFL).

Peptide Sequence	Amino acid positions	
	NEFL	NEFM
ALYEQEIR	137-144	n/a
LAAEDATNEK	148-158	n/a
QNADISAMQDTINK	340-353	n/a
EYQDLLNVK	370-379	383-391
LLEGEETR	392-399	404-411
VQSLQDEVAFLR	n/a	224-236

Our finding is in keeping with previous studies, although we do not find an age related increase of plasma NEFL. In contrast to other NEFL investigations we found a significant association between *APOE* ε4 and plasma NEFL, however a partial correlation to account for *APOE* genotype did not change our overall NEFL association. As previously hypothesised, it is possible that observed elevation of plasma NEFL is a reflection of CNS injury and not that of Aβ SUVR itself. It has been shown that CSF concentrations of NEFL (and therefore plasma NEFL) are not driven by pathological Aβ [625]. In support of this, the small number of AD and MCI subjects with low Aβ SUVR (Suspected Non Amyloid Pathology; SNAP) in our study continued to demonstrate high levels of NEFL (data not shown). Moreover, in other studies, NEFL measures have been seen to correlate with cognitive decline and therefore our finding maybe driven by the significant difference of MMSE between our Aβ- and Aβ+ groups (Table 5-1). However, our result still remained significant

when correlating NEFL with Aβ SUVR in only cognitively normal individuals where no difference in cognition is observed. As the Aβ cascade hypothesis suggests that Aβ deposition is the main initiator behind events that result in neuronal death, a clear link between elevations of NEFL in response to NAB can be made. Therefore, our data indicates that plasma NEFL could be an early marker of CNS injury that is consequence of preclinical Aβ deposition.

5.5.5 G protein coupled receptors

G protein coupled receptors (GPCRs) are essential membrane proteins that convert extracellular signals into intracellular responses, including responses to hormones, neurotransmitters, vision, olfaction and taste signals [630]. Substantial evidence points towards GPCRs and GPCR related proteins in the pathogenesis of AD, notably Aβ plaques formation [631] as well as α-secretase, β-secretase and γ-secretase activity [632-633]. Our data highlights the association of four GPCRs (probable G-protein coupled receptor 115 (GPR115), olfactory receptor 52I2 (OR52I2), ELMO domain containing 2 (ELOMD2) and G protein signalling modulator (GPSM2)) to have decreased peripheral expression in related to elevated Aβ SUVR. Although these specific GPCR's have not been directly related to AD pathology, it does indicate a more global alteration of GPCRs in response to NAB.

GPR3, a close relative of GPR115, participates in the mediation of Aβ generation by affecting the activity of the γ-secretase complex [634-635]. GPR3 is strongly expressed in neurons in the hippocampus, entorhinal cortex and thalamus in the normal human brain and its expression is increased in patients with sporadic AD [634]. Furthermore, olfactory disruption is a well-documented event in dementia [146] and has been considered to be an early clinical event in AD [636]. Olfactory function impairment tests alone or as part of battery of clinical examinations has been shown to predict MCI conversion to AD with high accuracy [637]. Furthermore, evidence from Tg2576 AD mouse model studies suggest that olfactory deficits may stem from non-fibrillar Aβ toxicity [638]. OR52I2 is a GPCR olfactory receptor that acts to initiate a neuronal response that perceives smell. It is therefore interesting that our plasma data demonstrates a decrease in those with elevated Aβ. Unlike GPR115, ELOMD2 and GPSM2, OR52I2 has been described as a part of the plasma proteome previously [565].

5.5.6 Other plasma protein groups of the multi-analyte classifier

V-type proton ATPase 116kDA subunit (ATP6V0A2), forkhead-associated domain-containing protein 1 (FHAD1) and dynein heavy chain 10 (DNAH10) were all significantly associated with Aβ SUVR in all univariate analysis and were all seen to have increased expression in the Aβ+ group.

ATP6V0A2 is involved in pH homeostasis and intracellular transport and has been described to reside in endosomes and in a compartment overlapping with the *trans*-Golgi network, a major secretory pathway that directs newly synthesised proteins. A mutation in the gene encoding for ATP6V0A2 causes autosomal recessive cutis laxa type II, which has major disruption of the golgi trafficking system [639]. Golgi trafficking defects have been previously described in AD [640], PD [641] and more recently has been hypothesised to underpin abnormal accumulation of Aβ [642].

The specific role of FHAD1 has not been elucidated however the family of forkhead-associated (FHA) domains have been shown to have major roles in a range of biological functions such as cell cycle controls and DNA damage repair [643]. More recently, FHA has been linked to immune responses and the signalling pathways leading to NF-κB activation [643]. Therefore, our observation of increase plasma expression of FHAD1 in conjunction with the decreased expression of RELA, described above, could indicate faulty NF-κB activity.

DNAH10 and as well as rootletin (CROCC) were included in the twenty-plasma protein panel for Aβ prediction. Interestingly, both these proteins are components of the primary ciliary root structure. Moreover, cilia and flagella associated protein 43 (WDR96) also primary cilia root protein was significant with Aβ at the univariate level. Primary cilia are solitary organelles that protrude from the cell surface in most mammalian cell types and the ciliary rootlet links the base of the cilium to the cell body. Increasing evidence suggests that primary cilia are key coordinators of homeostasis and signalling pathways and when defective are a major cause of human diseases and developmental disorders [644-645]. Several studies have implicated ciliary and basal body proteins in the regulation of Wnt signalling. The Wnt-planar cell polarity (Wnt-PCP) pathway has been shown to mediate many of the major

neurotoxic effects of Aβ and many aspects of AD neuropathology, including synapse loss and subsequent cognitive decline [646]. Although the structural components of the ciliary rootlet have been described very little is known about their function [647]. A hypothetical function suggests a role as a critical support structure for the cilia, especially in situations where mechanical stress is expected to be high [648]. Therefore, a deficit in the support structure of cilia could lead to the neurotoxic effects of Aβ via the Wnt-PCP pathway. Although CROCC is the major component of the cilia root, we found a stronger association of DNAH10 and Aβ. DNAH10 is primarily linked to respiratory cilia, although its expression has been observed in the brain. A variant in the DNAH10 gene has been linked to Charcot Marie Tooth disease, an inherited peripheral neuropathy [649].

E3 ubiquitin-protein ligase (UBR1) was shown to be increased in Aβ+ subjects however; this association was lost when examined in cognitively normal subjects only. Ubiquitin-protein ligases, like UBR1, are of particular importance in disease as they determine the targeting specificity of the ubiquitin system [650]. Such molecules have been found to be mutated, absent or malfunction in some hereditary forms of neurodegenerative disorders and indeed the presence of ubiquitin-positive, intra or extracellular inclusion are found in a number of neurodegenerative diseases [651]. In the same manner, secreted phosphoprotein 24 (SPP2) and histone RNA hairpin-binding protein (SLBP) were not associated with the cognitively normal group but decreased in relationship was observed with NAB as a whole group. This suggests that these three protein groups are more associated with NAB in established disease. SPP2 is a member of the cystatin superfamily with a genetic link to degeneration of the retina [652] whereas SLBP is an essential RNA binding protein essential for the coordination of histone gene expression with DNA synthesis.

5.5.7 Identification and replication of brain-derived proteins in plasma

Cerebrovascular pathology is common in normal aging and this is often marked by noticeable damage at the BBB. This process seems to be exacerbated and accelerated during AD and other dementias where vascular impairment is common [487]. Various mechanisms have been suggested as a source of the BBB dysfunction in AD, with accumulation of Aβ in the vascular walls [653] and a link to *APOE* genotype being

described [69]. Under normal conditions, processes at the BBB endothelial cells are meant to prevent the unregulated leakage of plasma proteins into the CNS. Several alterations in a dysfunctional BBB are observed at these endothelial cells, such as, loosening of the tight junctions, increased pinocytosis and subsequent increased barrier permeability [487]. Therefore, ion balance, nutritional transport and the modulation of peripheral extravasation are impaired leading to secondary neuronal injury and neurodegeneration.

We have already hypothesised this peripheral extravasation by observing decreased plasma FGγ in AD vulnerable individuals. We believe, supported by others, that the movement of FGγ (and other coagulation by-products) into the CNS (Chapter 3), in response to a dysfunctional BBB, enhances the aggregation of Aβ fibrillisation and inflammation by depositing as insoluble fibrin [490-491, 654]. As well as the influx of potentially neurotoxic peripheral molecules into the CNS, it has been suggested that there is a bidirectional movement of proteins across the dysfunctional BBB [655]. It must be noted that even under normal physiological conditions, substances are still able to cross the vascular BBB, and blood-CSF barrier, into the blood circulation by a variety of mechanisms [655]. Therefore, plasma could be a rich source of brain-derived proteins (BDP) that have the potential for being biomarkers of CNS injury related to neurodegeneration and/or BBB integrity.

There has been some effort to target hypothesised BDPs in the plasma as alternative non-invasive assessment of BBB dysfunction. Currently, the gold standard measurement for BBB damage is the calculation of the CSF/plasma albumin ratio (Qalb) and this has been widely reported to be increased in AD (reviewed in [350]). S100B has been the leading candidate of BBB integrity in the periphery [519, 525]. S100B is primary synthesised in the brain by the end feet process of the astrocytes and is quickly released from the brain into the blood when the BBB is disrupted [656]. However, we describe no detection of S100B in the AIBL-2/KARVIAH cohorts despite its identification in the method development phase. This may be attributed to AIBL-2/KARVIAH being a predominantly cognitively normal cohort and therefore minimal BBB dysfunction has occurred. In support of this, Qalb has been shown to be unchanged in preclinical and prodromal AD as well as having no relation to Aβ SUVR [657]. We were able to measure other candidates of BBB integrity (GFAP and

ENO2) which are also seen to be markers of astroglial and neuronal injury respectively. We found no difference in detectable GFAP between Aβ- and Aβ+ individuals, which is in line with more recent evidence [536]. However, a significant increase of γ-Enolase (ENO2, also known as NSE) with increased Aβ and this in parallel with increased plasma ENO2 being increased with BBB dysfunction [541], MCI [357] and other neurodegenerative disorders [658]. However, this finding needs to be taken with caution; 1) the participant numbers with measured ENO2 in this study were sparse (n = 30) and 2) ENO2 is sensitive to the effects of haemolysis and storage conditions [659].

We utilised the Human Protein Atlas (HPA) as a guide to generate a list of protein groups highly expressed in the CNS and hypothesised these to be primarily brain-derived. Cross referencing with our plasma data we generated evidence of 157 "BDP" protein groups circulating in plasma (Chapter 4) and here we replicate the peripheral expression of 120 protein groups, and due to increased sample size a further 52 BDP groups were identified in the AIBL-2 and KARVIAH cohorts. However, peripheral expressions of these protein groups were inconsistently measured in these cohorts. It was observed that only 14/172 were present in >50% of the data (Table 5-20 and Table 5-21) and these included axonal neuronal, astrocytic, and synaptic protein groups, of which, NEFL and NEUROG2 were found be associated with increased Aβ SUVR. The inconsistent measurement of BDP in this plasma dataset is not surprising given their likely low concentration levels being at the limits of detection for this MS methodology Furthermore, the inclusion of only a small number of MCI/AD subjects infers a small number individuals with active BBB impairment. Nonetheless, we have consistently identified the existence of a number of suspected BDPs, within plasma, across two independent studies and three distinct cohorts.

BDPs that fell below the 50% cut-off for the inclusion into statistical analysis pipeline were analysed separately for their association with Aβ. Postsynaptic density protein 95 (DLG4) was the protein group most significant this analyse. DLG4 (also known as PSD-95) is a post-synaptic protein, which plays an important role in synaptic plasticity and synaptic changes during long-term potentiation [660]. We observe a decreased level of DLG4, which is in keeping with CSF studies in

prodromal AD [661]. β-synuclein (SNCB) was also found to be significantly decreased in the Aβ+ group (Figure 5-18). As described in Chapter 4, SNCB is found predominately in the pre-synaptic terminal and highly homologous to α-synuclein. SNCB is thought to inhibit SNCA aggregation and therefore may protect the CNS from the toxic effects of SNCA. It is also interesting to find Down syndrome cell adhesion molecule protein (DSCAM) associated with NAB. Although no previous association made with AD or Aβ, DSCAM is associated with patients that develop Down's syndrome (DS). Individuals with DS have an extremely high incidence of early-onset dementia with an age dependant accumulation of Aβ. Another protein group found to be associated with Aβ is myelin basic protein (MBP). MBP has been hypothesised as a marker of axonal injury [359] and has been shown to co-localise with Aβ plaques in the AD brain [662-663]. MBP has been detected in the CSF and plasma [565] however these levels have yet to be associated with disease.

The detection of suspected BDP groups in plasma is encouraging and we propose that selected BDPs should be further investigated, even if not to be associated with Aβ in this current study. Protein groups which have an origin at or in neurones, axons, dendrites or synapses should be investigated as a priority (Table 5-28). There will be two significant challenges in investigating these BDP in more detail. Firstly, it is clear that the methodology applied here it not sensitive enough to measure BDP consistently in all subjects, although it is was successful in uncovering plasma expression of BDPs. A more targeted approach should be employed for the consistent measurement of these protein groups. Targeted MS-SRM derived from the peptide data generated here would be possible and the opportunity to identify multiple targets simultaneously is a major advantage. However, MS-SRM is largely dependent on the quality and number of peptides previously identified. An approach that is more likely to be successfully would be a custom ultra-sensitive single molecule digital array, such as SIMOA or Singulex, although the quality of this assay would be determine on paired antibodies available for a given target. Secondly, evidence presented in Table 4-9, Table 5-20 and Table 5-21 clearly demonstrate a number of BDPs have evidence for peripheral tissue expression, despite being minimal in most cases. Therefore, it is critical to elucidate the origin of the peripheral signal and to determine if it is truly brain-derived. Lastly, the sample cohort used to measure BDPs is likely to be a confounding factor. The stage of

dementia, age, *APOE* genotype, BBB integrity, TBI, vascular disease and autoimmune diseases are all likely influence the level of BDP in the periphery.

Table 5-28: Examples of BDP detected in plasma in this study that should be further investigated as blood-biomarkers for neurodegeneration and CNS injury.

Protein Name	Gene Name	Process or structure that could be affected in disease	Peripheral Tissue Expression (HPA)
Beta-Synuclein	*SCNB*	Synapse	No
Chromosome 4 open reading frame 50	*C4orf50*	Unknown	No
Growth Associated Protein 43	*GAP43*	Synapse	Yes
Kinesin-like protein 1A	*KIF1A*	Axon	No
Microtubule-associated protein 2	*MAP2*	Dendrite	No
Mylein Basic Protein	*MBP*	Axon	Yes
Neurone Specific Enolase	*ENO2*	Neuron	Yes
Oligodendrocyte-myelin glycoprotein	*OMG*	Axon	No
Oligodendrocytic Myelin Paranodal And Inner Loop Protein	*OPALIN*	Axon	No
Postsynaptic density protein 95	*DLG4*	Synapse	Yes
Proteolipid Protein 1	*PLP1*	Axon	Yes
Spectrin Breakdown Products	*n/a*	Neuron	No
Synapsin I	*SYN1*	Synapse	Yes
Synaptosome Associated Protein 25	*SNAP-25*	Synapse	Yes
Synaptotagmin 1	*SYT1*	Synapse	No
Syntaxin 1A	*STX1A*	Synapse	No
Tropomodulin 2 (neuronal)	*TMOD2*	Neuron	No
Ubiquitin C-Terminal Hydrolase L1	*UCHL1*	Neuron	Yes

5.5.8 Conclusion

Plasma proteins associating with brain Aβ burden have previously been shown to have the potential to act as biomarkers of early AD related pathology. However, attempts in profiling plasma for AD endophenotypes related species have been limited to pathway driven immunoassays and gel-based proteomics, which lack statistical power and proteome coverage. Using an unbiased LC-MS/MS profiling technique, this investigation identifies biomarker signatures, in plasma, that differ between individuals with and without neuropathological hallmarks of AD. At the single analyte level we identified numerous candidate biomarkers, which continued

to point towards activation of the coagulation system in relation to AD and Aβ burden. AD related proteins such as Amyloid beta A4 protein, Neurofilament light and RE1-silencing transcription factor were also readily quantified and found to be statistically related to Aβ SUVR. Furthermore, a large number of novel putative markers were correlated with Aβ pathology in cognitively normal individuals as well as the identification of protein groups proposed to be exclusively brain-derived that warrant further investigation.

Using a variable reduction analysis and support vector machine learning analysis, a twenty-plasma protein classifier was built and was able to predict Aβ positive individuals with a high accuracy (86.6%) in an independent cohort that consisted of cognitively normal individuals. This panel most likely needs to be refined, simplified and certainly validated in independent cohort by independent laboratories. Furthermore, efforts need to be made to successfully translate this panel to a simplified assay suitable for population screening. At the very least, the prediction of Aβ by these biomarkers in healthy elderly individuals, nearing comparable levels of core CSF measures, offers potential in preclinical stratification for clinical trials and early intervention targets worthy of further investigation.

Statement of collaborative work

Dr. Alejo Nevado-Holgado (Oxford University) edited the code for PRQ-2. Dr. Nevado-Holgado also developed the final multivariate classifier for Aβ prediction demonstrated here. I am again grateful to Dr. Malcolm Ward, Steve Lynham and the Centre of Excellence for Mass Spectrometry at King's College London for access to instrumentation. Lastly, I am grateful to Professor Ralph Martins for the access to the AIBL-2 and KARVIAH cohorts as well as the opportunity to conduct a proportion of this work in his laboratory at Edith Cowan University, Western Australia.

CHAPTER 6

DISCUSSIONS AND CONCLUSIONS

6.1 Overall summary

Recently, research has shown that it is possible to detect a peripheral signal of AD or AD related pathology. Whilst it remains unclear if these signals are causative factors, a direct reflection of AD pathology or secondary factors in response to CNS changes, it is now apparent that plasma is a valuable source of potential biomarkers of the disease. The majority of research has focused upon the predictability of differentially expressed proteins to classify diagnostic groups. These studies have highlighted candidate biomarkers and pathways that have high sensitivity and specificity; however these approaches have inherent limitations. The clinical heterogeneity in AD and active neuropathology in "healthy controls" is overlooked with these approaches. It is therefore possible that a "case versus control" design may reflect secondary changes derived from cohort specific variables, with limited involvement in the primary disease. A recent adjustment in the approach for plasma biomarkers has seen the use of established surrogate markers of AD as the primary outcome measurement. This includes stratification of studies based upon *APOE* genotype, cognitive decline, brain atrophy and more recently neocortical Aβ burden (NAB).

The primary aim of this work was to discover and validate plasma biomarkers of *in vivo* NAB, as a preclinical and/or prodromal surrogate risk for developing clinical AD. Recent evidence from anti-Aβ therapeutic trials suggest that intervention at only the earliest stages will be beneficial for those at risk. Phase III trials targeting Aβ reported that approximately 20% of trial participants actually had little or no Aβ when studied retrospectively and this is likely to increase substantially in studies involving only cognitively normal individuals. Therefore, biomarkers that can accurately identify suitable participants for such trials and track pathological progression would be of critical value. The considerable progress in the development of Aβ PET tracers and the standardisation of CSF sampling in evaluating *in vivo*

NAB has seen their routine implementation within research, therapeutic and clinical settings. However, a blood-based biomarker that is cost-effective and more broadly available than these techniques would be more practical and of use to the wider research community. Prior to this work only a small number of studies had investigated a blood-based signature for NAB [373, 437, 552]. These initial studies were restricted to predefined assay panels or 2DGE, a lengthy technique limited to identifying only a small number of candidates in limited sample sets. This thesis aimed to expand upon these two proteomic approaches; firstly, an unbiased 1DGE proteomic screen examined 78 subjects with either high or low Aβ pathology with surrogate measurements by ^{11}C-PiB (Chapter 3). Despite this preliminary study being the largest MS proteomic screen of Aβ related blood-biomarkers to date, with replicated candidates being discovered, it became apparent that limitations existed. Therefore, a methodical review aimed to investigate the weaknesses of this study and to identify suitable improvements while maintaining its strengths. A refined unbiased proteomic methodology which incorporated immunodepletion, TMT10plex peptide labelling and high-resolution peptide separation (rather than protein) demonstrated significantly improved number of quantifiable targets and increase plasma concentration detection (Chapter 4). It was also apparent that this methodology had the sensitivity to detect hypothesised brain-derived proteins and proteins with known involvement in neurodegenerative pathogenesis centrally, typically at the pg/mL concentration level. Following this huge methodological improvement, a secondary discovery and replication phase was performed on two independent cohorts with the focus on Aβ pathology in more cognitively normal cohorts (Chapter 5).

This project has thus used two discovery proteomic strategies for the identification of biologically relevant plasma biomarkers of Aβ. Being similar in strategy and the considerable overlap of analytes being measured between the two techniques, they could each provide a form of replication. However, inherent differences would render them complementary. The first discovery phase (Chapter 3) primarily focused on the classical plasma proteome (>1µg/mL) and fractionation was based at the protein level. This ensured that potential protein modifications and fragments observed by differing MW on a 1DGE could be measured as separate entities. The second discovery phase (Chapter 5) was a more comprehensive screen, not only covering the "classical plasma proteome" but inclusive of the much desired "tissue

leakage" level (pg/mL – ng/mL) as described by Anderson and colleagues [501]. Furthermore, the use of peptide fractionation and peptide labelling in this technique ensured that individual protein coverage was considerably higher and expression was considered to be a global view and not from a fragment or MW specific entity.

The first discovery phase (Chapter 3) highlighted a number of protein targets which were able to distinguish (uncorrected *P* value <0.05) between extreme high and low Aβ pathology, with the complement and coagulation pathways being a prominent feature. An MS 1DGE workflow is a discovery methodological tool and currently would not be suitable for a clinical setting. Therefore, an assay-based approach more applicable to a clinical setting was utilised as a replication tool. To minimise the loss of putative candidates due to cohort differences and to remove false positives, we performed a "technical replication" where the same LC-MS/MS subjects were re-analysed using an ELISA method. Three proteins technically replicated the findings from the LC-MS/MS discovery (FGγ, α2m and FHR-1). The large number of protein groups that did not pass technical replication highlights the importance to recognise the intrinsic differences between MS and antibody approaches in biomarker research. Most importantly, it is feasible that the LC-MS/MS peptides used for protein identification and quantification does not match the epitope measured by immunoassay. Next, the confounding influence of heterophilic antibodies generating false or elevated signal within immunoassays was not investigated in this study and lastly, spike/recovery tests need to determine the accuracy of commercial immunoassays. Furthermore, immunoassays cannot always distinguish modified or truncated forms of a same protein as seen by our MS 1DGE approach.

Only FGγ remained significantly related to Aβ in two independent cohorts; firstly, in the UCSF cohort (subject stratification by ^{11}C-PiB) and also in the EMIF-AD cohort where patients were stratified according to CSF $A\beta_{1-42}$ measures. This was the first blood-based study that utilised core CSF biomarkers as an endophenotype stratification. Further to this, a model with defined concentration cut-offs for FGγ was proposed. The model, which included only FGγ ng/mL and age, had a sensitivity 59%, specificity 78% for neocortical Aβ positivity, when initially tested. However, the same model, with exact concentration FGγ ng/mL cut-offs, was used to predict Aβ positivity in EMIF-AD with disappointing findings (sensitivity 44%, specificity

59%). Interestingly, the performance of the classifier seemed to improve in asymptomatic individuals (sensitivity 50%, specificity 61%). Further still, if the EMIF-AD cohort was adjusted to be more representative of elevated NAB found in the normal ageing population, reported by recent Aβ therapeutic trials (A4 and EPAD), a reasonable negative predictive value (NPV) of 74% was observed. The small positive predictive value (PPV = 32%) indicates that many of the positive results from an FGγ test are possibly false positives. It would be essential to follow up any positive result with a more reliable test (PET/CSF biomarkers) to obtain a more accurate assessment of Aβ. The strength in this FGγ blood test seems to rest in the superior performance of specificity and NPV suggesting that an FGγ blood test would be more useful in rejecting participants for Aβ therapeutic trials rather than selection.

The second discovery phase (Chapter 5) again highlighted a number of single analyte targets for the prediction of *in vivo* Aβ. Firstly, a number of plasma proteins demonstrated an association with Aβ in the presence of cognitively impaired individuals whereas subsets of proteins were exclusively or more significantly associated with asymptomatic subjects with elevated Aβ. Many protein groups displayed opposite direction of coefficients to those described in the first discovery phase. It is common to find conflicting relationships reported in blood-biomarker studies and this highlights the complexity of the relationship of these proteins may have with disease and the peripheral ageing processes. It is important to determine exactly which form of the protein is being measured and also to consider disease status used as the primary outcome measure as well as pre-analytical cohort differences. Despite these discrepancies, apoA1 and ITIH4 were protein groups found to be commonly associated with Aβ between the two LC-MS/MS studies. LC-MS/MS analysis in the AIBL-2 and KARVIAH cohorts continued to support the significant involvement of the coagulation and complement pathways with NAB as well as verification of brain-derived proteins circulating in plasma. The variable measurement of these brain-derived proteins across a large cohort meant that a reliable association with Aβ could not be concluded. Instead, this dataset is a valuable reference source of potential CNS related biomarkers that are detectable in blood and therefore hypothesis-driven investigation using targeted assays should be conducted to investigate the meaning of their peripheral expression.

The prominent finding in Chapter 5 was the independent replication of a multi-protein panel for NAB. Given the complexity of AD and AD-related pathology, it is likely a multi-analyte panel would be more accurate in addressing the heterogeneity of the disease. However, a trade-off between number of analytes to explain disease complexity and a reduced panel for biomarker simplicity would need to be negotiated. As with Chapter 3, we aimed to build the simplest model to predict Aβ pathology. In the AIBL-2 cohort, an SVM learning technique performed multivariate classification to train a predictive model. In addition to this, LASSO was used to remove correlating variables, while retaining the most significant protein group to represent certain clusters. The trained twenty-plasma protein model was then tested in the KARVAIH cohort achieving an accuracy of 81%, increasing to 86.6% using just the first 14 features. The most encouraging aspect of this discovery panel was the ability to predict elevated Aβ in purely asymptomatic individuals. If one was to train the predictive panel in only the asymptomatic individuals from AIBL-2 not only an anticipated reduction in variables but a potential increase in predictive accuracy when tested in the KARVIAH cohort. As previously discussed, certain considerations need to be addressed with this panel. Firstly, analytical variability was considerably reduced in this study with two cohorts being simultaneously measured and therefore future replication is unlikely to gain the same level of accuracy. Secondly, this panel would need to be translated to a more applicable platform for more general research and clinical use. As this has been previously shown to be troublesome, more effort and attention in tailoring assay panels based upon the epitopes and peptide data recognised by the LC-MS/MS discoveries would yield greater success. At the very least, the presence of this putative panel of biomarkers in the asymptomatic group indicates that there is potential in blood-based screening at preclinical stage of AD and highlights early intervention targets and pathways worthy of further investigation.

6.1.1 FGγ as peripheral marker for AD pathology

Unbiased LC-MS/MS has highlighted a number of coagulation factors in both discovery studies. The initial discovery highlighted FGγ, FGβ, FGα, plasminogen and prothrombin all to be nominally associated with elevated Aβ. In the second discovery phase coagulation related protein groups included kallikrein, factor XIII

and factor X. Prothrombin and HABP2 were statistically related to Aβ SUVR and were included in the multi-analyte model for Aβ prediction. Although the replication of a single analyte was not possible between these two LC-MS/MS studies the significant involvement of coagulation and fibrinolysis is evident.

The relationship between decreased plasma FGγ and Aβ surrogate markers was extensively replicated by immunoassay. FGγ and its relationship to AD related phenotypes is not a novel finding [373, 417, 436, 664] with Kiddle and colleagues [552] reporting it to be among an elite list of plasma candidates consistently related to AD. Further to this, a systematic review demonstrated that plasma FGγ was most likely to be specific to AD [665]. Given this evidence, more recent studies [375] and our data that demonstrates the unbiased discovery and replication in a further three independent cohorts, we believe that FGγ is the most replicated putative blood-biomarker for AD related phenotypes.

However, even within our own laboratory, FGγ is not always found to be related to AD phenotypes. The second discovery phase (Chapter 5) did not find FGγ or any fibrinogen chains related to Aβ and this could well be attributed to methodological differences between the two studies. Further to this, the incorporated immunodepletion strategy demonstrated that a small percentage of FGγ peptides are removed from plasma in the "albuminome" (Table 4-5). Encouragingly, the serine protease (prothrombin or thrombin (*F2*)) that converts fibrinogen to fibrin was found to be highly associated with Aβ. Furthermore, a recent targeted approach failed to find any association of plasma FGγ with Aβ as measured by F^{18} flutemetamol (Baird AL et al., in review). This inconsistency is likely to be confounded by the cross sectional examination of different disease stages studied in these investigations and also the differing methods of sample collection and storage. However, the relationship of cardiovascular risk and AD should also be considered. Elevated levels of fibrinogen and other coagulation factors have been related to a number of cardiovascular diseases which are secondary risk factors for AD [666-669] and also normal ageing (reviewed in [670]), whereas our data indicates a decreased level in association of NAB. Indeed, there have been a few reports of whole fibrinogen levels being increased with cognitive decline [404, 483]. These contradictory findings may point towards specific cleavage products for fibrinogen having a bidirectional

association with AD and Aβ. Yet, our data demonstrates that all coagulation factors measured, regardless of significance, have a negative coefficient with NAB. The role of cardiovascular risk will inevitably have a large influence on coagulation factor levels which was not accounted for in these studies. This could be partially responsible for the low sensitivity and specificity in FGγ in predicting Aβ. It would therefore be advised to assess plasma FGγ with AD phenotypes taking into account cardiovascular risk factors.

The direct relationship of fibrinogen and Aβ in the CNS and *in vitro* studies would still support the notion that our peripheral signal, in part, could be a reflection of NAB. However, evidence from the literature would deem this relationship to be fully dependable on a dysfunctional blood-brain barrier. It is widely reported that fibrinogen is an exclusive plasma protein that is excluded from the CNS by the BBB; however, there is a rapid movement of fibrinogen across a dysfunctional BBB which is converted by thrombin and in-turn deposited as insoluble Fibrin in the CNS [484, 671]. This deposition of fibrin has been shown to have a spatial relationship with Aβ, with many studies demonstrating co-deposition in the AD brain [484-486, 654, 672]. Fibrinogen also binds strongly to Aβ *in vitro* and increases fibrinogen aggregation and Aβ fibrillisation [484, 486]. It is evident that Aβ accumulation in the CNS can be both a cause and consequence of BBB dysfunction. The deposition of Aβ in the vessel walls of arteries, arterioles and capillaries from the toxic presence and incomplete clearance of Aβ can lead to blood vessel weakening and BBB impairment (reviewed in [673]). Furthermore, neurotoxicity, activated microglia and perivascular astrocytic damage induced by Aβ accumulation are all reported to cause injury to the BBB [653]. Therefore, a case can be made for a disruption of BBB initiated by NAB causing the extravasation of fibrinogen into the CNS that induces further Aβ deposition and neuronal damage. Nonetheless, various mechanisms for BBB dysfunction have been reported (reviewed in [654]) and therefore the influx of fibrinogen into the CNS can be induced by a number of mechanisms in response to a number of neurological conditions and events. Studies reporting measures of FGγ in the CSF have been limited. Acute neuroinflammatory conditions have reported elevated fibrinogen in the CSF but no change between chronic conditions (e.g. Multiple Sclerosis) and healthy controls [674]. Interestingly, a splicing variant of FGγ (FGγ A precursor) has

been previously reported as elevated in the CSF of AD and MCI subjects [492]. This could almost point to the breakdown of the blood-CSF barrier as well as the BBB.

It is evident that the movement of fibrinogen can only happen in response to an event that alters the BBB and that it could be concluded that our observed reduction of FGγ could be in response to BBB abnormality. BBB studies in AD have led to conclude that a subset, but not all AD patients, have disruptions of the BBB and for that reason plasma FGγ may not be specific for AD. However, it is also clear that once inside the CNS fibrinogen has a considerable amount of interaction with AD pathology and exacerbates its development. We hypothesise that the decrease of plasma FGγ is initially an early marker in response to BBB permeability (Figure 6-1). Furthermore, if substantial neocortical Aβ pathology is present within the CNS, a decrease in plasma FGγ would be more dramatic (Figure 6-1). The FGγ concentration cut-offs we presented (<944ng/mL) would only be applicable for these cohorts and that longitudinal baseline assessment of FGγ should be made on an individual basis due to various confounding influences. A sustained deviation away from the baseline may indicate BBB dysfunction and potentially elevated NAB.

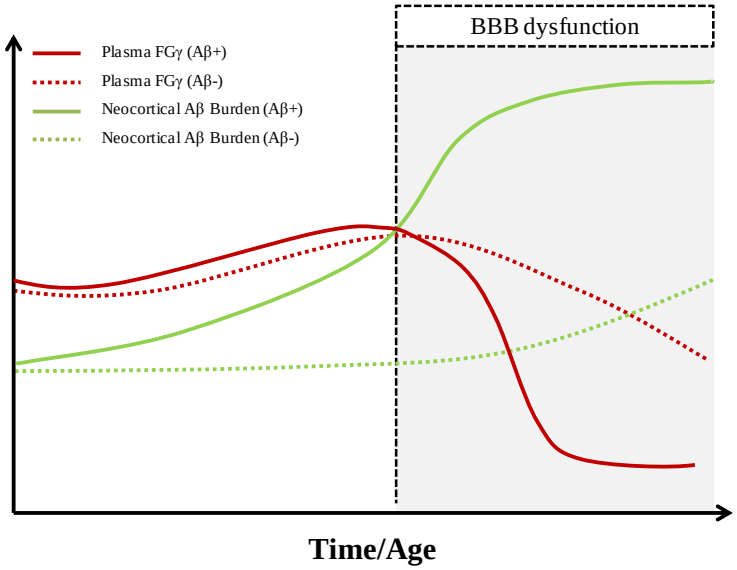

Figure 6-1: Hypothetical curve of plasma FGγ in response to BBB damage with Aβ+ and Aβ- individuals. The hypothesis presented assumes BBB dysfunction. Over time an expected increase in plasma FGγ due to age-related cardiovascular involvement. This trajectory is likely to continue if no BBB impairment is apparent. In response to an event that causes BBB dysfunction we would expect an immediate decrease in plasma FGγ. In Aβ+ individuals the influx of fibrinogen (FGγ) would interact and exacerbate the already increasing levels of neocortical Aβ observed in typical AD development, this would reflect in a more dramatic decrease in levels of plasma FGγ (red solid line). In Aβ- individuals an anticipated reduction in plasma FGγ may still be expected in response to BBB dysfunction however, with less NAB in the CNS the decrease in plasma FGγ would be less dramatic (red dashed line).

6.1.2 Multi-analyte marker of Aβ pathology

It is unlikely that a single marker alone will be able to explain heterogeneity demonstrated in AD in response to elevated Aβ. As previously discussed, a single marker, such as FGγ, has the potential to be confounded by a number of factors. A multivariate signature approach has been taken by many research groups and two studies have reported a multivariate model for Aβ prediction [436-437]. Here, we have presented a prediction model which seems to outperform these previously described models, although the studies cannot be directly compared. It is likely that the differences in platforms used between these studies will account for the differences in proteins included for prediction models. However, plasma Aβ was a common a feature. Burnham and Kiddle both utilised immunoassays to specifically target $A\beta_{1-42}$

in plasma and although it cannot be determined, our MS/MS data suggests peptides that are located within the region of toxic Aβ fragments are associated with NAB. This supports the concept of many in the biomarker field that the levels of plasma Aβ alone are not themselves diagnostic but has a role to play as part of a multi-analyte panel.

Using unbiased MS, this panel converges plasma proteins of varying abundances, differing mechanisms and novel or previously reported putative candidates for AD. As mentioned before, *APP* processing and the coagulation cascade are represented in this panel. Further to this, inflammation and complement proteins, transcription factors and GPCR's are deemed to be important in Aβ prediction. There is also the inclusion of CNS protein groups, NEFL and NEUROG2, the former being widely reported as a marker for axonal injury in a number of diseases. The broad diversity of this panel would have a greater opportunity to explain the variability in AD and its pathology. Although this panel has been described for elevation of NAB and tested in cognitively normal individuals, the cohorts utilised in this study are enriched for future AD risk and therefore this panel may well be more specific for Aβ in relation to AD. This would be of great use in therapeutic trials that continue to target Aβ in relation to AD. As further replication in similar cohorts would be necessary, the performance of this panel in suspected non-Aβ pathology (SNAP) AD subjects and other dementias of elevated Aβ would be valuable to determine the biomarker specificity for AD.

An ideal biomarker for AD has been previously described as being able to; detect a fundamental pathological feature, be validated in neuropathologically confirmed cases, have a sensitivity and specificity >80%, be reliable, reproducible, non-invasive, simple to perform and inexpensive [675]. While at the early stages, the biomarker panel presented in Chapter 5 would follow this outlined criterion. In reality, the further replication in differing cohorts of this biomarker panel would most likely reduce in accuracy for a number of factors (preanalytical, platform and cohort differences). A blood-based signature for AD and AD pathology is not expected to outperform or replace CSF or neuroimaging biomarkers but act as the first-step in a multi-stage diagnosis which will inevitably include further

confirmation by these modalities. However, higher accuracy at the initial stage is critical in reducing costs, recruit time and false positives for a clinical trial setting.

APOE status is a substantial risk factor for AD and Aβ accumulation. The association of several plasma proteins with NAB was shown to be partly confounded by the number of *APOE* ε4 individuals included in this study. However, at the univariate level plasma proteins included in this panel were found to be still highly associated with Aβ when accounting for *APOE* status. We conclude that the addition of *APOE* genotype in our model is unlikely to improve prediction accuracy however other genetic risk factors have not yet been explored. Although it was chosen for *APOE* not to be statistically corrected for, age and gender were included in a GLM adjustment. In a clinical setting, it is highly likely that these variables, particularly age, will have an effect on a number if not all protein levels included in this model. Although not possible in this study, further investigations should determine concentration cut-off for these significant proteins with age and gender related boundaries.

6.2 Ethical implications for preclinical testing of AD

Conducting preclinical AD trials presents a variety of novel ethical and policy challenges. An issue that is particularly relevant for this study would be revealing biomarker status (particularly healthy individuals) to participant's active in research studies. The suitable use of this information is much debated and while disease modifying treatments for AD currently do not exist a screening tool appears to have limited benefits to currently affected individuals. Therefore, many would argue that preclinical testing should remain within research protocols and the results should not be shared with subjects until suitable intervention become known.

From an ethical position, the knowledge of one's biological status could induce considerable stress, which could significantly affect the individual's well-being [676]. This will also have implications for the research or clinical study they are actively participating in. Using genetic biomarkers as an example, the REVEAL study has demonstrated that the knowledge of *APOE* status did not have a significant increase in anxiety compared with those who did not learn their *APOE* status [677]. However, those who were informed of being carriers of *APOE* ε4 demonstrated higher levels of distress over a one-year period [677]. The impact of knowing and the constant reminder of one's genetic risk or biomarker status for AD over a longer period would need to be studied and elucidated further. There was also a clear link that individuals who demonstrated emotional stress prior to enrolment were more likely to have difficulties after disclosure of biomarker status [677]. This finding points towards a cognitive pre-assessment and biomarker status being given on an individual basis.

In contrast to these standpoints, the REVEAL study also demonstrated that *APOE* ε4 aware individuals made efforts to introduce risk reducing interventions into their daily lives with significant benefits [678]. A further argument for the transparency in biomarker disclosure is that it would better replicate the actual clinical practice for future drug prescription for at risk individuals [676]. Currently, the A4 and API intervention trials have or intend to disclose biomarker status prior to trial participant inclusion [677, 679]. A European-wide study presented a positive public response to preclinical AD testing, demonstrating 2/3 people would receive a medical test if it would reveal if they would develop AD at later stage (http://www.alzheimer-

europe.org/Research/Value-of-Knowing). However, in contrast to this, reports from the DIAN study for those at risk for familial AD often do not want to learn the results from genetic testing [680]. Preclinical screening can help relieve uncertainty in individuals who have ageing concerns, particularly those with suspected inherited risks for AD. For some individuals the stress of uncertainty may be more considerable than the stress of knowing. Furthermore, an early diagnosis of definite AD (if made possible) will help individuals to implement future plans, whether this is obtaining relevant care packages and altering educational/career or family plans.

While it is clear that identifying individuals in the preclinical/prodromal stage of the disease will drastically aid AD research and clinical trials, it is imperative to carefully consider the individuals involved in these studies. Informed consent should always be obtained with appropriate support, counselling and advice being available not only throughout the studying but also after its conclusion. Currently, there are no guidelines for the disclosure of biomarkers status in such studies however recent recommendations [676] point towards the study type dictating the acceptable approach. Observational research studies should avoid disclosure as it is likely to impact on the cognitive performance on the participant having an impact on future research developments. Disclosure should be considered in intervention studies to protect biomarker negative subjects from preventable risks and stress, although the examined population will be a major factor in this decision (i.e. autosomal dominant AD).

6.3 Future Studies

Despite the first studies searching for putative plasma markers for AD occurring over 10 years ago, blood-based biomarkers that reflect dementia and its pathology is still an emerging field. As technology and longitudinal ageing cohorts continue to develop, large scale discovery and candidate replication studies will need to be repeated. The results from these studies have provided more evidence in a growing body of literature. This includes the conformation of previously identified single markers, offering novel candidates and novel classifiers. More work is clearly needed and suggestions for future studies are outlined below.

6.3.1 Independent verification of LC-MS/MS classifier

The most promising result from this body of work was the high accuracy of predicting NAB using a multi-analyte panel in a cognitively normal cohort. As previously discussed there are various aspects to consider in the replication of this classifier. Firstly, the reduced analytical variance has likely contributed to increased accuracy and secondly, it could be argued that this panel would to need to be converted to a more accessible platform to increase participant numbers and determine individual protein concentration cut-offs. If the analytical platform is altered then a technical replication in the AIBL-2 and KARVIAH participants would be required to ensure that the classifier is still performing to a high accuracy. If this was to be successful, the validation in independent cohorts and preferably by independent users would be essential. Independent cohorts that actively utilise Aβ biomarkers (imaging or CSF) in cognitively normal individuals are limited, however the Baltimore Longitudinal Study of Ageing (BLSA, www.blsa.nih.gov), the Swedish BIOFINDER (www.biofinder.se) and European Medical Informatics Framework (www.emif.eu) are well characterised cohorts where this classifier could be rigorously tested.

It is recommended that a proposed classifier should be tested in its exact form to produce an unbiased assessment of its performance and therefore careful considerations of this classifier should be made before the attempt of validation. Firstly, the training of the classifier was performed in a mixed diagnosis cohort (AIBL-2) and therefore re-analysis using only cognitively healthy subjects, suitable

to the validation cohorts mentioned above, may foster opportunity for greater validation. Secondly, a total of 14 candidates were used to gain 86.6% accuracy in NAB prediction. It would be anticipated that the reduction in classifier size, at the cost of a small decrease in accuracy, may also have a greater chance of validation.

6.3.2 Longitudinal assessment of plasma protein classifier(s)

Both models proposed in this work come from cross-sectional investigations and this has utility for participant entry for clinical trials. However, there is also a need for a plasma biomarker that can track AD pathology over longer periods or in response to a clinical or therapeutic intervention. This has been assessed at the single analyte level [375, 430] but a panel of multiple markers, each reflecting different mechanisms, is likely to be better at tracking the disease course.

The AIBL study is a longitudinal cohort and since the initial baseline measures were obtained in 2009, seven years worth of imaging, clinical and cognitive assessments have been collected. The global assessment of the plasma proteome in AIBL-1 and AIBL-2 subjects also offers the opportunity to use baseline protein measures to predict future conversion. This may be based upon a change in Aβ status or a change in clinical classification determined by longitudinal assessment

The model proposing plasma FGγ and age as a predictor for Aβ demonstrated a modest level of accuracy in its replication and its limitation has been previously discussed. However, given the simplicity of the model and a successful conversion to an assay based platform it would be easy to implement it in a longitudinal study and test the proposed hypothesis (Figure 6-1). Recently, substantial evidence has accumulated that fibrinogen moves across a dysfunctional BBB and co-deposits (as Fibrin) with various pathologies, including Aβ, and inflicts a CNS autoimmune response. We propose to utilise the MRC London Neurodegenerative Disease Brain Bank which has collected longitudinal plasma samples and with corresponding *post mortem* tissue. We aim to measure the trajectory of plasma FGγ (and other coagulation factors) up to the time of death and blindly predict Aβ status (determined by Braak staging) using our FGγ test. Furthermore, we will correlate the final plasma

FGγ measure with neocortical Aβ/FGγ and utilise immunohistochemistry to determine the location FGγ deposition in relation to Aβ plaques.

6.3.3 Across neurodegeneration classifier

The accumulation of Aβ is not only associated with AD but also a number of other dementias. Single and multi-analyte putative biomarkers highlighted throughout these studies should be examined in cohorts that include a range of dementias with differing neuropathology. This would determine which biomarkers are specific for Aβ, AD or neurodegeneration as a whole.

6.3.4 Blood-brain barrier models to assess plasma FGγ curve

There are currently a number of animal models that mimic BBB dysfunction [681]. Their advantage is the reduced confounding variables that are found in human disease and also their estimated age of BBB impairment is documented. Therefore, a longitudinal assessment of plasma FGγ before, during and after known BBB dysfunction in these models would help to elucidate the trajectory of plasma FGγ. *Post mortem* analysis would determine if the levels of plasma FGγ correlate with severity of AD pathology.

6.3.5 Cellular models of novel blood-based biomarkers

Pathway analysis and individual proteins indicate a number of mechanisms highlighted in the multi-analyte prediction for Aβ. Efforts should be made to clarify the association of these plasma biomarkers roles in the disease process, or what mechanistic relationship it is to Aβ. The effects of biomarker proteins should be determined on an Aβ pathway activity in cell lines and in primary rodent neuronal cultures.

6.3.6 Interrogation of plasma expression of brain-derived proteins

The finding of a large collection of brain-derived proteins circulating within plasma warrants further investigation. These brain-derived proteins have the potential to be biomarkers not only of NAB or AD but they could be markers for BBB integrity or other neurodegenerative diseases if examined in appropriate cohorts. Firstly,

knowing that their peripheral expression does exist, investigation of expression using sensitive targeted assay is likely to be more successful than LC-MS/MS. Given their low abundance the use of the single molecule array (SiMoA) assays would be the ideal choice of platform. The SiMoA platform has been shown to successfully detect plasma tau at 0.02pg/mL [359]. Secondly, it should be explored if a suspected brain-derived protein has significant protein expression in range of peripheral tissues. Furthermore, an endophenotype approach stratified by CSF/plasma albumin ratio or even plasma FGγ as proposed here could be utilised do determine if these brain-derived protein are a reflection of BBB integrity. Lastly, the recent development of methods for isolation of neuronal-derived exosomes (NDEs) from plasma has allowed quantification of neuronal proteins contained as a part of their cargo [530]. The transport of brain-derived proteins via neuronal exosomes could be an alternative explanation for their expression in plasma other than BBB dysfunction or peripheral tissue expression.

6.3.7 Post translational modification and protein fragments

One of the major advantages of LC-MS/MS over other discovery platforms is the detailed peptide structural data that is generated. Our 1DGE experiments and numerous 2DGE experiments in the field have demonstrated that the same protein groups can be identified at various locations on a gel and this is indicative of multiple forms of the protein (modified and/or cleaved). The extensive LC-MS/MS data generated here offers the opportunity for the assessment of post-translational modification biomarkers in blood. In the same manner as Chapter 5, a discovery in AIBL-2 cohort can conduct global expression or protein specific expression of modifications such as phosphorylation, acetylation and glycosylation. Any observed differences could be assessed in KARVIAH cohort. A specific glycosylated peptide pattern in plasma clusterin has already been associated with AD-related hippocampal atrophy [682].

6.3.8 Cost benefit analysis of a blood-based classifier

It is widely accepted that, at this point, blood-based biomarkers are not viewed as potentially diagnostic but rather as a first in line for a multi-stage diagnostic process. In a clinical trial scenario, blood-based biomarkers are seen to increase access to

potential participants while simultaneously reducing the time burden and cost in screening. While the former is certainly true, the reduction in cost has yet to be proven. Firstly, the cost of a multi-analyte panel(s) is unknown and secondly, the anticipated lower accuracy for a fully validated blood-based biomarker would require substantially larger pool of testable subjects to achieve the desired number of "positive" participants for a clinical trial. Therefore, a side-by-side assessment of blood-based biomarker performance against an actual clinical trial population that was pre-screened by Aβ imaging and/or CSF Aβ would determine if the cost savings for the implementation of a blood-based screen could be worthwhile.

6.4 Limitations

6.4.1 Concentration thresholds

Threshold values for biomarkers must be determined for them to be of use as a diagnostic and/or screening tool. An attempt has been made to apply an ng/mL threshold for Aβ positivity using FGγ in Chapter 3, with modest results. This cut-off was based upon a single cohort and would need to be adjusted after testing multiple cohorts that differed in age, ethnicity and disease state to provide a more accurate estimate. In Chapter 5 proteomic profiling utilised TMT isobaric labelling as discovery and replication tool. This provided only relative quantification of proteins levels, therefore estimation of optimal thresholds could not be computed for the twenty-protein classifier. Using an MS calibrator or successful conversion to a quantifiable platform would be needed to determine concentration cut-offs, as well as boundaries for age and gender differences.

6.4.2 Cross-sectional analysis

All observations in this study have been cross-sectional, in that protein levels are representation at the specific point in time. Cross-sectional analyses are excellent hypothesis generating studies that can include large number of participants because it is not limited by the need for follow-up data, patient drop-outs or variables introduced between time-points. A drawback to cross-sectional analysis is that it cannot be determined, unless well documented, if these relative abundances of individual plasma proteins are stable or sensitive to dynamic change over time. "Short-term" longitudinal analysis would determine how these plasma proteins respond to circadian rhythm and cycles over a few a weeks. This would also help with the determination of concentration cut-offs and obvious outliers that may affect the result. Our multivariate classifier was replicated, with high accuracy, in an independent cohort and therefore we would cautiously conclude that these plasma proteins remain stable. In both cohorts, blood draws were made in the morning after fasting but small variations in other preanalytics did occur.

Longitudinal analysis over multiple time-points throughout a disease course would determine how this classifier performs in relation to disease progression.

6.4.3 Comorbidities and lifestyle risk factors

Ageing, independently of AD, has numerous associated comorbidities and lifestyle risk factors. A number of blood protein levels are likely to be sensitive to these conditions. Although exclusion criteria were implemented into the research cohorts the affect of our candidate protein markers with cardiovascular risk, secondary diseases or diet was not investigated.

6.4.4 Specificity of Aβ PET

Post mortem neuropathology analysis is still considered the most accurate indicator of AD; in this study predominantly *in vivo* Aβ PET was used as a surrogate for early development for AD. As previously discussed measures of NAB are not generally specific for AD and are often described in other dementias and mixed pathology dementias. Although plasma signatures presented here are discovered in AD enriched cohorts, they should be considered only as markers of Aβ deposition potentially useful for multiple disorders.

6.5 Future perspectives on the field

6.5.1 Standardisation

Undoubtedly the greatest challenge for the field of AD blood-biomarkers is the agreement and implementation of preanalytical guidelines that can be universally employed across cohorts and research laboratories. There is a large concern with the lack of reproducibility of findings across independent laboratories and within laboratory settings [683]. Initial guidelines in sample collection, processing and storage have been outlined [440], replicating the actions taken by the Global Biomarker Standardisation Consortium of CSF biomarkers [324, 684]. This step is arguably more critical for blood-based biomarkers and potentially analytical guidelines should be even stricter than those set out for CSF analysis. Blood is a highly complex biological system and there are numerous confounders that influence levels of potential candidate markers. Furthermore, because of its distance to the disease organ, the field of AD blood-based biomarkers (including lipidomics and metabolomics) currently does not have a gold standard biomarker in which standardisation can be extensively examined and referred to.

These initial guidelines are a promising advancement in the AD field. If widely adopted, cohort and inter-laboratory variability can be reduced and the prospect of discovering a reproducible blood-based biomarker for AD and its pathology will be significantly increased.

6.5.2 Endophenotype strategies for blood-based biomarkers for AD risk

The eventual aim for the AD blood-biomarker field would be to have a test that is specific for AD. In this study, we have used Aβ PET and CSF $A\beta_{1-42}$ as surrogates for AD risk and this has potential utility for anti-Aβ trials which mainly target AD subjects. However, it has been discussed how elevated Aβ biomarkers are not necessarily indicative of AD development. The use of MRI imaging also has limitations as an endophenotype design for AD. The emergence of tau PET tracers offers new avenues for blood-based biomarker research and should be explored alone and in combination with Aβ PET; however, lack of disease specificity is again liable to be a confounding factor. The AD genetics field are beginning to look

closely at “polygenic risk scores” [685-686] where joint effects of multiple previously identified genetic variants are weighted to give a single score. Polygenic risk scores have recently been proven to be successful in schizophrenia research [687]. In the same manner, and with the emergence of large longitudinal cohorts that are well characterised, the convergence of various imaging (Aβ, tau, FDG and structural MRI), CSF analysis, genetic risks, epigenetics, psychological assessment, comorbidities and lifestyle risk factors could be used create a single “polybiomarker risk score” for AD. An endophenotype study that is stratified based upon a single score of multiple modalities might not only identify a blood-based biomarker of neocortical pathology but one that is explicit to AD risk.

BIBLIOGRAPHY

1. Katzman R. Editorial: The prevalence and malignancy of Alzheimer disease. A major killer. *Arch Neurol* 1976; **33**(4)**:** 217-218.

2. Prince M, Bryce R, Albanese E, Wimo A, Ribeiro W, Ferri CP. The global prevalence of dementia: a systematic review and metaanalysis. *Alzheimers Dement* 2013; **9**(1)**:** 63-75 e62.

3. Scheltens P, Blennow K, Breteler MM, de Strooper B, Frisoni GB, Salloway S *et al.* Alzheimer's disease. *Lancet* 2016; **388**(10043)**:** 505-517.

4. Delaere P, Duyckaerts C, He Y, Piette F, Hauw JJ. Subtypes and differential laminar distributions of beta A4 deposits in Alzheimer's disease: relationship with the intellectual status of 26 cases. *Acta Neuropathol* 1991; **81**(3)**:** 328-335.

5. O'Brien RJ, Wong PC. Amyloid precursor protein processing and Alzheimer's disease. *Annu Rev Neurosci* 2011; **34:** 185-204.

6. Miller DL, Papayannopoulos IA, Styles J, Bobin SA, Lin YY, Biemann K *et al.* Peptide compositions of the cerebrovascular and senile plaque core amyloid deposits of Alzheimer's disease. *Arch Biochem Biophys* 1993; **301**(1)**:** 41-52.

7. Armstrong RA. The molecular biology of senile plaques and neurofibrillary tangles in Alzheimer's disease. *Folia Neuropathol* 2009; **47**(4)**:** 289-299.

8. Atwood CS, Martins RN, Smith MA, Perry G. Senile plaque composition and posttranslational modification of amyloid-beta peptide and associated proteins. *Peptides* 2002; **23**(7)**:** 1343-1350.

9. Zhang YW, Thompson R, Zhang H, Xu H. APP processing in Alzheimer's disease. *Mol Brain* 2011; **4:** 3.

10. Chow VW, Mattson MP, Wong PC, Gleichmann M. An overview of APP processing enzymes and products. *Neuromolecular Med* 2010; **12**(1)**:** 1-12.

11. Murphy MP, LeVine H, 3rd. Alzheimer's disease and the amyloid-beta peptide. *J Alzheimers Dis* 2010; **19**(1)**:** 311-323.

12. Masters CL, Cappai R, Barnham KJ, Villemagne VL. Molecular mechanisms for Alzheimer's disease: implications for neuroimaging and therapeutics. *J Neurochem* 2006; **97**(6)**:** 1700-1725.

13. Walsh DM, Selkoe DJ. A beta oligomers - a decade of discovery. *J Neurochem* 2007; **101**(5)**:** 1172-1184.

14. Ballard C, Gauthier S, Corbett A, Brayne C, Aarsland D, Jones E. Alzheimer's disease. *Lancet* 2011; **377**(9770)**:** 1019-1031.

15. Eikelenboom P, Zhan SS, van Gool WA, Allsop D. Inflammatory mechanisms in Alzheimer's disease. *Trends Pharmacol Sci* 1994; **15**(12)**:** 447-450.

16. McGeer PL, McGeer EG. The inflammatory response system of brain: implications for therapy of Alzheimer and other neurodegenerative diseases. *Brain Res Brain Res Rev* 1995; **21**(2)**:** 195-218.

17. Oltersdorf T, Fritz LC, Schenk DB, Lieberburg I, Johnson-Wood KL, Beattie EC *et al.* The secreted form of the Alzheimer's amyloid precursor protein with the Kunitz domain is protease nexin-II. *Nature* 1989; **341**(6238)**:** 144-147.

18. Tanzi RE, McClatchey AI, Lamperti ED, Villa-Komaroff L, Gusella JF, Neve RL. Protease inhibitor domain encoded by an amyloid protein precursor mRNA associated with Alzheimer's disease. *Nature* 1988; **331**(6156)**:** 528-530.

19. Ponte P, Gonzalez-DeWhitt P, Schilling J, Miller J, Hsu D, Greenberg B *et al.* A new A4 amyloid mRNA contains a domain homologous to serine proteinase inhibitors. *Nature* 1988; **331**(6156)**:** 525-527.

20. Salameh MA, Robinson JL, Navaneetham D, Sinha D, Madden BJ, Walsh PN *et al.* The amyloid precursor protein/protease nexin 2 Kunitz inhibitor domain is a highly specific substrate of mesotrypsin. *J Biol Chem* 2010; **285**(3)**:** 1939-1949.

21. Hardy JA, Higgins GA. Alzheimer's disease: the amyloid cascade hypothesis. *Science* 1992; **256**(5054)**:** 184-185.

22. Barage SH, Sonawane KD. Amyloid cascade hypothesis: Pathogenesis and therapeutic strategies in Alzheimer's disease. *Neuropeptides* 2015; **52:** 1-18.

23. Mawuenyega KG, Sigurdson W, Ovod V, Munsell L, Kasten T, Morris JC *et al.* Decreased clearance of CNS beta-amyloid in Alzheimer's disease. *Science* 2010; **330**(6012)**:** 1774.

24. Sperling RA, Aisen PS, Beckett LA, Bennett DA, Craft S, Fagan AM *et al.* Toward defining the preclinical stages of Alzheimer's disease: recommendations from the National Institute on Aging-Alzheimer's Association workgroups on diagnostic guidelines for Alzheimer's disease. *Alzheimers Dement* 2011; **7**(3)**:** 280-292.

25. Agostinho P, Cunha RA, Oliveira C. Neuroinflammation, oxidative stress and the pathogenesis of Alzheimer's disease. *Curr Pharm Des* 2010; **16**(25)**:** 2766-2778.

26. Luo Y, Sunderland T, Roth GS, Wolozin B. Physiological levels of beta-amyloid peptide promote PC12 cell proliferation. *Neurosci Lett* 1996; **217**(2-3)**:** 125-128.

27. Moya KL, Benowitz LI, Schneider GE, Allinquant B. The amyloid precursor protein is developmentally regulated and correlated with synaptogenesis. *Dev Biol* 1994; **161**(2)**:** 597-603.

28. Plant LD, Boyle JP, Smith IF, Peers C, Pearson HA. The production of amyloid beta peptide is a critical requirement for the viability of central neurons. *J Neurosci* 2003; **23**(13)**:** 5531-5535.

29. Pearson HA, Peers C. Physiological roles for amyloid beta peptides. *J Physiol* 2006; **575**(Pt 1)**:** 5-10.

30. Mileusnic R, Lancashire CL, Johnston AN, Rose SP. APP is required during an early phase of memory formation. *Eur J Neurosci* 2000; **12**(12)**:** 4487-4495.

31. Atwood CS, Obrenovich ME, Liu T, Chan H, Perry G, Smith MA *et al.* Amyloid-beta: a chameleon walking in two worlds: a review of the trophic and toxic properties of amyloid-beta. *Brain Res Brain Res Rev* 2003; **43**(1)**:** 1-16.

32. Goedert M, Sisodia SS, Price DL. Neurofibrillary tangles and beta-amyloid deposits in Alzheimer's disease. *Curr Opin Neurobiol* 1991; **1**(3)**:** 441-447.

33. Forman MS, Trojanowski JQ, Lee VM. Neurodegenerative diseases: a decade of discoveries paves the way for therapeutic breakthroughs. *Nat Med* 2004; **10**(10)**:** 1055-1063.

34. Dickson DW, Crystal HA, Bevona C, Honer W, Vincent I, Davies P. Correlations of synaptic and pathological markers with cognition of the elderly. *Neurobiol Aging* 1995; **16**(3)**:** 285-298; discussion 298-304.

35. Buee L, Bussiere T, Buee-Scherrer V, Delacourte A, Hof PR. Tau protein isoforms, phosphorylation and role in neurodegenerative disorders. *Brain Res Brain Res Rev* 2000; **33**(1)**:** 95-130.

36. Lee G, Neve RL, Kosik KS. The microtubule binding domain of tau protein. *Neuron* 1989; **2**(6)**:** 1615-1624.

37. Mandelkow EM, Mandelkow E. Biochemistry and cell biology of tau protein in neurofibrillary degeneration. *Cold Spring Harb Perspect Med* 2012; **2**(7)**:** a006247.

38. Iqbal K, Grundke-Iqbal I. Alzheimer neurofibrillary degeneration: significance, etiopathogenesis, therapeutics and prevention. *J Cell Mol Med* 2008; **12**(1)**:** 38-55.

39. Kopke E, Tung YC, Shaikh S, Alonso AC, Iqbal K, Grundke-Iqbal I. Microtubule-associated protein tau. Abnormal phosphorylation of a non-paired helical filament pool in Alzheimer disease. *J Biol Chem* 1993; **268**(32)**:** 24374-24384.

40. Grundke-Iqbal I, Iqbal K, Tung YC, Quinlan M, Wisniewski HM, Binder LI. Abnormal phosphorylation of the microtubule-associated protein tau (tau) in Alzheimer cytoskeletal pathology. *Proc Natl Acad Sci U S A* 1986; **83**(13)**:** 4913-4917.

41. Ittner A, Chua SW, Bertz J, Volkerling A, van der Hoven J, Gladbach A *et al.* Site-specific phosphorylation of tau inhibits amyloid-beta toxicity in Alzheimer's mice. *Science* 2016; **354**(6314)**:** 904-908.

42. Mudher A, Lovestone S. Alzheimer's disease-do tauists and baptists finally shake hands? *Trends Neurosci* 2002; **25**(1)**:** 22-26.

43. Blurton-Jones M, Laferla FM. Pathways by which Abeta facilitates tau pathology. *Curr Alzheimer Res* 2006; **3**(5)**:** 437-448.

44. Mi K, Johnson GV. The role of tau phosphorylation in the pathogenesis of Alzheimer's disease. *Curr Alzheimer Res* 2006; **3**(5)**:** 449-463.

45. Braak H, Braak E, Bohl J. Staging of Alzheimer-related cortical destruction. *Eur Neurol* 1993; **33**(6)**:** 403-408.

46. Nestor PJ, Scheltens P, Hodges JR. Advances in the early detection of Alzheimer's disease. *Nat Med* 2004; **10 Suppl:** S34-41.

47. Braak H, Thal DR, Ghebremedhin E, Del Tredici K. Stages of the pathologic process in Alzheimer disease: age categories from 1 to 100 years. *J Neuropathol Exp Neurol* 2011; **70**(11)**:** 960-969.

48. Ingelsson M, Fukumoto H, Newell KL, Growdon JH, Hedley-Whyte ET, Frosch MP *et al.* Early Abeta accumulation and progressive synaptic loss, gliosis, and tangle formation in AD brain. *Neurology* 2004; **62**(6)**:** 925-931.

49. Frost B, Jacks RL, Diamond MI. Propagation of tau misfolding from the outside to the inside of a cell. *J Biol Chem* 2009; **284**(19)**:** 12845-12852.

50. Pooler AM, Polydoro M, Maury EA, Nicholls SB, Reddy SM, Wegmann S *et al.* Amyloid accelerates tau propagation and toxicity in a model of early Alzheimer's disease. *Acta Neuropathol Commun* 2015; **3:** 14.

51. Lewis J, Dickson DW. Propagation of tau pathology: hypotheses, discoveries, and yet unresolved questions from experimental and human brain studies. *Acta Neuropathol* 2016; **131**(1)**:** 27-48.

52. Chartierharlin MC, Crawford F, Houlden H, Warren A, Hughes D, Fidani L *et al.* Early-Onset Alzheimers-Disease Caused by Mutations at Codon-717 of the Beta-Amyloid Precursor Protein Gene. *Nature* 1991; **353**(6347)**:** 844-846.

53. Murrell J, Farlow M, Ghetti B, Benson MD. A Mutation in the Amyloid Precursor Protein Associated with Hereditary Alzheimers-Disease. *Science* 1991; **254**(5028)**:** 97-99.

54. Citron M, Oltersdorf T, Haass C, Mcconlogue L, Hung AY, Seubert P *et al.* Mutation of the Beta-Amyloid Precursor Protein in Familial Alzheimers-Disease Increases Beta-Protein Production. *Nature* 1992; **360**(6405)**:** 672-674.

55. St George-Hyslop P, Haines J, Rogaev E, Mortilla M, Vaula G, Pericak-Vance M *et al.* Genetic evidence for a novel familial Alzheimer's disease locus on chromosome 14. *Nat Genet* 1992; **2**(4)**:** 330-334.

56. Van Broeckhoven C, Backhovens H, Cruts M, De Winter G, Bruyland M, Cras P *et al.* Mapping of a gene predisposing to early-onset Alzheimer's disease to chromosome 14q24.3. *Nat Genet* 1992; **2**(4)**:** 335-339.

57. Sherrington R, Froelich S, Sorbi S, Campion D, Chi H, Rogaeva EA *et al.* Alzheimer's disease associated with mutations in presenilin 2 is rare and variably penetrant. *Human Molecular Genetics* 1996; **5**(7)**:** 985-988.

58. De Jonghe C, Esselens C, Kumar-Singh S, Craessaerts K, Serneels S, Checler F *et al.* Pathogenic APP mutations near the gamma-secretase cleavage site differentially affect Abeta secretion and APP C-terminal fragment stability. *Hum Mol Genet* 2001; **10**(16)**:** 1665-1671.

59. Cruts M, Van Broeckhoven C. Presenilin mutations in Alzheimer's disease. *Hum Mutat* 1998; **11**(3)**:** 183-190.

60. Campion D, Dumanchin C, Hannequin D, Dubois B, Belliard S, Puel M *et al.* Early-onset autosomal dominant Alzheimer disease: prevalence, genetic heterogeneity, and mutation spectrum. *Am J Hum Genet* 1999; **65**(3)**:** 664-670.

61. Rademakers R, Cruts M, Van Broeckhoven C. Genetics of early-onset Alzheimer dementia. *ScientificWorldJournal* 2003; **3:** 497-519.

62. Corder EH, Saunders AM, Strittmatter WJ, Schmechel DE, Gaskell PC, Small GW *et al.* Gene dose of apolipoprotein E type 4 allele and the risk of Alzheimer's disease in late onset families. *Science* 1993; **261**(5123)**:** 921-923.

63. Bagyinszky E, Youn YC, An SS, Kim S. The genetics of Alzheimer's disease. *Clin Interv Aging* 2014; **9:** 535-551.

64. Van Cauwenberghe C, Van Broeckhoven C, Sleegers K. The genetic landscape of Alzheimer disease: clinical implications and perspectives. *Genet Med* 2016; **18**(5)**:** 421-430.

65. Saunders AM, Strittmatter WJ, Schmechel D, George-Hyslop PH, Pericak-Vance MA, Joo SH *et al.* Association of apolipoprotein E allele epsilon 4 with late-onset familial and sporadic Alzheimer's disease. *Neurology* 1993; **43**(8)**:** 1467-1472.

66. Farrer LA, Cupples LA, Haines JL, Hyman B, Kukull WA, Mayeux R *et al.* Effects of age, sex, and ethnicity on the association between apolipoprotein E genotype and Alzheimer disease. A meta-analysis. APOE and Alzheimer Disease Meta Analysis Consortium. *JAMA* 1997; **278**(16)**:** 1349-1356.

67. Bu G. Apolipoprotein E and its receptors in Alzheimer's disease: pathways, pathogenesis and therapy. *Nat Rev Neurosci* 2009; **10**(5)**:** 333-344.

68. Castellano JM, Kim J, Stewart FR, Jiang H, DeMattos RB, Patterson BW *et al.* Human apoE Isoforms Differentially Regulate Brain Amyloid-beta Peptide Clearance. *Science Translational Medicine* 2011; **3**(89).

69. Bell RD, Winkler EA, Singh I, Sagare AP, Deane R, Wu ZH *et al.* Apolipoprotein E controls cerebrovascular integrity via cyclophilin A. *Nature* 2012; **485**(7399)**:** 512-516.

70. Sando SB, Melquist S, Cannon A, Hutton ML, Sletvold O, Saltvedt I *et al.* APOE epsilon 4 lowers age at onset and is a high risk factor for Alzheimer's disease; a case control study from central Norway. *BMC Neurol* 2008; **8:** 9.

71. Riley KP, Snowdon DA, Saunders AM, Roses AD, Mortimer JA, Nanayakkara N. Cognitive function and apolipoprotein E in very old adults: findings from the Nun Study. *J Gerontol B Psychol Sci Soc Sci* 2000; **55**(2)**:** S69-75.

72. Wilson RS, Schneider JA, Barnes LL, Beckett LA, Aggarwal NT, Cochran EJ *et al.* The apolipoprotein E epsilon 4 allele and decline in different cognitive systems during a 6-year period. *Arch Neurol* 2002; **59**(7)**:** 1154-1160.

73. Genin E, Hannequin D, Wallon D, Sleegers K, Hiltunen M, Combarros O *et al.* APOE and Alzheimer disease: a major gene with semi-dominant inheritance. *Mol Psychiatry* 2011; **16**(9)**:** 903-907.

74. Altmann A, Tian L, Henderson VW, Greicius MD. Sex modifies the APOE-related risk of developing Alzheimer disease. *Ann Neurol* 2014; **75**(4)**:** 563-573.

75. Corder EH, Saunders AM, Risch NJ, Strittmatter WJ, Schmechel DE, Gaskell PC, Jr. *et al.* Protective effect of apolipoprotein E type 2 allele for late onset Alzheimer disease. *Nat Genet* 1994; **7**(2)**:** 180-184.

76. Mahley RW, Weisgraber KH, Huang Y. Apolipoprotein E4: a causative factor and therapeutic target in neuropathology, including Alzheimer's disease. *Proc Natl Acad Sci U S A* 2006; **103**(15)**:** 5644-5651.

77. Kim KW, Jhoo JH, Lee KU, Lee DY, Lee JH, Youn JY *et al.* Association between apolipoprotein E polymorphism and Alzheimer's disease in Koreans. *Neurosci Lett* 1999; **277**(3)**:** 145-148.

78. Grothe MJ, Villeneuve S, Dyrba M, Bartres-Faz D, Wirth M. Multimodal characterization of older APOE2 carriers reveals selective reduction of amyloid load. *Neurology* 2017.

79. Lambert JC, Heath S, Even G, Campion D, Sleegers K, Hiltunen M *et al.* Genome-wide association study identifies variants at CLU and CR1 associated with Alzheimer's disease. *Nat Genet* 2009; **41**(10)**:** 1094-1099.

80. Harold D, Abraham R, Hollingworth P, Sims R, Gerrish A, Hamshere ML *et al.* Genome-wide association study identifies variants at CLU and PICALM associated with Alzheimer's disease. *Nat Genet* 2009; **41**(10)**:** 1088-1093.

81. Lambert JC, Ibrahim-Verbaas CA, Harold D, Naj AC, Sims R, Bellenguez C *et al.* Meta-analysis of 74,046 individuals identifies 11 new susceptibility loci for Alzheimer's disease. *Nat Genet* 2013; **45**(12)**:** 1452-1458.

82. Jones L, Holmans PA, Hamshere ML, Harold D, Moskvina V, Ivanov D *et al.* Genetic evidence implicates the immune system and cholesterol metabolism in the aetiology of Alzheimer's disease. *PLoS One* 2010; **5**(11)**:** e13950.

83. Seshadri S, Fitzpatrick AL, Ikram MA, DeStefano AL, Gudnason V, Boada M *et al.* Genome-wide analysis of genetic loci associated with Alzheimer disease. *JAMA* 2010; **303**(18)**:** 1832-1840.

84. Naj AC, Jun G, Beecham GW, Wang LS, Vardarajan BN, Buros J *et al.* Common variants at MS4A4/MS4A6E, CD2AP, CD33 and EPHA1 are associated with late-onset Alzheimer's disease. *Nat Genet* 2011; **43**(5)**:** 436-441.

85. Hollingworth P, Harold D, Sims R, Gerrish A, Lambert JC, Carrasquillo MM *et al.* Common variants at ABCA7, MS4A6A/MS4A4E, EPHA1, CD33 and CD2AP are associated with Alzheimer's disease. *Nat Genet* 2011; **43**(5)**:** 429-435.

86. Escott-Price V, Bellenguez C, Wang LS, Choi SH, Harold D, Jones L *et al.* Gene-Wide Analysis Detects Two New Susceptibility Genes for Alzheimer's Disease. *PLoS One* 2014; **9**(6).

87. Hibar DP, Adams HH, Jahanshad N, Chauhan G, Stein JL, Hofer E *et al.* Novel genetic loci associated with hippocampal volume. *Nat Commun* 2017; **8:** 13624.

88. Jun G, Ibrahim-Verbaas CA, Vronskaya M, Lambert JC, Chung J, Naj AC *et al.* A novel Alzheimer disease locus located near the gene encoding tau protein. *Mol Psychiatry* 2016; **21**(1)**:** 108-117.

89. Guerreiro R, Wojtas A, Bras J, Carrasquillo M, Rogaeva E, Majounie E *et al.* TREM2 variants in Alzheimer's disease. *N Engl J Med* 2013; **368**(2)**:** 117-127.

90. Jonsson T, Stefansson H, Steinberg S, Jonsdottir I, Jonsson PV, Snaedal J *et al.* Variant of TREM2 associated with the risk of Alzheimer's disease. *N Engl J Med* 2013; **368**(2)**:** 107-116.

91. Abduljaleel Z, Al-Allaf FA, Khan W, Athar M, Shahzad N, Taher MM *et al.* Evidence of trem2 variant associated with triple risk of Alzheimer's disease. *PLoS One* 2014; **9**(3)**:** e92648.

92. Guerreiro RJ, Lohmann E, Bras JM, Gibbs JR, Rohrer JD, Gurunlian N *et al.* Using Exome Sequencing to Reveal Mutations in TREM2 Presenting as a Frontotemporal Dementia-like Syndrome Without Bone Involvement. *Jama Neurology* 2013; **70**(1)**:** 78-84.

93. Takahashi K, Rochford CDP, Neumann H. Clearance of apoptotic neurons without inflammation by microglial triggering receptor expressed on myeloid cells-2. *Journal of Experimental Medicine* 2005; **201**(4)**:** 647-657.

94. Mazzio EA, Soliman KF. Basic concepts of epigenetics: impact of environmental signals on gene expression. *Epigenetics* 2012; **7**(2)**:** 119-130.

95. Landgrave-Gomez J, Mercado-Gomez O, Guevara-Guzman R. Epigenetic mechanisms in neurological and neurodegenerative diseases. *Front Cell Neurosci* 2015; **9:** 58.

96. Marques SC, Oliveira CR, Pereira CM, Outeiro TF. Epigenetics in neurodegeneration: a new layer of complexity. *Prog Neuropsychopharmacol Biol Psychiatry* 2011; **35**(2)**:** 348-355.

97. Wang J, Yu JT, Tan MS, Jiang T, Tan L. Epigenetic mechanisms in Alzheimer's disease: implications for pathogenesis and therapy. *Ageing Res Rev* 2013; **12**(4)**:** 1024-1041.

98. Millan MJ. The epigenetic dimension of Alzheimer's disease: causal, consequence, or curiosity? *Dialogues Clin Neurosci* 2014; **16**(3)**:** 373-393.

99. Urdinguio RG, Sanchez-Mut JV, Esteller M. Epigenetic mechanisms in neurological diseases: genes, syndromes, and therapies. *Lancet Neurol* 2009; **8**(11)**:** 1056-1072.

100. Lee J, Ryu H. Epigenetic modification is linked to Alzheimer's disease: is it a maker or a marker? *Bmb Reports* 2010; **43**(10)**:** 649-655.

101. Mastroeni D, Grover A, Delvaux E, Whiteside C, Coleman PD, Rogers J. Epigenetic mechanisms in Alzheimer's disease. *Neurobiology of Aging* 2011; **32**(7)**:** 1161-1180.

102. Chouliaras L, Mastroeni D, Delvaux E, Grover A, Kenis G, Hof PR *et al.* Consistent decrease in global DNA methylation and hydroxymethylation in the hippocampus of Alzheimer's disease patients. *Neurobiology of Aging* 2013; **34**(9)**:** 2091-2099.

103. Smith AR, Smith RG, Condliffe D, Hannon E, Schalkwyk L, Mill J *et al.* Increased DNA methylation near TREM2 is consistently seen in the superior temporal gyrus in Alzheimer's disease brain. *Neurobiol Aging* 2016; **47:** 35-40.

104. Sanchez-Mut J, Graff J. Epigenetic Alterations in Alzheimer's Disease. *Front Behav Neurosci* 2015; **9**.

105. Lunnon K, Smith R, Hannon E, De Jager PL, Srivastava G, Volta M *et al.* Methylomic profiling implicates cortical deregulation of ANK1 in Alzheimer's disease. *Nature Neuroscience* 2014; **17**(9)**:** 1164-1170.

106. De Jager PL, Srivastava G, Lunnon K, Burgess J, Schalkwyk LC, Yu L *et al.* Alzheimer's disease: early alterations in brain DNA methylation at ANK1, BIN1, RHBDF2 and other loci. *Nature Neuroscience* 2014; **17**(9)**:** 1156-1163.

107. Zhang K, Schrag M, Crofton A, Trivedi R, Vinters H, Kirsch W. Targeted proteomics for quantification of histone acetylation in Alzheimer's disease. *Proteomics* 2012; **12**(8)**:** 1261-1268.

108. Narayan PJ, Lill C, Faull R, Curtis MA, Dragunow M. Increased acetyl and total histone levels in post-mortem Alzheimer's disease brain. *Neurobiol Dis* 2015; **74:** 281-294.

109. Aisen PS, Schneider LS, Sano M, Diaz-Arrastia R, van Dyck CH, Weiner MF *et al.* High-dose B vitamin supplementation and cognitive decline in Alzheimer disease: a randomized controlled trial. *JAMA* 2008; **300**(15)**:** 1774-1783.

110. Herrmann N, Lanctot KL, Rothenburg LS, Eryavec G. A placebo-controlled trial of valproate for agitation and aggression in Alzheimer's disease. *Dement Geriatr Cogn Disord* 2007; **23**(2)**:** 116-119.

111. Ferri CP, Prince M, Brayne C, Brodaty H, Fratiglioni L, Ganguli M *et al.* Global prevalence of dementia: a Delphi consensus study. *Lancet* 2005; **366**(9503)**:** 2112-2117.

112. Goate A, Chartier-Harlin MC, Mullan M, Brown J, Crawford F, Fidani L *et al.* Segregation of a missense mutation in the amyloid precursor protein gene with familial Alzheimer's disease. *Nature* 1991; **349**(6311)**:** 704-706.

113. Sundstrom A, Nilsson LG, Cruts M, Adolfsson R, Van Broeckhoven C, Nyberg L. Increased risk of dementia following mild head injury for carriers but not for non-carriers of the APOE epsilon4 allele. *Int Psychogeriatr* 2007; **19**(1)**:** 159-165.

114. Hamer M, Chida Y. Physical activity and risk of neurodegenerative disease: a systematic review of prospective evidence. *Psychol Med* 2009; **39**(1)**:** 3-11.

115. Karp A, Paillard-Borg S, Wang HX, Silverstein M, Winblad B, Fratiglioni L. Mental, physical and social components in leisure activities equally contribute to decrease dementia risk. *Dement Geriatr Cogn Disord* 2006; **21**(2)**:** 65-73.

116. Abbott RD, White LR, Ross GW, Masaki KH, Curb JD, Petrovitch H. Walking and dementia in physically capable elderly men. *JAMA* 2004; **292**(12)**:** 1447-1453.

117. Beydoun MA, Beydoun HA, Wang Y. Obesity and central obesity as risk factors for incident dementia and its subtypes: a systematic review and meta-analysis. *Obes Rev* 2008; **9**(3)**:** 204-218.

118. Anstey KJ, Mack HA, Cherbuin N. Alcohol consumption as a risk factor for dementia and cognitive decline: meta-analysis of prospective studies. *Am J Geriatr Psychiatry* 2009; **17**(7)**:** 542-555.

119. Barberger-Gateau P, Raffaitin C, Letenneur L, Berr C, Tzourio C, Dartigues JF *et al.* Dietary patterns and risk of dementia: the Three-City cohort study. *Neurology* 2007; **69**(20)**:** 1921-1930.

120. Ngandu T, von Strauss E, Helkala EL, Winblad B, Nissinen A, Tuomilehto J *et al.* Education and dementia - What lies behind the association? *Neurology* 2007; **69**(14)**:** 1442-1450.

121. Lee Y, Back JH, Kim J, Kim SH, Na DL, Cheong HK *et al.* Systematic review of health behavioral risks and cognitive health in older adults. *Int Psychogeriatr* 2010; **22**(2)**:** 174-187.

122. Anstey KJ, von Sanden C, Salim A, O'Kearney R. Smoking as a risk factor for dementia and cognitive decline: a meta-analysis of prospective studies. *Am J Epidemiol* 2007; **166**(4)**:** 367-378.

123. Nokia MS, Lensu S, Ahtiainen JP, Johansson PP, Koch LG, Britton SL *et al.* Physical exercise increases adult hippocampal neurogenesis in male rats provided it is aerobic and sustained. *J Physiol-London* 2016; **594**(7)**:** 1855-1873.

124. Speisman RB, Kumar A, Rani A, Foster TC, Ormerod BK. Daily exercise improves memory, stimulates hippocampal neurogenesis and modulates immune and neuroimmune cytokines in aging rats. *Brain Behav Immun* 2013; **28:** 25-43.

125. Rovio S, Kareholt I, Helkala EL, Viitanen M, Winblad B, Tuomilehto J *et al.* Leisure-time physical activity at midlife and the risk of dementia and Alzheimer's disease. *Lancet Neurol* 2005; **4**(11)**:** 705-711.

126. Kivipelto M, Ngandu T, Fratiglioni L, Viitanen M, Kareholt I, Winblad B *et al.* Obesity and vascular risk factors at midlife and the risk of dementia and Alzheimer disease. *Arch Neurol* 2005; **62**(10)**:** 1556-1560.

127. Lu YC, Day FR, Gustafsson S, Buchkovich ML, Na JB, Bataille V *et al.* y New loci for body fat percentage reveal link between adiposity and cardiometabolic disease risk. *Nature Communications* 2016; **7**.

128. Pedditizi E, Peters R, Beckett N. The risk of overweight/obesity in mid-life and late life for the development of dementia: a systematic review and meta-analysis of longitudinal studies. *Age and Ageing* 2016; **45**(1)**:** 14-21.

129. Fitzpatrick AL, Kuller LH, Lopez OL, Diehr P, O'Meara ES, Longstreth WT, Jr. *et al.* Midlife and late-life obesity and the risk of dementia: cardiovascular health study. *Arch Neurol* 2009; **66**(3)**:** 336-342.

130. Buchman AS, Wilson RS, Bienias JL, Shah RC, Evans DA, Bennett DA. Change in body mass index and risk of incident Alzheimer disease. *Neurology* 2005; **65**(6)**:** 892-897.

131. Anttila T, Helkala EL, Viitanen M, Kareholt I, Fratiglioni L, Winblad B *et al.* Alcohol drinking in middle age and subsequent risk of mild cognitive impairment and dementia in old age: a prospective population based study. *BMJ* 2004; **329**(7465)**:** 539.

132. Huang W, Qiu C, Winblad B, Fratiglioni L. Alcohol consumption and incidence of dementia in a community sample aged 75 years and older. *J Clin Epidemiol* 2002; **55**(10)**:** 959-964.

133. Ruitenberg A, van Swieten JC, Witteman JC, Mehta KM, van Duijn CM, Hofman A *et al.* Alcohol consumption and risk of dementia: the Rotterdam Study. *Lancet* 2002; **359**(9303)**:** 281-286.

134. Paul CA, Au R, Fredman L, Massaro JM, Seshadri S, Decarli C *et al.* Association of alcohol consumption with brain volume in the Framingham study. *Arch Neurol* 2008; **65**(10)**:** 1363-1367.

135. Valenzuela MJ, Sachdev P. Brain reserve and dementia: a systematic review. *Psychol Med* 2006; **36**(4)**:** 441-454.

136. Savva GM, Stephan BC. Epidemiological studies of the effect of stroke on incident dementia: a systematic review. *Stroke* 2010; **41**(1)**:** e41-46.

137. Vermeer SE, Hollander M, van Dijk EJ, Hofman A, Koudstaal PJ, Breteler MM. Silent brain infarcts and white matter lesions increase stroke risk in the general population: the Rotterdam Scan Study. *Stroke* 2003; **34**(5)**:** 1126-1129.

138. Newman AB, Fitzpatrick AL, Lopez O, Jackson S, Lyketsos C, Jagust W *et al.* Dementia and Alzheimer's disease incidence in relationship to cardiovascular disease in the Cardiovascular Health Study cohort. *J Am Geriatr Soc* 2005; **53**(7)**:** 1101-1107.

139. Lu FP, Lin KP, Kuo HK. Diabetes and the risk of multi-system aging phenotypes: a systematic review and meta-analysis. *PLoS One* 2009; **4**(1)**:** e4144.

140. Akomolafe A, Beiser A, Meigs JB, Au R, Green RC, Farrer LA *et al.* Diabetes mellitus and risk of developing Alzheimer disease: results from the Framingham Study. *Arch Neurol* 2006; **63**(11)**:** 1551-1555.

141. Butterfield DA, Di Domenico F, Barone E. Elevated risk of type 2 diabetes for development of Alzheimer disease: a key role for oxidative stress in brain. *Biochim Biophys Acta* 2014; **1842**(9)**:** 1693-1706.

142. Qiu C, Winblad B, Fratiglioni L. The age-dependent relation of blood pressure to cognitive function and dementia. *Lancet Neurol* 2005; **4**(8)**:** 487-499.

143. de Bruijn RF, Bos MJ, Portegies ML, Hofman A, Franco OH, Koudstaal PJ *et al.* The potential for prevention of dementia across two decades: the prospective, population-based Rotterdam Study. *BMC Med* 2015; **13:** 132.

144. Anstey KJ, Lipnicki DM, Low LF. Cholesterol as a risk factor for dementia and cognitive decline: a systematic review of prospective studies with meta-analysis. *Am J Geriatr Psychiatry* 2008; **16**(5)**:** 343-354.

145. McGuinness B, Craig D, Bullock R, Passmore P. Statins for the prevention of dementia. *Cochrane Database Syst Rev* 2009; (2)**:** CD003160.

146. Zhao XS, Peng J, Wu Q, Ren Z, Pan LH, Tang ZH *et al.* Imbalanced cholesterol metabolism in Alzheimer's disease. *Clinica Chimica Acta* 2016; **456:** 107-114.

147. Wiesmann M, Capone C, Zerbi V, Mellendijk L, Heerschap A, Claassen JAHR *et al.* Hypertension Impairs Cerebral Blood Flow in a Mouse Model for Alzheimer's Disease. *Current Alzheimer Research* 2015; **12**(10)**:** 914-922.

148. McGuinness B, Todd S, Passmore AP, Bullock R. Systematic review: Blood pressure lowering in patients without prior cerebrovascular disease for

prevention of cognitive impairment and dementia. *J Neurol Neurosurg Psychiatry* 2008; **79**(1)**:** 4-5.

149. Laurin D, Masaki KH, Foley DJ, White LR, Launer LJ. Midlife dietary intake of antioxidants and risk of late-life incident dementia: the Honolulu-Asia Aging Study. *Am J Epidemiol* 2004; **159**(10)**:** 959-967.

150. Gray SL, Anderson ML, Crane PK, Breitner JC, McCormick W, Bowen JD *et al.* Antioxidant vitamin supplement use and risk of dementia or Alzheimer's disease in older adults. *J Am Geriatr Soc* 2008; **56**(2)**:** 291-295.

151. Malouf R, Grimley Evans J. Folic acid with or without vitamin B12 for the prevention and treatment of healthy elderly and demented people. *Cochrane Database Syst Rev* 2008; (4)**:** CD004514.

152. Scarmeas N, Stern Y, Tang MX, Mayeux R, Luchsinger JA. Mediterranean diet and risk for Alzheimer's disease. *Ann Neurol* 2006; **59**(6)**:** 912-921.

153. Ravaglia G, Forti P, Lucicesare A, Pisacane N, Rietti E, Mangialasche F *et al.* Plasma tocopherols and risk of cognitive impairment in an elderly Italian cohort. *Am J Clin Nutr* 2008; **87**(5)**:** 1306-1313.

154. Papp KV, Walsh SJ, Snyder PJ. Immediate and delayed effects of cognitive interventions in healthy elderly: a review of current literature and future directions. *Alzheimers Dement* 2009; **5**(1)**:** 50-60.

155. McKhann G, Drachman D, Folstein M, Katzman R, Price D, Stadlan EM. Clinical diagnosis of Alzheimer's disease: report of the NINCDS-ADRDA Work Group under the auspices of Department of Health and Human Services Task Force on Alzheimer's Disease. *Neurology* 1984; **34**(7)**:** 939-944.

156. McKhann GM, Knopman DS, Chertkow H, Hyman BT, Jack CR, Jr., Kawas CH *et al.* The diagnosis of dementia due to Alzheimer's disease: recommendations from the National Institute on Aging-Alzheimer's Association workgroups on diagnostic guidelines for Alzheimer's disease. *Alzheimers Dement* 2011; **7**(3)**:** 263-269.

157. Albert MS, DeKosky ST, Dickson D, Dubois B, Feldman HH, Fox NC *et al.* The diagnosis of mild cognitive impairment due to Alzheimer's disease: recommendations from the National Institute on Aging-Alzheimer's Association workgroups on diagnostic guidelines for Alzheimer's disease. *Alzheimers Dement* 2011; **7**(3)**:** 270-279.

158. Dubois B, Feldman HH, Jacova C, Hampel H, Molinuevo JL, Blennow K *et al.* Advancing research diagnostic criteria for Alzheimer's disease: the IWG-2 criteria. *Lancet Neurol* 2014; **13**(6)**:** 614-629.

159. Knopman DS, DeKosky ST, Cummings JL, Chui H, Corey-Bloom J, Relkin N *et al.* Practice parameter: diagnosis of dementia (an evidence-based

review). Report of the Quality Standards Subcommittee of the American Academy of Neurology. *Neurology* 2001; **56**(9)**:** 1143-1153.

160. Price JL, Morris JC. Tangles and plaques in nondemented aging and "preclinical" Alzheimer's disease. *Ann Neurol* 1999; **45**(3)**:** 358-368.

161. Forstl H. Does Alzheimer's Disease Really Exist? *International Psychogeriatrics* 2010; **22**(5)**:** 848-849.

162. Zubenko GS, Maher B, Hughes HB, Zubenko WN, Stiffler JS, Kaplan BB *et al.* Genome-wide linkage survey for genetic loci that influence the development of depressive disorders in families with recurrent, early-onset, major depression. *Am J Med Genet B* 2003; **123B**(1)**:** 1-18.

163. Geldmacher DS, Ducharme J. Family Quality of Life in Dementia: Qualitative Approach to Family-Identified Care Priorities. *Gerontologist* 2009; **49:** 498-498.

164. Barker WW, Luis CA, Kashuba A, Luis M, Harwood DG, Loewenstein D *et al.* Relative frequencies of Alzheimer disease, Lewy body, vascular and frontotemporal dementia, and hippocampal sclerosis in the State of Florida Brain Bank. *Alzheimer Dis Assoc Disord* 2002; **16**(4)**:** 203-212.

165. Tarawneh R, Holtzman DM. The clinical problem of symptomatic Alzheimer disease and mild cognitive impairment. *Cold Spring Harb Perspect Med* 2012; **2**(5)**:** a006148.

166. Irwin DJ, Grossman M, Weintraub D, Hurtig HI, Duda JE, Xie SX *et al.* Neuropathological and genetic correlates of survival and dementia onset in synucleinopathies: a retrospective analysis. *Lancet Neurol* 2017; **16**(1)**:** 55-65.

167. Galvin JE, Pollack J, Morris JC. Clinical phenotype of Parkinson disease dementia. *Neurology* 2006; **67**(9)**:** 1605-1611.

168. Tarawneh R, Galvin JE. Distinguishing Lewy body dementias from Alzheimer's disease. *Expert Rev Neurother* 2007; **7**(11)**:** 1499-1516.

169. McKeith IG, Galasko D, Kosaka K, Perry EK, Dickson DW, Hansen LA *et al.* Consensus guidelines for the clinical and pathologic diagnosis of dementia with Lewy bodies (DLB): report of the consortium on DLB international workshop. *Neurology* 1996; **47**(5)**:** 1113-1124.

170. Salmon DP, Galasko D, Hansen LA, Masliah E, Butters N, Thal LJ *et al.* Neuropsychological deficits associated with diffuse Lewy body disease. *Brain Cogn* 1996; **31**(2)**:** 148-165.

171. Stavitsky K, Brickman AM, Scarmeas N, Torgan RL, Tang MX, Albert M *et al.* The progression of cognition, psychiatric symptoms, and functional

abilities in dementia with Lewy bodies and Alzheimer disease. *Arch Neurol* 2006; **63**(10)**:** 1450-1456.

172. Weiner MF, Hynan LS, Parikh B, Zaki N, White CL, 3rd, Bigio EH *et al.* Can alzheimer's disease and dementias with Lewy bodies be distinguished clinically? *J Geriatr Psychiatry Neurol* 2003; **16**(4)**:** 245-250.

173. Galvin JE, Malcom H, Johnson D, Morris JC. Personality traits distinguishing dementia with Lewy bodies from Alzheimer disease. *Neurology* 2007; **68**(22)**:** 1895-1901.

174. Chui HC. Subcortical ischemic vascular dementia. *Neurol Clin* 2007; **25**(3)**:** 717-740, vi.

175. Desmond DW, Moroney JT, Paik MC, Sano M, Mohr JP, Aboumatar S *et al.* Frequency and clinical determinants of dementia after ischemic stroke. *Neurology* 2000; **54**(5)**:** 1124-1131.

176. Sachdev PS, Brodaty H, Valenzuela MJ, Lorentz L, Looi JC, Wen W *et al.* The neuropsychological profile of vascular cognitive impairment in stroke and TIA patients. *Neurology* 2004; **62**(6)**:** 912-919.

177. Ratnavalli E, Brayne C, Dawson K, Hodges JR. The prevalence of frontotemporal dementia. *Neurology* 2002; **58**(11)**:** 1615-1621.

178. Powlishta KK, Storandt M, Mandernach TA, Hogan E, Grant EA, Morris JC. Absence of effect of depression on cognitive performance in early-stage Alzheimer disease. *Arch Neurol* 2004; **61**(8)**:** 1265-1268.

179. Mitchell AJ, Shiri-Feshki M. Rate of progression of mild cognitive impairment to dementia--meta-analysis of 41 robust inception cohort studies. *Acta Psychiatr Scand* 2009; **119**(4)**:** 252-265.

180. Petersen RC, Doody R, Kurz A, Mohs RC, Morris JC, Rabins PV *et al.* Current concepts in mild cognitive impairment. *Arch Neurol* 2001; **58**(12)**:** 1985-1992.

181. Winblad B, Palmer K, Kivipelto M, Jelic V, Fratiglioni L, Wahlund LO *et al.* Mild cognitive impairment--beyond controversies, towards a consensus: report of the International Working Group on Mild Cognitive Impairment. *J Intern Med* 2004; **256**(3)**:** 240-246.

182. Petersen RC. Mild cognitive impairment as a diagnostic entity. *J Intern Med* 2004; **256**(3)**:** 183-194.

183. Feldman. Behavioral symptoms in mild cognitive impairment (vol 62, pg 1199, 2004). *Neurology* 2004; **63**(4)**:** 764-764.

184. Jack CR, Shiung MM, Gunter JL, O'Brien PC, Weigand SD, Knopman DS *et al.* Comparison of different MRI brain atrophy, rate measures with clinical disease progression in AD. *Neurology* 2004; **62**(4)**:** 591-600.

185. Obler LK, Albert ML. Historical note: Jules Seglas on language in dementia. *Brain Lang* 1985; **24**(2)**:** 314-325.

186. Farlow MR, Cummings JL. Effective pharmacologic management of Alzheimer's disease. *American Journal of Medicine* 2007; **120**(5)**:** 388-397.

187. Rubin EH, Storandt M, Miller JP, Kinscherf DA, Grant EA, Morris JC *et al.* A prospective study of cognitive function and onset of dementia in cognitively healthy elders. *Arch Neurol-Chicago* 1998; **55**(3)**:** 395-401.

188. Tata AM, Velluto L, D'Angelo C, Reale M. Cholinergic system dysfunction and neurodegenerative diseases: cause or effect? *CNS Neurol Disord Drug Targets* 2014; **13**(7)**:** 1294-1303.

189. Godyn J, Jonczyk J, Panek D, Malawska B. Therapeutic strategies for Alzheimer's disease in clinical trials. *Pharmacol Rep* 2016; **68**(1)**:** 127-138.

190. Anand P, Singh B. A review on cholinesterase inhibitors for Alzheimer's disease. *Arch Pharm Res* 2013; **36**(4)**:** 375-399.

191. Folch J, Petrov D, Ettcheto M, Abad S, Sanchez-Lopez E, Garcia ML *et al.* Current Research Therapeutic Strategies for Alzheimer's Disease Treatment. *Neural Plast* 2016; **2016:** 8501693.

192. Weinreb O, Amit T, Bar-Am O, Youdim MB. A novel anti-Alzheimer's disease drug, ladostigil neuroprotective, multimodal brain-selective monoamine oxidase and cholinesterase inhibitor. *Int Rev Neurobiol* 2011; **100:** 191-215.

193. Chu LW. Alzheimer's disease: early diagnosis and treatment. *Hong Kong Med J* 2012; **18**(3)**:** 228-237.

194. Prentice H, Modi JP, Wu JY. Mechanisms of Neuronal Protection against Excitotoxicity, Endoplasmic Reticulum Stress, and Mitochondrial Dysfunction in Stroke and Neurodegenerative Diseases. *Oxid Med Cell Longev* 2015; **2015:** 964518.

195. Shi XD, Lin XT, Hu R, Sun N, Hao JR, Gao C. Toxicological Differences Between NMDA Receptor Antagonists and Cholinesterase Inhibitors. *Am J Alzheimers Dis* 2016; **31**(5)**:** 405-412.

196. Wang X, Blanchard J, Grundke-Iqbal I, Iqbal K. Memantine Attenuates Alzheimer's Disease-Like Pathology and Cognitive Impairment. *PLoS One* 2015; **10**(12)**:** e0145441.

197. Wilkinson D, Windfeld K, Colding-Jorgensen E. Safety and efficacy of idalopirdine, a 5-HT6 receptor antagonist, in patients with moderate Alzheimer's disease (LADDER): a randomised, double-blind, placebo-controlled phase 2 trial. *Lancet Neurol* 2014; **13**(11)**:** 1092-1099.

198. Woolley ML, Bentley JC, Sleight AJ, Marsden CA, Fone KC. A role for 5-ht6 receptors in retention of spatial learning in the Morris water maze. *Neuropharmacology* 2001; **41**(2)**:** 210-219.

199. Ramirez MJ, Lai MK, Tordera RM, Francis PT. Serotonergic therapies for cognitive symptoms in Alzheimer's disease: rationale and current status. *Drugs* 2014; **74**(7)**:** 729-736.

200. Chang WP, Huang X, Downs D, Cirrito JR, Koelsch G, Holtzman DM *et al.* Beta-secretase inhibitor GRL-8234 rescues age-related cognitive decline in APP transgenic mice. *FASEB J* 2011; **25**(2)**:** 775-784.

201. Ghosh AK, Osswald HL. BACE1 (beta-secretase) inhibitors for the treatment of Alzheimer's disease. *Chem Soc Rev* 2014; **43**(19)**:** 6765-6813.

202. May PC, Willis BA, Lowe SL, Dean RA, Monk SA, Cocke PJ *et al.* The potent BACE1 inhibitor LY2886721 elicits robust central Abeta pharmacodynamic responses in mice, dogs, and humans. *J Neurosci* 2015; **35**(3)**:** 1199-1210.

203. Imbimbo BP, Giardina GA. gamma-secretase inhibitors and modulators for the treatment of Alzheimer's disease: disappointments and hopes. *Curr Top Med Chem* 2011; **11**(12)**:** 1555-1570.

204. Doody RS, Raman R, Farlow M, Iwatsubo T, Vellas B, Joffe S *et al.* A phase 3 trial of semagacestat for treatment of Alzheimer's disease. *N Engl J Med* 2013; **369**(4)**:** 341-350.

205. Tong G, Castaneda L, Wang JS, Sverdlov O, Huang SP, Slemmon R *et al.* Effects of single doses of avagacestat (BMS-708163) on cerebrospinal fluid Abeta levels in healthy young men. *Clin Drug Investig* 2012; **32**(11)**:** 761-769.

206. Dockens R, Wang JS, Castaneda L, Sverdlov O, Huang SP, Slemmon R *et al.* A placebo-controlled, multiple ascending dose study to evaluate the safety, pharmacokinetics and pharmacodynamics of avagacestat (BMS-708163) in healthy young and elderly subjects. *Clin Pharmacokinet* 2012; **51**(10)**:** 681-693.

207. Eriksen JL, Sagi SA, Smith TE, Weggen S, Das P, McLendon DC *et al.* NSAIDs and enantiomers of flurbiprofen target gamma-secretase and lower Abeta 42 in vivo. *J Clin Invest* 2003; **112**(3)**:** 440-449.

208. Corbett GT, Gonzalez FJ, Pahan K. Activation of peroxisome proliferator-activated receptor alpha stimulates ADAM10-mediated proteolysis of APP. *Proc Natl Acad Sci U S A* 2015; **112**(27)**:** 8445-8450.

209. Fragkouli A, Tsilibary EC, Tzinia AK. Neuroprotective role of MMP-9 overexpression in the brain of Alzheimer's 5xFAD mice. *Neurobiol Dis* 2014; **70:** 179-189.

210. Pimenova AA, Thathiah A, De Strooper B, Tesseur I. Regulation of amyloid precursor protein processing by serotonin signaling. *PLoS One* 2014; **9**(1)**:** e87014.

211. Gauthier S, Aisen PS, Ferris SH, Saumier D, Duong A, Haine D *et al.* Effect of tramiprosate in patients with mild-to-moderate Alzheimer's disease: exploratory analyses of the MRI sub-group of the Alphase study. *J Nutr Health Aging* 2009; **13**(6)**:** 550-557.

212. Aisen PS, Gauthier S, Ferris SH, Saumier D, Haine D, Garceau D *et al.* Tramiprosate in mild-to-moderate Alzheimer's disease - a randomized, double-blind, placebo-controlled, multi-centre study (the Alphase Study). *Arch Med Sci* 2011; **7**(1)**:** 102-111.

213. Salloway S, Sperling R, Keren R, Porsteinsson AP, van Dyck CH, Tariot PN *et al.* A phase 2 randomized trial of ELND005, scyllo-inositol, in mild to moderate Alzheimer disease. *Neurology* 2011; **77**(13)**:** 1253-1262.

214. Matlack KE, Tardiff DF, Narayan P, Hamamichi S, Caldwell KA, Caldwell GA *et al.* Clioquinol promotes the degradation of metal-dependent amyloid-beta (Abeta) oligomers to restore endocytosis and ameliorate Abeta toxicity. *Proc Natl Acad Sci U S A* 2014; **111**(11)**:** 4013-4018.

215. Awasthi M, Singh S, Pandey VP, Dwivedi UN. Alzheimer's disease: An overview of amyloid beta dependent pathogenesis and its therapeutic implications along with in silico approaches emphasizing the role of natural products. *J Neurol Sci* 2016; **361:** 256-271.

216. Gilman S, Koller M, Black RS, Jenkins L, Griffith SG, Fox NC *et al.* Clinical effects of Abeta immunization (AN1792) in patients with AD in an interrupted trial. *Neurology* 2005; **64**(9)**:** 1553-1562.

217. Panza F, Solfrizzi V, Imbimbo BP, Logroscino G. Amyloid-directed monoclonal antibodies for the treatment of Alzheimer's disease: the point of no return? *Expert Opin Biol Ther* 2014; **14**(10)**:** 1465-1476.

218. Salloway S, Sperling R, Fox NC, Blennow K, Klunk W, Raskind M *et al.* Two phase 3 trials of bapineuzumab in mild-to-moderate Alzheimer's disease. *N Engl J Med* 2014; **370**(4)**:** 322-333.

219. Tayeb HO, Murray ED, Price BH, Tarazi FI. Bapineuzumab and solanezumab for Alzheimer's disease: is the 'amyloid cascade hypothesis' still alive? *Expert Opin Biol Ther* 2013; **13**(7)**:** 1075-1084.

220. Doody RS, Thomas RG, Farlow M, Iwatsubo T, Vellas B, Joffe S *et al.* Phase 3 trials of solanezumab for mild-to-moderate Alzheimer's disease. *N Engl J Med* 2014; **370**(4)**:** 311-321.

221. Valera E, Spencer B, Masliah E. Immunotherapeutic Approaches Targeting Amyloid-beta, alpha-Synuclein, and Tau for the Treatment of Neurodegenerative Disorders. *Neurotherapeutics* 2016; **13**(1)**:** 179-189.

222. Novakovic D, Feligioni M, Scaccianoce S, Caruso A, Piccinin S, Schepisi C *et al.* Profile of gantenerumab and its potential in the treatment of Alzheimer's disease. *Drug Des Devel Ther* 2013; **7:** 1359-1364.

223. Bohrmann B, Baumann K, Benz J, Gerber F, Huber W, Knoflach F *et al.* Gantenerumab: a novel human anti-Abeta antibody demonstrates sustained cerebral amyloid-beta binding and elicits cell-mediated removal of human amyloid-beta. *J Alzheimers Dis* 2012; **28**(1)**:** 49-69.

224. Jacobsen H, Ozmen L, Caruso A, Narquizian R, Hilpert H, Jacobsen B *et al.* Combined treatment with a BACE inhibitor and anti-Abeta antibody gantenerumab enhances amyloid reduction in APPLondon mice. *J Neurosci* 2014; **34**(35)**:** 11621-11630.

225. Jindal H, Bhatt B, Sk S, Singh Malik J. Alzheimer disease immunotherapeutics: then and now. *Hum Vaccin Immunother* 2014; **10**(9)**:** 2741-2743.

226. Nalivaeva NN, Fisk LR, Belyaev ND, Turner AJ. Amyloid-degrading enzymes as therapeutic targets in Alzheimer's disease. *Curr Alzheimer Res* 2008; **5**(2)**:** 212-224.

227. Baranello RJ, Bharani KL, Padmaraju V, Chopra N, Lahiri DK, Greig NH *et al.* Amyloid-beta protein clearance and degradation (ABCD) pathways and their role in Alzheimer's disease. *Curr Alzheimer Res* 2015; **12**(1)**:** 32-46.

228. Kontsekova E, Zilka N, Kovacech B, Novak P, Novak M. First-in-man tau vaccine targeting structural determinants essential for pathological tau-tau interaction reduces tau oligomerisation and neurofibrillary degeneration in an Alzheimer's disease model. *Alzheimers Res Ther* 2014; **6**(4)**:** 44.

229. Panza F, Seripa D, Solfrizzi V, Imbimbo BP, Santamato A, Lozupone M *et al.* Tau aggregation inhibitors: the future of Alzheimer's pharmacotherapy? *Expert Opin Pharmacother* 2016; **17**(4)**:** 457-461.

230. Jack CR, Jr., Knopman DS, Chetelat G, Dickson D, Fagan AM, Frisoni GB *et al.* Suspected non-Alzheimer disease pathophysiology--concept and controversy. *Nat Rev Neurol* 2016; **12**(2)**:** 117-124.

231. Klunk WE, Engler H, Nordberg A, Wang Y, Blomqvist G, Holt DP *et al.* Imaging brain amyloid in Alzheimer's disease with Pittsburgh Compound-B. *Ann Neurol* 2004; **55**(3)**:** 306-319.

232. Rowe CC, Ellis KA, Rimajova M, Bourgeat P, Pike KE, Jones G *et al.* Amyloid imaging results from the Australian Imaging, Biomarkers and Lifestyle (AIBL) study of aging. *Neurobiol Aging* 2010; **31**(8)**:** 1275-1283.

233. Villemagne VL, Pike KE, Chetelat G, Ellis KA, Mulligan RS, Bourgeat P *et al.* Longitudinal assessment of Abeta and cognition in aging and Alzheimer disease. *Ann Neurol* 2011; **69**(1)**:** 181-192.

234. Fagan AM, Roe CM, Xiong C, Mintun MA, Morris JC, Holtzman DM. Cerebrospinal fluid tau/beta-amyloid(42) ratio as a prediction of cognitive decline in nondemented older adults. *Arch Neurol* 2007; **64**(3)**:** 343-349.

235. Shaw LM, Vanderstichele H, Knapik-Czajka M, Clark CM, Aisen PS, Petersen RC *et al.* Cerebrospinal fluid biomarker signature in Alzheimer's disease neuroimaging initiative subjects. *Ann Neurol* 2009; **65**(4)**:** 403-413.

236. Mattsson N, Zetterberg H, Hansson O, Andreasen N, Parnetti L, Jonsson M *et al.* CSF biomarkers and incipient Alzheimer disease in patients with mild cognitive impairment. *JAMA* 2009; **302**(4)**:** 385-393.

237. Visser PJ, Verhey F, Knol DL, Scheltens P, Wahlund LO, Freund-Levi Y *et al.* Prevalence and prognostic value of CSF markers of Alzheimer's disease pathology in patients with subjective cognitive impairment or mild cognitive impairment in the DESCRIPA study: a prospective cohort study. *Lancet Neurol* 2009; **8**(7)**:** 619-627.

238. Jagust WJ, Bandy D, Chen K, Foster NL, Landau SM, Mathis CA *et al.* The Alzheimer's Disease Neuroimaging Initiative positron emission tomography core. *Alzheimers Dement* 2010; **6**(3)**:** 221-229.

239. Dickerson BC, Wolk DA. MRI cortical thickness biomarker predicts AD-like CSF and cognitive decline in normal adults. *Neurology* 2012; **78**(2)**:** 84-90.

240. Vemuri P, Wiste HJ, Weigand SD, Shaw LM, Trojanowski JQ, Weiner MW *et al.* MRI and CSF biomarkers in normal, MCI, and AD subjects: predicting future clinical change. *Neurology* 2009; **73**(4)**:** 294-301.

241. Jack CR, Jr., Knopman DS, Jagust WJ, Shaw LM, Aisen PS, Weiner MW *et al.* Hypothetical model of dynamic biomarkers of the Alzheimer's pathological cascade. *Lancet Neurol* 2010; **9**(1)**:** 119-128.

242. Jack CR, Jr., Knopman DS, Jagust WJ, Petersen RC, Weiner MW, Aisen PS *et al.* Tracking pathophysiological processes in Alzheimer's disease: an updated hypothetical model of dynamic biomarkers. *Lancet Neurol* 2013; **12**(2)**:** 207-216.

243. Jack CR, Jr., Lowe VJ, Senjem ML, Weigand SD, Kemp BJ, Shiung MM *et al.* 11C PiB and structural MRI provide complementary information in imaging of Alzheimer's disease and amnestic mild cognitive impairment. *Brain* 2008; **131**(Pt 3)**:** 665-680.

244. Fagan AM, Head D, Shah AR, Marcus D, Mintun M, Morris JC *et al.* Decreased cerebrospinal fluid Abeta(42) correlates with brain atrophy in cognitively normal elderly. *Ann Neurol* 2009; **65**(2)**:** 176-183.

245. Jack CR, Jr., Lowe VJ, Weigand SD, Wiste HJ, Senjem ML, Knopman DS *et al.* Serial PIB and MRI in normal, mild cognitive impairment and Alzheimer's disease: implications for sequence of pathological events in Alzheimer's disease. *Brain* 2009; **132**(Pt 5)**:** 1355-1365.

246. Bateman RJ, Xiong C, Benzinger TL, Fagan AM, Goate A, Fox NC *et al.* Clinical and biomarker changes in dominantly inherited Alzheimer's disease. *N Engl J Med* 2012; **367**(9)**:** 795-804.

247. Fagan AM, Mintun MA, Shah AR, Aldea P, Roe CM, Mach RH *et al.* Cerebrospinal fluid tau and ptau(181) increase with cortical amyloid deposition in cognitively normal individuals: implications for future clinical trials of Alzheimer's disease. *EMBO Mol Med* 2009; **1**(8-9)**:** 371-380.

248. Hunt A, Schonknecht P, Henze M, Toro P, Haberkorn U, Schroder J. CSF tau protein and FDG PET in patients with aging-associated cognitive decline and Alzheimer's disease. *Neuropsychiatr Dis Treat* 2006; **2**(2)**:** 207-212.

249. Lo RY, Hubbard AE, Shaw LM, Trojanowski JQ, Petersen RC, Aisen PS *et al.* Longitudinal change of biomarkers in cognitive decline. *Arch Neurol* 2011; **68**(10)**:** 1257-1266.

250. Minoshima S, Giordani B, Berent S, Frey KA, Foster NL, Kuhl DE. Metabolic reduction in the posterior cingulate cortex in very early Alzheimer's disease. *Ann Neurol* 1997; **42**(1)**:** 85-94.

251. Forster S, Grimmer T, Miederer I, Henriksen G, Yousefi BH, Graner P *et al.* Regional expansion of hypometabolism in Alzheimer's disease follows amyloid deposition with temporal delay. *Biol Psychiatry* 2012; **71**(9)**:** 792-797.

252. Landau SM, Mintun MA, Joshi AD, Koeppe RA, Petersen RC, Aisen PS *et al.* Amyloid deposition, hypometabolism, and longitudinal cognitive decline. *Ann Neurol* 2012; **72**(4)**:** 578-586.

253. Lehmann M, Ghosh PM, Madison C, Laforce R, Jr., Corbetta-Rastelli C, Weiner MW *et al.* Diverging patterns of amyloid deposition and hypometabolism in clinical variants of probable Alzheimer's disease. *Brain* 2013; **136**(Pt 3)**:** 844-858.

254. Chan D, Janssen JC, Whitwell JL, Watt HC, Jenkins R, Frost C *et al.* Change in rates of cerebral atrophy over time in early-onset Alzheimer's disease: longitudinal MRI study. *Lancet* 2003; **362**(9390)**:** 1121-1122.

255. Catafau AM, Bullich S. Amyloid PET imaging: applications beyond Alzheimer's disease. *Clin Transl Imaging* 2015; **3**(1)**:** 39-55.

256. Braak H, Braak E. Frequency of stages of Alzheimer-related lesions in different age categories. *Neurobiol Aging* 1997; **18**(4)**:** 351-357.

257. Villain N, Chetelat G, Grassiot B, Bourgeat P, Jones G, Ellis KA *et al.* Regional dynamics of amyloid-beta deposition in healthy elderly, mild cognitive impairment and Alzheimer's disease: a voxelwise PiB-PET longitudinal study. *Brain* 2012; **135**(Pt 7)**:** 2126-2139.

258. Bacskai BJ, Hickey GA, Skoch J, Kajdasz ST, Wang Y, Huang GF *et al.* Four-dimensional multiphoton imaging of brain entry, amyloid binding, and clearance of an amyloid-beta ligand in transgenic mice. *Proc Natl Acad Sci U S A* 2003; **100**(21)**:** 12462-12467.

259. Fodero-Tavoletti MT, Rowe CC, McLean CA, Leone L, Li QX, Masters CL *et al.* Characterization of PiB binding to white matter in Alzheimer disease and other dementias. *J Nucl Med* 2009; **50**(2)**:** 198-204.

260. Mosconi L, Berti V, Glodzik L, Pupi A, De Santi S, de Leon MJ. Pre-clinical detection of Alzheimer's disease using FDG-PET, with or without amyloid imaging. *J Alzheimers Dis* 2010; **20**(3)**:** 843-854.

261. Ikonomovic MD, Klunk WE, Abrahamson EE, Mathis CA, Price JC, Tsopelas ND *et al.* Post-mortem correlates of in vivo PiB-PET amyloid imaging in a typical case of Alzheimer's disease. *Brain* 2008; **131**(Pt 6)**:** 1630-1645.

262. Rabinovici GD, Jagust WJ. Amyloid imaging in aging and dementia: testing the amyloid hypothesis in vivo. *Behav Neurol* 2009; **21**(1)**:** 117-128.

263. Klunk WE. Amyloid imaging as a biomarker for cerebral beta-amyloidosis and risk prediction for Alzheimer dementia. *Neurobiol Aging* 2011; **32 Suppl 1:** S20-36.

264. Jansen K, Thamm M, Bock CT, Scheufele R, Kucherer C, Muenstermann D *et al.* High Prevalence and High Incidence of Coinfection with Hepatitis B, Hepatitis C, and Syphilis and Low Rate of Effective Vaccination against Hepatitis B in HIV-Positive Men Who Have Sex with Men with Known Date of HIV Seroconversion in Germany. *PLoS One* 2015; **10**(11)**:** e0142515.

265. Resnick SM, Sojkova J, Zhou Y, An Y, Ye W, Holt DP *et al.* Longitudinal cognitive decline is associated with fibrillar amyloid-beta measured by [11C]PiB. *Neurology* 2010; **74**(10)**:** 807-815.

266. Nelissen N, Van Laere K, Thurfjell L, Owenius R, Vandenbulcke M, Koole M *et al.* Phase 1 study of the Pittsburgh compound B derivative 18F-flutemetamol in healthy volunteers and patients with probable Alzheimer disease. *J Nucl Med* 2009; **50**(8)**:** 1251-1259.

267. Vandenberghe R, Adamczuk K, Dupont P, Laere KV, Chetelat G. Amyloid PET in clinical practice: Its place in the multidimensional space of Alzheimer's disease. *Neuroimage Clin* 2013; **2:** 497-511.

268. Choi SR, Golding G, Zhuang Z, Zhang W, Lim N, Hefti F *et al.* Preclinical properties of 18F-AV-45: a PET agent for Abeta plaques in the brain. *J Nucl Med* 2009; **50**(11)**:** 1887-1894.

269. Johnson KA, Sperling RA, Gidicsin CM, Carmasin JS, Maye JE, Coleman RE *et al.* Florbetapir (F18-AV-45) PET to assess amyloid burden in Alzheimer's disease dementia, mild cognitive impairment, and normal aging. *Alzheimers Dement* 2013; **9**(5 Suppl)**:** S72-83.

270. Clark CM, Schneider JA, Bedell BJ, Beach TG, Bilker WB, Mintun MA *et al.* Use of florbetapir-PET for imaging beta-amyloid pathology. *JAMA* 2011; **305**(3)**:** 275-283.

271. Shokouhi S, Claassen D, Riddle W. Imaging Brain Metabolism and Pathology in Alzheimer's Disease with Positron Emission Tomography. *J Alzheimers Dis Parkinsonism* 2014; **4**(2).

272. Thompson PW, Ye L, Morgenstern JL, Sue L, Beach TG, Judd DJ *et al.* Interaction of the amyloid imaging tracer FDDNP with hallmark Alzheimer's disease pathologies. *J Neurochem* 2009; **109**(2)**:** 623-630.

273. Smid LM, Kepe V, Vinters HV, Bresjanac M, Toyokuni T, Satyamurthy N *et al.* Postmortem 3-D brain hemisphere cortical tau and amyloid-beta pathology mapping and quantification as a validation method of neuropathology imaging. *J Alzheimers Dis* 2013; **36**(2)**:** 261-274.

274. Gomperts SN, Rentz DM, Moran E, Becker JA, Locascio JJ, Klunk WE *et al.* Imaging amyloid deposition in Lewy body diseases. *Neurology* 2008; **71**(12)**:** 903-910.

275. Lippa CF, Duda JE, Grossman M, Hurtig HI, Aarsland D, Boeve BF *et al.* DLB and PDD boundary issues: diagnosis, treatment, molecular pathology, and biomarkers. *Neurology* 2007; **68**(11)**:** 812-819.

276. Ikonomovic MD, Abrahamson EE, Price JC, Hamilton RL, Mathis CA, Paljug WR *et al.* Early AD pathology in a [C-11]PiB-negative case: a PiB-amyloid imaging, biochemical, and immunohistochemical study. *Acta Neuropathol* 2012; **123**(3)**:** 433-447.

277. Edison P, Archer HA, Gerhard A, Hinz R, Pavese N, Turkheimer FE *et al.* Microglia, amyloid, and cognition in Alzheimer's disease: An

[11C](R)PK11195-PET and [11C]PIB-PET study. *Neurobiol Dis* 2008; **32**(3)**:** 412-419.

278. Claassen DO, Lowe VJ, Peller PJ, Petersen RC, Josephs KA. Amyloid and glucose imaging in dementia with Lewy bodies and multiple systems atrophy. *Parkinsonism Relat Disord* 2011; **17**(3)**:** 160-165.

279. Mott RT, Dickson DW, Trojanowski JQ, Zhukareva V, Lee VM, Forman M *et al.* Neuropathologic, biochemical, and molecular characterization of the frontotemporal dementias. *J Neuropathol Exp Neurol* 2005; **64**(5)**:** 420-428.

280. Rabinovici GD, Jagust WJ, Furst AJ, Ogar JM, Racine CA, Mormino EC *et al.* Abeta amyloid and glucose metabolism in three variants of primary progressive aphasia. *Ann Neurol* 2008; **64**(4)**:** 388-401.

281. Jellinger KA, Attems J. Prevalence and pathogenic role of cerebrovascular lesions in Alzheimer disease. *J Neurol Sci* 2005; **229-230:** 37-41.

282. Johnson KA, Gregas M, Becker JA, Kinnecom C, Salat DH, Moran EK *et al.* Imaging of amyloid burden and distribution in cerebral amyloid angiopathy. *Ann Neurol* 2007; **62**(3)**:** 229-234.

283. Villemagne VL, McLean CA, Reardon K, Boyd A, Lewis V, Klug G *et al.* 11C-PiB PET studies in typical sporadic Creutzfeldt-Jakob disease. *J Neurol Neurosurg Psychiatry* 2009; **80**(9)**:** 998-1001.

284. Liberski PP. Amyloid plaques in transmissible spongiform encephalopathies (prion diseases). *Folia Neuropathol* 2004; **42 Suppl B:** 109-119.

285. Okamura N, Shiga Y, Furumoto S, Tashiro M, Tsuboi Y, Furukawa K *et al.* In vivo detection of prion amyloid plaques using [(11)C]BF-227 PET. *Eur J Nucl Med Mol Imaging* 2010; **37**(5)**:** 934-941.

286. Sabbagh MN, Fleisher A, Chen K, Rogers J, Berk C, Reiman E *et al.* Positron emission tomography and neuropathologic estimates of fibrillar amyloid-beta in a patient with Down syndrome and Alzheimer disease. *Arch Neurol* 2011; **68**(11)**:** 1461-1466.

287. Hardy J. The amyloid hypothesis for Alzheimer's disease: a critical reappraisal. *J Neurochem* 2009; **110**(4)**:** 1129-1134.

288. Jagust W, Reed B, Mungas D, Ellis W, Decarli C. What does fluorodeoxyglucose PET imaging add to a clinical diagnosis of dementia? *Neurology* 2007; **69**(9)**:** 871-877.

289. Chetelat G, Desgranges B, de la Sayette V, Viader F, Berkouk K, Landeau B *et al.* Dissociating atrophy and hypometabolism impact on episodic memory in mild cognitive impairment. *Brain* 2003; **126**(Pt 9)**:** 1955-1967.

290. Rossor MN, Kennedy AM, Frackowiak RS. Clinical and neuroimaging features of familial Alzheimer's disease. *Ann N Y Acad Sci* 1996; **777:** 49-56.

291. Villemagne VL, Chetelat G. Neuroimaging biomarkers in Alzheimer's disease and other dementias. *Ageing Res Rev* 2016; **30:** 4-16.

292. Mosconi L, Tsui WH, Herholz K, Pupi A, Drzezga A, Lucignani G *et al.* Multicenter standardized 18F-FDG PET diagnosis of mild cognitive impairment, Alzheimer's disease, and other dementias. *J Nucl Med* 2008; **49**(3)**:** 390-398.

293. La Joie R, Perrotin A, Barre L, Hommet C, Mezenge F, Ibazizene M *et al.* Region-Specific Hierarchy between Atrophy, Hypometabolism, and beta-Amyloid (A beta) Load in Alzheimer's Disease Dementia. *Journal of Neuroscience* 2012; **32**(46)**:** 16265-16273.

294. Cohen AD, Klunk WE. Early detection of Alzheimer's disease using PiB and FDG PET. *Neurobiology of Disease* 2014; **72:** 117-122.

295. Forsberg A, Engler H, Almkvist O, Blomquist G, Hagman G, Wall A *et al.* PET imaging of amyloid deposition in patients with mild cognitive impairment. *Neurobiol Aging* 2008; **29**(10)**:** 1456-1465.

296. Altmann A, Ng B, Landau SM, Jagust WJ, Greicius MD. Regional brain hypometabolism is unrelated to regional amyloid plaque burden. *Brain* 2015; **138**(Pt 12)**:** 3734-3746.

297. Drago V, Babiloni C, Bartres-Faz D, Caroli A, Bosch B, Hensch T *et al.* Disease tracking markers for Alzheimer's disease at the prodromal (MCI) stage. *J Alzheimers Dis* 2011; **26 Suppl 3:** 159-199.

298. Frisoni GB, Fox NC, Jack CR, Jr., Scheltens P, Thompson PM. The clinical use of structural MRI in Alzheimer disease. *Nat Rev Neurol* 2010; **6**(2)**:** 67-77.

299. Coimbra A, Williams DS, Hostetler ED. The role of MRI and PET/SPECT in Alzheimer's disease. *Curr Top Med Chem* 2006; **6**(6)**:** 629-647.

300. Adlard PA, Tran BA, Finkelstein DI, Desmond PM, Johnston LA, Bush AI *et al.* A review of beta-amyloid neuroimaging in Alzheimer's disease. *Front Neurosci* 2014; **8:** 327.

301. Ramani A, Jensen JH, Helpern JA. Quantitative MR imaging in Alzheimer disease. *Radiology* 2006; **241**(1)**:** 26-44.

302. Sperling RA, Dickerson BC, Pihlajamaki M, Vannini P, LaViolette PS, Vitolo OV *et al.* Functional alterations in memory networks in early Alzheimer's disease. *Neuromolecular Med* 2010; **12**(1)**:** 27-43.

303. Kvartsberg H, Portelius E, Andreasson U, Brinkmalm G, Hellwig K, Lelental N *et al.* Characterization of the postsynaptic protein neurogranin in paired cerebrospinal fluid and plasma samples from Alzheimer's disease patients and healthy controls. *Alzheimers Research & Therapy* 2015; **7**.

304. Chetelat G, Villemagne VL, Pike KE, Baron JC, Bourgeat P, Jones G *et al.* Larger temporal volume in elderly with high versus low beta-amyloid deposition. *Brain* 2010; **133**(11)**:** 3349-3358.

305. Bourgeat P, Chetelat G, Villemagne VL, Fripp J, Raniga P, Pike K *et al.* Beta-amyloid burden in the temporal neocortex is related to hippocampal atrophy in elderly subjects without dementia. *Neurology* 2010; **74**(2)**:** 121-127.

306. Fodero-Tavoletti MT, Okamura N, Furumoto S, Mulligan RS, Connor AR, McLean CA *et al.* 18F-THK523: a novel in vivo tau imaging ligand for Alzheimer's disease. *Brain* 2011; **134**(Pt 4)**:** 1089-1100.

307. Fodero-Tavoletti MT, Furumoto S, Taylor L, McLean CA, Mulligan RS, Birchall I *et al.* Assessing THK523 selectivity for tau deposits in Alzheimer's disease and non-Alzheimer's disease tauopathies. *Alzheimers Res Ther* 2014; **6**(1)**:** 11.

308. Villemagne VL, Furumoto S, Fodero-Tavoletti MT, Mulligan RS, Hodges J, Harada R *et al.* In vivo evaluation of a novel tau imaging tracer for Alzheimer's disease. *Eur J Nucl Med Mol Imaging* 2014; **41**(5)**:** 816-826.

309. Okamura N, Harada R, Furumoto S, Arai H, Yanai K, Kudo Y. Tau PET imaging in Alzheimer's disease. *Curr Neurol Neurosci Rep* 2014; **14**(11)**:** 500.

310. Chein M, Mugnier ML, Croitoru M. Visual reasoning with graph-based mechanisms: the good, the better and the best. *Knowl Eng Rev* 2013; **28**(3)**:** 249-271.

311. James OG, Doraiswamy PM, Borges-Neto S. PET imaging of tau pathology in Alzheimer's disease and tauopathies. *Frontiers in Neurology* 2015; **6**.

312. Su ZJ, Roncaroli F, Durrenberger PF, Coope DJ, Karabatsou K, Hinz R *et al.* The 18-kDa Mitochondrial Translocator Protein in Human Gliomas: An C-11-(R)PK11195 PET Imaging and Neuropathology Study. *Journal of Nuclear Medicine* 2015; **56**(4)**:** 512-517.

313. Arora A, Bhagat N. Insight into the Molecular Imaging of Alzheimer's Disease. *International Journal of Biomedical Imaging* 2016.

314. Carter SF, Scholl M, Almkvist O, Wall A, Engler H, Langstrom B *et al.* Evidence for Astrocytosis in Prodromal Alzheimer Disease Provided by C-11-Deuterium-L-Deprenyl: A Multitracer PET Paradigm Combining C-11-

Pittsburgh Compound B and F-18-FDG. *Journal of Nuclear Medicine* 2012; **53**(1)**:** 37-46.

315. Okello A, Edison P, Archer HA, Turkheimer FE, Kennedy J, Bullock R *et al.* Microglial activation and amyloid deposition in mild cognitive impairment: a PET study. *Neurology* 2009; **72**(1)**:** 56-62.

316. Yokokura M, Mori N, Yagi S, Yoshikawa E, Kikuchi M, Yoshihara Y *et al.* In vivo changes in microglial activation and amyloid deposits in brain regions with hypometabolism in Alzheimer's disease. *Eur J Nucl Med Mol Imaging* 2011; **38**(2)**:** 343-351.

317. Carter SF, Scholl M, Almkvist O, Wall A, Engler H, Langstrom B *et al.* Evidence for astrocytosis in prodromal Alzheimer disease provided by 11C-deuterium-L-deprenyl: a multitracer PET paradigm combining 11C-Pittsburgh compound B and 18F-FDG. *J Nucl Med* 2012; **53**(1)**:** 37-46.

318. Blennow K, Wallin A, Hager O. Low frequency of post-lumbar puncture headache in demented patients. *Acta Neurol Scand* 1993; **88**(3)**:** 221-223.

319. Peskind ER, Riekse R, Quinn JF, Kaye J, Clark CM, Farlow MR *et al.* Safety and acceptability of the research lumbar puncture. *Alzheimer Dis Assoc Disord* 2005; **19**(4)**:** 220-225.

320. Vanderstichele H, Bibl M, Engelborghs S, Le Bastard N, Lewczuk P, Molinuevo JL *et al.* Standardization of preanalytical aspects of cerebrospinal fluid biomarker testing for Alzheimer's disease diagnosis: a consensus paper from the Alzheimer's Biomarkers Standardization Initiative. *Alzheimers Dement* 2012; **8**(1)**:** 65-73.

321. Teunissen CE, Verwey NA, Kester MI, van Uffelen K, Blankenstein MA. Standardization of Assay Procedures for Analysis of the CSF Biomarkers Amyloid beta((1-42)), Tau, and Phosphorylated Tau in Alzheimer's Disease: Report of an International Workshop. *Int J Alzheimers Dis* 2010; **2010**.

322. Mattsson N, Zegers I, Andreasson U, Bjerke M, Blankenstein MA, Bowser R *et al.* Reference measurement procedures for Alzheimer's disease cerebrospinal fluid biomarkers: definitions and approaches with focus on amyloid beta42. *Biomark Med* 2012; **6**(4)**:** 409-417.

323. Mattsson N, Andreasson U, Persson S, Carrillo MC, Collins S, Chalbot S *et al.* CSF biomarker variability in the Alzheimer's Association quality control program. *Alzheimers Dement* 2013; **9**(3)**:** 251-261.

324. Carrillo MC, Blennow K, Soares H, Lewczuk P, Mattsson N, Oberoi P *et al.* Global standardization measurement of cerebral spinal fluid for Alzheimer's disease: an update from the Alzheimer's Association Global Biomarkers Consortium. *Alzheimers Dement* 2013; **9**(2)**:** 137-140.

325. Leinenbach A, Pannee J, Dulffer T, Huber A, Bittner T, Andreasson U *et al.* Mass spectrometry-based candidate reference measurement procedure for quantification of amyloid-beta in cerebrospinal fluid. *Clin Chem* 2014; **60**(7)**:** 987-994.

326. Blennow K, Hampel H. CSF markers for incipient Alzheimer's disease. *Lancet Neurol* 2003; **2**(10)**:** 605-613.

327. Jack CR, Jr., Albert MS, Knopman DS, McKhann GM, Sperling RA, Carrillo MC *et al.* Introduction to the recommendations from the National Institute on Aging-Alzheimer's Association workgroups on diagnostic guidelines for Alzheimer's disease. *Alzheimers Dement* 2011; **7**(3)**:** 257-262.

328. Schott JM, Petersen RC. New criteria for Alzheimer's disease: which, when and why? *Brain* 2015; **138**(Pt 5)**:** 1134-1137.

329. Blennow K, Dubois B, Fagan AM, Lewczuk P, de Leon MJ, Hampel H. Clinical utility of cerebrospinal fluid biomarkers in the diagnosis of early Alzheimer's disease. *Alzheimers Dement* 2015; **11**(1)**:** 58-69.

330. Strozyk D, Blennow K, White LR, Launer LJ. CSF Abeta 42 levels correlate with amyloid-neuropathology in a population-based autopsy study. *Neurology* 2003; **60**(4)**:** 652-656.

331. Andreasen N, Sjogren M, Blennow K. CSF markers for Alzheimer's disease: total tau, phospho-tau and Abeta42. *World J Biol Psychiatry* 2003; **4**(4)**:** 147-155.

332. Skoog I, Davidsson P, Aevarsson O, Vanderstichele H, Vanmechelen E, Blennow K. Cerebrospinal fluid beta-amyloid 42 is reduced before the onset of sporadic dementia: a population-based study in 85-year-olds. *Dement Geriatr Cogn Disord* 2003; **15**(3)**:** 169-176.

333. Gustafson DR, Skoog I, Rosengren L, Zetterberg H, Blennow K. Cerebrospinal fluid beta-amyloid 1-42 concentration may predict cognitive decline in older women. *J Neurol Neurosurg Psychiatry* 2007; **78**(5)**:** 461-464.

334. Stomrud E, Hansson O, Blennow K, Minthon L, Londos E. Cerebrospinal fluid biomarkers predict decline in subjective cognitive function over 3 years in healthy elderly. *Dement Geriatr Cogn Disord* 2007; **24**(2)**:** 118-124.

335. Blennow K, Wallin A, Agren H, Spenger C, Siegfried J, Vanmechelen E. Tau protein in cerebrospinal fluid: a biochemical marker for axonal degeneration in Alzheimer disease? *Mol Chem Neuropathol* 1995; **26**(3)**:** 231-245.

336. Kandimalla RJ, Prabhakar S, Wani WY, Kaushal A, Gupta N, Sharma DR *et al.* CSF p-Tau levels in the prediction of Alzheimer's disease. *Biol Open* 2013; **2**(11)**:** 1119-1124.

337. Koopman K, Le Bastard N, Martin JJ, Nagels G, De Deyn PP, Engelborghs S. Improved discrimination of autopsy-confirmed Alzheimer's disease (AD) from non-AD dementias using CSF P-tau(181P). *Neurochem Int* 2009; **55**(4)**:** 214-218.

338. Hampel H, Buerger K, Zinkowski R, Teipel SJ, Goernitz A, Andreasen N *et al.* Measurement of phosphorylated tau epitopes in the differential diagnosis of Alzheimer disease: a comparative cerebrospinal fluid study. *Arch Gen Psychiatry* 2004; **61**(1)**:** 95-102.

339. Hansson O, Zetterberg H, Buchhave P, Londos E, Blennow K, Minthon L. Association between CSF biomarkers and incipient Alzheimer's disease in patients with mild cognitive impairment: a follow-up study. *Lancet Neurol* 2006; **5**(3)**:** 228-234.

340. Masliah E. Recent advances in the understanding of the role of synaptic proteins in Alzheimer's Disease and other neurodegenerative disorders. *J Alzheimers Dis* 2001; **3**(1)**:** 121-129.

341. Scheff SW, Price DA, Schmitt FA, DeKosky ST, Mufson EJ. Synaptic alterations in CA1 in mild Alzheimer disease and mild cognitive impairment. *Neurology* 2007; **68**(18)**:** 1501-1508.

342. Thorsell A, Bjerke M, Gobom J, Brunhage E, Vanmechelen E, Andreasen N *et al.* Neurogranin in cerebrospinal fluid as a marker of synaptic degeneration in Alzheimer's disease. *Brain Res* 2010; **1362:** 13-22.

343. Kvartsberg H, Duits FH, Ingelsson M, Andreasen N, Ohrfelt A, Andersson K *et al.* Cerebrospinal fluid levels of the synaptic protein neurogranin correlates with cognitive decline in prodromal Alzheimer's disease. *Alzheimers Dement* 2015; **11**(10)**:** 1180-1190.

344. Hellwig K, Kvartsberg H, Portelius E, Andreasson U, Oberstein TJ, Lewczuk P *et al.* Neurogranin and YKL-40: independent markers of synaptic degeneration and neuroinflammation in Alzheimer's disease. *Alzheimers Res Ther* 2015; **7:** 74.

345. Brinkmalm A, Brinkmalm G, Honer WG, Frolich L, Hausner L, Minthon L *et al.* SNAP-25 is a promising novel cerebrospinal fluid biomarker for synapse degeneration in Alzheimer's disease. *Mol Neurodegener* 2014; **9:** 53.

346. Hall S, Ohrfelt A, Constantinescu R, Andreasson U, Surova Y, Bostrom F *et al.* Accuracy of a panel of 5 cerebrospinal fluid biomarkers in the differential diagnosis of patients with dementia and/or parkinsonian disorders. *Arch Neurol* 2012; **69**(11)**:** 1445-1452.

347. Scherling CS, Hall T, Berisha F, Klepac K, Karydas A, Coppola G *et al.* Cerebrospinal fluid neurofilament concentration reflects disease severity in frontotemporal degeneration. *Ann Neurol* 2014; **75**(1)**:** 116-126.

348. Skillback T, Farahmand B, Bartlett JW, Rosen C, Mattsson N, Nagga K *et al.* CSF neurofilament light differs in neurodegenerative diseases and predicts severity and survival. *Neurology* 2014; **83**(21)**:** 1945-1953.

349. Brettschneider J, Petzold A, Sussmuth SD, Ludolph AC, Tumani H. Axonal damage markers in cerebrospinal fluid are increased in ALS. *Neurology* 2006; **66**(6)**:** 852-856.

350. Olsson B, Lautner R, Andreasson U, Ohrfelt A, Portelius E, Bjerke M *et al.* CSF and blood biomarkers for the diagnosis of Alzheimer's disease: a systematic review and meta-analysis. *Lancet Neurol* 2016; **15**(7)**:** 673-684.

351. Suarez-Calvet M, Araque Caballero MA, Kleinberger G, Bateman RJ, Fagan AM, Morris JC *et al.* Early changes in CSF sTREM2 in dominantly inherited Alzheimer's disease occur after amyloid deposition and neuronal injury. *Sci Transl Med* 2016; **8**(369)**:** 369ra178.

352. O'Bryant SE, Edwards M, Johnson L, Hall J, Villarreal AE, Britton GB *et al.* A blood screening test for Alzheimer's disease. *Alzheimers Dement (Amst)* 2016; **3:** 83-90.

353. Villarreal AE, O'Bryant SE, Edwards M, Grajales S, Britton GB. Serum-based protein profiles of Alzheimer's disease and mild cognitive impairment in elderly Hispanics. *Neurodegener Dis Manag* 2016; **6**(3)**:** 203-213.

354. Hakobyan S, Harding K, Aiyaz M, Hye A, Dobson R, Baird A *et al.* Complement Biomarkers as Predictors of Disease Progression in Alzheimer's Disease. *Journal of Alzheimers Disease* 2016; **54**(2)**:** 707-716.

355. Doecke JD, Laws SM, Faux NG, Wilson W, Burnham SC, Lam CP *et al.* Blood-based protein biomarkers for diagnosis of Alzheimer disease. *Arch Neurol* 2012; **69**(10)**:** 1318-1325.

356. Leung R, Proitsi P, Simmons A, Lunnon K, Guntert A, Kronenberg D *et al.* Inflammatory proteins in plasma are associated with severity of Alzheimer's disease. *PLoS One* 2013; **8**(6)**:** e64971.

357. Hye A, Riddoch-Contreras J, Baird AL, Ashton NJ, Bazenet C, Leung R *et al.* Plasma proteins predict conversion to dementia from prodromal disease. *Alzheimers Dement* 2014; **10**(6)**:** 799-807 e792.

358. Rissin DM, Kan CW, Campbell TG, Howes SC, Fournier DR, Song L *et al.* Single-molecule enzyme-linked immunosorbent assay detects serum proteins at subfemtomolar concentrations. *Nature Biotechnology* 2010; **28**(6)**:** 595-599.

359. Zetterberg H, Wilson D, Andreasson U, Minthon L, Blennow K, Randall J *et al.* Plasma tau levels in Alzheimer's disease. *Alzheimers Res Ther* 2013; **5**(2)**:** 9.

360. Mattsson N, Zetterberg H, Janelidze S, Insel PS, Andreasson U, Stomrud E *et al.* Plasma tau in Alzheimer disease. *Neurology* 2016; **87**(17)**:** 1827-1835.

361. Kuhle J, Barro C, Andreasson U, Derfuss T, Lindberg R, Sandelius A *et al.* Comparison of three analytical platforms for quantification of the neurofilament light chain in blood samples: ELISA, electrochemiluminescence immunoassay and Simoa. *Clin Chem Lab Med* 2016; **54**(10)**:** 1655-1661.

362. Janelidze S, Stomrud E, Palmqvist S, Zetterberg H, van Westen D, Jeromin A *et al.* Plasma beta-amyloid in Alzheimer's disease and vascular disease. *Sci Rep* 2016; **6:** 26801.

363. Gisslen M, Price RW, Andreasson U, Norgren N, Nilsson S, Hagberg L *et al.* Plasma Concentration of the Neurofilament Light Protein (NFL) is a Biomarker of CNS Injury in HIV Infection: A Cross-Sectional Study. *EBioMedicine* 2016; **3:** 135-140.

364. Ljungqvist J, Zetterberg H, Mitsis M, Blennow K, Skoglund T. Serum Neurofilament Light Protein as a Marker for Diffuse Axonal Injury: Results from a Case Series Study. *J Neurotrauma* 2016.

365. Baird AL, Westwood S, Lovestone S. Blood-Based Proteomic Biomarkers of Alzheimer's Disease Pathology. *Front Neurol* 2015; **6:** 236.

366. Sattlecker M, Kiddle SJ, Newhouse S, Proitsi P, Nelson S, Williams S *et al.* Alzheimer's disease biomarker discovery using SOMAscan multiplexed protein technology. *Alzheimers Dement* 2014; **10**(6)**:** 724-734.

367. Kiddle SJ, Steves CJ, Mehta M, Simmons A, Xu X, Newhouse S *et al.* Plasma protein biomarkers of Alzheimer's disease endophenotypes in asymptomatic older twins: early cognitive decline and regional brain volumes. *Transl Psychiat* 2015; **5**.

368. Thompson A, Schafer J, Kuhn K, Kienle S, Schwarz J, Schmidt G *et al.* Tandem mass tags: a novel quantification strategy for comparative analysis of complex protein mixtures by MS/MS. *Anal Chem* 2003; **75**(8)**:** 1895-1904.

369. Nanjappa V, Thomas JK, Marimuthu A, Muthusamy B, Radhakrishnan A, Sharma R *et al.* Plasma Proteome Database as a resource for proteomics research: 2014 update. *Nucleic Acids Res* 2014; **42**(Database issue)**:** D959-965.

370. Guntert A, Campbell J, Saleem M, O'Brien DP, Thompson AJ, Byers HL *et al.* Plasma gelsolin is decreased and correlates with rate of decline in Alzheimer's disease. *J Alzheimers Dis* 2010; **21**(2)**:** 585-596.

371. Song F, Poljak A, Kochan NA, Raftery M, Brodaty H, Smythe GA *et al.* Plasma protein profiling of Mild Cognitive Impairment and Alzheimer's disease using iTRAQ quantitative proteomics. *Proteome Sci* 2014; **12**(1)**:** 5.

372. Hye A, Lynham S, Thambisetty M, Causevic M, Campbell J, Byers HL *et al.* Proteome-based plasma biomarkers for Alzheimer's disease. *Brain* 2006; **129**(Pt 11)**:** 3042-3050.

373. Thambisetty M, Tripaldi R, Riddoch-Contreras J, Hye A, An Y, Campbell J *et al.* Proteome-based plasma markers of brain amyloid-beta deposition in non-demented older individuals. *J Alzheimers Dis* 2010; **22**(4)**:** 1099-1109.

374. Ashton NJ, Kiddle SJ, Graf J, Ward M, Baird AL, Hye A *et al.* Blood protein predictors of brain amyloid for enrichment in clinical trials? *Alzheimers Dement (Amst)* 2015; **1**(1)**:** 48-60.

375. Westwood S, Leoni E, Hye A, Lynham S, Khondoker MR, Ashton NJ *et al.* Blood-Based Biomarker Candidates of Cerebral Amyloid Using PiB PET in Non-Demented Elderly. *J Alzheimers Dis* 2016; **52**(2)**:** 561-572.

376. Song F, Poljak A, Valenzuela M, Mayeux R, Smythe GA, Sachdev PS. Meta-analysis of plasma amyloid-beta levels in Alzheimer's disease. *J Alzheimers Dis* 2011; **26**(2)**:** 365-375.

377. Koyama A, Okereke OI, Yang T, Blacker D, Selkoe DJ, Grodstein F. Plasma amyloid-beta as a predictor of dementia and cognitive decline: a systematic review and meta-analysis. *Arch Neurol* 2012; **69**(7)**:** 824-831.

378. Olsson B, Lautner R, Andreasson U, Ohrfelt A, Portelius E, Bjerke M *et al.* CSF and blood biomarkers for the diagnosis of Alzheimer's disease: a systematic review and meta-analysis. *Lancet Neurology* 2016; **15**(7)**:** 673-684.

379. Locascio JJ, Fukumoto H, Yap L, Bottiglieri T, Growdon JH, Hyman BT *et al.* Plasma amyloid beta-protein and C-reactive protein in relation to the rate of progression of Alzheimer disease. *Arch Neurol* 2008; **65**(6)**:** 776-785.

380. Rembach A, Faux NG, Watt AD, Pertile KK, Rumble RL, Trounson BO *et al.* Changes in plasma amyloid beta in a longitudinal study of aging and Alzheimer's disease. *Alzheimers Dement* 2014; **10**(1)**:** 53-61.

381. Fei M, Jianghua W, Rujuan M, Wei Z, Qian W. The relationship of plasma Abeta levels to dementia in aging individuals with mild cognitive impairment. *J Neurol Sci* 2011; **305**(1-2)**:** 92-96.

382. Blasko I, Jungwirth S, Jellinger K, Kemmler G, Krampla W, Weissgram S *et al.* Effects of medications on plasma amyloid beta (Abeta) 42: longitudinal data from the VITA cohort. *J Psychiatr Res* 2008; **42**(11)**:** 946-955.

383. Mayeux R, Honig LS, Tang MX, Manly J, Stern Y, Schupf N *et al.* Plasma A[beta]40 and A[beta]42 and Alzheimer's disease: relation to age, mortality, and risk. *Neurology* 2003; **61**(9)**:** 1185-1190.

384. Chouraki V, Beiser A, Younkin L, Preis SR, Weinstein G, Hansson O *et al.* Plasma amyloid-beta and risk of Alzheimer's disease in the Framingham Heart Study. *Alzheimers Dement* 2015; **11**(3)**:** 249-257 e241.

385. Abdullah L, Paris D, Luis C, Quadros A, Parrish J, Valdes L *et al.* The influence of diagnosis, intra- and inter-person variability on serum and plasma Abeta levels. *Neurosci Lett* 2007; **428**(2-3)**:** 53-58.

386. Buerger K, Frisoni G, Uspenskaya O, Ewers M, Zetterberg H, Geroldi C *et al.* Validation of Alzheimer's disease CSF and plasma biological markers: the multicentre reliability study of the pilot European Alzheimer's Disease Neuroimaging Initiative (E-ADNI). *Exp Gerontol* 2009; **44**(9)**:** 579-585.

387. Ghersi-Egea JF, Gorevic PD, Ghiso J, Frangione B, Patlak CS, Fenstermacher JD. Fate of cerebrospinal fluid-borne amyloid beta-peptide: rapid clearance into blood and appreciable accumulation by cerebral arteries. *J Neurochem* 1996; **67**(2)**:** 880-883.

388. Freeman SH, Raju S, Hyman BT, Frosch MP, Irizarry MC. Plasma Abeta levels do not reflect brain Abeta levels. *J Neuropathol Exp Neurol* 2007; **66**(4)**:** 264-271.

389. Devanand DP, Schupf N, Stern Y, Parsey R, Pelton GH, Mehta P *et al.* Plasma Abeta and PET PiB binding are inversely related in mild cognitive impairment. *Neurology* 2011; **77**(2)**:** 125-131.

390. Tzen KY, Yang SY, Chen TF, Cheng TW, Horng HE, Wen HP *et al.* Plasma Abeta but not tau is related to brain PiB retention in early Alzheimer's disease. *ACS Chem Neurosci* 2014; **5**(9)**:** 830-836.

391. Huang Y, Potter R, Sigurdson W, Kasten T, Connors R, Morris JC *et al.* beta-amyloid dynamics in human plasma. *Arch Neurol* 2012; **69**(12)**:** 1591-1597.

392. Bjerner J, Bormer OP, Nustad K. The war on heterophilic antibody interference. *Clin Chem* 2005; **51**(1)**:** 9-11.

393. Lui JK, Laws SM, Li QX, Villemagne VL, Ames D, Brown B *et al.* Plasma amyloid-beta as a biomarker in Alzheimer's disease: the AIBL study of aging. *J Alzheimers Dis* 2010; **20**(4)**:** 1233-1242.

394. Randall J, Mortberg E, Provuncher GK, Fournier DR, Duffy DC, Rubertsson S *et al.* Tau proteins in serum predict neurological outcome after hypoxic brain injury from cardiac arrest: results of a pilot study. *Resuscitation* 2013; **84**(3)**:** 351-356.

395. Chiu MJ, Yang SY, Horng HE, Yang CC, Chen TF, Chieh JJ *et al.* Combined plasma biomarkers for diagnosing mild cognition impairment and Alzheimer's disease. *ACS Chem Neurosci* 2013; **4**(12)**:** 1530-1536.

396. Chiu MJ, Chen YF, Chen TF, Yang SY, Yang FP, Tseng TW *et al.* Plasma tau as a window to the brain-negative associations with brain volume and memory function in mild cognitive impairment and early Alzheimer's disease. *Hum Brain Mapp* 2014; **35**(7)**:** 3132-3142.

397. Sparks DL, Kryscio RJ, Sabbagh MN, Ziolkowski C, Lin Y, Sparks LM *et al.* Tau is reduced in AD plasma and validation of employed ELISA methods. *Am J Neurodegener Dis* 2012; **1**(1)**:** 99-106.

398. Krishnan S, Rani P. Evaluation of selenium, redox status and their association with plasma amyloid/tau in Alzheimer's disease. *Biol Trace Elem Res* 2014; **158**(2)**:** 158-165.

399. Wang T, Xiao S, Liu Y, Lin Z, Su N, Li X *et al.* The efficacy of plasma biomarkers in early diagnosis of Alzheimer's disease. *Int J Geriatr Psychiatry* 2014; **29**(7)**:** 713-719.

400. Henriksen K, Byrjalsen I, Christiansen C, Karsdal MA. Relationship between serum levels of tau fragments and clinical progression of Alzheimer's disease. *J Alzheimers Dis* 2015; **43**(4)**:** 1331-1341.

401. Diamandis EP, Yousef GM, Petraki C, Soosaipillai AR. Human kallikrein 6 as a biomarker of alzheimer's disease. *Clin Biochem* 2000; **33**(8)**:** 663-667.

402. Kalman J, Marki-Zay J, Juhasz A, Santha A, Dux L, Janka Z. Serum and cerebrospinal fluid cystatin C levels in vascular and Alzheimer's dementia. *Acta Neurol Scand* 2000; **101**(4)**:** 279-282.

403. Licastro F, Pedrini S, Davis LJ, Caputo L, Tagliabue J, Savorani G *et al.* Alpha-1-antichymotrypsin and oxidative stress in the peripheral blood from patients with probable Alzheimer disease: a short-term longitudinal study. *Alzheimer Dis Assoc Disord* 2001; **15**(1)**:** 51-55.

404. van Oijen M, Witteman JC, Hofman A, Koudstaal PJ, Breteler MMB. Fibrinogen is associated with an increased risk of Alzheimer disease and vascular dementia. *Stroke* 2005; **36**(12)**:** 2637-2641.

405. Liu HC, Hu CJ, Chang JG, Sung SM, Lee LS, Yuan RY *et al.* Proteomic identification of lower apolipoprotein A-I in Alzheimer's disease. *Dement Geriatr Cogn Disord* 2006; **21**(3)**:** 155-161.

406. Laske C, Leyhe T, Stransky E, Hoffmann N, Fallgatter AJ, Dietzsch J. Identification of a blood-based biomarker panel for classification of Alzheimer's disease. *Int J Neuropsychopharmacol* 2011; **14**(9)**:** 1147-1155.

407. Han X, Rozen S, Boyle SH, Hellegers C, Cheng H, Burke JR *et al.* Metabolomics in early Alzheimer's disease: identification of altered plasma sphingolipidome using shotgun lipidomics. *PLoS One* 2011; **6**(7)**:** e21643.

408. Ijsselstijn L, Dekker LJ, Stingl C, van der Weiden MM, Hofman A, Kros JM *et al.* Serum levels of pregnancy zone protein are elevated in presymptomatic Alzheimer's disease. *J Proteome Res* 2011; **10**(11)**:** 4902-4910.

409. Teunissen CE, Veerhuis R, De Vente J, Verhey FR, Vreeling F, van Boxtel MP *et al.* Brain-specific fatty acid-binding protein is elevated in serum of patients with dementia-related diseases. *Eur J Neurol* 2011; **18**(6)**:** 865-871.

410. Sun L, Tan MS, Hu N, Yu JT, Tan L. Exploring the value of plasma BIN1 as a potential biomarker for alzheimer's disease. *J Alzheimers Dis* 2013; **37**(2)**:** 291-295.

411. Muenchhoff J, Poljak A, Song F, Raftery M, Brodaty H, Duncan M *et al.* Plasma protein profiling of mild cognitive impairment and Alzheimer's disease across two independent cohorts. *J Alzheimers Dis* 2015; **43**(4)**:** 1355-1373.

412. Akuffo EL, Davis JB, Fox SM, Gloger IS, Hosford D, Kinsey EE *et al.* The discovery and early validation of novel plasma biomarkers in mild-to-moderate Alzheimer's disease patients responding to treatment with rosiglitazone. *Biomarkers* 2008; **13**(6)**:** 618-636.

413. Cutler P, Akuffo EL, Bodnar WM, Briggs DM, Davis JB, Debouck CM *et al.* Proteomic identification and early validation of complement 1 inhibitor and pigment epithelium-derived factor: Two novel biomarkers of Alzheimer's disease in human plasma. *Proteomics Clin Appl* 2008; **2**(4)**:** 467-477.

414. Johnstone D, Milward EA, Berretta R, Moscato P. Multivariate protein signatures of pre-clinical Alzheimer's disease in the Alzheimer's disease neuroimaging initiative (ADNI) plasma proteome dataset. *PLoS One* 2012; **7**(4)**:** e34341.

415. Gomez Ravetti M, Moscato P. Identification of a 5-protein biomarker molecular signature for predicting Alzheimer's disease. *PLoS One* 2008; **3**(9)**:** e3111.

416. O'Bryant SE, Hobson VL, Hall JR, Barber RC, Zhang S, Johnson L *et al.* Serum brain-derived neurotrophic factor levels are specifically associated with memory performance among Alzheimer's disease cases. *Dement Geriatr Cogn Disord* 2011; **31**(1)**:** 31-36.

417. Hu WT, Holtzman DM, Fagan AM, Shaw LM, Perrin R, Arnold SE *et al.* Plasma multianalyte profiling in mild cognitive impairment and Alzheimer disease. *Neurology* 2012; **79**(9)**:** 897-905.

418. Zhang J, Jia J, Qin W, Wang S. Combination of plasma tumor necrosis factor receptors signaling proteins, beta-amyloid and apolipoprotein E for the detection of Alzheimer's disease. *Neurosci Lett* 2013; **541:** 99-104.

419. Marksteiner J, Imarhiagbe D, Defrancesco M, Deisenhammer EA, Kemmler G, Humpel C. Analysis of 27 vascular-related proteins reveals that NT-proBNP is a potential biomarker for Alzheimer's disease and mild cognitive impairment: a pilot-study. *Exp Gerontol* 2014; **50:** 114-121.

420. Agarwal S, Ghanty P, Pal NR. Identification of a small set of plasma signalling proteins using neural network for prediction of Alzheimer's disease. *Bioinformatics* 2015; **31**(15)**:** 2505-2513.

421. Ray S, Britschgi M, Herbert C, Takeda-Uchimura Y, Boxer A, Blennow K *et al.* Classification and prediction of clinical Alzheimer's diagnosis based on plasma signaling proteins. *Nat Med* 2007; **13**(11)**:** 1359-1362.

422. Bazenet C, Lovestone S. Plasma biomarkers for Alzheimer's disease: much needed but tough to find. *Biomark Med* 2012; **6**(4)**:** 441-454.

423. Soares HD, Chen Y, Sabbagh M, Roher A, Schrijvers E, Breteler M. Identifying early markers of Alzheimer's disease using quantitative multiplex proteomic immunoassay panels. *Ann N Y Acad Sci* 2009; **1180:** 56-67.

424. Marksteiner J, Kemmler G, Weiss EM, Knaus G, Ullrich C, Mechtcheriakov S *et al.* Five out of 16 plasma signaling proteins are enhanced in plasma of patients with mild cognitive impairment and Alzheimer's disease. *Neurobiol Aging* 2011; **32**(3)**:** 539-540.

425. Bjorkqvist M, Ohlsson M, Minthon L, Hansson O. Evaluation of a previously suggested plasma biomarker panel to identify Alzheimer's disease. *PLoS One* 2012; **7**(1)**:** e29868.

426. Yang H, Lyutvinskiy Y, Herukka SK, Soininen H, Rutishauser D, Zubarev RA. Prognostic polypeptide blood plasma biomarkers of Alzheimer's disease progression. *J Alzheimers Dis* 2014; **40**(3)**:** 659-666.

427. Apostolova LG, Hwang KS, Avila D, Elashoff D, Kohannim O, Teng E *et al.* Brain amyloidosis ascertainment from cognitive, imaging, and peripheral blood protein measures. *Neurology* 2015; **84**(7)**:** 729-737.

428. Thambisetty M, Simmons A, Hye A, Campbell J, Westman E, Zhang Y *et al.* Plasma biomarkers of brain atrophy in Alzheimer's disease. *PLoS One* 2011; **6**(12)**:** e28527.

429. Velayudhan L, Killick R, Hye A, Kinsey A, Guntert A, Lynham S *et al.* Plasma transthyretin as a candidate marker for Alzheimer's disease. *J Alzheimers Dis* 2012; **28**(2)**:** 369-375.

430. Song F, Poljak A, Crawford J, Kochan NA, Wen W, Cameron B *et al.* Plasma apolipoprotein levels are associated with cognitive status and decline in a community cohort of older individuals. *PLoS One* 2012; **7**(6)**:** e34078.

431. Jongbloed W, van Dijk KD, Mulder SD, van de Berg WD, Blankenstein MA, van der Flier W *et al.* Clusterin Levels in Plasma Predict Cognitive Decline and Progression to Alzheimer's Disease. *J Alzheimers Dis* 2015; **46**(4)**:** 1103-1110.

432. Thambisetty M, An Y, Kinsey A, Koka D, Saleem M, Guntert A *et al.* Plasma clusterin concentration is associated with longitudinal brain atrophy in mild cognitive impairment. *Neuroimage* 2012; **59**(1)**:** 212-217.

433. Gupta VB, Doecke JD, Hone E, Pedrini S, Laws SM, Thambisetty M *et al.* Plasma apolipoprotein J as a potential biomarker for Alzheimer's disease: Australian Imaging, Biomarkers and Lifestyle study of aging. *Alzheimers Dement (Amst)* 2016; **3:** 18-26.

434. Furney SJ, Kronenberg D, Simmons A, Guntert A, Dobson RJ, Proitsi P *et al.* Combinatorial markers of mild cognitive impairment conversion to Alzheimer's disease--cytokines and MRI measures together predict disease progression. *J Alzheimers Dis* 2011; **26 Suppl 3:** 395-405.

435. Toledo JB, Da X, Bhatt P, Wolk DA, Arnold SE, Shaw LM *et al.* Relationship between plasma analytes and SPARE-AD defined brain atrophy patterns in ADNI. *PLoS One* 2013; **8**(2)**:** e55531.

436. Kiddle SJ, Thambisetty M, Simmons A, Riddoch-Contreras J, Hye A, Westman E *et al.* Plasma based markers of [11C] PiB-PET brain amyloid burden. *PLoS One* 2012; **7**(9)**:** e44260.

437. Burnham SC, Faux NG, Wilson W, Laws SM, Ames D, Bedo J *et al.* A blood-based predictor for neocortical Abeta burden in Alzheimer's disease: results from the AIBL study. *Mol Psychiatry* 2014; **19**(4)**:** 519-526.

438. Hwang KS, Lazaris AS, Eastman JA, Teng E, Thompson PM, Gylys KH *et al.* Plasma BDNF levels associate with Pittsburgh compound B binding in the brain. *Alzheimers Dement (Amst)* 2015; **1**(2)**:** 187-193.

439. Voyle N, Baker D, Burnham SC, Covin A, Zhang Z, Sangurdekar DP *et al.* Blood Protein Markers of Neocortical Amyloid-beta Burden: A Candidate Study Using SOMAscan Technology. *J Alzheimers Dis* 2015; **46**(4)**:** 947-961.

440. O'Bryant SE, Gupta V, Henriksen K, Edwards M, Jeromin A, Lista S *et al.* Guidelines for the standardization of preanalytic variables for blood-based biomarker studies in Alzheimer's disease research. *Alzheimers Dement* 2015; **11**(5)**:** 549-560.

441. Mapstone M, Cheema AK, Fiandaca MS, Zhong X, Mhyre TR, MacArthur LH *et al.* Plasma phospholipids identify antecedent memory impairment in older adults. *Nat Med* 2014; **20**(4)**:** 415-418.

442. Whiley L, Sen A, Heaton J, Proitsi P, Garcia-Gomez D, Leung R *et al.* Evidence of altered phosphatidylcholine metabolism in Alzheimer's disease. *Neurobiol Aging* 2014; **35**(2)**:** 271-278.

443. Proitsi P, Kim M, Whiley L, Simmons A, Sattlecker M, Velayudhan L *et al.* Association of blood lipids with Alzheimer's disease: A comprehensive lipidomics analysis. *Alzheimers Dement* 2016.

444. Desire L, Blondiaux E, Carriere J, Haddad R, Sol O, Fehlbaum-Beurdeley P *et al.* Blood transcriptomic biomarkers of Alzheimer's disease patients treated with EHT 0202. *J Alzheimers Dis* 2013; **34**(2)**:** 469-483.

445. Voyle N, Kim M, Proitsi P, Ashton NJ, Baird AL, Bazenet C *et al.* Blood metabolite markers of neocortical amyloid-beta burden: discovery and enrichment using candidate proteins. *Transl Psychiatry* 2016; **6:** e719.

446. Ellis KA, Bush AI, Darby D, De Fazio D, Foster J, Hudson P *et al.* The Australian Imaging, Biomarkers and Lifestyle (AIBL) study of aging: methodology and baseline characteristics of 1112 individuals recruited for a longitudinal study of Alzheimer's disease. *Int Psychogeriatr* 2009; **21**(4)**:** 672-687.

447. Pike KE, Savage G, Villemagne VL, Ng S, Moss SA, Maruff P *et al.* Beta-amyloid imaging and memory in non-demented individuals: evidence for preclinical Alzheimer's disease. *Brain* 2007; **130**(Pt 11)**:** 2837-2844.

448. Rowe CC, Ng S, Ackermann U, Gong SJ, Pike K, Savage G *et al.* Imaging beta-amyloid burden in aging and dementia. *Neurology* 2007; **68**(20)**:** 1718-1725.

449. Folstein MF, Folstein SE, McHugh PR. "Mini-mental state". A practical method for grading the cognitive state of patients for the clinician. *J Psychiatr Res* 1975; **12**(3)**:** 189-198.

450. Morris JC. The Clinical Dementia Rating (CDR): current version and scoring rules. *Neurology* 1993; **43**(11)**:** 2412-2414.

451. Rabinovici GD, Rosen HJ, Alkalay A, Kornak J, Furst AJ, Agarwal N *et al.* Amyloid vs FDG-PET in the differential diagnosis of AD and FTLD. *Neurology* 2011; **77**(23)**:** 2034-2042.

452. Bettcher BM, Watson CL, Walsh CM, Lobach IV, Neuhaus J, Miller JW *et al.* Interleukin-6, age, and corpus callosum integrity. *PLoS One* 2014; **9**(9)**:** e106521.

453. Woolley JD, Strobl EV, Shelly WB, Karydas AM, Ketelle RNR, Wolkowitz OM *et al.* BDNF Serum Concentrations Show No Relationship with Diagnostic Group or Medication Status in Neurodegenerative Disease. *Current Alzheimer Research* 2012; **9**(7)**:** 815-821.

454. Mulder C, Verwey NA, van der Flier WM, Bouwman FH, Kok A, van Elk EJ *et al.* Amyloid-beta(1-42), Total Tau, and Phosphorylated Tau as Cerebrospinal Fluid Biomarkers for the Diagnosis of Alzheimer Disease. *Clinical Chemistry* 2010; **56**(2)**:** 248-253.

455. Olsen JV, Schwartz JC, Griep-Raming J, Nielsen ML, Damoc E, Denisov E *et al.* A Dual Pressure Linear Ion Trap Orbitrap Instrument with Very High Sequencing Speed. *Molecular & Cellular Proteomics* 2009; **8**(12)**:** 2759-2769.

456. Carrillo B, Yanofsky C, Laboissiere S, Nadon R, Kearney RE. Methods for combining peptide intensities to estimate relative protein abundance. *Bioinformatics* 2010; **26**(1)**:** 98-103.

457. Tabb DL, Friedman DB, Ham AJ. Verification of automated peptide identifications from proteomic tandem mass spectra. *Nat Protoc* 2006; **1**(5)**:** 2213-2222.

458. Kuhn DJ, Hunsucker SA, Chen Q, Voorhees PM, Orlowski M, Orlowski RZ. Targeted inhibition of the immunoproteasome is a potent strategy against models of multiple myeloma that overcomes resistance to conventional drugs and nonspecific proteasome inhibitors. *Blood* 2009; **113**(19)**:** 4667-4676.

459. Sing T, Sander O, Beerenwinkel N, Lengauer T. ROCR: visualizing classifier performance in R. *Bioinformatics* 2005; **21**(20)**:** 3940-3941.

460. Huang DW, Sherman BT, Lempicki RA. Bioinformatics enrichment tools: paths toward the comprehensive functional analysis of large gene lists. *Nucleic Acids Research* 2009; **37**(1)**:** 1-13.

461. Huang DW, Sherman BT, Lempicki RA. Systematic and integrative analysis of large gene lists using DAVID bioinformatics resources. *Nature Protocols* 2009; **4**(1)**:** 44-57.

462. Ogata H, Goto S, Sato K, Fujibuchi W, Bono H, Kanehisa M. KEGG: Kyoto Encyclopedia of Genes and Genomes. *Nucleic Acids Research* 1999; **27**(1)**:** 29-34.

463. Schenk S, Schoenhals GJ, de Souza G, Mann M. A high confidence, manually validated human blood plasma protein reference set. *BMC Med Genomics* 2008; **1:** 41.

464. Villemagne VL, Burnham S, Bourgeat P, Brown B, Ellis KA, Salvado O *et al.* Amyloid beta deposition, neurodegeneration, and cognitive decline in sporadic Alzheimer's disease: a prospective cohort study. *Lancet Neurol* 2013; **12**(4)**:** 357-367.

465. Sabri O, Seibyl J, Rowe C, Barthel H. Beta-amyloid imaging with florbetaben. *Clin Transl Imaging* 2015; **3**(1)**:** 13-26.

466. Nordberg A, Rinne JO, Kadir A, Langstrom B. The use of PET in Alzheimer disease. *Nat Rev Neurol* 2010; **6**(2)**:** 78-87.

467. Jagust WJ, Landau SM, Shaw LM, Trojanowski JQ, Koeppe RA, Reiman EM *et al.* Relationships between biomarkers in aging and dementia. *Neurology* 2009; **73**(15)**:** 1193-1199.

468. Scheinin NM, Aalto S, Koikkalainen J, Lotjonen J, Karrasch M, Kemppainen N *et al.* Follow-up of [11C]PIB uptake and brain volume in patients with Alzheimer disease and controls. *Neurology* 2009; **73**(15)**:** 1186-1192.

469. Blennow K, Hampel H, Zetterberg H. Biomarkers in amyloid-beta immunotherapy trials in Alzheimer's disease. *Neuropsychopharmacology* 2014; **39**(1)**:** 189-201.

470. Sperling RA, Rentz DM, Johnson KA, Karlawish J, Donohue M, Salmon DP *et al.* The A4 Study: Stopping AD Before Symptoms Begin? *Science Translational Medicine* 2014; **6**(228).

471. Soares HD, Potter WZ, Pickering E, Kuhn M, Immermann FW, Shera DM *et al.* Plasma biomarkers associated with the apolipoprotein E genotype and Alzheimer disease. *Arch Neurol* 2012; **69**(10)**:** 1310-1317.

472. Petersen RC, Smith GE, Waring SC, Ivnik RJ, Tangalos EG, Kokmen E. Mild cognitive impairment: clinical characterization and outcome. *Arch Neurol* 1999; **56**(3)**:** 303-308.

473. Neary D, Snowden JS, Gustafson L, Passant U, Stuss D, Black S *et al.* Frontotemporal lobar degeneration: a consensus on clinical diagnostic criteria. *Neurology* 1998; **51**(6)**:** 1546-1554.

474. Fagan AM, Mintun MA, Mach RH, Lee SY, Dence CS, Shah AR *et al.* Inverse relation between in vivo amyloid imaging load and cerebrospinal fluid Abeta42 in humans. *Ann Neurol* 2006; **59**(3)**:** 512-519.

475. Zwan M, van Harten A, Ossenkoppele R, Bouwman F, Teunissen C, Adriaanse S *et al.* Concordance between cerebrospinal fluid biomarkers and [11C]PIB PET in a memory clinic cohort. *J Alzheimers Dis* 2014; **41**(3)**:** 801-807.

476. Leuzy A, Carter SF, Chiotis K, Almkvist O, Wall A, Nordberg A. Concordance and Diagnostic Accuracy of [11C]PIB PET and Cerebrospinal Fluid Biomarkers in a Sample of Patients with Mild Cognitive Impairment and Alzheimer's Disease. *J Alzheimers Dis* 2015; **45**(4)**:** 1077-1088.

477. Mattsson N, Insel PS, Landau S, Jagust W, Donohue M, Shaw LM *et al.* Diagnostic accuracy of CSF Ab42 and florbetapir PET for Alzheimer's disease. *Ann Clin Transl Neurol* 2014; **1**(8)**:** 534-543.

478. Vlassenko A, Fagan A, Jasielec M, Su Y, Xiong CJ, Holtzman D *et al.* Relationship between brain A beta deposition and CSF A beta 42 several years prior to amyloid positivity. *Journal of Nuclear Medicine* 2014; **55**.

479. Racine AM, Koscik RL, Nicholas CR, Clark LR, Okonkwo OC, Oh JM *et al.* Cerebrospinal fluid ratios with Abeta42 predict preclinical brain beta-amyloid accumulation. *Alzheimers Dement (Amst)* 2016; **2:** 27-38.

480. Mulder C, Verwey NA, van der Flier WM, Bouwman FH, Kok A, van Elk EJ *et al.* Amyloid-beta(1-42), total tau, and phosphorylated tau as cerebrospinal fluid biomarkers for the diagnosis of Alzheimer disease. *Clin Chem* 2010; **56**(2)**:** 248-253.

481. Sevigny J, Chiao P, Bussiere T, Weinreb PH, Williams L, Maier M *et al.* The antibody aducanumab reduces Abeta plaques in Alzheimer's disease. *Nature* 2016; **537**(7618)**:** 50-56.

482. Blacker D, Haines JL, Rodes L, Terwedow H, Go RC, Harrell LE *et al.* ApoE-4 and age at onset of Alzheimer's disease: the NIMH genetics initiative. *Neurology* 1997; **48**(1)**:** 139-147.

483. Xu G, Zhang H, Zhang S, Fan X, Liu X. Plasma fibrinogen is associated with cognitive decline and risk for dementia in patients with mild cognitive impairment. *International Journal of Clinical Practice* 2008; **62**(7)**:** 1070-1075.

484. Cortes-Canteli M, Zamolodchikov D, Ahn HJ, Strickland S, Norris EH. Fibrinogen and Altered Hemostasis in Alzheimer's Disease. *Journal of Alzheimers Disease* 2012; **32**(3)**:** 599-608.

485. Ryu JK, McLarnon JG. A leaky blood-brain barrier, fibrinogen infiltration and microglial reactivity in inflamed Alzheimer's disease brain. *J Cell Mol Med* 2009; **13**(9A)**:** 2911-2925.

486. Paul J, Strickland S, Melchor JP. Fibrin deposition accelerates neurovascular damage and neuroinflammation in mouse models of Alzheimer's disease. *J Exp Med* 2007; **204**(8)**:** 1999-2008.

487. Marques F, Sousa JC, Sousa N, Palha JA. Blood-brain-barriers in aging and in Alzheimer's disease. *Mol Neurodegener* 2013; **8:** 38.

488. Sagare A, Deane R, Bell RD, Johnson B, Hamm K, Pendu R *et al.* Clearance of amyloid-beta by circulating lipoprotein receptors. *Nat Med* 2007; **13**(9)**:** 1029-1031.

489. Cortes-Canteli M, Paul J, Norris EH, Bronstein R, Ahn HJ, Zamolodchikov D *et al.* Fibrinogen and beta-amyloid association alters thrombosis and fibrinolysis: a possible contributing factor to Alzheimer's disease. *Neuron* 2010; **66**(5)**:** 695-709.

490. Klohs J, Baltes C, Princz-Kranz F, Ratering D, Nitsch RM, Knuesel I *et al.* Contrast-enhanced magnetic resonance microangiography reveals remodeling of the cerebral microvasculature in transgenic ArcAbeta mice. *J Neurosci* 2012; **32**(5)**:** 1705-1713.

491. Ahn HJ, Zamolodchikov D, Cortes-Canteli M, Norris EH, Glickman JF, Strickland S. Alzheimer's disease peptide beta-amyloid interacts with fibrinogen and induces its oligomerization. *Proc Natl Acad Sci U S A* 2010; **107**(50)**:** 21812-21817.

492. Lee JW, Namkoong H, Kim HK, Kim S, Hwang DW, Na HR *et al.* Fibrinogen gamma-A chain precursor in CSF: a candidate biomarker for Alzheimer's disease. *BMC Neurol* 2007; **7:** 14.

493. Bauer J, Strauss S, Schreitergasser U, Ganter U, Schlegel P, Witt I *et al.* Interleukin-6 and Alpha-2-Macroglobulin Indicate an Acute-Phase State in Alzheimers-Disease Cortices. *Febs Letters* 1991; **285**(1)**:** 111-114.

494. Du Y, Ni B, Glinn M, Dodel RC, Bales KR, Zhang Z *et al.* alpha2-Macroglobulin as a beta-amyloid peptide-binding plasma protein. *J Neurochem* 1997; **69**(1)**:** 299-305.

495. Hughes SR, Khorkova O, Goyal S, Knaeblein J, Heroux J, Riedel NG *et al.* Alpha2-macroglobulin associates with beta-amyloid peptide and prevents fibril formation. *Proc Natl Acad Sci U S A* 1998; **95**(6)**:** 3275-3280.

496. Kovacs DM. alpha2-macroglobulin in late-onset Alzheimer's disease. *Exp Gerontol* 2000; **35**(4)**:** 473-479.

497. Saunders AJ, Bertram L, Mullin K, Sampson AJ, Latifzai K, Basu S *et al.* Genetic association of Alzheimer's disease with multiple polymorphisms in alpha-2-macroglobulin. *Hum Mol Genet* 2003; **12**(21)**:** 2765-2776.

498. Levinson SS, Miller JJ. Towards a better understanding of heterophile (and the like) antibody interference with modern immunoassays. *Clin Chim Acta* 2002; **325**(1-2)**:** 1-15.

499. Vanderstichele H, Stoops E, Vanmechelen E, Jeromin A. Potential sources of interference on Abeta immunoassays in biological samples. *Alzheimers Res Ther* 2012; **4**(5)**:** 39.

500. Sehlin D, Sollvander S, Paulie S, Brundin R, Ingelsson M, Lannfelt L *et al.* Interference from heterophilic antibodies in amyloid-beta oligomer ELISAs. *J Alzheimers Dis* 2010; **21**(4)**:** 1295-1301.

501. Anderson NL, Anderson NG. The human plasma proteome: history, character, and diagnostic prospects. *Mol Cell Proteomics* 2002; **1**(11)**:** 845-867.

502. Rifai N, Gillette MA, Carr SA. Protein biomarker discovery and validation: the long and uncertain path to clinical utility. *Nat Biotechnol* 2006; **24**(8)**:** 971-983.

503. Cao Z, Tang HY, Wang H, Liu Q, Speicher DW. Systematic comparison of fractionation methods for in-depth analysis of plasma proteomes. *J Proteome Res* 2012; **11**(6)**:** 3090-3100.

504. Whiteaker JR, Zhao L, Anderson L, Paulovich AG. An automated and multiplexed method for high throughput peptide immunoaffinity enrichment and multiple reaction monitoring mass spectrometry-based quantification of protein biomarkers. *Mol Cell Proteomics* 2010; **9**(1)**:** 184-196.

505. Gong Y, Li X, Yang B, Ying W, Li D, Zhang Y *et al.* Different immunoaffinity fractionation strategies to characterize the human plasma proteome. *J Proteome Res* 2006; **5**(6)**:** 1379-1387.

506. Bellei E, Bergamini S, Monari E, Fantoni LI, Cuoghi A, Ozben T *et al.* High-abundance proteins depletion for serum proteomic analysis: concomitant removal of non-targeted proteins. *Amino Acids* 2011; **40**(1)**:** 145-156.

507. Tu C, Rudnick PA, Martinez MY, Cheek KL, Stein SE, Slebos RJ *et al.* Depletion of abundant plasma proteins and limitations of plasma proteomics. *J Proteome Res* 2010; **9**(10)**:** 4982-4991.

508. Gianazza E, Miller I, Palazzolo L, Parravicini C, Eberini I. With or without you - Proteomics with or without major plasma/serum proteins. *J Proteomics* 2016; **140:** 62-80.

509. Geyer PE, Kulak NA, Pichler G, Holdt LM, Teupser D, Mann M. Plasma Proteome Profiling to Assess Human Health and Disease. *Cell Syst* 2016; **2**(3)**:** 185-195.

510. Roche S, Tiers L, Provansal M, Seveno M, Piva MT, Jouin P *et al.* Depletion of one, six, twelve or twenty major blood proteins before proteomic analysis: The more the better? *Journal of Proteomics* 2009; **72**(6)**:** 945-951.

511. Krishnan S, Gaspari M, Della Corte A, Bianchi P, Crescente M, Cerletti C *et al.* OFFgel-based multidimensional LC-MS/MS approach to the cataloguing of the human platelet proteome for an interactomic profile. *Electrophoresis* 2011; **32**(6-7)**:** 686-695.

512. Zhang Y, Li Y, Qiu F, Qiu Z. Comprehensive analysis of low-abundance proteins in human urinary exosomes using peptide ligand library technology, peptide OFFGEL fractionation and nanoHPLC-chip-MS/MS. *Electrophoresis* 2010; **31**(23-24)**:** 3797-3807.

513. Mena ML, Moreno-Gordaliza E, Moraleja I, Canas B, Gomez-Gomez MM. OFFGEL isoelectric focusing and polyacrylamide gel electrophoresis

separation of platinum-binding proteins. *J Chromatogr A* 2011; **1218**(9)**:** 1281-1290.

514. Manadas B, English JA, Wynne KJ, Cotter DR, Dunn MJ. Comparative analysis of OFFGel, strong cation exchange with pH gradient, and RP at high pH for first-dimensional separation of peptides from a membrane-enriched protein fraction. *Proteomics* 2009; **9**(22)**:** 5194-5198.

515. Waller LN, Shores K, Knapp DR. Shotgun proteomic analysis of cerebrospinal fluid using off-gel electrophoresis as the first-dimension separation. *J Proteome Res* 2008; **7**(10)**:** 4577-4584.

516. Hubner NC, Ren S, Mann M. Peptide separation with immobilized pI strips is an attractive alternative to in-gel protein digestion for proteome analysis. *Proteomics* 2008; **8**(23-24)**:** 4862-4872.

517. Piersma SR, Fiedler U, Span S, Lingnau A, Pham TV, Hoffmann S *et al.* Workflow comparison for label-free, quantitative secretome proteomics for cancer biomarker discovery: method evaluation, differential analysis, and verification in serum. *J Proteome Res* 2010; **9**(4)**:** 1913-1922.

518. Fang Y, Robinson DP, Foster LJ. Quantitative analysis of proteome coverage and recovery rates for upstream fractionation methods in proteomics. *J Proteome Res* 2010; **9**(4)**:** 1902-1912.

519. Marchi N, Cavaglia M, Fazio V, Bhudia S, Hallene K, Janigro D. Peripheral markers of blood-brain barrier damage. *Clin Chim Acta* 2004; **342**(1-2)**:** 1-12.

520. Uhlen M, Fagerberg L, Hallstrom BM, Lindskog C, Oksvold P, Mardinoglu A *et al.* Proteomics. Tissue-based map of the human proteome. *Science* 2015; **347**(6220)**:** 1260419.

521. Steinstrasser L, Jacobsen F, Hirsch T, Kesting M, Chojnacki C, Krisp C *et al.* Immunodepletion of high-abundant proteins from acute and chronic wound fluids to elucidate low-abundant regulators in wound healing. *BMC Res Notes* 2010; **3:** 335.

522. Riley NM, Mullen C, Weisbrod CR, Sharma S, Senko MW, Zabrouskov V *et al.* Enhanced Dissociation of Intact Proteins with High Capacity Electron Transfer Dissociation. *J Am Soc Mass Spectrom* 2016; **27**(3)**:** 520-531.

523. Li Z, Adams RM, Chourey K, Hurst GB, Hettich RL, Pan C. Systematic comparison of label-free, metabolic labeling, and isobaric chemical labeling for quantitative proteomics on LTQ Orbitrap Velos. *J Proteome Res* 2012; **11**(3)**:** 1582-1590.

524. Sinclair J, Timms JF. Quantitative profiling of serum samples using TMT protein labelling, fractionation and LC-MS/MS. *Methods* 2011; **54**(4)**:** 361-369.

525. Blyth BJ, Farhavar A, Gee C, Hawthorn B, He H, Nayak A *et al.* Validation of Serum Markers for Blood-Brain Barrier Disruption in Traumatic Brain Injury. *J Neurotraum* 2009; **26**(9)**:** 1497-1507.

526. Zetterberg H, Smith DH, Blennow K. Biomarkers of mild traumatic brain injury in cerebrospinal fluid and blood. *Nat Rev Neurol* 2013; **9**(4)**:** 201-210.

527. Di Battista AP, Buonora JE, Rhind SG, Hutchison MG, Baker AJ, Rizoli SB *et al.* Blood Biomarkers in Moderate-To-Severe Traumatic Brain Injury: Potential Utility of a Multi-Marker Approach in Characterizing Outcome. *Front Neurol* 2015; **6:** 110.

528. Kvartsberg H, Portelius E, Andreasson U, Brinkmalm G, Hellwig K, Lelental N *et al.* Characterization of the postsynaptic protein neurogranin in paired cerebrospinal fluid and plasma samples from Alzheimer's disease patients and healthy controls. *Alzheimers Res Ther* 2015; **7**(1)**:** 40.

529. Mayer CA, Brunkhorst R, Niessner M, Pfeilschifter W, Steinmetz H, Foerch C. Blood Levels of Glial Fibrillary Acidic Protein (GFAP) in Patients with Neurological Diseases. *PLoS One* 2013; **8**(4).

530. Goetzl EJ, Boxer A, Schwartz JB, Abner EL, Petersen RC, Miller BL *et al.* Low neural exosomal levels of cellular survival factors in Alzheimer's disease. *Ann Clin Transl Neurol* 2015; **2**(7)**:** 769-773.

531. Goetzl EJ, Kapogiannis D, Schwartz JB, Lobach IV, Goetzl L, Abner EL *et al.* Decreased synaptic proteins in neuronal exosomes of frontotemporal dementia and Alzheimer's disease. *Faseb Journal* 2016; **30**(12)**:** 4141-4148.

532. Czeiter E, Mondello S, Kovacs N, Sandor J, Gabrielli A, Schmid K *et al.* Brain Injury Biomarkers May Improve the Predictive Power of the IMPACT Outcome Calculator. *J Neurotraum* 2012; **29**(9)**:** 1770-1778.

533. Neselius S, Brisby H, Theodorsson A, Blennow K, Zetterberg H, Marcusson J. CSF-Biomarkers in Olympic Boxing: Diagnosis and Effects of Repetitive Head Trauma. *PLoS One* 2012; **7**(4).

534. Metting Z, Wilczak N, Rodiger LA, Schaaf JM, van der Naalt J. GFAP and S100B in the acute phase of mild traumatic brain injury. *Neurology* 2012; **78**(18)**:** 1428-1433.

535. Woodcock T, Morganti-Kossmann MC. The role of markers of inflammation in traumatic brain injury. *Frontiers in Neurology* 2013; **4**.

536. Mayer CA, Brunkhorst R, Niessner M, Pfeilschifter W, Steinmetz H, Foerch C. Blood levels of glial fibrillary acidic protein (GFAP) in patients with neurological diseases. *PLoS One* 2013; **8**(4)**:** e62101.

537. Zhou XH, Brakebusch C, Matthies H, Oohashi T, Hirsch E, Moser M *et al.* Neurocan is dispensable for brain development. *Molecular and Cellular Biology* 2001; **21**(17)**:** 5970-5978.

538. Berger RP, Adelson PD, Pierce MC, Dulani T, Cassidy LD, Kochanek PM. Serum neuron-specific enolase, S100B, and myelin basic protein concentrations after inflicted and noninflicted traumatic brain injury in children. *J Neurosurg* 2005; **103**(1)**:** 61-68.

539. Reddy PH, Mani G, Park BS, Jacques J, Murdoch G, Whetsell W, Jr. *et al.* Differential loss of synaptic proteins in Alzheimer's disease: implications for synaptic dysfunction. *J Alzheimers Dis* 2005; **7**(2)**:** 103-117; discussion 173-180.

540. Antonucci F, Corradini I, Fossati G, Tomasoni R, Menna E, Matteoli M. SNAP-25, a Known Presynaptic Protein with Emerging Postsynaptic Functions. *Front Synaptic Neurosci* 2016; **8:** 7.

541. Marchi N, Rasmussen P, Kapural M, Fazio V, Kight K, Mayberg MR *et al.* Peripheral markers of brain damage and blood-brain barrier dysfunction. *Restor Neurol Neurosci* 2003; **21**(3-4)**:** 109-121.

542. Kilpatrick DC, Chalmers JD. Human L-ficolin (ficolin-2) and its clinical significance. *J Biomed Biotechnol* 2012; **2012:** 138797.

543. Morris HR, Waite AJ, Williams NM, Neal JW, Blake DJ. Recent advances in the genetics of the ALS-FTLD complex. *Curr Neurol Neurosci Rep* 2012; **12**(3)**:** 243-250.

544. Meighan PC, Peng C, Varnum MD. Inherited macular degeneration-associated mutations in CNGB3 increase the ligand sensitivity and spontaneous open probability of cone cyclic nucleotide-gated channels. *Front Physiol* 2015; **6:** 177.

545. Thorsell A, Bjerke M, Gobom J, Brunhage E, Vanmechelen E, Andreasen N *et al.* Neurogranin in cerebrospinal fluid as a marker of synaptic degeneration in Alzheimer's disease. *Brain Research* 2010; **1362:** 13-22.

546. Kvartsberg H, Duits FH, Ingelsson M, Andreasen N, Ohrfelt A, Andersson K *et al.* Cerebrospinal fluid levels of the synaptic protein neurogranin correlates with cognitive decline in prodromal Alzheimer's disease. *Alzheimers & Dementia* 2015; **11**(10)**:** 1180-1190.

547. Remnestal J, Just D, Mitsios N, Fredolini C, Mulder J, Schwenk JM *et al.* CSF profiling of the human brain enriched proteome reveals associations of neuromodulin and neurogranin to Alzheimer's disease. *Proteomics Clin Appl* 2016; **10**(12)**:** 1242-1253.

548. Wellington H, Paterson RW, Portelius E, Tornqvist U, Magdalinou N, Fox NC *et al.* Increased CSF neurogranin concentration is specific to Alzheimer disease. *Neurology* 2016; **86**(9)**:** 829-835.

549. De Vos A, Jacobs D, Struyfs H, Fransen E, Andersson K, Portelius E *et al.* C-terminal neurogranin is increased in cerebrospinal fluid but unchanged in plasma in Alzheimer's disease. *Alzheimers & Dementia* 2015; **11**(12)**:** 1461-1469.

550. Diez-Guerra FJ. Neurogranin, a Link Between Calcium/Calmodulin and Protein Kinase C Signaling in Synaptic Plasticity. *IUBMB Life* 2010; **62**(8)**:** 597-606.

551. Yang J, Korley FK, Dai M, Everett AD. Serum neurogranin measurement as a biomarker of acute traumatic brain injury. *Clinical Biochemistry* 2015; **48**(13-14)**:** 843-848.

552. Kiddle SJ, Sattlecker M, Proitsi P, Simmons A, Westman E, Bazenet C *et al.* Candidate blood proteome markers of Alzheimer's disease onset and progression: a systematic review and replication study. *J Alzheimers Dis* 2014; **38**(3)**:** 515-531.

553. Razavi M, Frick LE, LaMarr WA, Pope ME, Miller CA, Anderson NL *et al.* High-throughput SISCAPA quantitation of peptides from human plasma digests by ultrafast, liquid chromatography-free mass spectrometry. *J Proteome Res* 2012; **11**(12)**:** 5642-5649.

554. Kim JS, Ahn HS, Cho SM, Lee JE, Kim Y, Lee C. Detection and quantification of plasma amyloid-beta by selected reaction monitoring mass spectrometry. *Anal Chim Acta* 2014; **840:** 1-9.

555. Kaneko N, Yamamoto R, Sato TA, Tanaka K. Identification and quantification of amyloid beta-related peptides in human plasma using matrix-assisted laser desorption/ionization time-of-flight mass spectrometry. *Proc Jpn Acad Ser B Phys Biol Sci* 2014; **90**(3)**:** 104-117.

556. Hu S, Loo JA, Wong DT. Human body fluid proteome analysis. *Proteomics* 2006; **6**(23)**:** 6326-6353.

557. Lovheim H, Elgh F, Johansson A, Zetterberg H, Blennow K, Hallmans G *et al.* Plasma concentrations of free amyloid beta cannot predict the development of Alzheimer's disease. *Alzheimers Dement* 2017.

558. Roher AE, Esh CL, Kokjohn TA, Castano EM, Van Vickle GD, Kalback WM *et al.* Amyloid beta peptides in human plasma and tissues and their significance for Alzheimer's disease. *Alzheimers & Dementia* 2009; **5**(1)**:** 18-29.

559. Li QX, Whyte S, Tanner JE, Evin G, Beyreuther K, Masters CL. Secretion of Alzheimer's disease Abeta amyloid peptide by activated human platelets. *Lab Invest* 1998; **78**(4)**:** 461-469.

560. Delvaux E, Bentley K, Stubbs V, Sabbagh M, Coleman PD. Differential processing of amyloid precursor protein in brain and in peripheral blood leukocytes. *Neurobiol Aging* 2013; **34**(6)**:** 1680-1686.

561. Tang K, Hynan LS, Baskin F, Rosenberg RN. Platelet amyloid precursor protein processing: a bio-marker for Alzheimer's disease. *J Neurol Sci* 2006; **240**(1-2)**:** 53-58.

562. Casoli T, Di Stefano G, Giorgetti B, Grossi Y, Balietti M, Fattoretti P *et al.* Release of beta-amyloid from high-density platelets: implications for Alzheimer's disease pathology. *Ann N Y Acad Sci* 2007; **1096:** 170-178.

563. Gowert NS, Donner L, Chatterjee M, Eisele YS, Towhid ST, Munzer P *et al.* Blood platelets in the progression of Alzheimer's disease. *PLoS One* 2014; **9**(2)**:** e90523.

564. McLoughlin DM, Miller CC. The FE65 proteins and Alzheimer's disease. *J Neurosci Res* 2008; **86**(4)**:** 744-754.

565. Liu X, Valentine SJ, Plasencia MD, Trimpin S, Naylor S, Clemmer DE. Mapping the human plasma proteome by SCX-LC-IMS-MS. *J Am Soc Mass Spectrom* 2007; **18**(7)**:** 1249-1264.

566. Tanahashi H, Tabira T. Characterization of an amyloid precursor protein-binding protein Fe65L2 and its novel isoforms lacking phosphotyrosine-interaction domains. *Biochem J* 2002; **367**(Pt 3)**:** 687-695.

567. Tanahashi H, Asada T, Tabira T. c954C-->T polymorphism in the Fe65L2 gene is associated with early-onset Alzheimer's disease. *Ann Neurol* 2002; **52**(5)**:** 691-693.

568. Lambert JC, Mann D, Goumidi L, Harris J, Pasquier F, Frigard B *et al.* A FE65 polymorphism associated with risk of developing sporadic late-onset alzheimer's disease but not with Abeta loading in brains. *Neurosci Lett* 2000; **293**(1)**:** 29-32.

569. Ciallella JR, Figueiredo H, Smith-Swintosky V, McGillis JP. Thrombin induces surface and intracellular secretion of amyloid precursor protein from human endothelial cells. *Thromb Haemost* 1999; **81**(4)**:** 630-637.

570. Akiyama H, Ikeda K, Kondo H, McGeer PL. Thrombin accumulation in brains of patients with Alzheimer's disease. *Neurosci Lett* 1992; **146**(2)**:** 152-154.

571. Choi-Miura NH, Yoda M, Saito K, Takahashi K, Tomita M. Identification of the substrates for plasma hyaluronan binding protein. *Biol Pharm Bull* 2001; **24**(2)**:** 140-143.

572. Mari D, Parnetti L, Coppola R, Bottasso B, Reboldi GP, Senin U *et al.* Hemostasis abnormalities in patients with vascular dementia and Alzheimer's disease. *Thromb Haemost* 1996; **75**(2)**:** 216-218.

573. Gupta A, Watkins A, Thomas P, Majer R, Habubi N, Morris G *et al.* Coagulation and inflammatory markers in Alzheimer's and vascular dementia. *Int J Clin Pract* 2005; **59**(1)**:** 52-57.

574. Rafnsson SB, Deary IJ, Smith FB, Whiteman MC, Rumley A, Lowe GD *et al.* Cognitive decline and markers of inflammation and hemostasis: the Edinburgh Artery Study. *J Am Geriatr Soc* 2007; **55**(5)**:** 700-707.

575. Bots ML, Breteler MMB, van Kooten F, Haverkate F, Meijer P, Koudstaal PJ *et al.* Coagulation and fibrinolysis markers and risk of dementia - The Dutch vascular factors in dementia study. *Haemostasis* 1998; **28**(3-4)**:** 216-222.

576. Wilson CJ, Cohen HJ, Pieper CF. Cross-linked fibrin degradation products (D-Dimer), plasma cytokines, and cognitive decline in community-dwelling elderly persons. *Journal of the American Geriatrics Society* 2003; **51**(10)**:** 1374-1381.

577. Carlsson F, Sandin C, Lindahl G. Human fibrinogen bound to Streptococcus pyogenes M protein inhibits complement deposition via the classical pathway. *Mol Microbiol* 2005; **56**(1)**:** 28-39.

578. Horstmann RD, Sievertsen HJ, Leippe M, Fischetti VA. Role of fibrinogen in complement inhibition by streptococcal M protein. *Infect Immun* 1992; **60**(12)**:** 5036-5041.

579. Amara U, Flierl MA, Rittirsch D, Klos A, Chen H, Acker B *et al.* Molecular Intercommunication between the Complement and Coagulation Systems. *Journal of Immunology* 2010; **185**(9)**:** 5628-5636.

580. Rogers J, Cooper NR, Webster S, Schultz J, Mcgeer PL, Styren SD *et al.* Complement Activation by Beta-Amyloid in Alzheimer-Disease. *P Natl Acad Sci USA* 1992; **89**(21)**:** 10016-10020.

581. Shen Y, Lue LF, Yang LB, Roher A, Kuo YM, Strohmeyer R *et al.* Complement activation by neurofibrillary tangles in Alzheimer's disease. *Neuroscience Letters* 2001; **305**(3)**:** 165-168.

582. Shen Y, Meri S. Yin and Yang: complement activation and regulation in Alzheimer's disease. *Progress in Neurobiology* 2003; **70**(6)**:** 463-472.

583. McGeer EG, McGeer PL. Innate immunity in Alzheimer's disease: a model for local inflammatory reactions. *Mol Interv* 2001; **1**(1)**:** 22-29.

584. Huber-Lang M, Sarma JV, Zetoune FS, Rittirsch D, Neff TA, McGuire SR *et al.* Generation of C5a in the absence of C3: a new complement activation pathway. *Nature Medicine* 2006; **12**(6)**:** 682-687.

585. Chen H, Lu J, Chen X, Yu H, Zhang L, Bao Y *et al.* Low serum levels of the innate immune component ficolin-3 is associated with insulin resistance and predicts the development of type 2 diabetes. *J Mol Cell Biol* 2012; **4**(4)**:** 256-257.

586. Li RX, Chen HB, Tu K, Zhao SL, Zhou H, Li SJ *et al.* Localized-statistical quantification of human serum proteome associated with type 2 diabetes. *PLoS One* 2008; **3**(9)**:** e3224.

587. Lu T, Aron L, Zullo J, Pan Y, Kim H, Chen Y *et al.* REST and stress resistance in ageing and Alzheimer's disease. *Nature* 2014; **507**(7493)**:** 448-454.

588. Pozzi D, Lignani G, Ferrea E, Contestabile A, Paonessa F, D'Alessandro R *et al.* REST/NRSF-mediated intrinsic homeostasis protects neuronal networks from hyperexcitability. *EMBO J* 2013; **32**(22)**:** 2994-3007.

589. Abner EL, Jicha GA, Shaw LM, Trojanowski JQ, Goetzl EJ. Plasma neuronal exosomal levels of Alzheimer's disease biomarkers in normal aging. *Ann Clin Transl Neurol* 2016; **3**(5)**:** 399-403.

590. Jones S. An overview of the basic helix-loop-helix proteins. *Genome Biol* 2004; **5**(6)**:** 226.

591. Ma Q, Sommer L, Cserjesi P, Anderson DJ. Mash1 and neurogenin1 expression patterns define complementary domains of neuroepithelium in the developing CNS and are correlated with regions expressing notch ligands. *J Neurosci* 1997; **17**(10)**:** 3644-3652.

592. Hodge RD, Kowalczyk TD, Wolf SA, Encinas JM, Rippey C, Enikolopov G *et al.* Intermediate progenitors in adult hippocampal neurogenesis: Tbr2 expression and coordinate regulation of neuronal output. *J Neurosci* 2008; **28**(14)**:** 3707-3717.

593. Ozen I, Galichet C, Watts C, Parras C, Guillemot F, Raineteau O. Proliferating neuronal progenitors in the postnatal hippocampus transiently express the proneural gene Ngn2. *Eur J Neurosci* 2007; **25**(9)**:** 2591-2603.

594. Deng W, Aimone JB, Gage FH. New neurons and new memories: how does adult hippocampal neurogenesis affect learning and memory? *Nat Rev Neurosci* 2010; **11**(5)**:** 339-350.

595. Mu Y, Gage FH. Adult hippocampal neurogenesis and its role in Alzheimer's disease. *Mol Neurodegener* 2011; **6:** 85.

596. Haughey NJ, Nath A, Chan SL, Borchard AC, Rao MS, Mattson MP. Disruption of neurogenesis by amyloid beta-peptide, and perturbed neural progenitor cell homeostasis, in models of Alzheimer's disease. *J Neurochem* 2002; **83**(6)**:** 1509-1524.

597. Bolos M, Hu Y, Young KM, Foa L, Small DH. Neurogenin 2 mediates amyloid-beta precursor protein-stimulated neurogenesis. *J Biol Chem* 2014; **289**(45)**:** 31253-31261.

598. Wyss-Coray T, Rogers J. Inflammation in Alzheimer disease-a brief review of the basic science and clinical literature. *Cold Spring Harb Perspect Med* 2012; **2**(1)**:** a006346.

599. Heppner FL, Ransohoff RM, Becher B. Immune attack: the role of inflammation in Alzheimer disease. *Nat Rev Neurosci* 2015; **16**(6)**:** 358-372.

600. Pahl HL. Activators and target genes of Rel/NF-kappaB transcription factors. *Oncogene* 1999; **18**(49)**:** 6853-6866.

601. Verma IM. Nuclear factor (NF)-kappaB proteins: therapeutic targets. *Ann Rheum Dis* 2004; **63 Suppl 2:** ii57-ii61.

602. Tilstra JS, Clauson CL, Niedernhofer LJ, Robbins PD. NF-kappaB in Aging and Disease. *Aging Dis* 2011; **2**(6)**:** 449-465.

603. Yamamoto Y, Gaynor RB. Role of the NF-kappaB pathway in the pathogenesis of human disease states. *Curr Mol Med* 2001; **1**(3)**:** 287-296.

604. Berenbaum F. Signaling transduction: target in osteoarthritis. *Curr Opin Rheumatol* 2004; **16**(5)**:** 616-622.

605. Alexandraki K, Piperi C, Kalofoutis C, Singh J, Alaveras A, Kalofoutis A. Inflammatory process in type 2 diabetes - The role of cytokines. *Diabetes Mellitus and Its Complications* 2006; **1084:** 89-117.

606. Valen G. Signal transduction through nuclear factor kappa B in ischemia-reperfusion and heart failure. *Basic Res Cardiol* 2004; **99**(1)**:** 1-7.

607. Cuaz-Perolin C, Billiet L, Bauge E, Copin C, Scott-Algara D, Genze F *et al.* Antiinflammatory and antiatherogenic effects of the NF-kappaB inhibitor acetyl-11-keto-beta-boswellic acid in LPS-challenged ApoE-/- mice. *Arterioscler Thromb Vasc Biol* 2008; **28**(2)**:** 272-277.

608. Steinman L. Nuanced roles of cytokines in three major human brain disorders. *J Clin Invest* 2008; **118**(11)**:** 3557-3563.

609. Perry VH, Cunningham C, Holmes C. Systemic infections and inflammation affect chronic neurodegeneration. *Nat Rev Immunol* 2007; **7**(2)**:** 161-167.

610. Holmes C, El-Okl M, Williams AL, Cunningham C, Wilcockson D, Perry VH. Systemic infection, interleukin 1beta, and cognitive decline in Alzheimer's disease. *J Neurol Neurosurg Psychiatry* 2003; **74**(6)**:** 788-789.

611. Hunot S, Brugg B, Ricard D, Michel PP, Muriel MP, Ruberg M *et al.* Nuclear translocation of NF-kappa B is increased in dopaminergic neurons of patients with Parkinson disease. *P Natl Acad Sci USA* 1997; **94**(14)**:** 7531-7536.

612. Ghosh A, Roy A, Liu X, Kordower JH, Mufson EJ, Hartley DM *et al.* Selective inhibition of NF-kappaB activation prevents dopaminergic neuronal loss in a mouse model of Parkinson's disease. *Proc Natl Acad Sci U S A* 2007; **104**(47)**:** 18754-18759.

613. Balistreri CR, Candore G, Accardi G, Colonna-Romano G, Lio D. NF-kappa B pathway activators as potential ageing biomarkers: targets for new therapeutic strategies. *Immun Ageing* 2013; **10**.

614. Trojanowski JQ, Walkenstein N, Lee VM. Expression of neurofilament subunits in neurons of the central and peripheral nervous system: an immunohistochemical study with monoclonal antibodies. *J Neurosci* 1986; **6**(3)**:** 650-660.

615. Petzold A. Neurofilament phosphoforms: surrogate markers for axonal injury, degeneration and loss. *J Neurol Sci* 2005; **233**(1-2)**:** 183-198.

616. Steinacker P, Feneberg E, Weishaupt J, Brettschneider J, Tumani H, Andersen PM *et al.* Neurofilaments in the diagnosis of motoneuron diseases: a prospective study on 455 patients. *J Neurol Neurosur Ps* 2016; **87**(1)**:** 12-20.

617. Idland AV, Sala-Llonch R, Borza T, Watne LO, Wyller TB, Braekhus A *et al.* CSF neurofilament light levels predict hippocampal atrophy in cognitively healthy older adults. *Neurobiol Aging* 2017; **49:** 138-144.

618. Pijnenburg YA, Janssen JC, Schoonenboom NS, Petzold A, Mulder C, Stigbrand T *et al.* CSF neurofilaments in frontotemporal dementia compared with early onset Alzheimer's disease and controls. *Dement Geriatr Cogn Disord* 2007; **23**(4)**:** 225-230.

619. Bjerke M, Zetterberg H, Edman A, Blennow K, Wallin A, Andreasson U. Cerebrospinal fluid matrix metalloproteinases and tissue inhibitor of metalloproteinases in combination with subcortical and cortical biomarkers in vascular dementia and Alzheimer's disease. *J Alzheimers Dis* 2011; **27**(3)**:** 665-676.

620. Zetterberg H, Skillback T, Mattsson N, Trojanowski JQ, Portelius E, Shaw LM *et al.* Association of Cerebrospinal Fluid Neurofilament Light Concentration With Alzheimer Disease Progression. *Jama Neurology* 2016; **73**(1)**:** 60-67.

621. Zetterberg H, Jacobsson J, Rosengren L, Blennow K, Andersen PM. Cerebrospinal fluid neurofilament light levels in amyotrophic lateral sclerosis: impact of SOD1 genotype. *European Journal of Neurology* 2007; **14**(12)**:** 1329-1333.

622. Norgren N, Rosengren L, Stigbrand T. Elevated neurofilament levels in neurological diseases. *Brain Res* 2003; **987**(1)**:** 25-31.

623. Holmberg B, Rosengren L, Karlsson JE, Johnels B. Increased cerebrospinal fluid levels of neurofilament protein in progressive supranuclear palsy and multiple-system atrophy compared with Parkinson's disease. *Movement Disord* 1998; **13**(1)**:** 70-77.

624. Teunissen CE, Khalil M. Neurofilaments as biomarkers in multiple sclerosis. *Mult Scler J* 2012; **18**(5)**:** 552-556.

625. Zetterberg H, Skillback T, Mattsson N, Trojanowski JQ, Portelius E, Shaw LM *et al.* Association of Cerebrospinal Fluid Neurofilament Light Concentration With Alzheimer Disease Progression. *JAMA Neurol* 2016; **73**(1)**:** 60-67.

626. Gaiottino J, Norgren N, Dobson R, Topping J, Nissim A, Malaspina A *et al.* Increased Neurofilament Light Chain Blood Levels in Neurodegenerative Neurological Diseases. *PLoS One* 2013; **8**(9).

627. Bacioglu M, Maia LF, Preische O, Schelle J, Apel A, Kaeser SA *et al.* Neurofilament Light Chain in Blood and CSF as Marker of Disease Progression in Mouse Models and in Neurodegenerative Diseases. *Neuron* 2016; **91**(1)**:** 56-66.

628. Lu CH, Macdonald-Wallis C, Gray E, Pearce N, Petzold A, Norgren N *et al.* Neurofilament light chain A prognostic biomarker in amyotrophic lateral sclerosis. *Neurology* 2015; **84**(22)**:** 2247-2257.

629. Rojas J, Karydas A, Bang J, Tsai R, Blennow K, Liman V *et al.* Plasma neurofilament light chain predicts disease progression in progressive supranuclear palsy. *Journal of Neurochemistry* 2016; **138:** 241-242.

630. Rosenbaum DM, Rasmussen SG, Kobilka BK. The structure and function of G-protein-coupled receptors. *Nature* 2009; **459**(7245)**:** 356-363.

631. Thathiah A, De Strooper B. G protein-coupled receptors, cholinergic dysfunction, and Abeta toxicity in Alzheimer's disease. *Sci Signal* 2009; **2**(93)**:** re8.

632. Thathiah A, Horre K, Snellinx A, Vandewyer E, Huang Y, Ciesielska M *et al.* beta-arrestin 2 regulates Abeta generation and gamma-secretase activity in Alzheimer's disease. *Nat Med* 2013; **19**(1)**:** 43-49.

633. Conn PJ, Lindsley CW, Meiler J, Niswender CM. Opportunities and challenges in the discovery of allosteric modulators of GPCRs for treating CNS disorders. *Nat Rev Drug Discov* 2014; **13**(9)**:** 692-708.

634. Thathiah A, Spittaels K, Hoffmann M, Staes M, Cohen A, Horre K *et al.* The orphan G protein-coupled receptor 3 modulates amyloid-beta peptide generation in neurons. *Science* 2009; **323**(5916)**:** 946-951.

635. Nelson CD, Sheng M. Gpr3 stimulates Abeta production via interactions with APP and beta-arrestin2. *PLoS One* 2013; **8**(9)**:** e74680.

636. Devanand DP, Michaels-Marston KS, Liu X, Pelton GH, Padilla M, Marder K *et al.* Olfactory deficits in patients with mild cognitive impairment predict Alzheimer's disease at follow-up. *Am J Psychiatry* 2000; **157**(9)**:** 1399-1405.

637. Conti MZ, Vicini-Chilovi B, Riva M, Zanetti M, Liberini P, Padovani A *et al.* Odor Identification Deficit Predicts Clinical Conversion from Mild Cognitive Impairment to Dementia Due to Alzheimer's Disease. *Arch Clin Neuropsych* 2013; **28**(5)**:** 391-399.

638. Wesson DW, Levy E, Nixon RA, Wilson DA. Olfactory Dysfunction Correlates with Amyloid-beta Burden in an Alzheimer's Disease Mouse Model. *Journal of Neuroscience* 2010; **30**(2)**:** 505-514.

639. Kornak U, Reynders E, Dimopoulou A, van Reeuwijk J, Fischer B, Rajab A *et al.* Impaired glycosylation and cutis laxa caused by mutations in the vesicular H+-ATPase subunit ATP6V0A2. *Nature Genetics* 2008; **40**(1)**:** 32-34.

640. Huse JT, Liu KN, Pijak DS, Carlin D, Lee VMY, Doms RW. beta-secretase processing in the trans-Golgi network preferentially generates truncated amyloid species that accumulate in Alzheimer's disease brain. *Journal of Biological Chemistry* 2002; **277**(18)**:** 16278-16284.

641. Mizuno Y, Hattori N, Kitada T, Matsumine H, Mori H, Shimura H *et al.* Familial Parkinson's disease alpha-synuclein and parkin. *Parkinson's Disease* 2001; **86:** 13-21.

642. Joshi G, Wang YZ. Golgi defects enhance APP amyloidogenic processing in Alzheimer's disease. *Bioessays* 2015; **37**(3)**:** 240-247.

643. Weng JH, Hsieh YC, Huang CCF, Wei TYW, Lim LH, Chen YH *et al.* Uncovering the Mechanism of Forkhead-Associated Domain-Mediated TIFA Oligomerization That Plays a Central Role in Immune Responses. *Biochemistry* 2015; **54**(40)**:** 6219-6229.

644. Gerdes JM, Davis EE, Katsanis N. The Vertebrate Primary Cilium in Development, Homeostasis, and Disease. *Cell* 2009; **137**(1)**:** 32-45.

645. Conroy PC, Saladino C, Dantas TJ, Lalor P, Dockery P, Morrison CG. C-NAP1 and rootletin restrain DNA damage-induced centriole splitting and facilitate ciliogenesis. *Cell Cycle* 2012; **11**(20)**:** 3769-3778.

646. Killick R, Ribe EM, Al-Shawi R, Malik B, Hooper C, Fernandes C *et al.* Clusterin regulates beta-amyloid toxicity via Dickkopf-1-driven induction of the wnt-PCP-JNK pathway. *Mol Psychiatr* 2014; **19**(1)**:** 88-98.

647. Jenkins PM, McEwen DP, Martens JR. Olfactory Cilia: Linking Sensory Cilia Function and Human Disease. *Chem Senses* 2009; **34**(5)**:** 451-464.

648. Yang J, Li TS. The ciliary rootlet interacts with kinesin light chains and may provide a scaffold for kinesin-1 vesicular cargos. *Experimental Cell Research* 2005; **309**(2)**:** 379-389.

649. Braathen GJ, Hoyer H, Busk OL, Tveten K, Skjelbred CF, Russell MB. Variants in the genes DCTN2, DNAH10, LRIG3, and MYO1A are associated with intermediate Charcot-Marie-Tooth disease in a Norwegian family. *Acta Neurologica Scandinavica* 2016; **134**(1)**:** 67-75.

650. Ardley HC, Robinson PA. The Role of Ubiquitin-Protein Ligases in Neurodegenerative Disease. *Neurodegenerative Diseases* 2004; **1**(2-3)**:** 71-87.

651. Kaytor MD, Warren ST. Aberrant protein deposition and neurological disease. *Journal of Biological Chemistry* 1999; **274**(53)**:** 37507-37510.

652. Liu Y, Chen X, Xu QH, Gao X, Tam POS, Zhao KX *et al.* SPP2 Mutations Cause Autosomal Dominant Retinitis Pigmentosa. *Sci Rep-Uk* 2015; **5**.

653. Erickson MA, Banks WA. Blood-brain barrier dysfunction as a cause and consequence of Alzheimer's disease. *J Cerebr Blood F Met* 2013; **33**(10)**:** 1500-1513.

654. Davalos D, Akassoglou K. Fibrinogen as a key regulator of inflammation in disease. *Semin Immunopathol* 2012; **34**(1)**:** 43-62.

655. Banks WA. Characteristics of compounds that cross the blood-brain barrier. *Bmc Neurology* 2009; **9**.

656. Kapural M, Krizanac-Bengez L, Barnett G, Perl J, Masaryk T, Apollo D *et al.* Serum S-100 beta as a possible marker of blood-brain barrier disruption. *Brain Research* 2002; **940**(1-2)**:** 102-104.

657. Janelidze S, Hertze J, Nagga K, Nilsson K, Nilsson C, Wennstrom M *et al.* Increased blood-brain barrier permeability is associated with dementia and diabetes but not amyloid pathology or APOE genotype. *Neurobiol Aging* 2016; **51:** 104-112.

658. Rosen C, Mattsson N, Johansson PM, Andreasson U, Wallin A, Hansson O *et al.* Discriminatory analysis of biochip-derived protein patterns in CSF and plasma in neurodegenerative diseases. *Frontiers in Aging Neuroscience* 2011; **3**.

659. Ramont L, Thoannes H, Volondat A, Chastang F, Millet MC, Maquart FX. Effects of hemolysis and storage condition on neuron-specific enolase (NSE) in cerebrospinal fluid and serum: implications in clinical practice. *Clinical Chemistry and Laboratory Medicine* 2005; **43**(11)**:** 1215-1217.

660. Meyer D, Bonhoeffer T, Scheuss V. Balance and stability of synaptic structures during synaptic plasticity. *Neuron* 2014; **82**(2)**:** 430-443.

661. Sultana R, Banks WA, Butterfield DA. Decreased Levels of PSD95 and Two Associated Proteins and Increased Levels of BCl2 and Caspase 3 in Hippocampus from Subjects with Amnestic Mild Cognitive Impairment: Insights into Their Potential Roles for Loss of Synapses and Memory, Accumulation of A beta, and Neurodegeneration in a Prodromal Stage of Alzheimer's Disease. *Journal of Neuroscience Research* 2010; **88**(3)**:** 469-477.

662. Zhan XH, Jickling GC, Ander BP, Stamova B, Liu DZ, Kao PF *et al.* Myelin Basic Protein Associates with A beta PP, A beta(1-42), and Amyloid Plaques in Cortex of Alzheimer's Disease Brain. *Journal of Alzheimers Disease* 2015; **44**(4)**:** 1213-1229.

663. Ou-Yang MH, Van Nostrand WE. The absence of myelin basic protein promotes neuroinflammation and reduces amyloid beta-protein accumulation in Tg-5xFAD mice. *J Neuroinflamm* 2013; **10**.

664. Choi J, Malakowsky CA, Talent JM, Conrad CC, Gracy RW. Identification of oxidized plasma proteins in Alzheimer's disease. *Biochem Biophys Res Commun* 2002; **293**(5)**:** 1566-1570.

665. Chiam JTW, Dobson RJB, Kiddle SJ, Sattlecker M. Are Blood-Based Protein Biomarkers for Alzheimer's Disease also Involved in Other Brain Disorders? A Systematic Review. *Journal of Alzheimers Disease* 2015; **43**(1)**:** 303-314.

666. Mikhailidis DP, Barradas MA, Jeremy JY, Dandona P. Fibrinogen enhances and albumin reduces RBC aggregation. *Angiology* 1987; **38**(8)**:** 615-616.

667. Ernst E, Resch KL. Fibrinogen as a cardiovascular risk factor: a meta-analysis and review of the literature. *Ann Intern Med* 1993; **118**(12)**:** 956-963.

668. Lominadze D, Dean WL, Tyagi SC, Roberts AM. Mechanisms of fibrinogen-induced microvascular dysfunction during cardiovascular disease. *Acta Physiol (Oxf)* 2010; **198**(1)**:** 1-13.

669. Deramecourt V, Slade JY, Oakley AE, Perry RH, Ince PG, Maurage CA *et al.* Staging and natural history of cerebrovascular pathology in dementia. *Neurology* 2012; **78**(14)**:** 1043-1050.

670. North BJ, Sinclair DA. The Intersection Between Aging and Cardiovascular Disease. *Circulation Research* 2012; **110**(8)**:** 1097-1108.

671. Ryu JK, Petersen MA, Murray SG, Baeten KM, Meyer-Franke A, Chan JP *et al.* Blood coagulation protein fibrinogen promotes autoimmunity and demyelination via chemokine release and antigen presentation. *Nat Commun* 2015; **6:** 8164.

672. Jantaratnotai N, Schwab C, Ryu JK, McGeer PL, McLarnon JG. Converging Perturbed Microvasculature and Microglial Clusters Characterize Alzheimer Disease Brain. *Current Alzheimer Research* 2010; **7**(7)**:** 625-636.

673. Attems J, Jellinger K, Thal DR, Van Nostrand W. Sporadic cerebral amyloid angiopathy. *Neuropath Appl Neuro* 2011; **37**(1)**:** 75-93.

674. Ehling R, di Pauli F, Lackner P, Kuenz B, Lutterotti A, Gneiss C *et al.* Fibrinogen is elevated in the CSF of acute neuroinflammatory diseases: a cross-sectional study. *Journal of Neurology* 2011; **258:** 213-214.

675. Frank RA, Galasko D, Hampel H, Hardy J, de Leon MJ, Mehta PD *et al.* Biological markers for therapeutic trials in Alzheimer's disease - Proceedings of the biological markers working group; NIA initiative on neuroimaging in Alzheimer's disease. *Neurobiology of Aging* 2003; **24**(4)**:** 521-536.

676. Molinuevo JL, Cami J, Carne X, Carrillo MC, Georges J, Isaac MB *et al.* Ethical challenges in preclinical Alzheimer's disease observational studies and trials: Results of the Barcelona summit. *Alzheimers Dement* 2016; **12**(5)**:** 614-622.

677. Green RC, Roberts JS, Cupples LA, Relkin NR, Whitehouse PJ, Brown T *et al.* Disclosure of APOE genotype for risk of Alzheimer's disease. *N Engl J Med* 2009; **361**(3)**:** 245-254.

678. Chao S, Roberts JS, Marteau TM, Silliman R, Cupples LA, Green RC. Health behavior changes after genetic risk assessment for Alzheimer disease: The REVEAL Study. *Alzheimer Dis Assoc Disord* 2008; **22**(1)**:** 94-97.

679. Harkins K, Sankar P, Sperling R, Grill JD, Green RC, Johnson KA *et al.* Development of a process to disclose amyloid imaging results to cognitively normal older adult research participants. *Alzheimers Res Ther* 2015; **7**(1)**:** 26.

680. Ryman DC, Acosta-Baena N, Aisen PS, Bird T, Danek A, Fox NC *et al.* Symptom onset in autosomal dominant Alzheimer disease: a systematic review and meta-analysis. *Neurology* 2014; **83**(3)**:** 253-260.

681. Sohet F, Daneman R. Genetic mouse models to study blood-brain barrier development and function. *Fluids Barriers CNS* 2013; **10**(1)**:** 3.

682. Liang HC, Russell C, Mitra V, Chung R, Hye A, Bazenet C *et al.* Glycosylation of Human Plasma Clusterin Yields a Novel Candidate Biomarker of Alzheimer's Disease. *Journal of Proteome Research* 2015; **14**(12)**:** 5063-5076.

683. O'Bryant SE, Lista S, Rissman RA, Edwards M, Zhang F, Hall J *et al.* Comparing biological markers of Alzheimer's disease across blood fraction and platforms: Comparing apples to oranges. *Alzheimers Dement (Amst)* 2016; **3:** 27-34.

684. Mattsson N, Andreasson U, Persson S, Carrillo MC, Collins S, Chalbot S *et al.* CSF biomarker variability in the Alzheimer's Association quality control program. *Alzheimers & Dementia* 2013; **9**(3)**:** 251-261.

685. Verhaaren BF, Vernooij MW, Koudstaal PJ, Uitterlinden AG, van Duijn CM, Hofman A *et al.* Alzheimer's disease genes and cognition in the nondemented general population. *Biol Psychiatry* 2013; **73**(5)**:** 429-434.

686. Harris SE, Davies G, Luciano M, Payton A, Fox HC, Haggarty P *et al.* Polygenic Risk for Alzheimer's Disease is not Associated with Cognitive Ability or Cognitive Aging in Non-Demented Older People. *Journal of Alzheimers Disease* 2014; **39**(3)**:** 565-574.

687. McIntosh AM, Gow A, Luciano M, Davies G, Liewald DC, Harris SE *et al.* Polygenic Risk for Schizophrenia Is Associated with Cognitive Change Between Childhood and Old Age. *Biol Psychiat* 2013; **73**(10)**:** 938-943.

APPENDICES

Appendix 1. LC-MS/MS protein group identifications extracted by PRQ-1 pre-processing pipeline for Chapter 3

Protein group MW isoforms (*n* = 381) identified by LC-MS/MS with TMT6plex protein quantification. These protein groups were extracted using the statistical pipeline PRQ-1 and post-PRQ-1 clean up.

UniProt ID	Protein Name	Gene Name	1DGE Fraction	Samples Present (%)
P42684	Abelson tyrosine-protein kinase 2	*ABL2*	7	62.50
P60709	Actin, cytoplasmic 1	*ACTB*	5	68.75
P43652	Afamin	*AFM*	3	93.75
P43652	Afamin	*AFM*	4	87.50
P43652	Afamin	*AFM*	5	87.50
P02768	Albumin	*ALB*	1	100
P02768	Albumin	*ALB*	2	100
P02768	Albumin	*ALB*	3	100
P02768	Albumin	*ALB*	4	100
P02768	Albumin	*ALB*	5	100
P02768	Albumin	*ALB*	6	100
P02768	Albumin	*ALB*	7	100
P02768	Albumin	*ALB*	8	100
P02768	Albumin	*ALB*	9	100
P02768	Albumin	*ALB*	10	68.75
P19652	Alpha-1-acid glycoprotein 2	*ORM2*	5	87.50
P19652	Alpha-1-acid glycoprotein 2	*ORM2*	6	75.00
P01011	Alpha-1-antichymotrypsin	*SERPINA3*	1	87.50
P01011	Alpha-1-antichymotrypsin	*SERPINA3*	2	100
P01011	Alpha-1-antichymotrypsin	*SERPINA3*	3	75.00
P01011	Alpha-1-antichymotrypsin	*SERPINA3*	4	87.50
P01011	Alpha-1-antichymotrypsin	*SERPINA3*	5	100
P01011	Alpha-1-antichymotrypsin	*SERPINA3*	6	62.50
P01011	Alpha-1-antichymotrypsin	*SERPINA3*	7	100
P01011	Alpha-1-antichymotrypsin	*SERPINA3*	8	81.25
P01011	Alpha-1-antichymotrypsin	*SERPINA3*	9	81.25
P04217	Alpha-1-B Glycoprotein	*A1BG*	4	81.25

P04217	Alpha-1-B Glycoprotein	*A1BG*	5	81.25
P08697	Alpha-2-antiplasmin	*SERPINF2*	5	75.00
P01023	Alpha-2-Macroglobulin (α2m)	*A2M*	1	100
P01023	Alpha-2-Macroglobulin (α2m)	*A2M*	2	100
P01023	Alpha-2-Macroglobulin (α2m)	*A2M*	3	100
P01023	Alpha-2-Macroglobulin (α2m)	*A2M*	4	62.50
P01023	Alpha-2-Macroglobulin (α2m)	*A2M*	5	100
P01023	Alpha-2-Macroglobulin (α2m)	*A2M*	6	75.00
P01023	Alpha-2-Macroglobulin (α2m)	*A2M*	7	100
P01023	Alpha-2-Macroglobulin (α2m)	*A2M*	8	87.50
P01023	Alpha-2-Macroglobulin (α2m)	*A2M*	9	75.00
P01008	Antithrombin-III	*SERPINC1*	4	81.25
P01008	Antithrombin-III	*SERPINC1*	5	100
P01008	Antithrombin-III	*SERPINC1*	6	68.75
P01008	Antithrombin-III	*SERPINC1*	7	62.50
P01008	Antithrombin-III	*SERPINC1*	8	81.25
P01008	Antithrombin-III	*SERPINC1*	9	100
P01008	Antithrombin-III	*SERPINC1*	10	81.25
P02647	Apolipoprotein A-I (ApoA1)	*APOA1*	2	100
P02647	Apolipoprotein A-I (ApoA1)	*APOA1*	3	75.00
P02647	Apolipoprotein A-I (ApoA1)	*APOA1*	5	75.00
P02647	Apolipoprotein A-I (ApoA1)	*APOA1*	6	100
P02647	Apolipoprotein A-I (ApoA1)	*APOA1*	7	93.75
P02647	Apolipoprotein A-I (ApoA1)	*APOA1*	8	100
P02647	Apolipoprotein A-I (ApoA1)	*APOA1*	9	93.75
P02647	Apolipoprotein A-I (ApoA1)	*APOA1*	10	68.75
P06727	Apolipoprotein A-IV (ApoA4)	*APOA4*	5	93.75
P06727	Apolipoprotein A-IV (ApoA4)	*APOA4*	6	56.25
P04114	Apolipoprotein B (ApoB)	*APOB*	1	100
P04114	Apolipoprotein B (ApoB)	*APOB*	2	93.75
P04114	Apolipoprotein B (ApoB)	*APOB*	3	93.75
P04114	Apolipoprotein B (ApoB)	*APOB*	5	75.00
P55056	Apolipoprotein C-IV	*APOC4*	8	87.50
P55056	Apolipoprotein C-IV	*APOC4*	9	93.75
P05090	Apolipoprotein D	*APOD*	6	87.50
P05090	Apolipoprotein D	*APOD*	7	87.50
P02649	Apolipoprotein E	*APOE*	6	93.75
P02649	Apolipoprotein E	*APOE*	7	68.75
P02649	Apolipoprotein E	*APOE*	8	100

P02649	Apolipoprotein E	*APOE*	9	93.75
P02649	Apolipoprotein E	*APOE*	10	56.25
P02749	Apolipoprotein H	*APOH*	5	62.50
O14791	Apolipoprotein L-1 (ApoL1)	*APOL1*	5	81.25
O14791	Apolipoprotein L-1 (ApoL1)	*APOL1*	6	68.75
O95445	Apolipoprotein M	*APOM*	7	87.50
O95445	Apolipoprotein M	*APOM*	8	87.50
O95445	Apolipoprotein M	*APOM*	9	50.00
P08519	Apolipoprotein(a)	*LPA*	1	62.50
P08519	Apolipoprotein(a)	*LPA*	2	68.75
O75882	Attractin	*ATRN*	2	62.50
P61769	Beta-2-microglobulin	*B2M*	9	87.50
P04003	C4b-binding protein alpha chain	*C4BPA*	1	100
P04003	C4b-binding protein alpha chain	*C4BPA*	2	100
P04003	C4b-binding protein alpha chain	*C4BPA*	3	100
P04003	C4b-binding protein alpha chain	*C4BPA*	4	93.75
P04003	C4b-binding protein alpha chain	*C4BPA*	5	100
P04003	C4b-binding protein alpha chain	*C4BPA*	6	93.75
P04003	C4b-binding protein alpha chain	*C4BPA*	7	100
P04003	C4b-binding protein alpha chain	*C4BPA*	9	50.00
P15169	Carboxypeptidase N catalytic chain	*CPN1*	5	56.25
P15169	Carboxypeptidase N catalytic chain	*CPN1*	9	68.75
O43866	CD5 antigen-like	*CD5L*	5	75.00
O43866	CD5 antigen-like	*CD5L*	6	56.25
O43866	CD5 antigen-like	*CD5L*	9	81.25
P00450	Ceruoplasmin	*CP*	2	87.50
P00450	Ceruoplasmin	*CP*	3	100
P00450	Ceruoplasmin	*CP*	4	81.25
P00450	Ceruoplasmin	*CP*	5	81.25
P00450	Ceruoplasmin	*CP*	6	75.00
P06276	Cholinesterase	*BCHE*	3	50.00
P10909	Clusterin	*CLU*	5	62.50
P10909	Clusterin	*CLU*	6	87.50
P12259	Coagulation factor V	*F5*	1	62.50
P00742	Coagulation factor X	*F10*	5	75.00
P02747	Complement C1q subcomponent subunit C	*C1QC*	1	87.50
P02747	Complement C1q subcomponent subunit C	*C1QC*	2	56.25
P02747	Complement C1q subcomponent subunit C	*C1QC*	6	50.00

P02747	Complement C1q subcomponent subunit C	*C1QC*	7	87.50
P00736	Complement C1r subcomponent	*C1R*	3	62.50
P09871	Complement C1s subcomponent	*C1S*	3	81.25
P09871	Complement C1s subcomponent	*C1S*	4	50.00
P06681	Complement C2	*C2*	3	87.50
P01024	Complement C3	*C3*	1	100
P01024	Complement C3	*C3*	2	100
P01024	Complement C3	*C3*	3	100
P01024	Complement C3	*C3*	4	100
P01024	Complement C3	*C3*	5	100
P01024	Complement C3	*C3*	6	100
P01024	Complement C3	*C3*	7	100
P01024	Complement C3	*C3*	8	93.75
P01024	Complement C3	*C3*	9	87.50
P0C0L4	Complement C4-A	*C4A*	1	56.25
P0C0L4	Complement C4-A	*C4A*	2	93.75
P0C0L4	Complement C4-A	*C4A*	3	100
P0C0L4	Complement C4-A	*C4A*	4	93.75
P0C0L4	Complement C4-A	*C4A*	5	100
P0C0L4	Complement C4-A	*C4A*	6	100
P0C0L4	Complement C4-A	*C4A*	7	100
P0C0L4	Complement C4-A	*C4A*	8	100
P0C0L4	Complement C4-A	*C4A*	9	100
P0C0L4	Complement C4-A	*C4A*	10	50.00
P01031	Complement C5	*C5*	1	100
P01031	Complement C5	*C5*	2	87.50
P13671	Complement component C6	*C6*	2	81.25
P13671	Complement component C6	*C6*	3	100
P13671	Complement component C6	*C6*	5	62.50
P10643	Complement component C7	*C7*	3	56.25
P07357	Complement component C8 alpha chain	*C8A*	5	75.00
P07360	Complement component C8 gamma chain	*C8G*	8	87.50
P02748	Complement component C9	*C9*	1	56.25
P02748	Complement component C9	*C9*	2	56.25
P02748	Complement component C9	*C9*	4	75.00
P00751	Complement factor B	*CFB*	1	56.25
P00751	Complement factor B	*CFB*	2	68.75
P00751	Complement factor B	*CFB*	3	100

P00751	Complement factor B	*CFB*	6	81.25
P00751	Complement factor B	*CFB*	8	68.75
P00751	Complement factor B	*CFB*	9	75.00
P00751	Complement factor B	*CFB*	10	50.00
P00746	Complement factor D	*CFD*	7	75.00
P08603	Complement factor H (CFH)	*CFH*	1	87.50
P08603	Complement factor H (CFH)	*CFH*	2	100
P08603	Complement factor H (CFH)	*CFH*	3	100
P08603	Complement factor H (CFH)	*CFH*	4	62.50
P08603	Complement factor H (CFH)	*CFH*	5	87.50
P08603	Complement factor H (CFH)	*CFH*	6	87.50
P08603	Complement factor H (CFH)	*CFH*	7	87.50
P08603	Complement factor H (CFH)	*CFH*	8	93.75
P08603	Complement factor H (CFH)	*CFH*	9	100
P08603	Complement factor H (CFH)	*CFH*	10	68.75
P05156	Complement factor I	*CFI*	6	62.50
Q03591	Complemet Factor H related protein 1 (FHR-1)	*CFHR1*	5	87.50
Q03591	Complemet Factor H related protein 1 (FHR-1)	*CFHR1*	6	68.75
Q03591	Complemet Factor H related protein 1 (FHR-1)	*CFHR1*	8	87.50
Q03591	Complemet Factor H related protein 1 (FHR-1)	*CFHR1*	9	68.75
P36980	Complemet Factor H related protein 2	*CFHR2*	6	75.00
P02741	C-reactive protein	*CRP*	1	50.00
P02679	Fibrinogen γ chain (FGγ)	*FGG*	3	81.25
P02679	Fibrinogen γ chain (FGγ)	*FGG*	5	93.75
P02679	Fibrinogen γ chain (FGγ)	*FGG*	6	62.50
P02671	Fibrinogen-α-Chain (FGα)	*FGA*	1	93.75
P02671	Fibrinogen-α-Chain (FGα)	*FGA*	2	100
P02671	Fibrinogen-α-Chain (FGα)	*FGA*	3	100
P02671	Fibrinogen-α-Chain (FGα)	*FGA*	4	100
P02671	Fibrinogen-α-Chain (FGα)	*FGA*	5	100
P02671	Fibrinogen-α-Chain (FGα)	*FGA*	6	100
P02671	Fibrinogen-α-Chain (FGα)	*FGA*	7	100
P02671	Fibrinogen-α-Chain (FGα)	*FGA*	8	100
P02671	Fibrinogen-α-Chain (FGα)	*FGA*	9	87.50
P02671	Fibrinogen-α-Chain (FGα)	*FGA*	10	50.00
P02675	Fibrinogen-β-Chain (FGβ)	*FGB*	1	81.25
P02675	Fibrinogen-β-Chain (FGβ)	*FGB*	2	93.75

P02675	Fibrinogen-β-Chain (FGβ)	*FGB*	3	93.75
P02675	Fibrinogen-β-Chain (FGβ)	*FGB*	4	87.50
P02675	Fibrinogen-β-Chain (FGβ)	*FGB*	5	100
P02675	Fibrinogen-β-Chain (FGβ)	*FGB*	6	87.50
P02675	Fibrinogen-β-Chain (FGβ)	*FGB*	7	100
P02675	Fibrinogen-β-Chain (FGβ)	*FGB*	8	87.50
P02675	Fibrinogen-β-Chain (FGβ)	*FGB*	9	87.50
P02675	Fibrinogen-β-Chain (FGβ)	*FGB*	10	50.00
P02751	Fibronectin	*FN1*	1	100
P02751	Fibronectin	*FN1*	2	93.75
P02751	Fibronectin	*FN1*	3	93.75
Q15485	Ficolin-2	*FCN2*	6	81.25
O75636	Ficolin-3	*FCN3*	6	75.00
P06396	Gelsolin	*GSN*	2	56.25
P06396	Gelsolin	*GSN*	3	93.75
P06396	Gelsolin	*GSN*	4	56.25
P06396	Gelsolin	*GSN*	5	75.00
P06396	Gelsolin	*GSN*	6	56.25
P22352	Glutathione Peroxidase 3	*GPX3*	7	87.50
P22352	Glutathione Peroxidase 3	*GPX3*	8	56.25
P00738	Haptoglobin (HP)	*HP*	2	68.75
P00738	Haptoglobin (HP)	*HP*	3	75.00
P00738	Haptoglobin (HP)	*HP*	5	100
P00738	Haptoglobin (HP)	*HP*	6	93.75
P00738	Haptoglobin (HP)	*HP*	7	81.25
P00738	Haptoglobin (HP)	*HP*	8	81.25
P00739	Haptoglobin-related protein	*HPR*	5	62.50
P00739	Haptoglobin-related protein	*HPR*	6	81.25
P00739	Haptoglobin-related protein	*HPR*	9	68.75
P02790	Hemopexin	*HPX*	1	62.50
P02790	Hemopexin	*HPX*	2	87.50
P02790	Hemopexin	*HPX*	3	100
P02790	Hemopexin	*HPX*	4	93.75
P02790	Hemopexin	*HPX*	5	100
P02790	Hemopexin	*HPX*	6	87.50
P02790	Hemopexin	*HPX*	7	87.50
P02790	Hemopexin	*HPX*	8	87.50
P02790	Hemopexin	*HPX*	9	56.25
P05546	Heparin cofactor 2	*SERPIND1*	4	68.75

P04196	Histidine-rich glycoprotein	*HRG*	1	75.00
P04196	Histidine-rich glycoprotein	*HRG*	3	68.75
P04196	Histidine-rich glycoprotein	*HRG*	4	75.00
P04196	Histidine-rich glycoprotein	*HRG*	5	62.50
P04196	Histidine-rich glycoprotein	*HRG*	6	56.25
P01876	Ig alpha-1 chain C region	*IGHA1*	1	93.75
P01876	Ig alpha-1 chain C region	*IGHA1*	2	93.75
P01876	Ig alpha-1 chain C region	*IGHA1*	3	87.50
P01876	Ig alpha-1 chain C region	*IGHA1*	4	93.75
P01876	Ig alpha-1 chain C region	*IGHA1*	5	93.75
P01876	Ig alpha-1 chain C region	*IGHA1*	6	100
P01876	Ig alpha-1 chain C region	*IGHA1*	7	100
P01876	Ig alpha-1 chain C region	*IGHA1*	8	100
P01876	Ig alpha-1 chain C region	*IGHA1*	9	93.75
P01877	Ig alpha-2 chain C region	*IGHA2*	2	75.00
P01877	Ig alpha-2 chain C region	*IGHA2*	3	81.25
P01877	Ig alpha-2 chain C region	*IGHA2*	4	81.25
P01877	Ig alpha-2 chain C region	*IGHA2*	5	87.50
P01877	Ig alpha-2 chain C region	*IGHA2*	6	56.25
P01860	Ig gamma-3 chain C region	*IGHG3*	1	93.75
P01860	Ig gamma-3 chain C region	*IGHG3*	2	81.25
P01860	Ig gamma-3 chain C region	*IGHG3*	3	100
P01860	Ig gamma-3 chain C region	*IGHG3*	4	87.50
P01860	Ig gamma-3 chain C region	*IGHG3*	5	100
P01860	Ig gamma-3 chain C region	*IGHG3*	6	81.25
P01860	Ig gamma-3 chain C region	*IGHG3*	7	100
P01768	Ig heavy chain V-III region CAM	n/a	3	50.00
P01768	Ig heavy chain V-III region CAM	n/a	4	50.00
P01768	Ig heavy chain V-III region CAM	n/a	5	68.75
P01768	Ig heavy chain V-III region CAM	n/a	6	56.25
P01768	Ig heavy chain V-III region CAM	n/a	8	62.50
P01768	Ig heavy chain V-III region CAM	n/a	9	68.75
P01781	Ig heavy chain V-III region GAL	n/a	2	56.25
P01781	Ig heavy chain V-III region GAL	n/a	3	81.25
P01781	Ig heavy chain V-III region GAL	n/a	5	68.75
P01781	Ig heavy chain V-III region GAL	n/a	6	62.50
P01781	Ig heavy chain V-III region GAL	n/a	8	68.75
P01781	Ig heavy chain V-III region GAL	n/a	9	68.75
P01780	Ig heavy chain V-III region JON	n/a	5	87.50

P01762	Ig heavy chain V-III region TRO	n/a	1	50.00
P01762	Ig heavy chain V-III region TRO	n/a	2	81.25
P01762	Ig heavy chain V-III region TRO	n/a	3	93.75
P01762	Ig heavy chain V-III region TRO	n/a	4	68.75
P01762	Ig heavy chain V-III region TRO	n/a	5	100
P01762	Ig heavy chain V-III region TRO	n/a	6	100
P01762	Ig heavy chain V-III region TRO	n/a	8	68.75
P01762	Ig heavy chain V-III region TRO	n/a	9	75.00
P01762	Ig heavy chain V-III region TRO	n/a	10	50.00
P01834	Ig kappa chain C region	*IGKC*	3	62.50
P01834	Ig kappa chain C region	*IGKC*	6	56.25
P01834	Ig kappa chain C region	*IGKC*	7	100
P06310	Ig kappa chain V-II region RPMI 6410	n/a	7	75.00
P06310	Ig kappa chain V-II region RPMI 6410	n/a	8	62.50
P04206	Ig kappa chain V-III region GOL	n/a	7	87.50
P18135	Ig kappa chain V-III region HAH	*IGKV3-20*	7	87.50
P18135	Ig kappa chain V-III region HAH	*IGKV3-20*	8	50.00
P01620	Ig kappa chain V-III region SIE	n/a	7	93.75
P04433	Ig kappa chain V-III region VG	*IGKV3D-11*	7	87.50
P04433	Ig kappa chain V-III region VG	*IGKV3D-11*	8	62.50
P01700	Ig lambda chain V-I region HA	n/a	3	68.75
P01700	Ig lambda chain V-I region HA	n/a	7	81.25
P01700	Ig lambda chain V-I region HA	n/a	8	68.75
P01700	Ig lambda chain V-I region HA	n/a	9	62.50
P0CG04	Ig lambda-1 chain C regions	*IGLC1*	2	56.25
P0CG04	Ig lambda-1 chain C regions	*IGLC1*	6	68.75
P0CG04	Ig lambda-1 chain C regions	*IGLC1*	7	75.00
P0CG04	Ig lambda-1 chain C regions	*IGLC1*	8	68.75
P0CG04	Ig lambda-1 chain C regions	*IGLC1*	9	56.25
P0CF74	Ig lambda-6 chain C region	*IGLC6*	7	50.00
A0M8Q6	Ig lambda-7 chain C region	*IGLC7*	7	75.00
P01871	Ig mu chain C region	*IGHM*	5	56.25
P01871	Ig mu chain C region	*IGHM*	6	75.00
P01871	Ig mu chain C region	*IGHM*	7	56.25
P01871	Ig mu chain C region	*IGHM*	8	50.00
P04220	Ig mu heavy chain disease protein	n/a	1	50.00
P04220	Ig mu heavy chain disease protein	n/a	2	62.50
P04220	Ig mu heavy chain disease protein	n/a	3	68.75

P04220	Ig mu heavy chain disease protein	n/a	4	62.50
P01591	Immunoglobulin J chain	*IGJ*	7	50.00
P19827	Inter-alpha-trypsin inhibitor heavy chain H1	*ITIH1*	1	100
P19827	Inter-alpha-trypsin inhibitor heavy chain H1	*ITIH1*	2	87.50
P19827	Inter-alpha-trypsin inhibitor heavy chain H1	*ITIH1*	3	100
P19827	Inter-alpha-trypsin inhibitor heavy chain H1	*ITIH1*	4	62.50
P19827	Inter-alpha-trypsin inhibitor heavy chain H1	*ITIH1*	5	50.00
P19827	Inter-alpha-trypsin inhibitor heavy chain H1	*ITIH1*	8	62.50
P19827	Inter-alpha-trypsin inhibitor heavy chain H1	*ITIH1*	9	62.50
P19823	Inter-alpha-trypsin inhibitor heavy chain H2	*ITIH2*	1	100
P19823	Inter-alpha-trypsin inhibitor heavy chain H2	*ITIH2*	2	93.75
P19823	Inter-alpha-trypsin inhibitor heavy chain H2	*ITIH2*	3	100
P19823	Inter-alpha-trypsin inhibitor heavy chain H2	*ITIH2*	4	75.00
P19823	Inter-alpha-trypsin inhibitor heavy chain H2	*ITIH2*	5	75.00
P19823	Inter-alpha-trypsin inhibitor heavy chain H2	*ITIH2*	8	56.25
Q06033	Inter-alpha-trypsin inhibitor heavy chain H3	*ITIH3*	1	75.00
Q06033	Inter-alpha-trypsin inhibitor heavy chain H3	*ITIH3*	2	56.25
Q06033	Inter-alpha-trypsin inhibitor heavy chain H3	*ITIH3*	3	75.00
Q14624	Inter-alpha-trypsin inhibitor heavy chain H4	*ITIH4*	1	56.25
Q14624	Inter-alpha-trypsin inhibitor heavy chain H4	*ITIH4*	2	87.50
Q14624	Inter-alpha-trypsin inhibitor heavy chain H4	*ITIH4*	3	100
Q14624	Inter-alpha-trypsin inhibitor heavy chain H4	*ITIH4*	5	93.75
Q14624	Inter-alpha-trypsin inhibitor heavy chain H4	*ITIH4*	6	56.25
P29622	Kallistatin	*SERPINA4*	1	75.00
P29622	Kallistatin	*SERPINA4*	5	56.25
P01042	Kininogen-1	*KNG1*	3	81.25
P02750	Leucine-rich alpha-2-glycoprotein	*LRG1*	5	87.50
Q9H8L6	Multimerin-2	*MMRN2*	8	50.00
P32119	Peroxiredoxin-2	*PRDX2*	7	62.50

P32119	Peroxiredoxin-2	*PRDX2*	8	75.00
P80108	Phosphatidylinositol-glycan-specific phospholipase D	*GPLD1*	3	68.75
P36955	Pigment epithelium-derived factor	*SERPINF1*	5	81.25
P03952	Plasma kallikrein	*KLKB1*	3	93.75
P00747	Plasminogen	*PLG*	1	62.50
P00747	Plasminogen	*PLG*	2	93.75
P00747	Plasminogen	*PLG*	3	100
P00747	Plasminogen	*PLG*	4	62.50
P00747	Plasminogen	*PLG*	5	87.50
P00747	Plasminogen	*PLG*	6	81.25
P00747	Plasminogen	*PLG*	7	93.75
P00747	Plasminogen	*PLG*	9	62.50
P02775	Platelet basic protein	*PPBP*	9	87.50
Q92620	Pre-mRNA-splicing factor	*DHX38*	2	87.50
Q92620	Pre-mRNA-splicing factor	*DHX38*	3	81.25
Q92620	Pre-mRNA-splicing factor	*DHX38*	5	62.50
P02760	Protein AMBP	*AMBP*	6	75.00
Q92954	Proteoglycan 4	*PRG4*	9	50.00
P00734	Prothrombin	*F2*	3	81.25
P00734	Prothrombin	*F2*	4	87.50
P00734	Prothrombin	*F2*	5	68.75
P00734	Prothrombin	*F2*	6	68.75
A6NIZ1	Ras-related protein Rap-1b-like protein	*RAP1BL*	7	62.50
P02753	Retinol-binding protein 4	*RBP4*	9	62.50
P02753	Retinol-binding protein 5	*RBP4*	7	87.50
P02753	Retinol-binding protein 6	*RBP4*	8	87.50
Q13103	Secreted phosphoprotein 24	*SPP2*	8	50.00
P02787	Serotransferrin	*TF*	1	87.50
P02787	Serotransferrin	*TF*	2	100
P02787	Serotransferrin	*TF*	3	100
P02787	Serotransferrin	*TF*	4	93.75
P02787	Serotransferrin	*TF*	5	100
P02787	Serotransferrin	*TF*	6	100
P02787	Serotransferrin	*TF*	7	100
P02787	Serotransferrin	*TF*	8	100
P02787	Serotransferrin	*TF*	9	100
P02787	Serotransferrin	*TF*	10	75.00
P35542	Serum amyloid A-4 protein	*SAA4*	8	100

P35542	Serum amyloid A-4 protein	*SAA4*	9	93.75
P35542	Serum amyloid A-4 protein	*SAA4*	10	56.25
P02743	Serum amyloid P-component	*APCS*	7	93.75
P27169	Serum paraoxonase/arylesterase 1	*PON1*	5	56.25
Q9H299	SH3 domain-binding glutamic acid-rich-like protein 3	*SH3BGRL3*	9	68.75
Q9H299	SH3 domain-binding glutamic acid-rich-like protein 3	*SH3BGRL3*	10	50.00
P02549	Spectrin alpha chain, erythrocytic 1	*SPTA1*	7	56.25
P35443	Thrombospondin-4	*THBS4*	8	68.75
P02766	Transthyretin	*TTR*	6	56.25
P02766	Transthyretin	*TTR*	8	93.75
P02766	Transthyretin	*TTR*	9	93.75
P02766	Transthyretin	*TTR*	10	56.25
P07225	Vitamin K-dependent protein S	*PROS1*	3	81.25
P04004	Vitronectin	*VTN*	9	50.00
P04275	von Willebrand factor	*VWF*	1	68.75
P04275	von Willebrand factor	*VWF*	2	75.00
P25311	Zinc-alpha-2-glycoprotein	*AZGP1*	5	87.50
P25311	Zinc-alpha-2-glycoprotein	*AZGP1*	6	75.00
P25311	Zinc-alpha-2-glycoprotein	*AZGP1*	7	62.50

Appendix 2. MS/MS spectra assignments for protein groups not selected for technical replication in Chapter 3.

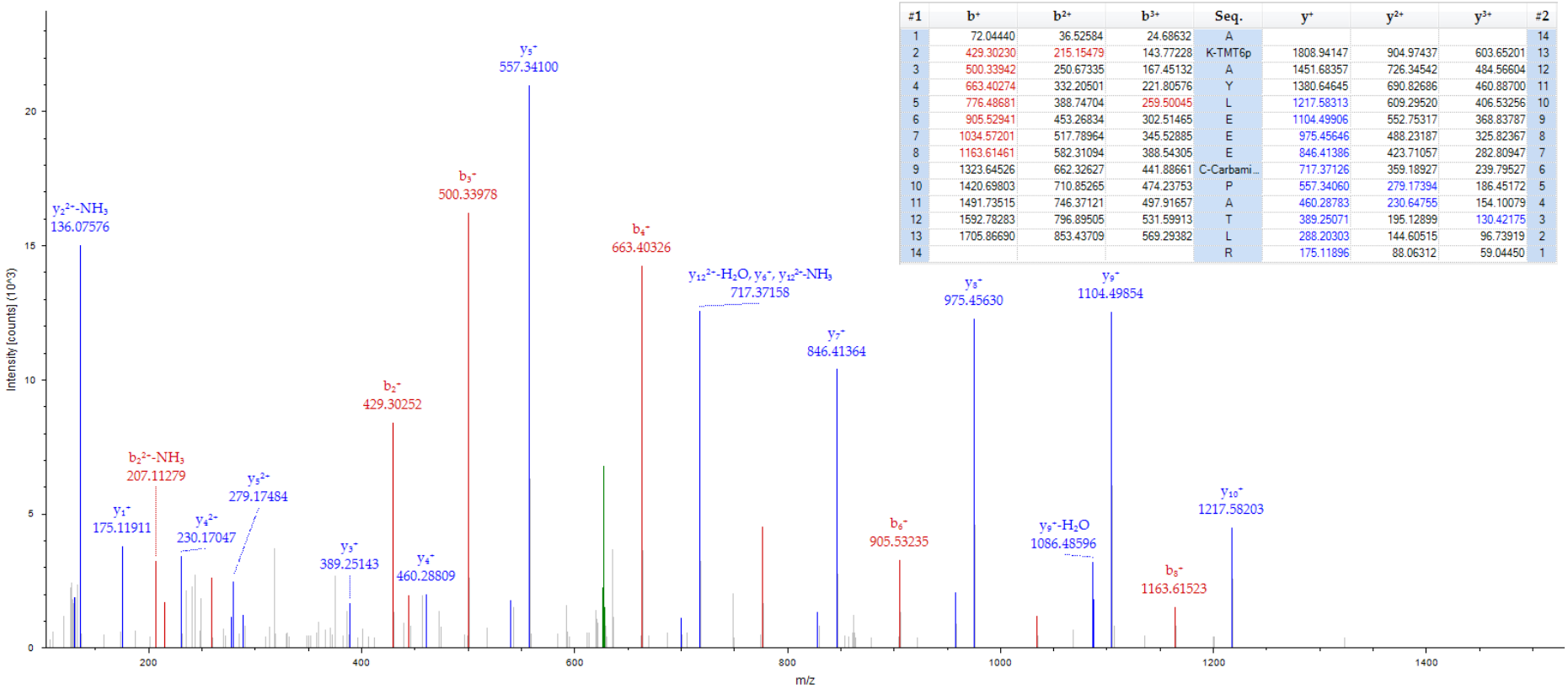

#1	b+	b2+	b3+	Seq.	y+	y2+	y3+	#2
1	72.04440	36.52584	24.68632	A				14
2	429.30230	215.15479	143.77228	K-TMT6p	1808.94147	904.97437	603.65201	13
3	500.33942	250.67335	167.45132	A	1451.68357	726.34542	484.56604	12
4	663.40274	332.20501	221.80576	Y	1380.64645	690.82686	460.88700	11
5	776.48681	388.74704	259.50045	L	1217.58313	609.29520	406.53256	10
6	905.52941	453.26834	302.51465	E	1104.49906	552.75317	368.83787	9
7	1034.57201	517.78964	345.52885	E	975.45646	488.23187	325.82367	8
8	1163.61461	582.31094	388.54305	E	846.41386	423.71057	282.80947	7
9	1323.64526	662.32627	441.88661	C-Carbami...	717.37126	359.18927	239.79527	6
10	1420.69803	710.85265	474.23753	P	557.34060	279.17394	186.45172	5
11	1491.73515	746.37121	497.91657	A	460.28783	230.64755	154.10079	4
12	1592.78283	796.89505	531.59913	T	389.25071	195.12899	130.42175	3
13	1705.86690	853.43709	569.29382	L	288.20303	144.60515	96.73919	2
14				R	175.11896	88.06312	59.04450	1

MS/MS spectrum of *m/z* 627.33 the $[M+3H]^{3+}$ molecular ion for a peptide of 1879.97 Da with corresponding sequence AKAYLEEECPATLR unique to zinc-alpha-2-glycoprotein identified in 1DGE fraction 7 as significant (*P* value <0.05) between PiB+ and PiB- groups.

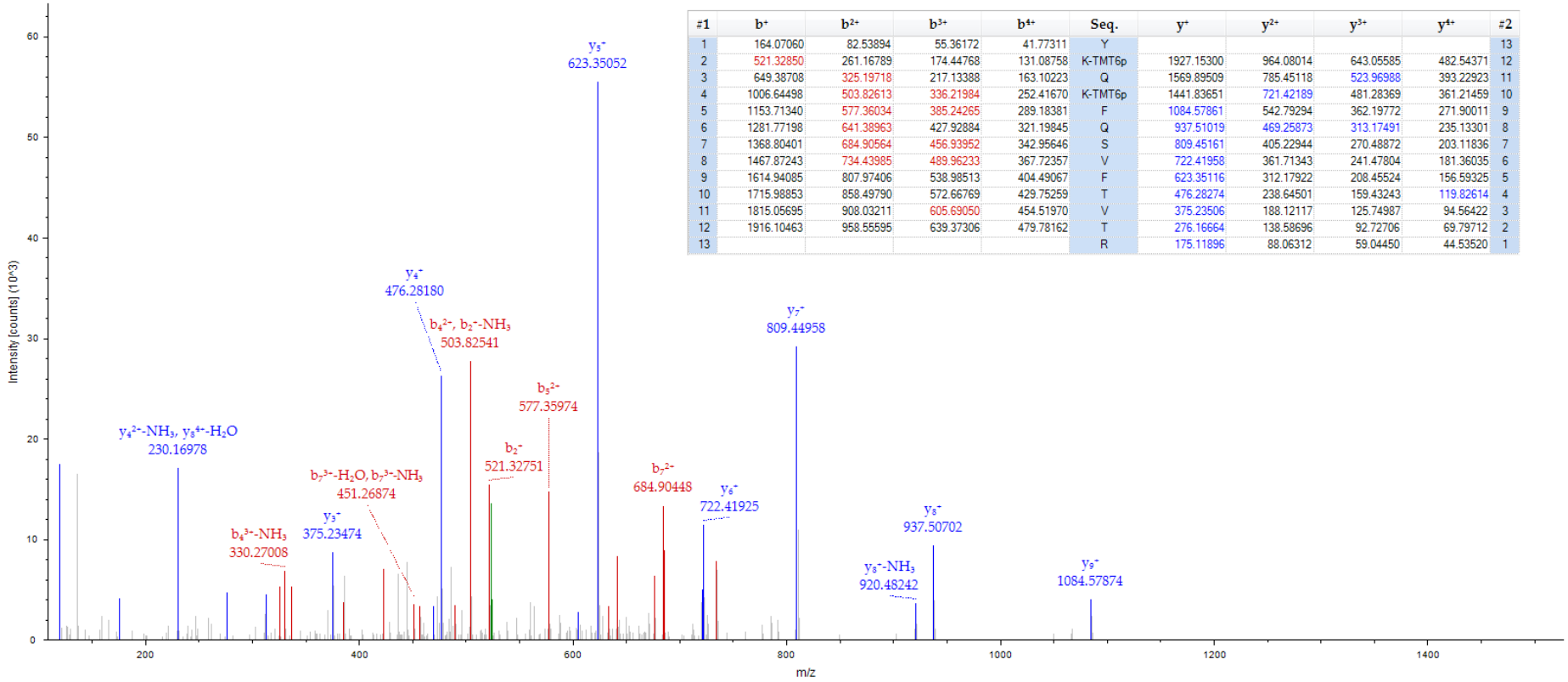

#1	b+	b2+	b3+	b4+	Seq.	y+	y2+	y3+	y4+	#2
1	164.07060	82.53894	55.36172	41.77311	Y					13
2	521.32850	261.16789	174.44768	131.08758	K-TMT6p	1927.15300	964.08014	643.05585	482.54371	12
3	649.38708	325.19718	217.13388	163.10223	Q	1569.89509	785.45118	523.96988	393.22923	11
4	1006.64498	503.82613	336.21984	252.41670	K-TMT6p	1441.83651	721.42189	481.28369	361.21459	10
5	1153.71340	577.36034	385.24265	289.18381	F	1084.57861	542.79294	362.19772	271.90011	9
6	1281.77198	641.38963	427.92884	321.19845	Q	937.51019	469.25873	313.17491	235.13301	8
7	1368.80401	684.90564	456.93952	342.95646	S	809.45161	405.22944	270.48872	203.11836	7
8	1467.87243	734.43985	489.96233	367.72357	V	722.41958	361.71343	241.47804	181.36035	6
9	1614.94085	807.97406	538.98513	404.49067	F	623.35116	312.17922	208.45524	156.59325	5
10	1715.98853	858.49790	572.66769	429.75259	T	476.28274	238.64501	159.43243	119.82614	4
11	1815.05695	908.03211	605.69050	454.51970	V	375.23506	188.12117	125.74987	94.56422	3
12	1916.10463	958.55595	639.37306	479.78162	T	276.16664	138.58696	92.72706	69.79712	2
13					R	175.11896	88.06312	59.04450	44.53520	1

MS/MS spectrum of *m/z* 523.30 the $[M+3H]^{3+}$ molecular ion for a peptide of 2090.21 Da with corresponding sequence YKQKFQSVFTVTR unique to complement C1q subcomponent subunit C identified in 1DGE fraction 2 as significant (*P* value <0.05) between PiB+ and PiB- groups.

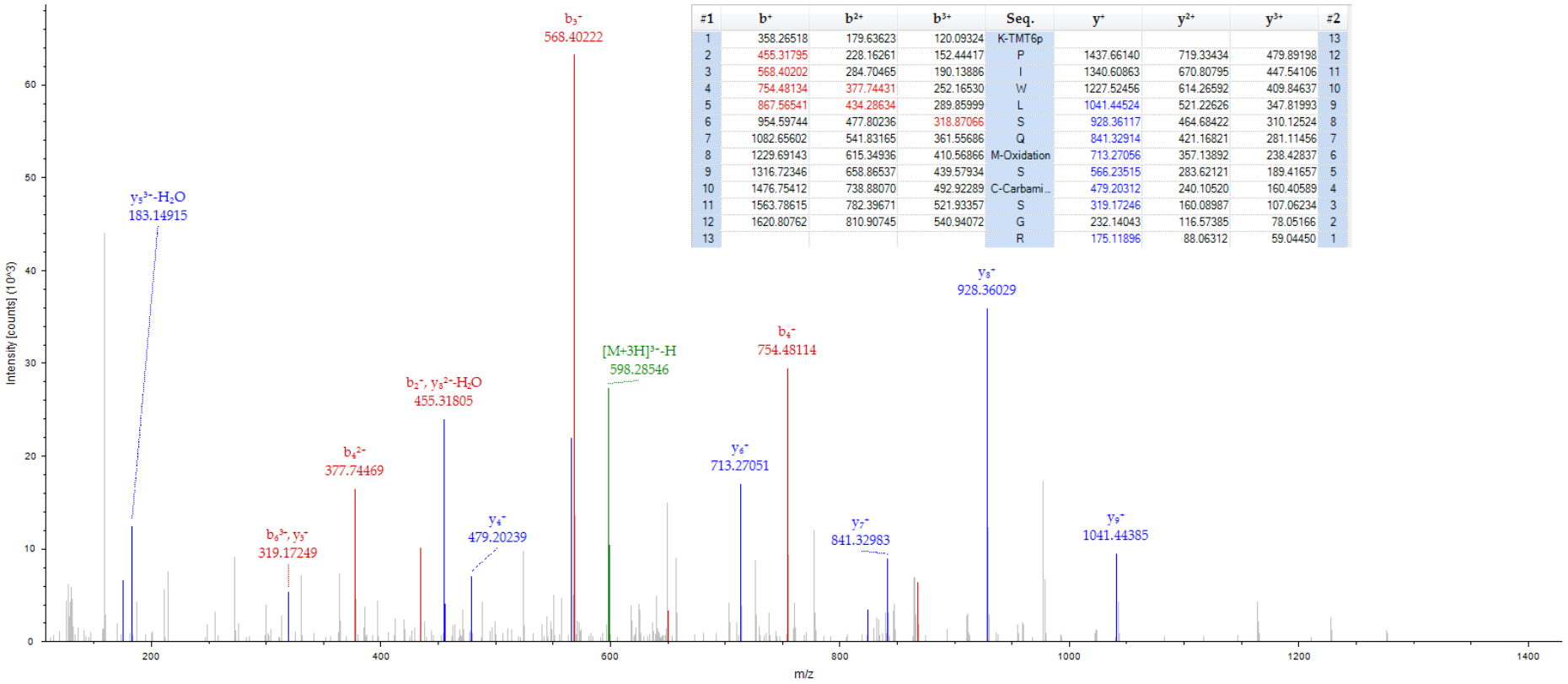

#1	b+	b2+	b3+	Seq.	y+	y2+	y3+	#2
1	358.26518	179.63623	120.09324	K-TMT6p				13
2	455.31795	228.16261	152.44417	P	1437.66140	719.33434	479.89198	12
3	568.40202	284.70465	190.13886	I	1340.60863	670.80795	447.54106	11
4	754.48134	377.74431	252.16530	W	1227.52456	614.26592	409.84637	10
5	867.56541	434.28634	289.85999	L	1041.44524	521.22626	347.81993	9
6	954.59744	477.80236	318.87066	S	928.36117	464.68422	310.12524	8
7	1082.65602	541.83165	361.55686	Q	841.32914	421.16821	281.11456	7
8	1229.69143	615.34936	410.56866	M-Oxidation	713.27056	357.13892	238.42837	6
9	1316.72346	658.86537	439.57934	S	566.23515	283.62121	189.41657	5
10	1476.75412	738.88070	492.92289	C-Carbami...	479.20312	240.10520	160.40589	4
11	1563.78615	782.39671	521.93357	S	319.17246	160.08987	107.06234	3
12	1620.80762	810.90745	540.94072	G	232.14043	116.57385	78.05166	2
13				R	175.11896	88.06312	59.04450	1

MS/MS spectrum of *m/z* 593.64 the $[M+3H]^{3+}$ molecular ion for a peptide of 1778.91 Da with corresponding sequence KPIWLSQMSCSGR unique to CD5 antigen-like identified in 1DGE fraction 5 as significant (*P* value <0.05) between PiB+ and PiB- groups.

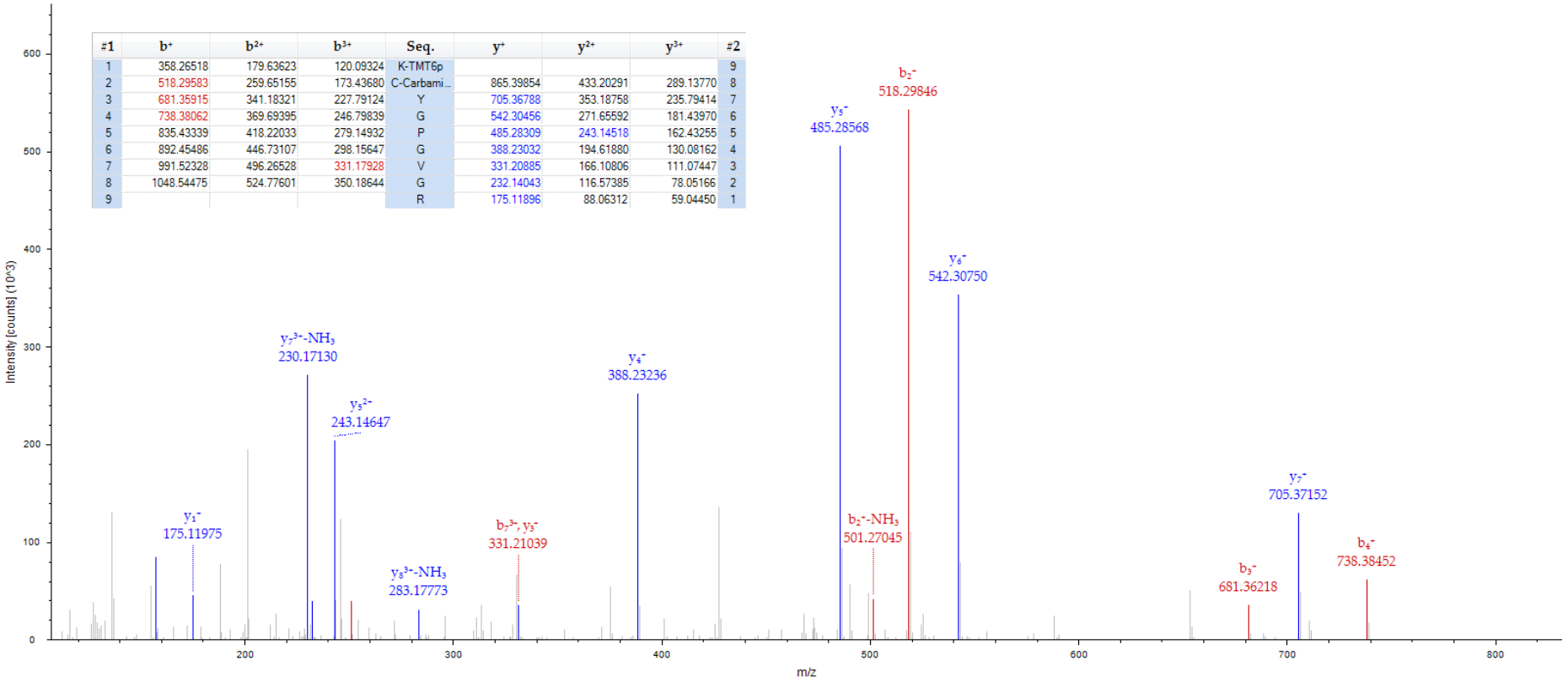

MS/MS spectrum of *m/z* 408.22 the $[M+3H]^{3+}$ molecular ion for a peptide of 1222.65 Da with corresponding sequence KCYGPGVGR unique to CD5 antigen-like identified in 1DGE fraction 5 as significant (*P* value <0.05) between PiB+ and PiB- groups.

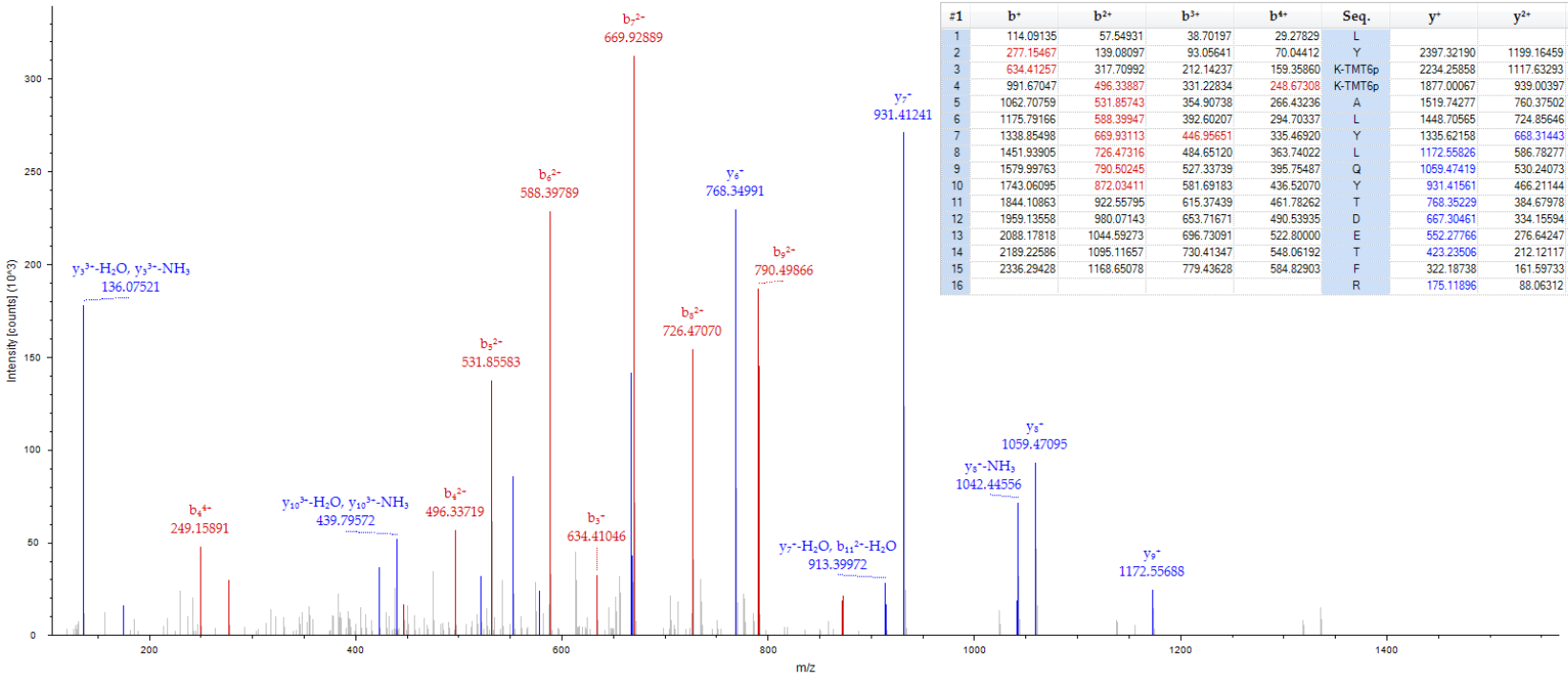

#1	b+	b2+	b3+	b4+	Seq.	y+	y2+	y3+	y4+	#2
1	114.09135	57.54931	38.70197	29.27829	L					16
2	277.15467	139.08097	93.05641	70.04412	Y	2397.32190	1199.16459	799.77882	600.08593	15
3	634.41257	317.70992	212.14237	159.35860	K-TMT6p	2234.25858	1117.63293	745.42438	559.32010	14
4	991.67047	496.33887	331.22834	248.67308	K-TMT6p	1877.00067	939.00397	626.33841	470.00563	13
5	1062.70759	531.85743	354.90738	266.43236	A	1519.74277	760.37502	507.25244	380.69115	12
6	1175.79166	588.39947	392.60207	294.70337	L	1448.70565	724.85646	483.57340	362.93187	11
7	1338.85498	669.93113	446.95651	335.46920	Y	1335.62158	668.31443	445.87871	334.66085	10
8	1451.93905	726.47316	484.65120	363.74022	L	1172.55826	586.78277	391.52427	293.89502	9
9	1579.99763	790.50245	527.33739	395.75487	Q	1059.47419	530.24073	353.82958	265.62401	8
10	1743.06095	872.03411	581.69183	436.52070	Y	931.41561	466.21144	311.14339	233.60936	7
11	1844.10863	922.55795	615.37439	461.78262	T	768.35229	384.67978	256.78895	192.84353	6
12	1959.13558	980.07143	653.71671	490.53935	D	667.30461	334.15594	223.10639	167.58161	5
13	2088.17818	1044.59273	696.73091	522.80000	E	552.27766	276.64247	184.76407	138.82487	4
14	2189.22586	1095.11657	730.41347	548.06192	T	423.23506	212.12117	141.74987	106.56422	3
15	2336.29428	1168.65078	779.43628	584.82903	F	322.18738	161.59733	108.06731	81.30230	2
16					R	175.11896	88.06312	59.04450	44.53520	1

MS/MS spectrum of *m/z* 628.35 the $[M+4H]^{4+}$ molecular ion for a peptide of 2510.40 Da with corresponding sequence LYKKALYLQYTDETFR unique to ceruoplasmin identified in 1DGE fraction 2 as significant (*P* value <0.05) between PiB+ and PiB- groups.

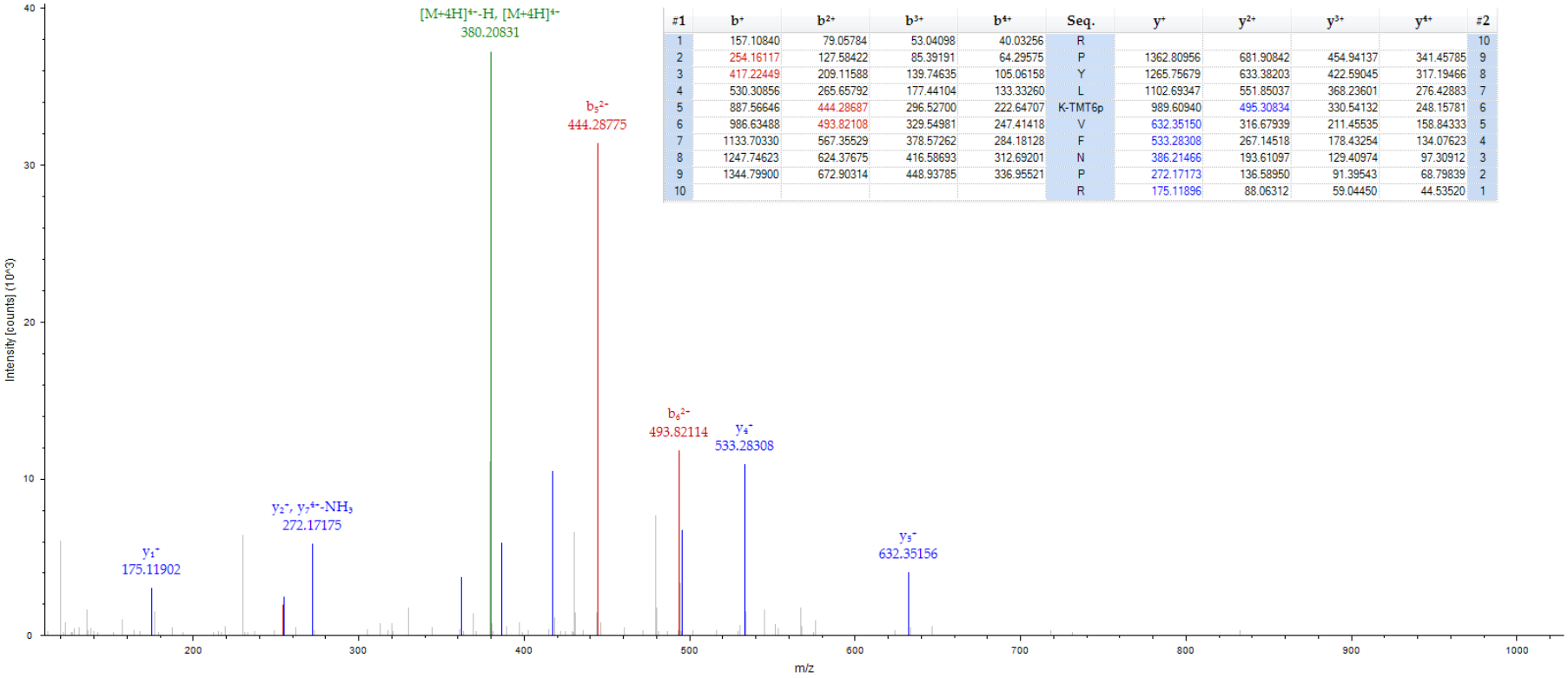

#1	b⁺	b²⁺	b³⁺	b⁴⁺	Seq.	y⁺	y²⁺	y³⁺	y⁴⁺	#2
1	157.10840	79.05784	53.04098	40.03256	R					10
2	254.16117	127.58422	85.39191	64.29575	P	1362.80956	681.90842	454.94137	341.45785	9
3	417.22449	209.11588	139.74635	105.06158	Y	1265.75679	633.38203	422.59045	317.19466	8
4	530.30856	265.65792	177.44104	133.33260	L	1102.69347	551.85037	368.23601	276.42883	7
5	887.56646	444.28687	296.52700	222.64707	K-TMT6p	989.60940	495.30834	330.54132	248.15781	6
6	986.63488	493.82108	329.54981	247.41418	V	632.35150	316.67939	211.45535	158.84333	5
7	1133.70330	567.35529	378.57262	284.18128	F	533.28308	267.14518	178.43254	134.07623	4
8	1247.74623	624.37675	416.58693	312.69201	N	386.21466	193.61097	129.40974	97.30912	3
9	1344.79900	672.90314	448.93785	336.95521	P	272.17173	136.58950	91.39543	68.79839	2
10					R	175.11896	88.06312	59.04450	44.53520	1

MS/MS spectrum of *m/z* 380.48 the $[M+4H]^{4+}$ molecular ion for a peptide of 1518.91 Da with corresponding sequence RPYLKVFNPR unique to ceruoplasmin identified in 1DGE fraction 2 as significant (*P* value <0.05) between PiB+ and PiB- groups.

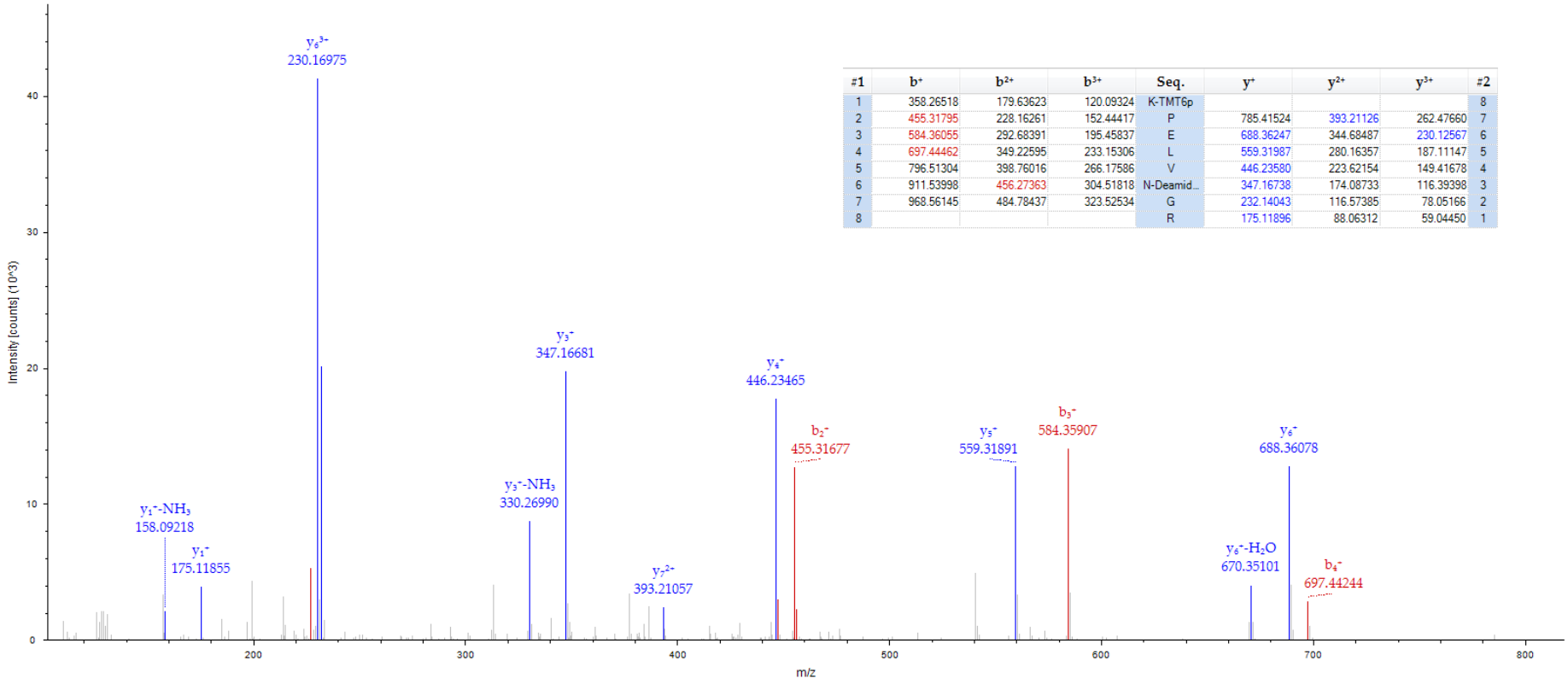

#1	b^+	b^{2+}	b^{3+}	Seq.	y^+	y^{2+}	y^{3+}	#2
1	358.26518	179.63623	120.09324	K-TMT6p				8
2	455.31795	228.16261	152.44417	P	785.41524	393.21126	262.47660	7
3	584.36055	292.68391	195.45837	E	688.36247	344.68487	230.12567	6
4	697.44462	349.22595	233.15306	L	559.31987	280.16357	187.11147	5
5	796.51304	398.76016	266.17586	V	446.23580	223.62154	149.41678	4
6	911.53998	456.27363	304.51818	N-Deamid...	347.16738	174.08733	116.39398	3
7	968.56145	484.78437	323.52534	G	232.14043	116.57385	78.05166	2
8				R	175.11896	88.06312	59.04450	1

MS/MS spectrum of *m/z* 381.56 the $[M+3H]^{3+}$ molecular ion for a peptide of 1142.67 Da with corresponding sequence KPELVNGR unique to C4b-binding protein alpha chain identified in 1DGE fraction 4 as significant (*P* value <0.05) between PiB+ and PiB- groups.

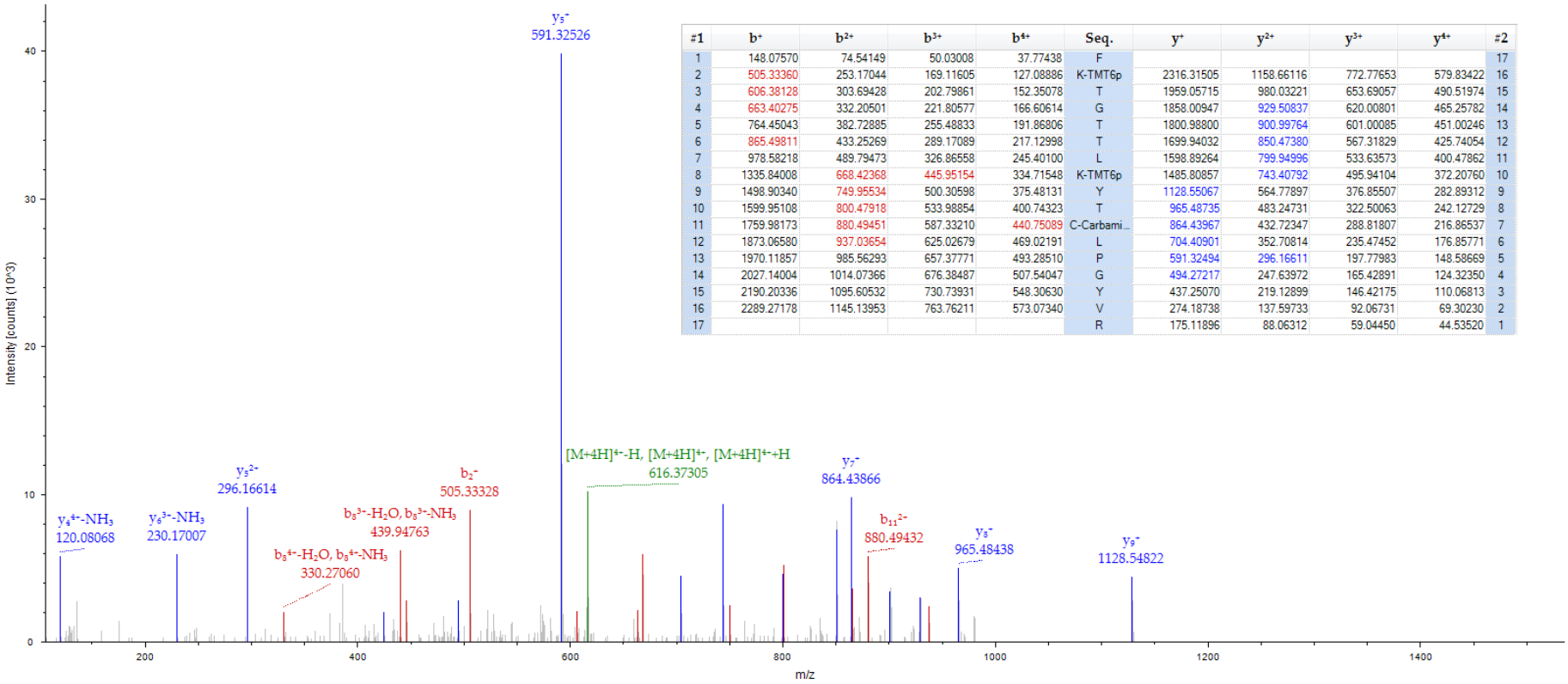

#1	b+	b2+	b3+	b4+	Seq.	y+	y2+	y3+	y4+	#2
1	148.07570	74.54149	50.03008	37.77438	F					17
2	505.33360	253.17044	169.11605	127.08886	K-TMT6p	2316.31505	1158.66116	772.77653	579.83422	16
3	606.38128	303.69428	202.79861	152.35078	T	1959.05715	980.03221	653.69057	490.51974	15
4	663.40275	332.20501	221.80577	166.60614	G	1858.00947	929.50837	620.00801	465.25782	14
5	764.45043	382.72885	255.48833	191.86806	T	1800.98800	900.99764	601.00085	451.00246	13
6	865.49811	433.25269	289.17089	217.12998	T	1699.94032	850.47380	567.31829	425.74054	12
7	978.58218	489.79473	326.86558	245.40100	L	1598.89264	799.94996	533.63573	400.47862	11
8	1335.84008	668.42368	445.95154	334.71548	K-TMT6p	1485.80857	743.40792	495.94104	372.20760	10
9	1498.90340	749.95534	500.30598	375.48131	Y	1128.55067	564.77897	376.85507	282.89312	9
10	1599.95108	800.47918	533.98854	400.74323	T	965.48735	483.24731	322.50063	242.12729	8
11	1759.98173	880.49451	587.33210	440.75089	C-Carbami...	864.43967	432.72347	288.81807	216.86537	7
12	1873.06580	937.03654	625.02679	469.02191	L	704.40901	352.70814	235.47452	176.85771	6
13	1970.11857	985.56293	657.37771	493.28510	P	591.32494	296.16611	197.77983	148.58669	5
14	2027.14004	1014.07366	676.38487	507.54047	G	494.27217	247.63972	165.42891	124.32350	4
15	2190.20336	1095.60532	730.73931	548.30630	Y	437.25070	219.12899	146.42175	110.06813	3
16	2289.27178	1145.13953	763.76211	573.07340	V	274.18738	137.59733	92.06731	69.30230	2
17					R	175.11896	88.06312	59.04450	44.53520	1

MS/MS spectrum of *m/z* 616.60 the $[M+4H]^{4+}$ molecular ion for a peptide of 2463.38 Da with corresponding sequence FKTGTTLKYTCLPGYVR unique to C4b-binding protein alpha chain identified in 1DGE fraction 4 as significant (*P* value <0.05) between PiB+ and PiB- groups.

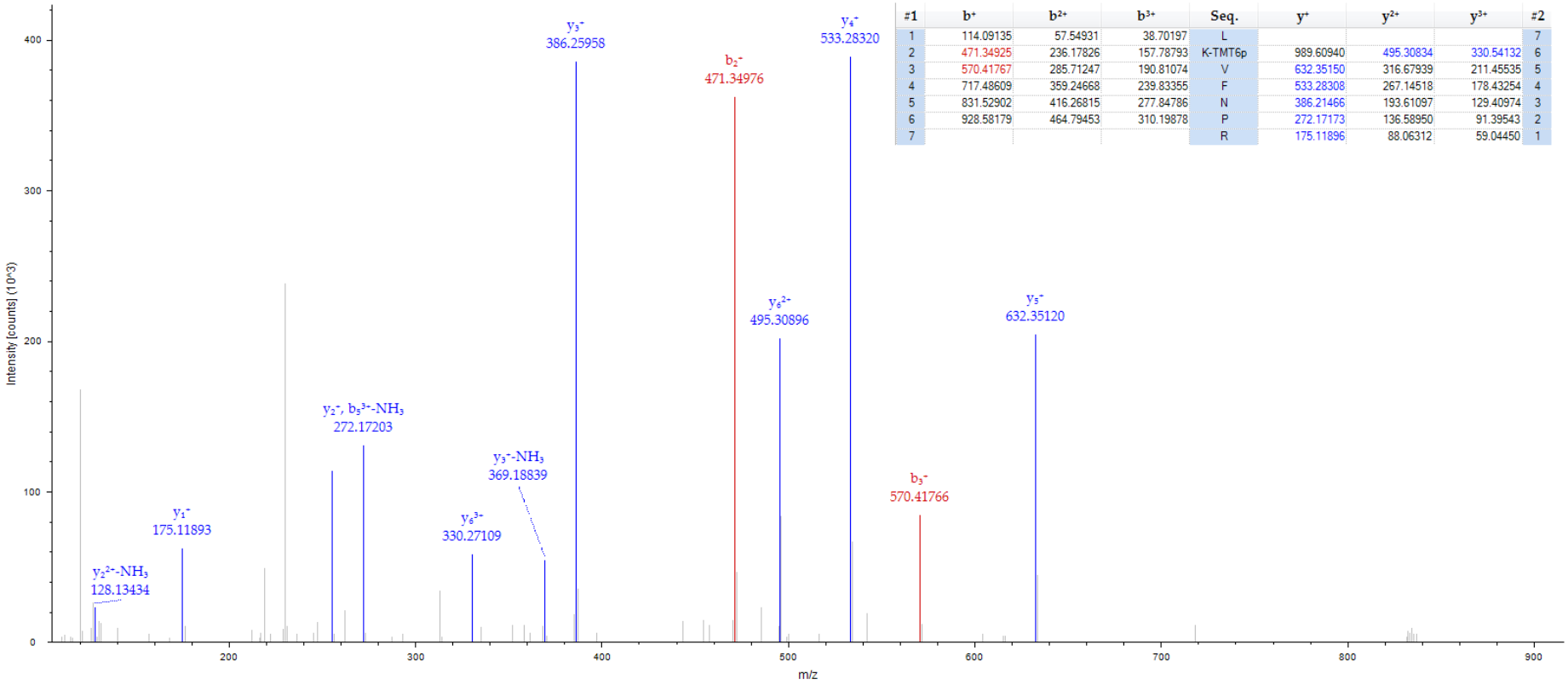

#1	b+	b2+	b3+	Seq.	y+	y2+	y3+	#2
1	114.09135	57.54931	38.70197	L				7
2	471.34925	236.17826	157.78793	K-TMT6p	989.60940	495.30834	330.54132	6
3	570.41767	285.71247	190.81074	V	632.35150	316.67939	211.45535	5
4	717.48609	359.24668	239.83355	F	533.28308	267.14518	178.43254	4
5	831.52902	416.26815	277.84786	N	386.21466	193.61097	129.40974	3
6	928.58179	464.79453	310.19878	P	272.17173	136.58950	91.39543	2
7				R	175.11896	88.06312	59.04450	1

MS/MS spectrum of *m/z* 368.23 the $[M+3H]^{3+}$ molecular ion for a peptide of 1102.69 Da with corresponding sequence LKVFNPR unique to pre-mRNA-splicing factor identified in 1DGE fraction 2 as significant (*P* value <0.05) between PiB+ and PiB- groups.

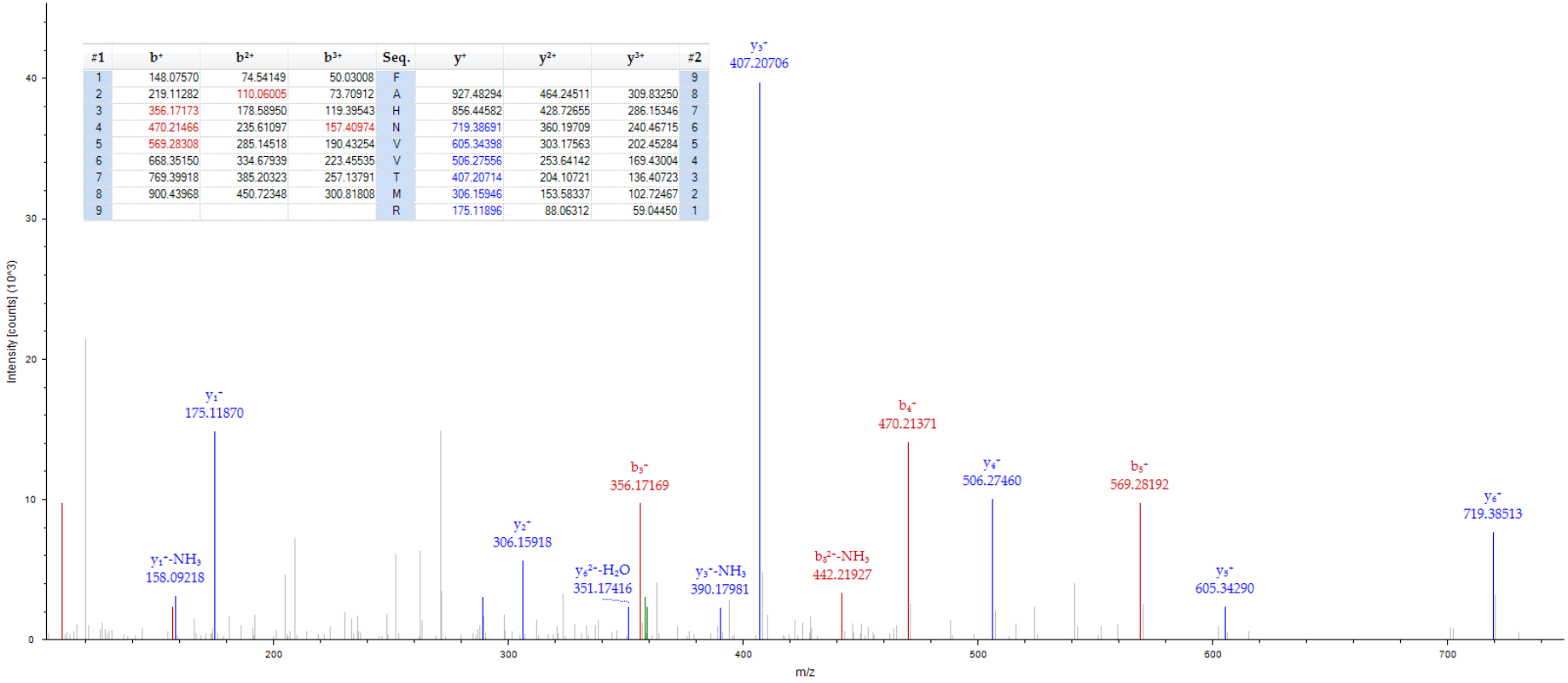

MS/MS spectrum of *m/z* 358.85 the $[M+3H]^{3+}$ molecular ion for a peptide of 1074.55 Da with corresponding sequence FAHNVVTMR unique to Inter-alpha-trypsin inhibitor heavy chain H3 identified in 1DGE fraction 2 as significant (*P* value <0.05) between PiB+ and PiB- groups.

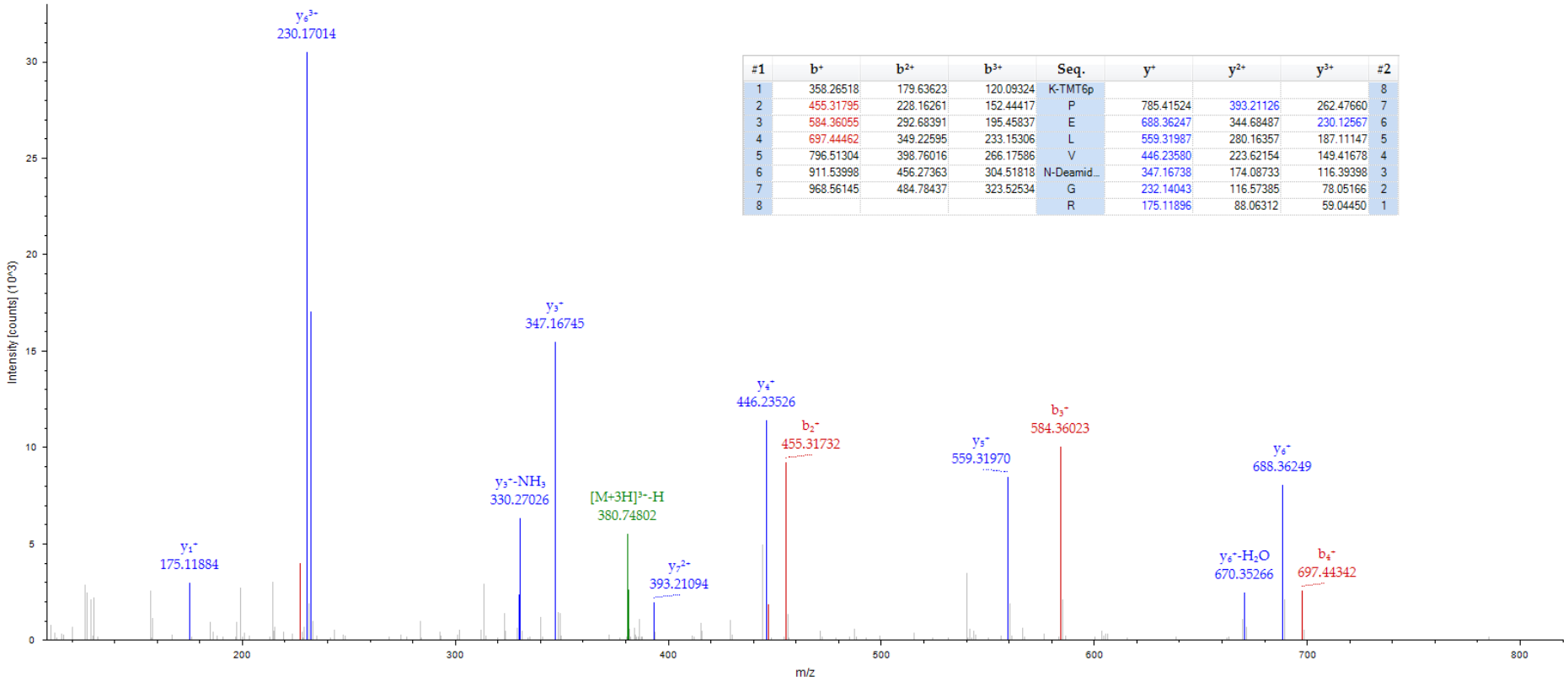

#1	b+	b2+	b3+	Seq.	y+	y2+	y3+	#2
1	358.26518	179.63623	120.09324	K-TMT6p				8
2	455.31795	228.16261	152.44417	P	785.41524	393.21126	262.47660	7
3	584.36055	292.68391	195.45837	E	688.36247	344.68487	230.12567	6
4	697.44462	349.22595	233.15306	L	559.31987	280.16357	187.11147	5
5	796.51304	398.76016	266.17586	V	446.23580	223.62154	149.41678	4
6	911.53998	456.27363	304.51818	N-Deamid...	347.16738	174.08733	116.39398	3
7	968.56145	484.78437	323.52534	G	232.14043	116.57385	78.05166	2
8				R	175.11896	88.06312	59.04450	1

MS/MS spectrum of *m/z* 381.56 the $[M+3H]^{3+}$ molecular ion for a peptide of 1142.67 Da with corresponding sequence KPELVNGR unique to C4b-binding protein alpha chain identified in 1DGE fraction 7 as significant (*P* value <0.05) between PiB+ and PiB- groups.

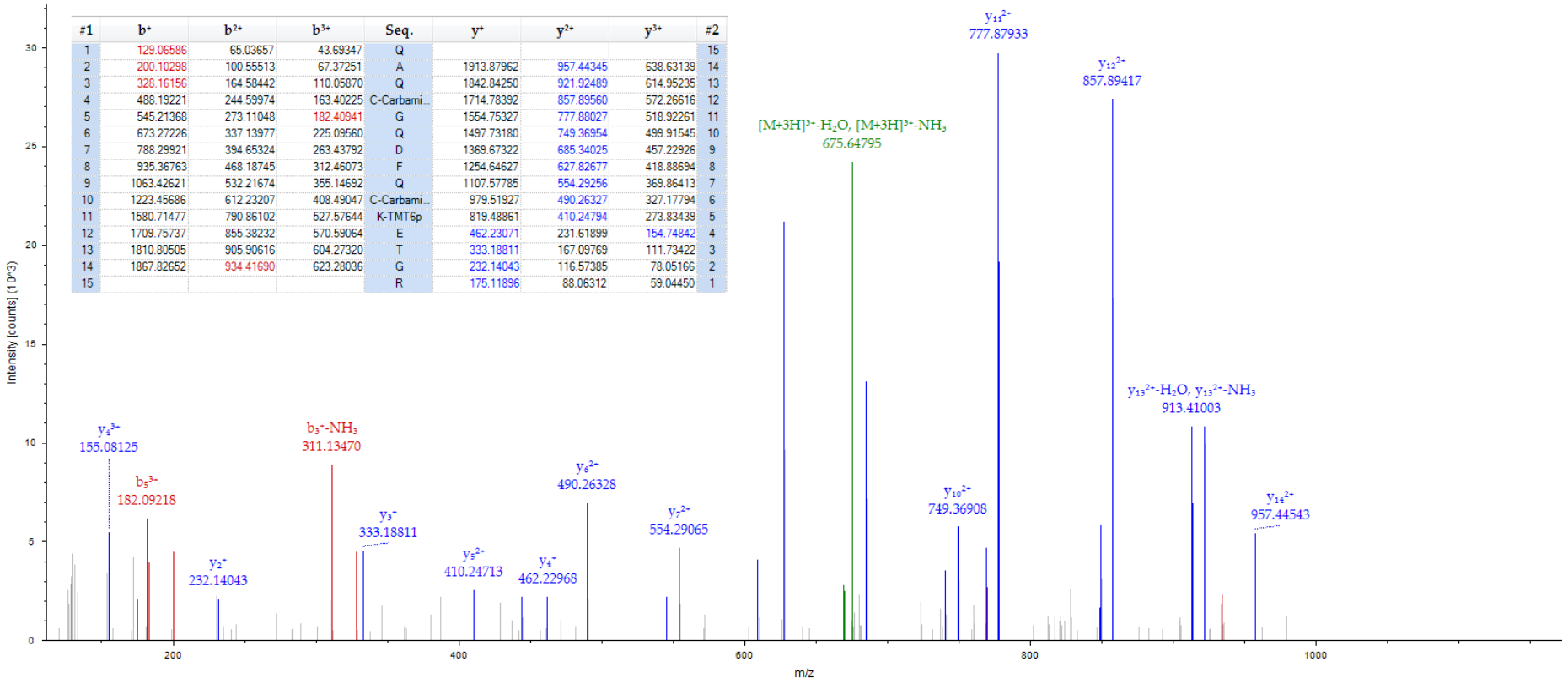

MS/MS spectrum of *m/z* 681.31 the $[M+3H]^{3+}$ molecular ion for a peptide of 2041.93 Da with corresponding sequence QAQCGQDFQCKETGR unique to complement component C8 alpha chain identified in 1DGE fraction 5 as significant (*P* value <0.05) between PiB+ and PiB- groups.

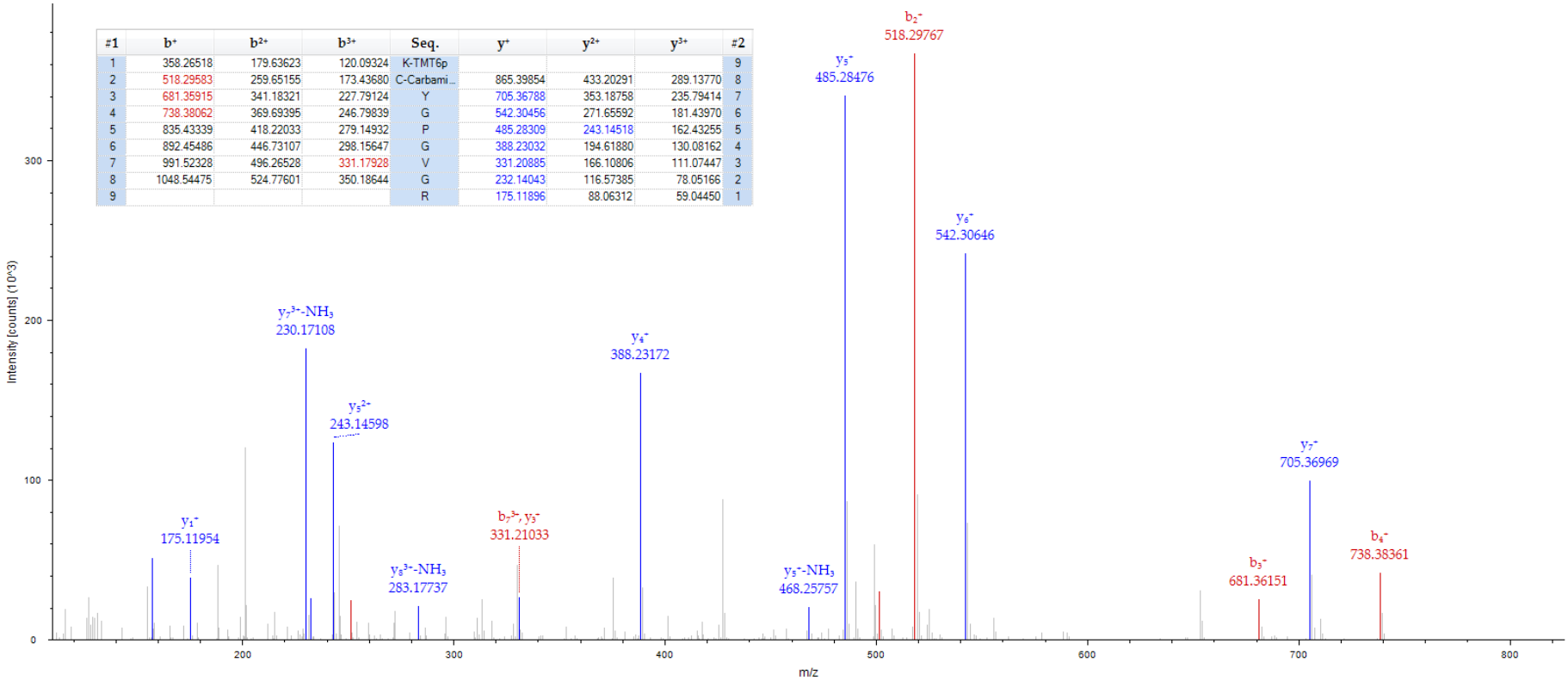

MS/MS spectrum of *m/z* 408.22 the $[M+3H]^{3+}$ molecular ion for a peptide of 1222.65 Da with corresponding sequence KCYGPGVGR unique to CD5 antigen-like identified in 1DGE fraction 6 as significant (*P* value <0.05) between PiB+ and PiB- groups.

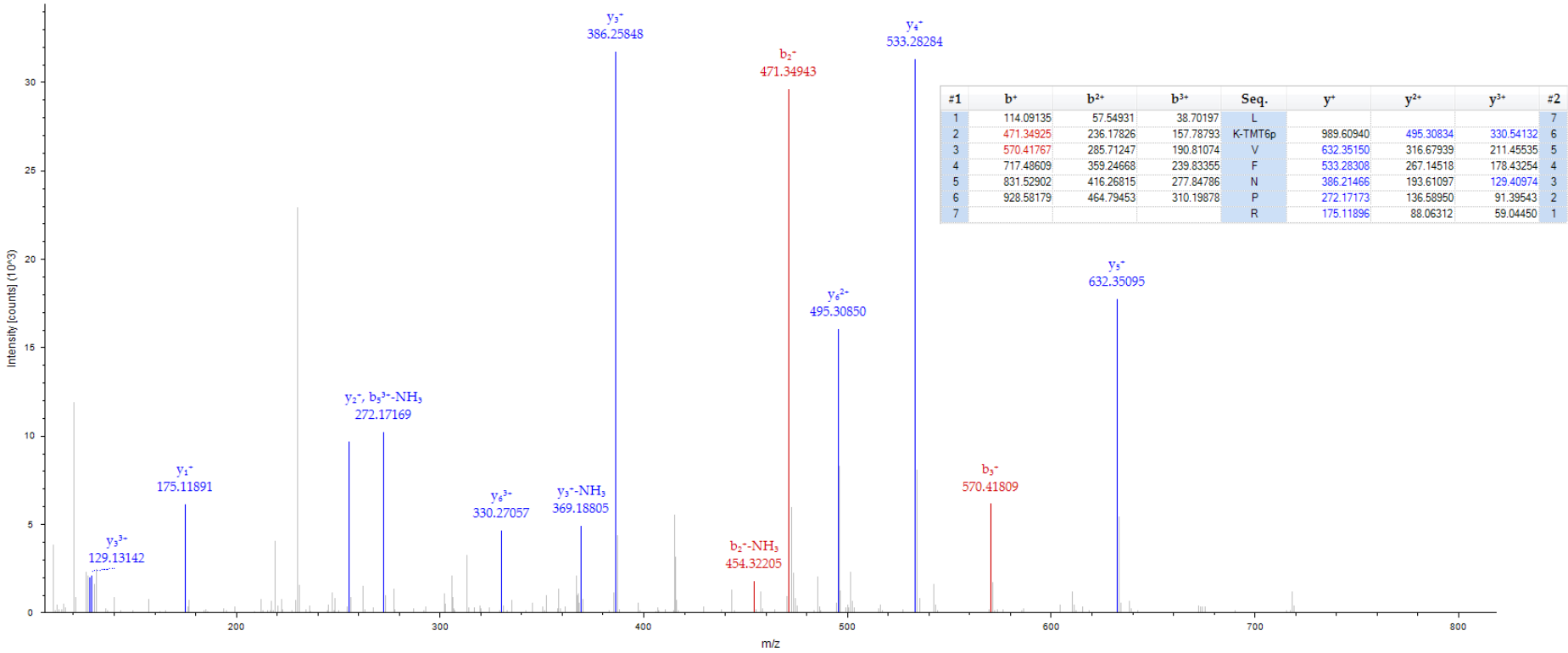

#1	b+	b2+	b3+	Seq.	y+	y2+	y3+	#2
1	114.09135	57.54931	38.70197	L				7
2	471.34925	236.17826	157.78793	K-TMT6p	989.60940	495.30834	330.54132	6
3	570.41767	285.71247	190.81074	V	632.35150	316.67939	211.45535	5
4	717.48609	359.24668	239.83355	F	533.28308	267.14518	178.43254	4
5	831.52902	416.26815	277.84786	N	386.21466	193.61097	129.40974	3
6	928.58179	464.79453	310.19878	P	272.17173	136.58950	91.39543	2
7				R	175.11896	88.06312	59.04450	1

MS/MS spectrum of *m/z* 368.23 the $[M+3H]^{3+}$ molecular ion for a peptide of 1102.69 Da with corresponding sequence LKVFNPR unique to pre-mRNA-splicing factor identified in 1DGE fraction 5 as significant (*P* value <0.05) between PiB+ and PiB- groups.

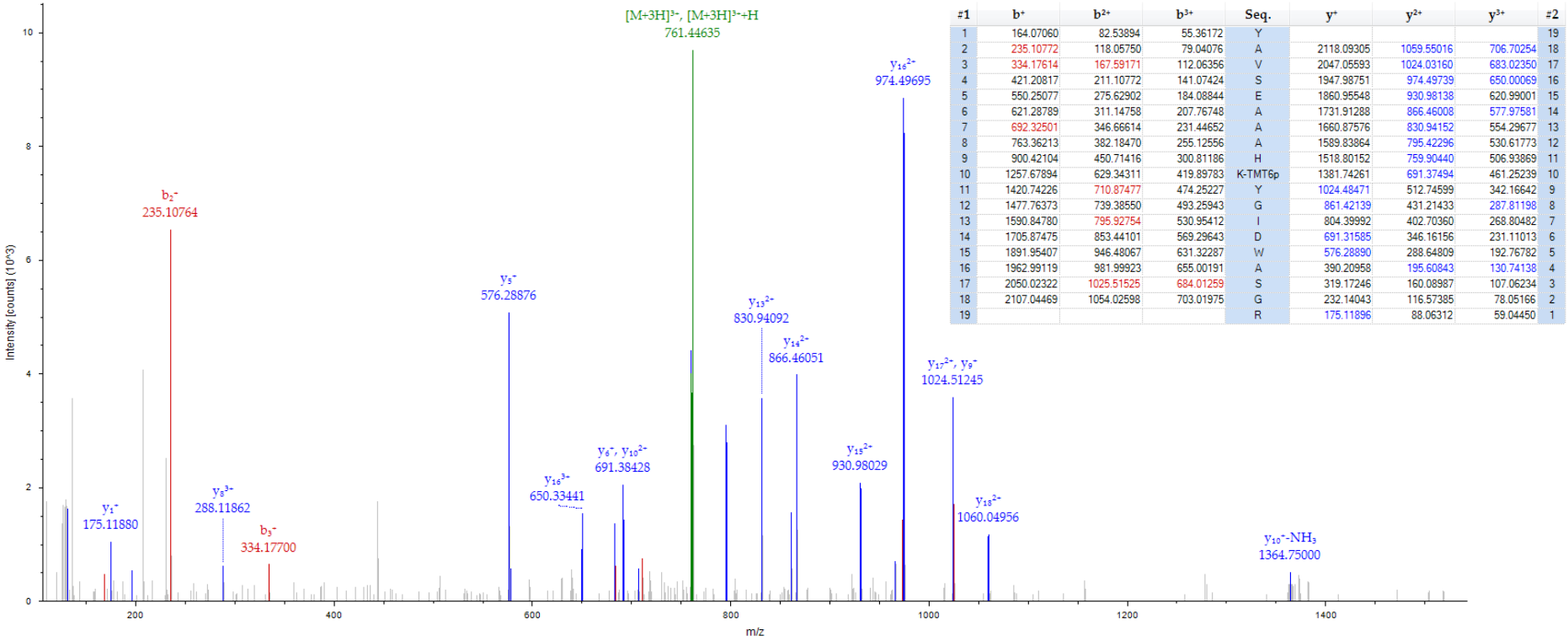

#1	b⁺	b²⁺	b³⁺	Seq.	y⁺	y²⁺	y³⁺	#2
1	164.07060	82.53894	55.36172	Y				19
2	235.10772	118.05750	79.04076	A	2118.09305	1059.55016	706.70254	18
3	334.17614	167.59171	112.06356	V	2047.05593	1024.03160	683.02350	17
4	421.20817	211.10772	141.07424	S	1947.98751	974.49739	650.00069	16
5	550.25077	275.62902	184.08844	E	1860.95548	930.98138	620.99001	15
6	621.28789	311.14758	207.76748	A	1731.91288	866.46008	577.97581	14
7	692.32501	346.66614	231.44652	A	1660.87576	830.94152	554.29677	13
8	763.36213	382.18470	255.12556	A	1589.83864	795.42296	530.61773	12
9	900.42104	450.71416	300.81186	H	1518.80152	759.90440	506.93869	11
10	1257.67894	629.34311	419.89783	K-TMT6p	1381.74261	691.37494	461.25239	10
11	1420.74226	710.87477	474.25227	Y	1024.48471	512.74599	342.16642	9
12	1477.76373	739.38550	493.25943	G	861.42139	431.21433	287.81198	8
13	1590.84780	795.92754	530.95412	I	804.39992	402.70360	268.80482	7
14	1705.87475	853.44101	569.29643	D	691.31585	346.16156	231.11013	6
15	1891.95407	946.48067	631.32287	W	576.28890	288.64809	192.76782	5
16	1962.99119	981.99923	655.00191	A	390.20958	195.60843	130.74138	4
17	2050.02322	1025.51525	684.01259	S	319.17246	160.08987	107.06234	3
18	2107.04469	1054.02598	703.01975	G	232.14043	116.57385	78.05166	2
19				R	175.11896	88.06312	59.04450	1

MS/MS spectrum of *m/z* 761.05 the $[M+3H]^{3+}$ molecular ion for a peptide of 2281.15 Da with corresponding sequence YAVSEAAAHKYGIDWASGR unique to ficolin-3 identified in 1DGE fraction 6 as significant (*P* value <0.05) between PiB+ and PiB- groups.

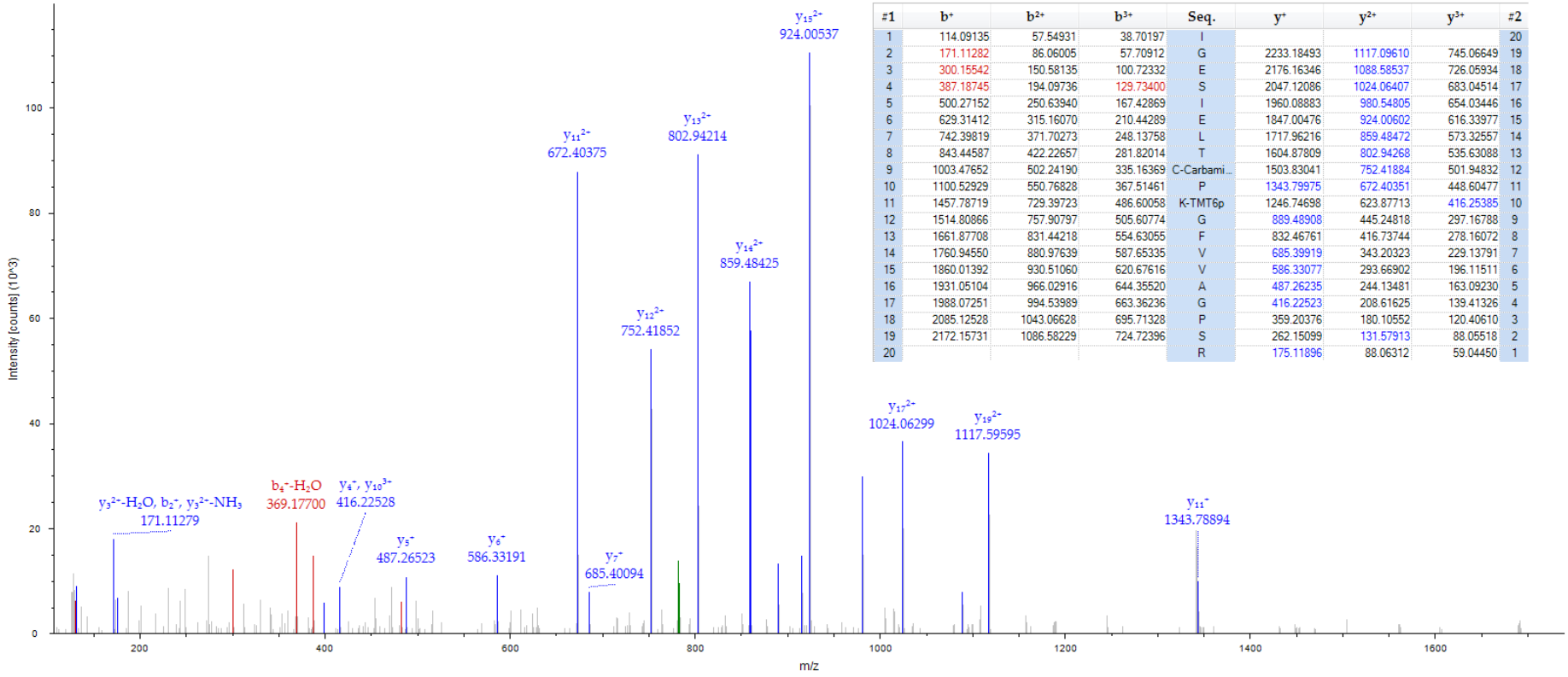

#1	b+	b2+	b3+	Seq.	y+	y2+	y3+	#2
1	114.09135	57.54931	38.70197	I				20
2	171.11282	86.06005	57.70912	G	2233.18493	1117.09610	745.06649	19
3	300.15542	150.58135	100.72332	E	2176.16346	1088.58537	726.05934	18
4	387.18745	194.09736	129.73400	S	2047.12086	1024.06407	683.04514	17
5	500.27152	250.63940	167.42869	I	1960.08883	980.54805	654.03446	16
6	629.31412	315.16070	210.44289	E	1847.00476	924.00602	616.33977	15
7	742.39819	371.70273	248.13758	L	1717.96216	859.48472	573.32557	14
8	843.44587	422.22657	281.82014	T	1604.87809	802.94268	535.63088	13
9	1003.47652	502.24190	335.16369	C-Carbami...	1503.83041	752.41884	501.94832	12
10	1100.52929	550.76828	367.51461	P	1343.79975	672.40351	448.60477	11
11	1457.78719	729.39723	486.60058	K-TMT6p	1246.74698	623.87713	416.25385	10
12	1514.80866	757.90797	505.60774	G	889.48908	445.24818	297.16788	9
13	1661.87708	831.44218	554.63055	F	832.46761	416.73744	278.16072	8
14	1760.94550	880.97639	587.65335	V	685.39919	343.20323	229.13791	7
15	1860.01392	930.51060	620.67616	V	586.33077	293.66902	196.11511	6
16	1931.05104	966.02916	644.35520	A	487.26235	244.13481	163.09230	5
17	1988.07251	994.53989	663.36236	G	416.22523	208.61625	139.41326	4
18	2085.12528	1043.06628	695.71328	P	359.20376	180.10552	120.40610	3
19	2172.15731	1086.58229	724.72396	S	262.15099	131.57913	88.05518	2
20				R	175.11896	88.06312	59.04450	1

MS/MS spectrum of *m/z* 782.75 the $[M+3H]^{3+}$ molecular ion for a peptide of 2346.25 Da with corresponding sequence IGESIELTCPKGFVVAGPSR unique to complement component C6 identified in 1DGE fraction 2 as significant (*P* value <0.05) between PiB+ and PiB- groups.

#1	b+	b2+	b3+	b4+	Seq.	y+	y2+	y3+	y4+	#2
1	114.09135	57.54931	38.70197	29.27829	L					16
2	277.15467	139.08097	93.05641	70.04412	Y	2397.32190	1199.16459	799.77882	600.08593	15
3	634.41257	317.70992	212.14237	159.35860	K-TMT6p	2234.25858	1117.63293	745.42438	559.32010	14
4	991.67047	496.33887	331.22834	248.67308	K-TMT6p	1877.00067	939.00397	626.33841	470.00563	13
5	1062.70759	531.85743	354.90738	266.43236	A	1519.74277	760.37502	507.25244	380.69115	12
6	1175.79166	588.39947	392.60207	294.70337	L	1448.70565	724.85646	483.57340	362.93187	11
7	1338.85498	669.93113	446.95651	335.46920	Y	1335.62158	668.31443	445.87871	334.66085	10
8	1451.93905	726.47316	484.65120	363.74022	L	1172.55826	586.78277	391.52427	293.89502	9
9	1579.99763	790.50245	527.33739	395.75487	Q	1059.47419	530.24073	353.82958	265.62401	8
10	1743.06095	872.03411	581.69183	436.52070	Y	931.41561	466.21144	311.14339	233.60936	7
11	1844.10863	922.55795	615.37439	461.78262	T	768.35229	384.67978	256.78895	192.84353	6
12	1959.13558	980.07143	653.71671	490.53935	D	667.30461	334.15594	223.10639	167.58161	5
13	2088.17818	1044.59273	696.73091	522.80000	E	552.27766	276.64247	184.76407	138.82487	4
14	2189.22586	1095.11657	730.41347	548.06192	T	423.23506	212.12117	141.74987	106.56422	3
15	2336.29428	1168.65078	779.43628	584.82903	F	322.18738	161.59733	108.06731	81.30230	2
16					R	175.11896	88.06312	59.04450	44.53520	1

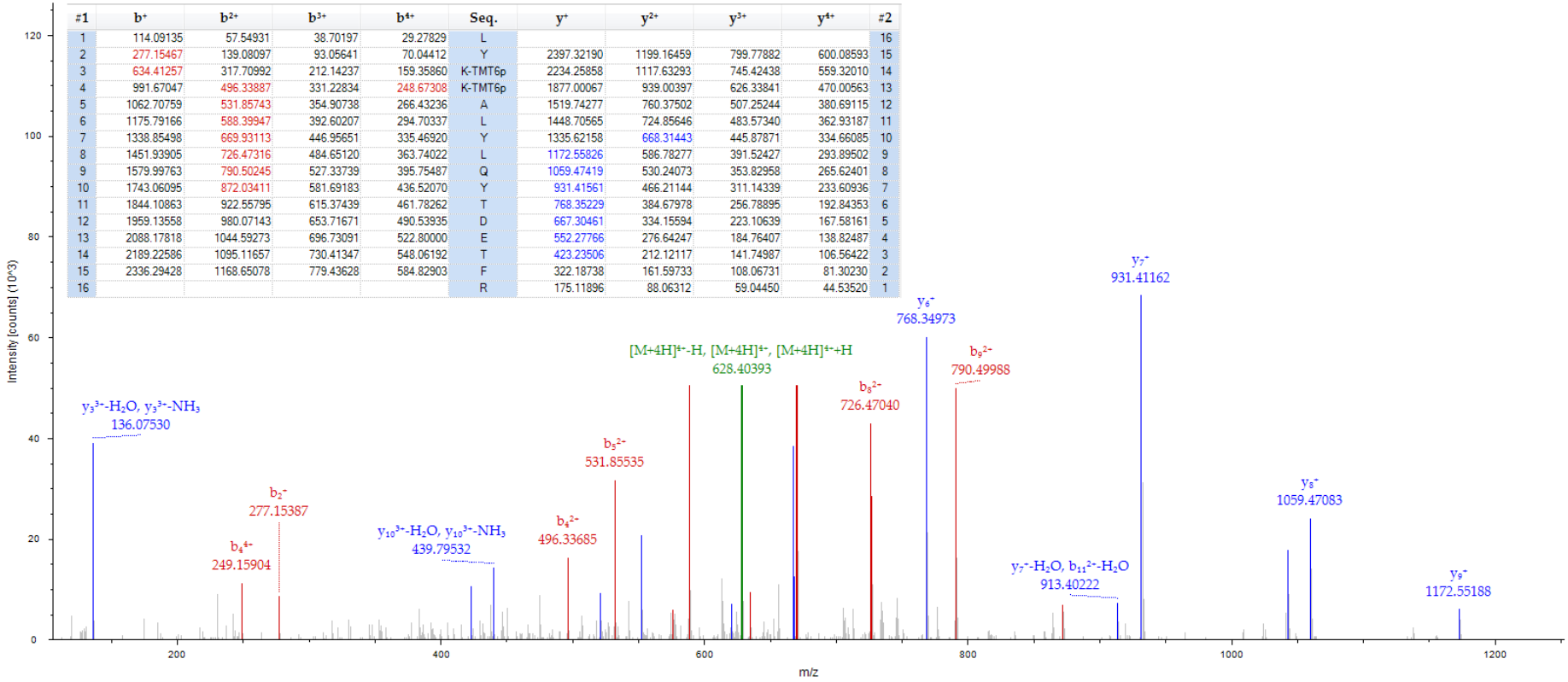

MS/MS spectrum of *m/z* 628.35 the $[M+3H]^{3+}$ molecular ion for a peptide of 2510.40 Da with corresponding sequence LYKKALYLQYTDETFR unique to ceruoplasmin identified in 1DGE fraction 6 as significant (*P* value <0.05) between PiB+ and PiB- groups.

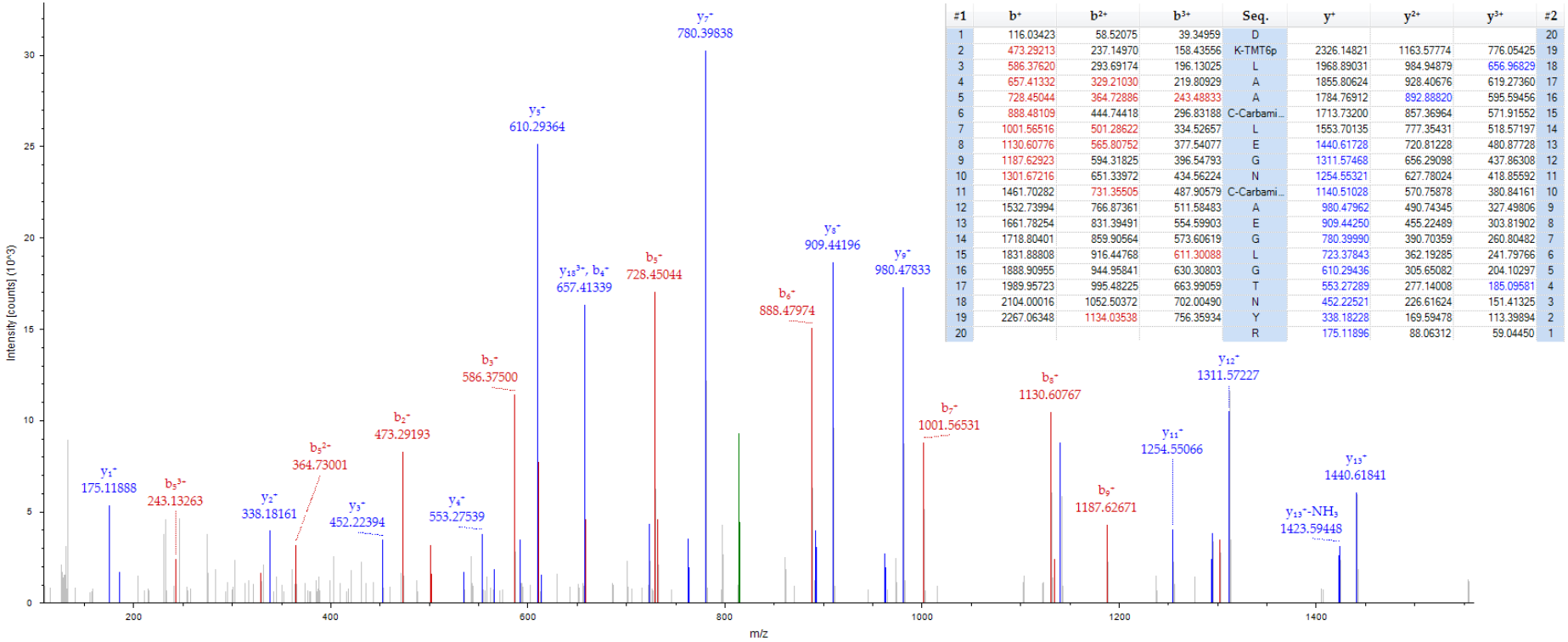

#1	b+	b2+	b3+	Seq.	y+	y2+	y3+	#2
1	116.03423	58.52075	39.34959	D				20
2	473.29213	237.14970	158.43556	K-TMT6p	2326.14821	1163.57774	776.05425	19
3	586.37620	293.69174	196.13025	L	1968.89031	984.94879	656.96829	18
4	657.41332	329.21030	219.80929	A	1855.80624	928.40676	619.27360	17
5	728.45044	364.72886	243.48833	A	1784.76912	892.88820	595.59456	16
6	888.48109	444.74418	296.83188	C-Carbami...	1713.73200	857.36964	571.91552	15
7	1001.56516	501.28622	334.52657	L	1553.70135	777.35431	518.57197	14
8	1130.60776	565.80752	377.54077	E	1440.61728	720.81228	480.87728	13
9	1187.62923	594.31825	396.54793	G	1311.57468	656.29098	437.86308	12
10	1301.67216	651.33972	434.56224	N	1254.55321	627.78024	418.85592	11
11	1461.70282	731.35505	487.90579	C-Carbami...	1140.51028	570.75878	380.84161	10
12	1532.73994	766.87361	511.58483	A	980.47962	490.74345	327.49806	9
13	1661.78254	831.39491	554.59903	E	909.44250	455.22489	303.81902	8
14	1718.80401	859.90564	573.60619	G	780.39990	390.70359	260.80482	7
15	1831.88808	916.44768	611.30088	L	723.37843	362.19285	241.79766	6
16	1888.90955	944.95841	630.30803	G	610.29436	305.65082	204.10297	5
17	1989.95723	995.48225	663.99059	T	553.27289	277.14008	185.09581	4
18	2104.00016	1052.50372	702.00490	N	452.22521	226.61624	151.41325	3
19	2267.06348	1134.03538	756.35934	Y	338.18228	169.59478	113.39894	2
20				R	175.11896	88.06312	59.04450	1

MS/MS spectrum of *m/z* 814.39 the $[M+3H]^{3+}$ molecular ion for a peptide of 2441.17 Da with corresponding sequence DKLAACLEGNCAEGLGTNYR unique to prothrombin identified in 1DGE fraction 6 as significant (*P* value <0.05) between PiB+ and PiB- groups.

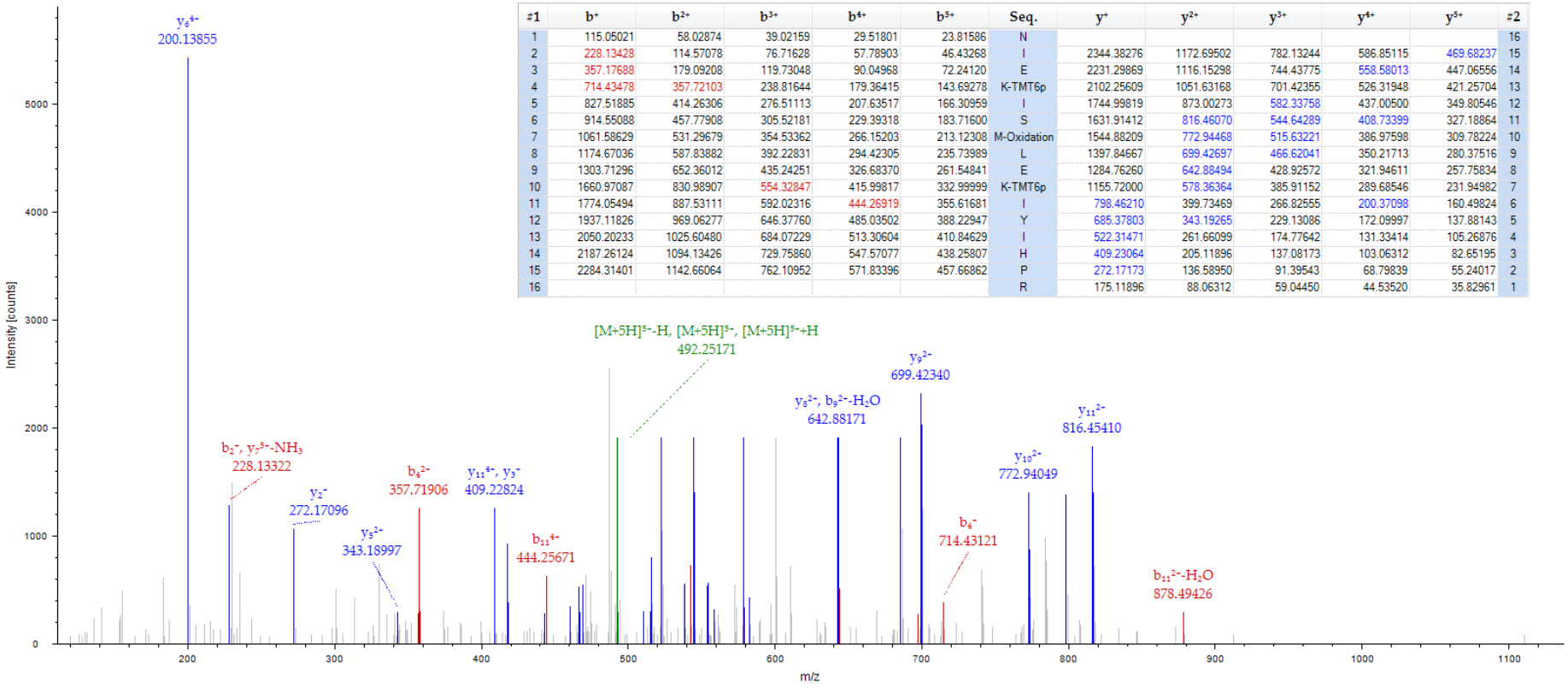

#1	b^+	b^{2+}	b^{3+}	b^{4+}	b^{5+}	Seq.	y^+	y^{2+}	y^{3+}	y^{4+}	y^{5+}	#2
1	115.05021	58.02874	39.02159	29.51801	23.81586	N						16
2	228.13428	114.57078	76.71628	57.78903	46.43268	I	2344.38276	1172.69502	782.13244	586.85115	469.68237	15
3	357.17688	179.09208	119.73048	90.04968	72.24120	E	2231.29869	1116.15298	744.43775	558.58013	447.06556	14
4	714.43478	357.72103	238.81644	179.36415	143.69278	K-TMT6p	2102.25609	1051.63168	701.42355	526.31948	421.25704	13
5	827.51885	414.26306	276.51113	207.63517	166.30959	I	1744.99819	873.00273	582.33758	437.00500	349.80546	12
6	914.55088	457.77908	305.52181	229.39318	183.71600	S	1631.91412	816.46070	544.64289	408.73399	327.18864	11
7	1061.58629	531.29679	354.53362	266.15203	213.12308	M-Oxidation	1544.88209	772.94468	515.63221	386.97598	309.78224	10
8	1174.67036	587.83882	392.22831	294.42305	235.73989	L	1397.84667	699.42697	466.62041	350.21713	280.37516	9
9	1303.71296	652.36012	435.24251	326.68370	261.54841	E	1284.76260	642.88494	428.92572	321.94611	257.75834	8
10	1660.97087	830.98907	554.32847	415.99817	332.99999	K-TMT6p	1155.72000	578.36364	385.91152	289.68546	231.94982	7
11	1774.05494	887.53111	592.02316	444.26919	355.61681	I	798.46210	399.73469	266.82555	200.37098	160.49824	6
12	1937.11826	969.06277	646.37760	485.03502	388.22947	Y	685.37803	343.19265	229.13086	172.09997	137.88143	5
13	2050.20233	1025.60480	684.07229	513.30604	410.84629	I	522.31471	261.66099	174.77642	131.33414	105.26876	4
14	2187.26124	1094.13426	729.75860	547.57077	438.25807	H	409.23064	205.11896	137.08173	103.06312	82.65195	3
15	2284.31401	1142.66064	762.10952	571.83396	457.66862	P	272.17173	136.58950	91.39543	68.79839	55.24017	2
16						R	175.11896	88.06312	59.04450	44.53520	35.82961	1

MS/MS spectrum of *m/z* 492.49 the $[M+5H]^{5+}$ molecular ion for a peptide of 2458.42 Da with corresponding sequence NIEKISMLEKIYIHPR unique to prothrombin identified in 1DGE fraction 6 as significant (*P* value <0.05) between PiB+ and PiB- groups.

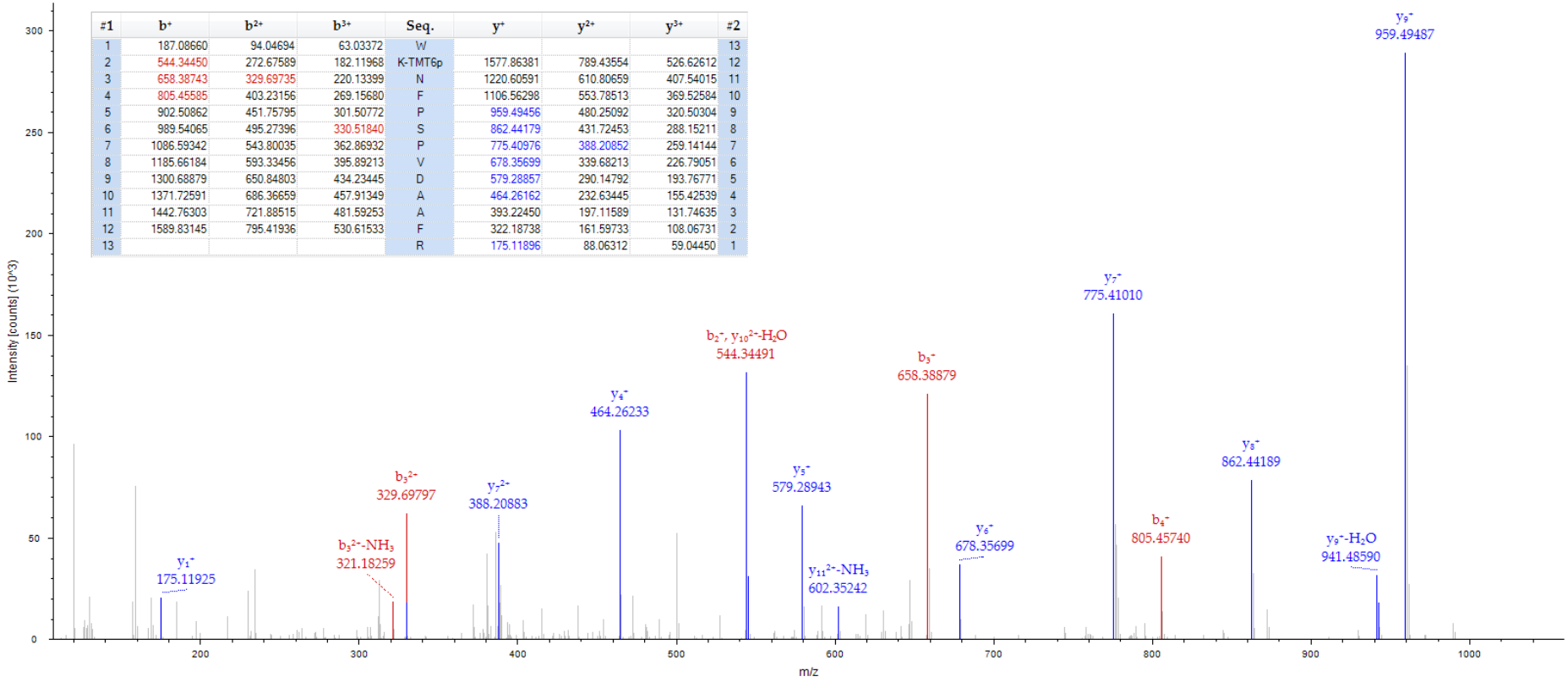

MS/MS spectrum of *m/z* 588.65 the $[M+3H]^{3+}$ molecular ion for a peptide of 1763.94 Da with corresponding sequence WKNFPSPVDAAFR unique to hemopexin identified in 1DGE fraction 6 as significant (*P* value <0.05) between PiB+ and PiB- groups.

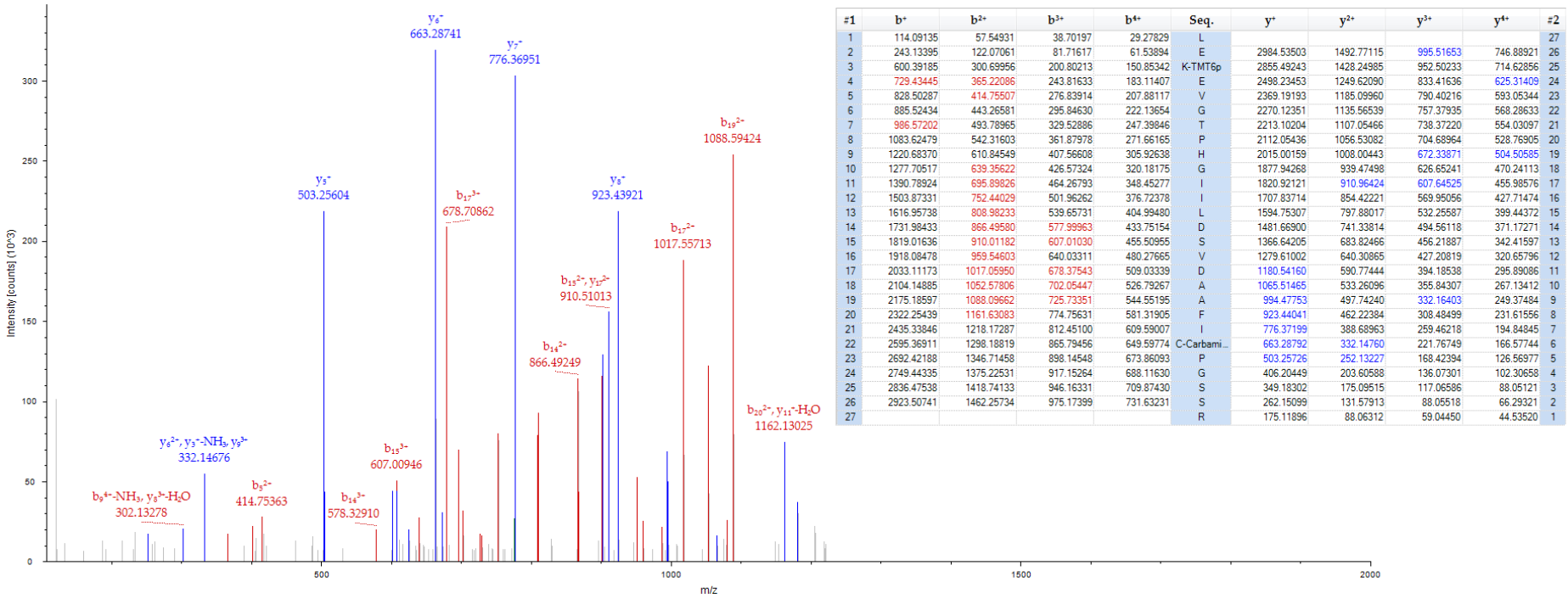

#1	b+	b2+	b3+	b4+	Seq.	y+	y2+	y3+	y4+	#2
1	114.09135	57.54931	38.70197	29.27829	L					27
2	243.13395	122.07061	81.71617	61.53894	E	2984.53503	1492.77115	995.51653	746.88921	26
3	600.39185	300.69956	200.80213	150.85342	K-TMT6p	2855.49243	1428.24985	952.50233	714.62856	25
4	729.43445	365.22086	243.81633	183.11407	E	2498.23453	1249.62090	833.41636	625.31409	24
5	828.50287	414.75507	276.83914	207.88117	V	2369.19193	1185.09960	790.40216	593.05344	23
6	885.52434	443.26581	295.84630	222.13654	G	2270.12351	1135.56539	757.37935	568.28633	22
7	986.57202	493.78965	329.52886	247.39846	T	2213.10204	1107.05466	738.37220	554.03097	21
8	1083.62479	542.31603	361.87978	271.66165	P	2112.05436	1056.53082	704.68964	528.76905	20
9	1220.68370	610.84549	407.56608	305.92638	H	2015.00159	1008.00443	672.33871	504.50585	19
10	1277.70517	639.35622	426.57324	320.18175	G	1877.94268	939.47498	626.65241	470.24113	18
11	1390.78924	695.89826	464.26793	348.45277	I	1820.92121	910.96424	607.64525	455.98576	17
12	1503.87331	752.44029	501.96262	376.72378	I	1707.83714	854.42221	569.95056	427.71474	16
13	1616.95738	808.98233	539.65731	404.99480	L	1594.75307	797.88017	532.25587	399.44372	15
14	1731.98433	866.49580	577.99963	433.75154	D	1481.66900	741.33814	494.56118	371.17271	14
15	1819.01636	910.01182	607.01030	455.50955	S	1366.64205	683.82466	456.21887	342.41597	13
16	1918.08478	959.54603	640.03311	480.27665	V	1279.61002	640.30865	427.20819	320.65796	12
17	2033.11173	1017.05950	678.37543	509.03339	D	1180.54160	590.77444	394.18538	295.89086	11
18	2104.14885	1052.57806	702.05447	526.79267	A	1065.51465	533.26096	355.84307	267.13412	10
19	2175.18597	1088.09662	725.73351	544.55195	A	994.47753	497.74240	332.16403	249.37484	9
20	2322.25439	1161.63083	774.75631	581.31905	F	923.44041	462.22384	308.48499	231.61556	8
21	2435.33846	1218.17287	812.45100	609.59007	I	776.37199	388.68963	259.46218	194.84845	7
22	2595.36911	1298.18819	865.79456	649.59774	C-Carbami...	663.28792	332.14760	221.76749	166.57744	6
23	2692.42188	1346.71458	898.14548	673.86093	P	503.25726	252.13227	168.42394	126.56977	5
24	2749.44335	1375.22531	917.15264	688.11630	G	406.20449	203.60588	136.07301	102.30658	4
25	2836.47538	1418.74133	946.16331	709.87430	S	349.18302	175.09515	117.06586	88.05121	3
26	2923.50741	1462.25734	975.17399	731.63231	S	262.15099	131.57913	88.05518	66.29321	2
27					R	175.11896	88.06312	59.04450	44.53520	1

MS/MS spectrum of *m/z* 775.15 he $[M+4H]^{4+}$ molecular ion for a peptide of 3097.61 Da with corresponding sequence LEKEVGTPHGIILDSVDAAFICPGSSR, unique to hemopexin identified in 1DGE fraction 5 as significant (*P* value <0.05) between PiB+ and PiB- groups.

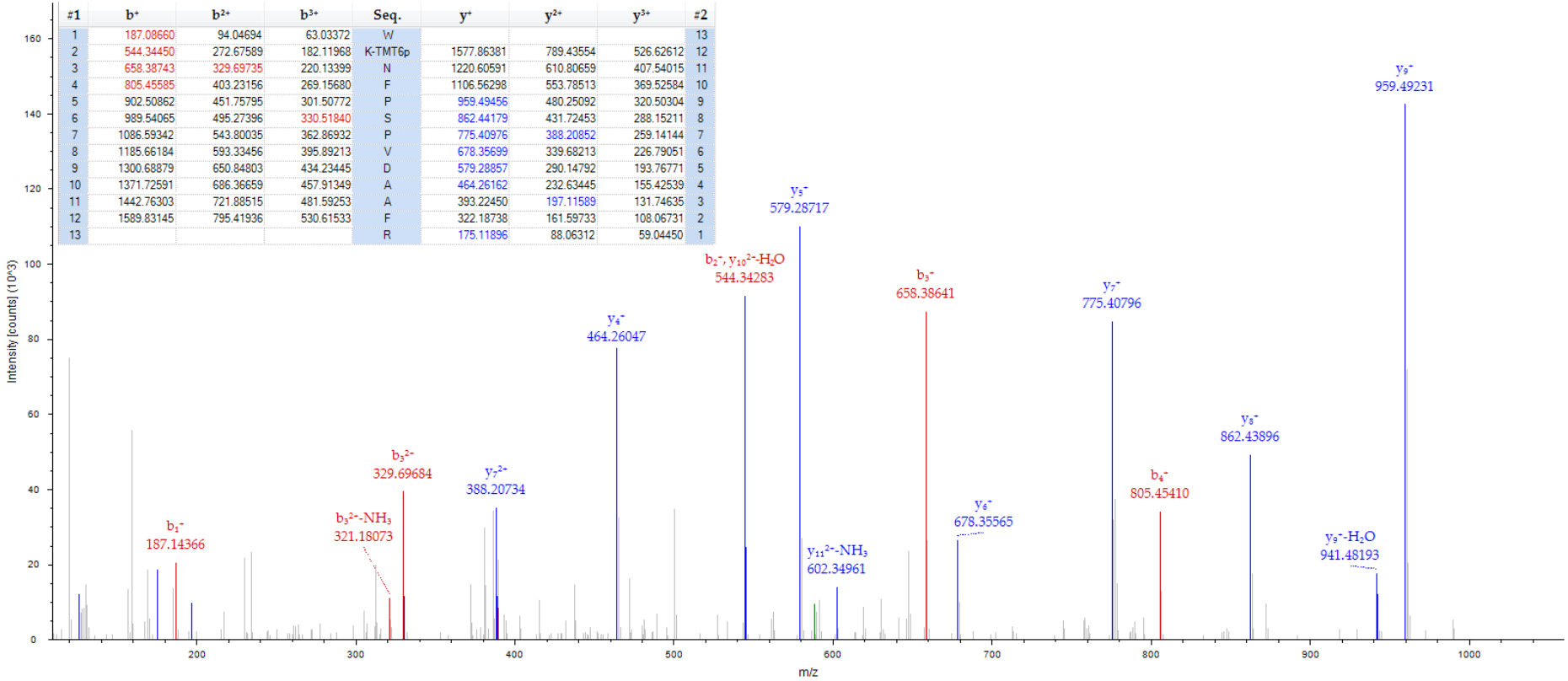

MS/MS spectrum of *m/z* 588.65 the $[M+3H]^{3+}$ molecular ion for a peptide of 1763.94 Da with corresponding sequence WKNFPSPVDAAFR unique to hemopexin identified in 1DGE fraction 5 as significant (*P* value <0.05) between PiB+ and PiB- group.

Appendix 3. Peptide profiles used for protein group MW isoforms identification (No TMT) and quantification (TMT) significantly associated with Aβ SUVR in Chapter 3.

Peptide sequences for protein group MW isoforms significantly associated with Aβ SUVR. Peptide identifications (No TMT) were used as supporting evidence for confident protein group assignment. Quantified (TMT) peptides were used for protein ratio scores and supporting evidence.

UniProt ID	Protein Name	Gene Name	1DGE Fraction	Peptide Identifications	Quantified (TMT) Peptides Identifications
P01023	alpha-2-Macroglobulin (α2m)	*A2M*	1	ATVLNYLPKCIR KPKMCPQLQQYEMHGPEGLR NQGNTWLTAFVLKTFAQAR QTVSWAVTPK VSVQLEASPAFLAVPVEKEQAPHCICANGR VVSMDENFHPLNELIPLVYIQDPKGNR	GEAFTLKATVLNYLPKCIR QKDNGCFR QLNYKHYDGSYSTFGER
P01023	alpha-2-Macroglobulin (α2m)	*A2M*	2	GEAFTLKATVLNYLPKCIR GHFSISIPVKSDIAPVAR KDTVIKPLLVEPEGLEK KPKMCPQLQQYEMHGPEGLR NQGNTWLTAFVLKTFAQAR	ATVLNYLPKCIR QKDNGCFR QLNYKHYDGSYSTFGER TGKAAQVTIQSSGTFSSKFQVDNNNR TITKLSFVKVDSHFR VVSMDENFHPLNELIPLVYIQDPKGNR
P01023	alpha-2-Macroglobulin (α2m)	*A2M*	2	KEYEMKLHTEAQIQEEGTVVELTGR KPKMCPQLQQYEMHGPEGLR VSVQLEASPAFLAVPVEKEQAPHCICANGR	GEAFTLKATVLNYLPKCIR QKDNGCFR QLNYKHYDGSYSTFGER TGKAAQVTIQSSGTFSSKFQVDNNNR TITKLSFVKVDSHFR VVSMDENFHPLNELIPLVYIQDPKGNR

P02647	apolipoprotein A-I (apoA1)	*APOA1*	5	EQLGPVTQEFWDNLEKETEGLR	QKVEPLR VKDLATVYVDVLKDSGR
P02647	apolipoprotein A-I (apoA1)	*APOA1*	6	EQLGPVTQEFWDNLEKETEGLR LAARLEALKENGGAR LHELQEKLSPLGEEMR LLDNWDSVTSTFSKLR QGLLPVLESFKVSFLSALEEYTKKLNTQ QKLHELQEKLSPLGEEMR VKDLATVYVDVLKDSGR	AKPALEDLR LAEYHAK LEALKENGGAR QKVEPLR VSFLSALEEYTKKLNTQ
P02647	apolipoprotein A-I (ApoA1)	*APOA1*	9		LEALKENGGAR QKVEPLR VKDLATVYVDVLKDSGR
P02647	apolipoprotein A-I (apoA1)	*APOA1*	10	LEALKENGGAR	EQLGPVTQEFWDNLEKETEGLR
P06727	apolipoprotein A-IV (apoA4)	*APOA4*	6	RVEPYGENFNKALVQQMEQLR QKLGPHAGDVEGHLSFLEKDLR	GNTEGLQKSLAELGGHLDQQVEEFR LLPHANEVSQKIGDNLR
O14791	apolipoprotein L1 (apoL1)	*APOL1*	5	LKSELEDNIR	KALDNLAR VTEPISAESGEQVER
P08519	apolipoprotein(a)	*LPA*	1	NPDSGKQPWCYTTDPCVR	TPAYYPNAGLIKNYCR
P04003	C4b-binding protein alpha chain	*C4BPA*	4	GVGWSHPLPQCEIVK	FKTGTTLKYTCLPGYVR KPELVNGR QSTLDKEL
P04003	C4b-binding protein alpha chain	*C4BPA*	7	WTPYQGCEALCCPEPKLNNGEITQHR	KPELVNGR
O43866	CD5 antigen-like	*CD5L*	5		KCYGPGVGR KPIWLSQMSCSGR LADGPGHCKGR

					VEVEQKGQWGTVCDDGWDIKDVAVLCR
O43866	CD5 antigen-like	*CD5L*	6		KCYGPGVGR KPIWLSQMSCSGR
P00450	ceruloplasmin	*CP*	2	FNKNNEGTYYSPNYNPQSR KERGPEEEHLGILGPVIWAEVGDTIR QKDVDKEFYLFPTVFDENESLLLEDNIR VTFHNKGAYPLSIEPIGVR	LYKKALYLQYTDETFR RPYLKVFNPR
P10909	clusterin	*CLU*	6		EILSVDCSTNNPSQAKLR KNPKFMETVAEKALQEYR RPHFFFPKSR
P02747	complement C1q subcomponent subunit C	*C1QC*	2		YKQKFQSVFTVTR
P01024	complement C3	*C3*	6	AEDLVGK FISLGEACKKVFLDCCNYITELR ISLPESLKR KCCEDGMR LDKACEPGVDYVYKTR QPSSAFAAFVKR SSKITHR TFISPIK YISKYELDKAFSDR	EGVQKEDIPPADLSDQVPDTESETR IFTVNHKLLPVGR KVLLDGVQNPR QPVPGQQMTLKIEGDHGAR TKKQELSEAEQATR VELLHNPAFCSLATTKR YYTYLIMNKGR
P01024	complement C3	*C3*	8	IFTVNHKLLPVGR SVQLTEKR	TKKQELSEAEQATR
P0C0L4	complement C4-A	*C4A*	1	CSVFYGAPSKSR GPEVQLVAHSPWLKDSLSR	DKGQAGLQR

P0C0L4	complement C4-A	*C4A*	7	GQVVKGSVFLR NNVPCSPKVDFTLSSER VEYGFQVKVLR	LLATLCSAEVCQCAEGKCPR MKFACYYPR
P13671	complement component C6	*C6*	2	GEVLDNSFTGGICKTVKSSR KLECNGENDCGDNSDER KMEILHPGKCLA KYNPIPSVQLMGNGFHFLAGEPR TECIKPVVQEVLTITPFQR TKAVCTR	IGESIELTCPKGFVVAGPSR
P07357	complement component C8 alpha chain	*C8A*	5	HTSLGPLEAKR	KVQTQAC
P00751	complement factor B	*CFB*	1	DAQYAPGYDKVKDISEVVTPR STGSWSTLKTQDQKTVR	DLLYIGKDR QKQVPAHAR
P08603	complement factor H (CFH)	*CFH*	6	KGEWVALNPLR	FQYKCNMGYEYSER TTCWDGKLEYPTCAK QMSKYPSGER
Q03591	complement factor H related protein 1 (FHR-1)	*CFHR1*	8	TTCWDGKLEYPTCAK	ITCTEEGWSPTPKCLR TGESAEFVCKR
P02671	fibrinogen α chain (FGα)	*FGA*	4	AQLVDMKR EVDLKDYEDQQKQLEQVIAKDLLPSR HQSACKDSDWPFCSDEDWNYKCPSGCR KVIEKVQHIQLLQKNVR	GKSSSYSKQFTSSTSYNR LEVDIDIKIR MKGLIDEVNQDFTNR TGKEKVTSGSTTTTR
P02679	fibrinogen γ chain (FGγ)	*FGG*	6	VGPEADKYR	KMLEEIMKYEASILTHDSSIR TSTADYAMFKVGPEADKYR
O75636	ficolin 3	*FCN3*	6		YAVSEAAAHKYGIDWASGR

P06396	gelsolin	*GSN*	5	IEGSNKVPVDPATYGQFYGGDSYIILYNYR	LKATQVSKGIR LFACSNKIGR
P00738	hapoglobin	*HP*	5	FTDHLKYVMLPVADQDQCIR	NANFKFTDHLKYVMLPVADQDQCIR QKVSVNER VMPICLPSKDYAEVGR
P00738	hapoglobin	*HP*	8	NYYKLR	VMPICLPSKDYAEVGR
P02790	hemopexin	*HPX*	5		LEKEVGTPHGIILDSVDAAFICPGSSR WKNFPSPVDAAFR
P02790	hemopexin	*HPX*	6		WKNFPSPVDAAFR
P04196	histidine-rich glycoprotein (HRG)	*HRG*	3		KYWNDCEPPDSR RPSEIVIGQCKVIATR
P19827	Inter-alpha-trypsin inhibitor heavy chain H3	*ITIH3*	2	DYIFGNYIER KLEQTKEALLR	FAHNVVTMR LWAYLTIEQLLEKR
Q92620	pre-mRNA-splicing factor	*DHX38*	2		LKVFNPR
Q92620	pre-mRNA-splicing factor	*DHX38*	5		LKVFNPR
P00734	prothrombin	*F2*	6	ETAASLLQAGYKGR KSPQELLCGASLISDR	DKLAACLEGNCAEGLGTNYR NIEKISMLEKIYIHPR
P02787	serotransferrin	*TF*	1	GKKSCHTAVGR MDAKMYLGYEYVTAIR SETKDLLFR	NTYEKYLGEEYVKAVGNLR SAGWNIPMGLLYNKINHCR
P25311	zinc-alpha-2-glycoprotein	*AZGP1*	7		AKAYLEEECPATLR

Appendix 4. Full list of protein groups (*n* = 1085) identified in >50% of samples and used for statistical association with neocortical Aβ burden in Chapter 5 (listed as gene names).

A1BG	*AKNA*	*APOC1*	*ATR*	*C10orf68*
A2M	*ALB*	*APOC2*	*ATRN*	*C12orf40*
ABCA1	*ALKBH8*	*APOC3*	*ATRX*	*C17orf100*
ABCA12	*ALMS1*	*APOC4*	*AZGP1*	*C1orf168*
ABCA13	*ALMS1P*	*APOD*	*B2M*	*C1orf173*
ABCA6	*ALOXE3*	*APOE*	*B3GALT2*	*C1orf222*
ABCC1	*ALS2CR11*	*APOF*	*B3GNT9*	*C1orf65*
ABCC8	*AMBP*	*APOH*	*BAIAP2*	*C1QA*
ABHD10	*ANK1*	*APOL1*	*BAZ2B*	*C1QB*
ABHD6	*ANK2*	*APOM*	*BCHE*	*C1QC*
ABL1	*ANK3*	*APP*	*BCORL1*	*C1R*
ABL2	*ANKRD12*	*ARAP1*	*BDNF*	*C1RL*
ACACB	*ANKRD18A*	*ARFGAP2*	*BDP1*	*C1S*
ACADVL	*ANKRD26*	*ARFGEF1*	*BICD1*	*C2*
ACCSL	*ANKRD32*	*ARFGEF2*	*BIRC2*	*C2orf16*
ACTB	*ANKRD36B*	*ARHGAP21*	*BIRC3*	*C2orf78*
ACVRL1	*ANKRD62*	*ARHGAP39*	*BIRC6*	*C3*
ADAM28	*ANPEP*	*ARHGEF1*	*BLOC1S6*	*C4A*
ADAMTSL1	*AP4E1*	*ARHGEF25*	*BNC2*	*C4B*
ADAT1	*APBA2*	*ARID4B*	*BOD1L1*	*C4BPA*
ADGB	*APBB3*	*ARID5B*	*BPTF*	*C4BPB*
AFM	*APC*	*ASH1L*	*BRCA1*	*C4orf21*
AGT	*APCS*	*ASNSD1*	*BRCA2*	*C5*
AHNAK	*APLP2*	*ASPM*	*BROMI*	*C5orf42*
AHNAK2	*APMAP*	*ASXL1*	*BRWD3*	*C6*
AHSG	*APOA1*	*ATAD2*	*BSN*	*C6orf10*
AIFM3	*APOA2*	*ATAD5*	*BTAF1*	*C6orf163*
AK9	*APOA4*	*ATF7IP2*	*BTD*	*C7*
AKAP6	*APOB*	*ATP13A2*	*BTK*	*C8A*
AKAP9	*APOBEC3G*	*ATP6V0A2*	*BTNL8*	*C8B*

C8G	*CD163*	*CFI*	*CPN1*	*DHX32*
C9	*CD44*	*CFL2*	*CPN2*	*DHX34*
C9orf126	*CD5L*	*CFP*	*CPS1*	*DIP2B*
CA5A	*CDC42EP4*	*CGNL1*	*CRABP2*	*DISP1*
CADPS2	*CDH13*	*CHD1*	*CRHR1*	*DKFZp571N1833*
CAGE1	*CDH2*	*CHD3*	*CRISP3*	*DKK3*
CAMP	*CDH5*	*CHD5*	*CROCC*	*DKKL1*
CAPRIN2	*CDK1*	*CHD7*	*CRTAC1*	*DMD*
CASC2	*CDK5RAP2*	*CHIT1*	*CRYAA*	*DMXL1*
CASP8AP2	*CDKL2*	*CHL1*	*CSDE1*	*DNA2*
CBR3	*CECR2*	*CKAP5*	*CSMD2*	*DNAH1*
CCDC101	*CENPE*	*CLEC3B*	*CST3*	*DNAH10*
CCDC146	*CENPF*	*CLIP1*	*CTAGE5*	*DNAH12*
CCDC147	*CENPQ*	*CLIP4*	*CTIF*	*DNAH14*
CCDC149	*CEP112*	*CLU*	*CUL3*	*DNAH17*
CCDC152	*CEP128*	*CMYA5*	*CUL9*	*DNAH2*
CCDC157	*CEP135*	*CNDP1*	*CUX1*	*DNAH3*
CCDC168	*CEP152*	*CNGB3*	*CWF19L2*	*DNAH5*
CCDC18	*CEP250*	*CNNM4*	*CYC1*	*DNAH6*
CCDC180	*CEP290*	*CNOT1*	*CYP2W1*	*DNAH8*
CCDC30	*CEP350*	*CNTLN*	*DAPK1*	*DNAH9*
CCDC39	*CEP85*	*CNTRL*	*DARS*	*DNAJC16*
CCDC66	*CEP89*	*COBLL1*	*DDX10*	*DNASE1L3*
CCDC73	*CFB*	*COL24A1*	*DDX19B*	*DNHD1*
CCDC77	*CFD*	*COL6A5*	*DDX47*	*DNM1L*
CCDC88C	*CFH*	*COLEC12*	*DDX49*	*DNM2*
CCDC9	*CFHR1*	*COMP*	*DEAF1*	*DNM3*
CCDC91	*CFHR2*	*COPS7B*	*DEFA1*	*DOCK10*
CCT3	*CFHR3*	*CP*	*DENND3*	*DOCK4*
CD14	*CFHR5*	*CPB2*	*DHRS9*	*DOCK5*

DOPEY2	*EPB41*	*FARSB*	*FYTTD1*	*GSN*
DOT1L	*EPHB2*	*FAT1*	*G6PD*	*GVINP1*
DPP9	*EPPK1*	*FAT2*	*GANC*	*HABP2*
DSC1	*EPRS*	*FAT4*	*GART*	*HACE1*
DSCAM	*ERBB4*	*FBLN1*	*GBF1*	*HAUS3*
DSP	*ERC1*	*FBXO3*	*GC*	*HBA1*
DST	*EVPL*	*FCGR3B*	*GCC2*	*HBB*
DTX3L	*EYS*	*FCN2*	*GCSAM*	*HBD*
DUOX1	*F10*	*FCN3*	*GFAP*	*HCN2*
DYNC1H1	*F11*	*FDXACB1*	*GINS1*	*HDAC3*
DYNC2H1	*F12*	*FER1L6*	*GIT2*	*HDAC9*
DZIP3	*F13A1*	*FES*	*GK*	*HEATR1*
ECM1	*F13B*	*FETUB*	*GLIPR1L1*	*HEATR3*
ECM29	*F2*	*FEZ2*	*GMFG*	*HECTD3*
EDF1	*F5*	*FGA*	*GNN*	*HECTD4*
EDRF1	*F9*	*FGB*	*GOLGA1*	*HEG1*
EFCAB5	*FAF1*	*FGF14*	*GOLGA2*	*HELZ*
EFCAB6	*FAM111B*	*FGG*	*GOLGA3*	*HERC1*
EFEMP1	*FAM160A2*	*FHAD1*	*GOLGA4*	*HERC2*
EFHC2	*FAM178A*	*FHOD3*	*GOLGA6C*	*HERC6*
EFHD2	*FAM179A*	*FLNC*	*GOLGB1*	*HGFAC*
EHBP1L1	*FAM184A*	*FMN2*	*GPLD1*	*HGS*
EHD1	*FAM184B*	*FN1*	*GPR115*	*HK1*
EIF2AK2	*FAM186A*	*FREM1*	*GPR126*	*HLTF*
EIF5B	*FAM188A*	*FRMPD1*	*GPR155*	*HMBOX1*
ELMOD2	*FAM76A*	*FRY*	*GPR98*	*HMGB4*
EMILIN2	*FAM81A*	*FSIP2*	*GPS1*	*HMGXB3*
EML5	*FAM83B*	*FUT8*	*GPSM2*	*HMMR*
ENTHD1	*FAN1*	*FYB*	*GPX3*	*HOXC13*
EOMES	*FANCM*	*FYCO1*	*GSE1*	*HOXD3*

HP	*IGKC*	*ITIH5*	*KIAA2026*	*LAMA3*
HPR	*IGLC2*	*ITPR1*	*KIDINS220*	*LAMA4*
HPS5	*IGLC3*	*ITPR2*	*KIF15*	*LATS2*
HPX	*IGLC6*	*IVL*	*KIF16B*	*LBP*
HRG	*IGLC7*	*IZUMO1*	*KIF20B*	*LCAT*
HRNR	*IGLL5*	*JAG1*	*KIF21B*	*LCP2*
HSP90AA5P	*IGSF9*	*JAK1*	*KIF3B*	*LDHA*
HSPA5	*IL10*	*JAK2*	*KIF4A*	*LDHB*
HSPD1	*IL10RA*	*JARID1B*	*KIF4B*	*LGALS3BP*
HYDIN	*IL13RA1*	*JMJD1C*	*KIF5C*	*LIMK1*
IAH1	*IL17RA*	*JPH1*	*KLKB1*	*LNPEP*
IBTK	*IL18RAP*	*JPH3*	*KMT2C*	*LOXHD1*
ICA1	*IL19*	*KALRN*	*KMT2D*	*LOXL4*
IFI44	*IL1RAP*	*KANK1*	*KNG1*	*LPA*
IFT74	*IL2*	*KANK2*	*KNTC1*	*LRG1*
IGF1	*IL3*	*KANSL1*	*KPNA7*	*LRP1*
IGF2	*ILF2*	*KCNH4*	*KRT1*	*LRP12*
IGFALS	*INCENP*	*KCNJ8*	*KRT10*	*LRP1B*
IGFBP3	*INPP4A*	*KDM2B*	*KRT13*	*LRP2*
IGFN1	*INPP5B*	*KDM3A*	*KRT18*	*LRP5*
IGHA1	*INPP5D*	*KDM5A*	*KRT2*	*LRP6*
IGHA2	*INTS3*	*KIAA0100*	*KRT20*	*LRRC43*
IGHD	*INTU*	*KIAA0196*	*KRT222*	*LRRC59*
IGHG1	*INVS*	*KIAA0753*	*KRT36*	*LRRC66*
IGHG2	*ISPD*	*KIAA1109*	*KRT5*	*LRRIQ3*
IGHG3	*ITGAM*	*KIAA1217*	*KRT6B*	*LRRK1*
IGHG4	*ITIH1*	*KIAA1328*	*KRT8*	*LRRN1*
IGHM	*ITIH2*	*KIAA1430*	*KRT9*	*LRSAM1*
IGHMBP2	*ITIH3*	*KIAA1524*	*KTN1*	*LTF*
IGJ	*ITIH4*	*KIAA1731*	*LAMA1*	*LUM*

LUZP1	*MMRN2*	*MYO1E*	*NKRF*	*PAEP*
LUZP2	*MOCOS*	*MYO5A*	*NKTR*	*PAK6*
LYST	*MPHOSPH8*	*MYO5B*	*NOL8*	*PAPD4*
MACF1	*MPZL3*	*MYO9A*	*NOLC1*	*PARP11*
MAN1A1	*MRAS*	*MYOM3*	*NPHP1*	*PARP4*
MAP1B	*MRPS28*	*MYT1L*	*NPY2R*	*PARPBP*
MAP2	*MST1*	*N4BP2*	*NPY5R*	*PBRM1*
MAP3K19	*MST1L*	*NALCN*	*NRAP*	*PCCA*
MAP3K7	*MTBP*	*NARG2*	*NRCAM*	*PCDH9*
MAP4	*MTDH*	*NAV1*	*NRGN*	*PCDHA3*
MAPK7	*MTFMT*	*NAV2*	*NRXN1*	*PCDHB15*
MAPK9	*MTHFR*	*NAV3*	*NRXN2*	*PCF11*
MAPKAPK5	*MTOR*	*NBEA*	*NSD1*	*PCLO*
MAPT	*MTRF1*	*NCAM1*	*NSRP1*	*PCNT*
MASP1	*MTX2*	*NCOR2*	*NUMA1*	*PCNX*
MASP2	*MUC12*	*NDUFAF6*	*NUP153*	*PCYOX1*
MAT1A	*MUC16*	*NEB*	*NUP214*	*PDS5A*
MCM3AP	*MUC2*	*NEFL*	*OBSCN*	*PELP1*
MDGA1	*MXRA5*	*NEFM*	*ODF2L*	*PEPD*
MDN1	*MYBBP1A*	*NEK1*	*OPHN1*	*PGAM2*
MED14	*MYCBP2*	*NEK3*	*OR4D9*	*PGLYRP2*
MED22	*MYH10*	*NEK9*	*OR52I2*	*PHLDB1*
MED30	*MYH11*	*NEMF*	*OR8G5*	*PI16*
MED30S	*MYH13*	*NEO1*	*ORC2*	*PI4KA*
MET	*MYH15*	*NEUROG2*	*ORM1*	*PIBF1*
MFN1	*MYH7*	*NF1*	*ORM2*	*PIEZO2*
MFSD6	*MYH7B*	*NHSL1*	*OSBPL10*	*PIGR*
MGA	*MYH9*	*NIN*	*OTOF*	*PIK3C2A*
MICALL2	*MYLK*	*NINL*	*P4HA3*	*PIK3C2B*
MKI67	*MYO18A*	*NIPBL*	*PABPC1*	*PIKFYVE*

PITPNA	*PRKCQ*	*RB1CC1*	*RRBP1*	*SERPINA7*
PIWIL1	*PRKDC*	*RBM44*	*RSF1*	*SERPINC1*
PKD1L2	*PROC*	*RBP4*	*RTTN*	*SERPIND1*
PKHD1	*PROS1*	*RC3H1*	*RUFY2*	*SERPINF1*
PKP4	*PRPH*	*RCOR3*	*RYR1*	*SERPINF2*
PLCB1	*PRSS1*	*RELA*	*RYR2*	*SERPING1*
PLCB2	*PRSS3*	*RERGL*	*RYR3*	*SETD2*
PLCH1	*PSMD1*	*REST*	*SAA1*	*SETD3*
PLCL1	*PSMD6*	*REV1*	*SAA2*	*SETDB1*
PLD2	*PTPN13*	*REV3L*	*SAA4*	*SF3B2*
PLEC	*PTPN22*	*RFC4*	*SACS*	*SGCA*
PLEKHA7	*PTPN23*	*RHBDF2*	*SAMD9*	*SGOL2*
PLG	*PTPRG*	*RIMBP3C*	*SARS*	*SH3GL1*
PLXDC2	*PZP*	*RIMS2*	*SBSN*	*SHANK1*
PLXNA2	*QSOX1*	*RIMS3*	*SCAPER*	*SHBG*
PLXND1	*R3HDM2*	*RIN2*	*SCARB1*	*SHROOM3*
PMFBP1	*RAB17*	*RLTPR*	*SCEL*	*SIGLEC16*
POLQ	*RAB3GAP2*	*RNASE4*	*SCN2A*	*SIPA1L1*
POM121L2	*RABEP1*	*RNF20*	*SCN7A*	*SIPA1L3*
PON1	*RAD18*	*RNF213*	*SCYL2*	*SIRPB2*
PON3	*RAD54B*	*RNH1*	*SELL*	*SLBP*
PPBP	*RALGAPA2*	*RNMTL1*	*SEMA3F*	*SLC16A10*
PPFIBP2	*RANBP2*	*ROBO1*	*SENP5*	*SLC25A14*
PPL	*RAPGEF2*	*ROCK2*	*SEPP1*	*SLC29A1*
PPP1R12A	*RAPGEF4*	*RPAP3*	*SERPINA1*	*SLC4A1AP*
PPP1R26	*RAPGEF6*	*RPL37A*	*SERPINA10*	*SLC4A7*
PRDM4	*RARA*	*RPL7*	*SERPINA3*	*SLC6A2*
PRDX2	*RARRES2*	*RPRD2*	*SERPINA4*	*SLK*
PRG4	*RASA2*	*RPS6KA3*	*SERPINA5*	*SLMAP*
PRKAG1	*RASGRF1*	*RRAGA*	*SERPINA6*	*SLTM*

SLX4IP	*SRRM1*	*TET1*	*TPR*	*UNC45A*
SMC2	*SSRP1*	*TET2*	*TRAK1*	*UNKL*
SMC3	*ST18*	*TET3*	*TRANK1*	*UPF1*
SMC4	*STAB2*	*TF*	*TRIL*	*URB1*
SMEK2	*STAG1*	*TFRC*	*TRIM65*	*USO1*
SMTN	*STARD9*	*TGFBI*	*TRIO*	*USP18*
SNAP25	*STAT1*	*THBS1*	*TRIP11*	*USP20*
SNCA	*STIM1*	*THBS3*	*TRPC1*	*USP21*
SND1	*STK31*	*THG1L*	*TRPM3*	*USP42*
SNRPB2	*STOX2*	*THUMPD2*	*TRRAP*	*USP43*
SNX15	*STX11*	*TIA1*	*TSEN2*	*UTP14C*
SOGA1	*STXBP3*	*TIAM2*	*TSHZ3*	*UTP20*
SOGA2	*STXBP5L*	*TIE1*	*TSLP*	*UTRN*
SORBS1	*SUPT6H*	*TIFA*	*TTC17*	*VASN*
SORBS3	*SYCP1*	*TIGD1*	*TTC28*	*VCAM1*
SOX15	*SYMPK*	*TIGD2*	*TTC7B*	*VCAN*
SPAG17	*SYN1*	*TLN1*	*TTLL6*	*VCL*
SPAG9	*SYNE1*	*TLN2*	*TTN*	*VEZT*
SPATA16	*SYNE2*	*TMEM131*	*TTR*	*VIL1*
SPATA21	*SYT16*	*TMEM57*	*TXLNG*	*VIM*
SPEF2	*SYTL2*	*TMF1*	*TYK2*	*VIPAS39*
SPERT	*TARBP1*	*TMPRSS11A*	*UACA*	*VPS11*
SPG11	*TBC1D16*	*TMTC3*	*UBA6*	*VPS13A*
SPHKAP	*TBC1D32*	*TNFRSF10C*	*UBR1*	*VPS13B*
SPP2	*TBC1D9*	*TNKS*	*UBR4*	*VPS13C*
SPTA1	*TBX18*	*TNXB*	*UBR5*	*VPS13D*
SPTB	*TCHH*	*TOP2A*	*UCHL5*	*VPS16*
SPTBN1	*TDRD1*	*TP63*	*UGGT1*	*VPS33B*
SPTBN2	*TDRD15*	*TPM3*	*ULK2*	*VTN*
SPTBN5	*TDRD6*	*TPM4*	*UNC13B*	*VWF*

WAPAL	*XIRP2*	*ZNF114*	*ZNF806*
WDFY3	*YTHDC2*	*ZNF292*	*ZNF835*
WDR33	*ZAR1L*	*ZNF454*	*ZNF92*
WDR87	*ZC3H12C*	*ZNF462*	*ZNF93*
WDR96	*ZC3H13*	*ZNF496*	*ZNF99*
WFDC3	*ZCCHC6*	*ZNF518A*	*ZPBP2*
WNK3	*ZFC3H1*	*ZNF536*	*ZRANB3*
XIAP	*ZFHX4*	*ZNF683*	*ZZEF1*
XIRP1	*ZNF106*	*ZNF804B*	